Superconducting Fluctuations In Boron-Doped Nanocrystalline Diamond Films: A Study of Disordered Granular Metals Using Diagrammatic Quantum Field Theory

by

David Tony Stewart Perkins

A thesis submitted to the
University of Birmingham
for the degree of
DOCTOR OF PHILOSOPHY

School of Physics and Astronomy
College of Engineering and Physical Sciences
University of Birmingham
1 July 2021

ABSTRACT

In this thesis, we demonstrate how to generalise the diagrammatic methods of quantum field theory commonly used for calculating transport phenomena in disordered homogeneous metals, such that they may be used for disordered granular metals. The predictions of our granular model are then compared to experimental resistance versus temperature data measured in boron-doped nanocrystalline diamond films. We find semi-quantitative agreement under the assumption of a constant phase breaking rate, τ_ϕ^{-1}, and explore the possible temperature dependence of τ_ϕ^{-1}. We find that our current model of a disordered granular metal does not generate a phase breaking mechanism which is able to quantitatively match theory to experiment. We suggest different avenues to explore theoretically and experimentally to determine the origin of the contributions to the fluctuation conductivity in BNCD, so that we better understand the onset of superconductivity in disordered granular metals.

DEDICATION

This thesis is dedicated to my Mum, Dad, and Sparky (my dog).

ACKNOWLEDGEMENTS

I would like to acknowledge my supervisor, Rob Smith, for helping me throughout my PhD when I became stuck on certain problems, and suggesting literature to look at when trying to understand new physics I had not yet encountered. Even if we did argue about notation when writing papers, Rob's level of pedantry and style presentation taught me a lot about how to present research in a coherent and interesting manner.

Along the same lines, I must thank Georgina Klemencic and Jonathan Fellows for inspiring my PhD project with their works on boron-doped nanocrystalline diamond. I am lucky to have worked in collaboration with Jon and George.

Next I would like to acknowledge my parents for dealing with my hermit-like behaviour when writing the majority of this thesis during the COVID-19 pandemic. They were understanding at times and infuriating at others... there again, they did provide a fair amount of food, so I probably shouldn't complain too much.

I'd also like to thank the University of Birmingham theory group's PhD students: Manjinder Kainth (Manny), Michael Clarke, Rory Whelan, Ben McCanna, Jordan Moodie, Robert Stanyon, George Bartlett, Chris Oliver, Jacob Spink, Rose Davies, Ewan McCulloch, Enrico Martello, Anda Xiong, and George McArdle for making the offices a fun working environment. We spent many, possibly too many, hours discussing problems that were anything but physics and more focussed on the latest strange thought that had been conjured up or interesting announcements regarding games and tech. The PhD students who came before me (Manny, Jordan, Rob, and George) also taught me the valuable life skills of how to juggle and how to solve Rubik's cubes quickly. I think my PB was around

the 41 to 42 second mark, though that's nothing compared to Manny and Jacob. I think I will miss the 2 hour lunches with the group.

I would also like to thank Manny in particular for creating the LaTeX template used to make this thesis. Without this template, I would have spent far longer than I would have liked arguing with LaTeX in trying to get my thesis to match the University of Birmingham's style.

Finally, I would like to thank Jordan Lightstone and William Jowett for being absolutely amazing friends. They helped me when I was in a bad place mentally, and I will be forever grateful to them for being there for me. I'm glad they're just as weird and strange as I am.

PUBLICATIONS

"*Fluctuation Spectroscopy in Granular Superconductors with Application to Boron-doped Nanocrystalline Diamond*" -

D. T. S. Perkins, G. M. Klemencic, J. M. Fellows, R. A. Smith

Physical Review B, Volume 104, Issue 9, Page 094513 (2021)

"*Phase Slips and Metastability in Granular Boron-Doped Nanocrystalline Diamond Microbridges*" -

G. M. Klemencic, D. T. S. Perkins, J. M. Fellows, C. M. Muirhead, R. A. Smith, S. Mandal, S. Manifold, M. Salman, S. R. Giblin, & O. A. Williams,

Carbon, Volume 175, Page 43 (2021)

"*Drude Conductivity of a Granular Metal*" -

D. T. S. Perkins & R. A. Smith,

Annals of Physics, Volume 418, Article 168170 (2020)

PREFACE

Throughout my PhD I found that locating good pieces of literature that were clear, open, and helpful in trying to improve my own understanding of condensed matter field theory was quite a challenge, and at times a real pain. My journey into diagrammatic field theory began with Rickayzen's book titled "Green's Functions and Condensed Matter Physics", or as the spine of the book I had would call it "Green's Fucntions..."... so I was off to a good start with a book with many typos and a few skimped over details. I guess the typos and errors in the book made me pay closer attention, and perhaps meant I had a better understanding of the material. Nevertheless, it was still infuriating to read at times! Though I would still recommend it as a first read into the area if you're willing to learn about the lesser known Green's "Fucntions".

I did find many other brilliant sources for learning quantum field theory for condensed matter, such as Altland and Simons; Abrikosov, Gorkov, and Dzyaloshinski (AGD); and Bruus and Flensberg, but this did take time. For example, in trying to understand impurity averaging for disordered metals near the beginning of my PhD, I found Altand and Simons fantastic for performing the averaging procedure in the context of path integrals. However, finding a good diagrammatic approach, that was not quite so hand wavey, only presented itself three years into my PhD courtesy of Bruus and Flensberg. Granted that one could continue with more complicated calculations by appreciating the notion behind the averaging, I felt quite disatisfied not seeing the full beauty (or horror) that lead to the results we so readily use.

Due to the penetrable literature (in my opinion) on different topics and ideas being

somewhat spread out through different textbooks and some papers, I have tried to compile all the pre-requisite ideas and methods that a student whose focus is diagrammatic field theory, like myself, would need or appreciate at the start of their PhD. Some of the most renown texts are amazing once you already have a decent understanding, looking at you AGD. Yet this is not helpful when it comes to trying to learn the subject at a postgraduate level for the first time. After having spent probably too long worrying about the fundamentals behind why field theory works, and why should I believe all the rules we have, I thought I would try and compile the knowledge I found so that future PhD students might find part of this thesis helpful in getting stuck into their research faster. This has lead me to write my thesis in an almost three part style.

The first part of my thesis will provide a pedagogical presentation of the building blocks of quantum field theory and how we can derive the rules to the well known Feynman diagrams, which may appear as just squiggles on a page to the uninitiated. In conjunction with this part, many of the appendices will serve as further in depth presentations of the ideas discussed in the text.

Following this, the second part deals with commonly considered transport problems related to the electrical conductivity in homogeneous metals. In these sections we discuss how to derive the Drude conductivity in detail, and how the effects of weak localisation, electron-electron interactions, and superconducting fluctuations lead to corrections. This part will serve as a good demonstration of how to perform diagrammatic calculations in disordered homogeneous metals, and will be a vital reference to all the analogous granular calculations we consider later. The final part will focus purely on my research on granular materials and how we can better understand the electrical conductivity in these systems using diagrammatic methods.

In short, for the student reading this work wanting to learn about field theory and diagrammatics I would advise them to read through chapter 2 and the appendices therein. For those students who want to understand transport in terms of disorder and electrical conductivity I would like to direct them to chapter 3 and the appendices referenced here.

For the worryingly keen students and examiner who wish continue reading or to skip the introductory material (respectively) I direct them to chapters 4 onwards.

CONTENTS

1 Introduction **1**

2 Green's Functions & Diagrammatic Methods For Homogeneous Systems **5**

2.1 Mathematical Properties of Green's Functions 6

2.2 Free Electron Green's Function 15

2.3 Single-Particle Interactions 18

2.4 Two-Particle Interactions 23

3 Transport Phenomena In Homogeneous Systems **35**

3.1 Impurity Scattering and Diagrammatics 36

3.2 Drude Conductivity 43

3.2.1 The Naïve Approach 51

3.2.2 A Careful Treatment 53

3.2.3 The Einstein Relation 57

3.3 Weak Localisation 58

3.3.1 The Cooperon & Diffuson 60

3.3.2 Weak Localisation Corrections 68

3.4 Electron-Electron Interactions – Coulomb 72

3.4.1 The Screened Coulomb Interaction and RPA 72

3.4.2 EEI Corrections to the Electrical Conductivity 75

3.5 Superconducting Fluctuations 80

3.5.1 The Pair Propagator 81
3.5.2 Fluctuation Conductivity – A Brief History 85
3.5.3 Fluctuation Conductivity 87
3.6 Phase Coherence Lifetime 100
3.6.1 Coulomb Phase Breaking Mechanism 102
3.6.2 Superconducting Fluctuations Phase Breaking Mechanism 110
3.7 Chapter Summary 121

4 Developing Diagrammatic Techniques For Granular Systems 123
4.1 What is a Granular Metal? 124
4.2 Tunnelling: A New Form of Disorder 126
4.2.1 Single-particle Green's Function 127
4.2.2 Single-electron Green's Function – With Averaging over Tunnelling Events 129
4.3 Two-particle Interactions 134
4.3.1 Two-particle Interactions – With Averaging Over Tunnelling Events 139

5 Transport Phenomena In Granular Systems 141
5.1 Drude Conductivity 141
5.1.1 A Classical model 142
5.1.2 Quantum Field Theory & Linear Response 144
5.1.3 The Naïve Approach 150
5.1.4 The Careful Approach 152
5.2 Weak Localisation 155
5.2.1 Granular Diffusive Propagators 155
5.2.2 Weak Localisation Correction in Granular Metals 163
5.3 Electron-Electron Interactions 167
5.3.1 The Screened Coulomb Interaction 167
5.3.2 EEI Corrections to the Electrical Conductivity 170

5.4 Superconducting Fluctuations . . . 178
5.4.1 The Pair Propagator . . . 180
5.4.2 Fluctuation Conductivity . . . 184
5.4.3 Discussion . . . 197
5.5 Phase Coherence Lifetime . . . 199
5.5.1 Coulomb Phase Breaking Mechanism . . . 200
5.5.2 Superconducting Fluctuation Phase Breaking Mechanism . . . 209
5.6 Chapter Summary . . . 214

6 Boron-Doped Nanocrystalline Diamond: Experimental Results 215
6.1 Data Analysis . . . 216
6.2 Theory Versus Experiment . . . 217
6.3 Discussion . . . 222

7 Conclusion 227

A Second Quantisation & the Pictures of Quantum Mechanics 233
A.1 Second Quantisation . . . 233
A.1.1 Single-Particle Operators . . . 239
A.1.2 Two-particle operators . . . 241
A.1.3 The Pictures of Quantum Mechanics . . . 243

B Wick's Theorem 253

C The Density Matrix 257

D Disorder Averaging, Self-Energy, and the Born approximation 261
D.1 Disorder Averaging - The Gruesome Details . . . 261
D.2 The First Order Born Approximation . . . 267
D.3 The Full Born Approximation . . . 273
D.4 The Self-Consistent Born Approximation . . . 275

D.5 Crossing Terms 278

E Kubo's Formula and Linear Response **281**

E.1 Electrical Current 284

F Observing Weak Localisation **289**

G Electron-Electron Interaction – Calculation Details **295**

G.1 Screened Coulomb and RPA 295

G.2 Cancellation of Diagrams A, B, and C 298

G.3 EEI Corrections in Different Dimensions 302

H The Pair Propagator: An Honest Derivation **307**

I Fluctuation Conductivity – Calculation Details **311**

I.1 Vanishing Zero Frequency Response – Homogeneous Metals 312

I.2 Non-Singular Contributions 324

I.3 AL Integration Details 326

I.4 Anomalous MT Integration Details 330

I.5 Regular MT & DOS Integration Details 331

I.6 Vanishing Zero Frequency Response – Granular Metals 333

I.6.1 EEI Side Note 340

J Phase Breaking Rates in Homogeneous Systems – Calculation Details **341**

J.1 Coulomb Contribution 341

J.1.1 Two Dimensions 346

J.1.2 Three Dimensions 349

J.2 Superconducting Fluctuations Contribution 351

J.2.1 Two Dimensional Systems 355

J.2.2 Three Dimensional Systems 356

K Lattices and Periodic Boundary Conditions **359**

L Analysis of Resistance versus Temperature Data for Various BNCD Films **363**

M Summin' About Sum Identities **369**

M.1 Matsubara Sums 369

M.2 Momentum Sums in the Diffusive Limit 372

M.2.1 A Single Green's Function 375

M.3 A Difference of coths 377

M.4 A Sum of a Product of Green's Functions in Spectral Function Form 378

N Special Functions **381**

N.1 The Digamma Function 381

N.2 The Hurwitz Zeta Function 382

References **382**

LIST OF FIGURES

2.1 Green's functions in complex frequency space 14

2.2 Diagrammatics for a single particle potential 22

2.3 Diagrammatic representation of first order numerator corrections due to two particle interactions 27

2.4 Disconnected and connected pieces of a diagram 28

2.5 Position-frequency energy conservation 31

3.1 Diagrammatic representation of disorder averaging of four impurity scattering events. 38

3.2 Diagrammatic representation of the simplified disorder-averaged self-energy and electron Green's function Dyson equation. 39

3.3 Self-consistent diagrammatic series for the disorder-averaged electron Green's function. 42

3.4 Current-Current correlator diagrams before disorder averaging. 47

3.5 Disorder average of the conductivity diagram. 49

3.6 Drude diagram for a homogeneous system. 50

3.7 Analytic structure of Drude integrand 52

3.8 Analytic structure of Drude frequency sum. 53

3.9 Visualisation of the paths a particle can take in weak localisation. 58

3.10 Generic ladder diagram of cooperons and diffusons. 60

3.11 Explicit particle and hole paths schematic for weak localisation. 61

3.12 Diagrammatic series of the open diffuson. 62
3.13 Diagrammatic series of the half closed diffuson. 65
3.14 Redrawing a maximally crossed diagram. 66
3.15 Diagrammatic series for the open and half closed cooperons. 67
3.16 Weak localisation correction to the electrical conductivity. 69
3.17 RPA series for the Screened Coulomb interaction. 73
3.18 Diagrams for corrections to the electrical conductivity due to the Coulomb interaction. 75
3.19 Sign choices of the EEI DOS type diagram with an additional diffuson. . . 77
3.20 Sign choices of the EEI MT type diagram with an additional diffuson. . . . 78
3.21 Example plots of electron-electron interaction corrections to the electrical conductivity and resistivity. 79
3.22 Diagrammatic series for the virtual Cooper pair propagator. 81
3.23 Fluctuation conductivity diagrams for a homogeneous metal. 85
3.24 Sign choices for the blocks appearing in the AL diagram. 88
3.25 Contour deformation for the AL diagram. 89
3.26 93
3.27 Sign choice of the anomalous MT diagrams contributing to fluctuation conductivity. 93
3.28 Sign choices of the regular MT diagrams contributing to fluctuation conductivity. 97
3.29 Sign choices of the fluctuation DOS diagrams contributing to conductivity. 99
3.30 Diagrammatic representation of the cooperon with explicit terms related to phase breaking. 101
3.31 Diagrammatic representation of Σ_ϕ due to the Coulomb interaction for homoegenous systems. 102
3.32 Contours used for analytic continuation of the frequency sums appearing in the Coulomb contribution to phase breaking rates. 106

3.33 Diagrammatic representation of Σ_ϕ due to the Coulomb interaction for homoegenous systems. 111
3.34 Contours used for analytic continuation of the Cooperon frequency sum appearing in the superocnducting fluctuation contribution to phase breaking rates. 113
3.35 Plots of the total phase breaking rates in 2D homogeneous superconductors. 118
3.36 Plots comparing Brenig et. al.'s approximation to their self-consistent equation for the phase breaking rate. 119
3.37 Plots of the phase breaking rate for 3D homogeneous metals with a superconducting transition. 120

4.1 Schematic drawings of realistic and model granular metals. 125
4.2 Diagrammatics for tunnelling within a single-particle Green's function. . . 128
4.3 Diagrammatic representation of the simplified tunnelling averaged self-energy and electron Green's function Dyson equation. 130
4.4 Diagrammatic representation of first order corrections due to two particle interactions in granular systems. 139

5.1 Granular metal circuit diagram. 142
5.2 Diagrammatic representation of the granular Drude conductivity. 149
5.3 Diagrammatic series for the granular diffuson used by Beloborodov et. al.. 156
5.4 Diagrammatic series for the granular diffuson 157
5.5 Diagrammatic series for the granular diffuson with a closed end 160
5.6 Diagrammatic series for the open and half closed cooperons in granular systems. 161
5.7 Weak localisation correction to the electrical conductivity in granular metals. 162
5.8 RPA series for the screened Coulomb interaction in granular metals. 168
5.9 Diagrams for corrections to the electrical conductivity due to the Coulomb interaction in granular metals. 170

5.10 Plots of analytical and numerical behaviour for high temperature EEI behaviour in granular metals. 176

5.11 Examples of alternative tunnelling event placements and correlations in the granular EEI diagrams. 177

5.12 Diagrammatic series for the virtual Cooper pair propagator in a granular metal. 181

5.13 Diagrams for corrections to the electrical conductivity due to superconducting fluctuations in granular metals. 185

5.14 Diagrammatic representation of the granular cooperon with explicit terms related to phase breaking. 199

5.15 Diagrammatic representation of Σ_ϕ due to the Coulomb interaction for granular systems. 201

5.16 Diagrammatic representation of Σ_ϕ due to the Coulomb interaction for granular systems. 208

5.17 Example plots of the phase breaking rate for a granular superconductor. . 212

6.1 Resistance versus temperature data taken from a 339nm BNCD film with fitting to high temperature behaviour. 216

6.2 Resistance versus temperature data taken from a 339nm BNCD film with fitting to high temperature behaviour. 217

6.3 Theoretical fluctuation conductivity predictions based upon experimental parameters in the absence of phase breaking. 218

6.4 Resistance versus temperature data taken from a 339nm BNCD film with fitting to high temperature behaviour. 220

6.5 Theoretical phase breaking rate in a 339nm BNCD film. 221

6.6 Theoretical fluctuation conductivity predictions based upon experimental parameters including a temperature dependent phase breaking rate. 221

D.1 Diagrammatic representation of disorder averaging of single impurity disribution. 262
D.2 Diagrammatic representation of disorder averaging of two and three impurity disributions. 264
D.3 Diagrammatic representation of disorder averaging of four impurity disributions. 266
D.4 Diagrammatic representation of the disorder-averaged self-energy and electron Green's function Dyson equation. 267
D.5 Self-energy for the disorderd electron gas in the full Born approximation. . 274
D.6 Second order corrections to the disorder-averaged electon Green's function. 278
D.7 Comparison of momentum (phase) space of impurity scattering crossed terms and non-crossed terms. 279

F.1 Sketch of experimental setup for observing oscillatory behaviour in weak localisation corrections in a varying magnetic field. 290

G.1 Sign choices of the EEI DOS diagram. 299
G.2 Sign choices of the EEI MT type diagram. 301

H.1 Diagrammatic series for the modified cooperon vertex part. 308
H.2 Alternate writing of the pair propagator diagrammatic series. 310

I.1 Fluctuation conductivity diagram sign choices for a homogeneous metal. . 314
I.2 Sign choices for the blocks appearing in the AL diagram. 317
I.3 Diagrams for corrections to the electrical conductivity due to superconducting fluctuations in granular metals. 333

J.1 Diagrammatic representation of Σ_ϕ due to the Coulomb interaction for homoegenous systems. 343
J.2 Diagrammatic representation of Σ_ϕ due to the Coulomb interaction for homoegenous systems. 350

L.1 Resistance versus temperature fittings for data taken from a 564nm BNCD film. 364
L.2 Resistance versus temperature fittings for data taken from a 204nm BNCD film. 365
L.3 Resistance versus temperature fittings for data taken from a 168nm BNCD film. 366
L.4 Resistance versus temperature fittings for data taken from a 160nm BNCD film. 367
L.5 Resistance versus temperature fittings for data taken from a 128nm BNCD film. 368

M.1 Deformation of the contour integral for Matsubara type sums. 370
M.2 Contour choices for diffusive momentum sum integral approximations. . . . 373

LIST OF TABLES

5.1 Summary of the regional behaviours of the DOS, anomalous MT, and AL contributions to the fluctuation conductivity of a granular metal in terms of the reduced temperature, η. The results here are given in units of e^2/a, and are taken in the limit of negligible phase breaking, $\tau_\phi^{-1} = 0$. 196

A.1 Summary of the relations between different quantum mechanical pictures. . 248

I.1 Ranges of ε that give a non-zero contribution to $K_{\alpha\beta}^{(F)}$. The brackets within each resultant cell gives the transformation we use to manipulate the Matsubara sums to obtain the results given in eq. I.8. For multiple transformations in the same cell, the order they are written is the order in which they are applied. 319

L.1 Summary of the T_c and a values found to various BNCD films, and the range of values Γ and E_{Th} might take. 363

M.1 Choices of Matsubara counting functions and their residues for fermionic and bosonic frequencies, $\varepsilon = (2n+1)\pi T$ and $\omega = 2\pi n T$ respectively. 372

CHAPTER 1

INTRODUCTION

Transport phenomena have been of great interest to physicists, chemists, biologists, and engineers over the past few centuries. In a very general sense, transport phenomena relate to the transfer of information from one point to another via some mechanism. Common examples include electrical conductivity, thermal conductivity, diffusion of gases, fluid flow, electrolysis, the list goes on. In this thesis, we focus on how information is transferred through granular metals via electrical currents.

The simplest model for a metal was originally proposed by Drude [1] in 1900, only three years after the discovery of the electron by J. J. Thomson [2]. In Drude's model, a metal was treated as an ideal gas of electrons in a positive background. Under the influence of an electric field, the electrons move in the same general direction through a field of impurities, colliding and scattering elastically off the impurities at a typical rate of τ_0^{-1}. With this simple picture of a metal, Drude was able to obtain an expression for the electrical conductivity of a metal in terms of measurable quantities,

$$\sigma_0 = \frac{n_e e^2 \tau_0}{m_e}, \tag{1.1}$$

where n_e is the number density of electrons, e is the magnitude of the electron charge, and m_e is the mass of an electron. This expression allowed the determination of τ_0^{-1} for a material, given experimental measurement of the system's conductance and dimensions.

We can view this as the first measure of disorder in a system: more impurities would lead to a larger scattering rate, and hence represent a more disordered (or less pure) metal. A natural question arising from Drude's formula is, how does the scattering rate (and hence the conductivity) change with temperature?

It turns out that a whole plethora of phenomena occur in metallic systems that can alter conductivity, some of which may be expected from a classical perspective, whilst others are inherently quantum mechanical. The most obvious effect of temperature is lattice vibrations, which were put on a firm mathematical footing in 1912 by Debye [3]. The Debye model of lattice vibrations [4] was phrased in terms of quantised sound waves (now known as phonons), having been inspired by Max Planck's quantisation of light. Thus, even the simplest physical picture leading to a temperature dependent resistance was quantum mechanical at its very core.

Throughout the 1900s and 1910s, it became clear that quantum mechanics was the underlying description for the physics of particles on the atomic and sub-atomic scales. With the development of "new" quantum mechanics (after Heisenberg [5] and Schrödinger[6]), in 1927 Sommerfeld extended Drude's original ideas to a weakly interacting electron gas obeying Fermi-Dirac statistics [7]. Using these ideas, Drude's formula for σ_0 can be obtained from the Boltzmann transport equation [8].

The development of microscopic quantum transport theory only began to take off with proliferation of quantum field theory (QFT) in the 1950s, when Matsubara [9] introduced finite temperature methods (statistical physics) into QFT. During this period, the focus of physics moved from a single-particle description of the universe to a many-particle one. This step had been hinted at since the conception of the phonon as a collective vibrational mode of a crystal lattice. Using Matsubara field theory, the linear response theory of Kubo [10], and the impurity averaging techniques of Edwards [11], Langer published a trilogy of papers [12, 13, 14] demonstrating how the Drude conductivity could be obtained in a fully microscopic manner (i.e. the Drude result survived QFT).

Using the machinery of Matsubara field theory, the period from the late 1950s to

the late 1980s saw the calculation of corrections to the electrical conductivity due to various mechanisms. By the end of the 1950s, the microscopic theory of superconductivity developed by Bardeen, Cooper, and Schrieffer (BCS) [15], had been rewritten in a field theoretic form by Nambu [16] and Gorkov [17]. This allowed for calculation of the electrical and thermal transport properties of the superconducting state. Paradoxically, it was only at the end of the 1960s that the divergence of the electrical conductivity at the onset of superconductivity was considered. These corrections to σ_0 were understood in terms of finite lifetime (virtual) Cooper pairs, and were calculated by Aslamazov and Larkin [18], Maki [19], and Thompson [20]; they are referred to as the fluctuation conductivity.

Continuing with this back to front path, the effects of disorder and (Coulomb) electron-electron interactions (EEIs) were not explained theoretically until the late 1970s. Altshuler and Aronov [21] determined and evaluated the Feynman diagrams describing the EEI corrections. The effects of localisation due to increasing disorder strength were calculated using scaling theory by Abrahams et. al. [22], and diagrammatically by Gorkov et. al. [23].

In parallel to this work, since the 1960s, physicists also explored the electronic transport properties of granular materials, from both theoretical and experimental perspectives. Early works (for reviews, see [24] and [25]) focussed primarily on the metal-insulator transition (MIT), whilst more recent work (for a review, see [26]) in the late 1990s and 2000s considered disordered granular metals far from the MIT. It was found that many of the results for disordered homogeneous metals, those originally considered in the early to mid 20^{th} century, could be translated across to granular systems by a simple replacement of the effective diffusion constant. However, novel temperature dependence of the electrical conductivity in granular metals was also predicted theoretically, with some of the most surprising differences appearing in the effects of superconducting fluctuations.

In 2008, Lerner et. al. [27] predicted three regions of behaviour to exist in the fluctuation conductivity close to T_c. These three regions occur when the characteristic size of a virtual Cooper pair was much smaller than the typical grain size, comparable to

the grain size, and much larger than the grain size. It was only recently that this was observed experimentally by Klemencic et. al. [28], who measured the change in resistance of boron-doped nanocrystalline diamond (BNCD) films, as they were cooled from room temperature to below $T_c \lesssim 4$K. In their data, they observed power law crossovers in the reduced temperature, $\eta = (T - T_c)/T_c$, dependence of the fluctuation conductivity, from $-1/2$ to -3 to $-1/2$. These changes in behaviour can be related to dimensional crossovers from 3D to quasi-0D to 3D, which disagreed with Lerner et. al.'s theory only in the *far-from-T_c region*.

The objective of this thesis is to explain the observations of Klemencic et. al.. To do this we must first understand how to calculate the various contributions to the electrical conductivity in disordered homogeneous metals, before trying to calculate their granular analogues. This thesis is therefore structured as follows: chapter 2 presents an overview of diagrammatic QFT in condensed matter physics. Chapter 3 shows how these ideas can be applied to disordered homogeneous metals to calculate the electrical conductivity contributions generated by various physical processes. After this, chapter 4 extends the ideas of chapter 2 to granular systems, and provides the set of diagrammatic rules used to perform the calculations that follow. Chapter 5 is analogous to chapter 3, and demonstrates how to calculate the Drude conductivity of a granular metal, before considering the corrections to this result arising from the same phenomena discussed in chapter 3. We then compare our theory for superconducting fluctuations in granular metals to Klemencic et. al.'s experimental results in chapter 6, and discuss how our theory can be refined or adjusted. Finally, in chapter 7 we conclude the findings of this thesis.

CHAPTER 2

GREEN'S FUNCTIONS & DIAGRAMMATIC METHODS FOR HOMOGENEOUS SYSTEMS

Green's functions provide a natural building block in the construction of quantum field theory (QFT). The general concept of a Green's function remains unchanged in QFT, that being the solution of a differential equation with a delta function source term. In addition to this, the Green's function now describes the propagation of a single particle from $(\mathbf{r}', t')$ to $(\mathbf{r}, t)$ in the simplest case, and the collective behaviour of multiple particles in more complex situations.

Two approaches can be taken in generating the necessary Green's functions for a problem; first being a diagrammatic description, which will be the focus of this thesis; whilst the second uses a path integral phrasing of the partition function. Both methods are equivalent, but carry advantages over the other. Diagrammatic theories are only applicable when a perturbative expansion of the problem exists. However, they can allow us to consider higher order corrections with greater ease compared to the path integral formulation. When a perturbative expansion doesn't exist, we may only use the path integral approach. This allows us to access powerful techniques such as renormalisation.

This chapter closely follows the structure of refs. [29, 30]. We first outline the types of Green's functions encountered in QFT and their mathematical properties in section 2.1. Following, we construct the single electron Green's function for free particles in section 2.2. Lastly, sections 2.3 and 2.4 provide a derivation of the diagrammatic rules for single particle and two particle interactions, respectively.

2.1 Mathematical Properties of Green's Functions

We concern ourselves with three types of Green's function: the retarded Green's function, G^R, the advanced Green's function, G^A, and the temperature Green's function, G, defined by ($\hbar = 1$)

$$G^R(t,t') = -i\,\langle [A(t), B(t')]_\eta \rangle\,\Theta(t-t'), \tag{2.1a}$$

$$G^A(t,t') = -i\,\langle [A(t), B(t')]_\eta \rangle\,\Theta(t'-t), \tag{2.1b}$$

$$\begin{aligned} G(\tau,\tau') &= -\langle T_\tau\{A(\tau)B(\tau')\}\rangle \\ &= -\langle A(\tau)B(\tau')\rangle\,\Theta(\tau-\tau') \\ &\quad + \eta\,\langle B(\tau')A(\tau)\rangle\,\Theta(\tau'-\tau), \end{aligned} \tag{2.1c}$$

where $A(t)$ and $B(t')$ are Heisenberg operators at times t and t' respectively, $\Theta(t)$ is the Heaviside function, and the square brackets represent

$$[A,B]_\eta = AB + \eta BA, \qquad \eta = \begin{cases} +1, & \text{for fermioninc operators} \\ -1, & \text{for bosonic operators} \end{cases}. \tag{2.2}$$

The angled brackets denote averaging over the density matrix, ρ, for a system in the grand canonical ensemble (GCE),

$$\langle ... \rangle = \mathrm{Tr}\left[\rho\, ...\right], \qquad \rho = \frac{1}{\mathcal{Z}} e^{-\beta(H-\mu N)}, \qquad \mathcal{Z} = \mathrm{Tr}\left[e^{-\beta(H-\mu N)}\right]. \tag{2.3}$$

where H is the system's Hamiltonian, μ is the chemical potential, N is the number operator, $\beta = 1/T$ is the inverse of temperature ($k_B = 1$), and $\mathcal{Z}$ is the partition function. The trace is defined as the sum of the diagonal elements of a matrix, $\widehat{O}$, in the basis of a complete set of states, $\{\phi_n\}$,

$$\mathrm{Tr}[\,\widehat{O}\,] = \sum_{\phi_n} \langle \phi_n | \,\widehat{O}\, | \phi_n \rangle \,. \tag{2.4}$$

Clearly the trace is basis independent, but we typically choose the eigenbasis for ease of calculation.

In the temperature Green's function τ is imaginary time, related to real time via the Wick rotation $t = -i\tau$. Lastly, T_τ denotes imaginary time ordering, such that operators occurring at later times appear to the left of operators occurring at earlier times.

All three of these Green's functions can be related to each other, but the temperature Green's function is particularly useful for introducing statistical mechanics into quantum mechanical problems. The choice $t = -i\tau$ transforms the grand canonical unitary time evolution operator (assuming a time-independent Hamiltonian), $\mathcal{U} = e^{-i(H-\mu N)t} = e^{-(H-\mu N)\tau}$, to a form resembling ρ.[1] An operator in the GCE is thus evolved in imaginary time according to

$$A(\tau) = \mathcal{U}^\dagger(-i\tau) A(0) \mathcal{U}(-i\tau) = e^{(H-\mu N)\tau} A(0) e^{-(H-\mu N)\tau}. \tag{2.5}$$

Imaginary time therefore provides a natural link between time evolution and statistical mechanics.[2]

[1] When in the GCE we wish to treat μ as being a fixed parameter, allowing the particle number to vary. Consequently, we wish to deal with operators that keep μ fixed and change the number of particles in the system. Keeping particle number fixed, operators evolve according to the normal time evolution operator $e^{-H\tau}$, whilst GCE operators changing the particle number (and keeping μ fixed) evolve according to the grand canonical time evolution operator, $e^{-(H-\mu N)\tau}$, see [30].

Alternatively, we can consider the density matrix in the canonical ensemble, $\sim e^{-\beta H}$, and compare it to the density matrix in the GCE, $\sim e^{-\beta(H-\mu N)}$, and demand that the time evolution operator maintain a similar form to these in their respective pictures. Hence in the GCE this amounts to considering time evolution of a state according to $H - \mu N$, and so our Schrödinger equation (assuming particle number is conserved) becomes $(H - \mu N)\phi = \widetilde{E}\phi$.

[2] Note that $\mathcal{U}^\dagger(-i\tau) \neq \mathcal{U}(-i\tau)^\dagger$, as the Hermitian conjugation acts at different times compared to the

All Green's functions with just two time arguments can be shown to depend only on the time difference. This is seen by considering the correlator

$$\begin{aligned} C(t,t') &= \langle A(t)B(t')\rangle \\ &= \frac{1}{\mathcal{Z}}\mathrm{Tr}\left[e^{-\beta(H-\mu N)}e^{i(H-\mu N)t}A(0)e^{-i(H-\mu N)t}e^{i(H-\mu N)t'}B(0)e^{-i(H-\mu N)t'}\right]. \end{aligned} \tag{2.6}$$

Clearly the cyclic nature of the trace combined with the commutation of the exponents allows the exponentials to be grouped to produce $(H-\mu N)(t'-t)$ in the exponents. Thus,

$$\begin{aligned} C(t,t') &= \frac{1}{\mathcal{Z}}\mathrm{Tr}\left[e^{-\beta(H-\mu N)}e^{i(H-\mu N)(t'-t)}A(0)e^{-i(H-\mu N)(t-t')}B(0)\right] \\ &= \langle A(t-t')B(0)\rangle \\ &= C(t-t'). \end{aligned} \tag{2.7}$$

This property makes it convenient to consider the temporal Fourier transform; for some general Green's function

$$\mathcal{G}(\Omega) = \int_{-\infty}^{+\infty} dt\, \mathcal{G}(t)\, e^{i\Omega t}. \tag{2.8}$$

Examining the retarded Green's function, assuming $\langle [A(t), B(0)]_\eta \rangle$ does not grow exponentially with time and $\Omega \in \mathbb{C}$, the integral only converges provided that $\mathrm{Im}[\Omega] > 0$. This is a consequence of the retarded Green's function being non-zero only for $t \in [0, +\infty]$. Hence, $\mathcal{G}(\Omega)$ is analytic in the upper-half plane and may be related to $G^R(\omega)$ through

$$G^R(\omega) = \mathcal{G}(\omega + i\delta), \tag{2.9}$$

where δ is a positive infinitesimal, and $\omega \in \mathbb{R}$. We may therefore write the Fourier

input of the argument. In the first case, we take $t = -i\tau$ after conjugating $\mathcal{U}(t)$, whilst in the second case we take $t = -i\tau$ before taking the conjugate of $\mathcal{U}(t)$. It is trivial to see that $\mathcal{U}(-i\tau)^\dagger = \mathcal{U}^\dagger(i\tau)$.

transform, and its inverse, for the retarded Green's function as

$$\begin{aligned} G^R(\omega) &= \int_{-\infty}^{+\infty} dt\, G^R(t)\, e^{i(\omega+i\delta)t}, \\ G^R(t) &= \int_{-\infty}^{+\infty} \frac{d\omega}{2\pi}\, G^R(\omega)\, e^{-i(\omega+i\delta)t}. \end{aligned} \tag{2.10}$$

An alternative representation of a Green's function is its spectral form. Consider eq. 2.8 and replace the trace in $G^R(t)$ with a sum over the many-body eigenstates of the system's grand canonical (GC) Hamiltonian [29], $(H-\mu N)\,|m\rangle = (E_m - \mu N_m)\,|m\rangle = \widetilde{E}_m\,|m\rangle$,

$$\begin{aligned} G^R(\omega) &= -\frac{i}{\mathcal{Z}} \int_0^{+\infty} dt\, e^{i(\omega+i\delta)t} \sum_m \langle m|\, e^{-\beta(H-\mu N)} [A(t), B(0)]_\eta\, |m\rangle \\ &= -\frac{i}{\mathcal{Z}} \int_0^{+\infty} dt\, e^{i(\omega+i\delta)t} \sum_{m,n} \left(e^{-\beta\widetilde{E}_m} + \eta e^{-\beta\widetilde{E}_n} \right) A_{mn} B_{nm} e^{i(\widetilde{E}_m - \widetilde{E}_n)t}, \\ &= -\frac{1}{\mathcal{Z}} \sum_{m,n} \frac{e^{-\beta\widetilde{E}_m} + \eta e^{-\beta\widetilde{E}_n}}{\widetilde{E}_n - \widetilde{E}_m - \omega - i\delta} A_{mn} B_{nm}, \end{aligned} \tag{2.11}$$

where $A_{mn} = \langle m|\, A(0)\, |n\rangle$, and we inserted the identity $\mathcal{I} = \sum_n |n\rangle\langle n|$ between $A(0)$ and $B(0)$. The final line of eq. 2.11 is known as the frequency Lehmann representation of a Green's function [31]. Note this assumes that H and N commute in order for the state to be an eigenstate of both operators, and so the particle number is conserved according to Heisenberg's equation of motion. Given $\widetilde{E}_m \in \mathbb{R}$ we write

$$G^R(\omega) = \int_{-\infty}^{+\infty} dx \frac{\mathcal{A}(x)}{\omega + i\delta - x}, \tag{2.12a}$$

$$\mathcal{A}(x) = \frac{1+\eta e^{-\beta x}}{\mathcal{Z}} \sum_{m,n} e^{-\beta\widetilde{E}_m}\, A_{mn} B_{nm}\, \delta(x + \widetilde{E}_m - \widetilde{E}_n). \tag{2.12b}$$

Eq. 2.12a is the spectral form of the Green's function, with $\mathcal{A}(x)$ being the spectral function.[3]

[3]Some texts define the spectral function as containing an additional factor of 2π so that the integral over x is normalised by a factor of $(2\pi)^{-1}$. This is just worth noting for understanding potential discrepancies with other texts.

To interpret this physically, let us consider the case where $A = c_{\mathbf{k}}^\dagger$ and $B = c_{\mathbf{k}}$ are creation and annihilation operators, respectively, for a particle with momentum $\mathbf{k}$. The Green's function associated to this is known as a single-particle Green's function, as it describes the propagation of a single particle. In this case the spectral function is

$$\mathcal{A}(\mathbf{k},\omega) = \frac{1+\eta e^{-\beta\omega}}{\mathcal{Z}} \sum_{m,n} e^{-\beta\widetilde{E}_m} \mid \langle m| \, c_{\mathbf{k}}^\dagger \, |n\rangle \mid^2 \delta(\omega + \widetilde{E}_m - \widetilde{E}_n). \tag{2.13}$$

First we note that $\mid \langle m| \, c_{\mathbf{k}}^\dagger \, |n\rangle \mid^2$ is the probability of finding the system in the state $|m\rangle$ after the addition of a particle with momentum $\mathbf{k}$ to the initial state $|n\rangle$. This also makes $\mathcal{A}(\omega)$ a real function.[4] Next we see that the delta function enforces energy conservation, $\widetilde{E}_m = \widetilde{E}_n + \omega$, that is to say the particle carries an energy ω relative to the chemical potential. Therefore, the spectral function describes all possible transitions from state $|n\rangle$ to state $|m\rangle$ upon the addition of a particle with momentum $\mathbf{k}$ and energy $(\omega + \mu)$. As such it is closely tied to the probability of these transitions. In the case of transport phenomena where most of the electrons involved are close to the Fermi surface, we expect that the spectral function will be strongly peaked about the Fermi energy.

A useful sum rule can then be obtained from $\mathcal{A}(x)$,

$$\int_{-\infty}^{+\infty} dx \, \mathcal{A}(x) = \langle [A(0), B(0)]_\eta \rangle \, . \tag{2.14}$$

Assuming that A and B are non-singular operators so the above is finite, we see in the limit $|\omega| \to \infty$ eq. 2.12a becomes

$$G^R(\omega) \sim \frac{\langle [A(0), B(0)]_\eta \rangle}{\omega}. \tag{2.15}$$

Therefore, $G^R(\omega)$ tends to zero like ω^{-1} for non-zero $\langle [A(0), B(0)]_\eta \rangle$, or faster in the case $\langle [A(0), B(0)]_\eta \rangle$ vanishes.

These ideas can be applied entirely equivalently to the advanced Green's function.

[4] This is true for the spectral function of any single particle Green's function.

The temporal Fourier transform now requires the complex frequency to be in the lower half plane to ensure convergence, $\omega - i\delta$, so we can relate $G^A(\omega)$ to $\mathcal{G}(\Omega)$ via

$$G^A(\omega) = \mathcal{G}(\omega - i\delta), \tag{2.16}$$

and so the Fourier transform and inverse Fourier transform relations for the advanced Green's function are

$$\begin{aligned} G^A(\omega) &= \int_{-\infty}^{+\infty} dt\, G^A(t)\, e^{i(\omega - i\delta)t}, \\ G^A(t) &= \int_{-\infty}^{+\infty} \frac{d\omega}{2\pi}\, G^A(\omega)\, e^{-i(\omega - i\delta)t}. \end{aligned} \tag{2.17}$$

Furthrmore, it is trivial to show that the advanced Green's function written in spectral form is

$$G^A(\omega) = \int_{-\infty}^{+\infty} dx \frac{\mathcal{A}(x)}{\omega - i\delta - x}. \tag{2.18}$$

Clearly, the retarded and advanced Green's functions are related via $\mathcal{G}(\Omega)$. Therefore, $\mathcal{G}(\Omega)$ is analytic in the upper-half plane and equal to $G^R(\omega)$ as $\mathrm{Im}[\Omega] \to 0^+$, as well as being analytic in the lower-half plane and equal to $G^A(\omega)$ as $\mathrm{Im}[\Omega] \to 0^-$. Lastly, $\mathcal{G}(\Omega)$ is not analytic at all points on the real axis due to the difference between the retarded and advanced Green's functions,

$$G^R(\omega) - G^A(\omega) = \int_{-\infty}^{+\infty} dx\, \mathcal{A}(x) \left[\frac{1}{\omega + i\delta - x} - \frac{1}{\omega - i\delta - x} \right] = -2\pi i \mathcal{A}(\omega). \tag{2.19}$$

Here made use of the Plemelj formula,

$$\int_{-\infty}^{+\infty} dx \frac{\mathcal{A}(x)}{\omega \pm i\delta - x} = \mp i\pi \mathcal{A}(\omega) + \mathcal{P} \int_{-\infty}^{+\infty} dx \frac{\mathcal{A}(x)}{\omega - x}, \tag{2.20}$$

where $\mathcal{P}$ denotes the principal part of the integral. Given this break of analyticity, we introduce a branch cut along the real axis. The relation in eq. 2.19 simplifies in the case of single-particle Green's functions, as the retarded and advanced forms are simply

complex conjugates of each other. In this case, the spectral function can be written easily in terms of the retarded Green's function,

$$\mathcal{A}(\omega) = -\frac{1}{\pi}\mathrm{Im}\left[G^R(\omega)\right]. \tag{2.21}$$

We now turn our attention to the temperature Green's function. Like the previous Green's functions, this too depends only on the difference $\tau - \tau'$. A very important difference the temperature Green's function has in comparison to the others is that its convergence is only guaranteed on a finite interval, $-\beta < \tau - \tau' < \beta$ [31]. To demonstrate this we write $G(\tau - \tau')$ in its temporal Lehmann representation,

$$\begin{aligned} G(\tau - \tau') = &-\frac{1}{\mathcal{Z}}\sum_{m,n} e^{-\widetilde{E}_m(\beta-\tau+\tau')}e^{-\widetilde{E}_n(\tau'-\tau)}A_{mn}B_{nm}\Theta(\tau-\tau') \\ &+\frac{\eta}{\mathcal{Z}}\sum_{m,n} e^{-\widetilde{E}_n(\beta+\tau-\tau')}e^{-\widetilde{E}_m(\tau'-\tau)}A_{mn}B_{nm}\Theta(\tau'-\tau). \end{aligned} \tag{2.22}$$

When $\tau - \tau' > 0$ we can see the first line requires $\tau - \tau' < \beta$ to ensure the sum converges exponentially for large energies. In a similar vein, the second line is relevant for $\tau - \tau' < 0$ and easily converges for $-\beta < \tau - \tau'$.[5]

Let us define the general argument of the temperature Green's function on the interval. Next we consider when this argument is negative by taking $\tau' = \beta$,

$$\begin{aligned} G(\tau-\beta) &= \eta\left\langle B(0)A(\tau-\beta)\right\rangle \\ &= \frac{\eta}{\mathcal{Z}}\mathrm{Tr}\left[e^{-\beta H}B(0)e^{H(\tau-\beta)}A(0)e^{H(\beta-\tau)}\right] \\ &= \frac{\eta}{\mathcal{Z}}\mathrm{Tr}\left[e^{-\beta H}A(0)e^{-H\tau}B(0)e^{H\tau}\right] \\ &= \eta\left\langle A(0)B(\tau)\right\rangle = -\eta G(\tau). \end{aligned} \tag{2.23}$$

[5]For bosons $\mu \leq 0$, hence $\widetilde{E}_n > 0$ is guaranteed, so the exponent of the surviving piece will be negative for all accessible states. For fermions $\mu > 0$, so $\widetilde{E}_n < 0$ for states below the Fermi level. However, the number of states accessible in this region is limited and have a finite range of energies in comparison to the infinite number of states with an unbound range of energies above the Fermi level. Thus the sum will converge, as for higher energies the summand decays exponentially for higher energies, provided $A_{mn}B_{nm}$ is well behaved and does not grow exponentially.

Hence, the temperature Green's function is periodic for bosons, $G(\tau) = G(\tau + \beta)$, and anti-periodic for fermions, $G(\tau) = -G(\tau + \beta)$, over the interval $-\beta < \tau - \tau' \leq \beta$.

These periodic properties suggest the use of Fourier analysis, however $G(\tau)$ is not periodic for all $\tau \in \mathbb{R}$. Despite this lack of global periodicity, our range of concern is only over the interval where we observe (anti-)periodic behaviour. Therefore, we can construct a periodic function, that is periodic for all real numbers, defined by $G(\tau)$ on the interval $-\beta < \tau < \beta$. We can then perform Fourier analysis on this new function to find a Fourier series definition of $G(\tau)$ for $-\beta < \tau < \beta$. Using these ideas we can write the temporal Fourier series definition for $G(\tau)$ as,

$$G(\tau) = T \sum_{\nu} G(i\nu) e^{-i\nu\tau}, \qquad \text{for} \qquad -\beta < \tau < \beta, \tag{2.24a}$$

$$G(i\nu) = \int_0^\beta d\tau G(\tau) e^{i\nu\tau}, \tag{2.24b}$$

where $\nu = 2\pi n T$ and $\nu = (2n+1)\pi T$ $(n \in \mathbb{Z})$ in the bosonic and fermionic cases respectively. The frequency ν is known as a Matsubara frequency and $G(i\nu)$ a Matsubara Green's function.[6] In general, when considering Matsubara frequencies, we adopt the convention where ω and Ω are used exclusively for bosonic frequencies, whilst ε is used for fermionic frequencies.

Furthermore, we may also write $G(i\nu)$ in spectral form; starting from eq. 2.1c and following the same steps as for the retarded Green's function we find,

$$G(i\nu) = \int_{-\infty}^{+\infty} dx \frac{\mathcal{A}(x)}{i\nu - x}, \tag{2.25}$$

where ν can be a fermionic or bosonic Matsubara frequency. Although it appears that we can obtain the retarded and advanced Green's functions from $G(i\nu)$ by analytic continuation of ν, $i\nu \to \omega \pm i\delta$, we have to ensure it leads to a unique solution. Analytic

[6] We use $G(i\nu)$ to denote the use of Matsubara Green's functions with i written explicity in the argument alonside the generic Matsubara frequency ν. This is not to be confused for the continuous frequency used in the retarded and advanced Green's functions.

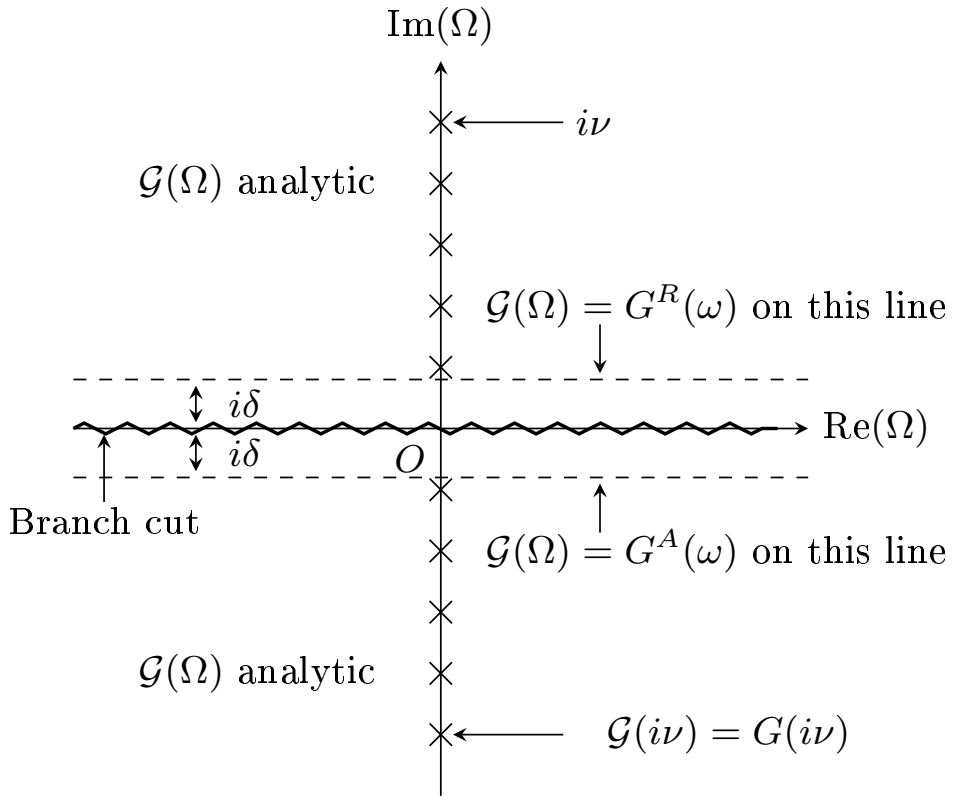

Figure 2.1: Relationship between $\mathcal{G}(\Omega)$, $G^{R,A}(\omega)$, and $G(i\nu)$ in complex frequency space.

continuation alone cannot guarantee the generation of a single unique function. However, recalling that $G^R(\omega)$ and $G^A(\omega)$ must decay as fast as, or faster than, ω^{-1} as $|\omega| \to \infty$ (eq. 2.15), a unique solution can be obtained [29]. Thus, there exists a unique function, $\mathcal{G}(\Omega)$, of the complex variable Ω, that satisfies the following

$$\mathcal{G}(i\nu) = G(i\nu), \forall\, \nu, \qquad \text{and,} \qquad \lim_{|\Omega|\to\infty} \Omega\, \mathcal{G}(\Omega) = C, \tag{2.26}$$

where C is some finite number. Fig. 2.1 shows how the different Green's functions discussed in this section are related to each other in complex frequency space.

Having provided a brief summary of the mathematical properties of Green's functions necessary for QFT calculations, we shall now move on to their physical interpretation. The next section shall discuss Green's functions as propagators and how to obtain their functional form.

2.2 Free Electron Green's Function

As mentioned in this chapter's introduction, a Green's function can be interpreted as the probability amplitude for a particle starting at $(\mathbf{r}', \tau')$ being found at $(\mathbf{r}, \tau)$. Thus a Green's function describes particle propagation from $(\mathbf{r}', \tau')$ to $(\mathbf{r}, \tau)$, and so is also referred to as a propagator. This is most easily seen from the perspective of a temperature Green's function. We define the single-particle temperature Green's function as

$$\mathscr{G}_{\sigma\sigma'}(\mathbf{r}, \tau; \mathbf{r}', \tau') = -\left\langle T_\tau \left\{ \psi_\sigma(\mathbf{r}, \tau) \psi^\dagger_{\sigma'}(\mathbf{r}', \tau') \right\} \right\rangle, \tag{2.27}$$

where $\psi_\sigma(\mathbf{r}, \tau)$ is the field operator for an electron with spin σ, and the averaging is taken with respect to some general GC Hamiltonian $\mathscr{H}$.[7] See appendix A for a review of field operators, second quantisation, and their representation in imaginary time.

We change the basis of the field operators from continuous real space to discrete momentum space by assuming periodic boundary conditions for a system of volume $\mathcal{V}$,[8]

$$\psi_\sigma(\mathbf{r}, \tau) = \frac{1}{\sqrt{\mathcal{V}}} \sum_{\mathbf{k}} e^{i\mathbf{k}\cdot\mathbf{r}} c_{\mathbf{k}\sigma}(\tau), \qquad \psi^\dagger_\sigma(\mathbf{r}, \tau) = \frac{1}{\sqrt{\mathcal{V}}} \sum_{\mathbf{k}} e^{-i\mathbf{k}\cdot\mathbf{r}} c^\dagger_{\mathbf{k}\sigma}(\tau), \tag{2.28}$$

where $c^\dagger_{\mathbf{k}\sigma}(\tau)$ and $c_{\mathbf{k}\sigma}(\tau)$ are the creation and annihilation operators for a particle in state $\mathbf{k}$ with spin σ at time τ respectively. Our single-particle Green's function thus becomes

$$\mathscr{G}_{\sigma\sigma'}(\mathbf{r}, \tau; \mathbf{r}', \tau') = -\frac{1}{\mathcal{V}} \sum_{\mathbf{k},\mathbf{p}} e^{i\mathbf{k}\cdot\mathbf{r}} e^{-i\mathbf{p}\cdot\mathbf{r}'} \left\langle T_\tau \left\{ c_{\mathbf{k}\sigma}(\tau) c^\dagger_{\mathbf{p}\sigma'}(\tau') \right\} \right\rangle, \tag{2.29}$$

though it may appear we have not gained much ground here. However, since we are

[7] Note that $\psi^\dagger(\mathbf{r}, \tau) \neq \psi(\mathbf{r}, \tau)^\dagger$, as the Hermitian conjugation acts at different times compared to the Wick rotation being applied. In the first case, we take $t = -i\tau$ after conjugating $\psi(\mathbf{r}, t)$, whilst in the second case we take $t = -i\tau$ before taking the conjugate of $\psi(\mathbf{r}, t)$. It is trivial to see that $\psi(\mathbf{r}, \tau)^\dagger = \psi^\dagger(\mathbf{r}, -\tau)$.

[8] Normally the field operators are written in some new basis with wave functions $\phi_\alpha(\mathbf{r})$ appearing as the coefficients of the annihilation operators, c_α, and $\phi^*_\alpha(\mathbf{r})$ for the creation operators, $c^\dagger_\alpha$, see appendix A. However, since we will be wishing to deal with translationally invariant systems, the most natural basis to transform to is that of plane waves (free particles), as these have well defined momentum states and respect the symmetries of the system.

looking at systems with translational invariance,[9] momentum conservation dictates that only averages of equivalent momenta survive,

$$\left\langle c_{\mathbf{k}\sigma} c^{\dagger}_{\mathbf{p}\sigma'} \right\rangle = \left\langle c_{\mathbf{k}\sigma} c^{\dagger}_{\mathbf{k}\sigma} \right\rangle \delta_{\mathbf{kp}} \delta_{\sigma\sigma'}. \tag{2.30}$$

Here we also noted that only averages of particles with equivalent spin survive.

Therefore, we arrive at a much simpler form for the free single-particle Green's function, which we denote as $G^{(0)}_{\sigma\sigma}$,

$$G^{(0)}_{\sigma\sigma'}(\mathbf{r}-\mathbf{r}', \tau-\tau') = \frac{1}{\mathcal{V}} \sum_{\mathbf{k}} e^{i\mathbf{k}\cdot(\mathbf{r}-\mathbf{r}')} G^{(0)}_{\sigma}(\mathbf{k}, \tau-\tau') \delta_{\sigma\sigma'}, \tag{2.31a}$$

$$G^{(0)}_{\sigma}(\mathbf{k}, \tau-\tau') = -\left\langle T_{\tau}\left\{ c_{\mathbf{k}\sigma}(\tau) c^{\dagger}_{\mathbf{k}\sigma}(\tau') \right\} \right\rangle. \tag{2.31b}$$

Though we have only dealt explicitly with the temperature Green's function here, the retarded and advanced single-particle Green's functions can be defined analogously, and exhibit the same properties.

A general note to be made is that eq. 2.31a is the general definition for the momentum space Green's function of a system with translational invariance. That is to say,

$$\mathscr{G}_{\sigma\sigma'}(\mathbf{r}-\mathbf{r}', \tau-\tau') = \frac{1}{\mathcal{V}} \sum_{\mathbf{k}} e^{i\mathbf{k}\cdot(\mathbf{r}-\mathbf{r}')} \mathscr{G}_{\sigma}(\mathbf{k}, \tau-\tau') \delta_{\sigma\sigma'} \tag{2.32}$$

Only in problems where we do not have translational invariance do we choose a different basis of wave functions as prefactors to the creation and annihilation operators when replacing the field operators.[10] For all the problems we consider though, we either start with or restore translational invariance at some point, thus allowing us to use the momentum Green's function.

[9] In disordered metals we may treat the electrons as being nearly free, and so we use the free electron Green's function as a building block for these systems.

[10] For example, in the quantum Hall effect the wave functions are Landau levels, which are far from plane waves. So using a plane wave basis would only create difficulties, especially since the total momentum, $\mathbf{k}$, is no longer a good quantum number. In other cases, it may be more beneficial to decompose our field operators in terms of Bloch waves.

Based upon ref. [31], let's now consider the free electron gas in the grand canonical ensemble, whose GC Hamiltonian is

$$\mathscr{H}_0 = H_0 - \mu N = \sum_\sigma \sum_{\mathbf{k}} \xi_{\mathbf{k}} c^\dagger_{\mathbf{k}\sigma} c_{\mathbf{k}\sigma}, \qquad \text{where,} \qquad \xi_{\mathbf{k}} = \frac{k^2}{2m_e} - \mu, \tag{2.33}$$

μ is the chemical potential (Fermi energy), m_e is the electron mass, and we have set $\hbar = 1$. Using $c_{\mathbf{k}\sigma}(\tau) \equiv \mathcal{U}^\dagger(-i\tau) c_{\mathbf{k}\sigma} \mathcal{U}(-i\tau) = e^{-\xi_{\mathbf{k}}\tau} c_{\mathbf{k}\sigma}$ and taking $\tau' = 0$, eq. 2.31b becomes

$$G^{(0)}_\sigma(\mathbf{k}, \tau) = -e^{-\xi_{\mathbf{k}}\tau} \left\langle c_{\mathbf{k}\sigma} c^\dagger_{\mathbf{k}\sigma} \right\rangle \Theta(\tau) + e^{-\xi_{\mathbf{k}}\tau} \left\langle c^\dagger_{\mathbf{k}\sigma} c_{\mathbf{k}\sigma} \right\rangle \Theta(-\tau). \tag{2.34}$$

The Matsubara Green's function associated to eq. 2.34 is given by using eq. 2.24b,

$$\begin{aligned} G^{(0)}_\sigma(\mathbf{k}, i\varepsilon) &= -\int_0^\beta d\tau\, e^{-\tau(\xi_{\mathbf{k}} - i\varepsilon)} \left\langle c_{\mathbf{k}\sigma} c^\dagger_{\mathbf{k}\sigma} \right\rangle \\ &= \frac{\left\langle c_{\mathbf{k}\sigma} c^\dagger_{\mathbf{k}\sigma} \right\rangle}{i\varepsilon - \xi_{\mathbf{k}}} \left[1 - e^{-\beta(\xi_{\mathbf{k}} - i\varepsilon)}\right] \\ &= \frac{\left\langle c_{\mathbf{k}\sigma} c^\dagger_{\mathbf{k}\sigma} \right\rangle}{i\varepsilon - \xi_{\mathbf{k}}} \left[1 + e^{-\beta\xi_{\mathbf{k}}}\right]. \end{aligned} \tag{2.35}$$

At this point we recall for electrons $\{c_{\mathbf{k}\sigma}, c^\dagger_{\mathbf{k}\sigma}\} = 1$, and the occupation factor of a state $\mathbf{k}$ is given by $\left\langle c^\dagger_{\mathbf{k}\sigma} c_{\mathbf{k}\sigma} \right\rangle$.[11] This leads us to

$$G^{(0)}_\sigma(\mathbf{k}, i\varepsilon) = \frac{1}{i\varepsilon - \xi_{\mathbf{k}}}. \tag{2.36}$$

Thus we have obtained the free electron Matsubara Green's function.[12]

Since the free electron Matsubara Green's function doesn't have any spin dependence, we will drop the explicit spin label on the Green's function and add the appropriate multiplicative factors due to spin summation where necessary for the remainder of this chapter. Additionally, the free particle label will now become a subscript (i.e: $G^{(0)}_\sigma \to G_0$).

[11] For fermions the occupation factor is the Fermi-Dirac distribution, $f(\xi_{\mathbf{k}}) = (1 + e^{\beta\xi_{\mathbf{k}}})^{-1}$, whilst for bosons it is the Bose-Einstein distribution, $n(\xi_{\mathbf{k}}) = (e^{\beta\xi_{\mathbf{k}}} - 1)^{-1}$.

[12] The Green's function for non-interacting bosons has the same form as eq. 2.36, and follows the same argument as given here.

The retarded and advanced Green's functions are easily obtained from eq. 2.36 by analytic continuation $i\varepsilon \to \omega \pm i\delta$,

$$G_0^R(\mathbf{k},\omega) = \frac{1}{\omega + i\delta - \xi_{\mathbf{k}}} = G_0^A(\mathbf{k},\omega)^*. \tag{2.37}$$

These Green's functions serve as the basic building blocks for all subsequent calculations. To understand the effects of disorder, electron-electron interactions, superconducting fluctuations, and more, we require eq. 2.36 as the zeroth order term in the perturbation series. Before we explore these phenomena, let us first obtain the rules governing diagrammatic field theory.

2.3 Single-Particle Interactions

In this section we shall consider the effects of a single-particle potential, $U(\mathbf{r})$, upon the single-particle Green's function. This process is done perturbatively, generating corrections to the complete single-particle Green's function based upon the free particle Green's function and a number of interactions with $U(\mathbf{r})$. We shall closely follow ref. [29] here, and demonstrate how diagrammatics can be associated to the perturbative expansion.

The GC Hamiltonian of concern is given by

$$\mathscr{H}_1(\mathbf{r}_1) = -\frac{1}{2m}\nabla_1^2 - \mu + U(\mathbf{r}_1), \tag{2.38}$$

whose corresponding Schrödinger equation is

$$-\frac{\partial\phi(\mathbf{r},\tau)}{\partial\tau} = \mathscr{H}_1(\mathbf{r})\phi(\mathbf{r},\tau). \tag{2.39}$$

Let us show that the single-particle Green's function is indeed a Green's function in the classical sense for the Schrödinger equation in the absence of two-particle interactions.[13]

[13]It can be shown that the single-particle Green's function also acts as a Green's function in the classical sense when interactions are present, however this generates a dependence of the single-particle Green's

We wish to show that the single-particle Green's function solves the Schrödinger equation with a delta function source,

$$\left[\frac{\partial}{\partial\tau_1} + \mathscr{H}_1(\mathbf{r}_1)\right] G(\mathbf{r}_1,\tau_1;\mathbf{r}_2,\tau_2;U) = -\delta^{(d)}(\mathbf{r}_1-\mathbf{r}_2)\delta(\tau_1-\tau_2), \tag{2.40}$$

subject to the boundary condition

$$G(\mathbf{r}_1,\mathbf{r}_2;\tau_1-\tau_2+\beta;U) = -\eta G(\mathbf{r}_1,\mathbf{r}_2;\tau_1-\tau_2;U). \tag{2.41}$$

Here d is the number of dimensions, $0 \leq \tau_1,\tau_2 \leq \beta$, and we have appreciated that the Green's function only depends upon time differences.[14] Acting the time derivative upon the Green's function produces (suppressing spin indices)

$$\begin{aligned}\frac{\partial}{\partial\tau_1}G(\mathbf{r}_1,\mathbf{r}_2;\tau_1-\tau_2+\beta;U) = &-\left\langle\left[\psi(\mathbf{r}_1,\tau_1-\tau_2),\psi^\dagger(\mathbf{r}_2,0)\right]_\eta\right\rangle\delta(\tau_1-\tau_2)\\ &+\left\langle T_\tau\left\{\frac{\partial}{\partial\tau_1}\psi(\mathbf{r}_1,\tau_1-\tau_2)\,\psi^\dagger(\mathbf{r}_2,0)\right\}\right\rangle.\end{aligned} \tag{2.42}$$

The δ function allows us to set $\tau_1=\tau_2$ in the first term, hence we may use the equal-time commutation relation $[\psi(\mathbf{r},\tau),\psi^\dagger(\mathbf{r}',\tau)]_\eta = \delta^{(d)}(\mathbf{r}-\mathbf{r}')$ to obtain the delta function product we are aiming for,

$$\begin{aligned}\frac{\partial}{\partial\tau_1}G(\mathbf{r}_1,\mathbf{r}_2;\tau_1-\tau_2;U) = &-\delta^{(d)}(\mathbf{r}_1-\mathbf{r}_2)\delta(\tau_1-\tau_2)\\ &-\left\langle T_\tau\left\{\frac{\partial}{\partial\tau_1}\psi(\mathbf{r}_1,\tau_1-\tau_2)\psi^\dagger(\mathbf{r}_2,0)\right\}\right\rangle.\end{aligned} \tag{2.43}$$

Next we use the Heisenberg equation of motion (see appendix A.1)

$$\frac{\partial}{\partial\tau_1}\psi(\mathbf{r}_1,\tau_1-\tau_2) = \mathscr{H}_1\psi(\mathbf{r}_1,\tau_1-\tau_2) - \psi(\mathbf{r}_1,\tau_1-\tau_2)\mathscr{H}_1, \tag{2.44}$$

function upon the two-particle Green's function. See [29] for details.

[14] We have included U in the Green's function's argument to explicitly denote the presence of single-particle interactions.

and write $\mathscr{H}_1$ in its second-quantised form,

$$\mathscr{H}_1 = \int d^d r \psi^\dagger(\mathbf{r}) \left[-\frac{\nabla^2}{2m} - \mu + U(\mathbf{r}) \right] \psi(\mathbf{r}). \tag{2.45}$$

We then manipulate the first term of eq. 2.44 by using eq. 2.45 to show

$$\begin{aligned} \mathscr{H}_1 \psi(\mathbf{r}_1, \tau_1 - \tau_2) &= e^{\mathscr{H}_1(\tau_1-\tau_2)}\, \mathscr{H}_1\, \psi(\mathbf{r}_1)\, e^{-\mathscr{H}_1(\tau_1-\tau_2)} \\ &= e^{\mathscr{H}_1(\tau_1-\tau_2)} \int d^d r \Bigg\{ \eta[\delta^{(d)}(\mathbf{r}-\mathbf{r}_1) - \psi(\mathbf{r}_1)\psi^\dagger(\mathbf{r})] \\ &\qquad \times \left[-\frac{\nabla^2}{2m} - \mu + U(\mathbf{r}) \right] (-\eta) \psi(\mathbf{r}) e^{-\mathscr{H}_1(\tau_1-\tau_2)} \Bigg\} \\ &= -\mathscr{H}_1(\mathbf{r}_1)\psi(\mathbf{r}_1, \tau_1 - \tau_2) + \psi(\mathbf{r}_1, \tau_1 - \tau_2)\mathscr{H}_1. \end{aligned} \tag{2.46}$$

Substituting this into eq. 2.44, and then substituting the result into eq. 2.43 we find,

$$\begin{aligned} \frac{\partial}{\partial \tau_1} G(\mathbf{r}_1, \mathbf{r}_2; \tau_1 - \tau_2; U) = &- \delta^{(d)}(\mathbf{r}_1 - \mathbf{r}_2)\delta(\tau_1 - \tau_2) \\ &+ \mathscr{H}_1(\mathbf{r}_1) \left\langle T_\tau \left\{ \psi(\mathbf{r}_1, \tau_1 - \tau_2)\psi^\dagger(\mathbf{r}_2, 0) \right\} \right\rangle. \end{aligned} \tag{2.47}$$

Recognising the second term above as $-\mathscr{H}_1(\mathbf{r}_1)G(\mathbf{r}_1, \mathbf{r}_2; \tau_1 - \tau_2; U)$, we simply rearrange eq. 2.47 to arrive at eq. 2.40. Therefore, the single-particle Green's function truly is a Green's function in the classical sense for the Schrödinger equation.

Let us introduce the notation $x = (\mathbf{r}, \tau)$ for convenience. In which case eq. 2.40 becomes

$$\left[\frac{\partial}{\partial \tau_1} + \mathscr{H}_1(x_1) \right] G(x_1, x_2; U) = -\delta(x_1 - x_2). \tag{2.48}$$

We now note that the free particle Green's function, $G_0(x_1, x_2) = G(x_1, x_2; U = 0)$, satisfies

$$\left[\frac{\partial}{\partial \tau_1} + \mathscr{H}_0(x_1) \right] G_0(x_1, x_2) = -\delta(x_1 - x_2), \tag{2.49}$$

where $\mathscr{H}_0(x_1)$ is $\mathscr{H}(x_1; U = 0)$.

From eq. 2.48 we see

$$\begin{aligned}\left[\frac{\partial}{\partial\tau_1}+\mathscr{H}_0(x_1)\right]G(x_1,x_2;U) &= -\delta(x_1-x_2)-\int dx_3\,\delta(x_1-x_3)U(x_3)G(x_3,x_2;U),\\ &= \left[\frac{\partial}{\partial\tau_1}+\mathscr{H}_0(x_1)\right]\left[G_0(x_1,x_2)+\int dx_3\,G_0(x_1,x_3)U(x_3)G(x_3,x_2;U)\right],\end{aligned} \tag{2.50}$$

thus yielding the integral equation defining the complete single-particle Green's function

$$G(x_1,x_2;U)=G_0(x_1,x_2)+\int dx_3 G_0(x_1,x_3)U(x_3)G(x_3,x_2;U). \tag{2.51}$$

In the second line of eq. 2.50 we used eq. 2.49 to replace the delta functions. The integrals appearing here represent

$$\int dx=\int_0^\beta d\tau\int_{V_d}d^dr, \tag{2.52}$$

where V_d is all space.

By continuing to substitute $G(x_1,x_2;U)$ into itself in eq. 2.52, we may write full Green's function as a sum of terms increasing in the number of interactions with the background potential,

$$G(x_1,x_2;U)=G_0(x_1,x_2)+\sum_{n=1}^{\infty}G_n(x_1,x_2;U), \tag{2.53}$$

where

$$\begin{aligned}G_n(x_1,x_2;U)=\int dx_3\int dx_4\,...\int dx_{n+2}\Big[&G_0(x_1,x_3)U(x_3)G_0(x_3,x_4)U(x_4)\times...\\ &...\times U(x_n)G_0(x_{n+2},x_2)\Big].\end{aligned} \tag{2.54}$$

This quickly becomes very cumbersome to write out, and so we represent expressions such as eqs. 2.53 and 2.54 by diagrams, as shown in fig. 2.2. Here each thin solid line represents the free particle Green's function, and hence propagation between the coordinates at either end of the line. The direction of propagation is given by the arrow on the line. The thick solid line represents the full Green's function, whilst each cross

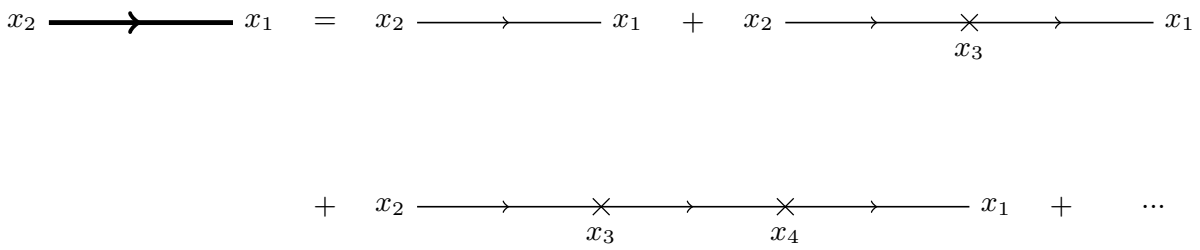

Figure 2.2: Diagrammatic representation of eq. 2.53.

denotes an interaction with the single particle potential.

Let us describe what is happening in the case of $G_1(x_1, x_2; U)$, represented by the second term in fig. 2.2. We first see the free particle propagating from x_2 to x_3, where it interacts with the potential at x_3. The free particle then continues to move from x_3 to x_1, and so the overall propagation is from x_2 to x_1 as expected from the argument of $G(x_1, x_2; U)$.

Currently, this diagrammatic representation seems to only be useful if we already know what the mathematical expression for the Green's function is. However, we can use intuition and physical understanding to construct more complex diagrams instead of following the procedure. This is particularly useful when considering physical phenomena like electron-electron interactions and the role of disorder in transport. To understand how the mathematical expressions are related to diagrams, we must construct and understand the diagrammatic rules associated to a problem. For the case at hand, the rules we employ are:

1. For each solid line directed from vertex x_m to x_n we associate a factor of $G_0(x_n, x_m)$.

2. For each cross located at vertex x_l, introduce a factor of $U(x_l)$.

3. Integrate the resulting expression over all internal vertices (i.e: for the n^{th} order contribution, x_3, x_4, ..., x_{n+2} are all internal vertices, whilst x_1 and x_2 are external vertices[15]).

[15]Here x_2 and x_1 are always external vertices, as they represent the start and end points of the full Green's function, and hence the start and end of the complete description of particle propagation. These are fixed and do not vary, where as the internal vertices may vary in position, hence the integration accounting for all possible internal space-time positions.

It is clear from these rules that we can easily reconstruct the series described by eqs. 2.53 and 2.54.

We may also distinguish between whether the Green's function describes particle or hole propagation. From the definition of the temperature Green's function we see that for $\tau_1 > \tau_2$, $G(x_1, x_2; U) = \left\langle \psi_\sigma(x_1)\psi^\dagger_\sigma(x_2)\right\rangle$ and hence describes particle propagation. Whilst for $\tau_1 < \tau_2$, $G(x_1, x_2; U) = -\eta \left\langle \psi^\dagger_\sigma(x_2)\psi_\sigma(x_1)\right\rangle$ and thus describes hole propagation. We note that the single-particle interaction here is not spin dependent, and so $G(x_1, x_2; U)$ has no spin dependence like the free particle Green's function.

In this subsection we outlined, constructed, and justified the diagrammatic rules for a system of non-interacting particles that were subject to a single-particle potential. In the next subsection we shall introduce two-particle interactions into the Hamiltonian, and derive the diagrammatic rules associated to these types of systems.

2.4 Two-Particle Interactions

Here we shall construct the diagrammatic rules for general two-particle interactions described by the GC Hamiltonian

$$\begin{aligned}
\mathscr{H} &= \mathscr{H}_1 + H_{\text{int}}, \\
\mathscr{H}_1 &= \sum_\sigma \int d^d r\, \psi^\dagger_\sigma(\mathbf{r}) \left[-\frac{1}{2m}\nabla^2 - \mu + U(\mathbf{r})\right] \psi_\sigma(\mathbf{r}), \\
H_{\text{int}} &= \frac{1}{2}\sum_{\sigma,\sigma'} \int d^d r \int d^d r'\, \psi^\dagger_\sigma(\mathbf{r})\psi^\dagger_{\sigma'}(\mathbf{r}')V(\mathbf{r}-\mathbf{r}')\psi_{\sigma'}(\mathbf{r}')\psi_\sigma(\mathbf{r}),
\end{aligned} \tag{2.55}$$

where $V(\mathbf{r}-\mathbf{r}')$ is the two-particle interaction potential. In order to proceed we must change the picture of quantum mechanics we wish to work in.

Thus far we have been working in the Heisenberg picture, where all time dependence is on the operators. However, to understand two-particle interactions we need to consider the interaction picture (see appendix A for a summary of the different pictures of quantum

mechanics). In this case, our Green's function may be written as

$$\mathscr{G}_{\alpha\alpha'}(x_1,x_2) = -\frac{\left\langle T_\tau\left\{\widetilde{\psi}_\alpha(x_1)\widetilde{\psi}^\dagger_{\alpha'}(x_2)\mathcal{S}(\beta)\right\}\right\rangle_0}{\langle\mathcal{S}(\beta)\rangle_0}, \tag{2.56}$$

where $\widetilde{\psi}^\dagger$ and $\widetilde{\psi}$ are the creation and annihilation operators in the interaction picture. The $\mathcal{S}$-matrix is defined as

$$\mathcal{S}(\tau) = T_\tau\left\{\exp\left(-\int_0^\tau d\tau' \widetilde{H}_{\rm int}(\tau')\right)\right\}, \tag{2.57}$$

with

$$\widetilde{H}_{\rm int}(\tau) = e^{\mathscr{H}_1\tau}H_{\rm int}e^{-\mathscr{H}_1\tau}. \tag{2.58}$$

The angular brackets $\langle ...\rangle_0$ denote averaging with respect to $\mathscr{H}_1$,

$$\langle ...\rangle_0 = \frac{1}{\mathcal{Z}_0}\mathrm{Tr}\left[e^{-\beta\mathscr{H}_1}...\right], \qquad \mathcal{Z}_0 = \mathrm{Tr}\left[e^{-\beta\mathscr{H}_1}\right]. \tag{2.59}$$

We now expand the $\mathcal{S}$-matrix in powers of the interaction Hamiltonian,

$$\mathcal{S}(\beta) = 1 + \sum_{n=1}^{\infty}\frac{(-1)^n}{n!}\int_0^\beta d\tau_1 ... \int_0^\beta d\tau_n T_\tau\left\{\widetilde{H}_{\rm int}(\tau_1)...\widetilde{H}_{\rm int}(\tau_n)\right\}, \tag{2.60}$$

and substitute it into the numerator of eq. 2.56. This gives

$$\begin{aligned}\mathscr{G}_{\alpha\alpha'}(x_1,x_2) = -\frac{1}{\langle\mathcal{S}(\beta)\rangle_0}\Bigg(&\left\langle T_\tau\left\{\widetilde{\psi}_\alpha(x_1)\widetilde{\psi}^\dagger_{\alpha'}(x_2)\right\}\right\rangle_0 \\ &+\sum_{n=1}^{\infty}\frac{(-1)^n}{n!}\int_0^\beta d\tau_1' ... \int_0^\beta d\tau_n'\left\langle T_\tau\left\{\widetilde{\psi}_\alpha(x_1)\widetilde{\psi}^\dagger_{\alpha'}(x_2)\widetilde{H}_{\rm int}(\tau_1')...\widetilde{H}_{\rm int}(\tau_n')\right\}\right\rangle\Bigg).\end{aligned} \tag{2.61}$$

If we also expanded $\langle\mathcal{S}(\beta)\rangle_0^{-1}$in powers of $H_{\rm int}$ we would easily identify

$$\begin{aligned}\mathscr{G}^{(0)}_{\alpha\alpha'}(x_1,x_2) &= -\left\langle T_\tau\left\{\widetilde{\psi}_\alpha(x_1)\widetilde{\psi}^\dagger_{\alpha'}(x_2)\right\}\right\rangle_0 = -\left\langle T_\tau\left\{\widetilde{\psi}_\alpha(x_1)\widetilde{\psi}^\dagger_{\alpha}(x_2)\right\}\right\rangle_0\delta_{\alpha\alpha'} \\ &= G(x_1,x_2;U)\delta_{\alpha\alpha'} = \mathscr{G}^{(0)}_{\alpha}(x_1,x_2)\delta_{\alpha\alpha'},\end{aligned} \tag{2.62}$$

which is just the Green's function without two-body interactions, as expected. Thus, the sum generated after this expansion therefore describes the two-particle interaction corrections to the Green's function. Let us analyse the first order correction in detail.

Focussing on the numerator of eq. 2.56, we write its first order correction explicitly as

$$\begin{aligned}\mathscr{G}^{(1,\mathrm{num})}_{\alpha\alpha'}(x_1,x_2) &= -\frac{1}{2}\sum_{\sigma,\sigma'}\int_0^\beta d\tau'\int d^dr'\int d^dr''\Big\langle T_\tau\Big\{\widetilde{\psi}_\alpha(x_1)\widetilde{\psi}^\dagger_{\alpha'}(x_2)\\ &\qquad\times\widetilde{\psi}^\dagger_\sigma(\mathbf{r}',\tau')\widetilde{\psi}^\dagger_{\sigma'}(\mathbf{r}'',\tau')V(\mathbf{r}'-\mathbf{r}'')\widetilde{\psi}_\sigma(\mathbf{r}'',\tau')\widetilde{\psi}_{\sigma'}(\mathbf{r}',\tau')\Big\}\Big\rangle_0\\ &= -\frac{1}{2}\sum_{\sigma,\sigma'}\int dx'\int dx''\Big\langle T_\tau\Big\{\widetilde{\psi}_\alpha(x_1)\widetilde{\psi}^\dagger_{\alpha'}(x_2)\widetilde{\psi}^\dagger_\sigma(x')\widetilde{\psi}^\dagger_{\sigma'}(x'')\\ &\qquad\times W(x'-x'')\widetilde{\psi}_\sigma(x'')\widetilde{\psi}_\sigma(x')\Big\}\Big\rangle_0,\end{aligned} \tag{2.63}$$

where the superscript denotes the numerator part and

$$W(x'-x'') = V(\mathbf{r}'-\mathbf{r}'')\delta(\tau'-\tau''). \tag{2.64}$$

At this point we make use of Wick's theorem (see appendix B for a short explanation of Wick's theorem) to split the average up into averages of pairs of creation and annihilation operators, thus forming an expression in terms of the Green's function we in principle know, $\mathscr{G}^{(0)}_{\sigma\sigma'}$. This procedure yields

$$\begin{aligned}&\Big\langle T_\tau\Big\{\widetilde{\psi}_\alpha(x_1)\widetilde{\psi}^\dagger_{\alpha'}(x_2)\widetilde{\psi}^\dagger_\sigma(x')\widetilde{\psi}^\dagger_{\sigma'}(x'')W(x'-x'')\widetilde{\psi}_{\sigma'}(x'')\widetilde{\psi}_\sigma(x')\Big\}\Big\rangle_0\\ &\quad=\Big[\Big\langle T_\tau\Big\{\widetilde{\psi}_\alpha(x_1)\widetilde{\psi}^\dagger_{\alpha'}(x_2)\Big\}\Big\rangle_0\Big\langle T_\tau\Big\{\widetilde{\psi}_\sigma(x')\widetilde{\psi}^\dagger_\sigma(x')\Big\}\Big\rangle_0\Big\langle T_\tau\Big\{\widetilde{\psi}_{\sigma'}(x'')\widetilde{\psi}^\dagger_{\sigma'}(x'')\Big\}\Big\rangle_0\\ &\quad-\eta\Big\langle T_\tau\Big\{\widetilde{\psi}_\alpha(x_1)\widetilde{\psi}^\dagger_{\alpha'}(x_2)\Big\}\Big\rangle_0\Big\langle T_\tau\Big\{\widetilde{\psi}_\sigma(x')\widetilde{\psi}^\dagger_{\sigma'}(x'')\Big\}\Big\rangle_0\Big\langle T_\tau\Big\{\widetilde{\psi}_{\sigma'}(x'')\widetilde{\psi}^\dagger_\sigma(x')\Big\}\Big\rangle_0\\ &\quad-\eta\Big\langle T_\tau\Big\{\widetilde{\psi}_\alpha(x_1)\widetilde{\psi}^\dagger_\sigma(x')\Big\}\Big\rangle_0\Big\langle T_\tau\Big\{\widetilde{\psi}_\sigma(x')\widetilde{\psi}^\dagger_{\sigma'}(x'')\Big\}\Big\rangle_0\Big\langle T_\tau\Big\{\widetilde{\psi}_{\sigma'}(x'')\widetilde{\psi}^\dagger_{\alpha'}(x_2)\Big\}\Big\rangle_0\\ &\quad+\Big\langle T_\tau\Big\{\widetilde{\psi}_\alpha(x_1)\widetilde{\psi}^\dagger_\sigma(x')\Big\}\Big\rangle_0\Big\langle T_\tau\Big\{\widetilde{\psi}_\sigma(x')\widetilde{\psi}^\dagger_{\alpha'}(x_2)\Big\}\Big\rangle_0\Big\langle T_\tau\Big\{\widetilde{\psi}_{\sigma'}(x'')\widetilde{\psi}^\dagger_{\sigma'}(x'')\Big\}\Big\rangle_0\\ &\quad-\eta\Big\langle T_\tau\Big\{\widetilde{\psi}_\alpha(x_1)\widetilde{\psi}^\dagger_{\sigma'}(x'')\Big\}\Big\rangle_0\Big\langle T_\tau\Big\{\widetilde{\psi}_{\sigma'}(x'')\widetilde{\psi}^\dagger_\sigma(x')\Big\}\Big\rangle_0\Big\langle T_\tau\Big\{\widetilde{\psi}_\sigma(x')\widetilde{\psi}^\dagger_{\alpha'}(x_2)\Big\}\Big\rangle_0\\ &\quad+\Big\langle T_\tau\Big\{\widetilde{\psi}_\alpha(x_1)\widetilde{\psi}^\dagger_{\sigma'}(x'')\Big\}\Big\rangle_0\Big\langle T_\tau\Big\{\widetilde{\psi}_{\sigma'}(x'')\widetilde{\psi}^\dagger_{\alpha'}(x_2)\Big\}\Big\rangle_0\Big\langle T_\tau\Big\{\widetilde{\psi}_\sigma(x')\widetilde{\psi}^\dagger_\sigma(x')\Big\}\Big\rangle_0\Big]\\ &\qquad\times W(x'-x'').\end{aligned} \tag{2.65}$$

Since x' and x'' are just dummy variables, it is clear that they can just be interchanged freely. Hence the third and fifth terms may be set equal, and the fourth and sixth terms may also be set equal in the above expression. Replacing the averages appearing in eq. 2.65 with Green's functions in the absence of two particle interactions, we find

$$\begin{aligned} -\Big[&\mathscr{G}^{(0)}_{\alpha}(x_1,x_2)\mathscr{G}^{(0)}_{\sigma}(x',x')\mathscr{G}^{(0)}_{\sigma'}(x'',x'')\delta_{\alpha\alpha'} \\ &+ 2\mathscr{G}^{(0)}_{\alpha}(x_1,x')\mathscr{G}^{(0)}_{\alpha'}(x',x_2)\mathscr{G}^{(0)}_{\sigma'}(x'',x'')\delta_{\alpha\sigma}\delta_{\sigma\alpha'} \\ &- \eta\mathscr{G}^{(0)}_{\alpha}(x_1,x_2)\mathscr{G}^{(0)}_{\sigma}(x',x'')\mathscr{G}^{(0)}_{\sigma}(x'',x')\delta_{\alpha\alpha'}\delta_{\sigma\sigma'} \\ &- 2\eta\mathscr{G}^{(0)}_{\alpha}\mathscr{G}^{(0)}_{\sigma}(x',x'')\mathscr{G}^{(0)}_{\alpha'}(x'',x_2)\delta_{\alpha\sigma}\delta_{\sigma\sigma'}\delta_{\sigma'\alpha'}\Big]W(x'-x''). \end{aligned} \tag{2.66}$$

Substituting this into $\mathscr{G}^{(1,\mathrm{num})}_{\alpha\alpha'}$ produces

$$\begin{aligned} \mathscr{G}^{(1,\mathrm{num})}_{\alpha\alpha'}(x_1,x_2) = \delta_{\alpha\alpha'}\int dx'\int dx''\Bigg[&\frac{1}{2}\sum_{\sigma,\sigma'}\mathscr{G}_0(x_1,x_2)\mathscr{G}_0(x',x')\mathscr{G}_0(x'',x'') \\ &- \eta\frac{1}{2}\sum_{\sigma}\mathscr{G}_0(x_1,x_2)\mathscr{G}_0(x',x'')\mathscr{G}_0(x'',x') + \sum_{\sigma'}\mathscr{G}_0(x_1,x')\mathscr{G}_0(x',x_2)\mathscr{G}_0(x'',x'') \\ &- \eta\mathscr{G}_0(x_1,x')\mathscr{G}_0(x',x'')\mathscr{G}_0(x'',x_2)\Bigg]W(x'-x''), \end{aligned} \tag{2.67}$$

where we accounted for the lack of spin dependence in $\mathscr{G}^{(0)}_{\alpha}$ and replaced it with $\mathscr{G}_0$. From this we can see that the full Green's function will only be non-zero for $\alpha = \alpha'$, since the interactions here are not spin dependent. Hence, let us only consider the case where $\alpha = \alpha'$ and drop the subscript α and α'.

Now we are in a situation where we begin to introduce a diagrammatic representation. Each term of eq. 2.67 is displayed respectively in fig. 2.3, with the wavy lines representing the interaction $W(x'-x'')$ and the solid lines being particle propagators described by $\mathscr{G}_0$. Interpreting these diagrams physically, fig. 2.3a represents the particle of concern passing through the system whilst two background particles interact by exciting one another, before returning to the same state. Fig. 2.3b is similar to the previous, but the background particles now exchange states by interacting with each other. Fig. 2.3c describes the particle of interest interacting with a background particle by exciting it, before the back-

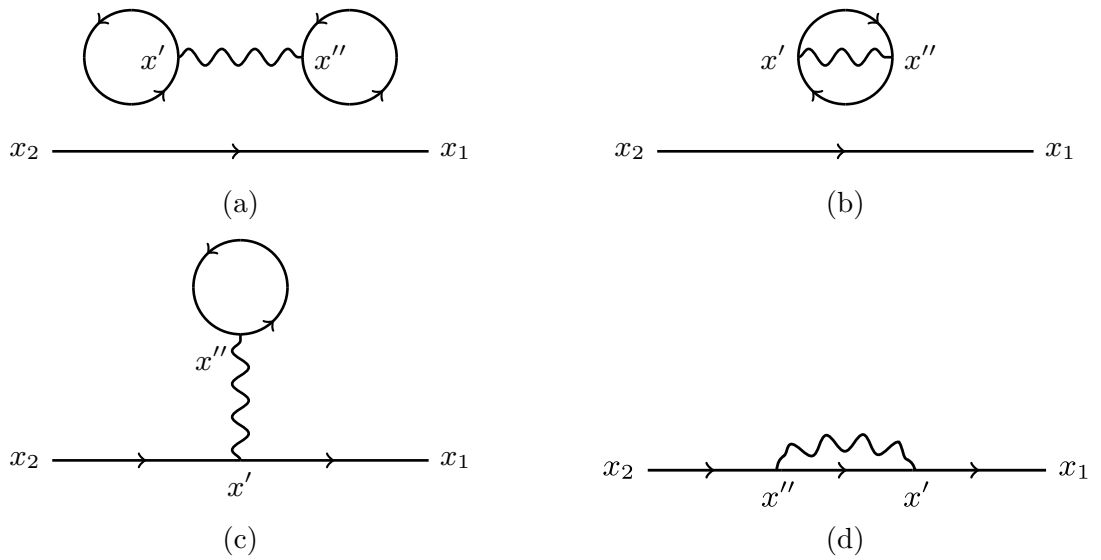

Figure 2.3: Diagrammatic representation of eq. 2.67.

ground particle relaxes back into its original state. Lastly, fig. 2.3d represents the original particle entering the system and interacting with a background particle by exciting it and replacing it, thus leaving the background particle to continue moving through the system, whilst the original particle occupies the state it kicked the other particle from.

It is clear two families of diagrams exist; one where all internal vertices are connected directly, or via each other, to the external vertices; and another where not all internal vertices are connected directly or indirectly to the external vertices. The former are called connected diagrams, whilst the latter are known as disconnected diagrams. Figs. 2.3a and 2.3b are examples of disconnected diagrams, where as figs. 2.3c and 2.3d are connected diagrams.

Let us now make use of the general expansion of the S-matrix in eq. 2.60. At the n^{th} order of expansion of $\mathscr{G}$'s numerator, we have n interaction Hamiltonians, each carrying two internal vertices connected to each other via an interaction. These internal vertices can then be joined to other internal vertices due to the other interaction Hamiltonians, or to the external vertices. If we consider choosing $n-m$ of these interaction Hamiltonians to be disconnected from the external vertices (i.e: no connected path to x_1 or x_2 at all), this leaves m interaction Hamiltonians to form the connected part of the diagram. We provide a visualisation of this in fig. 2.4. Clearly this has $\frac{n!}{m!(n-m)!}$ ways of being constructed and

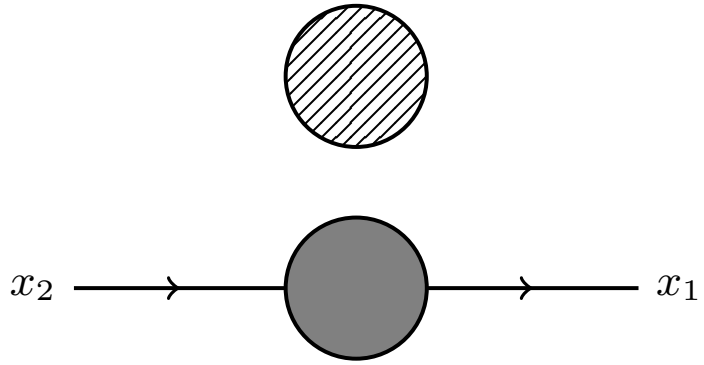

Figure 2.4: A general diagram with external vertices x_1 and x_2, where the grey bubble represents a generic set of interactions forming the connected piece. Where as the hatched bubble represents set of interactions forming the disconnected piece.

contributes $\mathscr{G}^{(n,m)}_{\text{num}}$ to the n^{th} order piece, $\mathscr{G}^{(n,\text{num})}$. Therefore we may write the expression associated to such a diagram as

$$\begin{aligned}\mathscr{G}^{(n,m)}_{\text{num}}(x_1,x_2) = &-\frac{(-1)^n}{m!(n-m)!}\\ &\times\int_0^\beta d\tau'_1\ldots\int_0^\beta d\tau'_m\Bigg[\left\langle T_\tau\left\{\widetilde{\psi}_\alpha(x_1)\widetilde{\psi}^\dagger_\alpha(x_2)\widetilde{H}_{\text{int}}(\tau'_1)\ldots\widetilde{H}_{\text{int}}(\tau'_m)\right\}\right\rangle_0^{\text{con}}\\ &\times\int_0^\beta d\tau'_{m+1}\ldots\int_0^\beta d\tau'_n\left\langle T_\tau\left\{\widetilde{H}_{\text{int}}(\tau'_{m+1})\ldots\widetilde{H}_{\text{int}}(\tau'_n)\right\}\right\rangle_0^{\text{discon}}\Bigg],\end{aligned}\tag{2.68}$$

where $\langle\ldots\rangle_0^{\text{con}}$ is the average with respect to $\mathscr{H}_1$ and forms the connected piece of the diagram, whilst $\langle\ldots\rangle_0^{\text{discon}}$ is the average with respect to $\mathscr{H}_1$ and forms the disconnected piece of the diagram. The $n!$ due to multiplicity is cancelled by the $n!$ in the denominator of the S-matrix expansion in eq. 2.61.

Next we consider a fixed connected piece and sum over all possible disconnected pieces, so we sum over all $l = n - m$ keeping m fixed. The contribution from this is simply

$$\begin{aligned}\mathscr{G}_{m,\text{num}}(x_1,x_2) = &\sum_l \mathscr{G}^{(l+m,m)}_{\text{num}}(x_1,x_2)\\ &-\frac{(-1)^m}{m!}\int_0^\beta d\tau'_1\ldots\int_0^\beta d\tau'_m\Bigg[\left\langle T_\tau\left\{\widetilde{\psi}_\alpha(x_1)\widetilde{\psi}^\dagger_\alpha(x_2)\widetilde{H}_{\text{int}}(\tau'_1)\ldots\widetilde{H}_{\text{int}}(\tau'_m)\right\}\right\rangle_0^{\text{con}}\\ &\times\left(1+\sum_{l=1}^\infty\frac{(-1)^l}{l!}\int_0^\beta d\tau''_1\ldots\int_0^\beta d\tau''_l\left\langle T_\tau\left\{\widetilde{H}_{\text{int}}(\tau''_1)\ldots\widetilde{H}_{\text{int}}(\tau''_l)\right\}\right\rangle_0^{\text{discon}}\right)\Bigg].\end{aligned}\tag{2.69}$$

To obtain the full Green's function, $\mathscr{G}$, from this we simply sum over all possible connected

pieces,

$$\mathscr{G}(x_1, x_2) = \frac{1}{\langle \mathcal{S}(\beta) \rangle_0} \sum_{m=0}^{\infty} \mathscr{G}_{m,\text{num}}(x_1, x_2). \tag{2.70}$$

Now, we note that the disconnected expression in eq. 2.69 is constant and independent of m, and is exactly equivalent to the expanded form of $\langle \mathcal{S}(\beta) \rangle$ given in eq. 2.60. The disconnected superscript does not change the averaging procedure, but rather clarifies which part of the diagram the average represents. However, the connected superscript does change things by neglecting disconnected diagrams generated by Wick's theorem. Thus, eq. 2.70 simplifies to

$$\begin{aligned} \mathscr{G}(x_1, x_2) &= \widetilde{G}_0(x_1, x_2) \\ &- \sum_{m=1}^{\infty} \frac{(-1)^m}{m!} \int_0^\beta d\tau_1' ... \int_0^\beta d\tau_m' \left\langle T_\tau \left\{ \widetilde{\psi}_\alpha(x_1) \widetilde{\psi}_\alpha^\dagger(x_2) \widetilde{H}_{\text{int}}(\tau_1') ... \widetilde{H}_{\text{int}}(\tau_m') \right\} \right\rangle_0^{\text{con}}. \end{aligned} \tag{2.71}$$

Therefore, only connected diagrams contribute to the Green's function.

This result is not surprising, as background processes are not of concern to the particle passing through the system. Hence, any diagrams that describe background processes irrelevant to the original particle should not contribute to the particle's dynamics. Given that the connected diagram already describes all relevant interactions with the particle that occur, the disconnected diagrams only repeat the connected piece's contribution with additional background processes and are therefore redundant.

We may now write the rules for diagrammatics describing two-particle interactions [29, 30]:

1. Create all connected, topologically inequivalent diagrams with 2^n internal vertices at n^{th} order, and two external vertices. At each internal vertex, two solid lines and a wavy line meet.

2. To each solid line we associate the propagator in the absence of two particle interactions, $\mathscr{G}^{(0)}_{\sigma\sigma'}(x_a, x_b)$, where the line moves from position x_b and spin σ' to position x_a and spin σ.

3. Each wavy line represents an interaction and carries a factor of $-W(x_a - x_b)$.

4. We now integrate over all internal positions, $\{x_m\}$, and sum over all internal spin indices.

5. For each closed fermion loop we introduce an extra factor of (-1).

6. For any Green's functions with their time arguments being equivalent, we take $\mathscr{G}_0(\mathbf{r}_a, \mathbf{r}_b, \tau)$ in the limit $\tau = \tau_a - \tau_b \to 0^-$.

These rules are given in real space and imaginary time. We have already shown that the Green's functions only depend upon time differences, meaning we may replace the temperature Green's functions by the Fourier series in terms of Matsubara Green's functions. This takes us into a Matsubara frequency picture. Furthermore, we shall consider systems with translational invariance so that we may move into a momentum space representation. This is particularly relevant to the phenomena we consider in disordered media, as they may be regarded as possessing translational invariance after averaging over all possible impurity distributions.

To move to a momentum-energy picture, we first write out our Green's functions and interaction in terms of their Fourier series,

$$\begin{aligned} \mathscr{G}^{(0)}_{\sigma\sigma'}(\mathbf{r}_a, \mathbf{r}_b, \tau' - \tau'') &= T \sum_{\nu} \mathscr{G}^{(0)}_{\sigma\sigma'}(\mathbf{r}_a, \mathbf{r}_b, i\nu) e^{-i\nu(\tau' - \tau'')}, \\ W(x' - x'') = V(\mathbf{r}' - \mathbf{r}'')\delta(\tau' - \tau'') &= V(\mathbf{r}' - \mathbf{r}'') T \sum_{\omega} e^{-i\omega(\tau' - \tau'')}, \end{aligned} \tag{2.72}$$

where ω is a bosonic Matsubara frequency and ν is a fermionic or bosonic Matsubara frequency depending on the particle being described by the Green's function.

Substituting these into the expansion in eq. 2.71 we find that each internal τ_n has three different Matsubara frequencies associated to it. One from the interaction, and one from each Green's function entering the vertex. The integral over this imaginary time

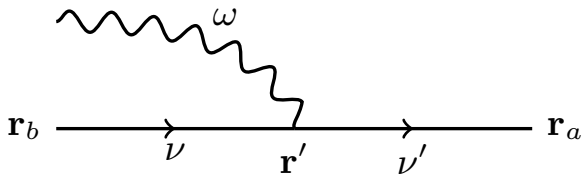

Figure 2.5: Example of the position frequency diagrammatic representation, illustrating energy conservation at the vertex.

component then has the form

$$\int_0^\beta d\tau_n e^{-i\tau_n(\omega+\nu-\nu')} = \delta_{\omega+\nu\,,\,\nu'}, \tag{2.73}$$

where ω is the frequency from the interaction entering the vertex, whilst ν and ν' are from the Green's functions entering and leaving the vertex respectively. The case where ω is leaving the vertex is analogous to this (let $\omega \to -\omega$), and we can clearly see that the frequency entering a vertex must be equal to the frequency (energy) leaving the vertex. Fig. 2.5 demonstrates this conservation of energy at the vertex.

Consequently the diagrammatic rules are adjusted upon moving into frequency space. Our propagators now carry an energy (ν, ω, ε, etc), such that each vertex conserves energy, and we sum over all internal energies. This replaces the labelling of end points with imaginary times, and the integrals over all internal imaginary times.

Let us now consider a system with translational invariance. We may write the Matsubara Green's functions in terms of their spatial Fourier series,

$$\begin{aligned} \mathscr{G}^{(0)}_{\sigma\sigma'}(\mathbf{r}_a - \mathbf{r}_b, i\nu) = \frac{1}{\mathcal{V}}\sum_{\mathbf{k}} \mathscr{G}^{(0)}_{\sigma\sigma'}(\mathbf{k}, i\nu)e^{i\mathbf{k}\cdot(\mathbf{r}_a-\mathbf{r}_b)} \to \frac{1}{(2\pi)^d}\int d^dk \mathscr{G}^{(0)}_{\sigma\sigma'}(\mathbf{k}, i\nu)e^{i\mathbf{k}\cdot(\mathbf{r}_a-\mathbf{r}_b)}, \\ V(\mathbf{r}' - \mathbf{r}'') = \frac{1}{\mathcal{V}}\sum_{\mathbf{q}} V(\mathbf{q})e^{i\mathbf{q}\cdot(\mathbf{r}'-\mathbf{r}'')} \to \frac{1}{(2\pi)^d}\int d^dq V(\mathbf{q})e^{i\mathbf{q}\cdot(\mathbf{r}'-\mathbf{r}'')}, \end{aligned} \tag{2.74}$$

where the last step in both lines approximates the sum as an integral, which is valid when the momentum states are close together such that the summand is slowly varying. Using this and eq. 2.72 we see that real space integrals in eq. 2.71 only have three momenta associated to a single internal position, $\mathbf{r}_n$, one from the interaction and two from the

Green's functions as the vertex. This produces integrals of the form

$$\int d^d r_n e^{i\mathbf{r}_n\cdot(\mathbf{q}+\mathbf{k}-\mathbf{k}')} = \begin{cases} \mathcal{V}\,\delta_{\mathbf{q}+\mathbf{k},\mathbf{k}'}, & \text{discrete momenta} \\ \delta^{(d)}(\mathbf{q}+\mathbf{k}-\mathbf{k}'), & \text{continuous momenta,} \end{cases} \tag{2.75}$$

where $\mathbf{q}$ is the momentum entering the vertex from the interaction, whilst $\mathbf{k}$ and $\mathbf{k}'$ are the momenta entering and leaving the vertex due to the particle propagators, respectively. As before, each propagator now carries a momentum across it, which replaces the position labels at the vertices. We can easily see that eq. 2.75 ensures each vertex conserves momentum.

Having now moved to momentum-frequency space, our diagrammatic rules have become [29, 30]:

1. Create all connected, topologically inequivalent diagrams with 2^n internal vertices at n^{th} order, and two external vertices. At each internal vertex, two solid lines and a wavy line meet.

2. To each solid line we associate the propagator in the absence of two particle interactions, $\mathscr{G}^{(0)}_{\sigma\sigma'}(\mathbf{k}, i\nu)$, which moves from spin state σ' to σ, whilst carrying a momentum $\mathbf{k}$ and an Matsubara frequency ν, such that momentum and energy are conserved at each vertex.

3. Each wavy line represents an interaction and carries a factor of $-V(\mathbf{q}, i\omega)$.

4. We now sum over all internal Matsubara frequencies, ν, and introduce a factor of T for each internal frequency summed over.

5. We next sum (integrate) over all internal momenta, $\mathbf{k}$, and introduce a factor of $\mathcal{V}^{-1}$ ($(2\pi)^{-d}$) for each internal momentum summed (integrated) over.

6. Sum over all internal spin indices. This is equivalent to just multiplying by a factor of $(2S+1)$ for each closed particle loop, where S is the particle's spin, and neglecting the spin indices and sums.

7. For each closed fermion loop we introduce an extra factor of (-1).

These rules will be used throughout this thesis in calculating the effects of various phenomena on the electrical transport properties of disordered metals. Given these diagrammatic rules, we are simply left with determining the interaction, $V(\mathbf{q}, i\omega)$, relevant to the physical process we wish to understand. In the case of EEIs this is just the Coulomb interaction, whilst for superconducting fluctuations the propagator describing virtual Cooper pairs becomes the effective interaction propagator.[16]

In this section we have outlined the mathematical properties underlying Green's functions, and explained why they describe particle propagation. With this picture in mind, we calculated the Green's function for a free particle. With the knowledge of the free particle propagator we proceeded to consider the perturbation expansion of the single-particle Green's function in terms of a background single-particle interaction. Doing so we derived the diagrammatic rules for particle propagation in the presence of a single-particle interaction. Lastly, we generalised these ideas further to generate the diagrammatic rules for particle propagation subject to a two-particle interaction. Using these rules, we shall move onto modelling disordered metallic systems.

[16]It is common in the literature when writing problems of this nature in terms of momentum sums, to suppress the factor of $\mathcal{V}^{-1}$. This is done for notational ease, as most sums will eventually be replaced by integrals. Nonetheless, these factors are accounted for in the literature though rarely written explicitly.

CHAPTER 3

TRANSPORT PHENOMENA IN HOMOGENEOUS SYSTEMS

The processes governing the transfer of energy and information through a system have been of great interest to mathematicians, physicists, and chemists for many centuries. One of the most famous of these people was the German physicist Paul Drude [1], who applied Boltzmann's kinetic theory of gases to the electrons in a metal to obtain the renowned Drude formula for the electrical conductivity of a metal,

$$\sigma_0 = \frac{n_e e^2 \tau_0}{m_e}, \tag{3.1}$$

where n_e is the number density of electrons in the metal, and τ_0 is the elastic scattering rate of electrons interacting with impurities in the metal. However, it was observed that this relation held well for high temperatures (comparable to room temperature), but broke down for low temperatures implying there were other physical mechanisms playing a role in these settings. With the quantum revolution of the 1920s, this result survived in the form of the Drude-Sommerfeld model, where the old classical description of colliding particles was replaced by a gas of weakly interacting electrons obeying Fermi-Dirac statistics [8, 4].

It was not until the 1950s that microscopic quantum transport theory began to be developed. This approach started with Matsubara [9] developing finite temperature QFT,

followed by Kubo [10] and Greenwood [32] deriving the linear response of the electrical conductivity to an externally applied electric field. Shortly afterwards, Edwards [11] introduced a method to include impurities in the metal, whilst Abrikosov and Gorkov [33] showed that the regular Drude result, in principle, could be obtained via zero temperature QFT in the absence of two-particle interactions and with the inclusion of impurities. Finally, Langer [12, 13, 14] demonstrated, with strict rigour, that diagrammatic QFT could be used to obtain the regular Drude result for zero and finite temperatures.

Let us begin this chapter by introducing impurities into our model of a metal, so that we may reproduce the calculation of the Drude conductivity from diagrammatic QFT. Only then may we understand how to calculate the electrical conductivity for a system with more complex physics present. After this, we shall explore the effects of weak localisation in section 3.3, before considering the role of electron-electron interactions (EEIs) in section 3.4. Following this, we will derive the corrections due to superconducting fluctuations in section 3.5. Finally, we shall consider the role of phase breaking mechanisms in section 3.6.

3.1 Impurity Scattering and Diagrammatics

The importance of impurities was realised within Drude's original model of a metal. Here they were treated as fixed points that electrons could scatter off with some characteristic scattering rate, τ_0^{-1}. Including these into QFT was not an easy task and was first achieved by Edwards [11] in 1958, quickly followed by Abrikosov and Gorkov [33] in 1959. Today multiple approaches exist to tackle disorder in systems, but they all share the idea of averaging over all possible distributions of the impurities. We shall follow the averaging procedure described by Rickayzen [29] and Bruus and Flensberg [31], as this is the most intuitive route to including impurities, and shares many similarities with the ideas presented in the original papers [11, 33]. Other approaches to averaging do exist: the path integral formulation of QFT allows for use of the replica trick [34]; nonlinear sigma models

(NLσM) provide an alternative route for those wishing to maintain complete mathematical rigour (see [34, 35, 36] for details), however, we will avoid using this method in this thesis.

Let us begin by considering the Hamiltonian in eq. 2.38 with the single particle potential,

$$U(\mathbf{r},\tau) = \sum_{i=1}^{N_{\text{imp}}} V(\mathbf{r}-\mathbf{R}_i)\delta(\tau), \tag{3.2}$$

which describes a set of N_{imp} identical impurities, with the i^{th} impurity being located at $\mathbf{R}_i$. Each impurity is thus described by the potential $V(\mathbf{r}-\mathbf{R}_i)$. Clearly the Green's function describing this system is given by the diagram in fig. 2.2, albeit only for a single realisation of the impurity distribution. Given that we cannot know the exact position of all impurities in a material, and that we are interested in the system's macroscopic properties, we perform an ensemble average over all possible impurity distributions. We refer to this as either impurity averaging or disorder averaging. Thus the Green's function we wish to consider is defined as

$$G(x,x') = \langle G(x;x';U)\rangle^{(0)}_{\text{dis}} = -\left\langle T_\tau\{\psi(x')\psi^\dagger(x)\}\right\rangle_{\text{dis}}, \tag{3.3}$$

where $\langle ...\rangle^{(0)}_{\text{dis}}$ denotes disorder averaging alone, and $\langle ...\rangle_{\text{dis}}$ denotes combined thermal and disorder averaging.

Applying this average will not affect the free electron Green's functions, now denoted by G_0, appearing in the perturbation series of the disorder-averaged Green's function, and hence the average will simply pass through them. The only objects affected by this procedure will be the $U(x)$ appearing as internal functions in the integrals defined in eq. 2.54. Thus the problem of impurity averaging reduces to evaluating averages of the form

$$\begin{aligned} \langle U(x_1)\rangle^{(0)}_{\text{dis}}, \qquad & \langle U(x_1)U(x_2)\rangle^{(0)}_{\text{dis}}, \\ \langle U(x_1)U(x_2)U(x_3)\rangle^{(0)}_{\text{dis}}, \qquad & \langle U(x_1)U(x_2)U(x_3)U(x_4)\rangle^{(0)}_{\text{dis}}. \end{aligned} \tag{3.4}$$

This averaging procedure is simply the average of a quantity over all possible positions of

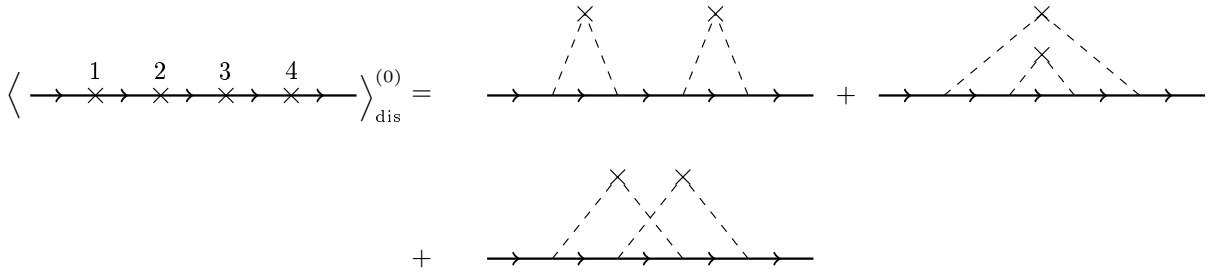

Figure 3.1: Diagrammatic representation of the fourth order correction to the disordered-averaged electron Green's function.

the impurities that it contains.

We make the additional assumption that the concentration of impurities is not too high, allowing us to treat the impurity positions as independent and random.[1] Furthermore, we shall only consider s-wave scattering for our problems.[2] To illustrate this process requires a lot of time and tedious algebra, so we give the details of performing the disorder average in appendix D, and simply state the consequences here. In brief, this averaging procedure can be summed up as assuming that the average of impurity events has a Gaussian distribution,

$$\langle U(x_1)\rangle^{(0)}_{\text{dis}} = 0, \qquad \langle U(x_1)U(x_2)\rangle^{(0)}_{\text{dis}} = \frac{1}{2\pi N(0)\tau_0}\delta(x_1 - x_2). \tag{3.5}$$

The end results of averaging generates the additional diagrammatic rules,

1. Only an even number of scattering events contributes after disorder averaging, so we consider diagrams where $2n$ ($n \in \mathbb{Z}_0^+$) crosses are present. Consider fig. 2.2 with all odd orders removed.

2. Consider all possible combinations where we pair all crosses, with paired crosses connected via a dotted line. Next, replace the two crosses on the Green's functions with a single cross in the centre of the dashed line, see fig. 3.1. This dashed line

[1] Being more specific, what we mean by a sufficiently low concentration of impurities is that $n_{\text{imp}}/n_e \ll 1$, where n_{imp} is the number density of impurities.

[2] All this means is that scattering is spherically symmetric, hence $|u(\mathbf{k}, \mathbf{k}')|$ depends only upon the magnitude of the momentum exchange, $|\mathbf{k} - \mathbf{k}'|$. To include angular dependence in scattering we refer the reader to Rickayzen [29], and Bruus and Flensberg [31].

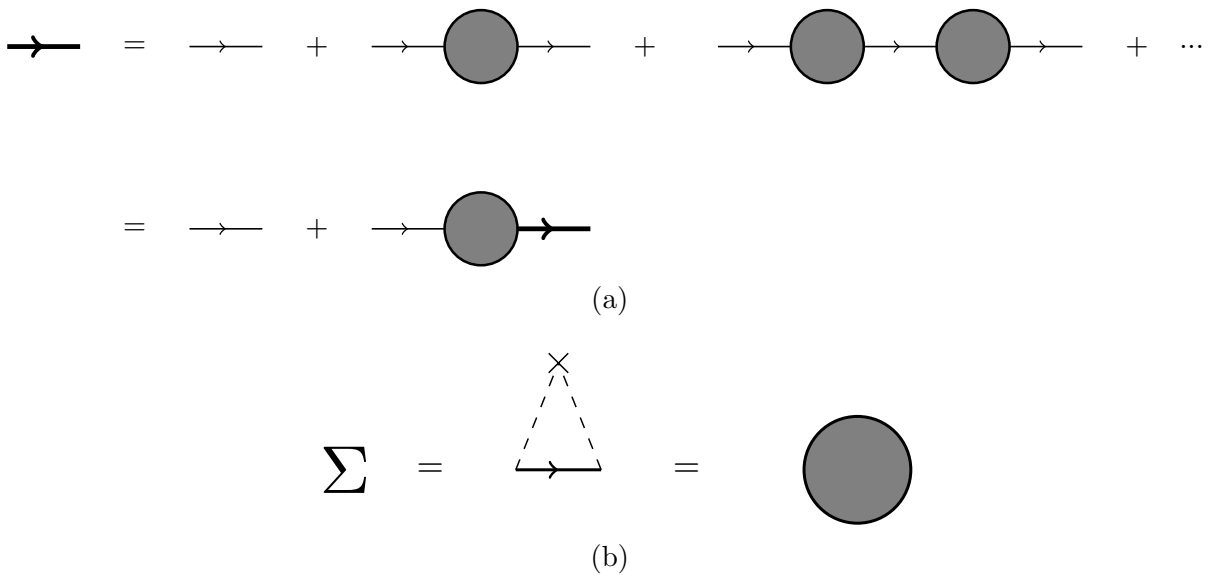

Figure 3.2: (a): Diagrammatic representation of the disorder-averaged electron Green's function, where the thin solid lines are G_0 propagators, and the thick solid lines are the disorder-averaged electron Green's function, G. (b): Diagrammatic series for the self-energy describing impurity averaging. Here the solid line represents G_0.

can transfer momentum but not Matsubara frequency, obeying the usual conservation laws, and forms a constant effective two-body interaction in energy-momentum space, with magnitude

$$\frac{1}{2\pi N(0)\tau_0}, \tag{3.6}$$

where $N(0)$ is the single spin density of states per unit volume at the Fermi surface.

3. For weakly disordered metals, where $k_F l \gg 1$ (l is the mean free path), terms involving overlapping (crossed) two-body scattering interactions are sub-dominant at all orders, and so may be neglected; for example, see the third term of fig. 3.1.

Nested diagrams, such as that shown in the second term of fig. 3.1, give a vanishing result, as will be explained shortly. After applying these rules and neglecting insignificant diagrams, we are left with calculating the Green's function shown in fig. 3.2a. The grey circle is known as the self-energy, Σ, and allows for an easier calculation of the disorder-averaged electron Green's function.[3]

[3]We have given a very simple example of a self-energy here. A more complete definition and treatment of the self-energy is given in appendix D.

In general, the self-energy allows us to write our Green's function as

$$\begin{aligned} G(x,x') = G_0(x,x') &+ \int dx_1 \int dx_2\, G_0(x,x_1)\Sigma(x_1,x_2)G_0(x_2,x') \\ &+ \int dx_1 \int dx_2 \int dx_3 \int dx_4\, G_0(x,x_1)\Sigma(x_1,x_2)G_0(x_2,x_3)\Sigma(x_3,x_4)G_0(x_4,x') \\ &+ ..., \end{aligned} \tag{3.7}$$

which may be rewritten as

$$G(x,x') = G_0(x,x') + \int dx_1 \int dx_2\, G_0(x,x_1)\Sigma(x_1,x_2)G(x_2,x'). \tag{3.8}$$

We may further simplify the problem by noting that averaging over all possible impurity distributions creates a system possessing translational invariance. Given that $G(x,x')$ must respect the symmetries of the system, it too must have translational invariance and therefore only a single momentum argument when written as a Fourier series. Similar reasoning means that the self-energy also possesses translational invariance. Consequently, we may write[4]

$$G(\mathbf{k},i\varepsilon) = G_0(\mathbf{k},i\varepsilon) + G_0(\mathbf{k},i\varepsilon)\Sigma(\mathbf{k},i\varepsilon)G(\mathbf{k},i\varepsilon), \tag{3.9}$$

where we have also performed a temporal Fourier transform to obtain Matsubara Green's functions. Eq. 3.9 is known as a Dyson equation. Therefore we arrive at a simple form for the disorder-averaged electron Green's function,

$$G(\mathbf{k},i\varepsilon) = \frac{1}{G_0(\mathbf{k},i\varepsilon)^{-1} - \Sigma(\mathbf{k},i\varepsilon)}. \tag{3.10}$$

The benefit of this form is that all of the Green's function's properties are determined by Σ, and so we need only focus on calculating this more primitive object. Fig. 3.2a represents eq. 3.9 in momentum-frequency space, or eqs. 3.7 and 3.8 in real space and imaginary time; fig. 3.2b shows the diagrammatic series for $\Sigma(\mathbf{k},i\varepsilon)$.

[4]We have not discussed temporal invariance, but it should be noted that this is possessed by the free electron Green's functions. Therefore the self-energy and the disorder-averaged electron Green's function will also have temporal invariance.

We now calculate Σ. Fig. 3.2b gives the self-energy to be

$$\Sigma(i\varepsilon) = \frac{1}{2\pi N(0)\tau_0}\frac{1}{\mathcal{V}}\sum_{\mathbf{k}'} G_0(\mathbf{k}', i\varepsilon) = -\frac{1}{2\pi N(0)\tau_0}\frac{1}{\mathcal{V}}\sum_{\mathbf{k}'}\frac{i\varepsilon + \xi_{\mathbf{k}'}}{\varepsilon^2 + \xi_{\mathbf{k}'}^2}, \tag{3.11}$$

where we have noted that the self-energy will have no momentum dependence. Since we want to focus on the most significant (i.e: singular) contributions to the self-energy, we focus on energies close to the Fermi surface, $\xi_{\mathbf{k}'}/\varepsilon_F \ll 1$ (ε_F is the Fermi energy). We may therefore approximate the sum in eq. 3.11 by an integral, whose limits are extended to $\pm\infty$. This allows us to write

$$\Sigma(i\varepsilon) = -\frac{1}{2\pi N(0)\tau_0}\int_{-\infty}^{+\infty} d\xi' N(\xi')\frac{i\varepsilon + \xi'}{\varepsilon^2 + \xi'^2} \simeq -\frac{1}{2\pi\tau_0}\int_{-\infty}^{+\infty} d\xi'\frac{i\varepsilon + \xi'}{\varepsilon^2 + \xi'^2}, \tag{3.12}$$

where $N(\xi')$ is the single spin density of states per unit volume at energy ξ'. In the final part of eq. 3.12, we accounted for the fact we are only interested in behaviour close the Fermi surface, and took $N(\xi')$ to be approximately constant about the Fermi energy. The second term of the integral vanishes due to oddness; the first term can be evaluated trivially to yield

$$\Sigma(i\varepsilon) = -\frac{i}{2\tau_0}\mathrm{sgn}(\varepsilon). \tag{3.13}$$

This therefore produces the disorder-averaged electron Green's function,

$$G(\mathbf{k}, i\varepsilon) = \frac{1}{i\varepsilon - \xi_{\mathbf{k}} + \frac{i}{2\tau_0}\mathrm{sgn}(\varepsilon)}. \tag{3.14}$$

If we wanted to include nested diagrams into our calculation of this Green's function, we would simply need to replace G_0 with G in the self-energy to generate a self-consistent solution, see fig. 3.3. Doing so eq. 3.11 becomes

$$\Sigma(i\varepsilon) = \frac{1}{2\pi N(0)\tau_0}\frac{1}{\mathcal{V}}\sum_{\mathbf{k}'} G(\mathbf{k}', i\varepsilon) = \frac{1}{2\pi N(0)\tau_0}\frac{1}{\mathcal{V}}\sum_{\mathbf{k}'}\frac{1}{i\varepsilon - \xi_{\mathbf{k}'} - \Sigma(i\varepsilon)}. \tag{3.15}$$

To solve this we use the ansatz $\mathrm{Im}[\Sigma(i\varepsilon)] = -\gamma\mathrm{sgn}(\varepsilon)$, where $\gamma > 0$, as done in [34]. The

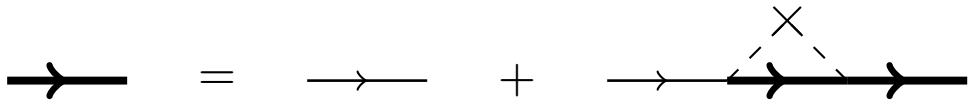

Figure 3.3: Self-consistent diagrammatic series for the disorder-averaged electron Green's function, which includes all forms of nested diagrams involving two correlated impurity scatterings.

real part is not of interest as we can absorb this into a redefinition of the chemical potential. Therefore, looking at the imaginary part of eq. 3.15 and replacing the momentum sum by an integral approximated about the Fermi surface, we see

$$\begin{aligned}\mathrm{Im}[\Sigma(i\varepsilon)] &= -\frac{1}{2\pi\tau_0}\int_{-\infty}^{+\infty} d\xi' \frac{\varepsilon+\gamma\mathrm{sgn}(\varepsilon)}{(\varepsilon+\gamma\mathrm{sgn}(\varepsilon))^2+\xi'^2} \\ &= -\frac{\mathrm{sgn}(\varepsilon)}{2\pi\tau_0}\int_{-\infty}^{+\infty} d\xi' \frac{|\varepsilon|+\gamma}{(|\varepsilon|+\gamma)^2+\xi'^2} \\ &= -\frac{\mathrm{sgn}(\varepsilon)}{2\tau_0}.\end{aligned} \tag{3.16}$$

For this to be true, we must have $\gamma = 1/(2\tau_0)$.

This result leads to exactly the same Green's function we found in eq. 3.14. To demonstrate this we rewrite eq. 3.10 as

$$G(\mathbf{k}, i\varepsilon) = \frac{1}{i\varepsilon - \xi_{\mathbf{k}} - \mathrm{Re}[\Sigma(i\varepsilon)] - i\,\mathrm{Im}[\Sigma(i\varepsilon)]}. \tag{3.17}$$

As stated earlier, we can absorb $\mathrm{Re}[\Sigma(i\varepsilon)]$ as a shift to the chemical potential in $\xi_{\mathbf{k}}$. Finally, by substituting eq. 3.16 in for $\mathrm{Im}[\Sigma(i\varepsilon)]$ we recover eq. 3.14. Clearly this means that nested diagrams can be treated as vanishing.

This Green's function allows us to extract new information by transforming to both momentum-time space, and position-frequency space.[5] In the former we find the retarded Green's function to be

$$G^R(\mathbf{k}, t) = -i\, e^{-i\xi_{\mathbf{k}} t}\, e^{-t/(2\tau_0)}\, \Theta(t). \tag{3.18}$$

The exponential decay in time shows that an electron remains in the definite momentum

[5] Details of these calculations are given in appendix D.

state $\mathbf{k}$ for a time on the scale of τ_0. We can interpret this as the typical time an electron travels without scattering from an impurity. Similarly, in the second case we see

$$G^R(\mathbf{r},\omega) = -\frac{\pi N(0)}{k_F r}\, e^{ik_F r}\, e^{-r/(2l)}, \tag{3.19}$$

where $l = v_F\tau_0$ (v_F is the Fermi velocity). This demonstrates that an electron wave function decays exponentially on the scale of l, after which the electron loses memory of its initial state. In other words, the electron typically travels a distance l before scattering from an impurity.

In summary, we have provided the results of including disorder diagrammatically and calculated the propagator for an electron in a disordered system, this led to an electron propagator that describes a confined electron wave function,[6] that scatters into a new momentum state on a time scale of τ_0, or equivalently after travelling a distance comparable to l. We shall now move on to calculating the electrical conductivity of a metal by including different physical mechanisms. We shall start simply by reproducing the Drude result, before including electron-electron interactions and the superconducting fluctuations.

3.2 Drude Conductivity

When considering the Drude result, one might ask: "Why calculate something we already know the answer to using more convoluted means?". This question partially answers itself. When using more sophisticated methods to understand more complicated mechanisms, to have faith in these methods we must be able to reproduce the simplest result. If we were to trudge on with diagrammatic QFT without rigorously verifying that it can generate the Drude result, which we know to be correct in the high temperature limit from observation,

[6]Note that for a specific realisation of impurities that the eigenstates are still extended propagating solutions in the case of weak disorder. In this case, we do not have translational invariance, and hence momentum is not a quantum number labelling the eigenstates. The exponential decay only arises as a result of the impurity averaging procedure, and so the effective eigenstates are confined. In contrast to previously, translational invariance has been artificially restored and so momentum becomes an artificial quantum number for these effective eigenstates. These are short lived states as a consequence.

then all further corrections would harbour an essence of mystery and magic as to why they work. This philosophy was clearly shared by Langer [12, 13, 14], whose work we will shall expand upon shortly. First let us derive the diagrammatic rules surrounding electrical conductivity following Rickayzen's methodology [29].

We start from the definition of the electrical conductivity tensor, $\sigma_{\alpha\beta}$, as the response of the macroscopic current density, $\mathbf{J}$, to the applied electric field, $\mathbf{E}$, for a d dimensional system

$$J_\alpha(\mathbf{r},t) = \sum_\beta \int_{-\infty}^{+\infty} dt' \int d^d r' \sigma_{\alpha\beta}(\mathbf{r}-\mathbf{r}', t-t') E_\beta(\mathbf{r}', t'). \tag{3.20}$$

For simplicity we choose to work in the Coulomb gauge (zero scalar field), so that the electric field is described solely in terms of the vector potential, $\mathbf{A}(\mathbf{r},t)$,

$$\mathbf{E} = -\frac{\partial \mathbf{A}}{\partial t}. \tag{3.21}$$

Performing a temporal Fourier transform on eq. 3.20 using eq. 3.21 yields

$$J_\alpha(\mathbf{r},\omega) = i\omega \sum_\beta \int d^d r' \sigma_{\alpha\beta}(\mathbf{r}-\mathbf{r}', \omega) A_\beta(\mathbf{r}', \omega). \tag{3.22}$$

Hence, the conductivity is related to the linear response of the current to the vector potential, a field which is easily included into quantum mechanics via minimal coupling. The Hamiltonian corresponding to a disordered system in the presence of $\mathbf{A}(\mathbf{r},\omega)$ is simply ($c = 1$)

$$\mathscr{H} = \sum_\sigma \int d^d r\, \psi_\sigma^\dagger(\mathbf{r}) \left[\frac{(-i\nabla - e\mathbf{A}(\mathbf{r},t))^2}{2m_e} + U(\mathbf{r}) - \mu \right] \psi_\sigma(\mathbf{r}), \tag{3.23}$$

which may be rewritten as $\mathscr{H} = \mathscr{H}_0 + H'$, where $\mathscr{H}_0$ is the Hamiltonian in the absence of $\mathbf{A}$ and

$$H'(t) = \int d^d r\, \mathbf{j}(\mathbf{r},t) \cdot \mathbf{A}(\mathbf{r},t). \tag{3.24}$$

Here $\mathbf{j}(\mathbf{r},t)$ is the microscopic current density defined as[7]

$$\mathbf{j}(\mathbf{r},t) = \mathbf{j}_0(\mathbf{r}) - \frac{e^2}{m_e}\sum_\sigma \psi^\dagger_\sigma(\mathbf{r})\psi_\sigma(\mathbf{r})\mathbf{A}(\mathbf{r},t), \tag{3.25a}$$

$$\mathbf{j}_0(\mathbf{r}) = -\frac{ie}{2m}\sum_\sigma \left[\psi^\dagger_\sigma(\mathbf{r})\nabla\psi_\sigma(\mathbf{r}) - \left\{\nabla\psi^\dagger_\sigma(\mathbf{r})\right\}\psi_\sigma(\mathbf{r})\right]. \tag{3.25b}$$

To obtain the macroscopic current from the microscopic current, we take the thermal average of $\mathbf{j}(\mathbf{r})$, followed by the disorder average. By applying Kubo's formula for linear response,[8] we obtain

$$\begin{aligned} J_\alpha(\mathbf{r},t) = \langle j_{0,\alpha}(\mathbf{r},t)\rangle_{0,\text{dis}} &- \frac{n_e e^2}{m_e}A_\alpha(\mathbf{r},t) \\ &- \sum_\beta \int_{-\infty}^{+\infty} dt' \int d^d r'\, \mathcal{G}^R_{\alpha\beta}(\mathbf{r},t;\mathbf{r}',t')A_\beta(\mathbf{r}',t'), \end{aligned} \tag{3.26}$$

where $n_e = \sum_\sigma \langle \widetilde{\psi}^\dagger_\sigma(\mathbf{r})\widetilde{\psi}_\sigma(\mathbf{r})\rangle_{0,\text{dis}}$ is the electron number density, and $\langle ...\rangle_{0,\text{dis}}$ denotes thermal averaging with respect to $\mathscr{H}_0$ and disorder averaging. The retarded Green's function is just the retarded current-current correlator

$$\mathcal{G}^R_{\alpha\beta}(\mathbf{r},t;\mathbf{r}',t') = -i\Big\langle \Big[\widetilde{j}_{0,\alpha}(\mathbf{r},t), \widetilde{j}_{0,\beta}(\mathbf{r}',t')\Big]\Big\rangle_{0,\text{dis}}\Theta(t-t'), \tag{3.27}$$

with $\widetilde{j}_{0,\alpha}$ denoting the α^{th} component of the current density operator with no external field in the interaction picture. Specifically,

$$\widetilde{\mathbf{j}}_0(\mathbf{r},t) = -\frac{ie}{2m_e}\sum_\sigma \left[\widetilde{\psi}^\dagger_\sigma(\mathbf{r},t)\nabla\widetilde{\psi}_\sigma(\mathbf{r},t) - \left\{\nabla\widetilde{\psi}^\dagger_\sigma(\mathbf{r},t)\right\}\widetilde{\psi}_\sigma(\mathbf{r},t)\right]. \tag{3.28}$$

Clearly, the first term of eq. 3.26 must vanish, as this is the average current in the absence of an applied field.

As a final step, we recall that the retarded Green's function depends only upon time

[7] We can also find the current density operator using functional differentiation, $\mathbf{j}(\mathbf{r},t) = \delta H'(t)/\delta A(\mathbf{r},t)$.
[8] See appendix E for the general Kubo formula and how it is applied to the electrical current.

differences, $t - t'$, and perform a temporal Fourier transform on eq. 3.26. Disorder averaging recovers translational invariance, allowing us to perform a spatial Fourier transform with ease. Applying both Fourier transforms yields

$$J_\alpha(\mathbf{q},\omega) = -\sum_\beta K^R_{\alpha\beta}(\mathbf{q},\omega)A_\beta(\mathbf{q},\omega), \tag{3.29a}$$

where

$$K^R_{\alpha\beta}(\mathbf{q},\omega) = \frac{n_e e^2}{m_e}\delta_{\alpha\beta} + \mathcal{G}^R_{\alpha\beta}(\mathbf{q},\omega), \tag{3.29b}$$

and $K^R_{\alpha\beta}$ is commonly referred to as the (retarded) electromagnetic response function.[9] The first term in $K^R_{\alpha\beta}$ is referred to as the diamagnetic term, whilst the second term is known as the paramagnetic contribution.

From the spatial Fourier transform of eq. 3.22 and eq. 3.29, we see that the electromagnetic response function is related to the conductivity tensor via

$$K^R_{\alpha\beta}(\mathbf{q},\omega) = -i\omega\sigma_{\alpha\beta}(\mathbf{q},\omega), \tag{3.30}$$

for real frequency ω. Given that we will be working in the Matsubara formalism throughout this thesis, we identify the equivalent relation in terms of the bosonic Matsubara frequency Ω,[10] which is obtained by letting $\omega \to i\Omega$,

$$K_{\alpha\beta}(\mathbf{q},i\Omega) = \Omega\sigma_{\alpha\beta}(\mathbf{q},i\Omega). \tag{3.31}$$

Clearly, in the limit of DC conductivity ($\omega, \Omega = 0$), the response function must vanish for a normal system. If this were not the case, the conductivity tensor would diverge as the frequency tends to zero, and hence the system would be superconducting. When performing diagrammatic calculations of the conductivity, it is of the utmost importance that the response function vanishes when dealing with a normal state material, otherwise

[9] In general this is a type of linear response function, and these ideas can be applied in a variety of cases.

[10] The applied electric field is bosonic in nature, and thus carries a bosonic Matsubara frequency.

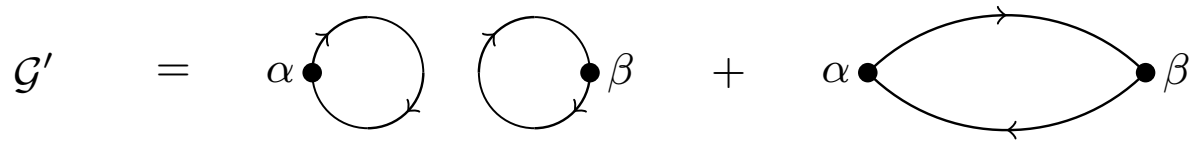

Figure 3.4: Diagrammatic representation $\mathcal{G}'(\mathbf{r}_1, \tau; \mathbf{r}'_1, \tau')$, where the solid lines are electron Green's functions for a specific impurity distribution, G'. The black dots denote the current vertices and their vector components, α and β.

the model being applied cannot be the correct description for the system. As such, we must always bear in mind that we have to include all diagrams of a certain order to ensure this happens.[11]

To calculate $K^R_{\alpha\beta}$ we must first find $\mathcal{G}^R_{\alpha\beta}$. This is most easily done by considering its corresponding temperature Green's function prior to disorder averaging,

$$\mathcal{G}'_{\alpha\beta}(\mathbf{r}_1, \tau; \mathbf{r}'_1, \tau') = -\left\langle T_\tau \left\{ \widetilde{j}_{0,\alpha}(\mathbf{r}_1, \tau) \widetilde{j}_{0,\beta}(\mathbf{r}'_1, \tau') \right\} \right\rangle_0, \tag{3.32}$$

where $\langle ... \rangle_0$ means thermal averaging with respect to $\mathscr{H}_0$ only. By substituting $\widetilde{\mathbf{j}}_0$ into $\mathcal{G}'_{\alpha\beta}$, we may write

$$\begin{aligned} \mathcal{G}'_{\alpha\beta}(\mathbf{r}_1, \tau; \mathbf{r}'_1, \tau') = \frac{e^2}{4m_e^2} \lim_{\substack{\mathbf{r}_2 \to \mathbf{r}_1 \\ \mathbf{r}'_2 \to \mathbf{r}'_1}} \Big[& (\nabla_{2'} - \nabla_{1'})_\beta (\nabla_2 - \nabla_1)_\alpha \\ & \times \sum_{\sigma,\sigma'} \left\langle T_\tau \left\{ \widetilde{\psi}_\sigma(\mathbf{r}_2, \tau) \widetilde{\psi}_{\sigma'}(\mathbf{r}'_2, \tau') \widetilde{\psi}^\dagger_{\sigma'}(\mathbf{r}'_1, \tau') \widetilde{\psi}^\dagger_\sigma(\mathbf{r}_1, \tau) \right\} \right\rangle_0 \Big], \end{aligned} \tag{3.33}$$

where the limit is applied after the gradient operators act. Wick's theorem allows for two possible contractions of the thermal average inside the spin sums,

$$G'(\mathbf{r}'_2, \tau'; \mathbf{r}'_1, \tau') G'(\mathbf{r}_2, \tau; \mathbf{r}_1, \tau) - G'(\mathbf{r}_2, \tau; \mathbf{r}'_1, \tau') G'(\mathbf{r}'_2, \tau'; \mathbf{r}_1, \tau) \delta_{\sigma\sigma'}, \tag{3.34}$$

where we have suppressed spin indices for ease of notation (the Green's functions do not

[11] Order here typically refers to the loop order of the diagram. This is most easily determined by counting the number of "small" momenta involved in the sums. We shall return to this idea later as there are no small momenta involved in the basic Drude calculation.

have any explicit spin dependence), and

$$G'(\mathbf{r},\tau;\mathbf{r}',\tau') = -\left\langle T_\tau \left\{ \widetilde{\psi}_\sigma(\mathbf{r},\tau)\widetilde{\psi}^\dagger_\sigma(\mathbf{r}',\tau') \right\} \right\rangle_0, \tag{3.35}$$

is the electron Green's function for a specific impurity distribution. These contractions are presented diagrammatically in fig. 3.4. The black dots represent the current vertices and hence act as our external vertices where momentum and Matsubara frequency may enter from the applied field. In real space the current vertices are simply

$$\hat{\mathbf{j}}_0(\mathbf{r}_1,\tau) = \frac{e}{2m_e} \lim_{\mathbf{r}_2\to\mathbf{r}_1} (\nabla_2 - \nabla_1). \tag{3.36}$$

The first of these two possible contractions leads to the term $\langle \widetilde{j}_{0,\alpha}(\mathbf{r}_1,\tau)\rangle_0 \langle \widetilde{j}_{0,\beta}(\mathbf{r}'_1,\tau')\rangle_0$, which clearly vanishes as $\langle \widetilde{j}_{0,\alpha}\rangle_0$ is just the microscopic current in the absence of an electric field. At this point we average over impurity distributions, such that

$$\begin{aligned} \mathcal{G}_{\alpha\beta}(\mathbf{r}_1,\tau;\mathbf{r}'_1,\tau') &= \left\langle \mathcal{G}'_{\alpha\beta}(\mathbf{r}_1,\tau;\mathbf{r}'_1,\tau') \right\rangle^{(0)}_{\text{dis}} \\ &= -\frac{e^2}{4m_e^2} \lim_{\substack{\mathbf{r}_2\to\mathbf{r}_1 \\ \mathbf{r}'_2\to\mathbf{r}'_1}} \Big[(\nabla_{2'} - \nabla_{1'})_\beta (\nabla_2 - \nabla_1)_\alpha \\ &\qquad \times \sum_{\sigma,\sigma'} \langle G'(\mathbf{r}_2,\tau;\mathbf{r}'_1,\tau') G'(\mathbf{r}'_2,\tau';\mathbf{r}_1,\tau) \rangle^{(0)}_{\text{dis}} \, \delta_{\sigma\sigma'} \Big]. \end{aligned} \tag{3.37}$$

This leads to an infinite number of diagrams to be considered, examples of which are given in fig. 3.5. However, we shall apply the same approximations we applied in finding the disorder-averaged electron Green's function in the previous subsection. In addition, we shall neglect the effects of interference between the two Green's functions in eq. 3.37, which is equivalent to assuming s-wave scattering. The inclusion of interference terms yields the same Drude result with $\tau_0 \to \tau_{\text{tr}}$ (the transport relaxation time), and other corrections which are significantly smaller (weak localisation).

These interference terms arise from both Green's functions sharing the same impurity distribution. So when performing our disorder average, we have to consider impurities

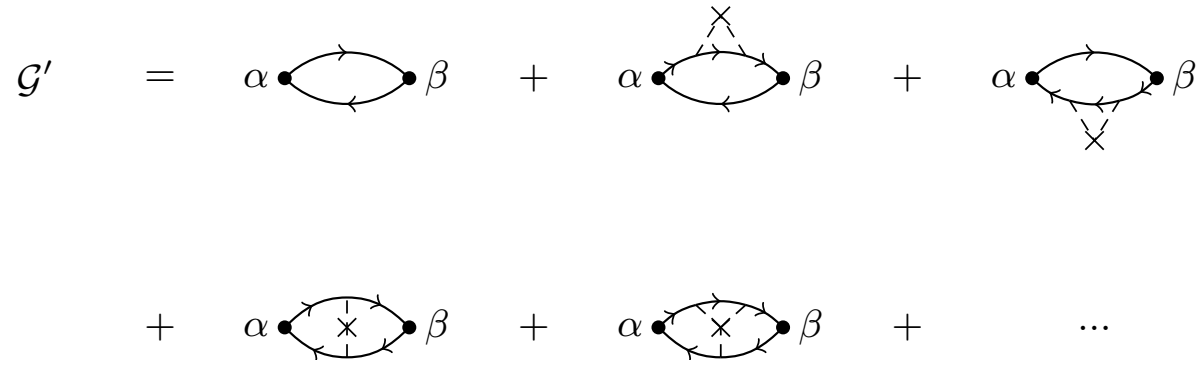

Figure 3.5: Examples of diagrams that arise from the complete disorder average of $\mathcal{G}'$, and not ignoring certain terms. The solid lines represent free electron Green's functions, G_0.

contained within both Green's functions simultaneously. This results in correlated scattering events between the Green's functions. A discussion of the terms that lead to the replacement $\tau_0 \to \tau_{tr}$ can be found in [29, 31]. We shall now focus purely on a metal containing only s-wave scatterers, so that

$$\begin{aligned}\mathcal{G}(\mathbf{r}_1,\tau;\mathbf{r}_1',\tau') \simeq -\frac{e^2}{4m_e^2}\lim_{\substack{\mathbf{r}_2\to\mathbf{r}_1\\ \mathbf{r}_2'\to\mathbf{r}_1'}}\Big[&(\nabla_{2'}-\nabla_{1'})_\beta(\nabla_2-\nabla_1)_\alpha\\ &\times\sum_{\sigma,\sigma'}\langle G'(\mathbf{r}_2,\tau;\mathbf{r}_1',\tau')\rangle_{\text{dis}}^{(0)}\langle G'(\mathbf{r}_2',\tau';\mathbf{r}_1,\tau)\rangle_{\text{dis}}^{(0)}\delta_{\sigma\sigma'}\Big]\\ =-\frac{e^2}{4m_e^2}\lim_{\substack{\mathbf{r}_2\to\mathbf{r}_1\\ \mathbf{r}_2'\to\mathbf{r}_1'}}\Big[&(\nabla_{2'}-\nabla_{1'})_\beta(\nabla_2-\nabla_1)_\alpha\\ &\times\sum_{\sigma,\sigma'}G(\mathbf{r}_2,\tau;\mathbf{r}_1',\tau')G(\mathbf{r}_2',\tau';\mathbf{r}_1,\tau)\delta_{\sigma\sigma'}\Big],\end{aligned} \tag{3.38}$$

where $G(\mathbf{r}_2,\tau;\mathbf{r}_1',\tau')$ is the disorder-averaged electron Green's function in real space and imaginary time.

After impurity averaging we regain translational invariance. Given that the Green's function already possesses temporal invariance, it is beneficial to move to momentum-frequency space in the usual Matsubara formalism. Doing so we find,

$$\mathcal{G}_{\alpha\beta}(\mathbf{q},i\Omega)=\frac{2e^2}{4m_e^2}\sum_{\mathbf{k}}T\sum_{\varepsilon}(2k_\alpha+q_\alpha)(2k_\beta+q_\beta)G(\mathbf{k}+\mathbf{q},i\varepsilon+i\Omega)G(\mathbf{k},i\varepsilon), \tag{3.39}$$

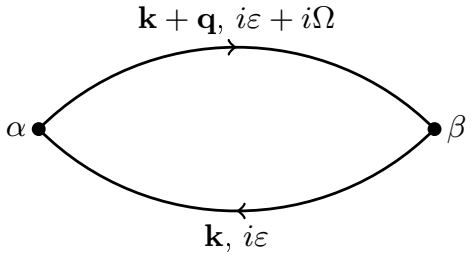

Figure 3.6: Fully labelled Drude diagram describing eq. 3.39. The solid lines represent disorder-averaged electron Green's functions.

where the extra factor of 2 comes from the spin sums, $G(\mathbf{k}, i\varepsilon)$ is the disorder-averaged electron Green's function of eq. 3.14, Ω is the bosonic Matsubara frequency of the external electric field, and ε is a fermionic Matsubara frequency.[12] We have suppressed the factor of $\mathcal{V}^{-1}$ for notational convenience as we will replace the sum by an integral, at which point this factor is naturally absorbed.[13] Finally, we identify the current vertices in momentum space as carrying the factor

$$\frac{e}{2m_e}(2\mathbf{k}+\mathbf{q}). \tag{3.40}$$

Considering a uniform electric field, we may set $\mathbf{q}=\mathbf{0}$. This simplifies eq. 3.39 to

$$\mathcal{G}_{\alpha\beta}(i\Omega) = 2\sum_{\mathbf{k}} T\sum_{\varepsilon} \frac{ek_\alpha}{m_e}\frac{ek_\beta}{m_e} G(\mathbf{k}, i\varepsilon+i\Omega)G(\mathbf{k}, i\varepsilon), \tag{3.41}$$

with each current vertex now carrying a factor of ek_α/m_e.

At this point we draw attention to a technical aspect of the Drude calculation. If we simply swapped the order of momentum and frequency sums, so that we may perform the momentum sum first, we would find that the diamagnetic term of the electromagnetic response function would not be cancelled, and hence the system would appear to be superconducting. Only by treating these sums carefully, and appreciating their insufficient rate of convergence, can we show that the diamagnetic term is indeed cancelled by the paramagnetic term, leaving only terms of order Ω and higher. This technical point was

[12] Whilst we have been explicit here, we shall assume that all future occurrences of ε as a Matsubara frequency are fermionic, whilst ω and Ω will always be bosonic, unless otherwise stated.

[13] This is a standard convention in the literature.

first openly acknowledged and dealt with by Langer's trilogy of papers [12, 13, 14]. We present here the same style of argument used in [37], where both naïve and rigorous approaches are given to demonstrate the delicate nature of this calculation.

3.2.1 The Naïve Approach

We start with the assumption that we may interchange summation orders without consequence. Replacing the momentum sum by an integral linearised about the Fermi surface gives,[14]

$$\mathcal{G}_{\alpha\beta}(i\Omega) = \frac{2e^2N(0)}{m_e^2}\,T\sum_{\varepsilon}\int d\hat{\Omega}_d\,k_{F\alpha}\,k_{F\beta} \times\int_{-\infty}^{+\infty}\frac{d\xi}{\left[\xi-i\varepsilon-i\Omega-\frac{i}{2\tau_0}\mathrm{sgn}(\varepsilon+\Omega)\right]\left[\xi-i\varepsilon-\frac{i}{2\tau_0}\mathrm{sgn}(\varepsilon)\right]}, \tag{3.42}$$

where $d\hat{\Omega}_d$ is the normalised d-dimensional angular element. Without loss of generality we assume $\Omega > 0$, meaning that the only non-zero contribution to the integral occurs when $\varepsilon + \Omega > 0$ and $\varepsilon < 0$, i.e. $-\Omega < \varepsilon < 0$. All other choices of ε lead to both poles of the integrand lying in the same half plane, so when evaluating the integral via complex analysis the contour can be closed in a half plane containing no poles, and hence the integral vanishes. We illustrate this point in fig. 3.7. Computing the ξ integral using the

[14] The use of linearise here may seem odd, as it does not appear that we have linearised anything in this integral. What this linearisation refers to, is the linearisation of the spectrum, $\varepsilon_{\mathbf{k}}$ or $\xi_{\mathbf{k}}$, near the Fermi surface. If we say that we are close to the Fermi surface, then we can consider a small displacement, $\mathbf{q}$, away from $\mathbf{k}_F$, such that $|\mathbf{q}| \ll k_F$. In any case, we can write $\varepsilon_{\mathbf{k}_F+\mathbf{q}} = (\mathbf{k}_F+\mathbf{q})^2/(2m_e)$. In the limit of small $\mathbf{q}$, we can approximate this expression as $\varepsilon_{\mathbf{k}_F+\mathbf{q}} \simeq \mathbf{v}_F\cdot(\mathbf{k}_F+2\mathbf{q})/2$, or equivalently $\xi_{\mathbf{k}_F+\mathbf{q}} \simeq \mathbf{v}_F\cdot\mathbf{q}$. Hence, both spectra appear linear in variations about the Fermi surface.

The consequence of this linearisation here, is to set $\mathbf{k} = \mathbf{k}_F$ where possible, and to only keep small variations where they are not dominated. For example, $N(\xi) \sim (\xi+\varepsilon_F)^{(d-2)/2}$, meaning linearising ξ about the Fermi surface will do very little as it is small compared to the additive term of ε_F next to it. Thus, we can simply take $N(\xi) \simeq N(0)$. In contrast, the ξ terms appearing in the Green's functions are not actively compared to another energy scale that is much larger. Hence, we may replace them with the linearised forms of ξ without them being insignificant. In short, this entire approximation comes down to treating ξ as small compared to the Fermi energy, and ignoring it where appropriate.

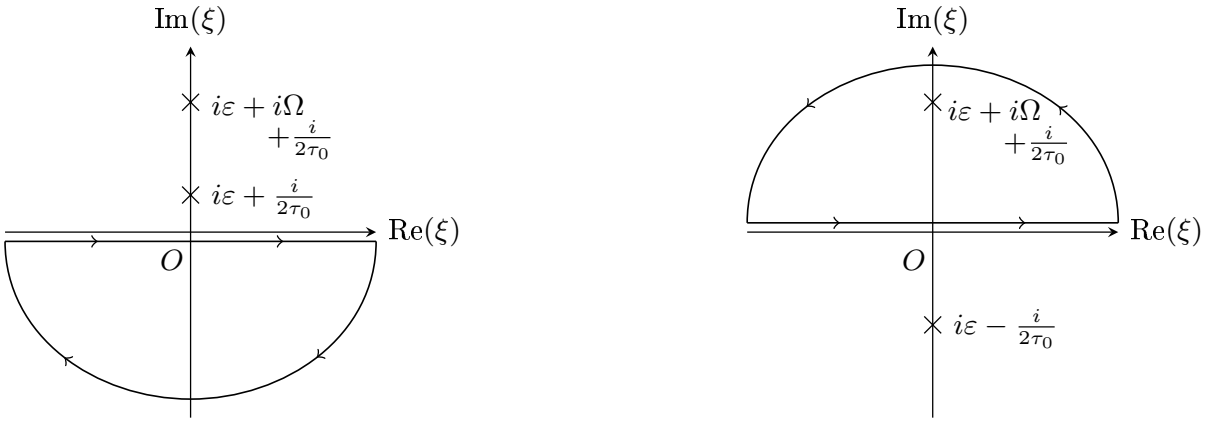

Figure 3.7: Left: the contour from analytic continuation can be closed in an empty half-plane when ε and $\varepsilon+\Omega$ have the same sign. Right: when ε and $\varepsilon+\Omega$ have opposite signs, both half-planes contain a pole, so any choice of contour will enclose a pole.

method of residues, we see that

$$\mathcal{G}_{\alpha\beta}(i\Omega) = \frac{2e^2N(0)}{m_e^2}T\sum_{\varepsilon}\Theta(-\varepsilon(\varepsilon+\Omega))\int d\hat{\Omega}_d\, k_{F\alpha}\, k_{F\beta}\frac{2\pi\tau_0}{1+\Omega\tau_0}. \tag{3.43}$$

The Heaviside function enforces the condition that ε and $\varepsilon+\Omega$ have opposite signs.

The angular integral is performed trivially to yield $k_F^2\delta_{\alpha\beta}/d$, while the ε sum produces the contribution

$$T\sum_{\varepsilon}\Theta(-\varepsilon(\varepsilon+\Omega)) = T\sum_{-\Omega<\varepsilon<0}1 = T\sum_{n=-\frac{\Omega}{2\pi T}}^{-1}1 = \frac{\Omega}{2\pi}. \tag{3.44}$$

The resulting response function is then

$$K_{\alpha\beta}(i\Omega) = \left[\frac{n_e e^2}{m_e} + \frac{\Omega}{1+\Omega\tau_0}\frac{n_e e^2\tau_0}{m_e}\right]\delta_{\alpha\beta}. \tag{3.45}$$

Clearly the diamagnetic term has not been cancelled, and $K_{\alpha\beta}$ does not vanish in the zero frequency limit. If we were allowed to simply ignore the diamagnetic term, then performing analytic continuation to the upper half plane, $i\Omega \to \omega + i\delta$ (ω is a continuous

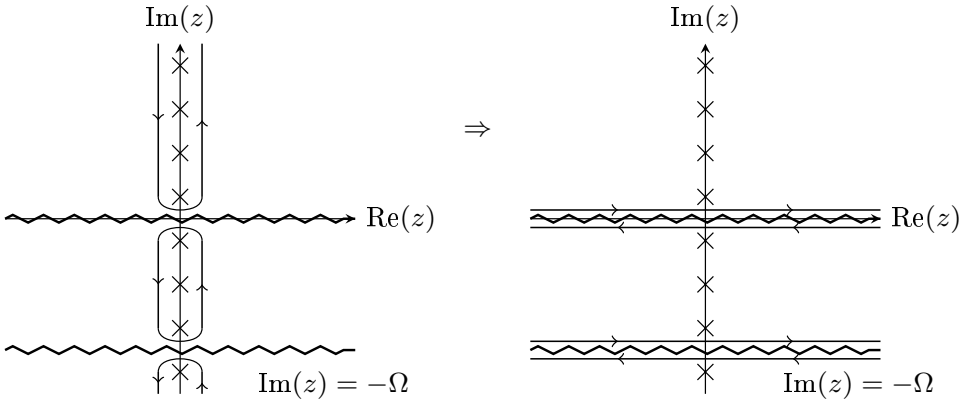

Figure 3.8: Analytic structure of the ε sum in eq. 3.41. The zigzags represent branch cuts along the real axis and the line where $\mathrm{Im}(z) = -\Omega$, due to the Green's functions $G(\mathbf{k}, i\varepsilon)$ and $G(\mathbf{k}, i\varepsilon + i\Omega)$ respectively. Crosses denote poles.

real frequency), would yield a conductivity tensor of the form

$$\sigma_{\alpha\beta}(\omega) = \frac{n_e e^2 \tau_0}{m_e} \frac{1}{1 - i\omega\tau_0} \delta_{\alpha\beta}, \tag{3.46}$$

which is the correct result for the AC Drude conductivity. We now need to understand how to cancel the diamagnetic term so that we can have confidence in this method of calculating the electrical conductivity.

3.2.2 A Careful Treatment

For this careful treatment of the electrical conductivity, we use the ideas presented by Rickayzen [29] and Altland and Simons [34].

In order to compute the frequency sum first, we begin by analytically continuing the sum into complex frequency space using the relation,

$$T \sum_{\varepsilon} F(i\varepsilon) = -\frac{1}{2\pi i} \oint_C dz F(z) f(z), \tag{3.47}$$

where $F(i\varepsilon)$ is some generic function, $f(z)$ is the Fermi function, and C is the contour enclosing the poles along the imaginary axis (located at $z = i\varepsilon$) in the anti-clockwise

direction (see the left diagram in fig. 3.8).[15] We may deform the contour to run either side of the branch cuts along the real axis and $\mathrm{Im}(z) = -\Omega$, as illustrated in fig. 3.8, to yield

$$\begin{aligned}\mathcal{G}_{\alpha\beta}(i\Omega) =& \frac{e^2 N(0) i}{\pi m_e^2} \int d\hat{\Omega}_d \, k_{F\alpha} \, k_{F\beta} \int_{-\infty}^{+\infty} d\xi \\ &\times \Bigg\{ \int_{-\infty}^{+\infty} dz \left[G^R(\mathbf{k}, z) - G^A(\mathbf{k}, z) \right] G^R(\mathbf{k}, z + i\Omega) f(z) \\ &\quad + \int_{-\infty - i\Omega}^{+\infty - i\Omega} dz \left[G^R(\mathbf{k}, z + i\Omega) - G^A(\mathbf{k}, z + i\Omega) \right] G^A(\mathbf{k}, z) f(z) \Bigg\}.\end{aligned} \tag{3.48}$$

Here we have again linearised the momentum integral about the Fermi surface. We next shift $z \to z - i\Omega$ in the second frequency integral, noting that $f(z - i\Omega) = f(z)$, and then analytically continue $i\Omega \to \omega + i\delta$, to obtain

$$\begin{aligned}\mathcal{G}^R_{\alpha\beta}(\omega) =& \frac{e^2 N(0) i}{\pi m_e^2} \int d\hat{\Omega}_d \, k_{F\alpha} \, k_{F\beta} \int_{-\infty}^{+\infty} d\xi \\ &\times \int_{-\infty}^{+\infty} dz \left[G^R(\mathbf{k}, z) - G^A(\mathbf{k}, z) \right] \left[G^R(\mathbf{k}, z + \omega) + G^A(\mathbf{k}, z - \omega) \right] f(z).\end{aligned} \tag{3.49}$$

Let us first concentrate on the $G^R G^R$ term. We initially consider the case where $\omega = 0$, for which the integral has the form

$$\begin{aligned}\int_{-\infty}^{+\infty} d\xi \int_{-\infty}^{+\infty} dz \, G^R(\mathbf{k}, z)^2 f(z) &= \int_{-\infty}^{+\infty} d\xi \int_{-\infty}^{+\infty} \frac{dz}{\left(z - \xi + \frac{i}{2\tau_0} \right)^2} f(z) \\ &= - \int_{-\infty}^{+\infty} d\xi \int_{-\infty}^{+\infty} dz \frac{d}{dz} \left[\frac{1}{z - \xi + \frac{i}{2\tau_0}} \right] f(z).\end{aligned} \tag{3.50}$$

Performing integration by parts on the z integral generates a vanishing boundary term and shifts the derivative onto $f(z)$. Due to the presence of $f'(z)$, which falls off exponentially at infinity, there is now sufficient convergence to interchange the order of integration.

[15] This way of dealing with sums is explored in greater depth in appendix M.

Thus the $G^R G^R$ term gives rise to the contribution

$$\int_{-\infty}^{+\infty} dz \, \frac{df}{dz} \int_{-\infty}^{+\infty} \frac{d\xi}{z - \xi + \frac{i}{2\tau_0}} = \int_{-\infty}^{+\infty} dz \, \frac{df}{dz}(-i\pi) = i\pi. \tag{3.51}$$

We now consider the case $\omega \neq 0$ by expanding $G^R(\mathbf{k}, z + \omega)$ as a power series in ω,

$$\begin{aligned} G^R(\mathbf{k}, z+\omega) G^R(\mathbf{k}, z) &= \sum_{n=0}^{\infty} \frac{(-1)^n \omega^n}{\left(z - \xi_{\mathbf{k}} + \frac{i}{2\tau_0}\right)^{n+2}} \\ &= \frac{d}{dz} \sum_{n=0}^{\infty} \frac{(-1)^{n+1}}{n+1} \frac{\omega^n}{\left(z - \xi_{\mathbf{k}} + \frac{i}{2\tau_0}\right)^{n+1}}. \end{aligned} \tag{3.52}$$

Proceeding as before, we perform integration by parts upon the z integral with eq. 3.52 as the integrand; this again shifts the derivative onto $f(z)$ allowing us to swap the orders of integration. At this point it is clear that all terms of the sum with $n \geq 1$ fall off sufficiently rapidly at infinity so that they contribute nothing to the integral.[16] Therefore, all non-trivial behaviour of the $G^R G^R$ term comes from the $n = 0$ piece, and has already been derived in the $\omega = 0$ case.

An entirely equivalent approach can be used for the $-G^A G^A$ term to produce an identical contribution of $i\pi$. Thus, the completely retarded and advanced pieces of eq. 3.49 lead to the contribution

$$\frac{e^2 N(0) i}{\pi m_e^2} \int d\hat{\Omega}_d \, k_{F\alpha} \, k_{F\beta} (2\pi i) = -\frac{n e^2}{m_e} \delta_{\alpha\beta}, \tag{3.53}$$

where we note that $n = 2N(0)k_F^2/(m_e d)$. Recalling eq. 3.29b, we see that this contribution exactly cancels the diamagnetic term appearing in the electromagnetic response function. Let us now compute the $G^R G^A$ terms of eq. 3.49 to check that no unexpected divergences remain.

[16] This is most easily seen by using the calculus of residues on the ξ integral, and noting that only the $n = 0$ term falls off logarithmically. Hence, even if the full contour is closed in the empty half plane, the contour at infinity gives a non-zero result. All other terms vanish faster than ξ^{-1} at infinity, meaning that the contour at infinity gives no contribution and so the full contour may be closed in the half plane containing no poles.

We combine the two $G^R G^A$ terms by letting $z \to z + \omega$ in the $G^R(\mathbf{k}, z)G^A(\mathbf{k}, z - \omega)$ piece, to give

$$\int_{-\infty}^{+\infty} d\xi \int_{-\infty}^{+\infty} dz\, G^R(\mathbf{k}, z + \omega)G^A(\mathbf{k}, z)[f(z + \omega) - f(z)]. \tag{3.54}$$

Conveniently, the difference between Fermi functions falls off exponentially at infinity, allowing us to swap the order of integration without consequence. We therefore perform the ξ integral first, followed by the z integral, before finally evaluating the angular integral. By using eqs. 3.29b and 3.53, and the relation

$$\int_{-\infty}^{+\infty} dz\, [f(z + \omega) - f(z)] = \omega, \tag{3.55}$$

we find

$$K^R_{\alpha\beta}(\omega) = \frac{n_e e^2 \tau_0}{m_e} \frac{-i\omega}{1 - i\omega\tau_0} \delta_{\alpha\beta}. \tag{3.56}$$

It is clear that the response function vanishes in the limit $\omega = 0$, and hence the system described is in the normal state.

Finally, by recalling that $K^R_{\alpha\beta}(\omega) = -i\omega\sigma_{\alpha\beta}(\omega)$, we arrive at the familiar AC Drude conductivity

$$\sigma_{\alpha\beta}(\omega) = \frac{n_e e^2 \tau_0}{m_e} \frac{1}{1 - i\omega\tau_0} \delta_{\alpha\beta}. \tag{3.57}$$

The DC Drude conductivity given in eq. 3.1 is then reproduced by considering the diagonal components of $\sigma_{\alpha\beta}(\omega = 0)$.

In summary, we have shown that diagrammatic QFT can be used to successfully reproduce the well-known Drude formula, although issues of convergence do arise. Nonetheless, with due care and attention, we can work around these difficulties so that no problems in the methodology remain, and we can put faith into this approach to calculating the electrical conductivity. Thankfully, when considering more complicated effects, convergence issues do not arise, as we have a large enough number of Green's functions to ensure that the integrands decay rapidly enough at infinity. So, from here on, we may freely swap the

orders of integration over frequency and momentum.[17] As a final point, we introduce a useful relation, after which we shall evaluate the corrections to the electrical conductivity that arise at low temperatures.

3.2.3 The Einstein Relation

An alternative way to write the electrical conductivity of a system in the absence of interference and interactions is via the Einstein relation [38],

$$\sigma = 2e^2 N(0)\mathcal{D}, \tag{3.58}$$

where $\mathcal{D}$ is the diffusion constant. For a d dimensional system

$$\mathcal{D} = \frac{v_F^2 \tau_0}{d}. \tag{3.59}$$

Substituting this into the Einstein relation gives the familiar Drude conductivity.

One advantage to using this relation is that it allows us to compare the sizes of conductivity corrections to the Drude result with greater ease, as they are typically written in terms of $\mathcal{D}$ as opposed to the the electron number density. Comparison of σ_0 to the corrections will allow us to identify any parameters that lead to the corrections being parametrically small, and in what dimensionalities the corrections are small.

Finally, this relation will prove extremely useful when trying to relate homogeneous and granular systems. In the granular analogue to the Drude conductivity, we will find that $\mathcal{D}$ will be replaced by an effective (tunnelling) diffusion constant.

[17] It is quite ironic that the simplest result, or rather the system with the simplest physics, has the most involved calculation in the sense that it requires the most appreciation of technical mathematics.

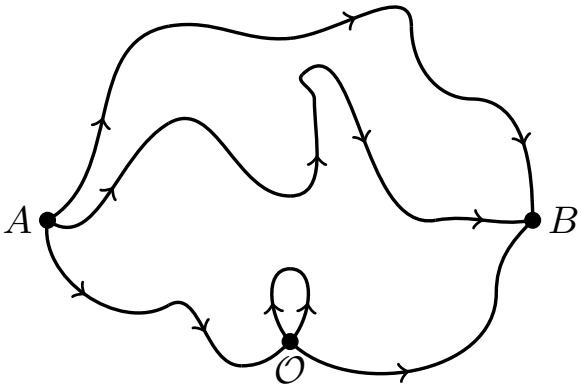

Figure 3.9: Example paths taken by a particle taken from A to B. The point $\mathcal{O}$ is a point of self-intersection for the bottom path.

3.3 Weak Localisation

Before we consider the more obvious effects of electron-electron interactions on the electrical conductivity, let us continue to focus on one-body effects. Specifically, in this section we will turn our attention to the effects of quantum interference. Put simply, this is the interference between all possible paths a particle can take when propagating from one point to another. We illustrate this idea of paths in fig. 3.9.

To get a more physical handle on this phenomenon, let us use the interpretation given in [39] and consider the probability of a particle travelling from point A to point B,

$$P(A \to B) = \Big| \sum_i A_i \Big|^2 = \sum_i |A_i|^2 + \sum_{i \neq j} A_i A_j^*, \tag{3.60}$$

where A_i is the probability amplitude of the particle travelling along the i^{th} path. The first term of the final expression in eq. 3.60 is just the sum of probabilities of the particle travelling down each possible path, whilst the second term represents interference between the different paths. Most paths have very little interference with one another due to a lack of coherence, and so their contribution to the probability is negligible. However, certain paths are coherent with each other, such as the self-intersecting path illustrated at the bottom of fig. 3.9. Consequently, we cannot neglect the contribution of these paths to the probability, and it is these terms that lead to quantum interference in disordered media.

Looking at the self-intersecting path in fig. 3.9 more closely, we can see that the particle can traverse the loop in either the clockwise or anticlockwise direction. Let us assign the probability amplitudes $\widetilde{A}_1$ and $\widetilde{A}_2$ to the two different directions, which are associated with a particle moving from A to $\mathcal{O}$. The probability of finding the particle at $\mathcal{O}$ by travelling these paths is then

$$|\widetilde{A}_1|^2 + |\widetilde{A}_2|^2 + 2\mathrm{Re}[\widetilde{A}_1\widetilde{A}_2^*] = 4|\widetilde{A}_1|^2, \tag{3.61}$$

where we used the fact that both paths are equally likely and (phase) coherent with one another, so $\widetilde{A}_1 = \widetilde{A}_2$. Therefore the probability of finding a particle at the point of self-intersection is twice that of a pair of independent paths. Hence, the particle has an enhanced probability of being found at the point $\mathcal{O}$. Consequently, the probability of finding the particle at B must be reduced, and so we expect the effects of quantum interference to lead to a reduction in the electrical conductivity.[18]

Given that a particle is more likely to be found at points of self-intersection, we can think of it as becoming localised about these points. We therefore refer to this phenomenon as localisation. The scattering strength then defines whether the particles are strongly confined or not. For weak scattering, particles are only weakly localised, that is to say that the wave function is significant inside a somewhat extended region, with characteristic size ξ_{loc} (localisation length), about the point $\mathcal{O}$ and negligible beyond this region. If the scattering is strong, then the particles are confined to a much smaller region and ξ_{loc} is much smaller. By continuing to increase the scattering strength we can induce a metal-insulator transition (MIT) due to Anderson localisation [40]. We shall not discuss the role of MITs in this thesis as our focus is on materials deep inside the metallic regime.[19] This limit of weak scattering we consider thus gives rise to the name of weak localisation

[18]It might seem like we could construct a similar counter-argument using paths that self-intersect at the point B. However, the point B is the point of observation, so once a particle passes through B for the first time we are no longer concerned with any subsequent motion of the particle as it has now reached the point of interest.

[19]For the reader wishing to learn more about the Anderson transition, Lee and Ramikrishnan [41] provide a good review of weak localisation and a discussion of how renormalisation groups may be used to move to the strong scattering limit.

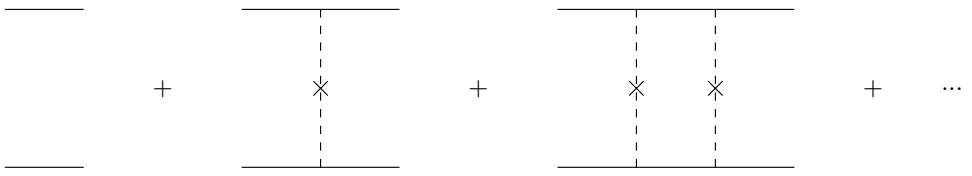

Figure 3.10: Generic form of a ladder diagram for impurity scattering.

(WL).[20] These ideas are a brief overview of those detailed in [39, 43].

So how can we include the effects of quantum interference in diagrammatic calculations? To do this we will need to construct a pair of two-body propagators that describe the diffusive motion of electrons and holes in metals. We call the particle-particle (hole-hole) propagator a cooperon, whilst the particle-hole propagator is referred to as a diffuson. These propagators play a vital role in all phenomena in disordered media, due to the infinitely many ways we may choose to correlate the impurity scattering events in different Green's functions. Hence, before we delve into the diagrammatic calculation of the weak localisation correction to conductivity, let us first derive these propagators.

3.3.1 The Cooperon & Diffuson

We might expect that the diagrams for interference appear as a sum of ladders of impurity lines between a pair of particle lines, or a particle and hole line, with each successive term adding an extra rung. This idea is illustrated in fig. 3.10, and is correct in the weak scattering limit we are considering. The details on how to derive these propagators' diagrammatic series can be found in [34]. For now we shall give physical interpretations of these propagators, and how to calculate their diagrammatic series.

Following [34], both of these propagators appear in the calculation of the density-density correlator,

$$\langle \delta\rho(\mathbf{r},\tau)\delta\rho(\mathbf{0},0)\rangle_{\text{dis}}\,, \tag{3.62}$$

where $\delta\rho(\mathbf{r},\tau) = \rho(\mathbf{r},\tau) - \langle\rho(\mathbf{r},\tau)\rangle$ is the local fluctuation of the density. Considering the

[20] An equivalent interpretation of WL is given by Bergmann [42] in terms of coherent backscattering events.

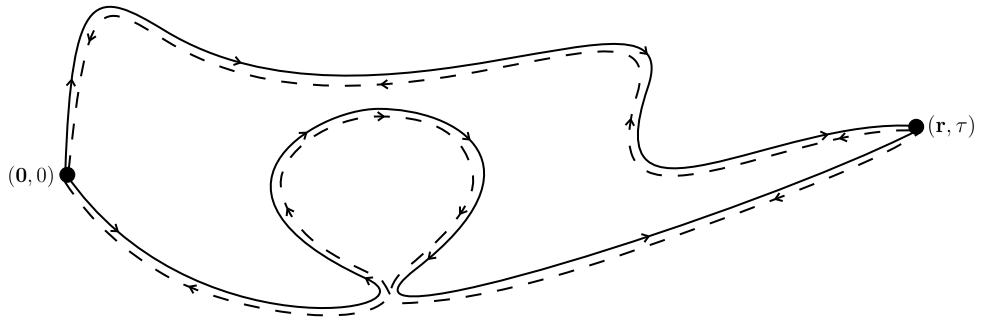

Figure 3.11: Explicit paths taken by particles and holes when travelling from one point to another. The solid line represents a particle's motion from $(\mathbf{0}, 0)$ to $(\mathbf{r}, \tau)$, whilst a dashed line represents a hole's motion from $(\mathbf{0}, 0)$ to $(\mathbf{r}, \tau)$. The arrows depict the direction taken in a particle interpretation of the paths. Hence, the solid lines point from $(\mathbf{0}, 0)$ to $(\mathbf{r}, \tau)$, whereas the dashed lines point from $(\mathbf{r}, \tau)$ to $(\mathbf{0}, 0)$ due to holes being particles travelling backwards in time.

quantum average explicitly in eq. 3.62, and applying Wick's theorem yields

$$\left\langle \left\langle \psi^\dagger(\mathbf{r}, \tau)\psi(\mathbf{0}, 0) \right\rangle \left\langle \psi(\mathbf{r}, \tau)\psi^\dagger(\mathbf{0}, 0) \right\rangle \right\rangle_{\text{dis}}^{(0)}, \tag{3.63}$$

which clearly describes a particle moving from $(\mathbf{0}, 0)$ to $(\mathbf{r}, \tau)$, and a hole moving from $(\mathbf{0}, 0)$ to $(\mathbf{r}, \tau)$. This correlator can be related to $P(A \to B)$, and so can be interpreted as the interference between the paths taken by the particle (which carry probability amplitudes A_i), with the paths taken by the hole (which carry probability amplitudes A_i^*).

The first term of eq. 3.60 corresponds to a particle traversing a path from $(\mathbf{0}, 0)$ to $(\mathbf{r}, \tau)$, whilst the hole traverses the same path in the same direction, as in the upper pair of paths in fig. 3.11. This is just particle-hole interference, and is described by the diffuson. If we consider the second term of eq. 3.60, the only significant contributions are from self-intersecting paths: the particle traverses the loop in one direction, the hole in the other, as shown in lower part of fig. 3.11, since we can interpret the hole as a particle moving in the opposite direction to the hole, this leads to particle-particle interference along the loop, which is described by the cooperon. In both cases, the leading-order behaviour is given by non-crossing impurity scattering lines between particle and hole lines (diffuson), or particle lines (cooperon).[21]

[21]Note that the impurity averaging still correlates the impurities inside a single Green's function at the

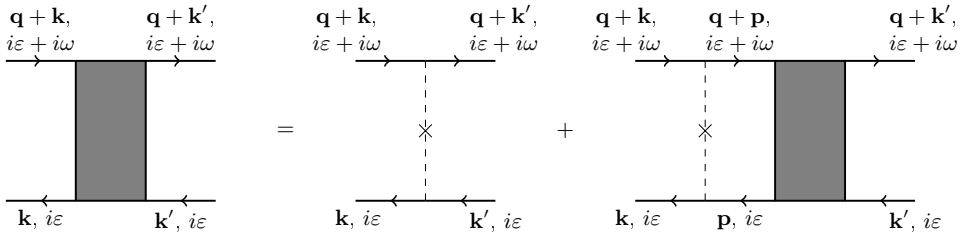

Figure 3.12: Diagrammatic series for the open diffuson, where the solid lines are disorder-averaged electron Green's functions and the grey region is the diffuson $\widetilde{D}(\mathbf{q}, i\varepsilon + i\omega, i\varepsilon)$.

We define the diffuson, $\widetilde{D}(\mathbf{q}, i\varepsilon + i\omega, i\varepsilon)$, via the diagrammatic series in fig. 3.12. As for the expansion of the electron Green's function, we are left with a Dyson equation,

$$\begin{aligned} \widetilde{D}(\mathbf{q}, i\varepsilon + i\omega, i\varepsilon) &= \frac{1}{2\pi N(0)\tau_0} + \frac{1}{2\pi N(0)\tau_0}\,\Sigma_D(\mathbf{q}, i\varepsilon + i\omega, i\varepsilon)\,\widetilde{D}(\mathbf{q}, i\varepsilon + i\omega, i\varepsilon) \\ \Rightarrow\ \widetilde{D}(\mathbf{q}, i\varepsilon + i\omega, i\varepsilon) &= \Big[2\pi N(0)\tau_0 - \Sigma_D(\mathbf{q}, i\varepsilon + i\omega, i\varepsilon)\Big]^{-1}, \end{aligned} \tag{3.64}$$

where

$$\Sigma_D(\mathbf{q}, i\varepsilon + i\omega, i\varepsilon) = \sum_{\mathbf{p}} G(\mathbf{p} + \mathbf{q}, i\varepsilon + i\omega) G(\mathbf{p}, i\varepsilon), \tag{3.65}$$

is the diffuson's self-energy. Note that ω must be a bosonic Matsubara frequency, so that ε and $\varepsilon + \omega$ are both fermionic Matsubara frequencies. This makes sense as the diffuson is a quasiparticle formed of two fermions, and hence we expect it to be bosonic in nature.

We now approximate the self-energy's momentum sum by an energy integral linearised around the Fermi surface. To do this, we first note that the energy appearing in the first Green's function above is a function of both $\mathbf{p}$ and $\mathbf{q}$, whilst the second Green's function depends only on $\mathbf{p}$. The main contribution to eq. 3.65 comes from energies, $\xi_{\mathbf{p}}$, within τ_0^{-1} of the Fermi energy; hence we are only interested in energies with $\xi_{\mathbf{p}} \ll \tau_0^{-1}$, or, equivalently, momenta such that $|\mathbf{p} - \mathbf{k}_F| \ll l^{-1}$.[22] This is due to $G(\mathbf{p}, i\varepsilon)$ having a similar form to a Lorentzian peaked around the Fermi surface with a width $\sim \tau_0^{-1}$ in energy, or $\sim l^{-1}$ in momentum. Given that $l^{-1} \ll k_F$ in the weak disorder limit, we may

same time. However, given that we can sum over all these possibilities, the disorder-averaged Green's function will simply be recreated, and so the scatterings between Green's functions will just be a ladder of scattering events will be between disorder-averaged Green's functions.

[22] In other words, only the electrons near the Fermi surface contribute to transport phenomena.

approximate $|\mathbf{p}| \sim k_F$, and take $|\mathbf{p}| = k_F$ where appropriate.[23] Since $\xi_{\mathbf{p}+\mathbf{q}}$ must also lie within this region, we approximate the integral in the limit of small $\mathbf{q}$, $|\mathbf{q}| \lesssim l^{-1} \ll k_F$.[24]

Using the fact that $|\mathbf{q}| \ll |\mathbf{p}| \sim k_F$, we approximate $\xi_{\mathbf{p}+\mathbf{q}} \simeq \xi_{\mathbf{p}} + \mathbf{v}_F \cdot \mathbf{q}$, where $\mathbf{v}_F$ is the Fermi velocity. We now replace the momentum sum in eq. 3.65 with an energy integral and an angular average,

$$\Sigma_D(\mathbf{q}, i\varepsilon + i\omega, i\varepsilon) = N(0) \int_{-\infty}^{+\infty} d\xi \int d\hat{\Omega}_d \left[\frac{1}{i\varepsilon - \xi + \frac{i}{2\tau_0}\mathrm{sgn}(\varepsilon)} \times \frac{1}{i\varepsilon + i\omega - \xi - \mathbf{v}_F \cdot \mathbf{q} + \frac{i}{2\tau_0}\mathrm{sgn}(\varepsilon + \omega)} \right]. \tag{3.66}$$

If the frequencies, $\varepsilon + \omega$ and ε, have the same sign, then both poles of the integrand in eq. 3.66 lie in the same half-plane of ξ. Since we have the freedom to choose a contour that encloses the empty half-plane, this integral vanishes. Consequently, all Green's functions that interfere with one another must have opposite frequency signs to generate non-zero contributions. The diffuson therefore carries the Heaviside factor $\Theta(-\varepsilon(\varepsilon + \omega))$.[25]

Let us now consider the case where $\varepsilon + \omega$ and ε have opposite signs, and assume that $\omega > 0$, i.e. $\varepsilon < 0$, $\varepsilon + \omega > 0$. The first Green's function in eq. 3.66 then has a pole in the lower half-plane at $\xi = i\varepsilon - i/(2\tau_0)$, whilst the second Green's function has a pole in the upper half-plane at $\xi = \mathbf{v}_F \cdot \mathbf{q} + i\varepsilon + i\omega + i/(2\tau_0)$. Evaluating the ξ integral by closing the contour in the lower half-plane gives,

$$\Sigma_D^{(\omega>0)}(\mathbf{q}, i\varepsilon + i\omega, i\varepsilon) = N(0) \int d\hat{\Omega}_d \, \frac{2\pi\tau_0}{1 + \omega\,\tau_0 + i\,\mathbf{v}_F \cdot \mathbf{q}\,\tau_0}. \tag{3.67}$$

[23] Since $\xi_{\mathbf{p}}$ is the variable we are integrating over, we don't want to set $|\mathbf{p}| = k_F$ inside it as this will just give $\xi_{\mathbf{p}} = 0$, meaning integration loses its purpose. Instead, we appreciate that $\xi_{\mathbf{p}}$ is small close to the Fermi surface, and so variations of $\xi_{\mathbf{p}}$ in this region are important. Hence, we treat $\xi_{\mathbf{p}}$ as though it is unaffected by this linearisation and neglect it when it is compared to a large energy scale, such as the Fermi energy, due to its small size in this region.

[24] The statement that $|\mathbf{q}| \lesssim l^{-1}$ sets l^{-1} as the absolute maximum value of $|\mathbf{q}|$ in the diffusive limit.

[25] Technically speaking, the self-energy carries this factor. However, in defining the open diffuson to carry this Heaviside factor we only neglect the first term (a single scattering event) of the series when the frequencies have the same sign. This is a negligible change, as a Dyson equation is analogous to a geometric series with a large result (courtesy of the diffusive limit defined in eq. 3.68). So by subtracting the first term from the result we find a negligible change. Hence, we can ignore the first term without much consequence.

At this point we make use of the *diffusive limit* to approximate this integral.[26] The diffusive limit is defined as

$$|\omega|,\, T \ll \frac{1}{\tau_0}, \qquad\qquad q \ll \frac{1}{l} \quad \Leftrightarrow \quad \mathcal{D}q^2 \ll \frac{1}{\tau_0}. \tag{3.68}$$

We now expand the integrand to leading order in ω and $\mathbf{q}$ (noting that $l = v_F\tau_0$),

$$\Sigma_D^{(\omega>0)}(\mathbf{q}, i\varepsilon + i\omega, i\varepsilon) = 2\pi N(0)\tau_0 \int d\hat{\Omega}_d \left(1 - \omega\,\tau_0 - i\,\mathbf{v}_F\cdot\mathbf{q}\,\tau_0 - (\mathbf{v}_F\cdot\mathbf{q})^2\tau_0^2\right). \tag{3.69}$$

To evaluate the angular averages, we note that

$$\int d\hat{\Omega}_d\, 1 = 1, \qquad\qquad \int d\hat{\Omega}_d\, (\mathbf{v}_F\cdot\mathbf{q}) = 0, \qquad\qquad \int d\hat{\Omega}_d\, (\mathbf{v}_F\cdot\mathbf{q})^2 = \frac{v_F^2 q^2}{d}, \tag{3.70}$$

and hence,

$$\Sigma_D^{(\omega>0)}(\mathbf{q}, i\varepsilon + i\omega, i\varepsilon) = 2\pi N(0)\tau_0 \left(1 - \omega\,\tau_0 - \frac{q^2 v_F^2}{d}\tau_0^2\right). \tag{3.71}$$

If we were to assume that $\omega < 0$, we would find that ω is replaced by $-\omega$ in eq. 3.71, so

$$\Sigma_D(\mathbf{q}, i\varepsilon + i\omega, i\varepsilon) = 2\pi N(0)\tau_0 \left(1 - |\omega|\,\tau_0 - \frac{q^2 v_F^2}{d}\tau_0^2\right). \tag{3.72}$$

From the diffuson self-energy above, we finally obtain the diffuson propagator,

$$\widetilde{D}(\mathbf{q}, i\varepsilon + i\omega, i\varepsilon) = \frac{1}{2\pi N(0)\tau_0^2}\frac{1}{\mathcal{D}q^2 + |\omega|}\Theta(-\varepsilon(\varepsilon+\omega)) \equiv \widetilde{D}(\mathbf{q}, i\omega)\Theta(-\varepsilon(\varepsilon+\omega)). \tag{3.73}$$

We introduce $\widetilde{D}(\mathbf{q}, i\omega)$ as a shorthand for the diffuson without the Heaviside function.

For convenience, we also define the diffuson for a diagram with a single closed end, as shown in fig. 3.13. For this we simply have to sum over the additional pair of internal Green's functions, which is equivalent to adding an extra factor of Σ_D. However, the order unity term will not be cancelled in this extra factor, and so we can neglect the ω

[26] With the sheer number of approximations and limits we take in condensed matter theory, physics begins to feel more like an art than a science. Then again, we do try to justify all that we do, and our results are usually in the ball park.

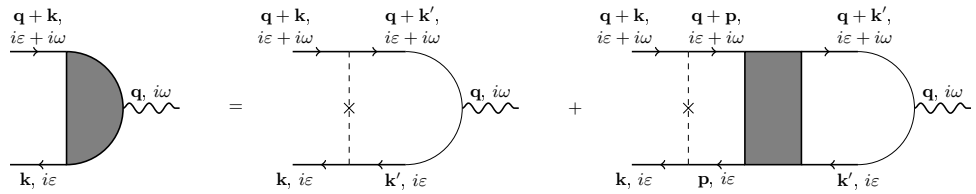

Figure 3.13: Diagrammatic series for the half closed diffuson, where the grey region on the left side of the equation is the diffuson $D(\mathbf{q}, i\varepsilon + i\omega, i\varepsilon)$. The wavy line is a generic interaction.

and $\mathcal{D}q^2$ terms in the diffusive limit. Therefore, we obtain this closed diffuson by simply multiplying $\widetilde{D}(\mathbf{q}, i\varepsilon + i\omega, i\varepsilon)$ by $2\pi N(0)\tau_0$ to give,

$$D(\mathbf{q}, i\varepsilon + i\omega, i\varepsilon) = \frac{1}{\tau_0}\frac{1}{\mathcal{D}q^2 + |\omega|}\Theta(-\varepsilon(\varepsilon + \omega)) \equiv D(\mathbf{q}, i\omega)\Theta(-\varepsilon(\varepsilon + \omega)). \tag{3.74}$$

This form of diffuson occurs most often in our calculations, as it corresponds to a vertex correction or the dressing of an interaction vertex.[27]

Alternatively, given $|\mathbf{q}| \ll |\mathbf{k}| \sim k_F$, we may neglect the small momentum, $\mathbf{q}$, appearing in the extra pair of Green's functions. We then use the identity

$$\sum_{\mathbf{k}} G^+(\mathbf{k})^m G^-(\mathbf{k})^n = 2\pi N(0)\tau_0 \frac{(m+n-2)!}{(m-1)!(n-1)!}(-i\tau_0)^{m-1}(i\tau_0)^{n-1} \tag{3.75}$$

where G^+ and G^- are disordered electron Green's functions with positive and negative Matsubara frequencies respectively, to evaluate momentum sum of the Green's functions. This identity is derived in appendix M.

At this point we turn our attention to the cooperon. So far we have ignored all terms involving crossed scattering events; let us consider a maximally crossed diagram. As usual, scatterings are paired, such that the leftmost scattering event on the top line is connected to the rightmost on the bottom line, and we proceed to pair the rest of the events so that the n^{th} leftmost event on the top is correlated to the n^{th} rightmost event on the bottom. We illustrate this idea in fig. 3.14. Due to the topological nature of

[27]The Heaviside appearing in the diffuson with a closed end is now exact, unlike the diffuson with two open ends. This is due to the two extra Green's functions being summed over. If they were of the same sign, then the integral would simply vanish as in the diffuson's self-energy.

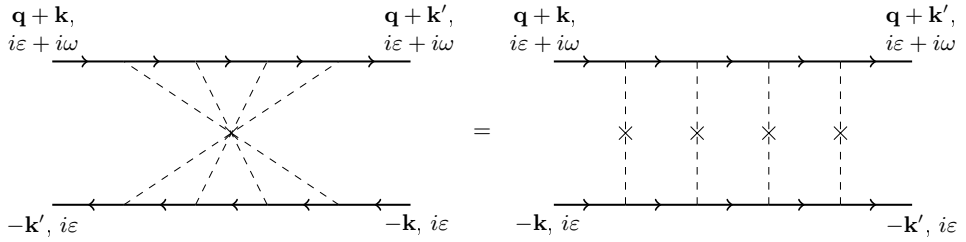

Figure 3.14: A maximally crossed diagram involving four sets of scattering events, and its unravelled form.

diagrammatics, we can unwrap maximally crossed diagrams to produce a ladder diagram between two particles, rather than a particle and a hole. In fact, the cooperon is related to the diffuson via the time reversal of one of the propagators.[28]

We therefore define the cooperon according to the series in fig. 3.15a. Following the same arguments as for the diffuson we quickly arrive at

$$\widetilde{C}(\mathbf{q}, i\varepsilon + i\omega, i\varepsilon) = \frac{1}{2\pi N(0)\tau_0^2}\frac{1}{\mathcal{D}q^2 + |\omega|}\Theta(-\varepsilon(\varepsilon+\omega)) \equiv \widetilde{C}(\mathbf{q}, i\omega)\Theta(-\varepsilon(\varepsilon+\omega)). \quad (3.76)$$

In a similar vein, we can define the cooperon with a closed side by the series in fig. 3.15b,

$$C(\mathbf{q}, i\varepsilon + i\omega, i\varepsilon) = \frac{1}{\tau_0}\frac{1}{\mathcal{D}q^2 + |\omega|}\Theta(-\varepsilon(\varepsilon+\omega)) \equiv C(\mathbf{q}, i\omega)\Theta(-\varepsilon(\varepsilon+\omega)). \quad (3.77)$$

Both of these diffusive propagators possess a pole as $\omega, |\mathbf{q}| \to 0$, usually referred to as a diffusive pole. In practice this is not an issue for the diffuson, but becomes problematic in calculations that involve the cooperon.[29] This arises due to the approximations we make when computing the diffusive momentum integral (the $\mathbf{q}$ integral), as explained in [31]. Usually we take the radial integral to be over the range $[0, \infty]$, where we would then find an infra-red divergence. However, the cooperon is related to phase coherence effects, and so cannot live longer than the time it takes particles to lose phase coherence; this is the phase coherence lifetime, τ_ϕ. We should therefore not include modes of infinitely

[28] Hence the change of propagator direction and reversal of momentum.

[29] The reason the diffuson is immune to this issue is related to Ward identities, which provide conservation laws to be obeyed by the propagators. In the case of the diffuson, the appropriate conserved quantity is particle number.

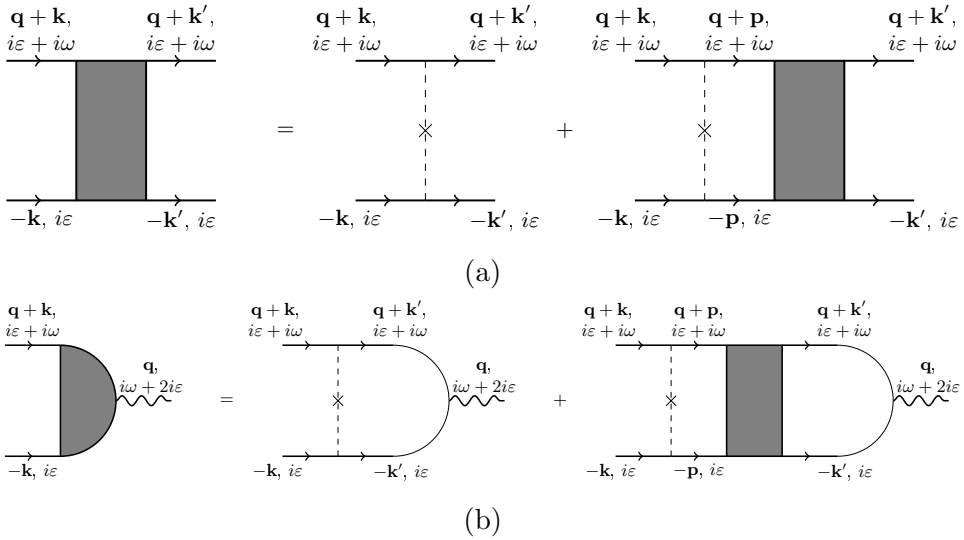

Figure 3.15: Diagrammatic series for the open cooperon (top) and half closed cooperon (bottom).

long wavelength in our integrals, but cut off the integrals at the phase coherence length $l_\phi = \sqrt{\mathcal{D}\tau_\phi}$ (i.e. $q_{\min} = l_\phi^{-1}$). This is the argument given in [31].

We can leave the lower limit of the integral unchanged, if we include the phase breaking rate, τ_ϕ^{-1}, in the denominator of the cooperon,

$$\widetilde{C}(\mathbf{q}, i\varepsilon + i\omega, i\varepsilon) = \frac{1}{2\pi N(0)\tau_0^2} \frac{1}{Dq^2 + |\omega| + \tau_\phi^{-1}} \Theta(-\varepsilon(\varepsilon + \omega)), \tag{3.78a}$$

$$C(\mathbf{q}, i\varepsilon + i\omega, i\varepsilon) = \frac{1}{\tau_0} \frac{1}{Dq^2 + |\omega| + \tau_\phi^{-1}} \Theta(-\varepsilon(\varepsilon + \omega)). \tag{3.78b}$$

An equivalent interpretation is given by Patton [44]. Here the cooperon is interpreted as the lifetime of a diffusive particle-particle mode. Specifically, the lifetime for a particle with momentum $\mathbf{q}$ is given by $\tau_0 C(q, \omega \to 0)$, which is just $1/(\mathcal{D}q^2)$ in the absence of phase breaking. However, as discussed above, this lifetime cannot exceed τ_ϕ, so these particle-particle modes must have an effective lifetime of $(\mathcal{D}q^2 + \tau_\phi^{-1})^{-1}$. From the nature of τ_ϕ, we can see the equivalence of Bergmann's interpretation of WL [42] as coherent backscattering events to the picture of self-intersecting paths.

Several physical mechanisms lead to phase breaking, with the total phase breaking rate

being given by their sum. Examples include elastic scattering from magnetic impurities, applied magnetic fields, inelastic EEI scattering, and superconducting fluctuations, which all decrease τ_ϕ. The exact temperature dependence of τ_ϕ^{-1} is thus quite non-trivial and extremely system-dependent. We will return to the calculation of τ_ϕ^{-1} in section 3.6. For the time being, we note that τ_ϕ^{-1} decreases with decreasing temperature.[30]

As a final remark about these diffusive propagators, let us consider the consequences of the Heaviside function appearing in both. When performing diagrammatic calculations, any cooperons or diffusons present will force the Matsubara frequencies of the Green's functions entering them to be of opposite sign. We can therefore break up the frequency sums of the diagrams into different regions, corresponding to the combinations of frequency signs that give a non-zero result. In general, these sign combinations will have to be treated separately, and then summed to give the total contribution of a single diagram. This organisation is used in all our calculations, and may be seen explicitly in the calculation of the EEI and superconducting fluctuation corrections in sections 3.4 and 3.5, as well as in appendices G and I. This is vital in allowing us to being able to compute the different diagrams in a tractable manner.

3.3.2 Weak Localisation Corrections

We start our calculation of the WL corrections by reconsidering the disorder average taken to obtain the Drude diagram. This time we consider interference between the Green's functions, which generates many contributions. The most singular of these comes from the maximally crossed diagrams, which can be unwrapped to produce the diagram in fig. 3.16.

The first to consider this diagram were Langer and Neal [45], although they did not resolve the apparent issue of divergence for systems of dimensionality two or less. It was only in the late 1970s that this seemingly ill-behaved correction was resolved. One

[30] τ_ϕ^{-1} is not generated naturally in the diagrammatic series' of fig. 3.15, and so we have inserted it artificially into the Cooperon here. Section 3.6 shows how to include the phase breaking rate diagrammatically, at least to leading order.

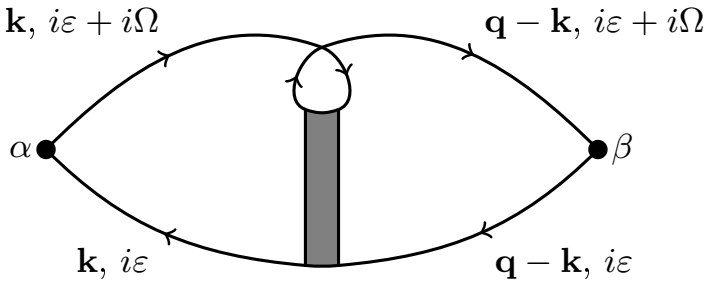

Figure 3.16: Diagrammatic representation of the WL correction to electrical conductivity.

approach was developed by Abrahams, Anderson, Licciardello, and Ramakrishnan [22].[31] This method was the scaling theory of localisation, which relies heavily upon our faith in physical intuition. To some, this approach may seem lacking in rigour and unsatisfying. Around the same time, Gor'kov, Larkin, and Khmel'nitskii [23] continued to treat the problem diagrammatically, and introduced an appropriate lower cut-off in the momentum sums to avoid the infrared divergence plaguing the corrections. This approach was also used by Abrahams and Ramakrishnan in a later paper [46].

We shall follow the Russian mindset when treating this problem, and stick to the diagrammatic approach. The response function for fig. 3.16 is

$$K_{\alpha\beta}(i\Omega) = \frac{2e^2}{m_e^2} T \sum_{\varepsilon} \sum_{\mathbf{k},\mathbf{q}} \Big[k_\alpha (q_\beta - k_\beta) G(\mathbf{k}, i\varepsilon + i\Omega) G(\mathbf{q}-\mathbf{k}, i\varepsilon + i\Omega) \times G(\mathbf{q}-\mathbf{k}, i\varepsilon) G(\mathbf{k}, i\varepsilon) \widetilde{C}(\mathbf{q}, i\varepsilon + i\Omega, i\varepsilon) \Big], \tag{3.79}$$

where, as usual, we assume $\Omega > 0$. The presence of the cooperon forces $\varepsilon < 0$ and $\varepsilon + \Omega > 0$, as these are the two frequencies entering the cooperon and must be of opposite sign. The main contribution comes from small q, as this is where the cooperon is most singular,[32] so we may approximate $q_\beta - k_\beta \simeq -k_\beta$ and $G(\mathbf{q}-\mathbf{k}, i\nu) \simeq G(\mathbf{k}, i\nu)$.

Eq. 3.79 therefore simplifies to

$$K_{\alpha\beta}(i\Omega) = -\delta_{\alpha\beta} \frac{2e^2 v_F^2}{d} T \sum_{-\Omega<\varepsilon<0} \sum_{\mathbf{k},\mathbf{q}} \frac{G(\mathbf{k}, i\varepsilon + i\Omega)^2 G(\mathbf{k}, i\varepsilon)^2}{2\pi N(0) \tau_0^2} \frac{1}{\mathcal{D}q^2 + \Omega + \tau_\phi^{-1}}. \tag{3.80}$$

[31] This group is sometimes referred to as the gang of four.

[32] Since one of the electron Green's functions depends only on $\mathbf{k}$, we take $\mathbf{k}$ to be close to k_F. Therefore the electron Green's functions with $\mathbf{q}-\mathbf{k}$ are most singular when $\mathbf{q}$ is small too.

Unlike the Drude calculation, we may freely interchange the orders of summation here without issue, as the summand is now sufficiently convergent.

We now make use of the identity in eq. 3.75, where in this case we replace $G(\mathbf{k}, i\varepsilon+i\Omega)$ with $G^+(\mathbf{k})$ and $G(\mathbf{k}, i\varepsilon)$ with $G^-(\mathbf{k})$. Applying eq. 3.75 to eq. 3.80 yields

$$K_{\alpha\beta}(i\Omega) = -\delta_{\alpha\beta}\, 4e^2\mathcal{D}T \sum_{-\Omega<\varepsilon<0} \sum_{\mathbf{q}} \frac{1}{\mathcal{D}q^2 + \Omega + \tau_\phi^{-1}}. \tag{3.81}$$

The Matsubara sum is the same as in eq. 3.44, and gives a multiplicative factor of $\Omega/(2\pi T)$. Thus our response function is

$$K_{\alpha\beta}(i\Omega) = -\delta_{\alpha\beta}\, \Omega \frac{2e^2\mathcal{D}}{\pi} \sum_{\mathbf{q}} \frac{1}{\mathcal{D}q^2 + \Omega + \tau_\phi^{-1}}. \tag{3.82}$$

We may now deduce the correction to electrical conductivity due to WL using eq. 3.31 to obtain,

$$\sigma_{WL}(i\Omega) = -\frac{2e^2\mathcal{D}}{\pi} \sum_{\mathbf{q}} \frac{1}{\mathcal{D}q^2 + \Omega + \tau_\phi^{-1}}. \tag{3.83}$$

We now focus on the DC conductivity, $\Omega = 0$, and consider the effect of dimensionality.

To progress further we approximate the momentum sum via an integral,

$$\sigma_{WL} = -\frac{2e^2\mathcal{D}}{\pi} \int \frac{d^d q}{(2\pi)^d} \frac{1}{\mathcal{D}q^2 + \tau_\phi^{-1}}. \tag{3.84}$$

Consider the situation where $\tau_\phi^{-1} = 0$ – we see that the integral diverges at the lower limit of its radial integral in 1D and 2D. In 3D, however, we have an ultra-violet divergence, regardless of the value of τ_ϕ^{-1}, which is cut-off by the diffusive limit.[33] This upper limit exists for 1D and 2D as well, due to being in the diffusive limit, but we take this to infinity

[33]The upper cut-off in the 3D integral is set by our use of the diffusive limit, $\mathcal{D}q^2 \ll \tau_0^{-1}$. We therefore set $q_{max}^{-1} = \sqrt{\mathcal{D}\tau_0}$. Note that this is much larger than other length scales present in these types of problems. Hence it may be set to infinity where divergences are not an issue.

where possible.[34] The weak localisation correction is thus

$$\sigma_{WL} = \begin{cases} -\dfrac{e^2}{\pi} l_\phi, & d = 1 \\ -\dfrac{e^2}{2\pi^2} \ln\left(\dfrac{\tau_\phi}{\tau_0}\right), & d = 2 \\ \dfrac{e^2}{2\pi^2}\left(\dfrac{1}{l_\phi} - \dfrac{1}{l}\right), & d = 3, \end{cases} \tag{3.85}$$

where $l_\phi = \sqrt{\mathcal{D}\tau_\phi}$ is the phase coherence length.[35]

Given that τ_ϕ^{-1} is smaller for lower temperatures, τ_ϕ and l_ϕ must therefore increase with decreasing temperature. Hence, σ_{WL} leads to a conductivity that decreases with decreasing temperature.

Finally, let us briefly mention experimental observation of WL. To observe WL phenomena experimentally, we can make use of an applied magnetic to destroy the phase coherence of self-intersecting paths. This reduces the WL correction, giving a negative magneto-resistance. Amongst the first to observe this phenomenon of negative magneto-resistance were Kawaji and Kawaguchi [47, 48].

Another observable effect is oscillatory behaviour in the magneto-resistance for a system with a ring geometry, as seen in the works of Sharvin et. al. [49] and Al'tshuler et. al. [50]. These experiments used a thin metallic cylinder threaded with a magnetic field so that they could focus on loops of fixed area/containing the same magnetic flux. When applying a magnetic field to a self-intersecting loop, the electron will pick up equal but opposite phases depending on which way it traverses the loop. Therefore, when the magnetic field corresponds to a $2\pi n$ phase shift, where $n \in \mathbb{Z}$, the interference will be constructive, whilst a $2\pi(n + 1/2)$ phase shift leads to destructive interference. The rest of this thesis does not focus on the role of magnetic fields, so we give further details of how to include a magnetic field in appendix F.

[34] Note that $l_\phi \gg l$.

[35] The prefactor to l^{-1} in the 3D result is not exactly what you would find upon doing the integrals. In truth, you would obtain $e^2\sqrt{3}/(\pi^3)$ as the prefactor, as we can set $\mathcal{D}q_{\max}^2 = \tau_0$. However, $\sqrt{3} \simeq 1.7$ and $\pi/2 \simeq 1.5$, hence the prefactors of l_ϕ^{-1} and l^{-1} are relatively close. Thus we set the prefactors equal, as the cut-off is defined with a sense of typical physicist hand waving.

In this section we have outlined how one introduces diffusion due to correlated scattering events between electron and hole propagators. Consequently, we studied the most singular contributions that arise due to diffusive modes in the limit of weak disorder. We found that they gave rise to a negative correction to the electrical conductivity, which can by physically attributed to the localisation of current carriers in the metal. Let us now introduce two-body interactions into our Hamiltonian.

3.4 Electron-Electron Interactions – Coulomb

The first two-body interaction we account for is the Coulomb interaction between electrons. In this section we shall outline how the Coulomb interaction is modified by the presence of many electrons and disorder, giving rise to the disorder-screened Coulomb interaction. Upon constructing the physically correct interaction, we shall calculate the corrections to the electrical conductivity due to its presence.

3.4.1 The Screened Coulomb Interaction and RPA

The bare Coulomb interaction is a long range force that decays radially as r^{-2}. The potential energy for this interaction between two charges located at $\mathbf{r}_1$ and $\mathbf{r}_2$, with charges q_1 and q_2 respectively, is[36]

$$V_0(\mathbf{r}-\mathbf{r}') = \frac{q_1 q_2}{|\mathbf{r}_1 - \mathbf{r}_2|}, \qquad \Rightarrow \qquad V_0(r) = \frac{q_1 q_2}{r}, \tag{3.86}$$

where the second expression emphasises that the interaction depends solely on the separation between the charges, $r = |\mathbf{r}_1 - \mathbf{r}_2|$. Since our charge carriers are electrons, we now set $q_1 = q_2 = e$.

[36]Here we work in Gaussian cgs units, in which $4\pi\varepsilon_0 = 1$, where ε_0 is the vacuum permittivity of free space.

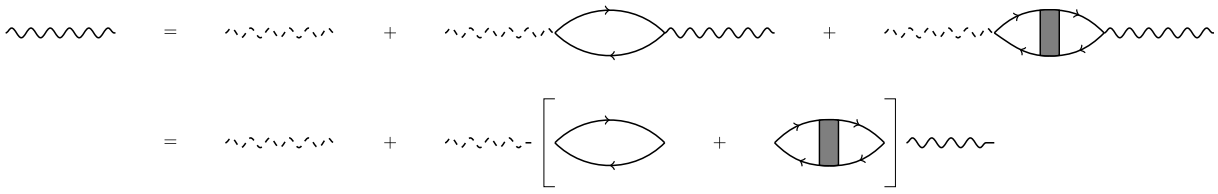

Figure 3.17: Diagrammatic series for the screened Coulomb interaction within RPA.

Taking the Fourier transform of $V_0(\mathbf{r}-\mathbf{r}')$ in different dimensions gives,

$$V_0(\mathbf{q}) = \begin{cases} \dfrac{4\pi e^2}{q^2}, & d=3 \\ \dfrac{2\pi e^2}{q}, & d=2 \\ -e^2\ln(q^2w^2), & d=1. \end{cases} \tag{3.87}$$

The cases of $d = 1$ and $d = 2$ are quasi-1D and quasi-2D interactions. These appear in thin wires and films respectively, where w, the transverse size of the system, is much smaller than the relevant length scale for the potential [39].

In the systems we consider, the electron density is sufficiently high to allow us to account for screening of the Coulomb interaction within the random phase approximation (RPA).[37] Using RPA we calculate the screened Coulomb interaction via the Dyson series shown in fig. 3.17, which corresponds to

$$V(\mathbf{q}, i\omega) = V_0(\mathbf{q}) - V_0(\mathbf{q})\Pi(\mathbf{q}, i\omega)V(\mathbf{q}, i\omega). \tag{3.88}$$

We refer to $\Pi(\mathbf{q}, i\omega)$ as the polarisation operator or bubble, which is given by

$$\begin{aligned} \Pi(\mathbf{q}, i\omega) = &-2T\sum_{\varepsilon}\sum_{\mathbf{k}} G(\mathbf{k}+\mathbf{q}, i\varepsilon+i\omega)G(\mathbf{k}, i\varepsilon) \\ &-2T\sum_{\varepsilon}\sum_{\mathbf{k},\mathbf{k}'}\Big[G(\mathbf{k}+\mathbf{q}, i\varepsilon+i\omega)G(\mathbf{k}, i\varepsilon)\widetilde{D}(\mathbf{q}, i\varepsilon+i\omega, i\varepsilon) \\ &\qquad\qquad \times G(\mathbf{k}'+\mathbf{q}, i\varepsilon+i\omega)G(\mathbf{k}', i\varepsilon)\Big]. \end{aligned} \tag{3.89}$$

[37] The ideas underpinning RPA are discussed in many books (see [29, 30, 31, 34, 39]), so we skip the in depth details here.

Let us start by considering the second term of eq. 3.89. The diffuson here means that the only non-zero contributions occur when ε and $\varepsilon + \omega$ are opposite in sign. We may then use eq. 3.75 to evaluate the momentum sums, noting that the most singular contributions come from small $\mathbf{q}$, so that we may neglect $\mathbf{q}$ inside the electron Green's functions. Evaluation of these momentum sums thus yields

$$-2T\sum_{\varepsilon}\frac{(2\pi N(0)\tau_0)^2}{2\pi N(0)\tau_0^2}\frac{\Theta(-\varepsilon(\varepsilon+\omega))}{\mathcal{D}q^2+|\omega|}=-2T\sum_{n=1}^{\frac{|\omega|}{2\pi T}}\frac{2\pi N(0)}{\mathcal{D}q^2+|\omega|}=-\frac{2N(0)|\omega|}{\mathcal{D}q^2+|\omega|}, \tag{3.90}$$

so that

$$\Pi(\mathbf{q},i\omega)=\Pi_0(\mathbf{q},i\omega)-\frac{2N(0)|\omega|}{\mathcal{D}q^2+|\omega|}. \tag{3.91}$$

In general the polarisation bubble obeys [51],

$$\lim_{\mathbf{q}\to\mathbf{0}}\lim_{\omega\to 0}\Pi(\mathbf{q},i\omega)=2N(0), \qquad \lim_{\omega\to 0}\lim_{\mathbf{q}\to\mathbf{0}}\Pi(\mathbf{q},i\omega)=0. \tag{3.92}$$

To satisfy eq. 3.92, we might guess that $\Pi_0(\mathbf{q},i\omega)=2N(0)$ in the diffusive limit; this is indeed the case, as demonstrated in appendix G. It follows that

$$\Pi(\mathbf{q},i\omega)=2N(0)\frac{\mathcal{D}q^2}{|\omega|+\mathcal{D}q^2}, \tag{3.93}$$

and hence

$$V(\mathbf{q},i\omega)=\frac{|\omega|+\mathcal{D}q^2}{(|\omega|+\mathcal{D}q^2)V_0(\mathbf{q})^{-1}+2N(0)\mathcal{D}q^2}. \tag{3.94}$$

Writing this for the different choices of dimensionality we have,

$$V(\mathbf{q},i\omega)=\frac{|\omega|+\mathcal{D}q^2}{2N(0)}\begin{cases}\dfrac{\kappa_3^2}{q^2(|\omega|+\mathcal{D}q^2)+\kappa_3^2\mathcal{D}q^2}, & d=3,\\ \dfrac{\kappa_2}{q(|\omega|+\mathcal{D}q^2)+\kappa_2\mathcal{D}q^2}, & d=2,\\ \dfrac{2e^2N(0)}{2e^2N(0)\mathcal{D}q^2-(|\omega|+\mathcal{D}q^2)\left[\ln(q^2w^2)\right]^{-1}}, & d=1,\end{cases} \tag{3.95}$$

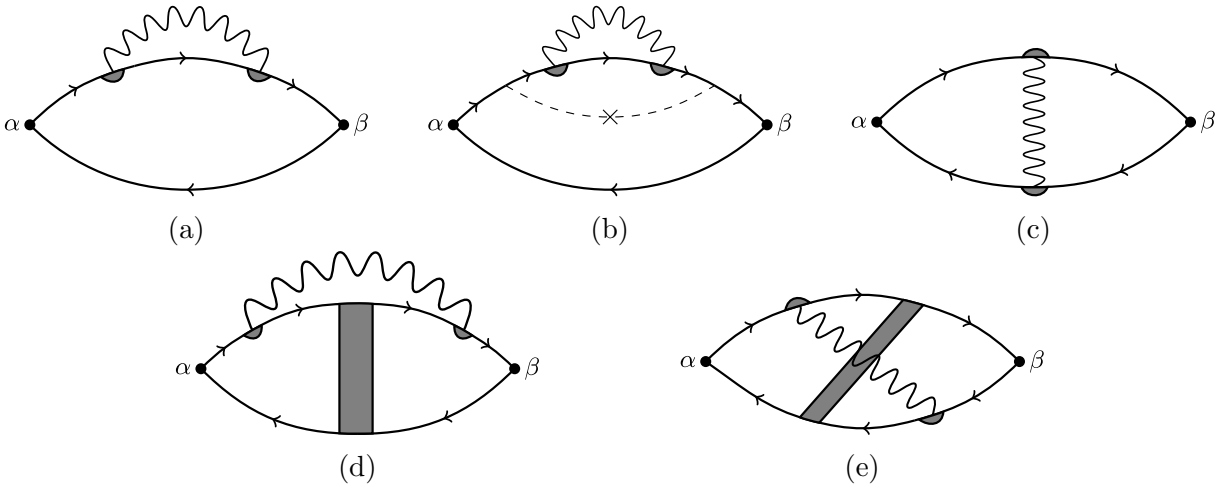

Figure 3.18: Leading order corrections to the electrical conductivity due to EEIs.

where κ_d is the d-dimensional Thomas-Fermi wave vector (inverse screening length),

$$\kappa_d = \begin{cases} \sqrt{8\pi N(0)e^2} = \sqrt{\dfrac{4m_e k_F e^2}{\pi}}, & d = 3, \\ 4\pi N(0)e^2 = 2m_e e^2, & d = 2. \end{cases} \tag{3.96}$$

Note that $\kappa_d \gg l^{-1}$ for the systems we consider, which means we can usually ignore the $V_0(\mathbf{q})^{-1}$ term in the denominator of eq. 3.94.[38] The screened Coulomb interaction then has the dimension independent form,

$$V(\mathbf{q}, i\omega) = \frac{1}{2N(0)} \frac{|\omega| + \mathcal{D}q^2}{\mathcal{D}q^2}. \tag{3.97}$$

Let us now consider its effect on the electrical conductivity.

3.4.2 EEI Corrections to the Electrical Conductivity

The leading order corrections to the conductivity are given by the diagrams in fig. 3.18 [39, 21]. The first three of these diagrams cancel exactly, as shown in appendix G; we therefore focus on calculating diagrams D and E.

[38] An example where we cannot ignore $V_0(\mathbf{q})^{-1}$ is the zero-bias anomaly in two dimensions.

These diagrams have the respective electromagnetic response functions,

$$\begin{aligned} K^{(D)}_{\alpha\beta}(i\Omega) = -\frac{4e^2}{m^2}T^2 \sum_{\varepsilon,\omega} \sum_{\mathbf{k},\mathbf{k}',\mathbf{q}} \Big[& k_\alpha k'_\beta V(\mathbf{q}, i\omega) G(\mathbf{k}, i\varepsilon + i\Omega) \\ & \times G(\mathbf{k}+\mathbf{q}, i\varepsilon + i\Omega + i\omega) G(\mathbf{k}, i\varepsilon) G(\mathbf{k}', i\varepsilon + i\Omega) \\ & \times G(\mathbf{k}'+\mathbf{q}, i\varepsilon + i\Omega + i\omega) G(\mathbf{k}', i\varepsilon) \\ & \times D(\mathbf{q}, i\varepsilon + i\Omega, i\varepsilon + i\Omega + i\omega)^2 \widetilde{D}(\mathbf{q}, i\varepsilon + i\Omega + i\omega, i\varepsilon) \Big], \end{aligned} \tag{3.98a}$$

$$\begin{aligned} K^{(E)}_{\alpha\beta}(i\Omega) = -\frac{4e^2}{m^2}T^2 \sum_{\varepsilon,\omega} \sum_{\mathbf{k},\mathbf{k}',\mathbf{q}} \Big[& k_\alpha (k'_\beta + q_\beta) V(\mathbf{q}, i\omega) G(\mathbf{k}, i\varepsilon + i\Omega) G(\mathbf{k}, i\varepsilon) \\ & \times G(\mathbf{k}+\mathbf{q}, i\varepsilon + i\Omega + i\omega) G(\mathbf{k}', i\varepsilon + i\omega) G(\mathbf{k}', i\varepsilon) \\ & \times G(\mathbf{k}'+\mathbf{q}, i\varepsilon + i\Omega + i\omega) D(\mathbf{q}, i\varepsilon + i\omega, i\varepsilon) \\ & \times D(\mathbf{q}, i\varepsilon + i\Omega, i\varepsilon + i\Omega + i\omega) \widetilde{D}(\mathbf{q}, i\varepsilon + i\Omega + i\omega, i\varepsilon) \Big]. \end{aligned} \tag{3.98b}$$

The factor of 4 in eq. 3.98a is due to a factor of 2 for spin, and an additional factor of 2 due to the equivalent diagram with the interaction on the lower electron Green's function. For eq. 3.98b the factor of 4 arises from a factor of 2 for spin, and an extra factor due to the equivalent diagram with the diffuson and interaction crossed in the opposite order.[39]

If we simply neglected the small momentum, $\mathbf{q}$, inside the electron Green's function these diagrams would vanish as the current vertices produce a single factor of k_α in each "fast" momentum sum, making the sums odd in their α component. We therefore expand our Green's functions to first order in $\mathbf{q}$ to extract the leading order behaviour.[40] This expansion is performed by taking $\xi_{\mathbf{k}+\mathbf{q}} \simeq \xi_{\mathbf{k}} + \mathbf{k}\cdot\mathbf{q}/m$ (the q^2 term is negligible as $q \ll k$),

[39] The diagram in fig. 3.18e has the diffuson connecting the bottom left and top right Green's functions, whilst the interaction links the top left and bottom right Green's functions. The other choice of orientation of the diffuson and interaction has the former connecting top left and bottom right, whilst the latter connects bottom left and top right.

[40] If we performed the same expansion for the first three diagrams, we would find that they are less singular and parametrically smaller than the expansion here. For diagrams A, B, and C we find that they would carry a factor of $(ql)^2$ inside the $\mathbf{q}$ summand compared to the $\mathbf{q} = \mathbf{0}$ case, which is small in the diffusive limit. As will be seen, the last two diagrams will contain an additional factor of $\mathcal{D}q^2/(\mathcal{D}q^2 + |\omega + \Omega|)$, which is naturally more singular than $(ql)^2$. Note, this is at order q^2, but this argument can be continued for higher orders.

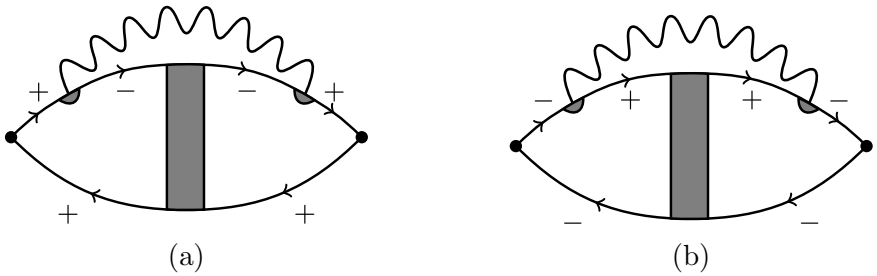

Figure 3.19: Sign choices for the Matsubara frequencies of the DOS diagram in fig. 3.18d. Panels a and b correspond to the D1 and D2 contributions respectively.

which allows us to write

$$G^{\pm}(\mathbf{k}+\mathbf{q}) = G^{\pm}(\mathbf{k}) \sum_{n=0}^{\infty} \left(\frac{\mathbf{k}\cdot\mathbf{q}}{m} G^{\pm}(\mathbf{k}) \right)^n . \tag{3.99}$$

We only need to retain the first-order term as all even orders will vanish due to being odd in the summand when accounting for the current vertices, and higher order terms are negligible. So, at leading order, these diagrams yield

$$\begin{aligned} K^{(D)}_{\alpha\beta}(i\Omega) = -\frac{4e^2}{m^4} T^2 \sum_{\varepsilon,\omega} \sum_{\mathbf{k},\mathbf{k}',\mathbf{q}} \Big[& k_\alpha(\mathbf{k}\cdot\mathbf{q}) k'_\beta(\mathbf{k}'\cdot\mathbf{q}) V(\mathbf{q}, i\omega) G(\mathbf{k}, i\varepsilon + i\Omega) \\ & \times G(\mathbf{k}, i\varepsilon + i\Omega + i\omega)^2 G(\mathbf{k}, i\varepsilon) G(\mathbf{k}', i\varepsilon + i\Omega) \\ & \times G(\mathbf{k}', i\varepsilon + i\Omega + i\omega)^2 G(\mathbf{k}', i\varepsilon) \\ & \times D(\mathbf{q}, i\varepsilon + i\Omega, i\varepsilon + i\Omega + i\omega)^2 \widetilde{D}(\mathbf{q}, i\varepsilon + i\Omega + i\omega, i\varepsilon) \Big], \end{aligned} \tag{3.100a}$$

$$\begin{aligned} K^{(E)}_{\alpha\beta}(i\Omega) = -\frac{4e^2}{m^2} T^2 \sum_{\varepsilon,\omega} \sum_{\mathbf{k},\mathbf{k}',\mathbf{q}} \Big[& k_\alpha(\mathbf{k}\cdot\mathbf{q}) k'_\beta(\mathbf{k}'\cdot\mathbf{q}) V(\mathbf{q}, i\omega) G(\mathbf{k}, i\varepsilon + i\Omega) G(\mathbf{k}, i\varepsilon) \\ & \times G(\mathbf{k}, i\varepsilon + i\Omega + i\omega)^2 G(\mathbf{k}', i\varepsilon + i\omega) G(\mathbf{k}', i\varepsilon) \\ & \times G(\mathbf{k}', i\varepsilon + i\Omega + i\omega)^2 D(\mathbf{q}, i\varepsilon + i\omega, i\varepsilon) \\ & \times D(\mathbf{q}, i\varepsilon + i\Omega, i\varepsilon + i\Omega + i\omega) \widetilde{D}(\mathbf{q}, i\varepsilon + i\Omega + i\omega, i\varepsilon) \Big]. \end{aligned} \tag{3.100b}$$

As usual, we approximate $\mathbf{k}$ to be around the Fermi surface, meaning $k_\alpha(\mathbf{k}\cdot\mathbf{q}) \simeq k_{F\alpha}(\mathbf{k}_F\cdot\mathbf{q})$ produces a factor of $k_F^2 q_\alpha/d$ inside the $\mathbf{q}$ sum upon performing the $\mathbf{k}$ sum.[41]

[41] This is most easily seen by writing $k_{F\alpha}(\mathbf{k}_F\cdot\mathbf{q}) = k_{F\alpha}k_{F\gamma}q_\gamma$ (using Einstein summation convention). The sum over $\mathbf{k}$ then produces $k_F^2\delta_{\alpha\gamma}q_\gamma/d = k_F^2 q_\alpha/d$.

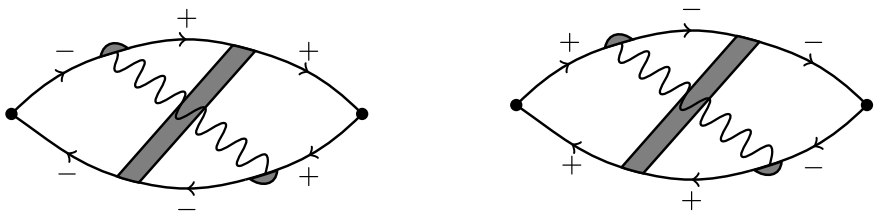

(a) (b)

Figure 3.20: Sign choices for the Matsubara frequencies of the diagram in fig. 3.18e. Panels a and b correspond to the E1 and E2 contributions respectively.

Next we consider the non-zero sign configurations for these diagrams enforced by the diffusons, which are shown in figs. 3.19 and 3.20 for $K^{(D)}_{\alpha\beta}$ and $K^{(E)}_{\alpha\beta}$, respectively. Upon performing the fast momentum and Fermi frequency sums, we arrive at

$$K^{(D1)}_{\alpha\beta}(i\Omega) = -16N(0)e^2\mathcal{D}^2T\sum_{\omega>\Omega}\sum_{\mathbf{q}}\frac{(\omega-\Omega)V(\mathbf{q},i\omega)}{(\mathcal{D}q^2+\omega)^2(\mathcal{D}q^2+\omega-\Omega)}q_\alpha q_\beta, \tag{3.101a}$$

$$K^{(D2)}_{\alpha\beta}(i\Omega) = -16N(0)e^2\mathcal{D}^2T\sum_{\omega>0}\sum_{\mathbf{q}}\frac{\omega V(\mathbf{q},i\omega)}{(\mathcal{D}q^2+\omega)^2(\mathcal{D}q^2+\omega-\Omega)}q_\alpha q_\beta, \tag{3.101b}$$

for diagram D, and

$$K^{(E1)}_{\alpha\beta}(i\Omega) = 16N(0)e^2\mathcal{D}^2T\sum_{\omega>\Omega}\sum_{\mathbf{q}}\frac{(\omega-\Omega)V(\mathbf{q},i\omega)}{(\mathcal{D}q^2+\omega)^2(\mathcal{D}q^2+\omega+\Omega)}q_\alpha q_\beta, \tag{3.102a}$$

$$K^{(E2)}_{\alpha\beta}(i\Omega) = 16N(0)e^2\mathcal{D}^2T\sum_{\omega>\Omega}\sum_{\mathbf{q}}\frac{(\omega-\Omega)V(\mathbf{q},i\omega)}{(\mathcal{D}q^2+\omega)^2(\mathcal{D}q^2+\omega-\Omega)}q_\alpha q_\beta, \tag{3.102b}$$

for diagram E. The total electromagnetic response function due to the EEIs is simply the sum of these contributions,

$$\begin{aligned}K_{\alpha\beta}(i\Omega) = -\frac{16N(0)e^2\mathcal{D}^2}{d}\,\delta_{\alpha\beta}\,T\Bigg[\sum_{0<\omega\leq\Omega}\omega+\sum_{\omega>\Omega}\Omega\Bigg]\\ \times\sum_{\mathbf{q}}\frac{q^2V(\mathbf{q},i\omega)}{(\mathcal{D}q^2+\omega)^2(\mathcal{D}q^2+\omega+\Omega)}.\end{aligned} \tag{3.103}$$

Here we used the fact that the summand factors multiplying $q_\alpha q_\beta$ have no angular dependence (i.e: they only depend upon q), meaning that the summand was odd in each

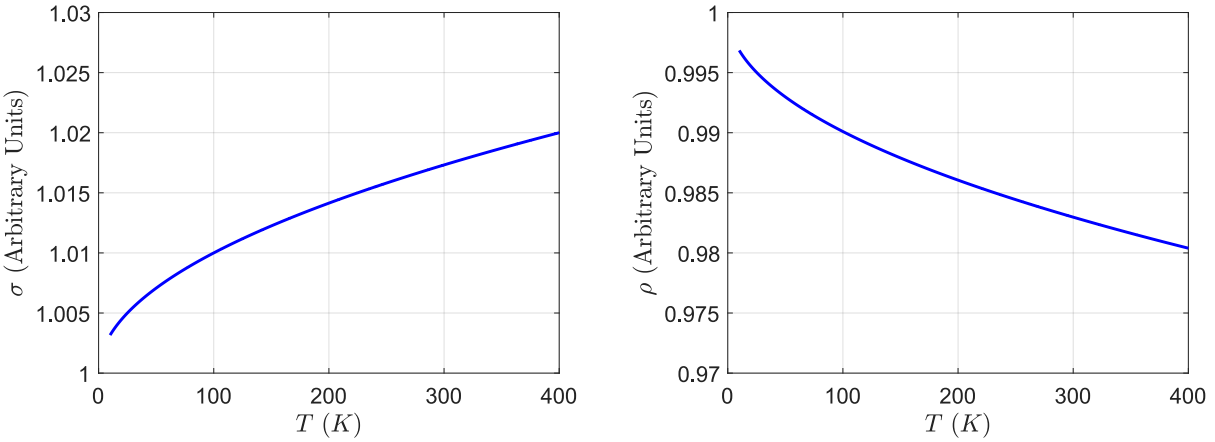

(a) (b)

Figure 3.21: Example curves of the resistivity, ρ, and conductivity, σ, for a typical metal with EEIs present in three dimensions.

component of $\mathbf{q}$ leading to a vanishing sum, unless $\alpha = \beta$.

At this point the choice of dimensionality dictates the approach we should take in evaluating these sums, so we leave mathematical details to appendix G. We find the EEI conductivity correction is then,

$$\sigma_{\text{EEI}} = -\frac{e^2}{2\pi^2}\left(\frac{T}{\mathcal{D}}\right)^{\frac{d}{2}-1} \times \begin{cases} \dfrac{\alpha_d}{(2\pi)^{2-\frac{d}{2}}}\dfrac{4-d}{2d}\zeta\left(2-\dfrac{d}{2},1\right), & d=1,3 \\ \ln\left(\dfrac{1}{2\pi T\tau_0}\right), & d=2, \end{cases} \tag{3.104}$$

where

$$\alpha_d = \begin{cases} 4\pi^2, & d=1 \\ 2\pi, & d=3, \end{cases} \tag{3.105}$$

and $\zeta(x,a)$ is the Hurwitz zeta function.[42] We note that coefficients have the numerical values,

$$\frac{\alpha_d}{(2\pi)^{2-\frac{d}{2}}}\frac{4-d}{2d}\zeta\left(\frac{d}{2},1\right) \simeq \begin{cases} 9.82, & d=1 \\ -0.61, & d=3, \end{cases} \tag{3.106}$$

which match those given Altshuler and Aronov [39].

Clearly in all dimensionalities, the EEI correction leads to a reduction in the conduc-

[42] See appendix N for details about the properties of $\zeta(x,a)$.

tivity with decreasing temperature. The temperature dependence is a simple power law, $\mathrm{sgn}(d-2)\,T^{\frac{d}{2}-1}$, in all except 2D, where it is logarithmic. Fig. 3.21 gives a visual reference for the shapes of curve we would expect to see in experiment when EEIs are present.

3.5 Superconducting Fluctuations

In this section, we introduce a second type of two-body interaction in the form of superconducting fluctuations, mediated by the BCS interaction. These act as a precursor to the superconducting transition. From observation, the $R(T)$ behaviour at the transition is not a step function, but rather a smooth curve with finite width and a definite shape, this is a consequence of superconducting fluctuations.

Physically, these fluctuations are the result of finite-lifetime (virtual) Cooper pairs. In this process electrons temporarily pair up, allowing for a superconducting channel to open, before being broken apart by natural thermal excitations. Due to the presence of these virtual Cooper pairs travelling without resistance, the conductivity naturally increases. These Cooper pairs survive for longer nearer the transition, and so the conductivity increases. This specific mechanism can be linked to the Aslamazov-Larkin (AL) contribution to the fluctuation conductivity. However, whilst electrons are preoccupied as Cooper pairs, the number of electrons available in the normal current channel is reduced, and so the conductivity due to normal state electrons decreases. This effect leads to the density of states (DOS) contribution. Finally, we can consider interference effects in both channels, although to give this a physical picture is not a simple task. These effects give rise to the Maki-Thompson (MT) contribution.

These contributions will be calculated in detail in section 3.5.3, and their origin in the literature explained in section 3.5.2. First we must understand how to construct the propagator for virtual Cooper pairs.

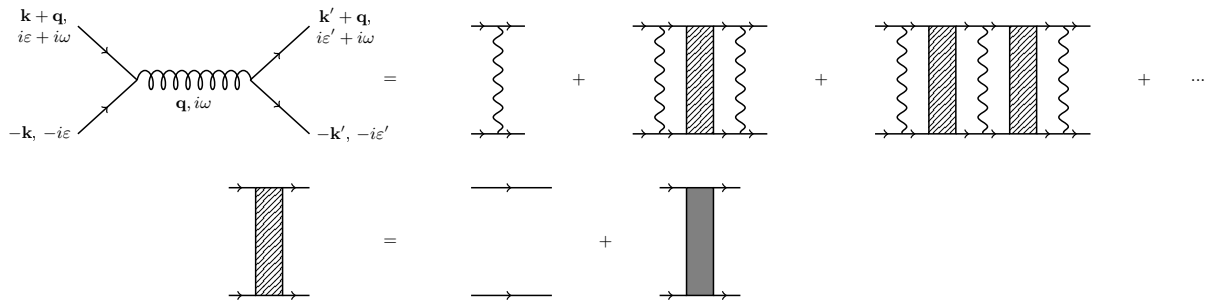

Figure 3.22: Diagrammatic series for the pair propagator mediated by BCS interactions (wavy lines). The BCS interaction allows for the exchange of momentum and frequency. The hatched region represents the addition of two electron Green's functions with no correlated scattering between them to the cooperon.

3.5.1 The Pair Propagator

The diagrammatic series for the pair propagator, $L(\mathbf{q}, i\omega)$, is given by the coiled line (spring) in fig. 3.22, which yields

$$L(\mathbf{q}, i\omega) = \lambda_0 + \lambda_0 \Pi_{fl}(\mathbf{q}, i\omega) L(\mathbf{q}, i\omega) \qquad \Rightarrow \qquad L(\mathbf{q}, i\omega) = \frac{1}{\lambda_0^{-1} - \Pi_{fl}(\mathbf{q}, i\omega)}, \quad (3.107)$$

where

$$\Pi_{fl}(\mathbf{q}, i\omega) = \Pi_{fl,0}(\mathbf{q}, i\omega) + \Pi_{fl,1}(\mathbf{q}, i\omega), \quad (3.108a)$$

$$\Pi_{fl,0}(\mathbf{q}, i\omega) = T \sum_{\varepsilon} \sum_{\mathbf{k}} G(\mathbf{k} + \mathbf{q}, i\varepsilon + i\omega) G(-\mathbf{k}, -i\varepsilon), \quad (3.108b)$$

$$\Pi_{fl,1}(\mathbf{q}, i\omega) = T \sum_{\varepsilon} \sum_{\mathbf{k}} G(\mathbf{k} + \mathbf{q}, i\varepsilon + i\omega) G(-\mathbf{k}, -i\varepsilon) C(\mathbf{q}, i\varepsilon + i\omega, i\varepsilon), \quad (3.108c)$$

is the fluctuation or pair polarisation operator. The pair propagator has the important property that it diverges at $T = T_c$ when $|\mathbf{q}| = 0 = \omega$,

$$\lim_{T \to T_c^+} L(\mathbf{q} = \mathbf{0}, \omega = 0; T) \to \infty. \quad (3.109)$$

Working in the diffusive limit, we may neglect $\Pi_{fl,0}$ without consequence, as shown in

appendix H.[43] The momentum sums in eq. 3.108c then yield

$$\Pi_{fl,1}(\mathbf{q}, i\omega) = 2\pi N(0) T \sum_{\varepsilon} \frac{\Theta(\varepsilon(\varepsilon+\omega))}{|\varepsilon| + |\varepsilon+\omega| + \mathcal{D}q^2 + \tau_\phi^{-1}}. \tag{3.110}$$

Let us assume $\omega \geq 0$ for the time being, so that

$$\begin{aligned} \Pi_{fl}^{(\omega>0)}(\mathbf{q}, i\omega) &= 2\pi N(0) T \left[\sum_{\varepsilon>0} + \sum_{\varepsilon<-\omega} \right] \frac{1}{|2\varepsilon+\omega| + \mathcal{D}q^2 + \tau_\phi^{-1}} \\ &= 4\pi N(0) T \sum_{\varepsilon>0} \frac{1}{2\varepsilon + \omega + \mathcal{D}q^2 + \tau_\phi^{-1}}. \end{aligned} \tag{3.111}$$

However, this sum is logarithmically divergent, so we introduce the Debye frequency, ω_D, as an upper cut-off, as this is the characteristic phonon energy. Hence,

$$\begin{aligned} \Pi_{fl}^{(\omega>0)}(\mathbf{q}, i\omega) &= N(0) \sum_{n=0}^{\frac{\omega_D}{2\pi T}} \frac{1}{n + \frac{1}{2} + \frac{\omega + \mathcal{D}q^2 + \tau_\phi^{-1}}{4\pi T}} \\ &= N(0) \left[\psi\left(\frac{\omega_D}{2\pi T} + \frac{3}{2} + \frac{\omega + \mathcal{D}q^2 + \tau_\phi^{-1}}{4\pi T} \right) - \psi\left(\frac{1}{2} + \frac{\omega + \mathcal{D}q^2 + \tau_\phi^{-1}}{4\pi T} \right) \right] \\ &\simeq N(0) \left[\ln\left(\frac{\omega_D}{2\pi T} \right) - \psi\left(\frac{1}{2} + \frac{\omega + \mathcal{D}q^2 + \tau_\phi^{-1}}{4\pi T} \right) \right], \end{aligned} \tag{3.112}$$

where $\psi(x)$ is the digamma function (see appendix N), and in the last line of eq. 3.112 we noted that $\omega_D \gg T, |\omega|, \mathcal{D}q^2, \tau_\phi^{-1}$. In the case where $\omega < 0$, we find the same result with $\omega \to -\omega$ in eq. 3.111, and so

$$\Pi_{fl}(\mathbf{q}, i\omega) \simeq N(0) \left[\ln\left(\frac{\omega_D}{2\pi T} \right) - \psi\left(\frac{1}{2} + \frac{|\omega| + \mathcal{D}q^2 + \tau_\phi^{-1}}{4\pi T} \right) \right], \tag{3.113}$$

Substituting this into eq. 3.107 leads to a somewhat cumbersome expression. This may be simplified using the definition of T_c in eq. 3.109, allowing us to write λ_0 in terms of T_c,

$$\lambda_0^{-1} = N(0) \left[\ln\left(\frac{\omega_D}{2\pi T_c} \right) - \psi\left(\frac{1}{2} + \frac{1}{4\pi T_c \tau_{\phi,c}} \right) \right]. \tag{3.114}$$

[43] This corresponds to the "dirty limit" of a superconductor.

When $\tau_\phi^{-1} = 0$, this gives us the BCS result for the unsuppressed transition temperature,

$$T_{c,0} = \frac{2\omega_D e^\gamma}{\pi} \exp\left(-\frac{1}{N(0)\lambda_0}\right), \tag{3.115}$$

where γ is the Euler-Mascheroni constant. In the general case where $\tau_\phi^{-1} \neq 0$, substituting eq. 3.113 and eq. 3.114 into eq. 3.107 gives

$$L(\mathbf{q}, i\omega) = \frac{1}{N(0)} \left[\ln\left(\frac{T}{T_c}\right) + \psi\left(\frac{1}{2} + \frac{|\omega| + \mathcal{D}q^2 + \tau_\phi^{-1}}{4\pi T}\right) - \psi\left(\frac{1}{2} + \frac{1}{4\pi T_c \tau_{\phi,c}}\right) \right]^{-1}. \tag{3.116}$$

This is the full pair propagator within the diffusive limit.[44]

Later on, we will only be concerned with cases involving small Cooper pair momenta and frequencies, so we may expand $L(\mathbf{q}, i\omega)$ in powers of $\mathcal{D}q^2$ and ω.[45] This yields

$$L(\mathbf{q}, i\omega) = \frac{1}{N(0)} \left[\ln\left(\frac{T}{T_c}\right) + \delta\psi + \psi'\left(\frac{1}{2} + \frac{1}{4\pi T\tau_\phi}\right) \frac{\mathcal{D}q^2 + |\omega|}{4\pi T} \right]^{-1}, \tag{3.117}$$

where

$$\delta\psi = \psi\left(\frac{1}{2} + \frac{1}{4\pi T\tau_\phi}\right) - \psi\left(\frac{1}{2} + \frac{1}{4\pi T_c \tau_{\phi,c}}\right). \tag{3.118}$$

In the case where phase breaking rates are negligible, $T\tau_\phi \gg 1$, we may write

$$L(\mathbf{q}, i\omega) = \frac{1}{N(0)} \left[\ln\left(\frac{T}{T_{c,0}}\right) + \frac{\pi}{8T}(\mathcal{D}q^2 + |\omega|) \right]^{-1}. \tag{3.119}$$

In the above, T_c is the general transition temperature for $\tau_\phi^{-1} \neq 0$, which is suppressed from the value $T_{c,0}$. To relate T_c to $T_{c,0}$, we use eq. 3.114, noting that λ_0 is a constant,

[44] We have not assumed anything about the size of $|\omega|$, $\mathcal{D}q^2$, or τ_ϕ^{-1} compared to T.

[45] It may seem like we are lacking rigour by treating the bosonic Matsubara frequency as continuous so that we may do a simple Taylor expansion (I.e: treating a discrete variable as continuous is not always okay). However, we can analytically continue our Matsubara pair propagator using $\omega \to \omega \pm i\delta$, perform the expansion in terms of the now continuous frequency, and move back to the Matsubara form using $\omega \pm i\delta \to \omega$. This will give exactly the same result as if we treated the Matsubara frequency as continuous for the purpose of expansion.

independent of the value of τ_ϕ^{-1}. It follows that

$$\begin{aligned} \ln\left(\frac{\omega_D}{2\pi T_{c,0}}\right) - \psi\left(\frac{1}{2}\right) &= \ln\left(\frac{\omega_D}{2\pi T_c}\right) - \psi\left(\frac{1}{2} + \frac{1}{4\pi T_c \tau_{\phi,c}}\right), \\ \Rightarrow \qquad \ln\left(\frac{T_c}{T_{c,0}}\right) &= \psi\left(\frac{1}{2}\right) - \psi\left(\frac{1}{2} + \frac{1}{4\pi T_c \tau_{\phi,c}}\right). \end{aligned} \tag{3.120}$$

Considering temperatures close to the transition, such that $(T - T_c)/T_c \ll 1$, we can replace the logarithm in the pair propagator with the reduced temperature, $\eta = (T - T_c)/T_c$. Hence, when $\tau_\phi^{-1} = 0$, we may approximate eq. 3.119 as

$$L(\mathbf{q}, i\omega) = \frac{1}{N(0)}\left[\eta + \frac{\pi}{8T}(\mathcal{D}q^2 + |\omega|)\right]^{-1}. \tag{3.121}$$

Furthermore, we may obtain the square of the virtual Cooper pair coherence length from the coefficient of q^2,

$$\xi_v = \sqrt{\frac{\pi\mathcal{D}}{8T_c\eta}} = \sqrt{\frac{\pi}{8d}}\sqrt{\frac{v_F l}{T_c\eta}}, \qquad T > T_c, \quad \eta \ll 1. \tag{3.122}$$

This is within agreement of the Ginzburg-Landau coherence length for Cooper pairs in a dirty 3D superconductor [52]. If we remove a factor of $\pi/(8T)$ from the denominator of eq. 3.121, the first term in the denominator becomes the Ginzburg-Landau relaxation rate [52],

$$\tau_{GL}^{-1} = \frac{8}{\pi}\frac{1}{T - T_c}, \qquad T > T_c, \quad \eta \ll 1. \tag{3.123}$$

This can be interpreted as the characteristic lifetime of a virtual Cooper pair.

The pair propagator thus provides information about the size and lifetime of the virtual Cooper pairs. These ideas will become very useful for building an intuitive picture for the superconducting fluctuation corrections in both homogeneous and granular metal.

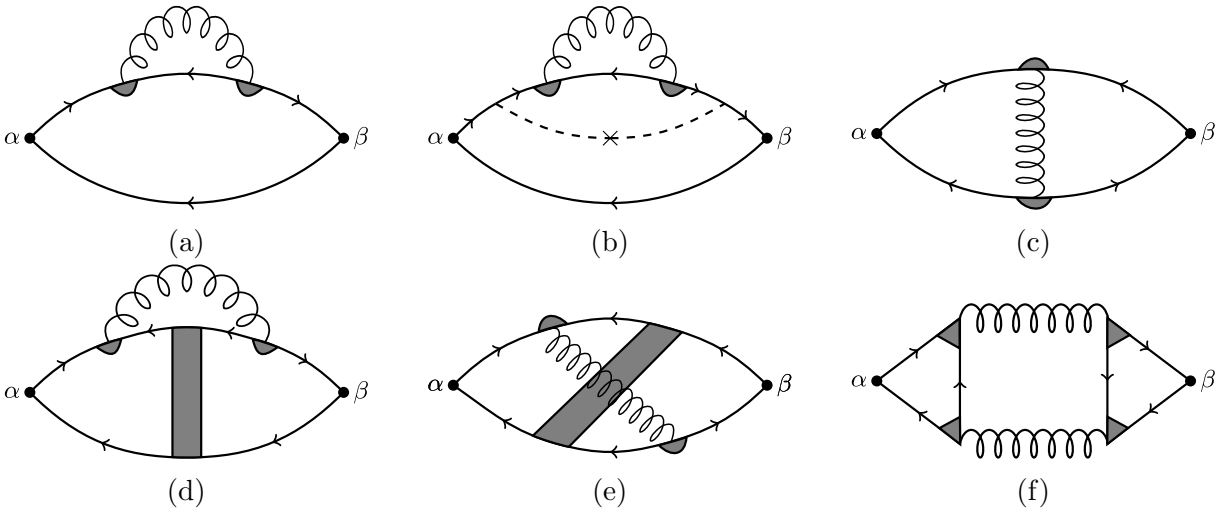

Figure 3.23: Diagrams describing the corrections to the electrical conductivity due to superconducting fluctuations.

3.5.2 Fluctuation Conductivity – A Brief History

In the previous subsection we constructed the propagator for the virtual Cooper pairs, which describes superconducting fluctuations. Let us now use this to calculate their effects on the electrical conductivity. These corrections can be grouped into three categories: Aslamazov-Larkin (AL), Maki-Thompson (MT), and density of states (DOS). The first of these was initially thought to be the most dominant contribution that led to an enhancement of the conductivity as one approached the transition from above, as discussed in the original paper by Aslamazov and Larkin [18]. The belief that the AL term was the most significant was due to the presence of two pair propagators in the diagram (fig. 3.23f), implying a more singular contribution when close to T_c.

This was not entirely the case however, as the diagram given by Aslamazov and Larkin which involved a pair propagator across the conductivity bubble, like that in fig. 3.23c, was shown to suffer infra-red divergence issues in its diffusive momentum integral within the work of Maki [19] in both one and two dimensions, suggesting that it may be as important or more important than the AL piece. This divergent result was clearly not physical, and was successfully dealt with by Thompson [20] by the inclusion of a phase breaking rate.

Thompson initially suggested that this phase breaking rate could arise from external phase breaking mechanisms, such as paramagnetic impurities and magnetic fields, and would lead to a suppression of the transition temperature. Soon after, Crow et. al. [53] measured the fluctuation conductivity in aluminium and lead films, and saw that the AL prediction was too small to explain their observations. By accounting for the Maki contribution with Thompson's correction, they were able to match the theory for zero magnetic field to experiment. To further demonstrate the sensitivity of the MT correction to magnetic fields, they also showed that at higher magnetic field strengths the MT contribution became smaller and the total fluctuation conductivity approached that predicted by Aslamazov and Larkin.

Whilst it might seem like a large success to have matched theory with experiment, the issue behind what governed the presence of the MT term and prevented its divergence was still not entirely resolved. What if no paramagnetic impurities or magnetic fields were present in the system? What if the electron-phonon interaction was relatively weak, so that it didn't disturb an electron's phase drastically? These qualms were settled later by Patton [44] and Keller and Korenman [54, 55], who argued and showed that phase breaking occurred naturally in the system without the need for external mechanisms.

Simply by the existence of virtual Cooper pairs there was a natural time scale, τ_n, that described the lifetime of an electron in the normal state, after which it would combine with another electron to form a virtual Cooper pair. Thus we have a natural lower cut-off in the diffusive momentum integral set by $l_n = v_F\tau_n$, which is just an example of the phase breaking mechanisms discussed towards the end of subsection 3.3.1. Using Patton's description [44], we can think of a system with superconduting fluctuations as having a decay rate, τ_n^{-1}, associated to the decay of electrons from the normal fluid to the superfluid of virtual Cooper pairs, whilst having a second decay rate, τ_s^{-1}, describing the decay of virtual Cooper pairs in the superfluid to electrons in the normal fluid.

Now that we have recapped some of the history behind the prediction and observation of superconducting fluctuations and their effects on the electrical conductivity, let us begin

to calculate their quantitative effects.[46]

3.5.3 Fluctuation Conductivity

The total fluctuation conductivity is given by the diagrams in fig. 3.23. Diagrams A, B, and D form the DOS corrections and so we expect these to give an overall negative contribution. Diagrams C and E are the MT contributions, and finally diagram F is the AL term. They can be shown to cancel in the zero external frequency limit, however this does not provide us with any new observable information and serves as a check that we have included all relevant diagrams. Therefore, we present the proof of their cancellation in appendix I. Furthermore, only diagrams A, B, C, and F give singular contributions, so these are the ones we shall calculate explicitly here. We proceed in calculating these diagrams in decreasing complexity, starting with the AL diagram, followed by the MT diagram, and finishing with the DOS terms.

The AL term

The AL diagram contains two blocks of Green's function which are independent of one another (see appendix I for details). These blocks may be written as

$$B_\alpha(\mathbf{q}, i\omega, i\Omega) = T\sum_{\varepsilon}\sum_{\mathbf{k}}\Bigg[\frac{k_\alpha}{m}G(\mathbf{k}, i\varepsilon + i\Omega)G(\mathbf{k}, i\varepsilon)G(\mathbf{q}-\mathbf{k}, i\omega - i\varepsilon) \times C(\mathbf{q}, i\varepsilon + i\Omega, i\omega - i\varepsilon)C(\mathbf{q}, i\varepsilon, i\omega - i\varepsilon)\Bigg], \tag{3.124}$$

where we have included the factor of k_α/m from the current vertex inside a single block. The response function associated to this diagram is then

$$K^{(F)}_{\alpha\beta}(i\Omega) = -4e^2T\sum_{\omega}\sum_{\mathbf{q}}B_\alpha(\mathbf{q}, i\omega, i\Omega)B_\beta(\mathbf{q}, i\omega, i\Omega)L(\mathbf{q}, i\omega + i\Omega)L(\mathbf{q}, i\omega). \tag{3.125}$$

[46] This is the point at which we use all the ideas we have applied before, and just shut up and calculate.

(a) (b)

Figure 3.24: Sign choices of the blocks appearing in the AL diagram. Panel a corresponds to $B_\alpha^{(a)}(\mathbf{q},0,0)$ ($\varepsilon<0$), whilst panel b corresponds to $B_\alpha^{(b)}(\mathbf{q},0,0)$ ($\varepsilon>0$).

Due to the presence of two pair propagators, when in the vicinity of T_c, all important ω and Ω dependence comes from the analytic structure of the pair propagators rather than the weak frequency dependence of the blocks [56]. Hence, we may set $\Omega=\omega=0$ inside the blocks to extract the leading order correction of the AL diagram. Thus we are left with evaluating,

$$B_\alpha(\mathbf{q},0,0)=T\sum_{\varepsilon}\sum_{\mathbf{k}}\frac{k_\alpha}{m}G(\mathbf{k},i\varepsilon)G(\mathbf{k},i\varepsilon)G(\mathbf{q}-\mathbf{k},-i\varepsilon)C(\mathbf{q},i\varepsilon,-i\varepsilon)^2. \tag{3.126}$$

As usual we work in the diffusive limit and consider $\mathbf{k}$ close to the Fermi surface. Naturally, we would neglect the small momentum $\mathbf{q}$ in the electron Green's function in this case, however, the $\mathbf{k}$ sum would vanish due to being odd in k_α. Therefore, we expand the electron Green's function in the same manner as we did for the EEI calculation, making use of eq. 3.99 with $\mathbf{q}\to-\mathbf{q}$.

Next we need to appreciate the different sign choices enforced by the cooperons on a block. These are illustrated in fig. 3.24, and each yield,

$$\begin{aligned}B_\alpha^{(a)}(\mathbf{q},0,0)=B_\alpha^{(b)}(\mathbf{q},0,0)&=-\frac{T}{\tau_0^2}\sum_{\varepsilon>0}\sum_{\mathbf{k}}\frac{k_{F\alpha}(\mathbf{k}_F\cdot\mathbf{q})}{m^2}\frac{G^-(\mathbf{k})^2G^+(\mathbf{k})^2}{(\mathcal{D}q^2+2\varepsilon+\tau_\phi^{-1})^2},\\ B_\alpha(\mathbf{q},0,0)&=B_\alpha^{(a)}(\mathbf{q},0,0)+B_\alpha^{(b)}(\mathbf{q},0,0)\end{aligned} \tag{3.127}$$

where we have accounted for the expansion of the electron Green's function to first order. Evaluating the $\mathbf{k}$ sum produces a factor of $4\pi N(0)\tau_0^3 v_F^2 q_\alpha/d$. We then perform the ε

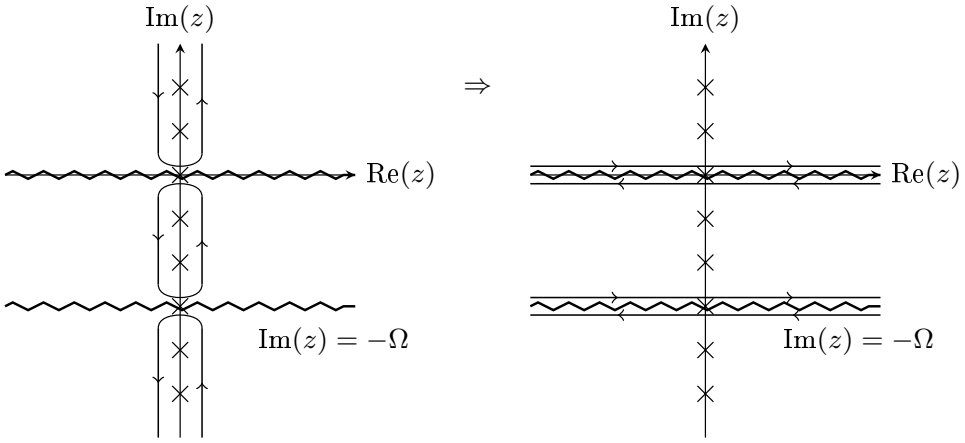

Figure 3.25: Left is the contour initially used to perform the analytic continuation of the ω sum for the AL diagram. Right shows the deformed contour we use to compute the integral. The zigzag lines represent the branch cuts at $\mathrm{Im}[z] = 0, i\Omega$.

making use of the digamma function derivative

$$B_\alpha(\mathbf{q}, 0, 0) = -\frac{N(0)\mathcal{D}q_\alpha}{2\pi T}\psi'\left(\frac{1}{2} + \frac{\mathcal{D}q^2 + \tau_\phi^{-1}}{4\pi T}\right). \tag{3.128}$$

Since we are only interested in the most singular contributions, we only consider small $\mathbf{q}$, hence we neglect the $\mathcal{D}q^2$ in the digamma derivative,

$$B_\alpha(\mathbf{q}, 0, 0) = -\frac{N(0)\mathcal{D}q_\alpha}{2\pi T}\psi'\left(\frac{1}{2} + \frac{1}{4\pi T\tau_\phi}\right). \tag{3.129}$$

Therefore, our response function becomes

$$K_{\alpha\beta}^{(F)}(i\Omega) = -\frac{e^2 N(0)^2\mathcal{D}^2}{\pi^2 T}\psi'\left(\frac{1}{2} + \frac{1}{4\pi T\tau_\phi}\right)^2 \sum_\omega \sum_{\mathbf{q}} q_\alpha q_\beta L(\mathbf{q}, i\omega)L(\mathbf{q}, i\omega + i\Omega). \tag{3.130}$$

To deal with the analytic structure of the pair propagators we must analytically continue the frequency sum to a contour integral in complex frequency space. Thus we use the standard Matsubara counting function trick detailed in appendix M.1,

$$T\sum_\omega F(\omega) = \frac{1}{4\pi i}\oint_C dz \coth\left(\frac{z}{2T}\right) F(-iz), \tag{3.131}$$

for some generic function of the bosonic Matsubara frequency ω, $F(\omega)$. Therefore,

$$\begin{aligned} K^{(F)}_{\alpha\beta}(i\Omega) =& i\frac{e^2N(0)^2\mathcal{D}^2}{4\pi^3T^2}\psi'\left(\frac{1}{2}+\frac{1}{4\pi T\tau_\phi}\right)^2 \\ &\times\sum_{\mathbf{q}} q_\alpha q_\beta \oint_C dz \coth\left(\frac{z}{2T}\right) L(\mathbf{q},z)L(\mathbf{q},z+i\Omega), \end{aligned} \tag{3.132}$$

where the contour C is illustrated on the left set axes in fig. 3.25. We then deform this contour to that shown on the right hand side of fig. 3.25. The form the pair propagator takes inside each region of the complex plane is defined by whether its frequency argument is above or below its branch cut,

$$L(\mathbf{q},z) = \begin{cases} L^R(\mathbf{q},z), & \mathrm{Im}(z)>0 \\ L^A(\mathbf{q},z), & \mathrm{Im}(z)<0, \end{cases} \tag{3.133}$$

where

$$L^R(\mathbf{q},z) = L^A(\mathbf{q},z)^* = \frac{1}{N(0)}\left[\ln\left(\frac{T}{T_c}\right)+\delta\psi+\psi'\left(\frac{1}{2}+\frac{1}{4\pi T\tau_\phi}\right)\frac{\mathcal{D}q^2-iz}{4\pi T}\right]^{-1}. \tag{3.134}$$

Note that we have already accounted for the fact that we are only interested in small momenta and frequencies in writing this line.

Let us focus on reshaping the contour integral into a more tractable form,

$$\begin{aligned} I(\mathbf{q},i\Omega) =& \oint_C dz \coth\left(\frac{z}{2T}\right) L(\mathbf{q},z)L(\mathbf{q},z+i\Omega) \\ =& \int_{-\infty}^{+\infty} dz \coth\left(\frac{z}{2T}\right)\left[L^R(\mathbf{q},z)-L^A(\mathbf{q},z)\right]L^R(\mathbf{q},z+i\Omega) \\ &+\int_{-\infty-i\Omega}^{+\infty-i\Omega} dz \coth\left(\frac{z}{2T}\right)\left[L^R(\mathbf{q},z+i\Omega)-L^A(\mathbf{q},z+i\Omega)\right]L^A(\mathbf{q},z) \\ =& \int_{-\infty}^{+\infty} dz \coth\left(\frac{z}{2T}\right)\Big\{\left[L^R(\mathbf{q},z)-L^A(\mathbf{q},z)\right]L^R(\mathbf{q},z+i\Omega) \\ &\qquad +\left[L^R(\mathbf{q},z)-L^A(\mathbf{q},z)\right]L^A(\mathbf{q},z-i\Omega)\Big\}, \end{aligned} \tag{3.135}$$

where, in moving from the third line to the fourth line, we let $z \to z - i\Omega$ in the second term and made use of the fact that $\coth(x)$ is unchanged by a shift $x \to z + n\pi i$ ($n \in \mathbb{Z}$), alongside $\Omega = 2\pi nT$ being a bosonic Matsubara frequency. Now that we have dealt with the analytic structure of the pair propagators such that all integrals lie on a single interval we may analytically continue the external frequency $i\Omega \to \Omega + i\delta$ to give the retarded response function.[47] This yields,

$$I^R(\mathbf{q}, \Omega) = 2i \int_{-\infty}^{+\infty} dz \coth\left(\frac{z}{2T}\right) \left[L^R(\mathbf{q}, z+\Omega) + L^A(\mathbf{q}, z-\Omega)\right] \mathrm{Im}\left[L^R(\mathbf{q}, z)\right], \quad (3.136)$$

and so

$$K^{(F),R}_{\alpha\beta}(\Omega) = i\frac{e^2 N(0)^2 \mathcal{D}^2}{4\pi^3 T^2} \psi'\left(\frac{1}{2} + \frac{1}{4\pi T\tau_\phi}\right)^2 \sum_{\mathbf{q}} q_\alpha q_\beta I^R(\mathbf{q}, \Omega). \quad (3.137)$$

Given that all diagrams cancel when $\Omega = 0$, we are free to expand eq. 3.137 to order Ω to obtain the DC conductivity correction, $K^R_{\alpha\beta}(\Omega) = -i\Omega\sigma_{\alpha\beta}(\Omega)$. Hence,

$$\sigma^{AL}_{\alpha\beta} = -\frac{e^2 N(0)^2 \mathcal{D}^2}{4\pi^3 T^2} \psi'\left(\frac{1}{2} + \frac{1}{4\pi T\tau_\phi}\right)^2 \sum_{\mathbf{q}} q_\alpha q_\beta \frac{\partial}{\partial\Omega} I^R(\mathbf{q}, \Omega)\Big|_{\Omega=0}. \quad (3.138)$$

Evaluating the derivative produces,

$$\begin{aligned} \frac{\partial}{\partial\Omega} I^R(\mathbf{q}, \Omega)\Big|_{\Omega=0} &= -4\int_{-\infty}^{+\infty} dz \coth\left(\frac{z}{2T}\right) \mathrm{Im}\left[L^R(\mathbf{q}, z)\right] \frac{\partial}{\partial z} \mathrm{Im}\left[L^R(\mathbf{q}, z)\right] \\ &= -\frac{1}{T}\int_{-\infty}^{+\infty} dz \,\mathrm{cosech}^2\left(\frac{z}{2T}\right) \mathrm{Im}\left[L^R(\mathbf{q}, z)\right]^2, \end{aligned} \quad (3.139)$$

where we used integration by parts to get the second line. Substituting this into eq. 3.138 and noting that the conductivity tensor is zero unless $\alpha = \beta$, $\sigma^{AL}_{\alpha\beta} = \delta_{\alpha\beta}\sigma_{AL}$, we obtain

$$\sigma_{AL} = \frac{e^2 N(0)^2 \mathcal{D}^2}{4\pi^3 T^3} \psi'\left(\frac{1}{2} + \frac{1}{4\pi T\tau_\phi}\right)^2 \sum_{\mathbf{q}} \frac{q^2}{d} \int_{-\infty}^{+\infty} dz \frac{\mathrm{Im}\left[L^R(\mathbf{q}, z)\right]^2}{\sinh^2\left(\frac{z}{2T}\right)}. \quad (3.140)$$

It turns out that phase breaking has little affect on the AL contribution, so for simplicity

[47] By mapping onto a single interval, we no longer have to worry about trying to be careful about the behaviour between $\mathrm{Im}[z] = 0$ and $\mathrm{Im}[z] = -i\Omega$.

let us set $\tau_\phi^{-1} = 0$ at this point.[48]

Next, we substitute in for $\mathrm{Im}[L^R(\mathbf{q}, z)]$, approximate the $\mathbf{q}$ sum via an integral over all space, and make the substitutions

$$\phi = \frac{\pi}{8T\epsilon}\, z, \qquad x^2 = \frac{\pi}{8T\epsilon}\, \mathcal{D}q^2, \qquad \epsilon = \ln\left(\frac{T}{T_c}\right). \tag{3.141}$$

This leaves us to evaluate

$$\begin{aligned}\sigma_{AL} = \frac{4e^2}{\pi d}\left(\frac{T}{\mathcal{D}}\right)^{\frac{d}{2}-1}\left(\frac{2}{\pi^3}\right)^{\frac{d}{2}}\Omega_d\ \epsilon^{\frac{d}{2}} \\ \times \int_0^{+\infty} dx \int_{-\infty}^{+\infty} d\phi \frac{\phi^2}{\sinh^2\left(\frac{4\epsilon}{\pi}\phi\right)} \frac{x^{d+1}}{\left[(1+x^2)^2+\phi^2\right]^2},\end{aligned} \tag{3.142}$$

where Ω_d is the d dimensional solid angle.[49] Lastly, we recall that we are interested only in temperatures close to T_c, meaning $\epsilon = \ln(T/T_c) \ll 1$. Thus the most singular contribution can be obtained by expanding, the ϕ integrand in powers of $\ln(T/T_c)$,

$$\frac{\phi^2}{\sinh^2\left(\frac{4\epsilon}{\pi}\phi\right)} = \frac{\pi^2}{16\epsilon^2} + \mathcal{O}(\eta^0). \tag{3.143}$$

Therefore, the leading order correction to the electrical conductivity due to the AL term is given by

$$\sigma_{AL} = \frac{\pi e^2}{2d}\left(\frac{T}{\mathcal{D}}\right)^{\frac{d}{2}-1}\left(\frac{2}{\pi^3}\right)^{\frac{d}{2}}\Omega_d\ \epsilon^{\frac{d}{2}-2}\int_0^{+\infty} dx \int_0^{+\infty} d\phi \frac{x^{d+1}}{\left[(1+x^2)^2+\phi^2\right]^2}, \tag{3.144}$$

where we also noted that the integral was even in ϕ.

To clarify what we mean by close to T_c, we introduce a quantity known as the reduced temperature, η,

$$\eta = \frac{T - T_c}{T_c}, \tag{3.145}$$

[48] Keeping $\tau_\phi^{-1} \neq 0$ is not difficult to deal with, but leads to some rather unpleasant expressions without providing any significant change.

[49] For the case of $d = 1$, this is just a factor of 2 as the integrand is spherically symmetric and so even in q when in one dimension. Therefore, we simply use this to rewrite the integral from 0 to $+\infty$, rather than $-\infty$ to $+\infty$.

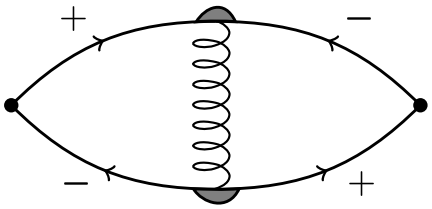

Figure 3.26

Figure 3.27: Sign choices for the Matsubara frequencies of the MT diagram in fig. 3.23c that give rise to the anomalous contribution.

which acts as a measure of distance from T_c. Hence, we define being close to T_c as being when $\eta \ll 1$. Conveniently, when $\eta \ll 1$ the logarithm can be approximated as

$$\ln\left(\frac{T}{T_c}\right) \simeq \eta. \tag{3.146}$$

Therefore, without needing to compute these integrals, we can see that the AL correction behaves as a simple power law in the reduced temperature,

$$\sigma_{AL} \sim \eta^{\frac{d}{2}-2}. \tag{3.147}$$

For the avid reader, details of evaluating these integrals are given in appendix I.3. We simply quote the results here,

$$\sigma_{AL} = e^2 \frac{\pi^2 \Omega_d}{128 d} \left(\frac{2}{\pi^3}\right)^{\frac{d}{2}} \left(\frac{T}{\mathcal{D}}\right)^{\frac{d}{2}-1} \eta^{\frac{d}{2}-2} \times \begin{cases} 3\pi, & d = 3 \\ 4, & d = 2 \\ \pi, & d = 1. \end{cases} \tag{3.148}$$

The $d = 2$ case coincides with the original result of Aslamzov and Larkin [18, 52]. In reality a system is 3D, so to regain 3D conductivities for the 1D and 2D cases, we simply divide the above by the film thickness, w, in 2D or by the cross-sectional area of the wire of radius a, πa^2, in 1D, where w and a are much less than the system size in the extended dimensions, L, that is $w, a \ll L$.

The MT term

The MT term has two types of contributions, one being the regular part and the other being the anomalous part. Let us deal with the anomalous part first, which arises from the sign configuration shown in fig. 3.27. This diagram has the response function[50]

$$\begin{aligned} K_{\alpha\beta}^{(C3)}(i\Omega) &= 16\pi N(0)e^2\mathcal{D}\delta_{\alpha\beta}T^2 \\ &\times \sum_{0<\omega<\Omega}\sum_{0<\varepsilon<\Omega-\omega}\sum_{\mathbf{q}} \frac{L(\mathbf{q},i\omega)}{(\mathcal{D}q^2+2\varepsilon+\omega+\tau_\phi^{-1})}\frac{1}{(\mathcal{D}q^2+2\Omega-2\varepsilon-\omega+\tau_\phi^{-1})} \\ &+ 8\pi N(0)e^2\mathcal{D}\delta_{\alpha\beta}T^2\sum_{0<\varepsilon<\Omega}\sum_{\mathbf{q}}\frac{L(\mathbf{q},0)}{(\mathcal{D}q^2+2\varepsilon+\tau_\phi^{-1})}\frac{1}{(\mathcal{D}q^2+2\Omega-2\varepsilon+\tau_\phi^{-1})}. \end{aligned} \tag{3.149}$$

Since there is only one pair propagator present, we need not worry about the analytic structure of the ω sum drastically. In fact, since we are only interested in behaviour close to T_c we can consider only the $\omega = 0$ piece of the response function, $\bar{K}_{\alpha\beta}^{(C3)}(i\Omega)$, to consider the leading order singular behaviour. This is equivalent to neglecting the dynamical effects of fluctuations [56]. This is the same as focusing on purely classical fluctuations, which are what dictate the BCS superconducting transition.

We may rewrite the $\omega = 0$ piece by using partial fractions to yield

$$\begin{aligned} \bar{K}_{\alpha\beta}^{(C3)}(i\Omega) &= 8\pi N(0)e^2\mathcal{D}\delta_{\alpha\beta}T^2\sum_{\mathbf{q}}\frac{L(\mathbf{q},0)}{\mathcal{D}q^2+\Omega+\tau_\phi^{-1}}\sum_{0<\varepsilon<\Omega}\frac{1}{\mathcal{D}q^2+2\varepsilon+\tau_\phi^{-1}} \\ &= 2N(0)e^2\mathcal{D}\delta_{\alpha\beta}T\sum_{\mathbf{q}}\left\{\frac{1}{\mathcal{D}q^2+\Omega+\tau_\phi^{-1}}\right. \\ &\qquad \left.\times\left[\psi\left(\frac{1}{2}+\frac{\mathcal{D}q^2+2\Omega+\tau_\phi^{-1}}{4\pi T}\right)-\psi\left(\frac{1}{2}+\frac{\mathcal{D}q^2+\tau_\phi^{-1}}{4\pi T}\right)\right]\right\}. \end{aligned} \tag{3.150}$$

We next expand to $\mathcal{O}(\Omega)$ to find the DC conductivity correction, as we know that all zeroth order pieces cancel, hence we may ignore the $\Omega = 0$ part of the expansion. To do this we analytically continue $i\Omega \to \Omega$ to consider the retarded response function, which does not generate any issues as the digamma function difference appearing in $\bar{K}_{\alpha\beta}^{(C3)}$ is sufficiently well behaved, then perform a standard Taylor series expansion in Ω. After

[50] Details on how to obtain this are given in appendix I.

finding the $\mathcal{O}(\Omega)$ piece, we can undo the analytic continuation by letting $\Omega \to i\Omega$ to consider the Matsubara response function. This process is rather long winded and gives the exact same result as if we had just treated the Matsubara frequncy Ω as continuous and differentiated with respect to it to find the first order term.[51] In future, when this is appropriate we shall do this rather than explain the process again.

Performing the expansion, using eq. 3.31, and writing $\sigma^{(C3)}_{\alpha\beta} = \delta_{\alpha\beta}\sigma^{(1)}_{MT}$, we find the DC correction to be

$$\sigma^{(1)}_{MT} = \frac{e^2 N(0)\mathcal{D}}{\pi} \sum_{\mathbf{q}} \frac{L(\mathbf{q},0)}{\mathcal{D}q^2 + \tau_\phi^{-1}} \psi'\left(\frac{1}{2} + \frac{\mathcal{D}q^2 + \tau_\phi^{-1}}{4\pi T}\right). \tag{3.151}$$

Clearly, if phase breaking was not accounted for the $\mathbf{q}$ sum would diverge in 1D and 2D. This diverging piece, cut-off by τ_ϕ^{-1}, gives rise to the anomalous MT contributions originally encountered by Maki [19]. Our interest in small momenta is further justified by the singular nature of this sum, and so we expand the digamma derivative in powers of $\mathcal{D}q^2 + \tau_\phi^{-1}$ to first order, as higher orders no longer produce results singular in $\epsilon \simeq \eta$ near T_c. The zeroth order piece is known as the anomalous MT conductivity, $\sigma^{(an)}_{MT}$, whilst the first order piece is known as a regular MT conductivity contribution, $\sigma^{(reg1)}_{MT}$. In this expansion we assume that τ_ϕ^{-1} is at most of order T. Hence we may write,

$$\sigma^{(1)}_{MT} = \sigma^{(an)}_{MT} + \sigma^{(reg1)}_{MT}, \tag{3.152a}$$

$$\sigma^{(an)}_{MT} = \frac{e^2 N(0)\mathcal{D}}{\pi} \psi'\left(\frac{1}{2}\right) \sum_{\mathbf{q}} \frac{L(\mathbf{q},0)}{\mathcal{D}q^2 + \tau_\phi^{-1}}, \tag{3.152b}$$

$$\sigma^{(reg1)}_{MT} = \frac{e^2 N(0)\mathcal{D}}{4\pi^2 T} \psi''\left(\frac{1}{2}\right) \sum_{\mathbf{q}} L(\mathbf{q},0). \tag{3.152c}$$

[51] When applying differentiation the variable with which you are differentiating with respect to should be continuous. This is because differentiation is a continuous process, is requires taking a limit of $\delta x \to 0$, which cannot be done for a discrete variable that hops suddenly from $n = 1$ to $n = 0$. Hence, we should be careful when we choose to differentiate with respect to a Matsubara frequency rather than a real continuous frequency.

To finish off our calculation of the anomalous MT term, we approximate the momentum sum by an integral, and treat τ_ϕ^{-1} as sufficiently small so that all digamma functions and their derivatives can be treated as having $\tau_\phi^{-1} = 0$. This allows us to use the same substitution for q as in eq. 3.141. This leaves us with,

$$\begin{aligned}\sigma_{MT}^{(an)} &= \frac{\pi e^2 \Omega_d}{2(2\pi)^d}\left(\frac{8T}{\pi\mathcal{D}}\right)^{\frac{d}{2}-1}\eta^{\frac{d}{2}-2}\int_0^{+\infty} dx \frac{x^{d-1}}{(x^2+\frac{\pi}{8T\tau_\phi\eta})(1+x^2)} \\ &= \frac{\pi e^2 \Omega_d}{2(2\pi)^d}\left(\frac{8T}{\pi\mathcal{D}}\right)^{\frac{d}{2}-1}\eta^{\frac{d}{2}-2}\frac{1}{1-\frac{\pi}{8T\tau_\phi\eta}}\int_0^{+\infty} dx\, x^{d-1}\left(\frac{1}{x^2+\frac{\pi}{8T\tau_\phi\eta}}-\frac{1}{1+x^2}\right).\end{aligned} \tag{3.153}$$

Given we assumed that $\tau_\phi^{-1} \ll T$, we can neglect it outside of the integral.[52] Hence,

$$\sigma_{MT}^{(an)} = \frac{\pi e^2 \Omega_d}{2(2\pi)^d}\left(\frac{8T}{\pi\mathcal{D}}\right)^{\frac{d}{2}-1}\eta^{\frac{d}{2}-2}\int_0^{+\infty} dx\, x^{d-1}\left(\frac{1}{x^2+\frac{\pi}{8T\tau_\phi\eta}}-\frac{1}{1+x^2}\right). \tag{3.154}$$

The inclusion of larger phase breaking rates is of more interest in the granular case, so we leave the discussion and effects of that for chapter 5.

The details behind evaluating the integral in eq. 3.154 are given in appendix I.4. Here we give the results,

$$\sigma_{MT}^{(an)} = \frac{e^2}{8}\left(\frac{8T}{\pi\mathcal{D}}\right)^{\frac{d}{2}-1}\eta^{\frac{d}{2}-2}\times\begin{cases}1, & d=3\\ \ln\left(\frac{8T\tau_\phi\eta}{\pi}\right), & d=2\\ 2\pi\sqrt{\frac{8T\tau_\phi\eta}{\pi}}, & d=1.\end{cases} \tag{3.155}$$

In writing the $d = 3$ case we have made use of the fact that τ_ϕ^{-1} is typically extremely small and negligible.[53] Whilst the 2D form may seem to have extremely non-trivial behaviour in terms of η, the logarithm is slowly varying and remains effectively constant close to T_c. Hence, we see that the anomalous MT term is just as singular as the AL term, and should not be neglected.

[52] Inside the integral it prevents divergence at the lower limit in one and two dimensions.

[53] This also shows that the phase breaking rate is not needed for a lower cut-off in the momentum sum in three dimensions.

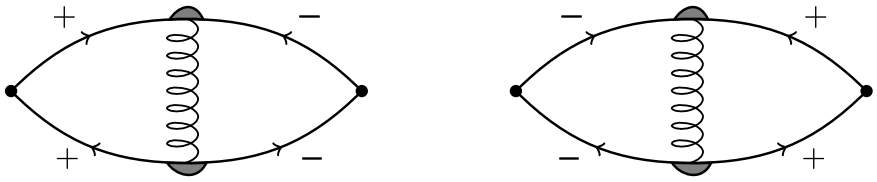

Figure 3.28: Sign choices for the Matsubara frequencies of the MT diagram in fig. 3.23c. Panels a and b correspond to the $K^{(C1)}_{\alpha\beta}(i\Omega)$ and $K^{(C2)}_{\alpha\beta}(i\Omega)$ respectively.

Before we return to $\sigma^{(reg1)}_{MT}$, let us consider the other sign configurations of the MT diagram, shown in fig. 3.28. They give equivalent contributions and again possess a simple pole structure in ω, so we can approximate their contributions by taking their $\omega = 0$ piece (details in appendix I.2),

$$\begin{aligned}\bar{K}^{(C1)}_{\alpha\beta}(i\Omega) &= \bar{K}^{(C2)}_{\alpha\beta}(i\Omega) \\ &= 8\pi N(0)e^2\mathcal{D}\delta_{\alpha\beta}T^2\sum_{\varepsilon>0}\sum_{\mathbf{q}}\frac{L(\mathbf{q},0)}{(\mathcal{D}q^2+2\varepsilon)}\frac{1}{(\mathcal{D}q^2+2\varepsilon+2\Omega)}.\end{aligned} \tag{3.156}$$

Performing the ε sums then expanding to first order in Ω gives their total DC conductivity contribution to be,

$$\sigma^{(reg2)}_{MT} = \sigma^{(C1)}_{MT} + \sigma^{(C2)}_{MT} = \frac{N(0)e^2\mathcal{D}}{4\pi^2T}\sum_{\mathbf{q}}L(\mathbf{q},0)\psi''\left(\frac{1}{2}+\frac{\mathcal{D}q^2+\tau_\phi^{-1}}{4\pi T}\right). \tag{3.157}$$

This is extremely similar in form to $\sigma^{(reg1)}_{MT}$. Since phase breaking rates are not a necessity in the calculation of the regular terms and do not affect it drastically, we set $\tau_\phi^{-1} = 0$ in these terms. Therefore, the two regular MT contributions to the conductivity are equivalent, so we may write,

$$\sigma^{(reg)}_{MT} = \sigma^{(reg1)}_{MT} + \sigma^{(reg2)}_{MT} = 2\sigma^{(reg1)}_{MT} = \frac{e^2N(0)\mathcal{D}}{2\pi^2T}\psi''\left(\frac{1}{2}\right)\sum_{\mathbf{q}}L(\mathbf{q},0). \tag{3.158}$$

Replacing the momentum sum by an integral and using the same substitution for q as

before gives ($\epsilon \simeq \eta$)

$$\sigma_{MT}^{(reg)} = \frac{e^2\Omega_d}{2\pi^2(2\pi)^d}\psi''\left(\frac{1}{2}\right)\left(\frac{8}{\pi}\right)^{\frac{d}{2}}\left(\frac{T}{\mathcal{D}}\right)^{\frac{d}{2}-1}\eta^{\frac{d}{2}-1}\int_0^{+\infty} dx\frac{x^{d-1}}{1+x^2}. \tag{3.159}$$

This integral diverges at the upper limit for $d = 2, 3$, so we introduce a cut-off, $x_{\max}$, based upon our approximation of the digamma functions,

$$\mathcal{D}q_{\max}^2 = 4\pi T \qquad\qquad x_{\max}^2 = \frac{\pi^2}{2\eta}. \tag{3.160}$$

The integral is then trivial to compute (see appendix I.5), and yields

$$\sigma_{MT}^{(reg)} = -e^2\frac{7\zeta(3)}{4\pi^3}\left(\frac{8}{\pi}\right)^{\frac{d}{2}}\left(\frac{T}{\mathcal{D}}\right)^{\frac{d}{2}-1}\times\begin{cases}\sqrt{2}, & d=3\\ \ln\left(\dfrac{\pi^2}{2\eta}\right), & d=2\\ \dfrac{2\pi}{\eta^{1/2}}, & d=1.\end{cases} \tag{3.161}$$

In writing the above we have used the identity $\psi''(1/2) = -14\zeta(3)$, where $\zeta(x)$ is the Riemann zeta function. This correction is clearly negative, and so reduces the conductivity due to interference effects. However, this is less singular than both the AL and anomalous MT terms, and so the conductivity still naturally diverges as we approach the transition.

The DOS term

The simplest diagram to compute is the DOS contribution. Here we find all behaviour of diagram A comes from the sign configurations shown in fig. 3.29, and that diagram B cancels half of the correction generated by fig. 3.29b.[54] Once again, the pole structure of the ω sum is simple and so we take the $\omega = 0$ pieces. The response functions we consider

[54]The details showing this are given in appendix I.1.

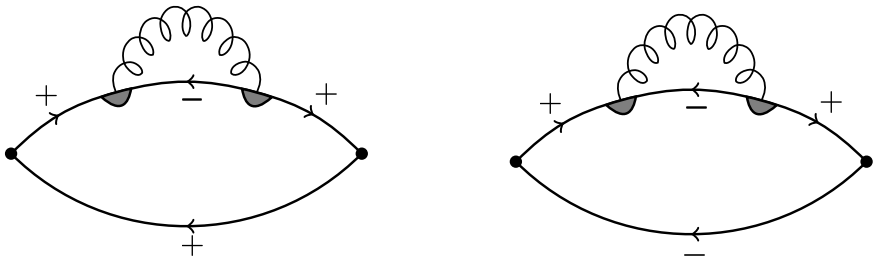

(a) (b)

Figure 3.29: Sign choices for the Matsubara frequencies of the DOS diagram in fig. 3.23a. Panels a and b correspond to the $K^{(A2)}_{\alpha\beta}(i\Omega)$ and $K^{(A3)}_{\alpha\beta}(i\Omega)$ respectively.

are then

$$\bar{K}^{(A2)}_{\alpha\beta}(i\Omega) = 8\pi N(0)e^2\mathcal{D}\delta_{\alpha\beta}T^2\sum_{\varepsilon>0}\sum_{\mathbf{q}}\frac{L(\mathbf{q},i\Omega)}{(\mathcal{D}q^2+2\varepsilon+2\Omega+\tau_\phi^{-1})^2}, \tag{3.162a}$$

$$\begin{aligned}\bar{K}^{(A3)}_{\alpha\beta}(i\Omega) &= -2\bar{K}^{(B)}_{\alpha\beta}(i\Omega)\\ &= -16\pi N(0)e^2\mathcal{D}\delta_{\alpha\beta}T^2\sum_{\mathbf{q}}\sum_{0<\varepsilon<\Omega}\frac{L(\mathbf{q},0)}{(\mathcal{D}q^2+2\varepsilon+\tau_\phi^{-1})^2}.\end{aligned} \tag{3.162b}$$

As before, we perform the ε sums and expand to first order in Ω, ignoring the zeroth order piece, to find the DC conductivity correction. Doing this we find that,

$$\sigma^{(A2)}_{DOS} = \sigma^{(A3)}_{DOS} + \sigma^{(B)}_{DOS} = \frac{1}{2}\sigma^{(A3)}_{DOS}, \tag{3.163}$$

and so the total correction from the DOS diagrams is found to be

$$\sigma_{DOS} = \frac{N(0)e^2\mathcal{D}}{2\pi^2T}\sum_{\mathbf{q}}L(\mathbf{q},0)\psi''\left(\frac{1}{2}+\frac{\mathcal{D}q^2+\tau_\phi^{-1}}{4\pi T}\right). \tag{3.164}$$

It is worth noting that this is simply twice the second regular MT part, $\sigma^{(reg2)}_{MT}$. Given that phase breaking mechanisms do not drastically change the DOS contributions we can neglect τ_ϕ^{-1} in eq. 3.164. As before, we focus on small momenta to find the leading order singular behaviour, so we also ignore the $\mathcal{D}q^2$ term appearing in the second digamma derivative. Upon accounting for these changes, we see that the DOS contribution is identical to the regular MT contribution with small phase breaking rates, eq. 3.158.

Therefore we follow the same steps taken in evaluating $\sigma_{MT}^{(reg)}$ to arrive at,

$$\sigma_{DOS} = -e^2 \frac{7\zeta(3)}{4\pi^3} \left(\frac{8}{\pi}\right)^{\frac{d}{2}} \left(\frac{T}{\mathcal{D}}\right)^{\frac{d}{2}-1} \times \begin{cases} \sqrt{2}, & d = 3 \\ \ln\left(\dfrac{\pi^2}{2\eta}\right), & d = 2 \\ \dfrac{2\pi}{\eta^{1/2}}, & d = 1. \end{cases} \tag{3.165}$$

The correction due to the DOS terms are negative, as expected. This lines up with the physical picture we gave earlier, when due to reducing the number of available current carries in the normal state, there would be some form of negative contribution to the conductivity. In reality, we see a transition and so the other positive contributions must overcome this. From our analysis of the AL and MT terms, we have shown that they are not only positive corrections but also more singular near T_c than the negative contributions arising from the regular MT and DOS corrections. Therefore, the set of diagrams we have calculated describe the on set of the superconducting transition.

In summary, we have presented the outline of the calculation of the superconducting fluctuation corrections to the DC electrical conductivity. In doing this, we created a propagator that described virtual Cooper pairs above T_c and showed that its zero momentum and frequency pole reproduced the BCS transition temperature. We also encountered in the case of the anomalous MT term in low dimensionalities that a cut-off was needed in the form of a phase breaking rate, τ_ϕ^{-1}. In a similar vein we saw a similar problem arise in the calculation of weak localisation corrections. Let us now discuss how we can find the temperature dependence of τ_ϕ^{-1}.

3.6 Phase Coherence Lifetime

We have mentioned and discussed the physical consequences of phase coherence numerous times leading up to this section, though we have not given any real insight as to how it might depend upon temperature, yet alone how to calculate such an object. In this section

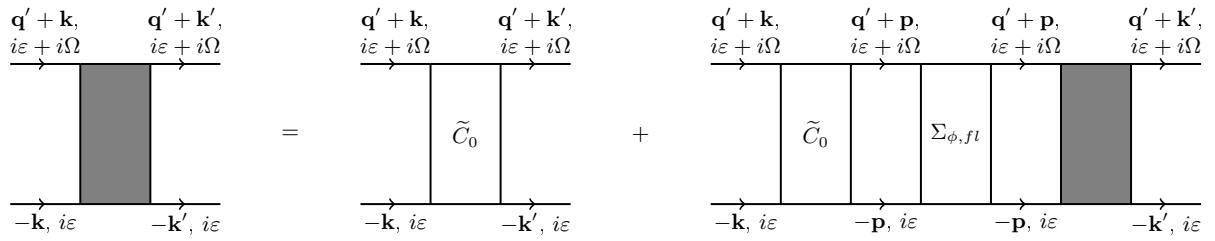

Figure 3.30: A more accurate diagrammatic representation of the cooperon, where Σ_ϕ contains the processes that generate τ_ϕ^{-1} in the cooperon, thus mitigating the need for a phenomenological insertion of phase breaking. $\widetilde{C}_0$ is the cooperon in the absence of phase breaking ($\tau_\phi^{-1} = 0$ in this part).

we will discuss two contributions to the phase breaking rate, τ_ϕ^{-1}, that appear naturally in the systems we consider: the first being due to Coulomb interactions, whilst the second arises from superconducting fluctuations. Their contributions were considered separately in 2D systems: Abrahams et. al. [57] calculated the Coulomb piece in 1981 using an exact eigenstates method, whilst Fukuyama and Abrahams [58] calculated the Coulomb piece in 1983 using diagrammatics, and Brenig et. al. [59] calculated the superconducting fluctuation piece in 1985 using diagrammatics in analogy to Fukuyama and Abrahams.

In both diagrammatic treatments, the cooperon series is modified to include diagrams that can be used to construct τ_ϕ^{-1} such that it can be written as the Dyson equation shown in fig. 3.30. Here the cooperon in the absence of phase breaking acts as the zeroth order component, whilst the object Σ_ϕ is related to τ_ϕ^{-1} and is defined in fig. 3.31 for Coulomb interactions.[55] The diagrams describing the contribution due to superconducting fluctuations are similar to those in fig. 3.31, but with a pair propagator in place of the Coulomb interaction and the Green's function between the interaction's start and end

[55]One might ask why we only consider diagrams where the interactions stays on the same Green's function line, and not an interaction that goes between the two lines. If we included this type of diagram, we would find that the impurity ladders to the right and left of the interaction would have different frequencies entering them.

If the top Green's function carried the frequency $i\varepsilon + i\omega$ and the bottom Green's function carried $i\varepsilon$, the interaction would move a frequency ω' from one to the other. After the interaction, we would then have $i\varepsilon + i\omega - i\omega'$ on the top and $i\varepsilon + i\omega'$ on the bottom. This means that the poles of impurity ladders either side (cooperons with $\tau_\phi^{-1} = 0$) would no longer line up. The first ladder would be most singular when $\omega = 0$, whilst the second ladder would be most singular for $\omega = 2\omega'$.

Compare this to the interaction staying to a single line, top or bottom, the impurity ladders either side of the interaction would have the same frequencies entering them, and so both have the same point of singularity. I.e: they are both most singular for $\omega = 0$. Consequently, these diagrams are far more dominant than the exchange interaction case.

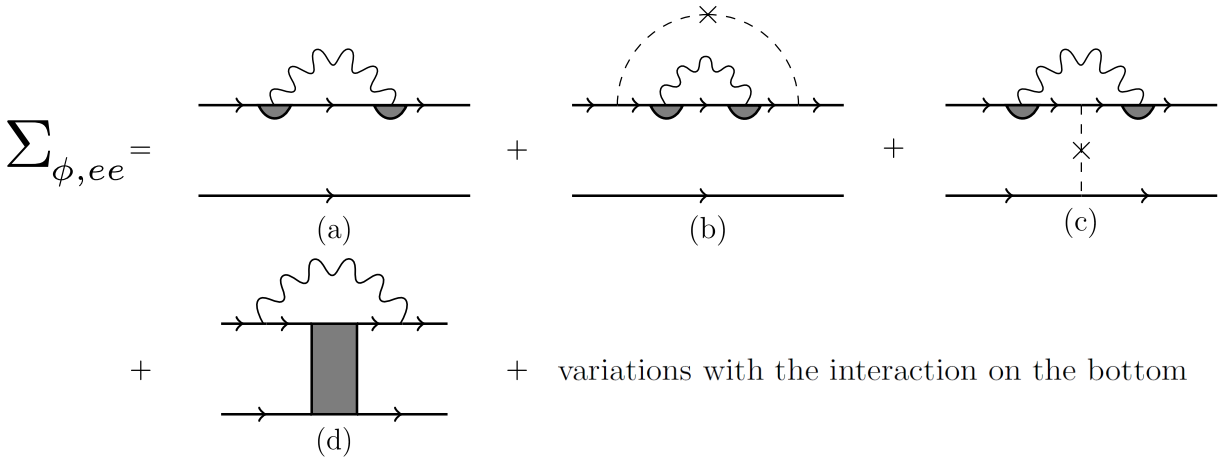

Figure 3.31: Diagrams describing the phase coherence corrections to the cooperon in homogeneous systems due to Coulomb interactions.

would instead travel from right to left. In either case due to the nature of disorder averaging, cooperons and diffusons will be generated within Σ_ϕ, and so we will eventually arrive at a self-consistency equation defining τ_ϕ^{-1}.

To start we shall consider the Coulomb correction in 2D, before we consider its effect in 3D to allow for comparison to the granular results we derive later. Afterwards, we consider the superconducting fluctuation contributions in a similar manner for both two and three dimensions.

3.6.1 Coulomb Phase Breaking Mechanism

For this treatment of the Coulomb contribution to τ_ϕ^{-1}, we shall follow Fukuyama and Abrahams' work [58] to re-derive their result for two dimensions, as well as providing our result for three dimensions, which coincides with that of Altshuler and Aronov [39]. Written mathematically we see the Dyson equation becomes

$$\widetilde{C}(\mathbf{q}', i\varepsilon + i\Omega, i\varepsilon) = \frac{1}{\widetilde{C}_0(\mathbf{q}', i\varepsilon + i\Omega, i\varepsilon)^{-1} - \Sigma_\phi}, \tag{3.166a}$$

where $\widetilde{C}_0(\mathbf{q}', i\varepsilon + i\Omega, i\varepsilon)$ is the cooperon in the absence of phase breaking. To recover eq. 3.78a from this, we therefore require

$$\frac{1}{\tau_\phi} = -\frac{\Sigma_\phi}{2\pi N(0)\tau_0^2}. \tag{3.167}$$

Hence, we may determine the temperature dependence of τ_ϕ^{-1} based on the diagrams given in fig. 3.31.

We begin by calculating diagrams A, B, and C of fig. 3.31, which can be written as

$$\Sigma^{(A)}_{\phi,ee} = -T\sum_{\mathbf{k},\mathbf{q}}\sum_{\omega}\Big[V(\mathbf{q}, i\omega)D(\mathbf{q}, i\varepsilon + i\Omega, i\varepsilon + i\Omega + i\omega)^2 G(\mathbf{k}, i\varepsilon + i\Omega)^2 \times G(\mathbf{k}+\mathbf{q}, i\omega + i\varepsilon + i\Omega)G(\mathbf{k}, i\varepsilon)\Big], \tag{3.168a}$$

$$\Sigma^{(B)}_{\phi,ee} = -T\sum_{\mathbf{k},\mathbf{k}',\mathbf{q}}\sum_{\omega}\left[\frac{V(\mathbf{q}, i\omega)}{2\pi N(0)\tau_0}D(\mathbf{q}, i\varepsilon + i\Omega, i\varepsilon + i\Omega + i\omega)^2 G(\mathbf{k}, i\varepsilon + i\Omega)^2 \times G(\mathbf{k}, i\varepsilon)G(\mathbf{k}', i\varepsilon + i\Omega)^2 G(\mathbf{k}'+\mathbf{q}, i\omega + i\varepsilon + i\Omega)\right], \tag{3.168b}$$

$$\Sigma^{(C)}_{\phi,ee} = -T\sum_{\mathbf{q}}\sum_{\omega}\left[\frac{V(\mathbf{q}, i\omega)}{2\pi N(0)\tau_0}D(\mathbf{q}, i\varepsilon + i\Omega, i\varepsilon + i\Omega + i\omega)^2 \times \left(\sum_{\mathbf{k}} G(\mathbf{k}, i\varepsilon + i\Omega)G(\mathbf{k}+\mathbf{q}, i\omega + i\varepsilon + i\Omega)G(\mathbf{k}, i\varepsilon)\right)^2\right], \tag{3.168c}$$

where Ω is the Matsubara frequency entering from the cooperon prior to Σ_ϕ. We have also neglected the small momentum, $\mathbf{q}'$, that would enter the Green's functions from the external cooperon as they are negligible compared to the fast momentum $\mathbf{k}$. The most singular contributions to these expressions clearly comes from small $\mathbf{q}$ ($|\mathbf{q}| \ll |\mathbf{k}| \simeq k_F$), and so we can proceed as we have done before by treating this momentum as our slow or diffusive mode.

With knowledge of the end result[56] we shall expand our Green's functions to first order in ω and second order in $\mathbf{q}$, as the leading order pieces of these diagrams cancel

[56]Perhaps there should be a spoiler warning here.

exactly.[57] We will also consider the case where $\Omega > 0$ without loss of generality, since we may consider the interactions on the Green's function entering with a positive frequency, meaning we are free to define as carrying an extra frequency of $\Omega > 0$ compared to the other Green's function entering the cooperon. By making this assumption, we must have $\varepsilon + \Omega > 0$ and $\varepsilon < 0$.

For ease of reading (and our own sanity), we again give the details of the calculation in appendix J. The sum of these diagrams yields,

$$\Sigma_{\phi,ee}^{(ABC)} = -T(2\pi N(0)\tau_0^2)^2 \sum_{\mathbf{q}} \sum_{\omega > \varepsilon + \Omega} \widetilde{D}(\mathbf{q}, i\omega) V(\mathbf{q}, i\omega), \tag{3.169}$$

where $\varepsilon + \Omega > 0$, and we have used the shorthand notation for the diffuson. We find a similar expression for diagram D in fig. 3.31. Starting from

$$\begin{aligned} \Sigma_{\phi,ee}^{(D)} = -T \sum_{\mathbf{q}} \sum_{\omega} & \widetilde{C}(\mathbf{q}, i\varepsilon + i\Omega + i\omega, i\varepsilon) V(\mathbf{q}, i\omega) \\ & \times \left(\sum_{\mathbf{k}} G(\mathbf{k}, i\varepsilon + i\Omega) G(\mathbf{k} + \mathbf{q}, i\varepsilon + \Omega + i\omega) G(\mathbf{k}, i\varepsilon) \right)^2 \end{aligned} \tag{3.170}$$

we evaluate the $\mathbf{k}$ sum by neglecting the $\mathbf{q}$ dependence in the Green's functions, before using eq. 3.75, to produce

$$\Sigma_{\phi,ee}^{(D)} = T(2\pi N(0)\tau_0^2)^2 \sum_{\mathbf{q}} \sum_{\omega > -(\varepsilon + \Omega)} \widetilde{C}(\mathbf{q}, i\Omega + i\omega) V(\mathbf{q}, i\omega). \tag{3.171}$$

The variants of the diagrams where the interaction appears on the bottom Green's function can be simply deduced from eq. 3.169 and eq. 3.171. We can see that for diagrams A, B, and C we dealt with $\varepsilon + \Omega > 0$ and $\varepsilon + \Omega + \omega < 0$, where as for their lower branch variants we require $\varepsilon + \omega > 0$ whilst $\varepsilon < 0$, so we expect the ω sum to the A, B, and C variants to be taken over $\omega < \varepsilon$. At the same time we would find $\omega \to -\omega$

[57] This will generate the leading order non-trivial behaviour that contributes to τ_ϕ^{-1}. The first order term of our expansion in $\mathbf{q}$ vanishes, as it carries an additional factor of $\mathbf{v}_F$ in the form $(\mathbf{v}_F \cdot \mathbf{q})$, and so will become odd in the fast momentum sum.

compared to the result in eq. 3.169. However, due to the summand being even in ω, we can let $\omega \to -\omega$ in the variant diagrams so that all values of ω considered are positive. For the variant of diagram D we cannot simply let $\omega \to -\omega$ as the cooperon depends on $\omega + \Omega$ and not just Ω. Hence, we cannot manipulate both ω sums involving the cooperon such that they are both solely taken over positive ω with the same summand. Therefore, the full leading order contribution of Coulomb interactions to Σ_ϕ is given by,

$$\begin{aligned}\Sigma_{\phi,ee} = -(2\pi N(0)\tau^2)^2 T \sum_{\mathbf{q}} \Bigg[\Bigg(\sum_{\omega > \varepsilon + \Omega} + \sum_{\omega > -\varepsilon} \Bigg) V(\mathbf{q}, i\omega) \widetilde{D}(\mathbf{q}, i\omega) \\ - \Bigg(\sum_{\omega > -(\varepsilon+\Omega)} + \sum_{\omega > \varepsilon} \Bigg) \widetilde{C}(\mathbf{q}, i\Omega + i\omega) V(\mathbf{q}, i\omega) \Bigg].\end{aligned} \tag{3.172}$$

Next, we analytically continue these sums to complex frequency space. The diffuson piece and cooperon pieces must be treated separately, due to the cooperon sum having terms in both half planes, whilst the diffuson's sums lie only in the upper half place. Starting with the diffuson sums, we need only consider one of the two diffuson sums in some detail as the other can be done in complete analogy. We may write,

$$T \sum_{\omega > -\varepsilon} V(\mathbf{q}, i\omega) \widetilde{D}(\mathbf{q}, i\omega) = \frac{1}{2\pi i} \oint_C dz\, n(z)\, V^R(\mathbf{q}, z) \widetilde{D}^R(\mathbf{q}, z), \tag{3.173}$$

where the superscript R denotes the retarded functions, $n(z)$ is the Bose-Einstein distribution, and the contour C is that shown in fig. 3.32a.

By deforming the contour to lie on the line $\mathrm{Im}(z) = -\varepsilon$ and noting that the integrand falls off sufficiently fast as $|z| \to \infty$, the integral will collapse,

$$\oint_C dz\, n(z)\, V^R(\mathbf{q}, z) \widetilde{D}^R(\mathbf{q}, z) = \int_{-\infty - i\varepsilon}^{+\infty - i\varepsilon} dz\, n(z)\, V^R(\mathbf{q}, z) \widetilde{D}^R(\mathbf{q}, z). \tag{3.174}$$

Letting $z \to z - i\varepsilon$, noting that $n(z - i\varepsilon) = -f(z)$,[58] where $l \in \mathbb{Z}$, and then analytically

[58] Recall that $\varepsilon = (2n+1)\pi T$, where $n \in Z$.

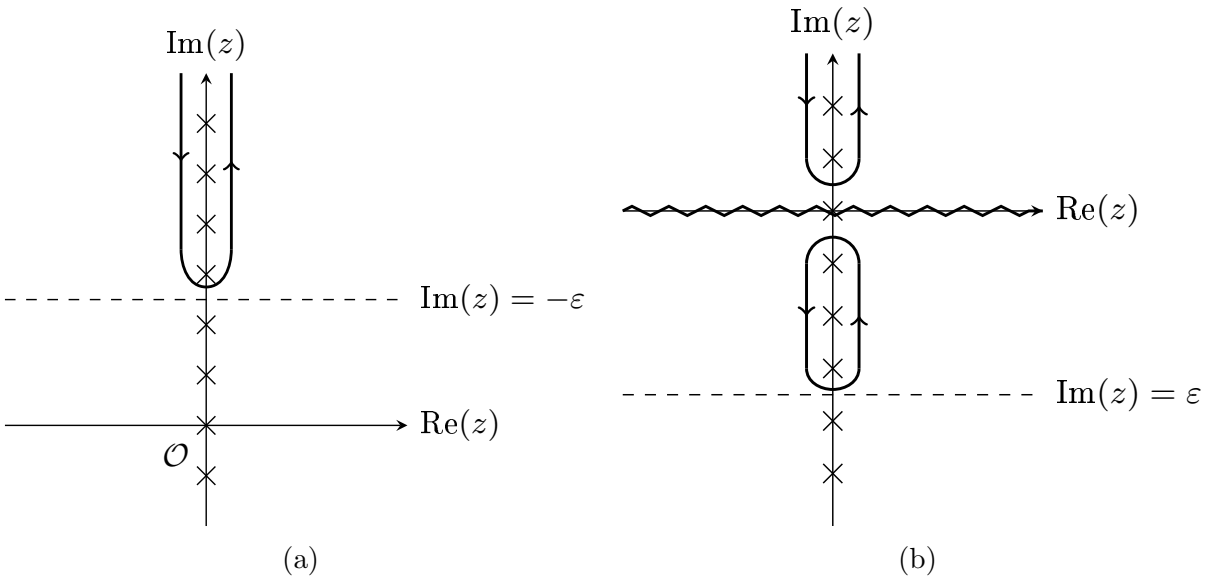

Figure 3.32: (a): contour used in the analytic continuation of the diffuson sum for $\omega > -\varepsilon$ in eq. 3.172. (b): contour used in the analytic continuation of the cooperon sum for $\omega > \varepsilon$ in eq. 3.172. The dashed line represents the cutoff in the frequency sums, and the zigzag represents a branch cut.

continuing the fermionic frequency, $i\varepsilon \to \varepsilon$, we end up at

$$\begin{aligned}\int_{-\infty-i\varepsilon}^{+\infty-i\varepsilon} dz\, n(z)\, V^R(\mathbf{q},z)\widetilde{D}^R(\mathbf{q},z) \to -\int_{-\infty}^{+\infty} dz f(z) V^R(\mathbf{q},z-\varepsilon)\widetilde{D}^R(\mathbf{q},z-\varepsilon) \\ = -\int_{-\infty}^{+\infty} dz f(z+\varepsilon) V^R(\mathbf{q},z)\widetilde{D}^R(\mathbf{q},z),\end{aligned} \tag{3.175}$$

where we let $z \to z+\varepsilon$ in obtaining the final line. Therefore, the original sum we considered in eq. 3.173 becomes

$$T\sum_{\omega>-\varepsilon} V(\mathbf{q},i\omega)\widetilde{D}(\mathbf{q},i\omega) \to -\int_{-\infty}^{+\infty} \frac{dz}{2\pi i} f(z+\varepsilon) V^R(\mathbf{q},z)\widetilde{D}^R(\mathbf{q},z) \tag{3.176}$$

We can follow the same ideas for the diffuson piece summed for $\omega > \varepsilon + \Omega$, however we will also need to analytically continue $i\Omega \to \Omega$ at the same time as we let $i\varepsilon \to \varepsilon$. After shifting the integral variable appropriately, this will produce a factor of $f(z-\varepsilon-\Omega)$ inside the integral instead of the $f(z+\varepsilon)$ we had before. Since we wish to consider the leading

order behaviour, we expand in powers of Ω and take the $\mathcal{O}(\Omega^0)$ piece. This leads to,

$$T\left(\sum_{\omega>\varepsilon+\Omega}+\sum_{\omega>-\varepsilon}\right)\widetilde{D}(\mathbf{q},i\varepsilon+i\Omega+i\omega,i\varepsilon+i\Omega)V(\mathbf{q},i\omega) \\ \rightarrow -\frac{1}{2\pi i}\int_{-\infty}^{+\infty}dz[f(z+\varepsilon)+f(z-\varepsilon)]V^R(\mathbf{q},z)\widetilde{D}^R(\mathbf{q},z). \tag{3.177}$$

Turning our attention towards the cooperon piece, we note that in analytically continuing the ω sums, we must introduce a branch cut along the real axis due to the screened Coulomb interaction changing from its advanced form in the lower half plane, to its retarded form in the upper half plane. Using the sum taken for $\omega > \varepsilon$ as an example, analytic continuation gives

$$T\sum_{\omega>\varepsilon}V(\mathbf{q},i\omega)\widetilde{C}(\mathbf{q},i\omega+i\Omega)=\frac{1}{2\pi i}\oint_{C'}dz\,n(z)\,V(\mathbf{q},z)\widetilde{C}^R(\mathbf{q},z+i\Omega), \tag{3.178}$$

where the contour C' is illustrated in fig. 3.32b. By deforming the contours to produce lines parallel to the branch cut and a line parallel to $\mathrm{Im}(z)=\varepsilon$ we see,

$$\oint_{C'}dz\,n(z)\,V(\mathbf{q},z)\widetilde{C}^R(\mathbf{q},z+i\Omega)=\int_{-\infty+i\varepsilon}^{+\infty+i\varepsilon}dz\,n(z)\,V^A(\mathbf{q},z)\widetilde{C}(\mathbf{q},z+i\Omega) \\ +\int_{-\infty}^{+\infty}dz\,n(z)\,\left[V^R(\mathbf{q},z)-V^A(\mathbf{q},z)\right]\widetilde{C}(\mathbf{q},z+i\omega). \tag{3.179}$$

We now shift $z\rightarrow z+i\varepsilon$ in the first integral, after which we analytically continue $i\varepsilon\rightarrow\varepsilon$ to then shift $z\rightarrow z-\varepsilon$. Following, we analytically continue $i\Omega\rightarrow\Omega$, expand in powers of Ω, and take the $\mathcal{O}(\Omega^0)$ term to isolate the most singular contribution, as in [58]. Hence,

$$\oint_{C'}dz\,n(z)\,V(\mathbf{q},z)\widetilde{C}^R(\mathbf{q},\,z+i\Omega) \\ \simeq\int_{-\infty}^{+\infty}dz\left\{2i\,n(z)\,\mathrm{Im}\left[V^R(\mathbf{q},z)\right]-f(z-\varepsilon)V^A(\mathbf{q},z)\right\}\widetilde{C}^R(\mathbf{q},z), \tag{3.180}$$

where we made use of $V^A(\mathbf{q},z)^*=V^R(\mathbf{q},z)$. In a similar manner we can show that the cooperon piece summed over $\omega>-(\varepsilon+\Omega)$ produces the same expression as above but

with $f(z+\varepsilon)$ instead of $f(z-\varepsilon)$. Thus, the cooperon piece of Σ_ϕ can be rewritten as,

$$\begin{aligned} T\left(\sum_{\omega>\varepsilon+\Omega}+\sum_{\omega>-\varepsilon}\right)&\widetilde{C}(\mathbf{q},i\varepsilon+i\Omega+i\omega,i\varepsilon+i\Omega)V(\mathbf{q},i\omega) \\ &\to\frac{2}{\pi}\int_{-\infty}^{+\infty}dz\,n(z)\,\mathrm{Im}\left[V^R(\mathbf{q},z)\right]\widetilde{C}^R(\mathbf{q},z) \\ &\quad-\frac{1}{2\pi i}\int_{-\infty}^{+\infty}dz[f(z+\varepsilon)+f(z-\varepsilon)]V^A(\mathbf{q},z)\widetilde{C}^R(\mathbf{q},z). \end{aligned} \tag{3.181}$$

Finally, by substituting eq. 3.177 and eq. 3.181 in to eq. 3.172, and then using eq. 3.167 we find,

$$\begin{aligned} \frac{1}{\tau_{\phi,ee}}=&N(0)\tau_0^2\sum_{\mathbf{q}}\Bigg[-2\int_{-\infty}^{+\infty}dz\Big\{\mathrm{Im}\left[V^R(\mathbf{q},z)\right] \\ &\times\Big([f(z+\varepsilon)+f(z-\varepsilon)]\widetilde{D}^R(\mathbf{q},z)+2n(z)\widetilde{C}^R(\mathbf{q},z)\Big)\Big\} \\ &+i\int_{-\infty}^{+\infty}dz[f(z+\varepsilon)+f(z-\varepsilon)]V^A(\mathbf{q},z)\left[\widetilde{D}^R(\mathbf{q},z)-\widetilde{C}^R(\mathbf{q},z)\right]\Bigg]. \end{aligned} \tag{3.182}$$

Clearly the most singular contributions come from small z, and so we shall approximate our integral in this limit. Therefore we may take

$$2n(z)\simeq\ \mathrm{cosech}\left(\frac{\beta z}{2}\right)\simeq 2\,\mathrm{cosech}(\beta z). \tag{3.183}$$

This is equivalent to assuming $\beta z\ll 1$, so our integral is now taken over the range $z\in[-T,+T]$. We further note that the Fermi functions are not singular for small z, and so terms containing $n(z)$ dominate over those with Fermi functions. Consequently, only the $n(z)\widetilde{C}^R(\mathbf{q},z)$ term is of any significant importance. Using these approximations we arrive at the result given in eq. 2.19 of [58], albeit with different limits,

$$\frac{1}{\tau_{\phi,ee}}\simeq-4N(0)\tau_0^2\sum_{\mathbf{q}}\int_{-T}^{+T}dz\frac{\widetilde{C}^R(\mathbf{q},z)}{\sinh(\beta z)}\mathrm{Im}\left[V^R(\mathbf{q},z)\right]. \tag{3.184}$$

From here onwards we will need to consider specific dimensionalities to obtain meaningful

results.

We provide the details of handling the integrals in appendix J and quote the results here.[59] In computing the integrals we assume that $\tau_\phi^{-1} \ll T$ in good metals, which we find to be true self-consistently. We give the results for two and three dimensions, as phase coherent effects are of distinct importance in two dimensions, and we will wish to consider phase breaking rates in three dimensional systems when we compare the theory of electrical conductivity in granular metals to the experimental results of BNCD.

2D Systems

Upon dealing with the integrals we reproduce Fukuyama and Abraham's [58] self-consistent equation for the Coulomb phase breaking rate for 2D disordered metals,

$$\frac{1}{\tau_{\phi,ee}} = \frac{T}{2\varepsilon_F \tau_0} \ln(\mathcal{D}\kappa_2^2 T \tau_\phi^2), \tag{3.185}$$

where $\kappa_2 = 4\pi N(0)e^2 = 2m_e e^2$ is the 2D Thomas-Fermi wave vector.[60] For systems without other phase breaking mechanisms present, we can find the leading order contribution to $\tau_{\phi,ee}^{-1}$ by letting substituting $\tau_{\phi,ee}$ into itself, and ignoring the nested logarithm, we recover Abraham et. al.'s [57, 58] result for 2D,

$$\frac{1}{\tau_{\phi,ee}} = \frac{T}{2\varepsilon_F \tau_0} \ln\left(\frac{T_1}{T}\right), \qquad T_1 = 4\varepsilon_F^2 \tau_0^2 \mathcal{D}\kappa^2. \tag{3.186}$$

As a final note for 2D, Altshuler and Aronov [39] obtain an alternative form for $\tau_{\phi,ee}^{-1}$ under the assumption that the thermal length, $L_T = \sqrt{\mathcal{D}/T}$, was much larger than the film thickness, t.[61] This lead them to

$$\frac{1}{\tau_{\phi,ee}} = \frac{T}{k_F l} \ln\left(\frac{k_F l}{2}\right). \tag{3.187}$$

[59] No integrals were harmed in this appendix during their handling.

[60] Note the Thomas-Fermi wave vector here is given in Gaussian cgs units. To regain the SI base units form, let $4\pi e^2 \to e^2/\varepsilon_0$.

[61] They also considered the case when $L_T \ll t$, however at sufficiently low temperatures this condition will no longer be true.

They obtained this result by including the vector potential into the cooperon and averaging over fluctuations in the electromagnetic field. This then generated a Schrödinger equation with an effective single-particle interaction, for which the cooperon was the appropriate Green's function.

3D Systems

For 3D, we find a result without the need to solve a self-consistent equation,

$$\frac{1}{\tau_{\phi,ee}} = \frac{1}{\sqrt{\varepsilon_F}} \left(\frac{3T}{2\varepsilon_F \tau_0} \right)^{3/2}. \tag{3.188}$$

This has exactly the same form as that given by Altshuler and Aronov [39].

Clearly, the phase breaking rate due to Coulomb interactions is small compared to the temperature when in a good metal due to the factor of $\varepsilon_F \tau_0 \gg 1$ appearing in the denominator. We can further see that we might expect $\tau_{\phi,ee}^{-1}$ to be even smaller in 3D than in 2D, due the small perturbative factor, $(\varepsilon_F \tau_0)^{-1}$, being to a higher power and the additional ratio of $\sqrt{T/\varepsilon_F}$.[62] Hence, we rarely expect $\tau_{\phi,ee}^{-1}$, and, in fact, τ_ϕ^{-1}, to be large enough to consider a non-zero value in most standard 3D metals. What we can see from these result though, is that the Coulombic phase breaking rate has a simple power law dependence upon the temperature, $T^{d/2}$. Let us now move on to considering the contribution of superconducting fluctuations to the phase breaking rate.

3.6.2 Superconducting Fluctuations Phase Breaking Mechanism

The calculation of the superconducting fluctuation contribution to τ_ϕ^{-1} was in first done by Keller and Korenman in 1971 and 1972 [54, 55]. Here they considered the corrections to the cooperon vertex piece in the context of the Maki-Thompson diagram, and showed how one could generate a phase breaking rate without the need for magnetic impurities, or external mechanisms. Their calculation showed that simply due to the natrual occurrance

[62] In good metals ε_F is typically at least of the order of 10^5K and as large as 10^6K in the best metals.

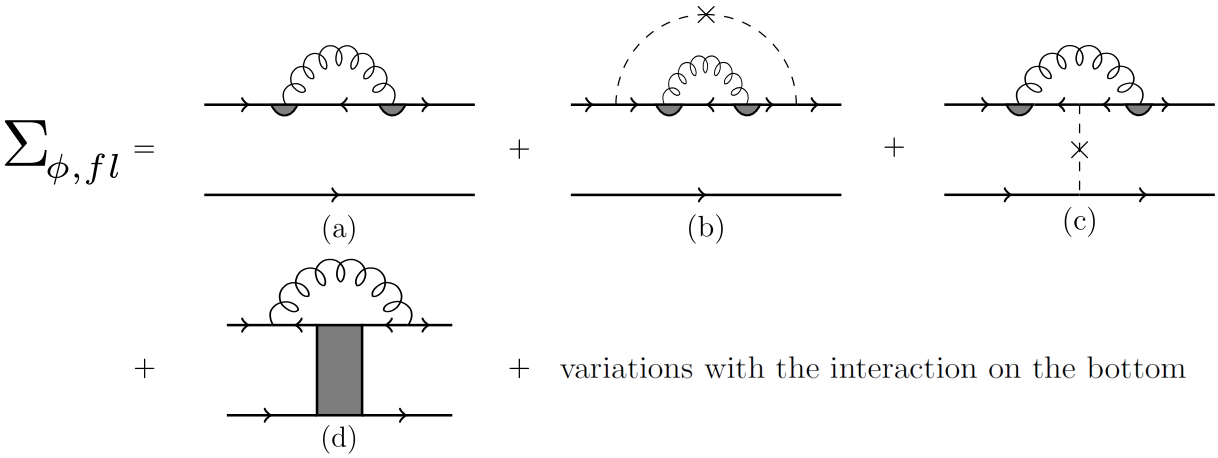

Figure 3.33: Diagrams describing the phase coherence corrections to the cooperon in homogeneous systems due to superconducting fluctuations.

of superconducting fluctuations, a phase breaking rate was generated. However, their calculation was not complete.

They considered diagrams of the form shown in diagrams A, B, and C of fig. 3.33, but did not account for diagram D. It also appears that they did not treat the problem self-consistently: in their diagrams A, B, and C, the cooperons appearing at the ends of the pair propagator were not those with $\tau_\phi^{-1} \neq 0$, but rather just simple impurity ladders. Furthermore, for a fully self-consistent treatment, the phase breaking rate due to Coulomb interactions should also be included. Consequently, they found a fluctuation phase breaking rate that diverged as one approached the transition from above,[63]

$$\frac{1}{\tau_{\phi,fl}} = \frac{2\ln 2}{k_F l}\frac{T}{\epsilon}, \qquad \epsilon = \ln\left(\frac{T}{T_c}\right). \tag{3.189}$$

This was pointed out to be unphysical by Brenig et. al. [59], as an infinite phase breaking rate would mean Cooper pairs could not form, and so there would be no superconducting transition. A larger τ_ϕ^{-1} leads to a greater suppression of T_c. Therefore, an infinite phase breaking rate would force T_c to zero.

The work of Brenig et. al. in 1985 [59] addresses this divergence by treating $\tau_{\phi,fl}^{-1}$ in a completely self-consistent manner. In doing so, they considered the diagrams shown

[63] As explained in ref. 22 of Brenig et. al. [59], this is give by $2L_2(0)$ Keller and Korenman's notation. This can be seen from eq. 14 of [55].

in fig. 3.33, in analogy to Fukuyama and Abraham's earlier treatment of the Coulomb contribution [58]. In their self-consistent treatment they included $\tau_{\phi,ee}^{-1}$ and found the total phase breaking rate due to Coulomb interactions and superconducting fluctuations. Let us now reproduce their calculation for two dimensions, and present a new result for three dimensions.

We leave the details of the calculation to appendix J, and provide the skeleton points of the calculation here. The methods employed there are extremely similar to those used in the calculation of $\tau_{\phi,ee}^{-1}$. We find that we must expand in powers of ω and $\mathbf{q}$ again to find a non-trivial result. After considering all possible sign configurations and variations with the propagator on the top or bottom line, we find,

$$\begin{aligned}\frac{1}{\tau_{\phi,fl}} =& (2\pi N(0)\tau_0^2)^2 T \sum_{\mathbf{q}} \sum_{\omega<\varepsilon+\Omega} \widetilde{C}(\mathbf{q}, i\omega - 2i\varepsilon - 2i\Omega)^2 L(\mathbf{q}, i\omega)(\mathcal{D}q^2 - \omega) \\ &+ (2\pi N(0)\tau_0^2)^2 T \sum_{\mathbf{q}} \sum_{\omega<-\varepsilon} \widetilde{C}(\mathbf{q}, i\omega + 2i\varepsilon)^2 L(\mathbf{q}, i\omega)(\mathcal{D}q^2 - \omega) \\ &- 2\pi N(0)\tau_0^2 T \sum_{\mathbf{q}} \sum_{\omega>\varepsilon+\Omega} \widetilde{D}(\mathbf{q}, i\omega - 2i\varepsilon - i\Omega) L(\mathbf{q}, i\omega) \\ &- 2\pi N(0)\tau_0^2 T \sum_{\mathbf{q}} \sum_{\omega>-\varepsilon} \widetilde{D}(\mathbf{q}, i\omega + 2i\varepsilon + i\Omega) L(\mathbf{q}, i\omega),\end{aligned} \tag{3.190}$$

where we again use the shorthand forms for the cooperon and diffuson. To analytically continue these frequency sums we appreciate that the cooperon sums consider poles in both half planes, so the contour we consider is shown in fig. 3.34, whilst the diffuson sums are relatively straightforward and use the contour shown in fig. 3.32a. We deform the cooperon contours to give integrals along the real axis and the line where $\mathrm{Im}(z) = \varepsilon + \omega$ (or $\mathrm{Im}(z) = -\varepsilon$, depending on the sum), and deform the diffuson contours to give an integral along the lines where $\mathrm{Im}(z) = \varepsilon + \omega$ and $\mathrm{Im}(z) = -\varepsilon$. Upon shifting all integrals to lie on the interval $z \in [-\infty, +\infty]$, and expanding to zeroth order in ε and Ω,[64] as in

[64] In the original Brenig et. al. paper [59], they set $\varepsilon, \varepsilon + \Omega \to 0$, which is equivalent to our expansion. We simply choose to think of this in terms of an expansion for the sake of familiarity.

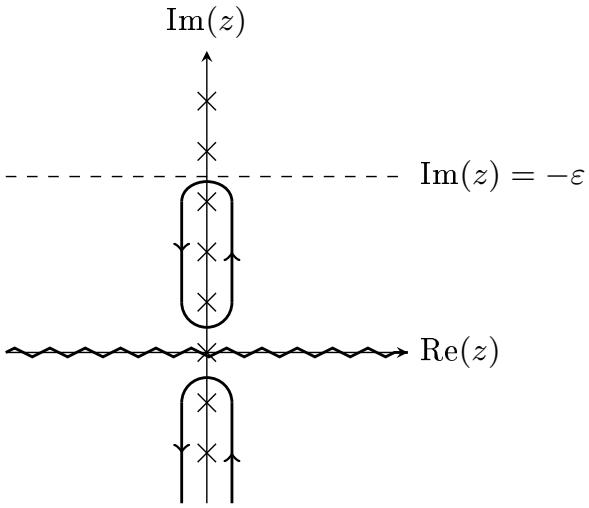

Figure 3.34: Here we show the type of contour used in analytically the bosonic sums involving a Cooperon in eq. 3.190.

the Coulomb calculation, we find

$$\frac{1}{\tau_{\phi,fl}} = 2N(0)\tau_0^2 \sum_{\mathbf{q}} \Bigg[4\pi N(0)\tau_0^2 \int_{-\infty}^{+\infty} dz\, n(z)\, \mathrm{Im}\left[L^R(\mathbf{q},z)\right] (\mathcal{D}q^2 + iz)\widetilde{C}^A(\mathbf{q},z)^2 \\ - 2\pi N(0)\tau_0^2 i \int_{-\infty}^{+\infty} dz f(z) L^R(\mathbf{q},z)(\mathcal{D}q^2 + iz)\widetilde{C}^A(\mathbf{q},z)^2 \\ + i\int_{-\infty}^{+\infty} dz f(z) L^R(\mathbf{q},z)\widetilde{D}^R(\mathbf{q},z) \Bigg]. \tag{3.191}$$

This is the same result given by Brenig et. al. [59] in their eq. 7 and eq. 8.

The most singular results occur at small z, and so the most dominant term arises from those containing $n(z)$. Hence, the leading order contribution to the phase breaking rate due to superconducting fluctuations is,

$$\frac{1}{\tau_{\phi,fl}} \simeq 8\pi N(0)^2 \tau_0^4 T \sum_{\mathbf{q}} \int_{-T}^{+T} \frac{dz}{z} \mathrm{Im}\left[L^R(\mathbf{q},z)\right] (\mathcal{D}q^2 + iz)\widetilde{C}^A(\mathbf{q},z)^2, \tag{3.192}$$

where we have taken $n(z) \simeq T/z$ for small z. Now, let us be precise in how we substitute in the pair propagator. Following Brenig et. al. [59], we expect the phase breaking rate to be small compared to the temperature, $\tau_\phi^{-1} \ll T$. In this case, the τ_ϕ^{-1} appearing in the digamma functions and their derivatives can be neglected. Therefore, the retarded

pair propagator can be taken as

$$L^R(\mathbf{q}, z) = \frac{1}{N(0)} \frac{1}{\ln\left(\frac{T}{T_c}\right) + \frac{\pi}{8T}(\mathcal{D}q^2 - iz)}. \tag{3.193}$$

It will be easier to phrase this problem in terms of the Ginzburg-Landau relaxation rate,

$$L^R(\mathbf{q}, z) = \frac{8T}{\pi N(0)} \frac{1}{\tau_{GL}^{-1} + \mathcal{D}q^2 - iz}. \tag{3.194}$$

Substituting this into eq. 3.192 and performing the frequency integral under the assumption $\tau_\phi^{-1} \ll T$ (details in appendix J) we arrive at,

$$\frac{1}{\tau_{\phi,fl}} = \frac{16T^2}{\pi N(0)} \sum_{\mathbf{q}} \left[1 + \frac{\mathcal{D}q^2}{\mathcal{D}q^2 + \tau_{GL}^{-1}}\right] \frac{1}{(\tau_\phi^{-1} + \tau_{GL}^{-1} + 2\mathcal{D}q^2)^2}. \tag{3.195}$$

We now need to consider the different dimensionalities separately (see appendix J). In any case, we will be left with a self-consistent equation to solve numerically. Specifically, we find

$$\frac{1}{\tau_{\phi,fl}} = \frac{16T^2\tau_\phi}{\pi k_F l} \left[\frac{\tau_{GL}^2}{\tau_{GL}^2 - \tau_\phi^2} + \frac{\tau_{GL}\tau_\phi}{(\tau_\phi - \tau_{GL})^2} \ln\left(\frac{2\tau_\phi}{\tau_\phi + \tau_{GL}}\right)\right], \tag{3.196}$$

for $d = 2$, which is the result derived by Brenig et. al. [59], and

$$\frac{1}{\tau_{\phi,fl}} = \frac{T^2}{\pi^2 N(0)\mathcal{D}^{3/2}} \sqrt{\frac{2}{\tau_{GL}^{-1} + \tau_\phi^{-1}}} \left[1 - \tau_{GL}^{-1} \left(\frac{\sqrt{2\tau_{GL}^{-1}} - \sqrt{\tau_{GL}^{-1} + \tau_\phi^{-1}}}{\tau_{GL}^{-1} - \tau_\phi^{-1}}\right)^2\right], \tag{3.197}$$

for $d = 3$. To give a final set of self-consistent equations, we will need to include the Coulomb contribution as well. The total phase breaking rate, τ_ϕ^{-1}, is simply the sum of the different contributions,

$$\frac{1}{\tau_\phi} = \frac{1}{\tau_{\phi,ee}} + \frac{1}{\tau_{\phi,fl}}. \tag{3.198}$$

Therefore, the full self-consistent equations come from adding eq. 3.185 to eq. 3.196 in

2D, and eq. 3.188 to eq. 3.197 in 3D. Thus, we arrive at

$$\frac{1}{\tau_\phi} = \left(\frac{3T}{k_F l}\right)^{3/2} \frac{1}{\sqrt{\varepsilon_F}} \left\{ 1 + 2\sqrt{\frac{T\tau_{GL}}{1+\tau_{GL}\tau_\phi^{-1}}} \left[1 - \left(\frac{\sqrt{2} - \sqrt{1+\tau_{GL}\tau_\phi^{-1}}}{1-\tau_{GL}\tau_\phi^{-1}} \right)^2 \right] \right\}, \quad (3.199)$$

for three dimensions, and a few possible expressions for two dimensions.[65]

Without making more approximations, we find our fully self-consistent solution in 2D to be

$$\frac{1}{\tau_\phi} = \frac{T}{k_F l} \ln(\mathcal{D}\kappa_2^2 T\tau_\phi^2) + \frac{16T^2\tau_\phi}{\pi k_F l} \left[\frac{\tau_{GL}^2}{\tau_{GL}^2 - \tau_\phi^2} + \frac{\tau_{GL}\tau_\phi}{(\tau_\phi - \tau_{GL})^2} \ln\left(\frac{2\tau_\phi}{\tau_\phi + \tau_{GL}}\right) \right]. \quad (3.200)$$

If we instead use the leading order form of $\tau_{\phi,ee}^{-1}$, we see

$$\frac{1}{\tau_\phi} = \frac{T}{k_F l} \ln\left(\frac{T_1}{T}\right) + \frac{16T^2\tau_\phi}{\pi k_F l} \left[\frac{\tau_{GL}^2}{\tau_{GL}^2 - \tau_\phi^2} + \frac{\tau_{GL}\tau_\phi}{(\tau_\phi - \tau_{GL})^2} \ln\left(\frac{2\tau_\phi}{\tau_\phi + \tau_{GL}}\right) \right]. \quad (3.201)$$

This is of a similar approach to Brenig et. al., who used the leading order form of the Coulomb contribution rather than its self-consistent solution.

Brenig et. al. [59] instead used the phase breaking rate for Coulomb obtained by Altshuler and Aronov [39], and so obtained the self-consistent equation,

$$\frac{1}{\tau_\phi} = \frac{T}{k_F l} \ln\left(\frac{k_F l}{2}\right) + \frac{16T^2\tau_\phi}{\pi k_F l} \left[\frac{\tau_{GL}^2}{\tau_{GL}^2 - \tau_\phi^2} + \frac{\tau_{GL}\tau_\phi}{(\tau_\phi - \tau_{GL})^2} \ln\left(\frac{2\tau_\phi}{\tau_\phi + \tau_{GL}}\right) \right]. \quad (3.202)$$

The advantage to using this version is that it is fairly material independent, as we only need to choose a value for $k_F l$ that describes a disorded metal, and not worry about the specfics that determine the diffusion constant for a specific material. However, we shall see that the three different 2D self-consistent equations produce rather different results when we use real experimental values.

Before we resort to numerics to decipher the self-consistent equations, we may attempt to extract the exact value of the phase breaking rate at the transition. In 2D we can only

[65] Note that we used $2\varepsilon_F\tau_0 = k_F l$ when including the Coulomb phase breaking rate.

do this when we replace $\tau_{\phi,ee}^{-1}$ by its leading order form or Brenig's form.[66] When $T = T_c$, $\tau_{GL} \to \infty$, and so we find for two dimensions,

$$\frac{1}{\tau_{\phi,c}} = \frac{T_c}{2k_F l}\left[\widetilde{\alpha} + \sqrt{\widetilde{\alpha}^2 + \frac{64k_F l}{\pi}}\right], \tag{3.203}$$

where

$$\widetilde{\alpha} = \begin{cases} \ln(k_F^2 l^2 \mathcal{D}\kappa_2^2), & \text{leading order} \\ \ln\left(\dfrac{k_F l}{2}\right), & \text{Brenig.} \end{cases} \tag{3.204}$$

This is clearly finite, and so corrects the divergence originally seen in the works of Keller and Korenman [54, 55]. It is possible to recover eq. 3.189 from eq. 3.196 by setting $\tau_\phi^{-1} = 0$ on the right hand side, as shown by Brenig et. al. [59].

Attempting to find a similar expression in three dimensions, we find ourselves facing a cubic. Naturally the answer will not be elegant and offers little insight. We can, however, see that τ_ϕ^{-1} is finite at the transition in 3D from the cubic generated. Verification of this is most easily done using Descartes' rule of signs to consider the cubic generated in terms of $x = \tau_\phi^{-1/2}$ for $x > 0$. We find that there is only one positive root, and either two negative real or two complex roots.

To look at the numerical solutions to the self-consistent equations, we will need some experimental parameters. For both 2D and 3D, we shall use values based upon the work of Gordon et. al. [60], who studied the role of phase breaking rates and the Maki-Thompson contribution in thin aluminium films.[67] In their works, they give the ratio of the room temperature resistance to the resistance at 4K, Γ, the Fermi velocity, resistance per square at 4.2K, $R_\square(4.2\text{K})$, and transition temperature for a $t = 15$nm thick film as (their sample 830),

$$\Gamma = 1.126, \qquad v_F = 1.3 \times 10^6 \text{ms}^{-1}, \qquad R_\square(4.2\text{K}) = 24.3\Omega, \qquad T_c = 1.84\text{K}. \tag{3.205}$$

[66] For the full self-consistent equation, we'd just end up with the another self-consistent equation.

[67] The values of parameters such as the diffusion constant, k_F, etc for thin films and bulk materials are typically in the same ball park.

In reality the system is 3D, so we use the 3D DOS and diffusion constant to find typical values for a thin superconducting metallic film. Our aim is to obtain expressions for $\mathcal{D}$, which relies upon knowing $N(0)$, κ_2, k_F, and l. Switching back into SI base units we may write,

$$\begin{aligned} N(0) &= \frac{1}{\pi^2\hbar^3}\sqrt{\frac{m_e^3}{2}}\sqrt{\varepsilon_F}, & \sigma_0 &= \frac{1}{R_\square(4.2\mathrm{K})t\Gamma}, \\ \mathcal{D} &= \frac{\sigma_0}{2e^2N(0)}, & \kappa_2 &= \frac{m_e e^2}{2\pi\varepsilon_0\hbar^2}, \end{aligned} \tag{3.206}$$

where we have used the Einstein relation for the diffusion constant, and ε_0 is the permittivity of free space. Substituting in the experimental values we find

$$\begin{aligned} &N(0) \simeq 4.72\times10^{46}\mathrm{J}^{-1}\mathrm{m}^{-3}, \qquad \sigma_0 \simeq 2.44\times10^{6}\Omega^{-1}\mathrm{m}^{-1}, \qquad \mathcal{D} \simeq 10^{-3}\mathrm{m}^2\mathrm{s}^{-1}, \\ &\frac{1}{\tau_0} \simeq 4.25\times10^{14}\mathrm{s}^{-1}, \qquad k_F \simeq 1.13\times10^{10}\mathrm{m}^{-1}, \qquad l \simeq 2.33\times10^{-9}\mathrm{m}, \end{aligned} \tag{3.207}$$

and hence the parameters we insert into eq. 3.200 are,

$$k_F l = 26, \qquad \kappa_2 = 3.8\times10^{10}\mathrm{m}^{-1} \quad \Rightarrow \quad \mathcal{D}\kappa_2^2 = 1.45\times10^{18}\mathrm{s}^{-1} = 1.1\times10^{7}\mathrm{K}, \tag{3.208}$$

where we moved back to natural units ($\hbar = 1$, $k_B = 1$) in the final equality of $\mathcal{D}\kappa_2^2$.

The plots in fig. 3.35 show the numerical solutions to the different 2D self-consistent equations over for the range $T \in [T_c, 3T_c]$. Eq. 3.200 is referred to as the full curve, eq. 3.201 is labelled as the leading order curve, and eq. 3.202 corresponds to the Brenig curve. Fig. 3.35 compares the three equations over the full range, and shows clearly that Brenig et. al.'s result grows near the transition. The other two cases do start to increase near the transition, albeit extremely little. This may be seen as evidence supporting the Altshuler-Aronov form for $\tau_{\phi,ee}^{-1}$, as this curve is closer in nature to the Keller-Korenman result for $\tau_{\phi,fl}^{-1}$. When it comes to granular systems later, however, a fully perturbative approach will still be taken, akin to that of Fukuyama and Abrahams [58], since it can still provide physical insight and act as a guide for less perturbative methods in the future.

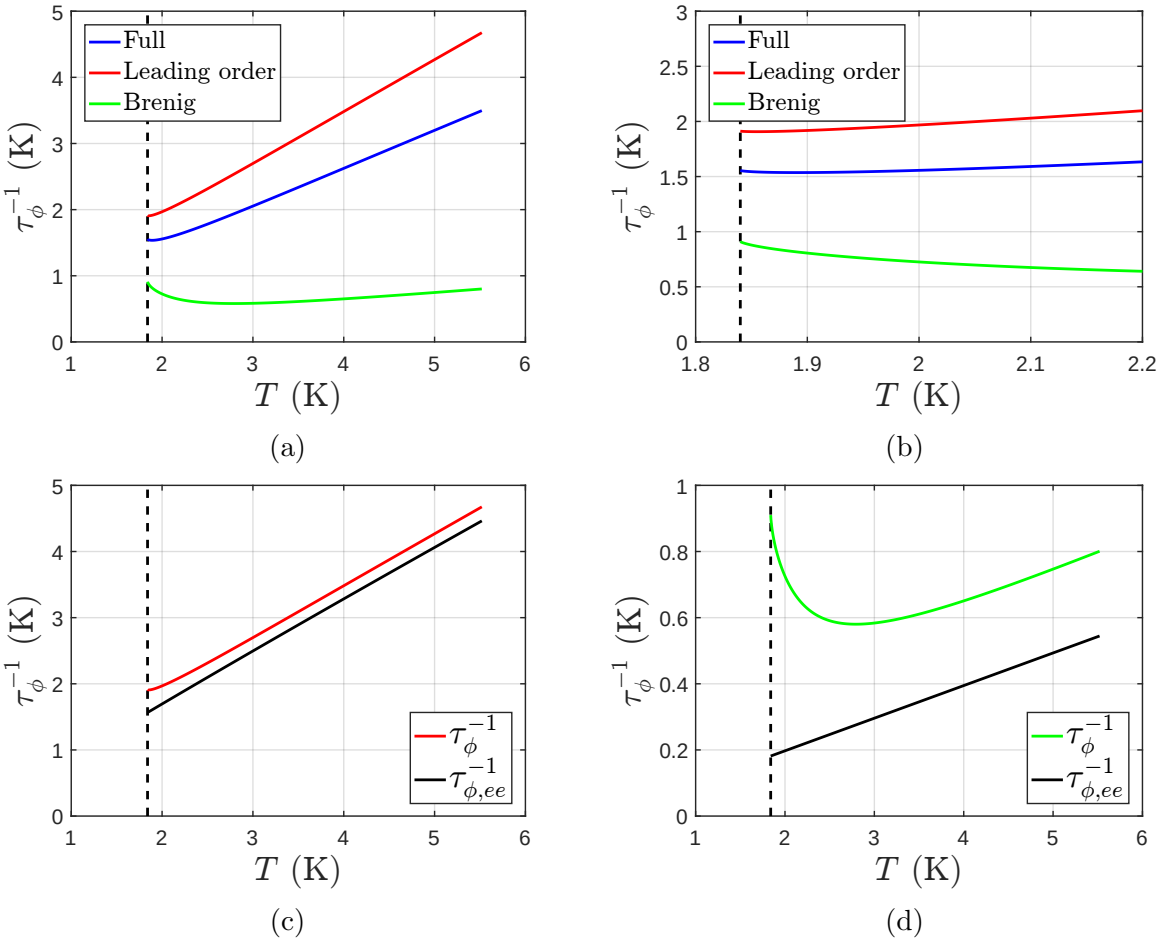

Figure 3.35: Numerical solutions to the 2D self-consistent equations for τ_ϕ^{-1}. The dashed line marks T_c. These plots are generated using values based on Gordon et. al.'s measurements [60]. (a): Total phase breaking rate for the different approximations we can solve self-consistently. The blue curve refers to the full self-consistent equation given in eq. 3.200, the red curve is the solution of the self-consistent equation using the leading order Coulomb phase breaking rate in eq. 3.201, and the green curve is the solution to Brenig et. al.'s self-consistent equation in eq. 3.202. (b): focus on the transition of panel a. (c): comparison of the leading order curve in panel a to the leading order Coulomb contribution (black). (d): comparison of the Brenig curve in panel a to the Brenig et. al.'s Coulomb contribution (black).

Fig. 3.35c and fig. 3.35d show that the total phase breaking rate tends to a form similar to the Coulomb phase breaking rate used in each case for high temperatures. We see that the curves are almost parallel, even extending the temperature range up to 100K, we find that the gradient only changes slightly. So, to leading order, τ_ϕ^{-1} and $\tau_{\phi,ee}^{-1}$ have the same temperature dependence for high temperatures, only their prefactors are slightly different and a near constant shift is required.

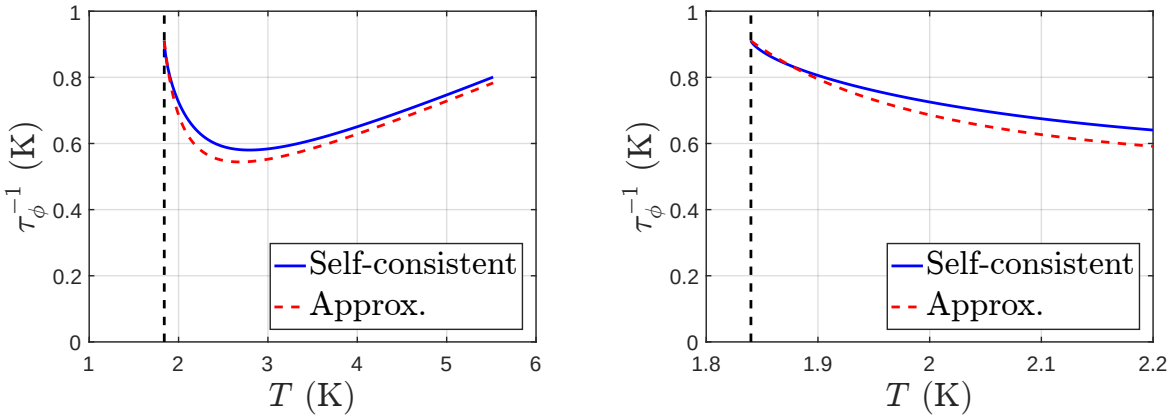

Figure 3.36: Comparison of Brenig et. al.'s [59] approximate function given in eq. 3.209 (dashed red line) compared to the solution of their self-consistent equation in eq. 3.202 (solid blue line). The dashed black line line marks T_c. (a): comparison over the range $T \in [T_c, 3T_c]$. (b): focussing in on the transition of panel a.

To approximate the curves generated by eq. 3.202, Brenig et. al. [59] gave the following function for the total phase breaking rate,

$$\frac{1}{\tau_\phi} = \frac{T}{k_F l}\left[\ln\left(\frac{k_F l}{2}\right) + \frac{2\ln 2}{\epsilon + \frac{2\ln 2}{\gamma}}\right], \tag{3.209}$$

where

$$\gamma = \frac{1}{2}\left[\sqrt{\left[\ln\left(\frac{k_F l}{2}\right)\right]^2 + \frac{64 k_F l}{\pi}} - \ln\left(\frac{k_F l}{2}\right)\right]. \tag{3.210}$$

We present eq. 3.209 compared to the Brenig et. al.'s self consistent equation in eq. 3.202 in fig. 3.36.

We can see that their approximate function has the same general shape as the self-consistent solution, though does deviate noticeably. In their own work, Brenig et. al. do state that this function is accurate to within 10% [59]. The way in which to obtain this function is neither clear or simple. We have therefore made mention of their result, and appreciate that it does give a similar curve to their self-consistent solution.

Moving on to the 3D case, we use the same experimental parameters as before, but in application to eq. 3.199. Fig. 3.37a shows that τ_ϕ^{-1} is generally small in 3D, and grows rapidly close to the transition. It is also clear that the phase breaking rate grows

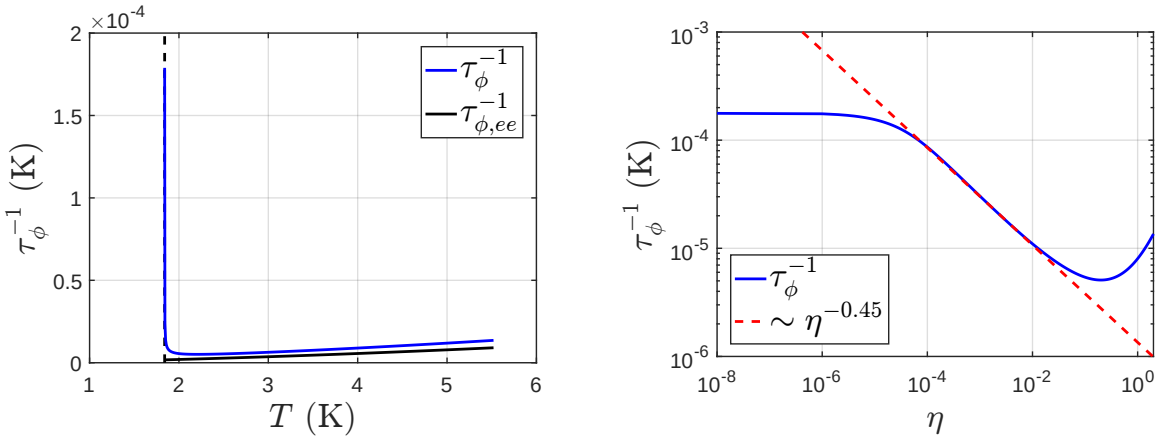

(a) (b)

Figure 3.37: (a): general temperature dependence of the total phase breaking rate in 3D (solid blue line) compared to the Coulomb phase breaking rate in 3D (solid black line). The dashed black line marks T_c. (b): reduced temperature dependence of the phase breaking rate in 3D (solid blue line). The dashed red line acts as a power law guide for an $\eta^{-0.45}$ power law.

for larger temperatures, though very slowly and hence remaining small. An interesting dependence can be seen by plotting this on a log-log scale against the reduced temperature, $\eta = (T - T_c)/T_c$, see fig. 3.37b. Here we see that τ_ϕ^{-1} changes very little extremely close to T_c, but grows approximately as $\eta^{-0.45}$ close to T_c ($10^{-4} \lesssim \eta \lesssim 10^{-2}$), before no longer depending on η in a simple manner.

Given that the curve in fig. 3.37b flattens out extremely close to T_c, it's clear that the phase breaking rate in 3D tends towards a finite non-zero value at the transition, as we expect from a physical standpoint. The rapid change in behaviour further away from the transition ($\eta \gtrsim 10^{-2}$), which is still close to T_c, can be attributed to the fluctuations in 3D systems being relatively small compared to their 2D and 1D counterparts, and so are quickly dominated by the Coulomb contribution to τ_ϕ^{-1}. As before, we see for higher temperatures the general T dependence of the curves is extremely similar, but the total phase breaking rate has a slightly more positive gradient than the Coulomb piece.

3.7 Chapter Summary

In this chapter we covered a large number of phenomena, and demonstrated how they can affect the transport of electrical current in disordered homogeneous metals.[68] We started by considering the effects of non-magnetic disorder described by single-particle potentials, and argued that to determine macroscopic quantities we would need to average over all possible distributions of the impurities.

Following this, we calculated the Drude conductivity using Kubo's formula for linear response, and showed how a diagrammatic language could be used to perform this calculation. This acted as a proof of concept for the diagrammatic approach, and served as the simplest stepping stone towards more complicated effects. The simplest correction to Drude arose in the form of weak localisation, which we were able to calculate by considering a maximally crossed diagram. This phenomenon was heavily reliant on the concept of phase coherence, and so we phenomenologically included a phase breaking rate, τ_ϕ^{-1}.

Afterwards, we considered the Coulomb interactions between electrons, which lead to a $T^{\frac{d}{2}-1}$ power law in the electrical conductivity for one and three dimensions, whilst we found a logarithmic dependence it two dimensions, $\ln(T\tau_0)$. Next we dealt with the effects of superconducting fluctuations, which appeared as virtual Cooper pairs above the transition. Here we demonstrated that diagrammatics could explain the divergence in σ we see near T_c, which grew as a simple power law in the reduced temperature, $\eta^{\frac{d}{2}-2}$. However, to avoid divergences for $d = 1, 2$, we were again forced to include a phase breaking rate.

The final section of this chapter addressed this seemingly benevolent being τ_ϕ^{-1}, and sought to understand its behaviour. Here we showed how one can calculated the temperature dependence of τ_ϕ^{-1} using only the effects that arose naturally in our systems, and not using other contributions due to more specific systems. Examples of these special cases could include Andreev reflection, magnetic impurities, etc.

[68] This was an extremely long chapter, I do apologise. I even started to wonder to myself if this chapter would ever end, and began to think perhaps not. Maybe that was the cabin fever of the pandemic and lockdown though. Nevertheless, here we are, we got there! Now for the next chapter.

Our aim is to translate as many of these results over to granular systems as possible. However, to do this we will first need to develop a diagrammatic language in which to do this. The next chapter will be a shorter analogous version of chapter 2, where we will show how to include a lattice of grains into the problem via the notion of tunnelling.

CHAPTER 4

DEVELOPING DIAGRAMMATIC TECHNIQUES FOR GRANULAR SYSTEMS

Everything we have dealt with so far has only been for homogeneous systems. In this chapter, we extend the digrammatic formalism derived in chapter 2 to granular systems. Consequently, this chapter will bear a lot of resemblance to chapter 2, though we will not have to provide the same level of detail, as direct comparison can be drawn between the methods taken to reach the end results.

Historically, much of work on the granular diagrammatic language was done by Beloborodov et. al. [61, 62, 63, 64, 65, 66], Biagini et. al. [67, 68], Skrzynski et. al. [69], and Efetov and Tschersich [70] in the late 1990s and early to mid 2000s, which culminated in Beloborodov et. al.'s 2007 review paper [26].[1] Within this plethora of works many ideas were discussed and methods used. Beloborodov et. al., Biagini et. al., and Skryzinksi et. al. primarily used diagrammatic methods to determine corrections to the electrical conductivity due to effects such as: superconducting fluctuations in strong magnetic fields [61, 62], superconducting fluctuations with larger intergranular coupling [69], weak locali-

[1] This list is by no means exhaustive, but refers to the main set of works that the ideas and methods of this thesis are based upon.

sation [63, 67], and Coulomb interactions [63, 64]. Further, Belobordov et. al. considered the effects of Coulomb interactions on MITs [65], whilst Biagini et. al. dealt with the corrections to the thermal conductivity due to superconducting fluctuations [68].

In contrast to the diagrammatic methods used in these papers, Efetov and Tschersich used the path integral formulation of QFT to understand the effects of Coulomb interactions at low temperatures on the electrical conductivity either side of the MIT [70]. Within their work, they derived the result for the granular Drude conductivity, a result that had been seemingly missing concrete proof in previous literature. However, the diagrammatic method was still not explicitly shown to obtain the granular Drude conductivity until the recent publication of Perkins and Smith [37]. After this brief history lesson, let us now outline the structure of this chapter.

We shall start by defining what we mean by a granular material and how we model such a system in section 4.1. Following this, we construct the diagrammatic rules needed to include tunnelling between grains in section 4.2, and how we treat tunnelling as a new form of disorder. Here we also derive the new single-electron Green's function. Finally, in section 4.3, we show how two-particle interactions may be included within a granular diagrammatic formalism.

4.1 What is a Granular Metal?

A granular metal is defined as being a collection of metallic islands embedded within an insulating, or less conductive, medium, which maintains metallic behaviour across the entire system. Alternatively, we can think of this in terms of dimensionless conductance. If the dimensionless conductance of an isolated grain is given by g_g, and the dimensionless conductance due to tunnelling between grains is given by g_T, then we define a granular metal as one satisfying,

$$1 \ll g_T \ll g_g. \tag{4.1}$$

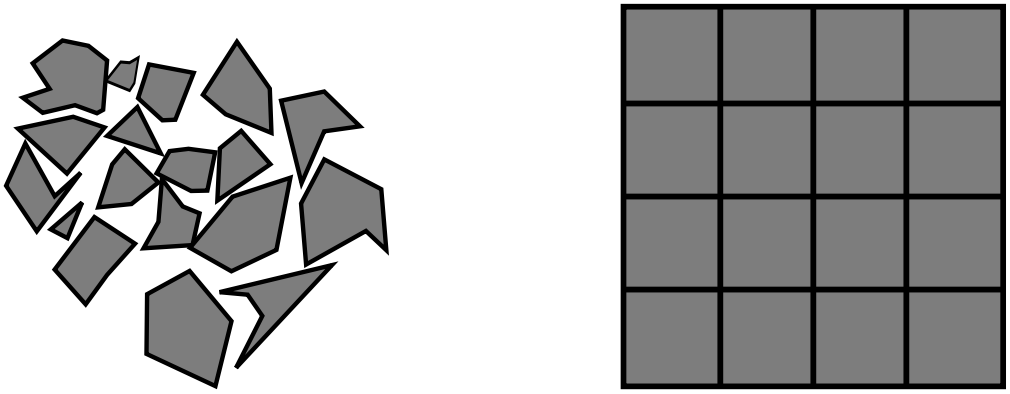

(a) (b)

Figure 4.1: (a): a generic example of a real 2D granular metal. (b): model of a 2D granular metal.

These dimensionless conductances can be written in terms of physical parameters characterising a granular metal,

$$g_T = \frac{\Gamma}{\delta}, \qquad g_g = \frac{E_{Th}}{\delta}, \tag{4.2}$$

where Γ is the tunnelling rate of electrons between grains at a single interface, $\delta = (N(0)a^d)^{-1}$ is the mean level spacing, a is the typical size of a grain,[2] and E_{Th} is the Thouless energy.[3]

In terms of modelling a granular metal, reality presents a messy picture, see fig. 4.1a. Disorder appears in many forms here: grain location, grain shapes, grain sizes, tunnelling probability, to list a few. However, as theorists, we need a nice and simple model to start analysing these systems. Thus we make the following set of assumptions,

- All grains are identical in shape and size. We assume the grains to be cubes with a characteristic size length of a.
- The impurities within a grain act solely within that grain.
- The grains form a lattice, which we assume to be simple cubic of side length a.

[2]Think of the mean level spacing as the inverse of the single spin DOS.

[3]The Thouless energy can be thought of as the energy scale associated to the rate at which a particle diffuses through a system, $\tau_D^{-1} = \mathcal{D}/L^2$ (L is the system's size), such that $E_{Th} = \hbar\tau_D^{-1}$.

We illustrate our effective model in fig. 4.1b. Whilst it may seem worrying that we take the grains to be the same size as the cubic lattice, it is not of concern in the mathematical model since we still enforce boundaries to the grains, which electrons can only cross via quantum tunnelling. The biggest advantage of this model is in its realisation of disorder. All disorder can be treated in terms of the tunnelling matrix elements appearing in the Hamiltonian, and so we only have to treat these matrix elements in a similar way to the impurities of section 3.1.

The assumptions we have made above are equivalent to those of Beloborodov et. al. [26], although we have assumed cubic grains as opposed to spherical grains. This choice is one of convenience, as more complicated problems become difficult to calculate when trying to account for spherical degeneracy within a radially symmetric sum. Let us now show how we include tunnelling into our Hamiltonian, whilst also maintaining the DOFs internal to a grain.[4]

4.2 Tunnelling: A New Form of Disorder

Generally, when considering a tunnelling problem we start from the tight binding model and tack on other parts describing the necessary physics.[5] The appropriate term to describe granular transport is thus,

$$H_T = \sum_{i,j} \sum_{\sigma} \sum_{\mathbf{k},\mathbf{p}} t_{ij}^{\mathbf{kp}} c_{i\mathbf{k}\sigma}^{\dagger} c_{j\mathbf{p}\sigma}, \tag{4.3}$$

where $t_{ij}^{\mathbf{kp}}$ is the tunnelling matrix element associated to an electron hopping from momentum state $\mathbf{p}$ on grain j, to momentum state $\mathbf{k}$ on grain i.[6] Naturally $t_{ij}^{\mathbf{kp}} = 0$ for $i = j$. Clearly, tunnelling is just another form of single-particle interaction.

[4] We refer to these as either intragranular DOFs or internal DOFs.

[5] We are no better than those before us, and this is exactly what we shall do.

[6] We adopt the convention that the final grain position will be the first grain label, whilst the starting grain position will be given by the second grain label. I.e. for a generic function F_{ji}, the particle moves from grain i to grain j. Using this notation, $\mathbf{R}_{ji} = \mathbf{R}_j - \mathbf{R}_i$ is the vector moving from grain i at $\mathbf{R}_i$ to grain j at $\mathbf{R}_j$.

Now, to construct our granular metal entirely, we need to add the presence of electrons and disorder within grains. The total Hamiltonian describing a granular metal, in the absence of two-particle interactions is then,

$$\begin{aligned}\mathscr{H}_1^{(T)} &= \sum_i \sum_\sigma \sum_{\mathbf{k}} \xi_{i\mathbf{k}} c^\dagger_{i\mathbf{k}\sigma} c_{i\mathbf{k}\sigma} + \sum_i \sum_\sigma \sum_{\mathbf{k},\mathbf{q}} U_i(\mathbf{q}) c^\dagger_{i\mathbf{k}+\mathbf{q}\sigma} c_{i\mathbf{k}\sigma} \\ &\quad + \sum_{i,j} \sum_\sigma \sum_{\mathbf{k},\mathbf{p}} t_{ij}^{\mathbf{kp}} c^\dagger_{i\mathbf{k}\sigma} c_{j\mathbf{p}\sigma} \\ &\equiv \mathscr{H}_g + H_T,\end{aligned} \tag{4.4}$$

where the first term describes free electrons bound to a single grain, the second term describes the disorder within a grain, and the third term is simply tunnelling between the grains. We use $\mathscr{H}_g$ to represent the Hamiltonian for the set of isolated grains with internal disorder.[7]

Before we delve into the disorder averaging over the $t_{ij}^{\mathbf{kp}}$, let us first demonstrate how we can generate a perturbative expansion in terms of these tunnelling events. The ideas we use are equivalent to those necessary for calculating the tunnelling current of a Josephson junction, and so we base our approach on Barone and Paternò's book [71] for a single tunnel junction.

4.2.1 Single-particle Green's Function

The major assumption we make, in line with Barone and Paternò [71], is

$$\left\langle c_{i\mathbf{k}\sigma} c^\dagger_{j\mathbf{p}\sigma'} \right\rangle_{\text{dis}} = \delta_{ij}\delta_{\sigma\sigma'}\delta_{\mathbf{kp}} \left\langle c_{i\mathbf{k}\sigma} c^\dagger_{i\mathbf{k}\sigma} \right\rangle_{\text{dis}}, \tag{4.5}$$

where $\langle ... \rangle_{\text{dis}}$ denotes averaging with respect to $\mathscr{H}_g$ and over the internal disorder. This is effectively saying that our theory must be built from the single-particle Green's functions internal to a grain.

[7] Recall that we use the font $\mathscr{H}$ to signify that we are in the grand canonical ensemble. When we see both fonts, $\mathscr{H}$ and H, used in the same equation, the part using $\mathscr{H}$ contains the chemical potential, and hence the knowledge that we are working in the GCE.

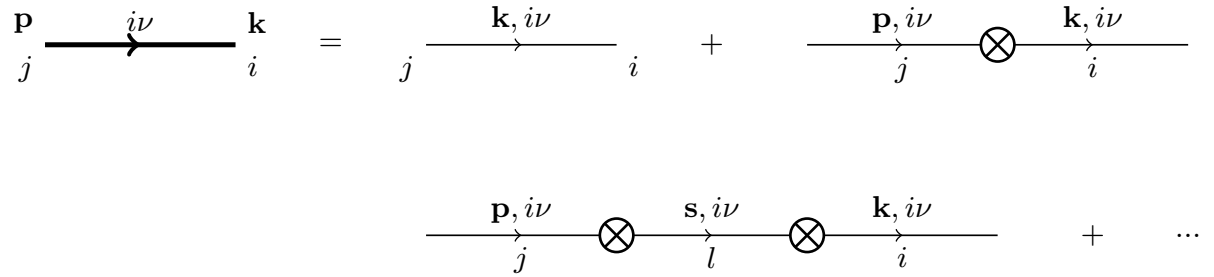

Figure 4.2: Diagrammatic representation of eq. 4.6, where we show the first three terms explicitly.

To obtain a diagrammatic expression for the single-electron Green's function, we start from its definition in the interaction picture (eq. 2.56), and treat H_T as our interacting perturbation. Using the expansion of the $\mathcal{S}$-matrix in eq. 2.60, recalling that all disconnected diagrams cancel, and lastly performing a Fourier series expansion in terms of fermionic Matsubara frequencies, we can see that the single-electron Green's function is simply given by a sum of consecutive tunnelling events made by the same electron,

$$\begin{aligned} G_{ij}(\mathbf{k},\mathbf{p},i\nu;H_T) = {} & \widetilde{G}_0(\mathbf{k},i\nu)\delta_{ij}\delta_{\mathbf{kp}} + t_{ij}^{\mathbf{kp}}\widetilde{G}_0(\mathbf{k},i\nu)\widetilde{G}_0(\mathbf{p},i\nu) \\ & + \sum_l \sum_{\mathbf{q}} t_{il}^{\mathbf{kq}} t_{lj}^{\mathbf{qp}} \widetilde{G}_0(\mathbf{k},i\nu)\widetilde{G}_0(\mathbf{q},i\nu)\widetilde{G}_0(\mathbf{p},i\nu) \\ & + \sum_{l,m} \sum_{\mathbf{s},\mathbf{q}} t_{il}^{\mathbf{kq}} t_{lm}^{\mathbf{sq}} t_{mj}^{\mathbf{qp}} \widetilde{G}_0(\mathbf{k},i\nu)\widetilde{G}_0(\mathbf{s},i\nu)\widetilde{G}_0(\mathbf{q},i\nu)\widetilde{G}_0(\mathbf{p},i\nu) + ..., \end{aligned} \tag{4.6}$$

where $\widetilde{G}_0$ is the homogeneous electron Green's function for a single isolated grain with translational invariance.[8] For the electronic transport problems we consider in chapter 5, $\widetilde{G}_0$ will simply be the homogeneous disorder-averaged electron Green's function from chapter 3 (eq. 3.14).

We write eq. 4.6 diagrammatically in fig. 4.2. This looks exactly like fig. 2.2, except now our single-particle scatterings have been replaced by tunnelling events. However, we cannot collapse this into a more useful form without averaging over the disordered set of tunnelling events. Before we do this, however, we can already deduce a new diagrammatic

[8] If the grains did not possess translational invariance, then we would not be able to write our tunnelling Hamiltonian in a form that tunnels from momentum state $\mathbf{p}$ in one grain to momentum state $\mathbf{k}$ in another.

rule for granular systems,

- All homogeneous Green's functions carry a grain label, which denotes the grain they belong to (i.e. $\widetilde{G}_0 \to \widetilde{G}_{0i}$). We then sum over all internal grain labels.

Thus, in the absence of averaging over tunnelling events, we find the following additional rules to those for single-particle interactions in homogeneous systems, under the premise that the single-particle interactions within each grain possess translational invariance:[9]

1. To each solid line we assign an additional grain index, denoted by a Latin character (e.g: i), on top of the momentum and frequency it already carries. This line represents the Green's function $\widetilde{G}_{0i}(\mathbf{k}, i\varepsilon)$.

2. Crossed circles represent tunnelling events, which introduce a factor of $t_{ij}^{\mathbf{kp}}$ to connect the Green's functions $\widetilde{G}_{0i}(\mathbf{k}, i\varepsilon)$ and $\widetilde{G}_{0j}(\mathbf{p}, i\varepsilon)$, which leave and enter the tunnelling event respectively.

3. Sum over all internal grain indices.

4.2.2 Single-electron Green's Function – With Averaging over Tunnelling Events

Let us now consider a disordered granular metal. In this case, by taking the impurity disorder average over each grain, we satisfy the need for translational invariance within a grain. As a result, $\widetilde{G}_0$ becomes the disorder-averaged electron Green's function in eq. 3.14. Our next step is to assign a statistical distribution to the tunnelling events.

Previously, we assumed a Gaussian distribution of impurity scattering events (eq. 3.5),

[9]This statement about internal translational invariance means we can write the homogeneous Green's functions in momentum space using only one momentum argument. This property can either be natural, or obtained by processes akin to disorder averaging.

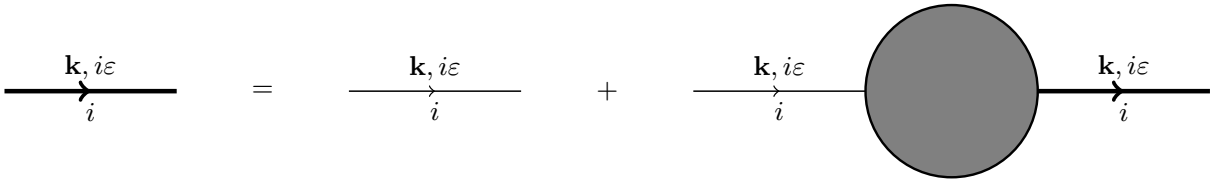

(a)

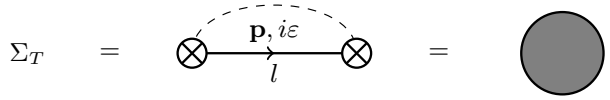

(b)

Figure 4.3: (a): Diagrammatic representation of the t-averaged electron Green's function, where the thin solid lines are $\widetilde{G}_{0i}$ propagators, and the thick solid lines are the t-averaged electron Green's function, G_i. (b): Diagrammatic series for the self-energy describing t-averaging. Here the solid line represents $\widetilde{G}_{0l}$.

so we assume an analogous distribution here,

$$\begin{aligned} \left\langle t_{ij}^{\mathbf{kp}} \right\rangle_{\mathrm{T}}^{(0)} &= 0, \\ \left\langle t_{ij}^{\mathbf{kp}} t_{lm}^{\mathbf{k'p'}} \right\rangle_{\mathrm{T}}^{(0)} &= \begin{cases} t^2(\delta_{im}\delta_{jl} + \delta_{il}\delta_{jm})\delta_{\mathbf{k}+\mathbf{k'},\mathbf{p}+\mathbf{p'}}, & \text{nearest neighbours} \\ 0, & \text{otherwise,} \end{cases} \end{aligned} \tag{4.7}$$

where $\langle ... \rangle_{\mathrm{T}}^{(0)}$ denotes the explicit averaging only over tunnelling events – t-averaging. In writing the average for two tunnelling events, we have assumed only nearest neighbour tunnelling is allowed.[10] Applying this average to eq. 4.6 we find an entirely equivalent set of diagrams to those in fig. 3.2, which we show in fig. 4.3. The dashed line connecting tunnelling events denotes their correlation. The t-averaged single-particle Green's function, $G_i(\mathbf{k}, i\varepsilon) = \langle G_{ij}(\mathbf{k}, \mathbf{p}, i\varepsilon; H_T) \rangle_T^{(0)}$, is therefore given by the Dyson equation

$$G_i(\mathbf{k}, i\varepsilon) = \widetilde{G}_{0i}(\mathbf{k}, i\varepsilon) + \widetilde{G}_{0i}(\mathbf{k}, i\varepsilon)\, \Sigma_T\, G_i(\mathbf{k}, i\varepsilon). \tag{4.8}$$

As in the homogeneous case, crossing terms will be negligible and nested diagrams vanish for the same reason.

[10] This is not an unreasonable assumption, and should always be our first port of call in these types of calculations.

The consequence of averaging is that each pair of tunnelling events correlated using eq. 4.7 produces a factor of $a^d t^2$.[11] This is in direct analogy to the factor of $(2\pi N(0)\tau_0)^{-1}$ that is produced in the homogeneous case (eq. 3.6). In the following, we shall write the factor of a^d generated by averaging explicitly, and so we now need to include the factors of $\mathcal{V}^{-1}$ for the momentum sums explicitly. Note, since the internal momenta are local to a grain, the volume appearing in the prefactor of momentum sums is just that of the grain, $\mathcal{V} = \mathcal{V}_g$ ($\mathcal{V}_g = a^d$ in our model). This is because the internal momentum is related to the size of the "internal system", or, in other words, the size of the grain.

The self-energy for the t-averaged Green's function is simply,

$$\Sigma_T = t^2 \sum_l \sum_{\mathbf{p}} \delta_{\langle il \rangle} \widetilde{G}_{0l}(\mathbf{p}, i\varepsilon), \tag{4.9}$$

where

$$\delta_{\langle il \rangle} = \begin{cases} 1, & i \text{ and } l \text{ are nearest neighbours} \\ 0, & \text{otherwise.} \end{cases} \tag{4.10}$$

Given that the grain index on $\widetilde{G}_{0l}$ is a formality to help picture the tunnelling processes occurring, and the homogeneous Green's function does not depend on the grain label, the sum over l combined with $\delta_{\langle il \rangle}$ simply produces a factor equal to the number of nearest

[11] The extra factor of a^d acts to cancel the a^{-d} that our original diagrammatic rules would generate due to the intragranular momentum sum that results from tunnelling to a grain and back. Put explicitly, for the case of two tunnelling events, we tunnel from grain i to grain j, before then tunnelling back to grain i. We can view the i label as external to the diagram, and j as an internal label to be summed over. The Green's functions at the start and end have the same intragranular momentum courtesy of our averaging procedure, whilst the Green's function in grain j has an independent momentum. The momentum appearing for the Green's function in j is internal to the diagram, and hence is summed over.

Consequently, our original homogeneous rules would say this carries a factor of a^{-d}. However, this momentum sum does not have the same origin as those generated in the homogeneous case. Rather, this momentum sum naturally appears in the Hamiltonian without a factor of a^{-d} in front of it. We can see that the series generated for the single-electron Green's function also reflects this in eq. 4.6: the tunnelling momentum sums do not carry a factor of a^{-d} with them. Hence, since only pairs of tunnelling events survive our averaging procedure, we correct the original homogeneous rules by including an extra factor of a^d for each pair of correlated tunnelling events. It is quite pleasant to see how this reflects the associated factor carried by a pair of impurity scattering events in homogeneous systems.

neighbours to the i^{th} grain. Hence,

$$\Sigma_T = zt^2 \sum_{\mathbf{p}} \widetilde{G}_0(\mathbf{p}, i\varepsilon), \tag{4.11}$$

where z is the coordination number of the granular lattice. The momentum sum is exactly the same as in eq. 3.11, but with no suppressed factor of $\mathcal{V}_g^{-1} = a^{-d}$,[12] and so

$$\Sigma_T = -izt^2 \pi N(0) a^d \text{sgn}(\varepsilon) = -\frac{iz\Gamma}{2}\text{sgn}(\varepsilon), \tag{4.12}$$

where Γ is the electron tunnelling rate at a single grain boundary, which is given by Fermi's golden rule

$$\Gamma = 2\pi N(0) a^d t^2. \tag{4.13}$$

The t-averaged single-electron Green's function is then given by the Dyson equation,

$$G_i(\mathbf{k}, i\varepsilon) = \frac{1}{\widetilde{G}_{0i}(\mathbf{k}, i\varepsilon)^{-1} - \Sigma_T}. \tag{4.14}$$

Hence, the t-averaged single-electron Green's function has an entirely analogous form to that of the homogeneous disorder-averaged electron Green's function (eq. 3.14),

$$G_i(\mathbf{k}, i\varepsilon) = \frac{1}{i\varepsilon - \xi_{\mathbf{k}} + \frac{i}{2\tau}\text{sgn}(\varepsilon)}, \tag{4.15a}$$

$$\frac{1}{\tau} = \frac{1}{\tau_0} + z\Gamma. \tag{4.15b}$$

In comparison to the homogeneous case, we see that τ_0^{-1}, the impurity scattering rate, has been replaced with the total scattering rate due to tunnelling and impurity scattering, τ^{-1}.

As part of our model of a disordered granular metal, whose disorder is both internal (impurities) and external (tunnelling) to a grain, we make the following assumption:

[12] Due to our explicit inclusion of volume factors now, this sum will produce a factor of $N(0)\mathcal{V}_g = N(0)a^d$ as opposed to the $N(0)$ we had in the previous chapter.

- An electron scatters many times off impurities internal to a grain, before tunnelling to the next grain, i.e. $\tau_0^{-1} \gg z\Gamma$.[13]

This assumption gives meaning to the idea of disorder within a grain. If tunnelling was to happen significantly more often than internal impurity scattering, the inclusion of internal disorder would become redundant, as the motion of electrons within a grain would become ballistic.

Given the extreme similarity to the single-electron Green's functions in homogeneous disordered metals, we might expect many granular results to appear similar to their homogeneous counterparts. However, before we see whether this is true or not, there are many more technical aspects we must cover. Let us first write down our new set of diagrammatic rules.

The set of rules due to averaged tunnelling events, which are in addition to those for disorder-averaged single-particle interactions in homogeneous systems, are thus,

1. To each solid line we assign an additional grain index, denoted by a Latin character (e.g: i), on top of the momentum and frequency it already carries. This line represents the Green's function $G_{0i}(\mathbf{k}, i\varepsilon)$.

2. Crossed circles represent tunnelling events, which introduce a factor of $t_{ij}^{\mathbf{kp}}$ to connect the Green's functions $G_{0i}(\mathbf{k}, i\varepsilon)$ and $G_{0j}(\mathbf{p}, i\varepsilon)$, which leave and enter the tunnelling event respectively.

3. Sum over all internal grain indices.

4. Only diagrams containing an even number of tunnelling events survive t-averaging.

5. Consider all possible combinations where we pair all tunnelling events, with paired events connected via a dotted line. This conserves intragranular momentum, but does not effect the energy of a Green's function, and so obeys the usual conserva-

[13] This is the same as assuming weak tunnelling, so the matrix elements $t_{ij}^{\mathbf{kp}}$ are small.

tion laws. This generates a constant effective two-body interaction in frequency–intragranular-momentum space, which is given by $t^2 a^d$.[14]

6. For weakly disordered systems, $k_F l \gg 1$ (l is the homogeneous mean free path), terms involving overlapping (crossed) two-body tunnelling interactions are sub-dominant at all orders, and so may be neglected.

Having stated the rules we play by for the single-particle interaction that is tunnelling, let us now derive the diagrammatic rules for two-particle interactions.

4.3 Two-particle Interactions

In chapter 2 we considered a generic two-particle interaction Hamiltonian for a homogeneous material. This interaction was included via H_{int} in eq. 2.55. For a granular metal, however, the particles can only exist within a grain and not between grains, hence they cannot be created/annihilated in all of position space. Instead, we should split the volume integrals up into a sum of volume integrals over each grain, and write all real space positions as a combination of lattice position and internal position within a grain,

$$\int d^d r \quad \rightarrow \quad \sum_i \int d^d y_i \,, \qquad\qquad \mathbf{r} = \mathbf{R}_i + \mathbf{y}_i \,, \tag{4.16}$$

where $\mathbf{y}_i$ is the position within the i^{th} grain, with the integral taken over the volume of the i^{th} grain. The field operators then become,

$$\psi_\sigma(\mathbf{R}_i + \mathbf{y}_i) \equiv \psi_{i\sigma}(\mathbf{y}), \tag{4.17}$$

[14]This is constant in both lattice position space and lattice momentum space. We will see more about lattice momentum space later.

and so,

$$\begin{aligned} H_{\text{int}} &= \frac{1}{2}\sum_{\sigma,\sigma'}\sum_{i,j}\int d^d y_i \int d^d y'_j\, \psi^\dagger_{i\sigma}(\mathbf{y})\psi^\dagger_{j\sigma'}(\mathbf{y}')V(\mathbf{R}_i+\mathbf{y}_i-\mathbf{R}_j-\mathbf{y}'_j)\psi_{j\sigma'}(\mathbf{y}')\psi_{i\sigma}(\mathbf{y}) \\ &= \frac{1}{2}\sum_{\sigma,\sigma'}\sum_{i,j}\int d^d y_i \int d^d y'_j\, \psi^\dagger_{i\sigma}(\mathbf{y})\psi^\dagger_{j\sigma'}(\mathbf{y}')V(\mathbf{R}_{ij}+\mathbf{y}_i-\mathbf{y}'_j)\psi_{j\sigma'}(\mathbf{y}')\psi_{i\sigma}(\mathbf{y}). \end{aligned} \tag{4.18}$$

For notational ease, we choose to write

$$V(\mathbf{R}_{ij}+\mathbf{y}_i-\mathbf{y}'_j) = V(\mathbf{R}_{ij},\mathbf{y}_i-\mathbf{y}'_j) = V_{ij}(\mathbf{y}_i-\mathbf{y}'_j). \tag{4.19}$$

We assume that each grain possesses translational invariance, meaning it is beneficial to replace the field operators with their second quantised counterparts using a plane wave basis that is local to a grain. Hence, we use eq. 2.28 with $\mathcal{V}=a^d$, and define the momenta according to the size and shape of the grain, as opposed to the entire system,

$$\psi_{i\sigma}(\mathbf{r},\tau) = \frac{1}{\sqrt{\mathcal{V}}}\sum_{\mathbf{k}} e^{i\mathbf{k}\cdot\mathbf{r}}c_{i\mathbf{k}\sigma}(\tau), \qquad \psi^\dagger_{i\sigma}(\mathbf{r},\tau) = \frac{1}{\sqrt{\mathcal{V}}}\sum_{\mathbf{k}} e^{-i\mathbf{k}\cdot\mathbf{r}}c^\dagger_{i\mathbf{k}\sigma}(\tau). \tag{4.20}$$

Further, we note that $V_{ij}(\mathbf{y}_i-\mathbf{y}'_j)$ has two layers of translational invariance: we can make a large translation that shifts the lattice, which does not affect the interaction due to the $\mathbf{R}_{ij}$ piece in its argument; we can make a small translation of the system that is of a size smaller than a grain, which does not affect the interaction due to the difference $\mathbf{y}_i-\mathbf{y}'_j$. We may therefore define two independent Fourier series expansions of the interaction: this leads to an internal momentum, $\mathbf{q}$, related to the change in internal position $\mathbf{y}_i-\mathbf{y}'_j$, and an external momentum, $\mathbf{Q}$, related to the change in lattice position, $\mathbf{R}_{ij}$. However, we often choose to remain in a mixed representation of internal momentum space and lattice position space.[15] Using these ideas, we have the following representations for a two-body

[15] I personally feel this is a more intuitive picture to work with when considering problems later on.

interaction with translational invariance,

$$V_{ij}(\mathbf{y}_i - \mathbf{y}'_j) = \frac{1}{\mathcal{V}} \sum_{\mathbf{q}} V_{ij}(\mathbf{q}) e^{i\mathbf{q}\cdot(\mathbf{y}_i - \mathbf{y}'_j)}, \tag{4.21a}$$

$$V_{ij}(\mathbf{q}) = \frac{1}{\mathcal{N}} \sum_{\mathbf{Q}} V(\mathbf{Q}, \mathbf{q}) e^{i\mathbf{Q}\cdot\mathbf{R}_{ij}}. \tag{4.21b}$$

We adopt the convention of using lower case letters for internal momenta, and capital letters for lattice momenta.

Substituting eq. 4.20 and eq. 4.21a into eq. 4.18, we arrive at

$$H_{\text{int}} = \frac{1}{2\mathcal{V}} \sum_{\sigma,\sigma'} \sum_{i,j} \sum_{\mathbf{k},\mathbf{p},\mathbf{q}} c^\dagger_{i\mathbf{k}+\mathbf{q}\sigma} c^\dagger_{i\mathbf{p}\sigma'} V_{ij}(\mathbf{q}) c_{i\mathbf{p}+\mathbf{q}\sigma'} c_{i\mathbf{k}\sigma}. \tag{4.22}$$

Now, the Green's function we wish to calculate is the full single-particle Green's function in the presence of two-particle interactions,[16]

$$\mathscr{G}^{(\alpha\alpha')}_{ji}(\mathbf{k}, \mathbf{p}; \tau_1, \tau_2) = -\frac{\left\langle T_\tau \left\{ \widetilde{c}_{i\alpha}(\mathbf{k}, \tau_1) \widetilde{c}^\dagger_{j\alpha'}(\mathbf{p}, \tau_2) \mathcal{S}(\beta) \right\} \right\rangle_0}{\langle \mathcal{S}(\beta) \rangle_0}, \tag{4.23}$$

where the $\mathcal{S}$-matrix has the same definition as before, the tildes on the creation and annihilation operators signify we are using the interaction picture, and

$$\langle ... \rangle_0 = \frac{1}{\mathcal{Z}_0} \text{Tr} \left[e^{-\beta \mathscr{H}_1^{(T)}} ... \right], \qquad \mathcal{Z}_0 = \text{Tr} \left[e^{-\beta \mathscr{H}_1^{(T)}} \right], \tag{4.24}$$

in analogy to eq. 2.59.

We can now perform an identical treatment to that given in chapter 2 to find the single-particle Green's function for a granular system, with two-body interactions and translationally invariant grains. In chapter 2, we could have chosen to start in momentum

[16] If we wanted to write this in a more similar form to eq. 2.56, we could put the momentum arguments in the subscript instead of the grain labels, and put $\mathbf{R}_i$ and $\mathbf{R}_j$ in the main argument instead of the momenta. Then by labelling $x_1 = (\mathbf{R}_i, \tau_1)$ and $x_2 = (\mathbf{R}_j, \tau_2)$, we find ourselves dealing with $\mathscr{G}^{(\alpha\alpha')}_{\mathbf{kp}}(x_1, x_2)$. Thus, we can apply exactly the same ideas as before, where the intragranular momenta are simply carried around as passengers.

space as opposed to position space for homogeneous systems, and found a near identical expression to that in eq. 4.22. The only major difference here is that we have the additional grain index on the creation and annihilation operators, along with the sums over grain position. If we simply ignored the presence of the momentum arguments on the operators, removed the momentum sums, and the factor of $\mathcal{V}^{-1}$ associated to these sums, this problem would look like the discretised version of section 2.4. Hence, we can apply the exact same set of steps used to obtain the diagrammatic rules in real space to obtain entirely analogous rules for a system situated on a lattice: our integrals over all internal positions in space would be replaced by a sum over all lattice positions.

To regain the granular nature is simple. We appreciate that the momentum arguments, sums, and factor of $\mathcal{V}^{-1}$ will only be passengers in the treatment mentioned above. Thus, we can re-insert the momentum arguments onto the operators, sum over all internal intragranular momenta, and introduce a factor of $\mathcal{V}^{-1}$ for each internal momentum sum, without any difficulty. Consequently, we find that the Green's function that acts as our diagrammatic building block, in analogy to eq. 2.62, is

$$\begin{aligned}\mathscr{G}_{0ij}^{(\sigma\sigma')}(\mathbf{k},\mathbf{p},i\nu) &= -\left\langle T_\tau\left\{\widetilde{c}_{i\sigma}(\mathbf{k},i\nu)\widetilde{c}_{j\sigma'}^{\dagger}(\mathbf{p},i\nu)\right\}\right\rangle_0 \\ &= -\left\langle T_\tau\left\{\widetilde{c}_{i\sigma}(\mathbf{k},i\nu)\widetilde{c}_{j\sigma}^{\dagger}(\mathbf{p},i\nu)\right\}\right\rangle_0 \delta_{\sigma\sigma'} \\ &= G_{ij}(\mathbf{k},\mathbf{p},i\nu;H_T)\delta_{\sigma\sigma'} = \mathscr{G}_{0ij}^{(\sigma)}(\mathbf{k},\mathbf{p},i\nu)\delta_{\sigma\sigma'},\end{aligned} \tag{4.25}$$

.

With this in mind, we may write down the diagrammatic rules for including two-particle interactions in the single-particle Green's function of a granular system, which has translational invariance within each grain,

1. Create all connected, topologically inequivalent diagrams with $2n$ internal vertices at n^{th} order, and two external vertices. At each internal vertex, two solid lines and a wavy line meet.

2. To each solid line we associate the propagator in the absence of two-particle inter-

actions, $\mathscr{G}_{0ij}^{(\sigma\sigma')}(\mathbf{k},\mathbf{p},i\nu)$, which moves from the state with intragranular momentum $\mathbf{p}$ and spin σ' in grain j, to the state with intragranular momentum $\mathbf{k}$ and spin σ in grain i, whilst carrying the Matsubara frequency ν, such that intragranular momentum, energy(frequency), and spin are conserved at each vertex.

3. Each wavy line represents an interaction and is associated to a factor of $-V_{ij}(\mathbf{q},i\omega)$, which carries an intragranular momentum $\mathbf{q}$ and Matsubara frequency ω from grain j to grain i.

4. We now sum over all internal Matsubara frequencies, ν, and introduce a factor of T for each internal frequency summed over.

5. We next sum (integrate) over all internal intragranular momenta, $\mathbf{k}$, and introduce a factor of $\mathcal{V}^{-1}$ ($(2\pi)^{-d}$) for each internal momentum summed (integrated) over.

6. Sum over all internal spin indices. This is equivalent to just multiplying by a factor of $(2S+1)$ for each closed particle loop, where S is the particle's spin, and neglecting the spin indices and sums.

7. Sum over all internal grain labels.

8. For each closed fermion loop we introduce an extra factor of (-1).

We give example diagrams in fig. 4.4, which are the first order corrections to the full single-particle Green's function,

$$\mathscr{G}_{ij}^{(\alpha\alpha'),(1a)}(\mathbf{k}_1,\mathbf{p}_1,i\nu) = -\frac{\eta}{\mathcal{V}^2}\sum_{l,m}\sum_{\sigma,\sigma'}\sum_{\mathbf{k},\mathbf{p}}\Big[V_{lm}(\mathbf{0},0)\mathscr{G}_{0,il}^{(\alpha\sigma)}(\mathbf{k}_1,\mathbf{k},i\nu) \times \mathscr{G}_{0,lj}^{(\sigma\alpha')}(\mathbf{k},\mathbf{p}_1,i\nu)\mathscr{G}_{0,mm}^{(\sigma'\sigma')}(\mathbf{p},\mathbf{p},i\nu)\Big], \tag{4.26a}$$

$$\mathscr{G}_{ij}^{(\alpha\alpha'),(1b)}(\mathbf{k}_1,\mathbf{p}_1,i\nu) = \frac{1}{\mathcal{V}^2}\sum_{l,m}\sum_{\sigma,\sigma'}\sum_{\mathbf{k},\mathbf{p}}\Big[V_{lm}(\mathbf{q},i\omega)\mathscr{G}_{0,im}^{(\alpha\sigma)}(\mathbf{k}_1,\mathbf{k},i\nu) \times \mathscr{G}_{0,lj}^{(\sigma'\alpha')}(\mathbf{p},\mathbf{p}_1,i\nu)\mathscr{G}_{0,ml}^{(\sigma\sigma')}(\mathbf{k}+\mathbf{q},\mathbf{p}+\mathbf{q},i\nu+i\omega)\Big]. \tag{4.26b}$$

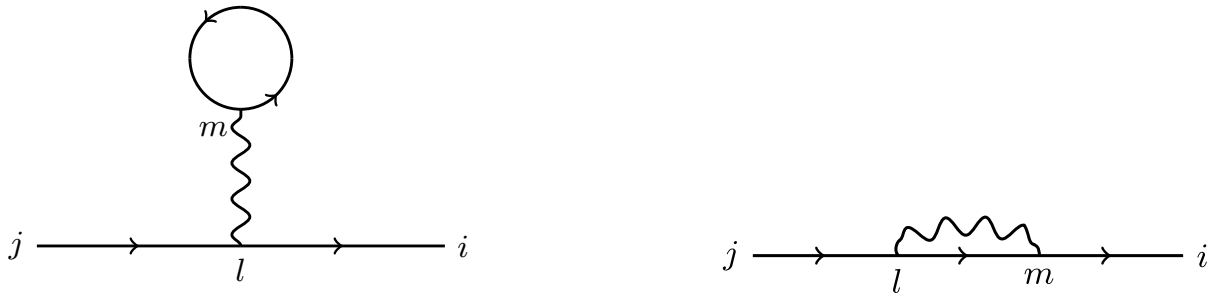

Figure 4.4: (a): Diagrammatic representation of eq. 4.26a. (b): Diagrammatic representation of eq. 4.26b.

4.3.1 Two-particle Interactions – With Averaging Over Tunnelling Events

The rules above are in the absence of t-averaging, and so look quite unpleasant, as do the resulting expressions. By applying t-averaging, rule 2 of the above set simplifies slightly as we no longer have to deal with non-interacting Green's functions that can start in one grain and end in another. The new non-interacting Green's function we use is then,

$$\begin{aligned}\mathscr{G}_{0i}^{(\sigma\sigma')}(\mathbf{k}, i\nu) &= \left\langle \mathscr{G}_{0ij}^{(\sigma\sigma')}(\mathbf{k}, \mathbf{p}, i\nu) \right\rangle_T^{(0)} \\ &= \langle G_{ij}(\mathbf{k}, \mathbf{p}, i\nu; H_T) \rangle_T^{(0)} \, \delta_{\sigma\sigma'} = G_i(\mathbf{k}, i\nu)\delta_{\sigma\sigma'} = \mathscr{G}_{0i}^{(\sigma)}(\mathbf{k}, i\nu)\delta_{\sigma\sigma'}.\end{aligned} \tag{4.27}$$

Therefore, the new second rule reads as:

- To each solid line we associate the propagator in the absence of two-particle interactions, $\mathscr{G}_{0i}^{(\sigma\sigma')}(\mathbf{k}, \mathbf{p}, i\nu)$, which starts and ends in grain i, and moves from the spin state σ' to the spin state σ, whilst carrying an intragranular momentum of $\mathbf{k}$ and Matsubara frequency of ν, such that intragranular momentum and energy(frequency) are conserved at each vertex.

Having outlined how to obtain the diagrammatic rules for granular systems, we are now in a position to start calculating the electrical conductivity of granular metals.

CHAPTER 5

TRANSPORT PHENOMENA IN GRANULAR SYSTEMS

In chapter 3 we discussed, and calculated, the corrections to the electrical conductivity of disordered homogeneous metals due to a variety of effects. Naturally, we expect these effects to also be present in granular materials. Therefore, this chapter will show how we calculate the analogous results in granular metals, and where we might expect new observations to occur that would not be seen in homogeneous systems.

We start this chapter by covering the details of the granular Drude conductivity calculation in section 5.1. We then consider the effects of interference and calculate the weak localisation corrections to the electrical conductivity in section 5.2. Next, we calculate the corrections due to EEIs via Coulomb in section 5.3, before considering superconducting fluctuations in section 5.4. Finally, in section 5.5, we obtain self-consistent expressions for the phase breaking rate.

5.1 Drude Conductivity

As was the case in homogeneous systems, the granular Drude conductivity result is one of the more awkward to calculate using QFT. The granular Drude result was quoted in

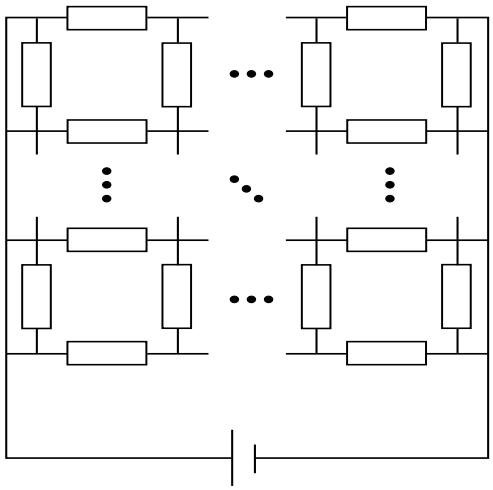

Figure 5.1: Circuit diagram interpretation of a granular metal in 2D.

the literature [61] to be,

$$\sigma_0^T = 2e^2 N(0)\Gamma a^2, \tag{5.1}$$

and was only explicitly calculated using path integral methods by Efetov and Tschersich [70]. A diagram was associated to the granular Drude conductivity in [64], but was not explicitly calculated until recently in the work of Perkins and Smith [37]. However, before we try to construct a field theory for granular electrical conductivity to verify this result, let us first start by considering a classical model to compare our answer to.

5.1.1 A Classical model

We can picture a granular system as a d-dimensional simple cubic lattice, where the vertices of a cube are left empty and we replace the lines connecting vertices with resistors, see fig. 5.1. In our model, all grains are identical, hence each resistor has the same resistance, R_T. If we wanted to measure the total resistance of this network, could imagine placing the granular sample between two metal plates (electrodes) that were connected to some source. This would mean that each grain at the surface of the sample would be in contact with the electrode, and so we would have the circuit diagram shown in fig. 5.1 in 2D. It is not difficult to see how this generalises for both 1D and 3D, let alone higher dimensions.

Clearly, all channels that run parallel to the plates will carry no current. This is because the voltage entering either side of a single resistor parallel to the plates is equal, meaning the potential difference across the resistor is zero. Therefore, all current runs in the channels perpendicular to the plates. If the sample has a length of n_x grains, the resistance of a single channel is then,

$$R_1 = (n_x - 1)R_T. \tag{5.2}$$

If the system has a width of n_y grains, the resistance of a single plane is given by adding $n_y - 1$ single channels in parallel,

$$\begin{aligned} \frac{1}{R_2} &= \sum_{m=1}^{n_y-1} \frac{1}{R_1} = \frac{n_y - 1}{R_1}, \\ \Rightarrow \qquad R_2 &= \frac{R_1}{n_y - 1} = \frac{n_x - 1}{n_y - 1} R_T. \end{aligned} \tag{5.3}$$

Finally, if the system has a height of n_z grains, the total resistance of the sample is given by adding $n_z - 1$ single planes in parallel,

$$R_3 = \frac{n_x - 1}{(n_y - 1)(n_z - 1)} R_T. \tag{5.4}$$

The conductivity associated to this material is thus,

$$\sigma_0^T = \frac{1}{\rho_0^T} = \frac{n_y n_z a^2}{n_x a} \frac{n_x - 1}{(n_y - 1)(n_z - 1)} R_T = \frac{n_y n_z}{n_x} \frac{n_x - 1}{(n_y - 1)(n_z - 1)} a R_T. \tag{5.5}$$

For the system to be classed as d-dimensional, it must be extended in each direction, meaning $n_x, n_y, n_z \gg 1$, and so

$$\sigma_0^T = \frac{1}{\rho_0^T} = a^{d-2} R_T. \tag{5.6}$$

Here we generalised from three dimensions to d dimensions.

Now, the resistance for a single tunnel junction is given by Barone and Paternò [71], which, written in our notation, is

$$R_T = \frac{1}{4\pi N(0)^2 a^{2d} t^2}, \tag{5.7}$$

where we have used the fact that the DOS for each grain are independent. Substituting eq. 5.7 into eq. 5.6, and recalling $\Gamma = 2\pi N(0) a^d t^2$, we recover the result given in eq. 5.1. Having found an expression for σ_0^T classically, let us now move onto formulating a QFT description of electrical conductivity in granular metals.

5.1.2 Quantum Field Theory & Linear Response

In this section we closely follow the work of Perkins and Smith [37]. To find an expression for the electrical conductivity, we need to calculate the linear response of the current density, $\mathbf{J}$, to the vector potential, $\mathbf{A}$, as in section 3.2. For this, we will need to define the perturbation to our Hamiltonian due to $\mathbf{A}$, as well as determine the electrical current operator for a granular system. In our case, the unperturbed Hamiltonian is given in eq. 4.4, which we write here as

$$\begin{aligned}\mathscr{H}_0 &= \sum_i \sum_\sigma \sum_{\mathbf{k}} \xi_{i\mathbf{k}} c^\dagger_{i\mathbf{k}\sigma} c_{i\mathbf{k}\sigma} + \sum_i \sum_\sigma \sum_{\mathbf{k},\mathbf{q}} U_i(\mathbf{q}) c^\dagger_{i\mathbf{k}+\mathbf{q}\sigma} c_{i\mathbf{k}\sigma} \\ &\quad + \sum_{i,j} \sum_\sigma \sum_{\mathbf{k},\mathbf{p}} t_{ij}^{\mathbf{kp}} c^\dagger_{i\mathbf{k}\sigma} c_{j\mathbf{p}\sigma} \\ &\equiv \mathscr{H}_g + H_T\end{aligned} \tag{5.8}$$

where the subscript on $\mathscr{H}_0$ denotes the vector potential's absence.

We include the vector potential into this Hamiltonian by means of the Peierls substitution [72, 73, 74],

$$t_{ij} \quad \rightarrow \quad t_{ij} \exp\left(ie \int_{\mathbf{R}_j}^{\mathbf{R}_i} d\mathbf{r} \cdot \mathbf{A}(\mathbf{r}, t) \right). \tag{5.9}$$

This assumes that the vector potential only exists between the grains, which is appropriate

for small grains. If we further assume that $\mathbf{A}(\mathbf{r},t)$ is roughly uniform in space, this substitution becomes

$$t_{ij} \quad \rightarrow \quad t_{ij}e^{ie\mathbf{R}_{ij}\cdot\mathbf{A}(t)}. \tag{5.10}$$

Substituting eq. 5.10 into eq. 5.8, and accounting for the fact we only allow nearest-neighbour hopping on a simple cubic lattice, we find

$$\begin{aligned}\mathscr{H}(t) = &\sum_i \sum_\sigma \sum_{\mathbf{k}} \xi_{i\mathbf{k}} c^\dagger_{i\mathbf{k}\sigma} c_{i\mathbf{k}\sigma} + \sum_i \sum_\sigma \sum_{\mathbf{k},\mathbf{q}} U_i(\mathbf{q}) c^\dagger_{i\mathbf{k}+\mathbf{q}\sigma} c_{i\mathbf{k}\sigma} \\ &+ \sum_{i,\alpha} \sum_\sigma \sum_{\mathbf{k},\mathbf{p}} \left[t^{\mathbf{kp}}_{i+\alpha i} c^\dagger_{i+\alpha\mathbf{k}\sigma} c_{i\mathbf{p}\sigma} e^{ieaA_\alpha(t)} + t^{\mathbf{kp}}_{ii+\alpha} c^\dagger_{i\mathbf{k}\sigma} c_{i+\alpha\mathbf{p}\sigma} e^{-ieaA_\alpha(t)} \right],\end{aligned} \tag{5.11}$$

where the sum over α is a sum over the axial directions (x, y, and z in 3D), and we noted that $\mathbf{R}_{ij} = \pm a\mathbf{e}_\alpha$ for nearest-neighbours i and $j = i \pm \alpha$. Since we are interested in linear response, we expand eq. 5.11 to first order in $\mathbf{A}(t)$, and neglect higher order terms,

$$\mathscr{H}(t) = \mathscr{H}_0 + iea \sum_\alpha A_\alpha(t) \sum_i \sum_\sigma \sum_{\mathbf{k},\mathbf{p}} \left[t^{\mathbf{kp}}_{i+\alpha i} c^\dagger_{i+\alpha\mathbf{k}\sigma} c_{i\mathbf{p}\sigma} - t^{\mathbf{kp}}_{ii+\alpha} c^\dagger_{i\mathbf{k}\sigma} c_{i+\alpha\mathbf{p}\sigma} \right]. \tag{5.12}$$

Clearly, the linear perturbation to the Hamiltonian we will use in Kubo's formula is

$$H' = iea \sum_\alpha A_\alpha(t) \sum_i \sum_\sigma \sum_{\mathbf{k},\mathbf{p}} \left[t^{\mathbf{kp}}_{i+\alpha i} c^\dagger_{i+\alpha\mathbf{k}\sigma} c_{i\mathbf{p}\sigma} - t^{\mathbf{kp}}_{ii+\alpha} c^\dagger_{i\mathbf{k}\sigma} c_{i+\alpha\mathbf{p}\sigma} \right]. \tag{5.13}$$

The current density operator associated to this Hamiltonian is given by[1]

$$\begin{aligned} j_\alpha(t) &= \frac{1}{a^d \mathcal{N}} \frac{\delta \mathscr{H}(t)}{\delta A_\alpha(t)} \\ &= \frac{iea^{1-d}}{\mathcal{N}} \sum_i \sum_\sigma \sum_{\mathbf{k},\mathbf{p}} \left[t^{\mathbf{kp}}_{i+\alpha i} c^\dagger_{i+\alpha\mathbf{k}\sigma} c_{i\mathbf{p}\sigma} e^{ieaA_\alpha(t)} - t^{\mathbf{kp}}_{ii+\alpha} c^\dagger_{i\mathbf{k}\sigma} c_{i+\alpha\mathbf{p}\sigma} e^{-ieaA_\alpha(t)} \right]. \end{aligned} \tag{5.14}$$

[1] We can also derive the current density using the discretised continuity equation.

We again expand this to first order in $A_\alpha(t)$ to consider linear response,

$$\begin{aligned} j_\alpha(t) &= j_{0,\alpha} + A_\alpha(t)\frac{e^2}{a^{d-2}\mathcal{N}}\sum_i \left[t^{\mathbf{kp}}_{i+\alpha i}c^\dagger_{i+\alpha\mathbf{k}\sigma}c_{i\mathbf{p}\sigma} + t^{\mathbf{kp}}_{ii+\alpha}c^\dagger_{i\mathbf{k}\sigma}c_{i+\alpha\mathbf{p}\sigma}\right] \\ &= j_{0,\alpha} + A_\alpha(t)\frac{e^2}{a^{d-2}\mathcal{N}}H_{T,\alpha}, \end{aligned} \tag{5.15}$$

where $j_{0,\alpha} = j_\alpha(t;\mathbf{A}=\mathbf{0})$, and $H_{T,\alpha}$ is the tunnelling Hamiltonian in the α^{th} direction in the absence of the vector potential (note that $H_T = \sum_\alpha H_{T,\alpha}$).

The macroscopic current density, $\mathbf{J}(t)$, is found by taking the thermal average of $\mathbf{j}(t)$, followed by the disorder average over internal impurities, and then the disorder average over tunnelling events,

$$\mathbf{J}(t) = \langle\langle\mathbf{j}(t)\rangle_{\text{dis}}\rangle^{(0)}_{\text{T}} \equiv \langle\mathbf{j}(t)\rangle_{\text{T}}\,. \tag{5.16}$$

Applying Kubo's formula for linear response, we obtain

$$J_\alpha(t) = \langle j_{0,\alpha}\rangle_{0,\text{T}} + A_\alpha(t)\frac{e^2}{a^{d-2}\mathcal{N}}\langle H_{T,\alpha}\rangle_{0,\text{T}} - \sum_\beta\int_{-\infty}^{+\infty}dt'\mathcal{G}^R_{\alpha\beta}(t,t')A_\beta(t'), \tag{5.17}$$

where $\langle ...\rangle_{0,\text{T}}$ denotes thermal averaging taken with respect to $\mathscr{H}_0$, before then applying the internal disorder average followed by the tunnelling disorder average. As in the homogeneous case,

$$\mathcal{G}^R_{\alpha\beta}(t,t') = -i\left\langle\left[\widetilde{j}_{0,\alpha}(t),\widetilde{j}_{0,\beta}(t')\right]\right\rangle_{0,\text{T}} a^d\mathcal{N}\Theta(t-t') \tag{5.18}$$

is the retarded current-current correlator.

Eq. 5.17 can be simplified quite drastically, by noting that $j_{0,\alpha}$ is the current operator in the absence of an applied field, hence its average should be zero. Next, the second term of eq. 5.17 also vanishes. This is a result of our averaging procedure for tunnelling events, as $H_{T,\alpha}$ only has terms containing a single factor $t^{\mathbf{kp}}_{ij}$. Hence, the macroscopic current is

$$J_\alpha(t) = -\sum_\beta\int_{-\infty}^{+\infty}dt'\mathcal{G}^R_{\alpha\beta}(t,t')A_\beta(t'). \tag{5.19}$$

Performing a temporal Fourier transform on eq. 5.19 yields

$$J_\alpha(\omega) = -\sum_\beta \mathcal{G}^R_{\alpha\beta}(\omega) A_\beta(\omega). \tag{5.20}$$

Hence, the retarded electromagnetic response function for a granular system is given by just the current-current correlator, $K^R_{\alpha\beta}(\omega) = \mathcal{G}^R_{\alpha\beta}(\omega)$, and has no diamagnetic piece that requires cancelling. Clearly, the same relations exist between the electromagnetic response function and the conductivity tensor as in the homogeneous case (see eq. 3.30 and eq. 3.31 with zero momentum).

To find $\mathcal{G}^R_{\alpha\beta}(\omega)$, we consider its temperature analogue,

$$\mathcal{G}_{\alpha\beta}(\tau,\tau') = -\left\langle T_\tau\{\widetilde{j}_{0,\alpha}(\tau), \widetilde{j}_{0,\beta}(\tau')\}\right\rangle_{0,\mathrm{T}} a^d \mathcal{N}, \tag{5.21}$$

where the τ and τ' appearing in the arguments are imaginary times. Writing eq. 5.21 in terms of creation and annihilation operators, we find

$$\begin{aligned}\mathcal{G}_{\alpha\beta}(\tau,\tau') = \frac{e^2}{a^{d-2}\mathcal{N}} \\ \times \sum_{i,j}\sum_{\sigma,\sigma'}\sum_{\substack{\mathbf{k},\mathbf{p},\\ \mathbf{k}',\mathbf{p}'}} \Big\langle T_\tau\Big\{ \left[t^{\mathbf{kp}}_{i+\alpha i} c^\dagger_{i+\alpha\mathbf{k}\sigma}(\tau) c_{i\mathbf{p}\sigma}(\tau) - t^{\mathbf{kp}}_{ii+\alpha} c^\dagger_{i\mathbf{k}\sigma}(\tau) c_{i+\alpha\mathbf{p}\sigma}(\tau)\right] \\ \times \left[t^{\mathbf{k}'\mathbf{p}'}_{j+\beta j} c^\dagger_{j+\beta\mathbf{k}'\sigma'}(\tau') c_{j\mathbf{p}'\sigma'}(\tau') - t^{\mathbf{k}'\mathbf{p}'}_{jj+\beta} c^\dagger_{j\mathbf{k}'\sigma'}(\tau') c_{j+\beta\mathbf{p}'\sigma'}(\tau')\right]\Big\}\Big\rangle_{0,\mathrm{T}}.\end{aligned} \tag{5.22}$$

Multiplying out the square brackets yields

$$\begin{aligned}&\left\langle T_\tau\{c^\dagger_{i+\alpha\mathbf{k}\sigma}(\tau) c_{i\mathbf{p}\sigma}(\tau) c^\dagger_{j+\beta\mathbf{k}'\sigma'}(\tau') c_{j\mathbf{p}'\sigma'}(\tau')\} t^{\mathbf{kp}}_{i+\alpha i} t^{\mathbf{k}'\mathbf{p}'}_{j+\beta j}\right\rangle_{0,\mathrm{T}} \\ &\quad + \left\langle T_\tau\{c^\dagger_{i\mathbf{k}\sigma}(\tau) c_{i+\alpha\mathbf{p}\sigma}(\tau) c^\dagger_{j\mathbf{k}'\sigma'}(\tau') c_{j+\beta\mathbf{p}'\sigma'}(\tau')\} t^{\mathbf{kp}}_{ii+\alpha} t^{\mathbf{k}'\mathbf{p}'}_{jj+\beta}\right\rangle_{0,\mathrm{T}} \\ &\quad\quad - \left\langle T_\tau\{c^\dagger_{i\mathbf{k}\sigma}(\tau) c_{i+\alpha\mathbf{p}\sigma}(\tau) c^\dagger_{j+\beta\mathbf{k}'\sigma'}(\tau') c_{j\mathbf{p}'\sigma'}(\tau')\} t^{\mathbf{kp}}_{ii+\alpha} t^{\mathbf{k}'\mathbf{p}'}_{j+\beta j}\right\rangle_{0,\mathrm{T}} \\ &\quad\quad\quad - \left\langle T_\tau\{c^\dagger_{i+\alpha\mathbf{k}\sigma}(\tau) c_{i\mathbf{p}\sigma}(\tau) c^\dagger_{j\mathbf{k}'\sigma'}(\tau') c_{j+\beta\mathbf{p}'\sigma'}(\tau')\} t^{\mathbf{kp}}_{i+\alpha i} t^{\mathbf{k}'\mathbf{p}'}_{jj+\beta}\right\rangle_{0,\mathrm{T}}.\end{aligned} \tag{5.23}$$

By applying Wick's theorem, we observe that the first two terms of eq. 5.23 vanish; this

is because our assumption in eq. 4.5 would lead a factor of $\delta_{i,j+\beta}\delta_{i+\alpha,j}$ in these terms. Hence, these terms can only be non-zero when $i = i + \alpha + \beta$, which is impossible since $\alpha, \beta > 0$ by definition. Thus, only the last two terms are non-zero, leading to

$$\begin{aligned} -\Bigg\langle &\Big\langle T_\tau\{c^\dagger_{i\mathbf{k}\sigma}(\tau)c_{j\mathbf{p}'\sigma'}(\tau')\}\Big\rangle_{0,\mathrm{dis}} \Big\langle T_\tau\{c_{i+\alpha\mathbf{p}\sigma}(\tau)c^\dagger_{j+\beta\mathbf{k}'\sigma'}(\tau')\}\Big\rangle_{0,\mathrm{dis}} t^{\mathbf{kp}}_{ii+\alpha}t^{\mathbf{k}'\mathbf{p}'}_{j+\beta j} \\ &+ \Big\langle T_\tau\{c^\dagger_{i+\alpha\mathbf{k}\sigma}(\tau)c_{j+\beta\mathbf{p}'\sigma'}(\tau')\}\Big\rangle_{0,\mathrm{dis}} \Big\langle T_\tau\{c_{i\mathbf{p}\sigma}(\tau)c^\dagger_{j\mathbf{k}'\sigma'}(\tau')\}\Big\rangle_{0,\mathrm{dis}} t^{\mathbf{kp}}_{i+\alpha i}t^{\mathbf{k}'\mathbf{p}'}_{jj+\beta}\Bigg\rangle^{(0)}_{\mathrm{T}}, \end{aligned} \tag{5.24}$$

where $\langle ... \rangle_{0,\mathrm{dis}}$ represents the thermal average taken with respect to $\mathscr{H}_0$, and averaging over internal disorder. If we were to substitute eq. 5.24 back into eq. 5.22, we would be able to identify the current vertices as contributing a factor of

$$\frac{ae\sqrt{a^d}}{\sqrt{\mathcal{N}}}t^{\mathbf{kp}}_{ii+\alpha}. \tag{5.25}$$

However, when we apply the t-average, this will change the current vertices to an effective form.

We apply the t-average, and rewrite eq. 5.24 in terms of the single-electron Green's functions defined in eq. 4.15a,

$$t^2\delta_{\alpha\beta}\delta_{ij}\delta_{\mathbf{k}+\mathbf{k}',\mathbf{p}+\mathbf{p}'}\delta_{\sigma\sigma'}\delta_{\mathbf{k}\mathbf{p}'}\delta_{\mathbf{p}\mathbf{k}'}\Big[G_i(\mathbf{k},\tau',\tau)G_{i+\alpha}(\mathbf{p},\tau,\tau') + G_{i+\alpha}(\mathbf{p},\tau,\tau')G_i(\mathbf{k},\tau',\tau)\Big]. \tag{5.26}$$

Here, we have neglected the case where the current vertices' tunnelling events are correlated with the tunnelling events inside the Green's functions, since this will generate a term of order t^4, which is clearly smaller than the above leading order term.

Finally, substituting eq. 5.26 into eq. 5.22, we arrive at

$$\begin{aligned} \mathcal{G}_{\alpha\beta}(\tau,\tau') = &\frac{e^2t^2}{a^{d-2}\mathcal{N}} \\ &\times \sum_i \sum_\sigma \sum_{\mathbf{k},\mathbf{p}} \Big[G_i(\mathbf{k},\tau',\tau)G_{i+\alpha}(\mathbf{p},\tau,\tau') + G_{i+\alpha}(\mathbf{p},\tau,\tau')G_i(\mathbf{k},\tau',\tau)\Big]. \end{aligned} \tag{5.27}$$

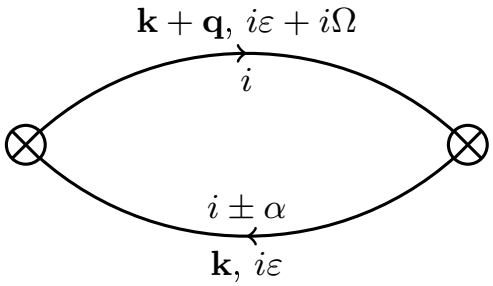

Figure 5.2: Granular Drude conuctivity diagram. We suppress the dashed line connecting the current vertices as there are no issues of ambiguity here.

We can obtain a more symmetric form for eq. 5.27, by letting $i \to i - \alpha$ in the second term of eq. 5.27's summand, as well as relabelling its momenta,

$$\begin{aligned}\mathcal{G}_{\alpha\beta}(\tau - \tau') = \frac{e^2 t^2}{a^{d-2}\mathcal{N}}\delta_{\alpha\beta} \\ \times \sum_i \sum_\sigma \sum_{\mathbf{k},\mathbf{p}} G_i(\mathbf{k}, \tau' - \tau)\Big[G_{i+\alpha}(\mathbf{p}, \tau - \tau') + G_{i-\alpha}(\mathbf{p}, \tau' - \tau)\Big].\end{aligned} \tag{5.28}$$

Here we have also accounted for the fact that single-particle Green's functions are always a function of time difference. To find the corresponding Matsubara expression, we first replace the electron Green's functions by their Matsubara Fourier series representations. After this, we write $\mathcal{G}_{\alpha\beta}(\tau - \tau')$ as a Matsubara Fourier series, and calculate its Fourier components in the usual manner. Doing so leads us to

$$\mathcal{G}_{\alpha\beta}(i\Omega) = \frac{2e^2 t^2}{a^{d-2}\mathcal{N}}\delta_{\alpha\beta} \sum_i \sum_{\mathbf{k},\mathbf{p}} T \sum_\varepsilon G_i(\mathbf{k}, i\varepsilon + i\Omega)\Big[G_{i+\alpha}(\mathbf{p}, i\varepsilon) + G_{i-\alpha}(\mathbf{p}, i\varepsilon)\Big], \tag{5.29}$$

where the factor of 2 comes from the spin sum.

We represent eq. 5.29 in fig. 5.2, where the crossed circles with α and β represent the tunnelling vertices, and the solid lines are the disorder and t-averaged electron Green's functions. Revisiting the form of the current vertices, we may now treat them as carrying a factor of

$$\frac{ae}{\sqrt{\mathcal{N}}} t_{ij}^{\mathbf{kp}}, \tag{5.30}$$

and allow the t-averaging procedure to produce a factor of a^d instead.

As explained in the homogeneous case, this diagram suffers divergences when we try to freely swap the order of summation. In fact, the situation appears worse here, as we have the same number of Green's functions but now an extra momentum integral. However, this is not the case and a naïve approach can obtain the correct answer, albeit employing a few tricks. For completeness, we also provide a rigorous method to calculate σ_0^T.

5.1.3 The Naïve Approach

Let us first evaluate eq. 5.29 by performing the momentum integrals first. Noting that $G_{i+\alpha}(\mathbf{p}, i\varepsilon) = G_{i-\alpha}(\mathbf{p}, i\varepsilon)$ to give the extra factor of 2, eq. 5.29 becomes

$$\begin{aligned}\mathcal{G}_{\alpha\beta}(i\Omega) &= \frac{4e^2t^2}{a^{d-2}\mathcal{N}}\delta_{\alpha\beta}\sum_i T\sum_\varepsilon\sum_{\mathbf{k}} G(\mathbf{k}, i\varepsilon + i\Omega)\sum_{\mathbf{p}} G(\mathbf{p}, i\varepsilon) \\ &= \frac{4e^2t^2}{a^{d-2}}\delta_{\alpha\beta}T\sum_\varepsilon\sum_{\mathbf{k}} G(\mathbf{k}, i\varepsilon + i\Omega)\sum_{\mathbf{p}} G(\mathbf{p}, i\varepsilon).\end{aligned} \tag{5.31}$$

We next replace each momentum sum by an integral linearised around the Fermi surface, and recall from eq. 3.11 and eq. 3.13 that,

$$\frac{1}{a^d}\sum_{\mathbf{k}} G(\mathbf{k}, i\varepsilon) = -i\pi N(0)\mathrm{sgn}(\varepsilon), \tag{5.32}$$

to write eq. 5.31 as,

$$\mathcal{G}_{\alpha\beta}(i\Omega) = -4\pi^2e^2N(0)^2a^{d+2}t^2\delta_{\alpha\beta}T\sum_\varepsilon \mathrm{sgn}(\varepsilon)\mathrm{sgn}(\varepsilon+\Omega). \tag{5.33}$$

Following Perkins and Smith [37], we use the fact that

$$\mathrm{sgn}(\varepsilon)\mathrm{sgn}(\varepsilon+\Omega) = 1 - 2\Theta(-\varepsilon(\varepsilon+\Omega)), \tag{5.34a}$$

and

$$T\sum_\varepsilon \Theta(-\varepsilon(\varepsilon+\Omega)) = T\sum_{-\Omega<\varepsilon<0} 1 = \frac{\Omega}{2\pi}, \tag{5.34b}$$

to get

$$\mathcal{G}_{\alpha\beta}(i\Omega) = -4\pi^2 e^2 N(0)^2 a^{d+2} t^2 \delta_{\alpha\beta} \left(T \sum_{\varepsilon} 1 - \frac{\Omega}{2\pi} \right). \tag{5.35}$$

Now, the Matsubara sum appearing in eq. 5.35 is clearly divergent. However, this sum can be argued to vanish using ideas of analytic continuation [37]. Let us consider the following sum for a generic Matsubara frequency,

$$T \sum_{\nu} \frac{1}{|\nu|^m} = \frac{T}{(2\pi T)^m} \sum_{n=-\infty}^{+\infty} \frac{1}{|n+c|^m} \equiv S(m,c), \tag{5.36}$$

where $c = 0$ for bosonic frequencies, and $c = 1/2$ for fermionic frequencies. This sum can be written in terms of Hurwitz zeta functions as so,

$$S(m,c) = \zeta(m,c) + \zeta(m,-c) - \frac{1}{c^m}. \tag{5.37}$$

The Hurwitz zeta function has the property that $\zeta(0,c) = 1/2 - c$, and so $S(0,c) = 0$. Therefore, we can make the argument that an infinite sum of unity over all Matsubara frequencies vanishes.[2]

Using this argument, eq. 5.35 is simply

$$\mathcal{G}_{\alpha\beta}(i\Omega) = 2\pi e^2 N(0)^2 a^{d+2} t^2 \, \Omega \, \delta_{\alpha\beta} = 2e^2 N(0) \Gamma a^2 \, \Omega \, \delta_{\alpha\beta}. \tag{5.38}$$

Given that $K_{\alpha\beta}(i\Omega) = \mathcal{G}_{\alpha\beta}(i\Omega)$ here, we can see that the response function indeed vanishes when $\Omega = 0$, and so describes a normal state system. Unlike the homogeneous case, we have not had to "hand-wave" the diamagnetic term away. In this circumstance though, the diamagnetic term vanishes and so does not cause any problems. Since $K_{\alpha\beta}(i\Omega) = \Omega\sigma_{\alpha\beta}$, we finally obtain

$$\sigma_0^T = 2e^2 N(0) \Gamma a^2. \tag{5.39}$$

[2] I'm so sorry you've had to see this beautiful abomination of a method for handling a divergent sum.

5.1.4 The Careful Approach

To treat this problem carefully, we must deal with the frequency sum first in eq. 5.29. We start by replacing the Matsubara sum by a contour integral, which has the same structure as in the homogeneous case, so we use the same contour and deformation shown in fig. 3.8. Thus, we may manipulate the frequency integral in the same way as before (see the working between eq. 3.48 and eq. 3.49). Upon replacing the momentum sums by integrals linearised around the Fermi surface, and performing the sum over i, we find the expression

$$\begin{aligned}\mathcal{G}^R_{\alpha\beta}(\omega) = &-\frac{e^2N(0)\Gamma a^2}{\pi^2 i}\int_{-\infty}^{+\infty}d\xi\int_{-\infty}^{+\infty}d\xi' \\ &\times\int_{-\infty}^{+\infty}dz f(z)\left[G^R(\mathbf{p},z)-G^A(\mathbf{p},z)\right]\left[G^R(\mathbf{k},z+\omega)+G^A(\mathbf{k},z-\omega)\right],\end{aligned} \tag{5.40}$$

where $\xi = \xi_{\mathbf{k}}$, $\xi' = \xi_{\mathbf{p}}$, and the extra factor of two comes from the lack of grain label dependence of the electron Green's functions, $G_{i+\alpha}(\mathbf{p}, i\varepsilon) = G_{i-\alpha}(\mathbf{p}, i\varepsilon)$.

The route we take in evaluating the integrals in eq. 5.40 is that taken by Perkins and Smith [37], which was inspired by the method Rickayzen [29] used to compute the homogeneous Drude conductivity. We introduce the function $g(\mathbf{k}, z)$ such that

$$G^R(\mathbf{k},z)-G^A(\mathbf{k},z) = 2i\,\mathrm{Im}\big[G^R(\mathbf{k},z)\big] \equiv -\frac{i}{\tau}g(\mathbf{k},z), \tag{5.41a}$$

$$G^R(\mathbf{k},z)+G^A(\mathbf{k},z) = 2\,\mathrm{Re}\big[G^R(\mathbf{k},z)\big] \equiv 2(\xi_{\mathbf{k}}-z)g(\mathbf{k},z), \tag{5.41b}$$

where

$$g(\mathbf{k},z) = g(z-\xi_{\mathbf{k}}) = \frac{1}{(z-\xi_{\mathbf{k}})^2+\frac{1}{4\tau^2}}. \tag{5.42}$$

We first demonstrate that $\mathcal{G}^R_{\alpha\beta}(\omega)$ vanishes when $\omega = 0$. In this case

$$\mathcal{G}^R_{\alpha\beta}(0) = \frac{2e^2N(0)\Gamma a^2}{\pi^2\tau}\int_{-\infty}^{+\infty}d\xi\int_{-\infty}^{+\infty}d\xi'\int_{-\infty}^{+\infty}dz f(z)g(z-\xi')g(z-\xi)(z-\xi). \tag{5.43}$$

Performing the ξ' integral by parts,

$$\begin{aligned}\mathcal{G}^R_{\alpha\beta}(0) = \frac{2e^2N(0)\Gamma a^2}{\pi^2\tau}\int_{-\infty}^{+\infty}d\xi\left[\xi'\int_{-\infty}^{+\infty}dz f(z)g(z-\xi')g(z-\xi)(z-\xi)\right]_{-\infty}^{+\infty}\\ -\frac{2e^2N(0)\Gamma a^2}{\pi^2\tau}\int_{-\infty}^{+\infty}d\xi\int_{-\infty}^{+\infty}d\xi'\xi'\frac{d}{d\xi'}\int_{-\infty}^{+\infty}dz f(z)g(z-\xi')g(z-\xi)(z-\xi).\end{aligned} \tag{5.44}$$

Clearly, the surface term vanishes as $g(z-\xi') \sim 1/\xi'^2$ for $\xi' \to \pm\infty$. Taking the ξ' derivative inside the z integral, it only acts on $g(z-\xi')$, and so we can replace the ξ' derivative of $g(z-\xi')$ with a z derivative at the cost of introducing a minus sign,

$$\mathcal{G}^R_{\alpha\beta}(0) = \frac{2e^2N(0)\Gamma a^2}{\pi^2\tau}\int_{-\infty}^{+\infty}d\xi\int_{-\infty}^{+\infty}d\xi'\xi'\int_{-\infty}^{+\infty}dz f(z)g(z-\xi)(z-\xi)\frac{d}{dz}g(z-\xi'). \tag{5.45}$$

Performing the z integral by parts, noticing the surface term vanishes again, we find

$$\begin{aligned}\mathcal{G}^R_{\alpha\beta}(0) = -\frac{2e^2N(0)\Gamma a^2}{\pi^2\tau}\int_{-\infty}^{+\infty}d\xi\int_{-\infty}^{+\infty}d\xi'\xi'\int_{-\infty}^{+\infty}dz\frac{df}{dz}g(z-\xi)(z-\xi)g(z-\xi')\\ -\frac{2e^2N(0)\Gamma a^2}{\pi^2\tau}\int_{-\infty}^{+\infty}d\xi\int_{-\infty}^{+\infty}d\xi'\xi'\int_{-\infty}^{+\infty}dz f(z)g(z-\xi')\frac{d}{dz}\Big[g(z-\xi)(z-\xi)\Big].\end{aligned} \tag{5.46}$$

The integrand of the first term of eq. 5.46 contains df/dz, which allows for sufficient convergence to exchange the orders of integration. However, we can avoid doing any integration by noting that the integrand has no poles in the space $(z,\xi) \in \mathbb{R}^2$, the z and ξ integrals have symmetric limits, df/dz is an even function of z, and $g(z-\xi)$ is an even function of $z-\xi$. With these facts in mind, we can see that the first term picks up a minus sign under the transformations $z \to -z$ and $\xi \to -\xi$. Therefore, the first term equals the negative of itself, and hence must vanish.

Turning to the second term of eq. 5.46, we see that it too vanishes,

$$\begin{aligned}&\int_{-\infty}^{+\infty}d\xi\int_{-\infty}^{+\infty}d\xi'\int_{-\infty}^{+\infty}dz f(z)g(z-\xi')\frac{d}{dz}\Big[g(z-\xi)(z-\xi)\Big]\\ &\quad= -\int_{-\infty}^{+\infty}d\xi\int_{-\infty}^{+\infty}d\xi'\int_{-\infty}^{+\infty}dz f(z)g(z-\xi')\frac{d}{d\xi}\Big[g(z-\xi)(z-\xi)\Big]\\ &\quad= -\int_{-\infty}^{+\infty}d\xi\frac{d}{d\xi}\int_{-\infty}^{+\infty}d\xi'\int_{-\infty}^{+\infty}dz f(z)g(z-\xi')g(z-\xi)(z-\xi),\end{aligned} \tag{5.47}$$

which, upon performing the above ξ integral, yields

$$-\left[\int_{-\infty}^{+\infty} d\xi' \int_{-\infty}^{+\infty} dz f(z)g(z-\xi')g(z-\xi)(z-\xi)\right]_{-\infty}^{+\infty} = 0. \tag{5.48}$$

Thus, $\mathcal{G}^R_{\alpha\beta}(0)$, and so $K^R_{\alpha\beta}(0)$, vanishes in the limit of zero external frequency. This confirms the system is in the normal state, and so this diagrammatic method passes the first test of validity.

To find the finite frequency response, we expand eq. 5.40 in powers of ω, to get

$$\mathcal{G}^R_{\alpha\beta}(\omega) = \frac{e^2 N(0)\Gamma a^{d+2}}{\pi^2\tau} \sum_{n=0}^{\infty} \omega^n I_n, \tag{5.49a}$$

$$I_n = \int_{-\infty}^{+\infty} d\xi \int_{-\infty}^{+\infty} d\xi' \int_{-\infty}^{+\infty} dz \, \frac{f(z)}{(z-\xi')^2 + \frac{1}{4\tau^2}} \left[\frac{(-1)^n}{\left(z-\xi+\frac{i}{2\tau}\right)^{n+1}} + \frac{1}{\left(z-\xi-\frac{i}{2\tau}\right)^{n+1}} \right]. \tag{5.49b}$$

Given $I_0 = 0$, the conductivity is thus

$$\sigma_0^T(\omega) = \frac{e^2 N(0)\Gamma a^2 i}{\pi^2\tau} \sum_{n=0}^{\infty} \omega^n I_{n+1}. \tag{5.50}$$

The DC conductivity is given by the $n = 0$ term of eq. 5.50,

$$\sigma_0^T = \frac{e^2 N(0)\Gamma a^2}{\pi^2\tau^2} \int_{-\infty}^{+\infty} d\xi \int_{-\infty}^{+\infty} d\xi' \int_{-\infty}^{+\infty} dz \, f(z)g(z-\xi')\frac{d}{dz}g(z-\xi). \tag{5.51}$$

Performing the z integral by parts yields,

$$\begin{aligned} \sigma_0^T = &- \frac{e^2 N(0)\Gamma a^2}{\pi^2\tau^2} \int_{-\infty}^{+\infty} d\xi \int_{-\infty}^{+\infty} d\xi' \int_{-\infty}^{+\infty} dz \, \frac{df}{dz} g(z-\xi')g(z-\xi) \\ &- \frac{e^2 N(0)\Gamma a^2}{\pi^2\tau^2} \int_{-\infty}^{+\infty} d\xi \int_{-\infty}^{+\infty} d\xi' \int_{-\infty}^{+\infty} dz \, f(z)g(z-\xi)\frac{d}{dz}g(z-\xi'). \end{aligned} \tag{5.52}$$

Clearly, the second term of eq. 5.52 is the negative of eq. 5.51, and so

$$\sigma_0^T = -\frac{e^2 N(0)\Gamma a^2}{2\pi^2\tau^2} \int_{-\infty}^{+\infty} d\xi \int_{-\infty}^{+\infty} d\xi' \int_{-\infty}^{+\infty} dz \frac{df}{dz} g(z-\xi')g(z-\xi). \tag{5.53}$$

With the factor of df/dz in the integrand, we now have sufficient convergence to swap the order of integration without issue. The energy integrals are trivial, each generating a factor of $2\pi\tau$, which leaves us with

$$\sigma_0^T = -2e^2 N(0)\Gamma a^2 \int_{-\infty}^{+\infty} dz \frac{df}{dz}. \tag{5.54}$$

The z integral produces a factor of -1, and so we arrive at the granular Drude conductivity, $\sigma_0^T = 2e^2 N(0)\Gamma a^2$. Regarding the AC Drude conductivity, it can be shown that all $n \neq 0$ terms in the sum of eq. 5.50 vanish (see [37] for details).

As a final note about the granular Drude result, we compare it to the Einstein relation in eq. 3.58. Doing so, we see that granular metals have an effective diffusion constant, $\mathcal{D}_T = \Gamma a^2$. We will see the same diffusion constant will appear in the granular analogues of the diffuson and cooperon.

5.2 Weak Localisation

The phenomenon of weak localisation depends entirely upon interference and phase coherence. We will therefore need to understand the role tunnelling plays in the diffuson and cooperon, before we can consider WL and more complicated corrections to the electrical conductivity. In section 5.2.1 we derive the granular diffuson and cooperon. Afterwards, in section 5.2.2, we calculate the granular WL correction to the conductivity.

5.2.1 Granular Diffusive Propagators

The granular cooperon and diffuson have already been derived by Beloborodov et. al. [26]; however their diagrammatic series appears to rely on nested diagrams, which can be included into the definition of the t-averaged electron Green's function or neglected upon physical grounds. Therefore, the inclusion of these diagrams in their derivation appears to double-count the contribution of these terms, see fig. 5.3.

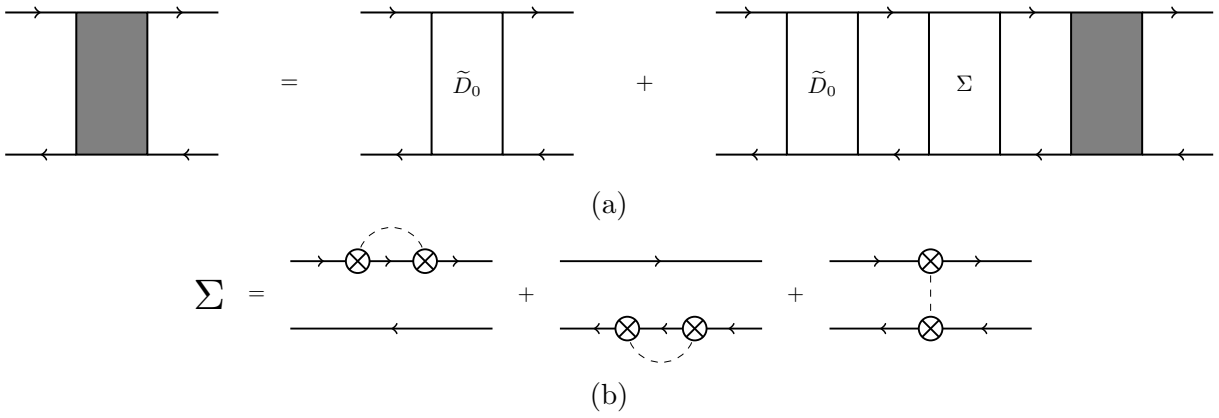

Figure 5.3: Diagrammatic series used by Beloborodov et. al. [26] for the granular diffuson. Here $\widetilde{D}_0$ is the homogeneous diffuson contained within a grain, and Σ is the diffuson's self energy.

To avoid this issue, and to provide a more natural derivation of the granular diffuson, we instead use the series defined in fig. 5.4. This treats internal disorder and tunnelling disorder at the same level, and so we can study how their strengths compare to one another. Writing this diagram mathematically, we have

$$\widetilde{D}_{ji}(\mathbf{q}, i\varepsilon + i\omega, i\varepsilon) = \widetilde{D}_{0ji} + \widetilde{D}_{0li}\,\Pi_{ml}(\mathbf{q}, i\varepsilon + i\omega, i\varepsilon)\,\widetilde{D}_{jm}(\mathbf{q}, i\varepsilon + i\omega, i\varepsilon), \tag{5.55a}$$

$$\widetilde{D}_{0ji} = \frac{1}{2\pi N(0)\tau_0}\delta_{ij} + t^2 a^d \delta_{\langle ij\rangle}, \tag{5.55b}$$

$$\Pi_{ml}(\mathbf{q}, i\varepsilon + i\omega, i\varepsilon) = \frac{\delta_{lm}}{a^d}\sum_{\mathbf{k}} G_l(\mathbf{k}+\mathbf{q}, i\varepsilon + i\omega) G_l(\mathbf{k}, i\varepsilon). \tag{5.55c}$$

The self-energy, Π_{lm}, is evaluated in exactly the same way as in section 3.3.1. We use a modified diffusive limit where τ replaces τ_0; in other words

$$\mathcal{D}q^2, |\omega|, T \ll \frac{1}{\tau}. \tag{5.56}$$

Using this limit yields

$$\Pi_{lm}(\mathbf{q}, i\varepsilon + i\omega, i\varepsilon) = 2\pi N(0)\tau(1 - |\omega|\tau - \mathcal{D}q^2\tau)\delta_{lm}, \tag{5.57}$$

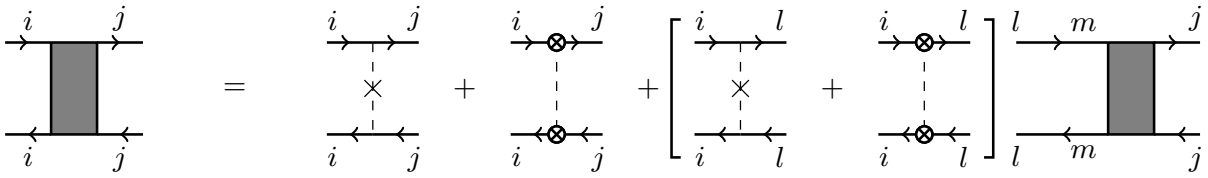

Figure 5.4: Granular diffuson diagrammatic series.

and the same condition that the two frequencies, ε and $\varepsilon + \omega$, must be opposite in sign.

To obtain a compact form for the diffuson, we recall that the granular lattice must be periodic by definition, so we may expand $\widetilde{D}_{0ji}$ as a Fourier series,

$$\widetilde{D}_{ji}(\mathbf{q}, i\varepsilon, i\varepsilon + i\Omega) = \frac{1}{\mathcal{N}} \sum_{\mathbf{Q}} \widetilde{D}(\mathbf{Q}, \mathbf{q}, i\varepsilon, i\varepsilon + i\Omega) e^{i\mathbf{Q}\cdot\mathbf{R}_{ji}}, \tag{5.58}$$

where $\mathcal{N}$ is the number of grains, and $\mathbf{R}_{ji} = \mathbf{R}_j - \mathbf{R}_i$ is the vector moving from grain i located at $\mathbf{R}_i$ to grain j located at $\mathbf{R}_j$. If we wanted to replace the $\mathbf{Q}$ sum by an integral, we would let (assuming a simple cubic lattice)[3]

$$\frac{1}{\mathcal{N}} \sum_{\mathbf{Q}} \to \left(\frac{a}{2\pi}\right)^d \int d^d Q. \tag{5.59}$$

Similarly, $\widetilde{D}_{0ji}$ and Π_{ml} may also be written as Fourier series.

Substituting the Fourier series expressions for $\widetilde{D}_{0ji}$, $\widetilde{D}_{0ji}$, and Π_{ml} into eq. 5.55a yields

$$\begin{aligned}
&\frac{1}{\mathcal{N}} \sum_{\mathbf{Q}} \widetilde{D}(\mathbf{Q}, \mathbf{q}, i\varepsilon, i\varepsilon + i\Omega) e^{i\mathbf{Q}\cdot\mathbf{R}_{ji}} \\
&\quad = \frac{1}{\mathcal{N}} \sum_{\mathbf{Q}} \widetilde{D}_0(\mathbf{Q}, \mathbf{q}, i\varepsilon, i\varepsilon + i\Omega) e^{i\mathbf{Q}\cdot\mathbf{R}_{ji}} \\
&\qquad + \frac{1}{\mathcal{N}} \sum_{l,m} \sum_{\mathbf{Q},\mathbf{P},\mathbf{K}} \Big[\widetilde{D}_0(\mathbf{K}, \mathbf{q}, i\varepsilon, i\varepsilon + i\Omega) \Pi(\mathbf{P}, \mathbf{q}, i\varepsilon, i\varepsilon + i\Omega) \\
&\qquad\qquad \times \widetilde{D}(\mathbf{Q}, \mathbf{q}, i\varepsilon, i\varepsilon + i\Omega) e^{i\mathbf{K}\cdot\mathbf{R}_{li}} e^{i\mathbf{P}\cdot\mathbf{R}_{ml}} e^{i\mathbf{Q}\cdot\mathbf{R}_{jm}} \Big].
\end{aligned} \tag{5.60}$$

[3]We give details of dealing with lattice-type problems and periodic boundaries within these systems in appendix K. This appendix should help to explain where the factors $\mathcal{N}$ appear and cancel.

This can be simplified by noting that grain label sums produce,

$$\begin{aligned}\sum_{l,m} e^{i\mathbf{K}\cdot\mathbf{R}_{li}} e^{i\mathbf{P}\cdot\mathbf{R}_{ml}} e^{i\mathbf{Q}\cdot\mathbf{R}_{jm}} &= \sum_{l,m} e^{i\mathbf{R}_l\cdot(\mathbf{K}-\mathbf{P})} e^{i\mathbf{R}_m\cdot(\mathbf{P}-\mathbf{Q})} e^{i(\mathbf{R}_j\cdot\mathbf{Q}-\mathbf{R}_i\cdot\mathbf{K})} \\ &= \mathcal{N}^2\, \delta_{\mathbf{K},\mathbf{P}}\, \delta_{\mathbf{Q},\mathbf{P}}\, e^{i\mathbf{Q}\cdot\mathbf{R}_{ji}}.\end{aligned} \tag{5.61}$$

Hence,

$$\begin{aligned}&\frac{1}{\mathcal{N}} \sum_{\mathbf{Q}} \widetilde{D}(\mathbf{Q},\mathbf{q},i\varepsilon,i\varepsilon+i\Omega) e^{i\mathbf{Q}\cdot\mathbf{R}_{ji}} \\ &\quad= \frac{1}{\mathcal{N}} \sum_{\mathbf{Q}} \Big[\widetilde{D}_0(\mathbf{Q},\mathbf{q},i\varepsilon,i\varepsilon+i\Omega) + \widetilde{D}_0(\mathbf{Q},\mathbf{q},i\varepsilon,i\varepsilon+i\Omega) \\ &\qquad\qquad \times \Pi(\mathbf{Q},\mathbf{q},i\varepsilon,i\varepsilon+i\Omega) \widetilde{D}(\mathbf{Q},\mathbf{q},i\varepsilon,i\varepsilon+i\Omega) \Big] e^{i\mathbf{Q}\cdot\mathbf{R}_{ji}}.\end{aligned} \tag{5.62}$$

For this to be true, the coefficients of the exponentials in each sum must be equal. Therefore, we arrive at a Dyson equation with exactly the same form as that we dealt with in the homogeneous case,

$$\begin{aligned}\widetilde{D}(\mathbf{Q},\mathbf{q},i\varepsilon,i\varepsilon+i\Omega) = \widetilde{D}_0(\mathbf{Q},\mathbf{q},i\varepsilon,&i\varepsilon+i\Omega) + \widetilde{D}_0(\mathbf{Q},\mathbf{q},i\varepsilon,i\varepsilon+i\Omega) \\ &\times \Pi(\mathbf{Q},\mathbf{q},i\varepsilon,i\varepsilon+i\Omega) \widetilde{D}(\mathbf{Q},\mathbf{q},i\varepsilon,i\varepsilon+i\Omega).\end{aligned} \tag{5.63}$$

The granular diffuson can thus be calculated using,

$$\widetilde{D}(\mathbf{Q},\mathbf{q},i\varepsilon,i\varepsilon+i\Omega) = \frac{1}{\widetilde{D}_0(\mathbf{Q},\mathbf{q},i\varepsilon,i\varepsilon+i\Omega)^{-1} - \Pi(\mathbf{Q},\mathbf{q},i\varepsilon,i\varepsilon+i\Omega)}. \tag{5.64}$$

Let us now determine $\widetilde{D}_0(\mathbf{Q},\mathbf{q},i\varepsilon,i\varepsilon+i\Omega)$ and $\Pi(\mathbf{Q},\mathbf{q},i\varepsilon,i\varepsilon+i\Omega)$ explicitly by writing their Kronecker deltas and nearest-neighbour deltas as Fourier series. Doing so, we find

$$\begin{aligned}\widetilde{D}_{0ji}(\mathbf{q},i\varepsilon,i\varepsilon+i\omega) = &\frac{1}{2\pi N(0)\tau_0} \frac{1}{\mathcal{N}} \sum_{\mathbf{Q}} e^{i\mathbf{Q}\cdot\mathbf{R}_{ji}} \\ &+ \frac{t^2 a^d}{\mathcal{N}} \sum_{\mathbf{Q}} \sum_{\alpha} \left(e^{i\mathbf{Q}\cdot(\mathbf{R}_{ji}+\mathbf{a}_\alpha)} + e^{i\mathbf{Q}\cdot(\mathbf{R}_{ji}-\mathbf{a}_\alpha)} \right),\end{aligned} \tag{5.65a}$$

$$\Pi_{ml}(\mathbf{q}, i\varepsilon, i\varepsilon+\omega) = (1-\omega\tau-\mathcal{D}q^2\tau)\frac{2\pi N(0)\tau}{\mathcal{N}}\sum_{\mathbf{Q}} e^{i\mathbf{Q}\cdot\mathbf{R}_{ml}}, \tag{5.65b}$$

where the second term in eq. 5.65a arises from the nearest-neighbour delta, $\delta_{\langle ij\rangle}$, and $\{\mathbf{a}_\alpha\}$ is the set of primitive lattice vectors. For a simple cubic lattice, these vectors are,

$$\mathbf{a}_\alpha = a\,\mathbf{e}_\alpha, \qquad\qquad \alpha = x, y, z, ... \tag{5.66}$$

The expression in eq. 5.65a can be simplified by introducing an object called the structure factor [4, 67],

$$\gamma_{\mathbf{Q}} = \frac{1}{z}\sum_{\alpha}\left(e^{i\mathbf{Q}\cdot\mathbf{a}_\alpha} + e^{-i\mathbf{Q}\cdot\mathbf{a}_\alpha}\right) \tag{5.67}$$

This allows us to re-express eq. 5.65a as,

$$\begin{aligned}
\widetilde{D}_{0ji}(\mathbf{q}, i\varepsilon+i\omega, i\varepsilon) &= \frac{1}{2\pi N(0)}\frac{1}{\mathcal{N}}\sum_{\mathbf{Q}}\left[\frac{1}{\tau_0} + z\Gamma\gamma_{\mathbf{Q}}\right]e^{i\mathbf{Q}\cdot\mathbf{R}_{ji}} \\
&= \frac{1}{2\pi N(0)}\frac{1}{\mathcal{N}}\sum_{\mathbf{Q}}\left[\frac{1}{\tau} + z\Gamma(\gamma_{\mathbf{Q}}-1)\right]e^{i\mathbf{Q}\cdot\mathbf{R}_{ji}} \\
&= \frac{1}{2\pi N(0)\tau}\frac{1}{\mathcal{N}}\sum_{\mathbf{Q}}\Big[1-\tau\Gamma\lambda_{\mathbf{Q}}\Big]e^{i\mathbf{Q}\cdot\mathbf{R}_{ji}},
\end{aligned} \tag{5.68}$$

where

$$\lambda_{\mathbf{Q}} = z(1-\gamma_{\mathbf{Q}}), \tag{5.69}$$

is used for notational convenience. From eq. 5.65b and eq. 5.68, we may deduce the Fourier series components we need to calculate the granular diffuson,

$$\widetilde{D}_0(\mathbf{Q}, \mathbf{q}, i\varepsilon, i\varepsilon+i\Omega) = \frac{1}{2\pi N(0)\tau}\left[1-\tau\Gamma\lambda_{\mathbf{Q}}\right], \tag{5.70a}$$

$$\Pi(\mathbf{Q}, \mathbf{q}, i\varepsilon, i\varepsilon+i\Omega) = 2\pi N(0)\tau(1-|\omega|\tau-\mathcal{D}q^2\tau). \tag{5.70b}$$

Finally, to get a simple form for the granular diffuson, we recall that $\tau_0^{-1} \gg z\Gamma$ and hence $\tau^{-1} \gg z\Gamma$. Therefore, we can expand $\widetilde{D}_0^{-1}$ in powers of $z\Gamma\tau$ and retain only terms

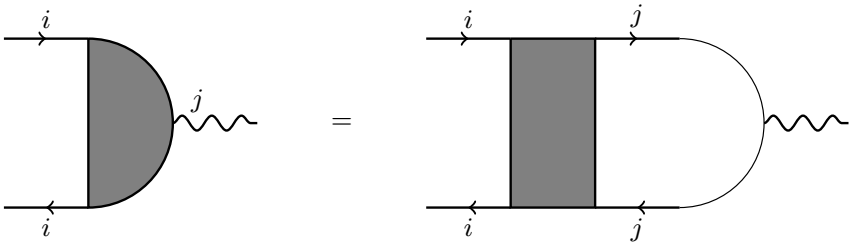

Figure 5.5: Granular diffuson diagrammatic series with a closed end. The wavy line is a generic interaction.

up to $\mathcal{O}(z\Gamma\tau)$.[4] This yields,

$$\widetilde{D}_0(\mathbf{Q},\mathbf{q},i\varepsilon,i\varepsilon+i\Omega)^{-1} = 2\pi N(0)\tau\left[1+\tau\Gamma\lambda_{\mathbf{Q}}\right]. \tag{5.71}$$

Thus we obtain the granular diffuson by substituting eq. 5.71 and eq. 5.70b into eq. 5.64,

$$\begin{aligned}\widetilde{D}(\mathbf{Q},\mathbf{q},i\varepsilon,i\varepsilon+i\omega) &= \frac{1}{2\pi N(0)\tau^2}\frac{1}{|\omega|+\mathcal{D}q^2+\Gamma\lambda_{\mathbf{Q}}}\Theta(-\varepsilon(\varepsilon+\omega)) \\ &\equiv \widetilde{D}(\mathbf{Q},\mathbf{q},\omega)\Theta(-\varepsilon(\varepsilon+\omega)),\end{aligned} \tag{5.72}$$

where, as before, we require the two frequencies entering the diffuson to be of opposite sign.

Clearly, this has an almost identical form to the homogeneous case, where $\mathcal{D}q^2$ has been replaced with $\mathcal{D}q^2+\Gamma\lambda_{\mathbf{Q}}$. By setting $\mathbf{q}=\mathbf{0}$, we recover Beloborodov et. al.'s result [26]. The diffuson we have derived here clearly has both sets of DOFs: those internal to a grain and those external to a grain, a result not previously seen in the literature.

Considering a diffuson with a closed end, see fig. 5.5, we find the same change in prefactor as with the homogeneous case,

$$\begin{aligned}D(\mathbf{Q},\mathbf{q},i\varepsilon+i\omega,i\varepsilon) &= \frac{1}{\tau}\frac{1}{|\omega|+\mathcal{D}q^2+\Gamma\lambda_{\mathbf{Q}}}\Theta(-\varepsilon(\varepsilon+\omega)) \\ &\equiv D(\mathbf{Q},\mathbf{q},i\omega)\Theta(-\varepsilon(\varepsilon+\omega)).\end{aligned} \tag{5.73}$$

The same is also true for the granular cooperons with open ends and a single closed end,

[4] The factor of $\lambda_{\mathbf{Q}}$ does not affect this expansion since $|\lambda_{\mathbf{Q}}|$ is, at most, of order unity in size.

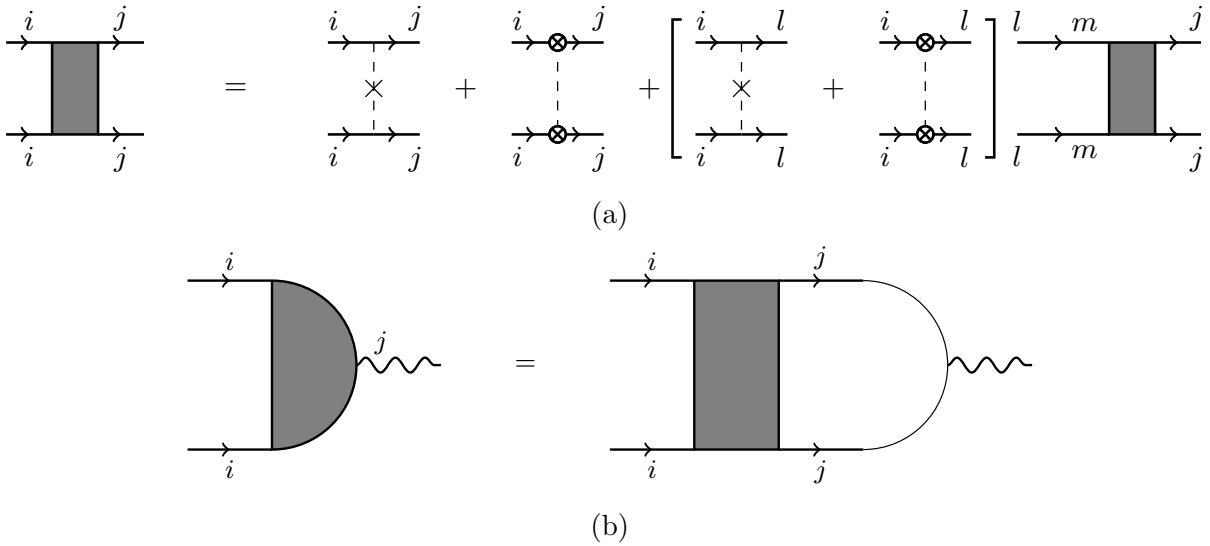

Figure 5.6: Diagrammatic series for the open cooperon (top) and half closed cooperon (bottom) in granular metals.

fig. 5.6a and fig. 5.6b respectively,

$$\begin{aligned}\widetilde{C}(\mathbf{Q},\mathbf{q},i\varepsilon+i\omega,i\varepsilon) &= \frac{1}{2\pi N(0)\tau^2}\frac{1}{|\omega|+\mathcal{D}q^2+\Gamma\lambda_{\mathbf{Q}}}\Theta(-\varepsilon(\varepsilon+\omega)) \\ &\equiv \widetilde{C}(\mathbf{Q},\mathbf{q},i\omega)\Theta(-\varepsilon(\varepsilon+\omega)).\end{aligned} \tag{5.74a}$$

$$\begin{aligned}C(\mathbf{Q},\mathbf{q},i\varepsilon+i\omega,i\varepsilon) &= \frac{1}{\tau}\frac{1}{|\omega|+\mathcal{D}q^2+\Gamma\lambda_{\mathbf{Q}}}\Theta(-\varepsilon(\varepsilon+\omega)) \\ &\equiv C(\mathbf{Q},\mathbf{q},i\omega)\Theta(-\varepsilon(\varepsilon+\omega)).\end{aligned} \tag{5.74b}$$

Before we proceed to consider two-body interactions, let us analyse the form of the external momentum contribution to the diffuson. In our models, we take the granular lattice to be simple cubic, meaning $z = 2d$, and eq. 5.67 can be rewritten as,

$$\gamma_{\mathbf{Q}} = \frac{1}{2d}\sum_{\alpha=1}^{d}\left(e^{i\mathbf{Q}\cdot\mathbf{a}_\alpha}+e^{-i\mathbf{Q}\cdot\mathbf{a}_\alpha}\right) = \frac{1}{d}\sum_{\alpha=1}^{d}\cos(Q_\alpha a), \tag{5.75}$$

where $\alpha = 1$ corresponds to the x-component, $\alpha = 2$ corresponds to the y-component, etc. Let us now consider the case of small $\mathbf{Q}$, $|\mathbf{Q}| \ll a^{-1}$. In this case, the structure factor

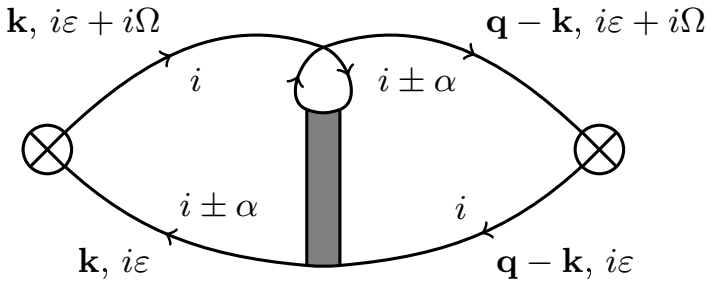

Figure 5.7: Diagrammatic representation of the WL correction to electrical conductivity in granular metals.

can be approximated as,

$$\gamma_{\mathbf{Q}} \simeq \frac{1}{d}\sum_{\alpha=1}^{d}\left(1-\frac{Q_\alpha^2 a^2}{2}\right) = 1-\frac{Q^2a^2}{2d}. \tag{5.76}$$

Hence, in this limit, the external momentum term can be replaced with,

$$\Gamma\lambda_{\mathbf{Q}} \simeq \Gamma a^2 Q^2. \tag{5.77}$$

This means that the diffuson, in the limit of small external momentum, has a dependence on $\mathbf{Q}$ almost identical to its dependence on $\mathbf{q}$. The only difference is the prefactor of Q^2 compared to q^2. For the internal momentum, the prefactor is the homogeneous diffusion constant, $\mathcal{D}$, whilst for the external momentum it is Γa^2. We therefore identify

$$\mathcal{D}_T = \Gamma a^2, \tag{5.78}$$

as the effective granular diffusion constant, as in the works of Beloborodov et. al. [26].

The limit we took to obtain this analogy can be rewritten in a form resembling the diffusive limit we have previously employed,

$$\mathcal{D}_T Q^2 \ll z\Gamma \qquad \Rightarrow \qquad Q \ll \frac{1}{a}, \tag{5.79}$$

since $z = \mathcal{O}(1)$ for real simple cubic lattices. We refer to this as the *granular diffusive*

limit. We now proceed to the calculation of the granular weak localisation correction.

5.2.2 Weak Localisation Correction in Granular Metals

The diagram describing the WL correction in granular metals is shown in fig. 5.7. This was calculated by Biagini et. al. [67], both with and without an applied external magnetic field. We shall only concern ourselves with the zero field case.

The expression associated to fig. 5.7 is,

$$\begin{aligned} K_{\alpha\alpha}(i\Omega) = -\frac{2e^2t^2}{a^{2d-2}\mathcal{N}} T \sum_i \sum_\varepsilon \sum_{\mathbf{k},\mathbf{p},\mathbf{q}} \Big[& G_i(\mathbf{k}, i\varepsilon + i\Omega) G_i(\mathbf{q}-\mathbf{k}, i\varepsilon) \\ & \times \Big\{ G_{i+\alpha}(\mathbf{p}, i\varepsilon) G_{i+\alpha}(\mathbf{q}-\mathbf{p}, i\varepsilon + i\Omega) \widetilde{C}_{ii+\alpha}(\mathbf{q}, i\varepsilon + i\Omega, i\varepsilon) \\ & + G_{i-\alpha}(\mathbf{p}, i\varepsilon) G_{i-\alpha}(\mathbf{q}-\mathbf{p}, i\varepsilon + i\Omega) \widetilde{C}_{ii-\alpha}(\mathbf{q}, i\varepsilon + i\Omega, i\varepsilon) \Big\} \Big]. \end{aligned} \tag{5.80}$$

The one subtlety in eq. 5.80 is in the minus sign prefactor. This is the result of one current vertex being reversed compared to the other. The current-current correlator can be thought of as measuring the response of an electron moving from one end of a material to the other, whilst a hole travels in the opposite direction, hence the electron line on the top in fig. 5.2, and hole line on the bottom. So we can picture the current vertices as pointing in opposite directions. To be clear, for Drude the left and right current vertices, $\mathbf{j}_L$ and $\mathbf{j}_R$ respectively, tunnel in opposite directions: $\mathbf{j}_L$ moves from grain $i \pm \alpha$ to grain i, whilst $\mathbf{j}_R$ goes from grain i to grain $i \pm \alpha$. Hence, we can think of the current-current correlator of physical concern as being given by a relation of the following nature,

$$\mathcal{G}_{\alpha\beta}(\tau - \tau') \sim - \left\langle T_\tau \{ j_{0,i+\alpha i}(\tau) j_{0,jj+\beta}(\tau') \} \right\rangle_{0,\mathrm{T}}, \tag{5.81}$$

where $j_{0,i+\alpha i}$ is the current vertex travelling from grain i to grain $i + \alpha$.[5]

[5]We say that we concern ourselves with the correlator of physical concern as the mathematics is not as enlightening. Mathematically speaking, the minus sign appears as the parts of the current-current correlator that will survive the averaging process, and generate tunnelling in the same direction, will be a result of current operator terms with the same sign multiplying together. For example, the first term of eq. 5.15 with α, multiplied into the first term of eq. 5.15 with β. This clearly differs by just a minus sign, compared to the result we find when the "cross terms" of opposite signs survive.

In contrast, one of the WL current vertices is flipped relative to the other: both $\mathbf{j}_L$ and $\mathbf{j}_R$ move from grain $i \pm \alpha$ to grain i. So we can think of $\mathbf{j}_R$ as having been reversed in its direction of travel compared to Drude. So the diagram in fig. 5.7 can be thought to have the following correlator,

$$\langle T_\tau \{ j_{0,i+\alpha i}(\tau) j_{0,j+\beta j}(\tau') \} \rangle_{0,\mathrm{T}} \,, \tag{5.82}$$

which is not of the current-current correlator's physical form in eq. 5.81. However, eq. 5.82 can be easily related to the physically relevant correlator, by noting that $j_{0,j+\beta j}(\tau') = -j_{0,jj+\beta}(\tau')$.[6] Therefore, the correlator in eq. 5.82 can be written as,

$$\langle T_\tau \{ j_{0,i+\alpha i}(\tau) j_{0,j+\beta j}(\tau') \} \rangle_{0,\mathrm{T}} = - \langle T_\tau \{ j_{0,i+\alpha i}(\tau) j_{0,jj+\beta}(\tau') \} \rangle_{0,\mathrm{T}} = -\mathcal{G}_{\alpha\beta}(\tau - \tau'). \tag{5.83}$$

Hence, given that $K_{\alpha\beta}(i\Omega) = \mathcal{G}_{\alpha\beta}(i\Omega)$, and $\mathcal{G}_{\alpha\beta}(i\Omega)$ is related to the correlator of fig. 5.7 by a minus sign, we can write the expression for the electromagnetic response function using our previous rules, with an additional factor of -1.

The result of this discussion is a new diagrammatic rule for calculating the electrical conductivity,

- If the current vertices describe tunnelling in opposite directions, then we need not change anything. If the current vertices describe tunnelling in the same direction, then the diagram produces an additional factor of -1.

Let us return to the calculation of the WL correction.

Noting the Heaviside function of the cooperon, we evaluate the fast momentum sums, $\mathbf{k}$ and $\mathbf{p}$, using eq. 3.75, but with τ in place of τ_0. Following this, the Matsubara sum is the same as in the homogeneous case, so we use the result from eq. 3.44. We then replace the remaining cooperons with their Fourier series expansions, and perform the sum over

[6] I.e. the current in one direction along a line, is just the negative of the current travelling in the opposite direction along the same line.

i. This leaves us with

$$K_{\alpha\alpha}(i\Omega) = -\frac{4N(0)e^2\tau^2\Gamma a^2}{a^d\mathcal{N}}\Omega\sum_{\mathbf{Q}}\sum_{\mathbf{q}}\widetilde{C}(\mathbf{Q},\mathbf{q},i\Omega)\cos(Q_\alpha a), \tag{5.84}$$

which obeys the requirement $K_{\alpha\alpha}(0) = 0$. The conductivity correction is therefore,

$$\sigma_{WL}(i\Omega) = -\frac{2e^2\Gamma a^2}{\pi a^d\mathcal{N}}\sum_{\mathbf{Q}}\sum_{\mathbf{q}}\frac{\cos(Q_\alpha a)}{\Omega + \mathcal{D}q^2 + \Gamma\lambda_{\mathbf{Q}} + \tau_\phi^{-1}}. \tag{5.85}$$

Note that Ω is still a Matsubara frequency here.

Let us discuss the importance of the internal and external momentum pieces appearing in the denominator. The energy scale of $\mathcal{D}q^2$ is set by the Thouless energy. For a system with characteristic size, L, see [27],

$$E_{Th} = \frac{\mathcal{D}}{L^2}. \tag{5.86}$$

For a homogeneous system, $L = L_0$ is large and so E_{Th} is small. However, for granular systems, each grain is much smaller than the size of a typical homogeneous system, $a \ll L_0$, and hence the Thouless energy of a single grain will be much larger than that of a homogeneous system.

Now, the momentum $\mathbf{q}$ is technically quantised, which is important due to the presence of the additional external momentum piece. So, let us consider a d-dimensional finite square well, with length L in each dimension, subject to the boundary condition that no current can pass through the system's surface. This boundary condition is a Neumann boundary condition, and requires the wave function's gradient to vanish at the surface. This yields,

$$\mathbf{q} = \frac{\pi}{L}(n_x, n_y, n_z) \qquad \Rightarrow \qquad \mathcal{D}q^2 = E_{Th}\pi^2(n_x^2 + n_y^2 + n_z^2) \tag{5.87}$$

in three dimensions, where $n_x, n_y, n_z \in \mathbb{Z}$. Clearly, $\mathcal{D}q^2$ will be much larger for any choice

of non-zero momentum in a granular system compared to a homogeneous system.

To understand why this is so important, we recall the presence of $\Gamma\lambda_{\mathbf{Q}}$ appearing next to $\mathcal{D}q^2$ in our diffusive propagators. From the conditions that define a granular metal in eq. 4.2, we must have $\Gamma \ll E_{Th}$. Hence, any choice of $\mathbf{q} \neq \mathbf{0}$ will dominate over the external momentum piece, and lead to a significantly less singular contribution from the diffusive propagators. Thus, the leading order behaviour will be given by the $\mathbf{q} = \mathbf{0}$ component of the internal momentum sum.

With this in mind, eq. 5.85 becomes,

$$\sigma_{WL}(i\Omega) = -\frac{2e^2\Gamma a^2}{\pi a^d \mathcal{N}} \sum_{\mathbf{Q}} \frac{\cos(Q_\alpha a)}{\Omega + \Gamma\lambda_{\mathbf{Q}} + \tau_\phi^{-1}}, \tag{5.88}$$

which has the same form as Biagini et. al. [67]. We are only interested in the DC response, so we set $\Omega = 0$, and we work in the granular diffusive limit, so $\cos(Q_\alpha a) \simeq 1$ and $\Gamma\lambda_{\mathbf{Q}} \simeq \Gamma a^2 Q^2$. Consequently, the granular WL correction is,

$$\sigma_{WL} = -\frac{2e^2\mathcal{D}_T}{\pi a^d \mathcal{N}} \sum_{\mathbf{Q}} \frac{1}{\mathcal{D}_T Q^2 + \tau_\phi^{-1}}. \tag{5.89}$$

This looks identical to the expression we had for the homogeneous case in eq. 3.83, where the previously suppressed $\mathcal{V}^{-1}$ factor has been replaced by $1/(\mathcal{N}a^d)$.

To evaluate the $\mathbf{Q}$ sum, we replace it by an integral and note that the radial integral no longer has an upper limit of π/a, but rather an upper limit of a^{-1} due to working in the granular diffusive limit. Thus, eq. 5.89 becomes,

$$\sigma_{WL} = -\frac{2e^2\mathcal{D}_T}{\pi} \frac{\Omega_d}{(2\pi)^d} \int_0^{a^{-1}} dQ \frac{Q^{d-1}}{\mathcal{D}_T Q^2 + \tau_\phi^{-1}}, \tag{5.90}$$

where Ω_d is the d-dimensional solid angle. Eq. 5.90 is the same as in the homogeneous

case, eq. 3.83, with $\mathcal{D} \to \mathcal{D}_T$. Performing this integral yields,[7]

$$\sigma_{WL} = \begin{cases} -\dfrac{e^2}{\pi^2} l_{\phi,T} \arctan\left(\dfrac{l_{\phi,T}}{a}\right), & d = 1 \\ -\dfrac{e^2}{2\pi^2} \ln\left(\Gamma\tau_\phi + 1\right), & d = 2 \\ \dfrac{e^2}{\pi^3}\left[\dfrac{1}{l_{\phi,T}} \arctan\left(\dfrac{l_{\phi,T}}{a}\right) - \dfrac{1}{a}\dfrac{\pi}{2}\right], & d = 3. \end{cases} \tag{5.91}$$

In the limit that $a \ll l_{\phi,T}$, which is equivalent to $\Gamma \ll \tau_\phi^{-1}$, eq. 5.91 becomes

$$\sigma_{WL} = \begin{cases} -\dfrac{e^2}{2\pi} l_{\phi,T}, & d = 1 \\ -\dfrac{e^2}{2\pi^2} \ln\left(\Gamma\tau_\phi\right), & d = 2 \\ \dfrac{e^2}{2\pi^2}\left[\dfrac{1}{l_{\phi,T}} - \dfrac{1}{a}\right], & d = 3. \end{cases} \tag{5.92}$$

This is exactly the same as the homogeneous results, with $\tau_0^{-1} \to \Gamma$, $l \to a$, and $\mathcal{D} \to \mathcal{D}_T$.

The apparent mapping from the homogeneous results to the granular results makes sense from a physical standpoint. Previously, τ_0^{-1} was the typical impurity scattering rate, whilst in granular metals the "scattering" mechanism that allows for transport is tunnelling, and so the associated rate is Γ. In a similar vein, a must be the analogue to l. Let us now move on to including the Coulomb interaction.

5.3 Electron-Electron Interactions

5.3.1 The Screened Coulomb Interaction

The Coulomb interaction in granular systems is a rather non-trivial problem, as the inclusion of both internal and external degrees of freedom will lead to cumbersome expressions for the bare Coulomb interaction. However, given we will be working in both the standard and granular diffusive limits, we expect that the disorder-screened Coulomb interaction

[7] We again choose a slightly different upper limit for the 3D case, as discussed in the footnotes of the homogeneous case.

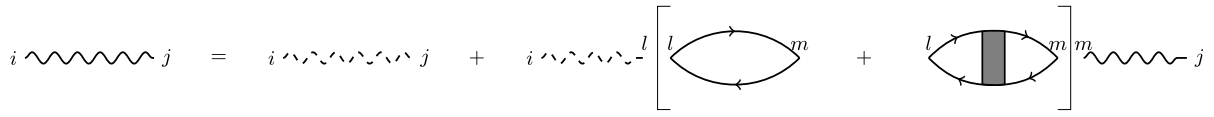

Figure 5.8: Diagrammatic series for the screened Coulomb interaction in a granular metal within RPA.

might have a similar form to what we found in section 3.4. Given the simple relation between the homogeneous and granular diffusons, the screened Coulomb interaction would naturally become,

$$V(\mathbf{Q}, \mathbf{q}, i\omega) = \frac{1}{2N(0)} \frac{\mathcal{D}_T Q^2 + \mathcal{D} q^2 + |\omega|}{\mathcal{D}_T Q^2 + \mathcal{D} q^2}. \tag{5.93}$$

However, since $E_{Th} \gg \Gamma$, any non-zero choice of the quantised momentum $\mathbf{q}$ will lead to a far less singular interaction. Hence, any terms resulting from terms with $\mathbf{q} \neq \mathbf{0}$ can be neglected in the problems we consider. Thus, eq. 5.93 can be replaced by the effective interaction

$$V(\mathbf{Q}, i\omega) = \frac{1}{2N(0)} \frac{\mathcal{D}_T Q^2 + |\omega|}{\mathcal{D}_T Q^2}. \tag{5.94}$$

This is indeed the form the screened Coulomb interaction takes in the granular diffusive limit, in accordance with the ideas presented by Beloborodov et. al. [63, 64, 26].

To see this from an RPA perspective, we refer to the series in fig. 5.8, which was originally considered by Beloborodov et. al. [26] in granular momentum space. The bare interaction they used is related to the charging energy between grains, $E_{c,ij}$,

$$V_{0,ij} = 2E_{c,ij} a^d = \frac{e^2}{\mathcal{C}_{ij}} a^d, \tag{5.95}$$

where $\mathcal{C}_{ij}$ is the capacitance matrix.[8] This works under the assumption that the internal DOFs are negligible, or rather that the long-range part of the Coulomb interaction is the important piece [63]. We could include $\mathbf{q}$ in these calculations; however, we will set it equal to zero at the end, and so serves us little benefit to continue including it.

[8]Eq. 5.95 differs from Beloborodov et. al.'s work by a factor of volume, this is to correct for a seeming dimensional discrepancy. This can be attributed to working in the intragranular momentum space, which would leads us to work with the internal momentum form of the Coulomb interaction, which carries an additional factor of volume compared to the position space bare Coulomb interaction.

The mathematical expression for fig. 5.8,

$$V_{ij}(i\omega) = V_{0,ij} + V_{0,lj}\Pi_{ml}(i\omega)V_{im}(i\omega), \tag{5.96a}$$

$$\begin{aligned}\Pi_{ml}(i\omega) = &-2T\sum_{\varepsilon}\sum_{\mathbf{k}} G(\mathbf{k}+\mathbf{q}, i\varepsilon + i\omega)G(\mathbf{k}, i\varepsilon) \\ &- 2T\sum_{\varepsilon}\sum_{\mathbf{k},\mathbf{k}'}\Big[G(\mathbf{k}+\mathbf{q}, i\varepsilon+i\omega)G(\mathbf{k}, i\varepsilon)\widetilde{D}(\mathbf{q}, i\varepsilon+i\omega, i\varepsilon) \\ &\times G(\mathbf{k}'+\mathbf{q}, i\varepsilon+i\omega)G(\mathbf{k}', i\varepsilon)\Big],\end{aligned} \tag{5.96b}$$

can be rewritten in lattice momentum space as

$$V(\mathbf{Q}, i\omega) = V_0(\mathbf{Q}) + V_0(\mathbf{Q})\Pi(\mathbf{Q}, i\omega)V(\mathbf{Q}, i\omega), \tag{5.97}$$

and clearly has the same form as the homogeneous case. It follows that

$$V(\mathbf{Q}, i\omega) = \frac{|\omega| + \Gamma\lambda_{\mathbf{Q}}}{V_0(\mathbf{Q})^{-1}(|\omega| + \Gamma\lambda_{\mathbf{Q}}) + 2N(0)\Gamma\lambda_{\mathbf{Q}}}. \tag{5.98}$$

Working in the granular diffusive limit, the capacitance matrix can be approximated so that $V_0(\mathbf{Q})$ has the same form as in homogeneous systems [26, 64],

$$V_0(\mathbf{Q}) = \begin{cases} \dfrac{4\pi e^2}{Q^2}, & d = 3 \\ \dfrac{2\pi e^2}{Q}, & d = 2 \\ -e^2\ln(Q^2w^2), & d = 1. \end{cases} \tag{5.99}$$

Substituting eq. 5.99 into eq. 5.97, and computing the polarisation operator as we did in the homogeneous case, we arrive at

$$V(\mathbf{Q}, i\omega) = \frac{|\omega| + \mathcal{D}_T Q^2}{2N(0)} \begin{cases} \dfrac{\kappa_3^2}{Q^2(|\omega| + \mathcal{D}_T Q^2) + \kappa_3^2\mathcal{D}_T Q^2}, & d = 3, \\ \dfrac{\kappa_2}{Q(|\omega| + \mathcal{D}_T Q^2) + \kappa_2\mathcal{D}_T Q^2}, & d = 2, \\ \dfrac{2e^2N(0)}{2e^2N(0)\mathcal{D}_T Q^2 - (|\omega| + \mathcal{D}_T Q^2)\left[\ln(Q^2w^2)\right]^{-1}}, & d = 1. \end{cases} \tag{5.100}$$

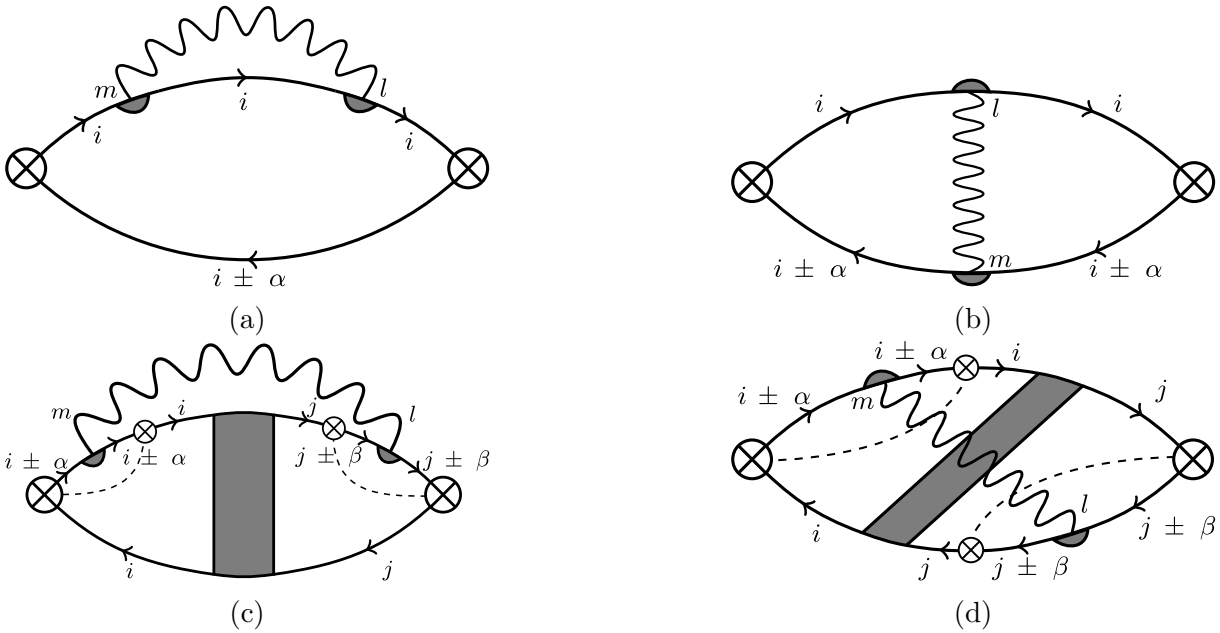

Figure 5.9: Leading order corrections to the electrical conductivity due to EEIs in granular metals.

Given that $\kappa_d \gg l^{-1}$, and $Q \ll a^{-1} \ll l^{-1}$ in the granular diffusive limit, eq. 5.100 can be approximated in the exact same way as before. Hence, we recover the result in eq. 5.94. Let us now consider the diagrams describing the EEI corrections to the electrical conductivity in a granular metal.

5.3.2 EEI Corrections to the Electrical Conductivity

The diagrams shown in fig. 5.9 describe the electrical conductivity corrections arising due to the Coulomb interaction. The specific placement of the tunnelling events in diagrams C and D must be included for such terms to exist. This is a direct result of the diffuson connecting the top and bottom parts of the conductivity bubble. The placement and correlation of these events give rise to the leading order contributions; any other choices of tunnelling event position and correlation would lead to higher order corrections. We will demonstrate the reasoning behind this once we have dealt with diagrams A and B.

In the homogeneous case, we had a third diagram that involved a single impurity scattering event correlated across one half of the conductivity bubble. We do not have an analogous diagram in the granular case though. We recall that diagram B of the

homogeneous EEI calculation cancelled half of the third sign configuration of diagram A in the homogeneous case. It turns out that in granular metals this cancellation is not needed, as the contribution of fig. 5.9a gives the granular analogue of the sum of diagrams A and B from the homogeneous case.

Now, the sum of these diagrams vanished for homogeneous metals. However, this is not exactly the case in the granular case, and leads to some questions about the limit in which these methods are applicable. Written in lattice position space, diagrams A (fig. 5.9a) and B (fig. 5.9b) are given, respectively, by

$$\begin{aligned} K^{(A)}_{\alpha\alpha}(i\Omega) = -\frac{8e^2a^2t^2T^2}{\mathcal{N}a^{2d}} \sum_{i,l,m} \sum_{\varepsilon,\omega} \sum_{\mathbf{k},\mathbf{p}} \Big[& V_{ml}(i\omega) G_i(\mathbf{k}, i\varepsilon + i\Omega)^2 G_i(\mathbf{k}, i\varepsilon + i\Omega + i\omega) \\ & \times \Big\{ G_{i+\alpha}(\mathbf{p}, i\varepsilon) + G_{i-\alpha}(\mathbf{p}, i\varepsilon) \Big\} D_{mi}(i\varepsilon + i\Omega, i\varepsilon + i\Omega + i\omega) \\ & \times D_{li}(i\varepsilon + i\Omega, i\varepsilon + i\Omega + i\omega) \Big], \end{aligned} \tag{5.101a}$$

$$\begin{aligned} K^{(B)}_{\alpha\alpha}(i\Omega) = -\frac{2e^2a^2t^2T^2}{\mathcal{N}a^{2d}} \sum_{i,l,m} \sum_{\varepsilon,\omega} \sum_{\mathbf{k},\mathbf{p}} \Big[& V_{ml}(i\omega) G_i(\mathbf{k}, i\varepsilon + i\Omega) G_i(\mathbf{p}, i\varepsilon + i\Omega + i\omega) \\ & \times D_{mi}(i\varepsilon + i\Omega, i\varepsilon + i\Omega + i\omega) \Big\{ G_{i+\alpha}(\mathbf{k}, i\varepsilon) G_{i+\alpha}(\mathbf{p}, i\varepsilon + i\omega) \\ & \times D_{li+\alpha}(i\varepsilon + i\Omega, i\varepsilon + i\Omega + i\omega) + G_{i-\alpha}(\mathbf{k}, i\varepsilon) G_{i-\alpha}(\mathbf{p}, i\varepsilon + i\omega) \\ & \times D_{li-\alpha}(i\varepsilon + i\Omega, i\varepsilon + i\Omega + i\omega) \Big\} \Big], \end{aligned} \tag{5.101b}$$

where we have suppressed the internal momentum argument of the diffusons due to it being equal to zero. These diagrams have the same sign configurations as those in the homogeneous case. We now follow the standard procedure for performing the fast internal momentum sums, shift to lattice momentum space, and evaluate the fermionic Matsubara frequency sum, to find

$$K^{(A)}_{\alpha\alpha}(i\Omega) + K^{(B)}_{\alpha\alpha}(i\Omega) = \frac{4N(0)e^2}{\mathcal{N}a^{d-2}d} T \sum_{\omega>\Omega} \sum_{\mathbf{Q}} (\omega - \Omega) V(\mathbf{Q}, i\omega) \frac{\Gamma\lambda_{\mathbf{Q}}}{(\omega + \Gamma\lambda_{\mathbf{Q}})^2}. \tag{5.102}$$

Clearly, eq. 5.102 does not vanish as it did in the homogeneous case. Worryingly though, we see that it does not vanish when $\Omega = 0$. Given that diagrams C and D correspond to diagrams D and E of the homogeneous calculation, and so vanish when $\Omega = 0$, the non-zero value of diagrams A and B in the zero frequency limit would imply that the set of diagrams in fig. 5.9 do not describe a normal state metal.

In the works of Beloborodov et. al. [26, 64], it is claimed that this gives rise to a high temperature behaviour unique to granular systems. This does not address the issue of the diagrams apparently failing to describe a normal state metal, however. We can reconcile this discrepancy by working in the granular diffusive limit, in which case

$$K^{(A)}_{\alpha\alpha}(i\Omega) + K^{(B)}_{\alpha\alpha}(i\Omega) = \frac{2e^2}{\mathcal{N}a^{d-2}d} T \sum_{\omega>\Omega} \sum_{\mathbf{Q}} \frac{\omega - \Omega}{\omega + \mathcal{D}_T Q^2}, \tag{5.103}$$

where we approximated $\Gamma\lambda_{\mathbf{Q}} \simeq \mathcal{D}_T Q^2$, and we substituted eq. 5.94 in for $V(\mathbf{Q}, i\omega)$. In this limit, eq. 5.103 corresponds to a higher order correction than the contributions of diagrams C and D. To see this we analyse the $\mathbf{Q}$ sum using power counting.

The process of power counting is simple and gives us an idea as to the style of behaviour we might expect from the result of an integral. For the $\mathbf{Q}$ sum in eq. 5.103, power counting gives a summand that is of the order Q^{-2}.[9] In contrast, the order produced by power counting diagrams C and D is Q^{-4}, and so the contribution of diagrams A and B is of a higher order. We therefore see that the contributions of diagrams A and B are not at leading order,[10] and so the diagrams in fig. 5.9 lead to vanishing response functions at the leading order when $\Omega = 0$.

Moving onto diagrams C and D, we may write their electromagnetic response functions

[9] To perform power counting, we simply note the largest power of Q occurring in numerator of the summand, and subtract from it the largest power Q appearing in the denominator. Assuming a spherically symmetric summand, the entire $\mathbf{Q}$ sum can then be thought of as being of the order Q^{d-2}, since we can think of the summand as an integral which introduces an additional factor Q^{d-1} into the integrand's numerator, which gives the integrand the order Q^{d-3}. Integration simply increases the power by 1, and so the entire sum/integral has the order Q^{d-2}.

[10] In short, we could have just treated $\Gamma\lambda_{\mathbf{Q}} = 0$ in the numerator of eq. 5.102.

as,

$$
\begin{aligned}
K^{(C)}_{\alpha\beta}(i\Omega) = -\frac{4e^2a^2t^4T^2}{\mathcal{N}a^{3d}} \sum_{\substack{i,j,\\ l,m}} \sum_{\varepsilon,\omega} \sum_{\substack{\mathbf{k},\mathbf{k}',\\ \mathbf{p},\mathbf{p}'}} \Big[& V_{ml}(i\omega) G_i(\mathbf{p}, i\varepsilon + i\Omega + i\omega) G_i(\mathbf{p}, i\varepsilon) \\
& \times \widetilde{D}_{ji}(i\varepsilon + i\Omega + i\omega, i\varepsilon) G_j(\mathbf{p}', i\varepsilon + i\Omega + i\omega) G_j(\mathbf{p}', i\varepsilon) \\
& \times \Big\{ G_{i+\alpha}(\mathbf{k}, i\varepsilon + i\Omega) G_{i+\alpha}(\mathbf{k}, i\varepsilon + i\Omega + i\omega) D_{mi+\alpha}(i\varepsilon + i\Omega, i\varepsilon + i\Omega + i\omega) \\
& \quad - G_{i-\alpha}(\mathbf{k}, i\varepsilon + i\Omega) G_{i-\alpha}(\mathbf{k}, i\varepsilon + i\Omega + i\omega) D_{mi-\alpha}(i\varepsilon + i\Omega, i\varepsilon + i\Omega + i\omega) \Big\} \\
& \times \Big\{ G_{j+\beta}(\mathbf{k}', i\varepsilon + i\Omega) G_{j+\beta}(\mathbf{k}', i\varepsilon + i\Omega + i\omega) D_{lj+\beta}(i\varepsilon + i\Omega, i\varepsilon + i\Omega + i\omega) \\
& \quad - G_{j-\beta}(\mathbf{k}', i\varepsilon + i\Omega) G_{j-\beta}(\mathbf{k}', i\varepsilon + i\Omega + i\omega) D_{lj-\beta}(i\varepsilon + i\Omega, i\varepsilon + i\Omega + i\omega) \Big\} \Big],
\end{aligned}
\tag{5.104a}
$$

$$
\begin{aligned}
K^{(D)}_{\alpha\beta}(i\Omega) = -\frac{4e^2a^2t^4T^2}{\mathcal{N}a^{3d}} \sum_{\substack{i,j,\\ l,m}} \sum_{\varepsilon,\omega} \sum_{\substack{\mathbf{k},\mathbf{k}',\\ \mathbf{p},\mathbf{p}'}} \Big[& V_{ml}(i\omega) G_i(\mathbf{p}, i\varepsilon + i\Omega + i\omega) G_i(\mathbf{k}, i\varepsilon) \\
& \times \widetilde{D}_{ji}(i\varepsilon + i\Omega + i\omega, i\varepsilon) G_j(\mathbf{p}', i\varepsilon + i\Omega + i\omega) G_j(\mathbf{p}', i\varepsilon) \\
& \times \Big\{ G_{i+\alpha}(\mathbf{k}, i\varepsilon + i\Omega) G_{i+\alpha}(\mathbf{k}, i\varepsilon + i\Omega + i\omega) D_{mi+\alpha}(i\varepsilon + i\Omega, i\varepsilon + i\Omega + i\omega) \\
& \quad - G_{i-\alpha}(\mathbf{k}, i\varepsilon + i\Omega) G_{i-\alpha}(\mathbf{k}, i\varepsilon + i\Omega + i\omega) D_{mi-\alpha}(i\varepsilon + i\Omega, i\varepsilon + i\Omega + i\omega) \Big\} \\
& \times \Big\{ G_{j+\beta}(\mathbf{k}, i\varepsilon + i\Omega) G_{j+\beta}(\mathbf{k}, i\varepsilon + i\Omega + i\omega) D_{lj+\beta}(i\varepsilon + i\Omega, i\varepsilon + i\Omega + i\omega) \\
& \quad - G_{j-\beta}(\mathbf{k}, i\varepsilon + i\Omega) G_{j-\beta}(\mathbf{k}, i\varepsilon + i\Omega + i\omega) D_{lj-\beta}(i\varepsilon + i\Omega, i\varepsilon + i\Omega + i\omega) \Big\} \Big].
\end{aligned}
\tag{5.104b}
$$

The minus sign appearing between the $\pm\alpha$ terms is due to the reversal of the tunnelling direction of the current vertex associated to α.[11] The same is also true for the minus sign appearing between the $\pm\beta$ terms. These diagrams have the same sign choices as their homogeneous analogues as the tunnelling events do not transfer frequency, so we can simply add tunnelling events to split Green's functions of the same sign in the sign choices shown in fig. 3.19 and fig. 3.20 for diagrams C and D respectively.

Evaluating each sign choice, we find that $K^{(C1)}_{\alpha\beta}$ and $K^{(D1)}_{\alpha\beta}$ cancel exactly, whilst $K^{(C2)}_{\alpha\beta}$

[11] See our discussion of this for the granular WL correction in section 5.2.2.

and $K^{(D2)}_{\alpha\beta}$ add to give

$$K^{(C)}_{\alpha\beta}(i\Omega) + K^{(D)}_{\alpha\beta}(i\Omega) = -\frac{16e^2N(0)\Gamma^2}{\mathcal{N}a^{d-2}} \times \sum_{\mathbf{Q}} T\left[\sum_{\omega>\Omega}\Omega + \sum_{0<\omega\leq\Omega}\omega\right] \frac{\sin(Q_\alpha a)\sin(Q_\beta a)V(\mathbf{Q},i\omega)}{(\omega+\Gamma\lambda_{\mathbf{Q}})^2(\omega+\Omega+\Gamma\lambda_{\mathbf{Q}})}. \tag{5.105}$$

This expression clearly equals zero when $\alpha \neq \beta$. Taking eq. 5.105 in the granular diffusive limit, $\sin(Q_\alpha a) \simeq Q_\alpha a$, and substituting eq. 5.94 in for $V(\mathbf{Q}, i\omega)$, yields

$$K^{(C)}_{\alpha\beta}(i\Omega) + K^{(D)}_{\alpha\beta}(i\Omega) = -\frac{8e^2\Gamma}{\mathcal{N}a^{d-2}d}\delta_{\alpha\beta} \times \sum_{\mathbf{Q}} T\left[\sum_{\omega>\Omega}\Omega + \sum_{0<\omega\leq\Omega}\omega\right] \frac{1}{(\omega+\mathcal{D}_T Q^2)(\omega+\Omega+\mathcal{D}_T Q^2)}. \tag{5.106}$$

Power counting gives the order of the $\mathbf{Q}$ summand to be Q^{-4}, as we stated earlier. Therefore, to leading order, the total electromagnetic response function due to EEIs is given by eq. 5.106,

$$K_{\alpha\beta}(i\Omega) = -\frac{8e^2\mathcal{D}_T}{\mathcal{N}a^d d}\delta_{\alpha\beta}\sum_{\mathbf{Q}} T\left[\sum_{\omega>\Omega}\Omega + \sum_{0<\omega\leq\Omega}\omega\right] \frac{1}{(\omega+\mathcal{D}_T Q^2)(\omega+\Omega+\mathcal{D}_T Q^2)}. \tag{5.107}$$

This is exactly the same expression we found in the homogeneous case (see eq. 3.97 and eq. 3.103), with $\mathcal{D} \to \mathcal{D}_T$ and the volume factor written explicitly. However, the major difference here is that when replacing the $\mathbf{Q}$ sum by an integral, the upper limit is set to a^{-1}, due to working in the granular diffusive limit.

In the homogeneous calculation, we set the upper limit of the q integral to infinity, despite the fact we were in the diffusive limit, meaning the upper cut-off should have been l^{-1}. However, the energy associated to the upper limit appearing in the integrand is given by $\mathcal{D}l^{-2}$, which is a much larger energy scale than the temperatures we concern ourselves with in typical transport experiments. Hence, extending the limit to infinity introduces small, but negligible, errors. Granular systems do not possess this luxury, however, as the upper limit of the Q integral has the associated energy of Γ, which can be higher or lower

than the temperature of the system. Hence, we must consider these limits separately.

Replacing the $\mathbf{Q}$ sum by an integral, performing said integral, and expanding to first order in Ω, we find

$$\sigma_{EEI} = -\frac{4\Omega_d e^2}{(2\pi)^d d} T \left[\lim_{\Omega\to 0} \sum_{0<\omega\leq\Omega} \frac{\omega}{\Omega} + \sum_{\omega>0} 1 \right] \times \begin{cases} \frac{a}{\omega}\sqrt{\frac{\Gamma}{\omega}} \arctan\left(\sqrt{\frac{\Gamma}{\omega}}\right) + \frac{\Gamma a}{\omega}\frac{1}{\Gamma+\omega}, & d=1 \\ \frac{1}{\omega} - \frac{1}{\omega+\Gamma}, & d=2 \\ \frac{1}{\sqrt{\mathcal{D}_T \omega}} \left[\arctan\left(\sqrt{\frac{\Gamma}{\omega}}\right) - \frac{\sqrt{\Gamma\omega}}{\Gamma+\omega} \right], & d=3. \end{cases} \tag{5.108}$$

These sums can only be done generally for $d = 2$,

$$\sigma_{EEI}^{(2D)} = -\frac{e^2}{2\pi^2}\left[\gamma + \psi\left(1+\frac{\Gamma}{2\pi T}\right) + \frac{\Gamma}{\pi T}\psi'\left(1+\frac{\Gamma}{2\pi T}\right)\right]. \tag{5.109}$$

For other dimensionalities, we will have to consider their expressions in eq. 5.108 in the different temperature limits present.

We first consider the low temperature limit, $T \ll \Gamma$, in which eq. 5.108 reproduces the same form of corrections as in the homogeneous case,

$$\sigma_{\mathrm{EEI}} = -\frac{e^2}{2\pi^2}\left(\frac{T}{\mathcal{D}_T}\right)^{\frac{d}{2}-1} \times \begin{cases} \frac{\alpha_d}{(2\pi)^{2-\frac{d}{2}}}\frac{4-d}{2d}\zeta\left(2-\frac{d}{2},1\right), & d=1,3 \\ \ln\left(\frac{\Gamma}{2\pi T}\right), & d=2. \end{cases} \tag{5.110}$$

This agrees with the result of Beloborodov et. al. [64].

Considering eq. 5.108 in the high temperature limit, $T \gg \Gamma$, yields

$$\sigma_{EEI} = -\frac{2\Omega_d \beta_d}{3(2\pi)^d d}\frac{e^2}{a^{d-2}}\frac{\Gamma}{T}, \qquad \text{where} \qquad \beta_d = \begin{cases} 1, & d=1 \\ \frac{3}{4}, & d=2 \\ \frac{1}{3}, & d=3. \end{cases} \tag{5.111}$$

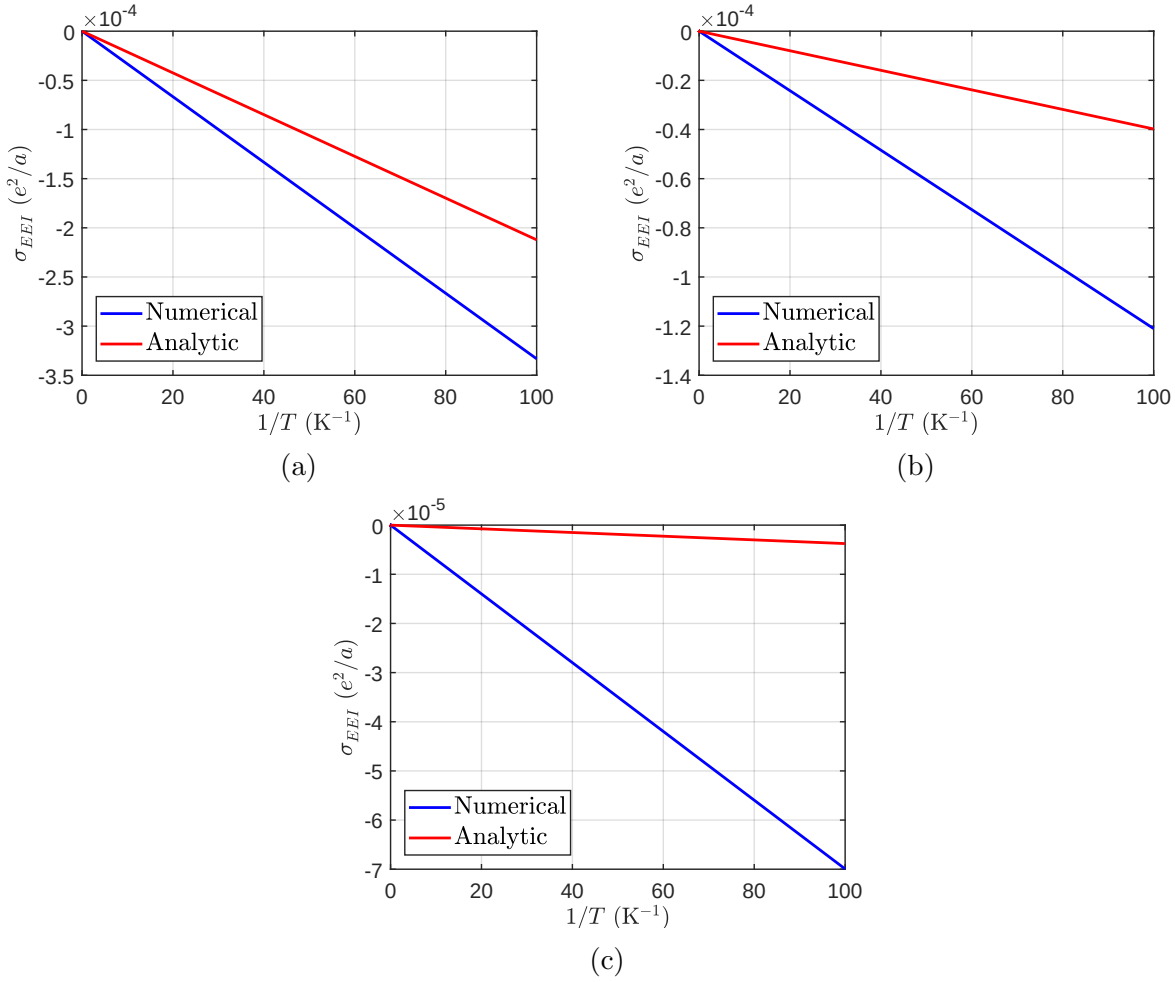

Figure 5.10: Numerical solutions to eq. 5.112a (numerical) in comparison to eq. 5.111 (analytical). (a), (b), and (c) correspond to 1D, 2D, and 3D respectively. Here we have used $\Gamma = 10^{-5}$K.

This is a result not discussed in the literature, and exhibits a temperature dependence independent of the system's dimensionality. This is similar to the result Beloborodov et. al. claim to get from diagrams A and B [64], where they found a logarithmic correction in the high temperature limit.

The T^{-1} behaviour in eq. 5.111 in the high temperature limit can even be seen outside of the granular diffusive limit. To see this, we instead perform the ω sums in eq. 5.105 first, to obtain

$$\sigma_{EEI} = -\frac{2e^2}{\mathcal{N}a^{d-2}\pi^2 d}\frac{\Gamma}{T}\sum_{\mathbf{Q}}\frac{\widetilde{\lambda}_{\mathbf{Q}}}{\lambda_{\mathbf{Q}}}\left[2\psi'\left(1+\frac{\Gamma\lambda_{\mathbf{Q}}}{2\pi T}\right)+\frac{\Gamma\lambda_{\mathbf{Q}}}{2\pi T}\psi''\left(1+\frac{\Gamma\lambda_{\mathbf{Q}}}{2\pi T}\right)\right] \tag{5.112a}$$

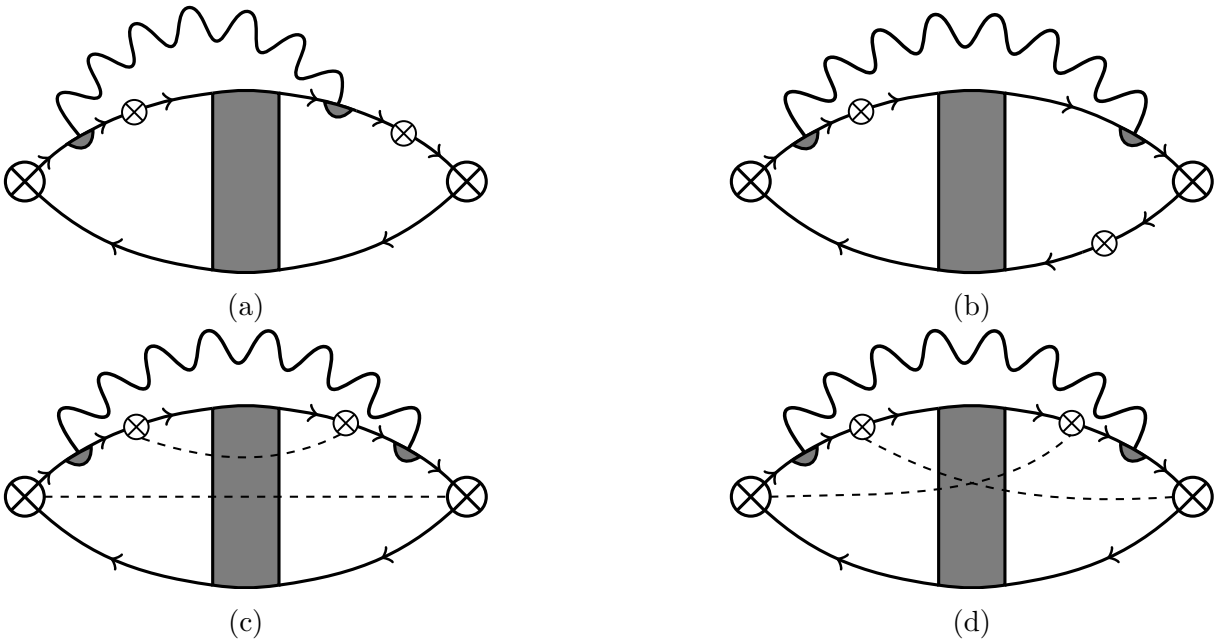

Figure 5.11: (a) and (b) give examples of alternative placements for the additional tunnelling events of diagram C. (c) and (d) give the alternative non-zero tunnelling event correlations of diagram C.

$$\widetilde{\lambda}_{\mathbf{Q}} = \sum_{\alpha=1}^{d} \sin^2(Q_\alpha a). \tag{5.112b}$$

We then replace the momentum sum by an integral, and perform it numerically. We present the numerical solution to eq. 5.112a in fig. 5.10 in one, two, and three dimensions, for comparison to the analytic solution obtained in eq. 5.111.

Now, earlier we mentioned different placements and correlations of the tunnelling events in diagrams C and D, and how these diagrams either vanish or are less singular. We give two types of alternative placements in fig. 5.11a and fig. 5.11b. These diagrams will naturally vanish, due to our ability to consider the extra tunnelling event on either the top or bottom of the bubble: the variant with a tunnelling event on the top half will carry an extra minus sign compared to when the tunnelling event is on the bottom. This is true regardless of the correlation we choose between the different tunnelling events.

Considering a different correlation of the tunnelling events, see fig. 5.11c and fig. 5.11d for examples, we find that these variants have one fewer grain label sums, and

hence we will have an additional lattice momentum compared to that of fig. 5.9c.[12] In assigning internal momenta to the electron lines, we are able to introduce two unique fast momenta, and two independent slow momenta. The slow momenta can be associated to the Coulomb interaction and the open diffuson that connects the top and bottom of the conductivity bubble. Clearly, the most singular terms generated by these diagrams arise from when the slow momenta are equal to zero.

To determine the size of these diagrams relative to that in fig. 5.9c we will need to evaluate the fast momentum sums. We note that each of these sums will have the form $G^+(\mathbf{k})^2 G^-(\mathbf{k})^2$, and so will each produce a factor $\sim N(0)\tau^2$. Therefore, accounting for volume factors, we see that these variant diagrams will carry a factor of $(\delta\tau)^2$ compared to those in fig. 5.9. Given that we concern ourselves with granular metals, we recall that $\delta \ll \Gamma \ll \tau^{-1}$. Hence, $(\delta\tau)^2$ is an extremely small prefactor, and so diagrams with correlations different to that of fig. 5.9c and fig. 5.9d lead to higher order corrections, and so can be neglected at leading order.

5.4 Superconducting Fluctuations

The effect of virtual Cooper pairs near T_c was the start of Beloborodov et. al.'s study of granular metals [61, 62]. In these works they focused heavily on the effects of strong magnetic fields, but did not consider the role of fluctuations in the absence of a field. A similar set of calculations were performed by Skrzynski et. al. [69] using a larger BCS interaction. In all of these works, the only DOFs included in two-body propagators were those of the lattice.[13]

In contrast to this, Lerner et. al. [27] approached the effects of virtual Cooper pairs in granular metals from the perspective of the internal DOFs. They focused on the

[12] This extra lattice momentum is carried by the open diffuson across the conductivity bubble.

[13] It is worth noting that the thermal conductivity correction due to fluctuations in granular metals has been calculated in the works of Biagini et. al. [68]. The approach used here appears to bear the greatest resemblance to the picture we have been working with for granular metals (i.e. setting up the problem in granular position space), but still focuses only on the lattice DOFs as in Beloborodov et. al.'s works [26].

zero field temperature dependence of these corrections, and worked in the case where $\Gamma \lesssim E_{Th} \lesssim T_c$. In their calculations they argued for the existence of three regions of behaviour in the reduced temperature dependence of the fluctuation corrections to the electrical conductivity, σ_{fl}, but did not show exactly how these regions were connected. The boundaries between these regions can be related to the electron tunnelling rate, and the Thouless energy of an isolated grain. Hence, we adopt the following naming convention,

- Close-to-T_c region: $\eta \lesssim \Gamma/T_c$
- Intermediate region: $\Gamma/T_c \lesssim \eta \lesssim E_{Th}/T_c$
- Far-from-T_c region: $E_{Th}/T_c \lesssim \eta \lesssim 1$.

We therefore expect crossovers between these regions to happen at $\eta \sim \Gamma/T_c$ (close-intermediate crossover) and $\eta \sim E_{Th}/T_c$ (intermediate-far crossover).

The methods used by Lerner et. al. were based upon the ideas and diagrams of Varlamov and Dorin [75], who calculated the effects of superconducting fluctuations on the single-particle tunnelling current of a single Josephson junction. Lerner et. al. predicted that, for 3D systems,

$$\sigma_{fl} \sim \begin{cases} \eta^{-1/2}, & \eta \lesssim \dfrac{\Gamma}{T_c} \\ \eta^{-3}, & \dfrac{\Gamma}{T_c} \lesssim \eta \lesssim \dfrac{E_{Th}}{T_c} \\ \eta^{-2}, & \dfrac{E_{Th}}{T_c} \lesssim \eta \lesssim 1. \end{cases} \tag{5.113}$$

However, their calculation relied upon a pair propagator confined to a single grain. As a result, their definition of the order of a process was based upon the number of single-grain pair propagators. Consequently, their diagram E, which resembles the usual MT diagram, requires two single grain pair-propagators and appears as a fourth order tunnelling process, and hence looks like a higher order correction. Because of this, they argued that higher order corrections (see their diagram D) should also be taken into account if they also possessed a sensitivity to phase coherence. In contrast, the methods we have developed

in this thesis allow us to construct a pair propagator that can tunnel between grains. It follows that diagrams such as Lerner et. al.'s diagram E appear within the infinite set of diagrams generated by considering the granular pair propagator.

Let us now outline how the granular pair propagator can be calculated with both internal and external DOFs present, and in doing so, see how the three regions of behaviour arise. After this, we shall calculate the correction σ_{fl} in granular metals. In these calculations, we closely follow the work of Perkins et. al. [76].

5.4.1 The Pair Propagator

To include superconductivity into our granular model we assume that the BCS interaction acts solely within a grain. This is equivalent to introducing the following term into the Hamiltonian,

$$H_{\mathrm{BCS}}^{(T)} = -\lambda_0 \sum_i \sum_{\mathbf{k},\mathbf{k}',\mathbf{q}} c_{i\mathbf{k}\uparrow}^\dagger c_{i\mathbf{q}-\mathbf{k}\downarrow}^\dagger c_{i\mathbf{q}-\mathbf{k}'\downarrow} c_{i\mathbf{k}'\uparrow}, \tag{5.114}$$

where we focus purely on singlet (s-wave) superconductivity. We find that the granular pair propagator is then given by the diagrammatic series in fig. 5.12, which can be written mathematically as

$$L_{ji}(\mathbf{q}, i\omega) = \lambda_0 \delta_{ij} + \lambda_0 \delta_{il} \Pi_{ml}(\mathbf{q}, i\omega) L_{jm}(\mathbf{q}, i\omega). \tag{5.115}$$

Expanding eq. 5.115 as a Fourier series in lattice momentum space, we find that the Fourier components are related by,

$$L(\mathbf{Q}, i\mathbf{q}, i\omega) = \lambda_0 + \lambda_0 \Pi(\mathbf{Q}, i\omega) L(\mathbf{Q}, \mathbf{q}, i\omega). \tag{5.116}$$

This is the usual Dyson equation, now with an extra granular momentum being carried around.

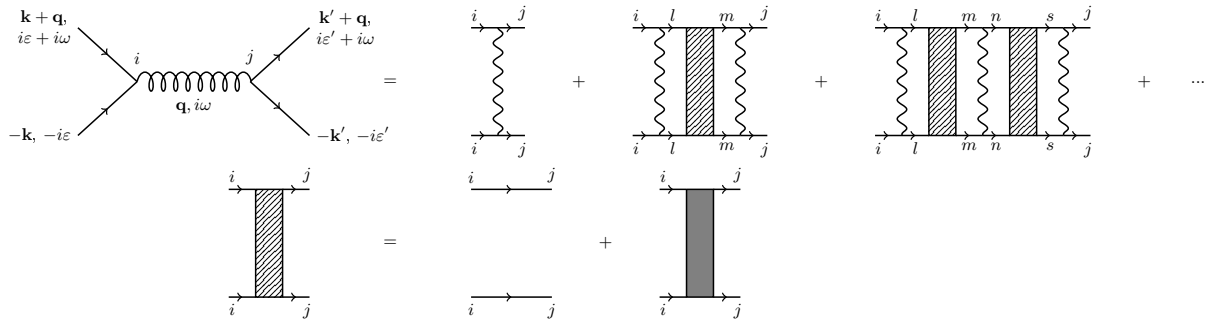

Figure 5.12: Diagrammatic series for the granular pair propagator mediated by BCS interactions (wavy lines). The BCS interaction does not allow for tunnelling between grains.

The granular fluctuation polarisation operator is given by,

$$\Pi_{fl}(\mathbf{Q},\mathbf{q},i\omega) = \Pi_{fl,0}(\mathbf{Q},\mathbf{q},i\omega) + \Pi_{fl,1}(\mathbf{Q},\mathbf{q},i\omega), \tag{5.117a}$$

$$\Pi_{fl,0}(\mathbf{Q},\mathbf{q},i\omega) = T\sum_{\varepsilon}\sum_{\mathbf{k}} G(\mathbf{k}+\mathbf{q},i\varepsilon+i\omega)G(-\mathbf{k},-i\varepsilon), \tag{5.117b}$$

$$\Pi_{fl,1}(\mathbf{Q},\mathbf{q},i\omega) = T\sum_{\varepsilon}\sum_{\mathbf{k}} G(\mathbf{k}+\mathbf{q},i\varepsilon+i\omega)G(-\mathbf{k},-i\varepsilon)C(\mathbf{Q},\mathbf{q},i\varepsilon+i\omega,i\varepsilon), \tag{5.117c}$$

where we have used the fact that the electron Green's functions are independent of the grain label. Eq. 5.117 is exactly the same as eq. 3.108, with the small change $\mathcal{D}q^2 \to \mathcal{D}q^2 + \Gamma\lambda_{\mathbf{Q}}$. The granular pair propagator is therefore trivial to derive,

$$L(\mathbf{Q},\mathbf{q},i\omega) = \frac{1}{N(0)}\left[\ln\left(\frac{T}{T_c}\right) + \psi\left(\frac{1}{2} + \frac{|\omega| + \mathcal{D}q^2 + \Gamma\lambda_{\mathbf{Q}} + \tau_\phi^{-1}}{4\pi T}\right) - \psi\left(\frac{1}{2} + \frac{1}{4\pi T_c\tau_{\phi,c}}\right)\right]^{-1}. \tag{5.118}$$

Now, for our calculations we shall work with an idealised version of Lerner et. al.'s considerations. In this case we shall assume,

$$\delta \ll \Gamma \ll E_{Th} \lesssim T_c. \tag{5.119}$$

In this case, given we are working with $T \geq T_c$, we may expand eq. 5.118 in terms of

$\Gamma\lambda_{\mathbf{Q}}$ without issue. As in the homogeneous case, we will be considering Cooper pairs with small frequencies, so we may also expand in powers of ω,

$$L(\mathbf{Q},\mathbf{q},i\omega)=\frac{1}{N(0)}\left[\epsilon(\mathbf{q},T)+\alpha_1(\mathbf{q},T)\frac{|\omega|+\Gamma\lambda_{\mathbf{Q}}}{4\pi T}\right]^{-1}, \tag{5.120}$$

where we have defined

$$\epsilon(\mathbf{q},T)=\ln\left(\frac{T}{T_c}\right)+\psi\left(\frac{1}{2}+\frac{\mathcal{D}q^2+\tau_\phi^{-1}}{4\pi T}\right)-\psi\left(\frac{1}{2}+\frac{1}{4\pi T_c\tau_{\phi,c}}\right), \tag{5.121a}$$

$$\alpha_n(\mathbf{q},T)=\psi^{(n)}\left(\frac{1}{2}+\frac{\mathcal{D}q^2+\tau_\phi^{-1}}{4\pi T}\right), \tag{5.121b}$$

for notational convenience. It is important to note that for $\eta\ll 1$, we can approximate $\epsilon(\mathbf{0},T)\simeq\eta$ when τ_ϕ^{-1} is sufficiently small. Later on, when we compare theory to experiment, we will be considering values of τ_ϕ^{-1} such that we cannot use this approximation, hence the introduction of this notation here.

For the case when $E_{Th}\ll T_c$, we can consider a large range of appropriately small momenta to justify an expansion in terms of $\mathcal{D}q^2$. In this case,

$$L(\mathbf{Q},\mathbf{q},i\omega)=\frac{1}{N(0)}\left[\bar{\epsilon}+\bar{\alpha}_1\frac{|\omega|+\mathcal{D}q^2+\Gamma\lambda_{\mathbf{Q}}}{4\pi T}\right]^{-1}, \tag{5.122}$$

where $\bar{\epsilon}=\epsilon(\mathbf{0},T)$ and $\bar{\alpha}_n=\alpha_n(\mathbf{0},T)$, which is the same as eq. 3.117 with $\mathcal{D}q^2\to\mathcal{D}q^2+\Gamma\lambda_{\mathbf{Q}}$. In the absence of phase breaking, eq. 5.122 collapses to

$$L(\mathbf{Q},\mathbf{q},i\omega)=\frac{1}{N(0)}\left[\ln\left(\frac{T}{T_{c,0}}\right)+\frac{\pi}{8T}(|\omega|+\mathcal{D}q^2+\Gamma\lambda_{\mathbf{Q}})\right]^{-1}. \tag{5.123}$$

For temperatures close to the transition, such that $\ln(T/T_{c,0})\simeq\eta$, we can see from the denominator of eq. 5.123 why three regions of behaviour exist. If we consider values of $\eta\ll\Gamma/T_c$ then the internal DOFs will give rise to a far less singular propagator, and hence less significant contributions to sums involving $L(\mathbf{Q},\mathbf{q},i\omega)$. Therefore, only the

$\mathbf{q} = \mathbf{0}$ term will be of any importance. If we consider $\Gamma/T_c \ll \eta \ll E_{Th}/T_c$, then the external DOFs become negligible in the pair propagator, whilst the internal DOFs still lead to less singular terms. In this case, only the $(\mathbf{Q}, \mathbf{q}) = (\mathbf{0}, \mathbf{0})$ piece of the propagator will be of any importance. Finally, if $E_{Th}/T_c \ll \eta \ll 1$, we may still neglect the external DOFs, however, we may now include the internal DOFs without generating less important contributions.[14]

To understand what these regions relate to physically, let us analyse the prefactors of the internal and external momentum pieces. By pulling out a factor of η from the denominator, these prefactors will become a coherence length. The prefactor of the internal q^2 piece is the same as in the homogeneous case,

$$\xi_{v,g} = \sqrt{\frac{\pi\mathcal{D}}{8T_c\eta}} = a\sqrt{\frac{\pi}{8}}\sqrt{\frac{E_{Th}}{T_c\eta}}, \qquad T > T_c, \quad \eta \ll 1, \tag{5.124}$$

and so represents the coherence length of a Cooper pair confined to a grain. Working in the granular diffusive limit, $\Gamma\lambda_{\mathbf{Q}} \simeq \mathcal{D}_T Q^2$, the prefactor of Q^2 introduces a new coherence length that is based on $\mathcal{D}_T$ rather than $\mathcal{D}$,

$$\xi_{v,T} = \sqrt{\frac{\pi\mathcal{D}_T}{8T_c\eta}} = a\sqrt{\frac{\pi}{8}}\sqrt{\frac{\Gamma}{T_c\eta}}, \qquad T > T_c, \quad \eta \ll 1, \tag{5.125}$$

which represents the coherence length of a Cooper pair across many grains.

We can see that the crossovers happen when $\xi_{v,T}$ and $\xi_{v,g}$ become comparable to the size of a grain. At the close-intermediate crossover, $\eta \sim \Gamma/T_c$, meaning $\xi_{v,T} \sim a$. We see a similar behaviour in internal coherence length at the intermediate-far crossover, $\eta \sim E_{Th}/T_c$, where $\xi_{v,g} \sim a$. To picture what is happening physically, let us consider moving away from T_c. In the close-to-T_c region, Cooper pairs have a typical size much greater than that of the grains, and so we associate the external coherence length to these Cooper pairs, $\xi_{v,T}$. As the temperature increases, the Cooper pairs and $\xi_{v,T}$ get smaller,

[14] In other words, terms with $\mathbf{q} \neq \mathbf{0}$ now become equally important, and we may keep $\mathbf{Q} = \mathbf{0}$ inside the propagator without any problems.

where they encounter the close-intermediate crossover when $\xi_{v,T}$ becomes comparable to a grain. So we may think of the close-to-T_c region as where Cooper pairs are much larger than a grain.

Continuing to higher temperatures, the Cooper pairs continue to get smaller and encounter the intermediate-far crossover when $\xi_{v,g} \sim a$. This means that the internal coherence length of a Cooper pair becomes comparable to the size of a grain at this crossover. For even higher temperatures, Cooper pairs again continue to get smaller, alongside $\xi_{v,g}$, such that we can think of Cooper pairs as being confined to a single grain,[15] and so we can associate the internal coherence length to the Cooper pairs in this region. We may therefore think of Cooper pairs in the far-from-T_c region as being much smaller than a grain, whilst the intermediate region describes Cooper pairs whose size is comparable to that of a grain. With this physical picture in mind, and having obtained the granular pair propagator, we now move onto calculate the fluctuation conductivity in granular metals.

5.4.2 Fluctuation Conductivity

The diagrams we use to calculate σ_{fl} are given in fig. 5.13. Their sum can be shown to vanish when the external frequency is set to zero in the granular diffusive limit, see appendix I.6. We also note that the contributions of diagrams C and D to the DC conductivity cancel, in analogy to the cancellation of diagrams D and E in the homogeneous case, see appendix I.2. We therefore focus on the detailed calculation of the DOS (diagram A), MT (diagram B), and AL (diagram E) terms. The set up of these calculations is entirely analogous to the homogeneous case, with the added complexity of the grain labels. We deal with the grain labels in exactly the same way as for all previous granular calculations, so we shall only provide the key details where the granular calculation differs from the homogeneous calculation.

We find the following response functions for DOS and MT diagrams in lattice momen-

[15] I.e. the temperature is large enough such that virtual Cooper pairs cannot travel a length greater than the size of a grain.

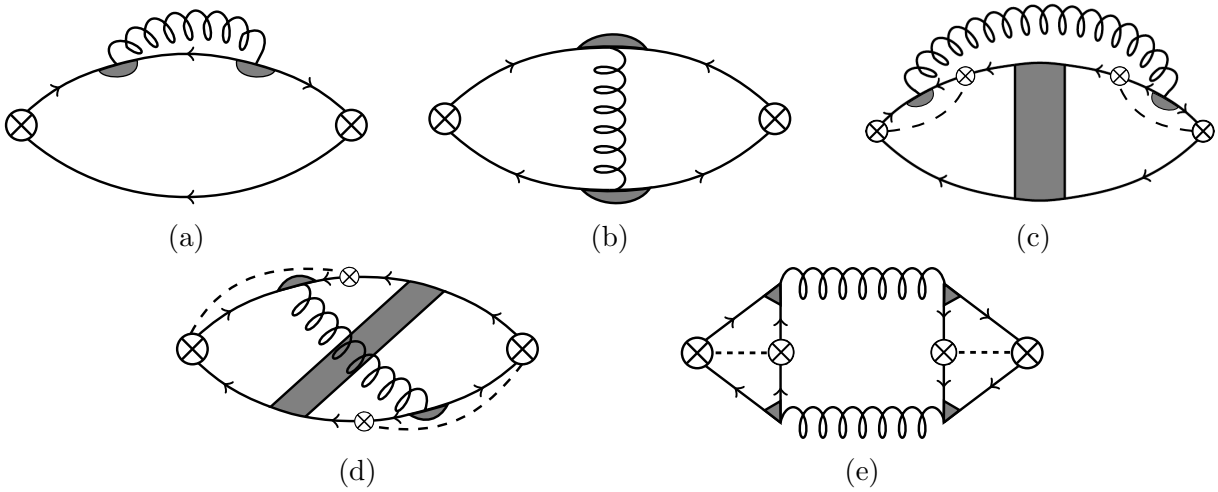

Figure 5.13: Leading order corrections to the electrical conductivity due to superconducting fluctuations.

tum space, respectively,

$$K^{(A)}_{\alpha\alpha}(i\Omega) = -\frac{8e^2a^2t^2}{\mathcal{N}a^{2d}}T^2\sum_{\varepsilon,\omega}\sum_{\mathbf{Q}}\sum_{\mathbf{k},\mathbf{p},\mathbf{q}}\Big[L(\mathbf{Q},\mathbf{q},i\omega)C(\mathbf{Q},\mathbf{q},i\varepsilon+i\Omega,i\omega-i\varepsilon-i\Omega)^2 \times G(\mathbf{k},i\varepsilon+i\Omega)^2G(\mathbf{q}-\mathbf{k},i\omega-i\varepsilon-i\Omega)G(\mathbf{p},i\varepsilon)\Big], \tag{5.126a}$$

$$K^{(B)}_{\alpha\alpha}(i\Omega) = \frac{4e^2a^2t^2}{\mathcal{N}a^{2d}}T^2\sum_{\varepsilon,\omega}\sum_{\mathbf{Q}}\sum_{\mathbf{k},\mathbf{p},\mathbf{q}}\Big[\cos(Q_\alpha a)L(\mathbf{Q},\mathbf{q},i\omega)C(\mathbf{Q},\mathbf{q},i\varepsilon,i\omega-i\varepsilon) \times C(\mathbf{Q},\mathbf{q},i\varepsilon+i\Omega,i\omega-i\varepsilon-i\Omega)G(\mathbf{k},i\varepsilon+i\Omega)^2 \times G(\mathbf{q}-\mathbf{k},i\omega-i\varepsilon-i\Omega)G(\mathbf{p},i\varepsilon)\Big], \tag{5.126b}$$

where we have accounted for the fact that the electron Green's functions are grain label independent. Note that the MT term has an extra minus sign due to the current vertices tunnelling in the same direction. Working in the granular diffusive limit, we may take $\cos(Q_\alpha a) \simeq 1$, and so $K^{(B)}_{\alpha\alpha}(i\Omega)$ now has the same form as its homogeneous analogue.

The AL diagram has the same block structure as before,

$$K^{(C)}_{\alpha\beta}(i\Omega) = -\frac{4e^2a^{2+d}t^4}{\mathcal{N}}T\sum_{\omega}\sum_{\mathbf{Q}}\sum_{\mathbf{q}}\Big[B_\alpha(\mathbf{Q},\mathbf{q},i\omega,i\Omega)B_\beta(\mathbf{Q},\mathbf{q},i\omega,i\Omega) \times L(\mathbf{Q},\mathbf{q},i\omega)L(\mathbf{Q},\mathbf{q},i\omega+i\Omega)\Big], \tag{5.127a}$$

$$B_\alpha(\mathbf{Q},\mathbf{q},i\omega,i\Omega) = \frac{2T}{a^{2d}}\sum_{\varepsilon}\sum_{\mathbf{k},\mathbf{p}}\Big[\sin(Q_\alpha a)C(\mathbf{Q},\mathbf{q},i\varepsilon+i\Omega,i\omega-i\varepsilon) \\ \times C(\mathbf{Q},\mathbf{q},i\varepsilon,i\omega-i\varepsilon)G(\mathbf{k},i\varepsilon+i\Omega)G(\mathbf{q}-\mathbf{k},i\omega-i\varepsilon) \\ \times G(\mathbf{p},i\varepsilon)G(\mathbf{q}-\mathbf{p},i\omega-i\varepsilon)\Big] \tag{5.127b}$$

In the granular diffusive limit, the $\sin(Q_\alpha a)$ appearing in the blocks can be replaced by $Q_\alpha a$, and so resembles the homogeneous AL diagram.

The sign choices we can make for the granular DOS, MT, and AL diagrams are the same as those for the homogeneous case. We may also apply the same assumptions made there: we only consider the $\omega = 0$ parts of the $K^{(A)}_{\alpha\alpha}(i\Omega)$ and $K^{(B)}_{\alpha\alpha}(i\Omega)$, we may set $\omega = \Omega = 0$ inside the block functions of the AL term, and we may neglect any $\mathbf{q}$ appearing in the electron Green's functions due to this being a small momentum compared to the other fast momenta.[16]

Once we have accounted for all non-zero sign configurations, we can perform the same analytic continuation as before for the AL term. The expressions we are left with for the DOS, MT, and AL terms can then be expanded to first order in Ω to find the fluctuation to the electrical DC conductivity, as we know that all $\mathcal{O}(\Omega^0)$ terms from all diagrams can be shown to cancel. We therefore find the following corrections to the electrical conductivity,

$$\sigma_{DOS} = \frac{N(0)\mathcal{D}_T e^2}{2\pi^2 T\mathcal{N}a^d}\sum_{\mathbf{Q}}\sum_{\mathbf{q}} L(\mathbf{Q},\mathbf{q},0)\psi''\left(\frac{1}{2}+\frac{\mathcal{D}q^2+\Gamma\lambda_{\mathbf{Q}}+\tau_\phi^{-1}}{4\pi T}\right), \tag{5.128a}$$

$$\sigma^{(1)}_{MT} = \frac{N(0)\mathcal{D}_T e^2}{\pi\mathcal{N}a^d}\sum_{\mathbf{Q}}\sum_{\mathbf{q}} \frac{L(\mathbf{Q},\mathbf{q},0)}{\mathcal{D}q^2+\Gamma\lambda_{\mathbf{Q}}+\tau_\phi^{-1}}\psi'\left(\frac{1}{2}+\frac{\mathcal{D}q^2+\Gamma\lambda_{\mathbf{Q}}+\tau_\phi^{-1}}{4\pi T}\right), \tag{5.128b}$$

$$\sigma^{(reg2)}_{MT} = \frac{N(0)\mathcal{D}_T e^2}{4\pi^2 T\mathcal{N}a^d}\sum_{\mathbf{Q}}\sum_{\mathbf{q}} L(\mathbf{Q},\mathbf{q},0)\psi''\left(\frac{1}{2}+\frac{\mathcal{D}q^2+\Gamma\lambda_{\mathbf{Q}}+\tau_\phi^{-1}}{4\pi T}\right), \tag{5.128c}$$

[16]Usually we would have to worry about whether this would lead to a vanishing contribution from a diagram, due to the current vertices carrying a factor of k_α in the homogeneous case. If this was the case, we would need to expand in powers of $\mathbf{q}$ to find the leading order contribution. We do not encounter this issue here though, as the granular current vertices have no factors related to the internal momenta. Hence, we may neglect the small momenta appearing inside the electron Green's functions without consequence.

$$\sigma_{AL} = \frac{N(0)^2\mathcal{D}_T^2 e^2}{4\pi^3 T^3 \mathcal{N} a^{d+2}} \sum_{\mathbf{Q}} \sum_{\mathbf{q}} \left[\sin^2(Q_\alpha a)\psi'\left(\frac{1}{2} + \frac{\mathcal{D}q^2 + \Gamma\lambda_{\mathbf{Q}} + \tau_\phi^{-1}}{4\pi T}\right)^2 \times \int_{-\infty}^{+\infty} dz \frac{\mathrm{Im}\left[L^R(\mathbf{Q},\mathbf{q},z)\right]^2}{\sinh^2\left(\frac{z}{2T}\right)} \right]. \tag{5.128d}$$

Comparing eq. 5.128a, eq.5.128b, eq. 5.128c, and eq. 5.128d to eq. 3.164, eq. 3.151, eq. 3.157, and eq. 3.140, respectively, we can see that they are complete analogues of their homogeneous counterparts. This becomes even more evident when we choose to work in the granular diffusive limit,

$$\sigma_{DOS} = \frac{N(0)\mathcal{D}_T e^2}{2\pi^2 T \mathcal{N} a^d} \sum_{\mathbf{Q}} \sum_{\mathbf{q}} \alpha_2(\mathbf{q},T) L(\mathbf{Q},\mathbf{q},0), \tag{5.129a}$$

$$\sigma_{MT}^{(an)} = \frac{N(0)\mathcal{D}_T e^2}{\pi \mathcal{N} a^d} \sum_{\mathbf{Q}} \sum_{\mathbf{q}} \alpha_1(\mathbf{q},T) \frac{L(\mathbf{Q},\mathbf{q},0)}{\mathcal{D}q^2 + \mathcal{D}_T Q^2 + \tau_\phi^{-1}}, \tag{5.129b}$$

$$\sigma_{MT}^{(reg1)} = \frac{N(0)\mathcal{D}_T e^2}{4\pi^2 T \mathcal{N} a^d} \sum_{\mathbf{Q}} \sum_{\mathbf{q}} \alpha_2(\mathbf{q},T) \frac{\mathcal{D}_T Q^2 L(\mathbf{Q},\mathbf{q},0)}{\mathcal{D}q^2 + \mathcal{D}_T Q^2 + \tau_\phi^{-1}}, \tag{5.129c}$$

$$\sigma_{MT}^{(reg2)} = \frac{N(0)\mathcal{D}_T e^2}{4\pi^2 T \mathcal{N} a^d} \sum_{\mathbf{Q}} \sum_{\mathbf{q}} \alpha_2(\mathbf{q},T) L(\mathbf{Q},\mathbf{q},0), \tag{5.129d}$$

$$\sigma_{AL} = \frac{N(0)^2\mathcal{D}_T^2 e^2}{4d\pi^3 T^3 \mathcal{N} a^d} \sum_{\mathbf{Q}} \sum_{\mathbf{q}} Q^2 \alpha_1(\mathbf{q},T)^2 \int_{-\infty}^{+\infty} dz \frac{\mathrm{Im}\left[L^R(\mathbf{Q},\mathbf{q},z)\right]^2}{\sinh^2\left(\frac{z}{2T}\right)}. \tag{5.129e}$$

Here we have also made use of the fact that we are working in the limit where $\Gamma \ll T_c \leq T$; the $\Gamma\lambda_{\mathbf{Q}}/(4\pi T)$ inside the digamma functions and their derivatives can be ignored in all conrtibutions, except for the $\sigma_{MT}^{(1)}$ term. For this piece we expanded the digamma function's derivative in powers of $\mathcal{D}_T Q^2$ to produce the anomalous and regular parts, $\sigma_{MT}^{(an)}$ and $\sigma_{MT}^{(reg1)}$ respectively.[17] Furthermore, in the limit $E_{Th} \ll T_c$ the expansion generating these terms can be performed in powers of $\mathcal{D}_T Q^2 + \mathcal{D}q^2$. In this case, the anomalous and

[17]We do not include τ_ϕ^{-1} in this expansion, as we will wish to consider large phase breaking rates in chapter 6 for comparison of theory to experiment.

regular parts become

$$\sigma_{MT}^{(an)} = \frac{\alpha_1(\mathbf{0},T)N(0)\mathcal{D}_T e^2}{\pi\mathcal{N}a^d}\sum_{\mathbf{Q}}\sum_{\mathbf{q}}\frac{L(\mathbf{Q},\mathbf{q},0)}{\mathcal{D}q^2+\mathcal{D}_T Q^2+\tau_\phi^{-1}}, \tag{5.130a}$$

$$\sigma_{MT}^{(reg1)} = \frac{\alpha_2(\mathbf{0},T)N(0)\mathcal{D}_T e^2}{4\pi^2 T\mathcal{N}a^d}\sum_{\mathbf{Q}}\sum_{\mathbf{q}}\frac{(\mathcal{D}_T Q^2+\mathcal{D}q^2)L(\mathbf{Q},\mathbf{q},0)}{\mathcal{D}q^2+\mathcal{D}_T Q^2+\tau_\phi^{-1}}. \tag{5.130b}$$

Let us now perform these integrals and sums for a 3D system, as this is what we will use for comparison to the experimental data of Klemencic et. al. [28] in chapter 6. We first calculate the DOS term, followed by the AL contribution, and finish with the MT correction. The η dependence for each of these terms within each region is summarised in table 5.1.

The DOS term

For all corrections we may replace the $\mathbf{Q}$ sum with an integral, and we choose to work in the granular diffusive limit. The granular momentum integral has one important difference when compared to the homogeneous momentum integral; the radial integral is no longer over the range $[0,\infty]$, but rather $[0,a^{-1}]$. Performing this integral yields,

$$\sigma_{DOS} = \frac{1}{\pi^3}\frac{e^2}{a}\sum_{\mathbf{q}}\frac{\alpha_2(\mathbf{q},T)}{\alpha_1(\mathbf{q},T)}\left[1-\sqrt{\frac{4\pi T\epsilon(\mathbf{q},T)}{\Gamma\alpha_1(\mathbf{q},T)}}\arctan\left(\sqrt{\frac{\Gamma\alpha_1(\mathbf{q},T)}{4\pi T\epsilon(\mathbf{q},T)}}\right)\right]. \tag{5.131}$$

The close-to-T_c behaviour is given by the $\mathbf{q}=\mathbf{0}$ component, as any $\mathbf{q}\neq\mathbf{0}$ contributions will be far less singular and thus less important,

$$\sigma_{DOS}^{(close)} = \frac{1}{\pi^3}\frac{e^2}{a}\frac{\bar{\alpha}_2}{\bar{\alpha}_1}\left[1-\sqrt{\frac{4\pi T\bar{\epsilon}}{\Gamma\bar{\alpha}_1}}\arctan\left(\sqrt{\frac{\Gamma\bar{\alpha}_1}{4\pi T\bar{\epsilon}}}\right)\right]. \tag{5.132}$$

The case where $\tau_\phi^{-1}=0$ yields

$$\sigma_{DOS}^{(close)} = -\frac{28\zeta(3)}{\pi^5}\frac{e^2}{a}\left[1-\sqrt{\frac{8T\eta}{\pi\Gamma}}\arctan\left(\sqrt{\frac{\pi\Gamma}{8T\eta}}\right)\right], \tag{5.133}$$

which, recalling $\eta \ll \Gamma/T_c$ deep inside the close-to-T_c region, can be approximated as,

$$\sigma_{DOS}^{(close)} = -\frac{28\zeta(3)}{\pi^5}\frac{e^2}{a}. \tag{5.134}$$

This result is the expected granular analogue of the 3D result in eq. 3.161. The slight difference between the homogeneous result and $\sigma_{DOS}^{(close)}$ is due to the upper cut-off in the momentum integral differing between the granular and homogeneous cases. This leads to an approximately constant result in granular metals, and a $T^{1/2}$ dependence in homogeneous systems. The important point here though, is that in both cases, the DOS correction has no dependence upon η, and does not diverge as $T \to T_c^+$. In fact, we can treat the homogeneous correction as approximately constant, since we may take $T \simeq T_c$ when $\eta \ll 1$.

The behaviour deep inside the intermediate region, such that $\Gamma/T_c \ll \eta \ll E_{Th}/T_c$, can be found by expanding eq. 5.132 in powers of $\sqrt{\Gamma/(T\epsilon(\mathbf{0},T))}$.[18] This is because all non-zero choices of $\mathbf{q}$ will still contribute less important terms. Performing this expansion gives[19]

$$\sigma_{DOS}^{(int)} = \frac{1}{12\pi^4}\frac{e^2}{a}\frac{\Gamma}{T}\frac{\bar{\alpha}_2}{\bar{\epsilon}}. \tag{5.135}$$

In the case of negligible phase breaking rates, this simplifies to

$$\sigma_{DOS}^{(int)} = -\frac{7\zeta(3)}{6\pi^4}\frac{e^2}{a}\frac{\Gamma}{T}\frac{1}{\eta}. \tag{5.136}$$

Finally, in the far-from-T_c region, we can begin to include non-zero values of $\mathbf{q}$ that are just as singular as the zero momentum piece. If the Thouless energy is sufficiently small that $E_{Th} \ll T_c$, we can consider large enough values of η that allow us to approximate the $\mathbf{q}$ sum as an integral. Let us consider the ideal case deep inside the far-from-T_c region, such that $E_{Th}/T_c \ll \eta \ll 1$.

[18] Since $\eta \gg \Gamma/T_c$, we can also take $\epsilon(\mathbf{q},T) \gg \Gamma/T_c$.

[19] We will have to expand the arctan to third order, as the first order term cancels with the 1 inside the brackets.

To find the behaviour here, we take eq. 5.135 and re-include the $\mathbf{q} \neq \mathbf{0}$ terms by letting $\bar{\alpha}_n \to \alpha_n(\mathbf{q}, T)$ and $\bar{\epsilon} \to \epsilon(\mathbf{q}, T)$, and sum this expression over all $\mathbf{q}$,

$$\sigma_{DOS}^{(far)} = \frac{1}{12\pi^4} \frac{e^2}{a} \frac{\Gamma}{T} \sum_{\mathbf{q}} \frac{\alpha_2(\mathbf{q}, T)}{\epsilon(\mathbf{q}, T)}. \tag{5.137}$$

Given we are considering $E_{Th}/T_c \ll \eta \ll 1$, we may neglect the $\mathbf{q}$ dependence inside all $\alpha_n(\mathbf{q}, T)$ appearing outside of $\epsilon(\mathbf{q}, T)$, as the digamma functions decay quickly for large arguments and the most singular behaviour comes from small momenta. Furthermore, this limit allows us to write

$$\epsilon(\mathbf{q}, T) \simeq \bar{\epsilon} + \frac{\bar{\alpha}_1}{4\pi T} \mathcal{D} q^2. \tag{5.138}$$

With these ideas in mind, eq. 5.137 becomes,

$$\sigma_{DOS}^{(far)} = \frac{\bar{\alpha}_2 e^2}{24\pi^6} \frac{\Gamma a^2}{T} \int_0^{q_c} dq \frac{q^2}{\bar{\epsilon} + \frac{\bar{\alpha}_1}{4\pi T} \mathcal{D} q^2}, \tag{5.139}$$

where we have replaced the sum by an integral. The upper cut-off is necessary to avoid a diverging result, and is defined by $\mathcal{D} q_c^2 = 4\pi T$. Performing the integral produces

$$\sigma_{DOS}^{(far)} = \frac{1}{3\pi^4} \frac{\bar{\alpha}_2}{\bar{\alpha}_1} \frac{e^2}{a} \sqrt{\frac{\Gamma^2 T}{\pi E_{Th}^3}} \left[1 - \sqrt{\frac{\bar{\epsilon}}{\bar{\alpha}_1}} \arctan\left(\sqrt{\frac{\bar{\alpha}_1}{\bar{\epsilon}}} \right) \right], \tag{5.140}$$

which clearly has the same form as the close-to-T_c behaviour in eq. 5.132. Considering $\tau_\phi^{-1} = 0$ and $\eta \ll 1$, eq. 5.140 can be approximated as

$$\sigma_{DOS}^{(far)} = -\frac{28\zeta(3)}{3\pi^6} \frac{e^2}{a} \sqrt{\frac{\Gamma^2 T}{\pi E_{Th}^3}}. \tag{5.141}$$

Thus we find that the far-from-T_c DOS correction is also independent of η, and can be treated as approximately constant.

Given our ability to analyse the the DOS correction deep within each region, we may summarise its behaviour for all $\eta \ll 1$. The most insightful summary we can provide is for a negligible phase breaking rate, otherwise we would not observe simple power laws

in terms of η. We therefore summarise the behaviour of the DOS correction deep within each region, in the absence of phase breaking, as

$$\sigma_{DOS} \sim -\frac{e^2}{a} \times \begin{cases} \text{const.}, & \eta \ll \dfrac{\Gamma}{T_c} \\ \dfrac{\Gamma}{T_c}\eta^{-1}, & \dfrac{\Gamma}{T_c} \ll \eta \ll \dfrac{E_{Th}}{T_c} \\ \text{const.} \times \sqrt{\dfrac{\Gamma^2 T_c}{E_{Th}^3}}, & \dfrac{E_{Th}}{T_c} \ll \eta \ll 1. \end{cases} \tag{5.142}$$

The AL term

We begin by performing the frequency integral in eq. 5.129e, which is dealt with in exactly the same manner as in the homogeneous case, so we shall not repeat those details here. We then replace the $\mathbf{Q}$ sum by an integral and let $x = Qa$,

$$\sigma_{AL} = \frac{\Gamma^2}{48\pi^5 T^2}\frac{e^2}{a}\sum_{\mathbf{q}} \alpha_1(\mathbf{q},T)^3 \int_0^1 dx \frac{x^4}{\left[\epsilon(\mathbf{q},T) + \frac{\alpha_1(\mathbf{q},T)\Gamma}{4\pi T}x^2\right]^3}. \tag{5.143}$$

Computing the x integral yields

$$\begin{aligned}\sigma_{AL} = \frac{T}{6\pi^2\Gamma}\frac{e^2}{a}\sum_{\mathbf{q}} \Bigg[& 3\sqrt{\frac{\Gamma\alpha_1(\mathbf{q},T)}{4\pi T\epsilon(\mathbf{q},T)}}\arctan\left(\sqrt{\frac{\Gamma\alpha_1(\mathbf{q},T)}{4\pi T\epsilon(\mathbf{q},T)}}\right) \\ & - \alpha_1(\mathbf{q},T)\Gamma\,\frac{5\alpha_1(\mathbf{q},T)\Gamma + 12\pi T\epsilon(\mathbf{q},T)}{[\alpha_1(\mathbf{q},T)\Gamma + 4\pi T\epsilon(\mathbf{q},T)]^2}\Bigg].\end{aligned} \tag{5.144}$$

From eq. 5.144, we see that the close-to-T_c AL behaviour is

$$\sigma_{AL}^{(close)} = \frac{T}{6\pi^2\Gamma}\frac{e^2}{a}\left[3\sqrt{\frac{\Gamma\bar{\alpha}_1}{4\pi T\bar{\epsilon}}}\arctan\left(\sqrt{\frac{\Gamma\bar{\alpha}_1}{4\pi T\bar{\epsilon}}}\right) - \bar{\alpha}_1\Gamma\,\frac{5\bar{\alpha}_1\Gamma + 12\pi T\bar{\epsilon}}{[\bar{\alpha}_1\Gamma + 4\pi T\bar{\epsilon}]^2}\right]. \tag{5.145}$$

When phase breaking rates are negligible, this becomes

$$\sigma_{AL}^{(close)} = \frac{1}{6\pi^2}\frac{T}{\Gamma}\frac{e^2}{a}\left[3\sqrt{\frac{\pi\Gamma}{8T\eta}}\arctan\left(\sqrt{\frac{\Gamma\pi}{8T\eta}}\right) - \pi\Gamma\,\frac{5\pi\Gamma + 24T\eta}{(\pi\Gamma + 8T\eta)^2}\right], \tag{5.146}$$

which can be approximated as

$$\sigma_{AL}^{(close)} = \frac{1}{8}\sqrt{\frac{T}{2\pi\Gamma}}\frac{e^2}{a}\frac{1}{\eta^{1/2}}, \tag{5.147}$$

when $\eta \ll \Gamma/T_c$. This is the same as the three-dimensional homogeneous result in eq. 3.148 with $\mathcal{D} \to \mathcal{D}_T$.

The behaviour in the intermediate region is found by expanding eq. 5.145 in powers of $\sqrt{\Gamma/(T_c\bar{\epsilon})}$, so to leading order

$$\sigma_{AL}^{(int)} = \frac{\bar{\alpha}_1^3}{240\pi^5}\frac{\Gamma^2}{T^2}\frac{e^2}{a}\frac{1}{\bar{\epsilon}^3}. \tag{5.148}$$

For $\tau_\phi^{-1} = 0$, this simplifies to

$$\sigma_{AL}^{(int)} = \frac{\pi}{1920}\frac{\Gamma^2}{T^2}\frac{e^2}{a}\frac{1}{\eta^3}. \tag{5.149}$$

Here we see that the AL contribution leads to a much more singular correction than in homogeneous systems, when deep inside the intermediate region.

The far-from-T_c behaviour can be found by re-including the $\mathbf{q}$ dependence into eq. 5.148, and summing over the internal momentum, as was done for the granular DOS correction. Applying the same expansions in terms of $\mathbf{q}$, we are left to evaluate

$$\sigma_{AL}^{(far)} = \frac{\bar{\alpha}_1^3}{240\pi^5}\frac{\Gamma^2}{T^2}\frac{e^2}{a}\sum_{\mathbf{q}}\frac{1}{\left[\bar{\epsilon} + \frac{\bar{\alpha}_1}{4\pi T}\mathcal{D}q^2\right]^3}. \tag{5.150}$$

We again replace the momentum sum by an integral, whose radial component is cut-off according to $\mathcal{D}q_c^2 = 4\pi T$,

$$\sigma_{AL}^{(far)} = \frac{\bar{\alpha}_1^3 e^2 a^2}{480\pi^7}\frac{\Gamma^2}{T^2}\int_0^{q_c} dq \frac{q^2}{\left[\epsilon(\mathbf{0},T) + \frac{\bar{\alpha}_1}{4\pi T}\mathcal{D}q^2\right]^3}. \tag{5.151}$$

In evaluating this integral we replace the upper limit by infinity without issue,[20] which

[20]Consider making the substitution $x = aq$, then the upper limit would become $x_c = \sqrt{4\pi T/E_{Th}}$,

yields

$$\sigma_{AL}^{(far)} = \frac{1}{1920}\sqrt{\frac{\Gamma^4}{2\pi E_{Th}^3 T}}\frac{1}{\bar{\epsilon}^{3/2}}. \tag{5.152}$$

When phase breaking mechanisms are negligible, eq. 5.152 becomes

$$\sigma_{AL}^{(far)} = \frac{1}{1920}\sqrt{\frac{\Gamma^4}{2\pi E_{Th}^3 T}}\frac{1}{\eta^{3/2}}. \tag{5.153}$$

We therefore summarise AL contribution to the granular fluctuation conductivity as,

$$\sigma_{AL} \sim \frac{e^2}{a} \times \begin{cases} \sqrt{\dfrac{T_c}{\Gamma}}\eta^{-1/2}, & \eta \ll \dfrac{\Gamma}{T_c} \\ \dfrac{\Gamma^2}{T_c^2}\eta^{-3}, & \dfrac{\Gamma}{T_c} \ll \eta \ll \dfrac{E_{Th}}{T_c} \\ \sqrt{\dfrac{\Gamma^4}{E_{Th}^3 T_c}}\eta^{-3/2}, & \dfrac{E_{Th}}{T_c} \ll \eta \ll 1. \end{cases} \tag{5.154}$$

The MT term

The contribution of $\sigma_{MT}^{(reg2)}$ is exactly half that of σ_{DOS}, so we shall not go through its calculation here. Let us first turn our attention to $\sigma_{MT}^{(reg1)}$ in eq. 5.129c, which can be written as

$$\sigma_{MT}^{(reg1)} = \frac{1}{2\pi^3}\frac{e^2}{a}\sum_{\mathbf{q}}\frac{\alpha_2(\mathbf{q},T)}{\alpha_1(\mathbf{q},T)}\Bigg[1 - \frac{\alpha_1(\mathbf{q},T)\Gamma\tau_\phi}{4\pi T\tau_\phi\epsilon(\mathbf{q},T) - \alpha_1(\mathbf{q},T)(1+\mathcal{D}q^2\tau_\phi)} \times \left(\frac{4\pi T\epsilon(\mathbf{q},T)}{\alpha_1(\mathbf{q},T)\Gamma}\right)^{3/2} \arctan\left(\sqrt{\frac{\alpha_1(\mathbf{q},T)\Gamma}{4\pi T\epsilon(\mathbf{q},T)}}\right)\Bigg] + S_\phi^{(reg)}, \tag{5.155a}$$

$$S_\phi^{(reg)} = \frac{1}{2\pi^3}\frac{e^2}{a}\sum_{\mathbf{q}}\Bigg[\frac{\alpha_2(\mathbf{q},T)\Gamma\tau_\phi}{4\pi T\tau_\phi\epsilon(\mathbf{q},T) - \alpha_1(\mathbf{q},T)(1+\mathcal{D}q^2\tau_\phi)} \times \left(\frac{1+\mathcal{D}q^2\tau_\phi}{\Gamma\tau_\phi}\right)^{3/2} \arctan\left(\sqrt{\frac{\Gamma\tau_\phi}{1+\mathcal{D}q^2\tau_\phi}}\right)\Bigg], \tag{5.155b}$$

where we note that $S_\phi^{(reg)} = 0$ when $\tau_\phi^{-1} = 0$.

which we take to be large in the case where $E_{Th} \ll T_c$.

In the close-to-T_c region,

$$\sigma_{MT}^{(reg1,close)} = \frac{1}{2\pi^3}\frac{e^2}{a}\frac{\bar{\alpha}_2}{\bar{\alpha}_1}\Bigg[1 - \frac{\bar{\alpha}_1\Gamma\tau_\phi}{4\pi T\tau_\phi\bar{\epsilon} - \bar{\alpha}_1} \times \left\{\left(\frac{4\pi T\bar{\epsilon}}{\bar{\alpha}_1\Gamma}\right)^{3/2}\arctan\left(\sqrt{\frac{\bar{\alpha}_1\Gamma}{4\pi T\bar{\epsilon}}}\right) - \frac{\arctan(\sqrt{\Gamma\tau_\phi})}{(\Gamma\tau_\phi)^{3/2}}\right\}\Bigg]. \tag{5.156}$$

When $\tau_\phi^{-1} = 0$, eq. 5.156 gives half of the DOS correction in the close region, see eq. 5.133, as expected.

Moving deep into the intermediate region,

$$\sigma_{MT}^{(reg1,int)} = \frac{1}{2\pi^3}\frac{e^2}{a}\frac{\bar{\alpha}_2}{\bar{\alpha}_1}\left[1 + \frac{\bar{\alpha}_1\Gamma\tau_\phi}{4\pi T\tau_\phi\bar{\epsilon} - \bar{\alpha}_1}\left(\frac{\arctan(\sqrt{\Gamma\tau_\phi})}{(\Gamma\tau_\phi)^{3/2}} - \frac{4\pi T\bar{\epsilon}}{\bar{\alpha}_1\Gamma} + \frac{1}{3}\right)\right]. \tag{5.157}$$

Eq. 5.157 becomes equal to half of the DOS correction when $\tau_\phi^{-1} = 0$, see eq. 5.136.

Finally, in the far-from-T_c region, re-including the non-zero $\mathbf{q}$ contributions leads to

$$\sigma_{MT}^{(reg1,far)} = S_\phi^{(reg)} + \frac{1}{2\pi^3}\frac{e^2}{a} \times \sum_{\mathbf{q}}\frac{\alpha_2(\mathbf{q},T)}{\alpha_1(\mathbf{q},T)}\left[1 + \frac{\alpha_1(\mathbf{q},T)\Gamma\tau_\phi}{4\pi T\tau_\phi\epsilon(\mathbf{q},T) - \alpha_1(\mathbf{q},T)(1+\mathcal{D}q^2\tau_\phi)}\left(\frac{1}{3} - \frac{4\pi T\epsilon(\mathbf{q},T)}{\alpha_1(\mathbf{q},T)\Gamma}\right)\right]. \tag{5.158}$$

Eq. 5.158 is only of use when E_{Th} is not significantly smaller than T_c. For the case where $E_{Th} \ll T_c$ we will instead need to use eq. 5.130b, whose $\mathbf{Q}$ sum can be evaluated to yield

$$\sigma_{MT}^{(reg1)} = \widetilde{S}_\phi^{(reg)} + \frac{\bar{\alpha}_2}{2\pi^3\bar{\alpha}_1}\frac{e^2}{a} \times \sum_{\mathbf{q}}\left[1 - \frac{4\pi\Gamma T\tau_\phi\bar{\alpha}_1\bar{\epsilon}}{4\pi T\tau_\phi\bar{\epsilon} - \bar{\alpha}_1}\sqrt{\frac{4\pi T\bar{\epsilon} + \bar{\alpha}_1\mathcal{D}q^2}{(\bar{\alpha}_1\Gamma)^3}}\arctan\left(\sqrt{\frac{\bar{\alpha}_1\Gamma}{4\pi T\bar{\epsilon} + \bar{\alpha}_1\mathcal{D}q^2}}\right)\right], \tag{5.159a}$$

$$\widetilde{S}_\phi^{(reg)} = \frac{1}{2\pi^3}\frac{e^2}{a}\sum_{\mathbf{q}}\frac{\bar{\alpha}_2\Gamma\tau_\phi}{4\pi T\tau_\phi\bar{\epsilon} - \bar{\alpha}_1}\sqrt{\frac{1+\mathcal{D}q^2\tau_\phi}{(\Gamma\tau_\phi)^3}}\arctan\left(\sqrt{\frac{\Gamma\tau_\phi}{1+\mathcal{D}q^2\tau_\phi}}\right). \tag{5.159b}$$

Clearly, eq. 5.159a collapses to half of the DOS contribution in eq. 5.141 when phase breaking rates are negligible.

In the far-from-T_c region, we may approximate $\widetilde{S}_\phi^{(reg)}$ by noting that $\mathcal{D}q^2\tau_\phi \gg \Gamma\tau_\phi$, and so we may expand the arctan appearing in $\widetilde{S}_\phi^{(reg1)}$ to first order in its argument to obtain the leading order behaviour. Consequently, eq. 5.159a becomes,

$$\sigma_{MT}^{(reg1,far)} = \frac{2}{3\pi^2}\frac{\bar{\alpha}_2 T\tau_\phi\Gamma\bar{\epsilon}}{4\pi T\tau_\phi\bar{\epsilon}-\bar{\alpha}_1}\frac{e^2}{a}\sum_{\mathbf{q}}\frac{1}{4\pi T\bar{\epsilon}+\bar{\alpha}_1\mathcal{D}q^2}. \tag{5.160}$$

We now replace the momentum sum by an integral, which can be evaluated to give

$$\sigma_{MT}^{(reg1,far)} = \frac{\bar{\alpha}_2}{12\pi^5\bar{\alpha}_1}\frac{e^2}{a}\left(\frac{4\pi T}{E_{Th}}\right)^{3/2}\frac{\Gamma\tau_\phi\bar{\epsilon}}{4\pi T\tau_\phi\bar{\epsilon}-\bar{\alpha}_1}\left[1-\sqrt{\frac{\bar{\epsilon}}{\bar{\alpha}_1}}\arctan\left(\sqrt{\frac{\bar{\alpha}_1}{\bar{\epsilon}}}\right)\right]. \tag{5.161}$$

If the phase breaking rate is negligible, eq. 5.161 becomes identical to half of the DOS contribution in eq. 5.141. Otherwise, we will have to compute the $\widetilde{S}_\phi^{(reg)}$ piece of $\sigma_{MT}^{(reg1,far)}$ numerically. From the above considerations we can see that $\sigma_{MT}^{(reg1)}$ will not lead to a singular contribution, and will behave in a similar manner to the DOS term.

Let us now consider the anomalous MT term given in eq. 5.129b,[21]

$$\begin{aligned}\sigma_{MT}^{(an)} = S_\phi^{(an)} - \frac{2T\tau_\phi}{\pi^2}\frac{e^2}{a}\sum_{\mathbf{q}}\Bigg[&\sqrt{\frac{4\pi T\epsilon(\mathbf{q},T)}{\Gamma\alpha_1(\mathbf{q},T)}}\arctan\left(\sqrt{\frac{\Gamma\alpha_1(\mathbf{q},T)}{4\pi T\epsilon(\mathbf{q},T)}}\right)\\ &\times\frac{\alpha_1(\mathbf{q},T)}{\alpha_1(\mathbf{q},T)(1+\mathcal{D}q^2\tau_\phi)-4\pi T\tau_\phi\epsilon(\mathbf{q},T)}\Bigg],\end{aligned} \tag{5.162a}$$

$$\begin{aligned}S_\phi^{(an)} = \frac{2T\tau_\phi}{\pi^2}\frac{e^2}{a}\sum_{\mathbf{q}}\Bigg[&\sqrt{\frac{1+\mathcal{D}q^2\tau_\phi}{\Gamma\tau_\phi}}\arctan\left(\sqrt{\frac{\Gamma\tau_\phi}{1+\mathcal{D}q^2\tau_\phi}}\right)\\ &\times\frac{\alpha_1(\mathbf{q},T)}{\alpha_1(\mathbf{q},T)(1+\mathcal{D}q^2\tau_\phi)-4\pi T\tau_\phi\epsilon(\mathbf{q},T)}\Bigg].\end{aligned} \tag{5.162b}$$

From eq. 5.162, we see that the close-to-T_c behaviour is given by

$$\sigma_{MT}^{(an,close)} = \frac{2T\tau_\phi}{\pi^2}\frac{e^2}{a}\frac{\bar{\alpha}_1}{\bar{\alpha}_1-4\pi T\tau_\phi\bar{\epsilon}}\left[\frac{\arctan(\sqrt{\Gamma\tau_\phi})}{\sqrt{\Gamma\tau_\phi}}-\sqrt{\frac{4\pi T\bar{\epsilon}}{\Gamma\bar{\alpha}_1}}\arctan\left(\sqrt{\frac{\Gamma\bar{\alpha}_1}{4\pi T\bar{\epsilon}}}\right)\right]. \tag{5.163}$$

[21] We do not need to consider the case where $E_{Th} \ll T_c$ separately to when $E_{Th} \ll T_c$ is not true, as the expansion used to generate the anomalous and regular pieces from $\sigma_{MT}^{(1)}$ only produces complications for the regular part.

Table 5.1: Summary of the regional behaviours of the DOS, anomalous MT, and AL contributions to the fluctuation conductivity of a granular metal in terms of the reduced temperature, η. The results here are given in units of e^2/a, and are taken in the limit of negligible phase breaking, $\tau_\phi^{-1} = 0$.

	Region		
	$\eta \ll \frac{\Gamma}{T_c}$	$\frac{\Gamma}{T_c} \ll \eta \ll \frac{E_{Th}}{T_c}$	$\frac{E_{Th}}{T_c} \ll \eta \ll 1$
σ_{DOS}	$-$const.	$-\frac{\Gamma}{T_c}\,\eta^{-1}$	$-\sqrt{\frac{\Gamma^2 T_c}{E_{Th}^3}} \times$ const.
$\sigma_{MT}^{(an)}$	$\sqrt{\frac{T_c}{\Gamma}}\,\eta^{-1/2}$	η^{-1}	$\sqrt{\frac{\Gamma^2 T_c}{E_{Th}^3}}\,\eta^{-1/2}$
σ_{AL}	$\sqrt{\frac{T_c}{\Gamma}}\,\eta^{-1/2}$	$\frac{\Gamma^2}{T_c^2}\,\eta^{-3}$	$\sqrt{\frac{\Gamma^4}{E_{Th}^3 T_c}}\,\eta^{-3/2}$

Deep inside the close-to-T_c region, when phase breaking rates are negligible, this expression simplifies to

$$\sigma_{MT}^{(an,close)} = \sqrt{\frac{T}{8\pi\Gamma}}\frac{e^2}{a}\frac{1}{\eta^{1/2}}, \tag{5.164}$$

which matches the homogeneous result for three dimensions, see eq. 3.155, with $\mathcal{D} \to \mathcal{D}_T$.

In the intermediate region we find,

$$\sigma_{MT}^{(an,int)} = \frac{2}{\pi^2}\frac{e^2}{a}\frac{\bar{\alpha}_1 T\tau_\phi}{\bar{\alpha}_1 - 4\pi T\tau_\phi\bar{\epsilon}}\left[\frac{\arctan(\sqrt{\Gamma\tau_\phi})}{\sqrt{\Gamma\tau_\phi}} - 1\right], \tag{5.165}$$

which simplifies to,

$$\sigma_{MT}^{(an,int)} = \frac{\bar{\alpha}_1}{2\pi^3}\frac{e^2}{a}\frac{1}{\eta}, \tag{5.166}$$

in the absence of phase breaking. Finally, in the far-from-T_c region, we approach $S_\phi^{(an)}$ with the same approximations we used for $\widetilde{S}_\phi^{(reg)}$. We are therefore left to evaluate

$$\sigma_{MT}^{(an,far)} = \frac{2\bar{\alpha}_1}{3\pi^2}T\Gamma\tau_\phi\frac{e^2}{a}\sum_{\mathbf{q}}\frac{1}{(1+\mathcal{D}q^2\tau_\phi)(4\pi T\bar{\epsilon} + \bar{\alpha}_1\mathcal{D}q^2)}. \tag{5.167}$$

Performing the momentum integral yields,

$$\sigma_{MT}^{(an,far)} = \frac{1}{6\pi^3}\frac{T}{E_{Th}}\frac{e^2}{a}\frac{\bar{\alpha}_1\Gamma\tau_\phi}{4\pi T\tau_\phi\bar{\epsilon}-\bar{\alpha}_1}\left[\sqrt{\frac{4\pi T\bar{\epsilon}}{\bar{\alpha}_1 E_{Th}}}-\frac{1}{\sqrt{E_{Th}\tau_\phi}}\right]. \tag{5.168}$$

When $\tau_\phi^{-1}=0$, eq. 5.168 becomes

$$\sigma_{MT}^{(an,far)} = \frac{1}{6}\frac{\Gamma}{E_{Th}}\sqrt{\frac{T}{8\pi^9 E_{Th}}}\frac{1}{\eta^{1/2}}. \tag{5.169}$$

The behaviour of the anomalous MT term within each region is thus,

$$\sigma_{MT}^{(an)} \sim \frac{e^2}{a}\times\begin{cases}\sqrt{\frac{T_c}{\Gamma}}\eta^{-1/2}, & \eta \ll \frac{\Gamma}{T_c}\\ \eta^{-1}, & \frac{\Gamma}{T_c}\ll\eta\ll\frac{E_{Th}}{T_c}\\ \sqrt{\frac{\Gamma^2 T_c}{E_{Th}^3}}\eta^{-1/2}, & \frac{E_{Th}}{T_c}\ll\eta\ll 1.\end{cases} \tag{5.170}$$

For ease of reference, we summarise the results for the reduced temperature dependence of the DOS, anomalous MT, and AL terms in table 5.1. These are true in the ideal case, $\Gamma \ll E_{Th} \ll T_c$, in the absence of phase breaking.

5.4.3 Discussion

From table 5.1, we can see that the η behaviour of the DOS and anomalous MT terms in the close-to-T_c and far-from-T_c regions is the same, unlike the AL term, whose power laws differ in the close and far regions. This is a consequence of the DOS and MT terms being $\mathcal{O}(t^2)$, whilst the AL term is $\mathcal{O}(t^4)$. In the granular diffusive limit, the terms at $\mathcal{O}(t^2)$ do not generate any extra factors of internal or external momenta when moving lattice position space to lattice momentum space. Hence, the Q and q integrals have the same form in the close-to-T_c and far-from-T_c regions, and thus give rise to the same power laws. In contrast, the AL term picks up additional factors of $\sin(Q_\alpha a)\simeq Q_\alpha a$ inside each block, due to being $\mathcal{O}(t^4)$. Clearly, the form of the Q and q integrals will now differ in

the close-to-T_c and far-from-T_c regions, with simple power counting informing us that the Q integral will generate an additional factor of η compared to the q integral.

Analysing the relative sizes of these terms, we see that the AL and MT terms are comparable and dominate in the close-to-T_c region, $\sigma_{AL} \sim \sigma_{MT}^{(an)}$. In the intermediate region, despite the AL correction being the most singular with an η^{-3} power law, we note that its prefactor makes it subdominant to the MT term in the absence of phase breaking. Comparing the intermediate forms for σ_{AL} and $\sigma_{MT}^{(an)}$ in this regime, we see that the AL term will dominate over the MT term only when $\eta < \Gamma/T_c$, which is clearly not in the region where we expect to see these power laws. Hence, the anomalous MT term dominates in this region. Comparing the AL and DOS terms, we see that the AL term will be dominant only when $\eta < \sqrt{\Gamma/T_c}$. Hence, the AL term will dominate over the DOS contribution in part of the intermediate region, if not the entire region. The range of this dominance will depend upon the size of $\sqrt{\Gamma/T_c}$ compared to E_{Th}/T_c.

In the far-from-T_c region, we again see that the MT term dominates of the AL piece, despite the more singular relation of AL. The AL term could only dominate over the anomalous MT contribution if $\eta < \Gamma/T_c$, which is not within this region. Comparing the AL and DOS terms, we see that the AL term can dominate when $\eta < (\Gamma/T_c)^{2/3}$, which may not lie within the far-from-T_c region. The range of AL dominance over the DOS term depends upon the size of E_{Th}/T_c compared to $(\Gamma/T_c)^{2/3}$.

Given these comparisons, we expect that the anomalous MT term will dominate in the intermediate and far-from-T_c region, whilst being comparable in size to the AL term in the close-to-T_c region. This leads us to expect the following observable fluctuation conductivity in experiments where the phase breaking rate is negligible,

$$\sigma_{fl} \sim \frac{e^2}{a} \times \begin{cases} \sqrt{\dfrac{T_c}{\Gamma}}\eta^{-1/2}, & \eta \ll \dfrac{\Gamma}{T_c} \\ \eta^{-1}, & \dfrac{\Gamma}{T_c} \ll \eta \ll \dfrac{E_{Th}}{T_c} \\ \sqrt{\dfrac{\Gamma^2 T_c}{E_{Th}^3}}\eta^{-1/2}, & \dfrac{E_{Th}}{T_c} \ll \eta \ll 1. \end{cases} \tag{5.171}$$

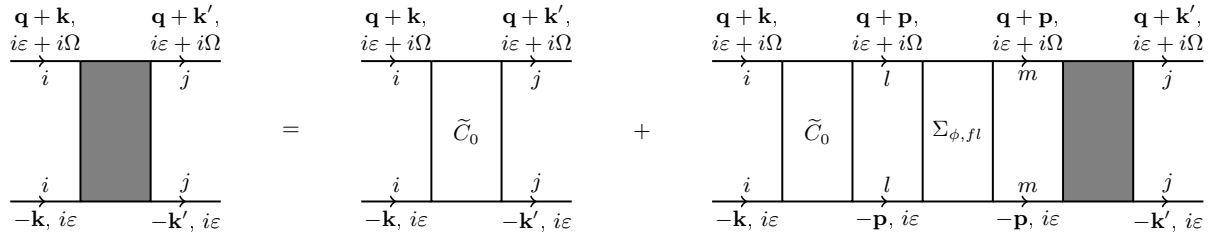

Figure 5.14: Diagrammatic series with the explicit inclusion of Σ_ϕ which accounts for the physical mechanisms generating a phase breaking rate in granular metals.

If we cannot neglect τ_ϕ^{-1}, the anomalous MT contribution will be suppressed, and the η^{-3} behaviour of the AL term may become observable in the intermediate region. This may occur for large enough phase breaking rates, such that the MT and DOS terms cancel almost exactly in the intermediate region; the MT and DOS terms have identical power laws in the intermediate region, and are opposite in sign. Another possibility is the modification of the anomalous MT term's power law due to a significant τ_ϕ^{-1}. To see whether the presence of phase breaking changes the power law of the MT term in any of the regions, we will need to perform the granular calculations analogous to those in section 3.6 to determine the temperature dependence of τ_ϕ^{-1} in granular superconductors.

5.5 Phase Coherence Lifetime

As in homogeneous systems, we found that phase breaking mechanisms were vital in order to prevent divergences occurring the in the both 1D and 2D granular WL corrections. The same is also true for 1D and 2D superconducting fluctuations. In the previous section, we included a phase breaking rate despite working in 3D, as we do not know with certainty whether phase breaking rates in granular systems are more prevalent than they are in homogeneous systems. When comparing the theory of granular superconducting fluctuations to experiment in chapter 6, we find that phase breaking may play an important role. We therefore need to understand its temperature dependence.

As in homogeneous systems, the phase breaking rate can be included into the cooperon diagrammatically via the object Σ_ϕ shown in fig. 5.14, where $\widetilde{C}_0$ is the granular cooperon

in the absence of phase breaking. We must now appreciate that Σ_ϕ allows an electron to travel from grain l to grain m, and so the Dyson equation associated to fig. 5.14 may be written as

$$\widetilde{C}_{ji}(\mathbf{q}, i\Omega) = \widetilde{C}_{0,ji}(\mathbf{q}, i\Omega) + \sum_{l,m} \widetilde{C}_{li}(\mathbf{q}, i\Omega)\Sigma_{\phi,ml}(\mathbf{q}, i\Omega)\widetilde{C}_{jm}(\mathbf{q}, i\Omega). \tag{5.172}$$

Moving to lattice momentum space, eq. 5.172 yields

$$\widetilde{C}(\mathbf{Q}, \mathbf{q}, i\Omega) = \frac{1}{\widetilde{C}_0(\mathbf{Q}, \mathbf{q}, i\Omega)^{-1} - \Sigma_\phi(\mathbf{Q}, \mathbf{q}, i\Omega)}. \tag{5.173}$$

To find τ_ϕ^{-1} we shall only consider the $(\mathbf{Q}, \mathbf{q}) = (\mathbf{0}, \mathbf{0})$ piece of $\Sigma_\phi(\mathbf{Q}, \mathbf{q}, i\Omega)$. This is in analogy to the homogeneous calculation in section 3.6, where we are only interested in the constant leading order behaviour of τ_ϕ^{-1}.[22] Hence, the phase breaking rate is given by

$$\frac{1}{\tau_\phi} = -\frac{\Sigma_\phi}{2\pi N(0)\tau_0^2}. \tag{5.174}$$

Let us now move on to consider the contributions of EEIs and superconducting fluctuations to the phase breaking rate.

5.5.1 Coulomb Phase Breaking Mechanism

The diagrams describing the phase breaking rate due to Coulomb interactions between electrons are given in fig. 5.15. Diagrams A-D look identical to those we considered in the homogeneous case, except that the cooperons and diffusons appearing here are now the granular diffusive propagators given in section 5.2.1. We also gain the additional diagrams E and F which are the tunnelling analogues of diagrams B and C. The calculation of these terms follows an identical procedure to that of the homogeneous case, so we skip all unnecessary details here.

[22] We do not set $\Omega = 0$ here, as the analytic structure of the frequency sums inside of Σ_ϕ is sensitive to the value of Ω before we analytically continue from Matsubara frequencies to continuous real frequencies.

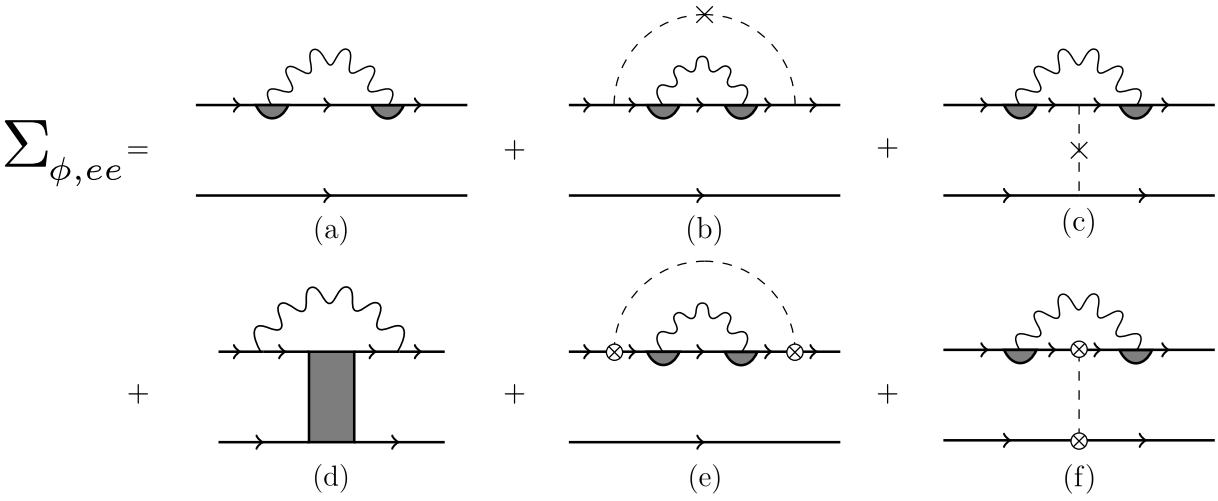

Figure 5.15: Diagrams describing the phase coherence corrections to the cooperon in granular systems due to Coulomb interactions.

Diagrams A, B, and C have the following expressions, respectively,

$$\Sigma^{(A)}_{\phi,ee,ii} = -\frac{T}{a^{2d}} \sum_{\omega} \sum_{l,m} \sum_{\mathbf{k}} \Big[G_i(\mathbf{k}, i\varepsilon + i\Omega)^2 G_i(\mathbf{k}, i\varepsilon + i\Omega + i\omega) G_i(\mathbf{k}, i\varepsilon) V_{ml}(i\omega) \times D_{mi}(i\varepsilon + i\Omega + i\omega, i\varepsilon + i\Omega) D_{li}(i\varepsilon + i\Omega + i\omega, i\varepsilon + i\Omega) \Big], \tag{5.175a}$$

$$\Sigma^{(B)}_{\phi,ee,ii} = -\frac{T}{2\pi N(0)\tau_0 a^{3d}} \sum_{\omega} \sum_{l,m} \sum_{\mathbf{k},\mathbf{k}'} \Big[G_i(\mathbf{k}, i\varepsilon + i\Omega)^2 G_i(\mathbf{k}, i\varepsilon) G_i(\mathbf{k}', i\varepsilon + i\Omega)^2 \times G_i(\mathbf{k}', i\varepsilon + i\Omega + i\omega) V_{ml}(i\omega) D_{mi}(i\varepsilon + i\Omega + i\omega, i\varepsilon + i\Omega) \times D_{li}(i\varepsilon + i\Omega + i\omega, i\varepsilon + i\Omega) \Big], \tag{5.175b}$$

$$\Sigma^{(C)}_{\phi,ee,ii} = -\frac{T}{2\pi N(0)\tau_0 a^{3d}} \times \sum_{\omega} \sum_{l,m} \Bigg[V_{ml}(i\omega) D_{mi}(i\varepsilon + i\Omega + i\omega, i\varepsilon + i\Omega) D_{li}(i\varepsilon + i\Omega + i\omega, i\varepsilon + i\Omega) \times \Bigg(\sum_{\mathbf{k}} G_i(\mathbf{k}, i\varepsilon + i\Omega) G_i(\mathbf{k}, i\varepsilon + i\Omega + i\omega) G_i(\mathbf{k}, i\varepsilon) \Bigg) \Bigg], \tag{5.175c}$$

where Ω is the external bosonic Matsubara frequency carried by the cooperon. These terms do not carry a small internal momentum associated to the Coulomb interaction, and hence we need only expand these terms to first order in ω as in the homogeneous case. Performing the fast momentum sums and moving to lattice momentum space, we

find the sum of $\Sigma^{(A)}_{\phi,ee}$, $\Sigma^{(B)}_{\phi,ee}$, and $\Sigma^{(C)}_{\phi,ee}$ to be

$$\Sigma^{(ABC)}_{\phi,ee,ii} = -\frac{(2\pi N(0)\tau^2)T\tau}{\mathcal{N}a^d}\sum_{\omega>\varepsilon+\Omega}\sum_{\mathbf{Q}}\Bigg\{V(\mathbf{Q},i\omega)D(\mathbf{Q},i\omega)^2 \times\left[2\left(1-\frac{\tau}{\tau_0}\right)^2+\omega\tau\left(4\frac{\tau}{\tau_0}-3\right)\right]\Bigg\}. \tag{5.176}$$

If we set $\tau=\tau_0$, eq. 5.176 is then identical to the homogeneous result if we had not expanded in $\mathbf{q}$ as well (see eq. 3.169).

Let us now consider the expressions for diagrams E and F,

$$\begin{aligned}\Sigma^{(E)}_{\phi,ee,ii} = -\frac{Tt^2}{a^{2d}}\sum_{\omega}\sum_{j,l,m}\sum_{\mathbf{k},\mathbf{k}'}\Big[&G_i(\mathbf{k},i\varepsilon+i\Omega)^2G_i(\mathbf{k},i\varepsilon)G_j(\mathbf{k}',i\varepsilon+i\Omega)^2\\ &\times G_j(\mathbf{k}',i\varepsilon+i\Omega+i\omega)V_{ml}(i\omega)D_{mj}(i\varepsilon+i\Omega+i\omega,i\varepsilon+i\Omega)\\ &\times D_{lj}(i\varepsilon+i\Omega+i\omega,i\varepsilon+i\Omega)\delta_{\langle ij\rangle}\Big],\end{aligned} \tag{5.177a}$$

$$\begin{aligned}\Sigma^{(F)}_{\phi,ee,ji} = -\frac{Tt^2}{a^{2d}}\sum_{\omega}\sum_{l,m}\sum_{\mathbf{k},\mathbf{k}'}\Big[&G_i(\mathbf{k},i\varepsilon+i\Omega)G_i(\mathbf{k},i\varepsilon+i\Omega+i\omega)G_i(\mathbf{k},i\varepsilon)\\ &\times G_j(\mathbf{k}',i\varepsilon+i\Omega)G_j(\mathbf{k}',i\varepsilon+i\Omega+i\omega)G_j(\mathbf{k}',i\varepsilon)V_{ml}(i\omega)\\ &\times D_{mi}(i\varepsilon+i\Omega+i\omega,i\varepsilon+i\Omega)D_{li}(i\varepsilon+i\Omega+i\omega,i\varepsilon+i\Omega)\delta_{\langle ji\rangle}\Big].\end{aligned} \tag{5.177b}$$

This time we do not expand in powers of ω, and simply perform the momentum sums in eq. 5.177. Upon moving to lattice momentum space this becomes,

$$\Sigma^{(E)}_{\phi,ee} = \frac{2\pi N(0)\tau^4Tz\Gamma}{\mathcal{N}a^d}\sum_{\omega>\varepsilon+\Omega}\sum_{\mathbf{Q}}V(\mathbf{Q},i\omega)D(\mathbf{Q},i\omega)^2, \tag{5.178a}$$

$$\Sigma^{(F)}_{\phi,ee}(\mathbf{K}) = \frac{2\pi N(0)\tau^4Tz\Gamma}{\mathcal{N}a^d}\sum_{\omega>\varepsilon+\Omega}\sum_{\mathbf{Q}}V(\mathbf{Q},i\omega)D(\mathbf{Q},i\omega)^2\gamma_{\mathbf{Q}+\mathbf{K}}. \tag{5.178b}$$

where we see that diagram F carries a lattice momentum external to the sums. Considering the Dyson equation for the granular cooperon in eq. 5.173, this external lattice momentum is just the lattice momentum carried by the entire cooperon. We therefore set $\mathbf{K}=\mathbf{0}$ to

allow for comparison to the homogeneous result, and hence

$$\Sigma^{(EF)}_{\phi,ee} = \Sigma^{(F)}_{\phi,ee} + \Sigma^{(F)}_{\phi,ee} = \frac{2\pi N(0)\tau^4 T z\Gamma}{\mathcal{N}a^d} \sum_{\omega>\varepsilon+\Omega} \sum_{\mathbf{Q}} V(\mathbf{Q}, i\omega) D(\mathbf{Q}, i\omega)^2 (1+\gamma_{\mathbf{Q}}). \quad (5.179)$$

To see how these diagrams give a result analogous to the homogeneous case, we next add eq. 5.176 to eq. 5.179,

$$\begin{aligned}\Sigma^{(ABCEF)}_{\phi,ee} = -\frac{(2\pi N(0)\tau^2)T\tau}{\mathcal{N}a^d} \sum_{\omega>\varepsilon+\Omega} \sum_{\mathbf{Q}} \Bigg\{ & V(\mathbf{Q}, i\omega) D(\mathbf{Q}, i\omega)^2 \\ & \times \left[2\left(1 - \frac{\tau}{\tau_0}\right) + \omega\tau\left(4\frac{\tau}{\tau_0} - 3\right) - z\Gamma\tau(1+\gamma_{\mathbf{Q}}) \right] \Bigg\}.\end{aligned} \quad (5.180)$$

Noting that

$$\frac{\tau}{\tau_0} = \frac{1}{1+z\Gamma\tau_0} \simeq 1 - z\Gamma\tau_0, \quad (5.181)$$

we now approximate eq. 5.180 to give

$$\begin{aligned}\Sigma^{(ABCEF)}_{\phi,ee} &= -\frac{(2\pi N(0)\tau_0^4)T}{\mathcal{N}a^d} \sum_{\omega>\varepsilon+\Omega} \sum_{\mathbf{Q}} V(\mathbf{Q}, i\omega) D(\mathbf{Q}, i\omega)^2 (\omega + \Gamma\lambda_{\mathbf{Q}}) \\ &= -\frac{(2\pi N(0)\tau_0^2)^2 T}{\mathcal{N}a^d} \sum_{\omega>\varepsilon+\Omega} \sum_{\mathbf{Q}} V(\mathbf{Q}, i\omega) \widetilde{D}(\mathbf{Q}, i\omega),\end{aligned} \quad (5.182)$$

where we recalled that $D(\mathbf{Q}, i\omega) = (2\pi N(0)\tau)\widetilde{D}(\mathbf{Q}, i\omega)$ in the final line of eq. 5.182. Comparing this to eq. 3.169, we see that the sum of diagrams A, B, C, E, and F give an entirely analogous result to the homogeneous diagrams of the same type.

Turning our attention towards diagram D, we may write

$$\begin{aligned}\Sigma^{(D)}_{\phi,ee,ji} = -\frac{T}{a^{3d}} \sum_{\omega} \sum_{\mathbf{k},\mathbf{k}'} \Bigg[& V_{ji}(i\omega) \widetilde{C}_{ji}(i\varepsilon + i\Omega + i\omega, i\varepsilon) G_i(\mathbf{k}, i\varepsilon) G_i(\mathbf{k}, i\varepsilon + i\Omega) \\ & \times G_i(\mathbf{k}, i\varepsilon + i\Omega + i\omega) G_j(\mathbf{k}', i\varepsilon) G_j(\mathbf{k}', i\varepsilon + i\Omega) G_j(\mathbf{k}', i\varepsilon + i\Omega + i\omega) \Bigg].\end{aligned} \quad (5.183)$$

Performing the momentum sums and shifting to lattice momentum space, we obtain

$$\Sigma^{(D)}_{\phi,ee}(\mathbf{K}) = \frac{(2\pi N(0)\tau^2)^2 T}{\mathcal{N}a^d} \sum_{\omega>-(\varepsilon+\Omega)} V(\mathbf{Q}, i\omega)\widetilde{C}(\mathbf{Q}+\mathbf{K}, i\Omega + i\omega). \tag{5.184}$$

As with diagram F, we set $\mathbf{K} = \mathbf{0}$ in eq. 5.184, and then approximating $\tau \simeq \tau_0$, leads to

$$\Sigma^{(D)}_{\phi,ee} = \frac{(2\pi N(0)\tau_0^2)^2 T}{\mathcal{N}a^d} \sum_{\omega>-(\varepsilon+\Omega)} V(\mathbf{Q}, i\omega)\widetilde{C}(\mathbf{Q}, i\Omega + i\omega). \tag{5.185}$$

Finally, the variants of these diagrams with the interaction appearing on the lower Green's function can be found in an entirely identical manner to the homogeneous case. This is due to the fact that tunnelling does not affect the frequency carried by a Green's function, and hence the diagrams in fig. 5.15 have the exact same frequency structure as those for the homogeneous calculation. Therefore, the phase breaking rate generated by the Coulomb interaction in granular metals is thus

$$\begin{aligned}\frac{1}{\tau_{\phi,ee}} = \frac{2\pi N(0)\tau_0^2 T}{\mathcal{N}a^d} \sum_{\mathbf{Q}} \Bigg[&\left(\sum_{\omega>\varepsilon+\Omega} + \sum_{\omega>-\varepsilon} \right) \widetilde{D}(\mathbf{Q}, i\omega) V(\mathbf{Q}, i\omega) \\ &- \left(\sum_{\omega>-(\varepsilon+\Omega)} + \sum_{\omega>\varepsilon} \right) \widetilde{C}(\mathbf{Q}, i\Omega + i\omega) V(\mathbf{Q}, i\omega) \Bigg],\end{aligned} \tag{5.186}$$

where we set $\tau \simeq \tau_0$ in the prefactor of the sums.

The process of analytically continuing the Matsubara sums in eq. 5.186 and expanding to $\mathcal{O}(\Omega^0)$ is entirely identical to the homogeneous case. We therefore simply read off the granular expression for $\tau^{-1}_{\phi,ee}$ from eq. 3.184,

$$\frac{1}{\tau_{\phi,ee}} \simeq -4N(0)\tau_0^2 \sum_{\mathbf{Q}} \int_{-T}^{+T} dz \frac{\widetilde{C}^R(\mathbf{Q}, z)}{\sinh(\beta z)} \mathrm{Im}\left[V^R(\mathbf{Q}, z)\right], \tag{5.187}$$

At this point we must consider each dimensionality specifically.

2D systems

In two dimensions,

$$\mathrm{Im}[V^R(\mathbf{Q},z)] \simeq \frac{2\pi e^2 \mathcal{D}_T \kappa_2 z}{(\kappa_2 \mathcal{D}_T Q^2)^2 + z^2}, \tag{5.188}$$

where we have assumed the granular diffusive limit and noted that $\kappa_2 \gg Q$. Replacing the momentum sum by an integral and evaluating the resulting expression yields

$$\frac{1}{\tau_{\phi,ee}} = \frac{e^2}{\pi \mathcal{D}_T \kappa_2} \int_{-T}^{+T} \frac{dz}{\sinh(\beta z)} \frac{z}{\tau_\phi^{-1} - iz - \frac{z^2}{\mathcal{D}_T \kappa_2^2}} \ln\left(\frac{\tau_\phi^{-1} - iz}{z^2} \frac{\mathcal{D}_T \kappa_2^2 \Gamma + z^2}{\Gamma + \tau_\phi^{-1} - iz} \right). \tag{5.189}$$

Since $\mathcal{D}_T \kappa_2^2$ is a large energy for disordered granular metals ($\mathcal{D}_T \kappa_2^2 \gg T$), and we are only interested in small values of z, we may safely neglect the $z^2/(\mathcal{D}_T \kappa_2^2)$ term appearing in the denominator outside of the logarithm of the above integrand. We may also approximate $z/\sinh(\beta z) \simeq T$, as we are only interested in small values of z (see appendix J.1). Inside the logarithm, we may neglect the z^2 appearing in the numerator if $\mathcal{D}_T \kappa_2^2 \Gamma \gg z^2$. For the latter to be true requires $\kappa_2 a \gg z/\Gamma$, which is guaranteed when $\Gamma \gg T$. If $\Gamma \ll T$, it is not immediately clear whether we may neglect the z^2 or not. For now let us assume that $\kappa_2 a \gg z/\Gamma$, in which this case eq. 5.189 becomes

$$\frac{1}{\tau_{\phi,ee}} = \frac{T}{4\pi^2 g_T} \int_{-T}^{+T} \frac{dz}{\tau_\phi^{-1} - iz} \ln\left(\frac{\tau_\phi^{-1} - iz}{z^2} \frac{\mathcal{D}_T \kappa_2^2 \Gamma}{\Gamma + \tau_\phi^{-1} - iz} \right), \tag{5.190}$$

where we noted that $\mathcal{D}_T \kappa_2 / e^2 = 4\pi g_T$.

To recover the granular analogue of the homogeneous result, we assume $\Gamma \gg T \gg \tau_\phi^{-1}$ so that $\Gamma \gg T^2 \tau_\phi$, and hence eq. 5.190 can be approximated as

$$\begin{aligned} \frac{1}{\tau_{\phi,ee}} &= \frac{T}{4\pi^2 g_T} \int_{-T}^{+T} \frac{dz}{\tau_\phi^{-1} - iz} \ln\left(\frac{\tau_\phi^{-1} - iz}{z^2} \mathcal{D}_T \kappa_2^2 \right) \\ &= \frac{T}{2\pi^2 g_T} \int_0^T dz\, \mathrm{Re}\left[\frac{1}{\tau_\phi^{-1} - iz} \ln\left(\frac{\tau_\phi^{-1} - iz}{z^2} \mathcal{D}_T \kappa_2^2 \right) \right]. \end{aligned} \tag{5.191}$$

This expression is identical to eq. J.21 for the homogeneous case with $\mathcal{D} \to \mathcal{D}_T$. We

therefore recover a self-consistent equation with the same form as that for homogeneous systems,

$$\frac{1}{\tau_{\phi,ee}} = \frac{1}{4\pi}\frac{T}{g_T}\ln(\mathcal{D}_T\kappa_2^2 T\tau_\phi^2). \tag{5.192}$$

Clearly there are many different limits we can consider due to the large number of energy scales we have to play with. To write everything in terms of energy scales, we introduce the Coulomb energy scale,

$$V_c = \frac{4\pi e^2}{a} = \kappa_2 a\delta. \tag{5.193}$$

This is a large energy scale: for a system with $a \sim 10^{-7}$m, we have $V_c \sim 10^3$K. Using this, we can see that neglecting the z^2 term in the denominator of the logarithm's prefactor is equivalent to assuming $\tau_\phi^{-1} \gg T^2\delta/(V_c^2 g_T)$. Recalling that δ is our smallest energy scale, $g_T \gg 1$, and $V_c \gg T$ when considering low temperature phenomena, we see that this assumption is safe in the systems we concern ourselves with. Let us now consider another limit to demonstrate how granular and homogeneous systems may differ.[23]

We now take the limit where $T \gg \tau_\phi^{-1} \gg \Gamma, T^2\delta/(V_c^2 g_T)$, and so approximate the logarithm as

$$\begin{aligned}\ln\left(\frac{\tau_\phi^{-1} - iz}{z^2}\frac{\mathcal{D}_T\kappa_2^2\Gamma + z^2}{\Gamma + \tau_\phi^{-1} - iz}\right) &= \ln\left(1 + \frac{\mathcal{D}_T\kappa_2^2\Gamma}{z^2}\right) - \ln\left(1 + \frac{\Gamma}{\tau_\phi^{-1} - iz}\right) \\ &\simeq \ln\left(1 + \frac{\mathcal{D}_T\kappa_2^2\Gamma}{z^2}\right) - \frac{\Gamma}{\tau_\phi^{-1} - iz}.\end{aligned} \tag{5.194}$$

Substituting this into eq. 5.189, letting $z \to z\tau_\phi^{-1}$, and setting the upper limit of the integral to infinity, we find[24]

$$\frac{1}{\tau_{\phi,ee}} = \frac{T}{2\pi^2 g_T}\int_0^\infty \frac{1}{1+z^2}\ln\left(1 + \frac{\Gamma^2\tau_\phi^2\kappa_2^2 a^2}{z^2}\right). \tag{5.195}$$

[23] This thesis is already long enough. It would be unwise to explore all possible limiting behaviours.
[24] The integral involving the second term of eq. 5.194 simply vanishes.

Performing the frequency integral gives

$$\frac{1}{\tau_{\phi,ee}} = \frac{T}{4\pi g_T}\Big[\ln(1-\Gamma\tau_\phi^2\mathcal{D}_T\kappa_2^2) + 2\,\mathrm{artanh}(\Gamma\tau_\phi\kappa_2 a)\Big], \tag{5.196}$$

where $\mathrm{artanh}(x)$ is the inverse function of $\tanh(x)$. By writing the artanh term in terms of logarithms, we arrive at

$$\frac{1}{\tau_{\phi,ee}} = \frac{T}{2\pi g_T}\ln(1+\Gamma\tau_\phi\kappa_2 a). \tag{5.197}$$

This self-consistent equation differs quite drastically from that in eq. 5.192, and hence serves as a demonstration of novel phase breaking mechanisms that may be present in granular metals.

To determine which expression is the most appropriate for a system requires an understanding of its material properties. With this knowledge we may then apply the suitable limits to eq. 5.189. The limit we assumed in obtaining eq. 5.197 turns out to be unphysical for granular metals, as it subtly violates our assumption that $g_T \gg 1$. This is because $N(\xi) = m_e/(2\pi)$ is constant in 2D, and so δ is also fixed for a system with a given grain size. If $a \sim 10^{-7}$m, then $\delta \sim 0.6$K, so in assuming $\Gamma \ll \tau_\phi^{-1} \ll T$ we inadvertently take $\Gamma \ll \delta$ and hence $g_T \ll 1$. The assumption that $\tau_\phi^{-1} \gg T^2\delta/(V_c^2 g_T)$ may still hold for a carefully chosen set of parameters. In any case, the important idea illustrated by eq. 5.197 is that new self-consistent equations can be obtained from granular systems, and hence novel phase breaking behaviour may be observable in granular metals. We now turn our attention to 3D systems.

3D systems

Unlike 2D systems, we now have the ability to change the mean level spacing by adjusting the carrier concentration of a material. We will therefore be able to consider more limits

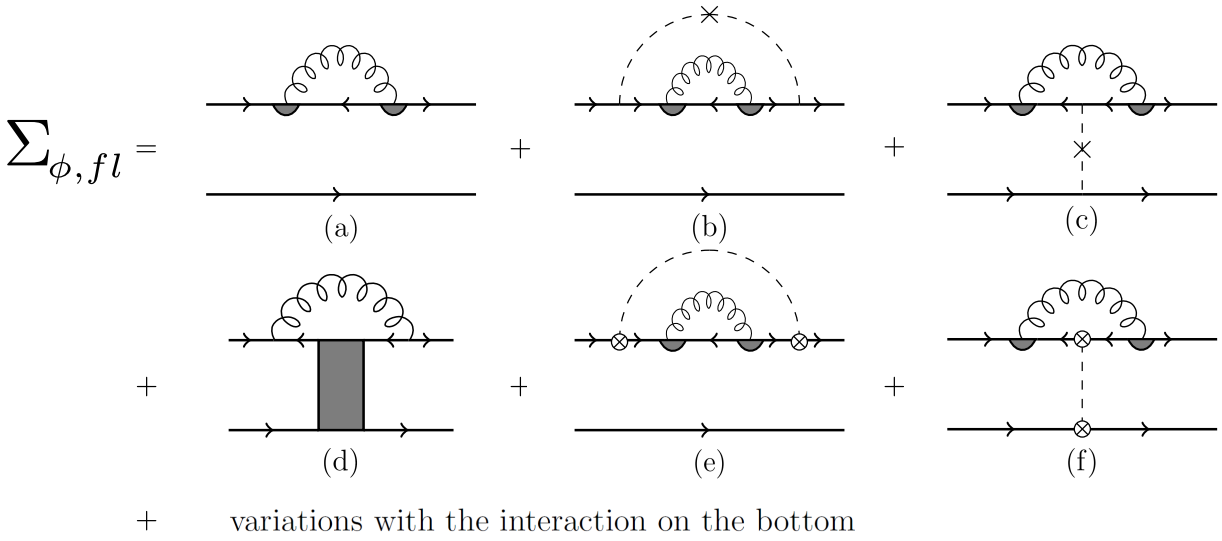

Figure 5.16: Diagrams describing the phase coherence corrections to the cooperon in granular systems due to superconducting fluctuations.

that are consistent with the granular metallic regime. In three dimensions,

$$\mathrm{Im}\left[V^R(\mathbf{Q},z)\right] \simeq -\frac{4\pi e^2 \mathcal{D}_T \kappa_3^2 z}{Q^2(\mathcal{D}_T^2\kappa_3^4 + z^2)}, \tag{5.198}$$

so substituting this into eq. 5.187, approximating $z/(\sinh(\beta z)) \simeq T$, and treating the momentum sum as an integral gives

$$\frac{1}{\tau_{\phi,ee}} = \frac{T}{\pi^3 g_T}\frac{1}{\sqrt{\Gamma\tau_\phi}}\int_0^{T\tau_\phi}\frac{dz}{1+\frac{z^2}{\tau_\phi^2\mathcal{D}_T^2\kappa_3^4}}\mathrm{Re}\left[\frac{1}{\sqrt{1-iz}}\arctan\left(\sqrt{\frac{\Gamma\tau_\phi}{1-iz}}\right)\right]. \tag{5.199}$$

We start by considering the limit $\Gamma \gg T \gg \tau_\phi^{-1}$, which allows us to recover the granular result analogous to the homogeneous case, see eq. 3.188,

$$\frac{1}{\tau_{\phi,ee}} = \frac{1}{\pi^2\sqrt{2\Gamma}}\frac{T^{3/2}}{g_T}. \tag{5.200}$$

If we instead take the limit $T \gg \tau_\phi^{-1} \gg \Gamma$, eq. 5.199 can be approximated as

$$\frac{1}{\tau_{\phi,ee}} = \frac{T}{\pi^3 g_T}\int_0^{T\tau_\phi}\frac{dz}{1+\frac{z^2}{\tau_\phi^2\mathcal{D}_T^2\kappa_3^4}}\mathrm{Re}\left[\frac{1}{1-iz}\right]. \tag{5.201}$$

Evaluating this integral, and noting that $\kappa_3^2 a^2 = 2V_c/\delta$, we arrive at a self-consistent equation for the 3D Coulomb phase breaking rate,

$$\frac{1}{\tau_{\phi,ee}} = \frac{4}{\pi^3}\frac{V_c^2\tau_\phi^2 g_T T}{1-4V_c^2\tau_\phi^2 g_T^2}\left[\frac{1}{2g_T V_c\tau_\phi}\arctan\left(\frac{T}{2V_c g_T}\right) - \arctan(T\tau_\phi)\right]. \tag{5.202}$$

In writing eq. 5.202, we have not let $T\tau_\phi \to \infty$ in the intergal limit. Given that $V_c \gg T$, our assumption $T \gg \tau_\phi^{-1}$, and that we may still take $g_T \gg 1$, this self-consistent equation can be simplified drastically to yield

$$\frac{1}{\tau_{\phi,ee}} = \frac{1}{\pi^3}\frac{T}{g_T}\arctan(T\tau_\phi) \simeq \frac{1}{2\pi^2}\frac{T}{g_T}. \tag{5.203}$$

Eq. 5.203 shows that we may obtain a result for τ_ϕ^{-1} unique to granular metals. Our next task is to understand the role of superconducting fluctuations in phase breaking for granular systems.

5.5.2 Superconducting Fluctuation Phase Breaking Mechanism

As in our calculation for σ_{fl} in section 5.4, we shall only consider 3D systems as this is what will be most relevant for comparison to the experimental results discussed in chapter 6. The diagrams describing $\tau_{\phi,fl}^{-1}$ are given in fig. 5.16, and can be shown to give

$$\frac{1}{\tau_{\phi,fl}} \simeq \frac{8\pi N(0)^2 T}{\mathcal{N}a^d\tau_0^{-4}}\sum_{\mathbf{Q}}\sum_{\mathbf{q}}\int_{-T}^{+T}dz\frac{\mathrm{Im}\left[L^R(\mathbf{Q},\mathbf{q},z)\right]}{z}(\Gamma\lambda_{\mathbf{Q}} + \mathcal{D}q^2 + iz)\widetilde{C}^A(\mathbf{Q},\mathbf{q},z)^2, \tag{5.204}$$

in analogy to eq. 3.192. As in the homogeneous case, we let $z \to z\tau_\phi^{-1}$, set $T\tau_\phi \to \infty$ in the integral limits, and ignore all τ_ϕ^{-1} dependence in the pair propagator's digamma functions and digamma function derivatives. By further assuming $Q \ll a^{-1}$, we find

$$\begin{aligned}\frac{1}{\tau_{\phi,fl}} =& \frac{16T^2}{\pi N(0)} \\ &\times \sum_{\mathbf{Q}}\sum_{\mathbf{q}}\left[1 + \frac{\mathcal{D}q^2 + \mathcal{D}_T Q^2}{\tau_{GL}^{-1} + \mathcal{D}q^2 + \mathcal{D}_T Q^2}\right]\frac{1}{\left[2(\mathcal{D}q^2 + \mathcal{D}_T Q^2) + \tau_{GL}^{-1} + \tau_\phi^{-1}\right]^2}.\end{aligned} \tag{5.205}$$

Here we have assumed the ideal case for superconducting fluctuation crossovers, where $\Gamma \ll E_{Th} \ll T_c$.

As we saw in the calculation of σ_{fl}, three regions of behaviour exist inside superconducting fluctuation contributions due to the nature of the pair propagator. The phase breaking rate is no exception to this, so we must consider the three different regions of behaviour separately here too. We apply the same ideas we have used throughout this thesis, so, for the sake of brevity, we simply give the end results. In the close-to-T_c region ($\tau_{GL}^{-1} \ll \Gamma$),

$$\frac{1}{\tau_{\phi,fl}} = \frac{8T^2}{\pi^3 g_T}\left[\frac{\tau_\phi^{-2} - 3\tau_{GL}^{-1}\tau_\phi^{-1} - 2\tau_{GL}^{-2}}{2(\tau_\phi^{-1} - \tau_{GL}^{-1})^2\sqrt{2\Gamma(\tau_{GL}^{-1} + \tau_\phi^{-1})}} \arctan\left(\sqrt{\frac{2\Gamma}{\tau_{GL}^{-1} + \tau_\phi^{-1}}}\right) + \frac{\tau_{GL}^{-1}}{(\tau_{GL}^{-1} - \tau_\phi^{-1})^2}\frac{\arctan(\sqrt{\Gamma\tau_{GL}})}{\sqrt{\Gamma\tau_{GL}}} + \frac{1}{2}\frac{\tau_\phi^{-1}}{\tau_{GL}^{-1} - \tau_\phi^{-1}}\frac{1}{2\Gamma + \tau_{GL}^{-1} + \tau_\phi^{-1}}\right], \tag{5.206}$$

which gives an equivalent expression to the homogeneous case, see eq. 3.197, in the limit $\Gamma \gg \tau_\phi^{-1}$,

$$\frac{1}{\tau_{\phi,fl}} = \frac{T^2}{\pi^2 g_T}\sqrt{\frac{2}{\Gamma(\tau_{GL}^{-1} + \tau_\phi^{-1})}}\left[1 - \tau_{GL}^{-1}\left(\frac{\sqrt{2\tau_{GL}^{-1}} - \sqrt{\tau_{GL}^{-1} + \tau_\phi^{-1}}}{\tau_{GL}^{-1} - \tau_\phi^{-1}}\right)^2\right]. \tag{5.207}$$

For a general granular system, eq. 5.206 is a clear indicator of behaviour not seen in homogeneous metals.

Moving onto the intermediate region ($\Gamma \ll \tau_{GL}^{-1} \ll E_{Th}$), eq. 5.206 yields

$$\frac{1}{\tau_{\phi,fl}} = \frac{8\delta}{3\pi^3}\frac{T^2}{(\tau_{GL}^{-1} + \tau_\phi^{-1})^2}. \tag{5.208}$$

Finally, in the far-from-T_c region ($E_{Th} \ll \tau_{GL}^{-1} \ll T_c$),

$$\frac{1}{\tau_{\phi,fl}} = \frac{T^2}{3\pi^4 g_T}\frac{1}{\sqrt{E_{Th}(\tau_{GL}^{-1} + \tau_\phi^{-1})}}\left[1 - \tau_{GL}^{-1}\left(\frac{\sqrt{2\tau_{GL}^{-1}} - \sqrt{\tau_{GL}^{-1} + \tau_\phi^{-1}}}{\tau_{GL}^{-1} - \tau_\phi^{-1}}\right)^2\right], \tag{5.209}$$

which has a form resembling the homogeneous 3D result, as expected in the far-from-T_c region.

In summary, we see that the superconducting fluctuation contribution to τ_ϕ^{-1} has three distinct regions of temperature dependence. The close-to-T_c behaviour only resembles the homogeneous 3D result in the limit $\Gamma \gg \tau_\phi^{-1}$, and produces a new self-consistent equation otherwise. In the intermediate region, we obtain another novel self-consistent equation unique to granular media, whilst in the far-from-T_c region, we find a result reflecting the system's dimensionality.

To see how the behaviour of τ_ϕ^{-1} changes compared to the homogeneous case, we plot numerical solutions to the self-consistent equations given by the sum of $\tau_{\phi,ee}^{-1}$ (eq. 5.203) and $\tau_{\phi,fl}^{-1}$ within each fluctuation region.[25] The results are shown in fig. 5.17a, where we have assumed the following parameters,

$$\delta = 10^{-5}\text{K}, \qquad \Gamma = 10^{-3}\text{K}, \qquad E_{Th} = 10^{-1}\text{K}, \qquad T_c = 10\text{K}. \tag{5.210}$$

We use these parameters as a demonstration of the behaviour we might see in granular materials.

In fig. 5.17a, the solid blue and solid red lines are calculated using eq. 5.206 and represent the close-to-T_c and intermediate behaviour. In contrast, the dashed black line is instead calculated using eq. 5.208 for $\tau_{\phi,fl}^{-1}$. By comparing the dashed black line with the solid red line, we see that the transition between close-to-T_c and intermediate behaviour is smooth and relatively quick.

The far-from-T_c behaviour (solid green line) is not connected to the intermediate curve, as this crossover is not trivial to compute analytically or numerically. For an accurate description, we would need to perform the $\mathbf{q}$ sum numerically, rather than treat it as an integral at all temperatures. If we were to treat the intragranular momentum sum as an integral (i.e. $\mathbf{q}$ is taken to be continuous), then we would introduce contributions arising from values of $\mathbf{q}$ that are smaller than the minimum non-zero intragranular momentum,

[25] By using eq. 5.203, we have assumed $T \gg \tau_\phi^{-1} \gg \Gamma$.

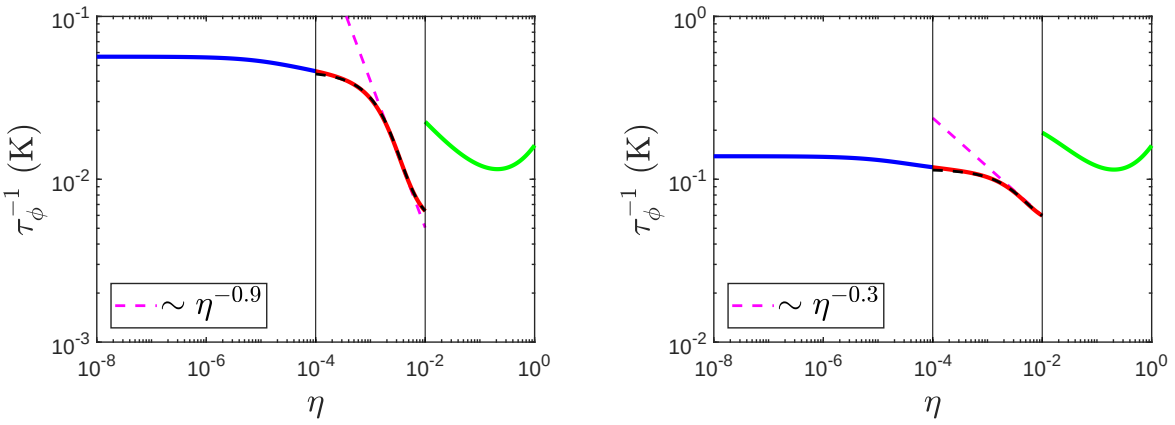

(a) (b)

Figure 5.17: The thin vertical black lines note the boundaries between the fluctuation behaviour regions. The solid blue and solid red lines show the self-consistent solution of the total phase breaking rate using eq. 5.206, in the close-to-T_c and intermediate regions respectively. The solid green line shows the self-consistent solution of the total phase breaking rate using eq. 5.209 in the far-from-T_c region. (a): solution using the parameters in eq. 5.210. (b): solution using the parameters in eq. 5.210, but with $\delta = 10^{-4}$K instead.

such that they would be comparable to $\mathbf{Q}$. This would give rise to more contributions that would appear as comparably singular to the $\mathbf{q} = \mathbf{0}$ term, which is not physically reasonable. We are therefore left with the unfortunate situation of not being able to plot a curve that is smooth over all regions of fluctuation behaviour. Thus, the green curve should only be used as a guide far away from the intermediate-far boundary. In a similar sense, the same is also true of the red curve within the intermediate region; we should use it as a guide far away from the intermediate-far boundary. The point at which we can consider the curve to be near-exact is not trivial to determine.

In the close-to-T_c region, τ_ϕ^{-1} varies extremely slowly, and can be treated as approximately constant. Upon entering the intermediate region, the phase breaking rate begins to decrease with an apparent $\eta^{-0.9}$ power law, before beginning to slow its rate of decrease as it approaches the intermediate-far boundary. In the far-from-T_c region, the phase breaking rate can be seen to continue decreasing, before starting to increase as we move away from T_c. As discussed above, the exact behaviour around the intermediate-far transition is not trivial to determine. We may, however, try to qualitatively analyse the

possible temperature dependence of τ_ϕ^{-1} between the two regions.

Given that τ_ϕ^{-1} begins to increase at higher temperatures deep inside the far-from-T_c region, and that the gradient of τ_ϕ^{-1} begins to increase in the intermediate region as the intermediate-far crossover is approached, it is reasonable to assume that the phase breaking rate has a natural minimum that exists near the intermediate-far crossover. The region this minimum lies in is not clear, and may vary depending on the parameters chosen. If the minimum lies inside the far-from-T_c region, we might expect the red curve to be a fairly good approximation of the intermediate behaviour far away from the intermediate-far crossover, and so the apparent $\eta^{-0.9}$ power law would still be visible over approximately one order of magnitude in η. In contrast, the minimum might exist in the intermediate region, and so the red curve will only be reliable further away from the intermediate-far crossover, in comparison to the previous situation. Additionally, the range over which we might expect the $\eta^{-0.9}$ power law will be reduced, and may not even be visible in this case.

From a more pessimistic perspective, the behaviour of τ_ϕ^{-1} might be more comparable to the green curve close to the intermediate-far crossover, even in the case where the minimum was located in the far-from-T_c region. Hence, the intermediate behaviour would appear drastically modified compared to that shown by the red curve in fig. 5.17a. To determine which of these pictures is correct requires an efficient way to perform the intragranular momentum sums without approximating them as an integral.

Finally, let us address the power law we see in the intermediate region. By using the same set of parameters as those listed in eq. 5.210, but taking $\delta = 10^{-4}$K instead, we plot the reduced temperature dependence of τ_ϕ^{-1} in fig. 5.17b. Here we find an $\eta^{-0.3}$ power law, and so the relation we see between the phase breaking rate and η appears to be non-trivial. To obtain a relation akin to Brenig et. al.'s [59], see eq. 3.209, does not seem feasible given the self-consistent forms of $\tau_{\phi,ee}^{-1}$ and $\tau_{\phi,fl}^{-1}$ in granular systems.

5.6 Chapter Summary

In summary, this chapter has presented the application of the diagrammatic methods derived in chapter 4 to describe the temperature dependence of the electrical conductivity in disordered granular metals. We started by presenting both a classical and field theoretic derivation of the granular equivalent of the Drude conductivity. After this we demonstrated how to obtain the granular cooperon and diffuson, so that we could calculate the weak localisation corrections to the electrical conductivity in granular metals. In these calculations we found straightforward mappings between the homogeneous and granular results by letting $\mathcal{D} \to \mathcal{D}_T$.

We then considered two-body interactions, choosing to tackle the Coulomb interaction first. Here we found that granular metals produced results analogous to the homogeneous case when $T \ll \Gamma$. However, this model gave a new and novel T^{-1} correction that was independent of dimensionality when $\Gamma \ll T$. Following this, we calculated the superconducting fluctuation corrections to the electrical conductivity in the case where $\Gamma \ll E_{Th} \ll T_c$, and saw that three regions of behaviour existed within the fluctuation conductivity. Each of these regions could be interpreted physically by comparing the size of a grain to the intergain and intragrain coherence lengths of a Cooper pair.

Finally, we calculated the temperature dependence of the phase breaking rate due to EEIs and virtual Cooper pairs. Here too, we found three regions of behaviour close to the superconducting transition. Let us now move on to comparing the predictions of this theory to experiment.

CHAPTER 6

BORON-DOPED NANOCRYSTALLINE DIAMOND: EXPERIMENTAL RESULTS

The work in this thesis was inspired by the experiments of Klemencic et. al. [28], who measured the electrical resistance of boron-doped nanocrystalline diamond (BNCD) films. Specfically, they looked at how the electrical resistance changed as the temperature was varied from room temperature, down to below the superconducting transition temperature of the BNCD films, $T_c \lesssim 4$K. Within their data, they saw superconducting fluctuation corrections characteristic of a 3D granular metal in the form of crossovers in the fluctuation conductance (3D-q0D-3D behaviour). Most interestingly, they saw the η^{-3} power law that we would expect from the AL contribution, and so used this as a fitting guide to determine T_c. After fitting an η^{-3} power law to a region, they saw very sharp changes to $\eta^{-1/2}$ behaviour either side of the η^{-3} region. These observations leave us with the following questions: what might be suppressing the anomalous MT term, such that the AL term can dominate? Is there a novel phase breaking rate that alters the anomalous MT behaviour to look like the AL term? Should we expect the crossovers to be sharp?

To answer these questions, we first reproduce Klemencic et. al.'s data analysis, using

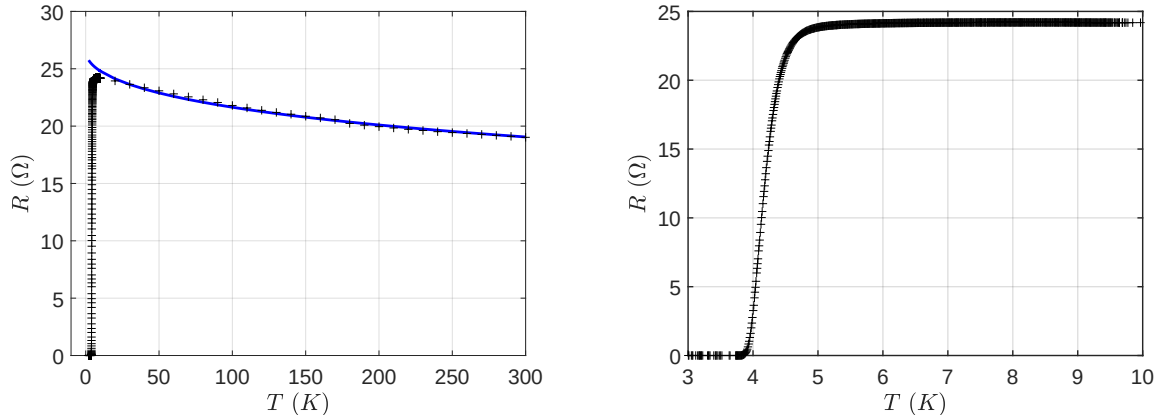

(a) (b)

Figure 6.1: The plots above show the data (crosses) taken by Klemencic et. al. [28] on a 339nm thick BNCD film. (a): Fitting 3D EEI corrections and Drude to high temperature behaviour. (b): focus on the superconducting transition.

the data they presented in [28]. Next, we compare this analysis to the theoretical predictions of chapter 5. Finally, we conclude this chapter with a discussion of the applicability of the theory to the BNCD films of Klemencic. et. al., and what further work may be required to deepen our understanding of granular superconductors.

6.1 Data Analysis

Fig. 6.1a presents the data taken by Klemencic et. al. [28] on a 339nm film, and shows a 3D EEI power law, $\sim T^{1/2}$, plus granular Drude fitting to the high temperature behaviour ($T \geq 10$K). To isolate the fluctuation behaviour, we simply subtract the conductance of this fitting away from the conductance data, which produces fig. 6.2a. Klemencic et. al. saw an η^{-3} power law behaviour, which is characteristic of the AL contribution in the intermediate region. We therefore fit the same power law over the region of η which appears to have this behaviour. By fitting a power law to the fluctuation data we are able to extract a value for T_c, which corresponds to the theoretical superconducting transition, rather than an arbitrary point that is a fraction of the normal state resistance.[1] For the 339nm film we find $T_c = 3.81$K.

[1]Sometimes T_c is defined experimentally as the temperature at which the resistance of a material is 90%, 50%, or 10% of its normal state value just above the transition (i.e. where η is not small).

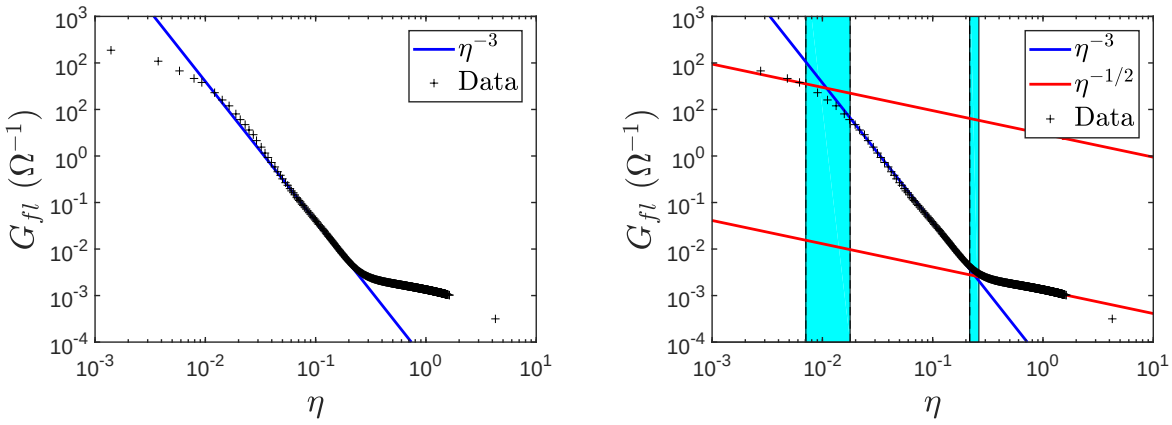

(a) (b)

Figure 6.2: The plots above show the fluctuation data we have generated from Klemencic et. al.'s data [28] from a 339nm BNCD film. (a): Here we guessed $T_c = 3.8$K, and have not applied any fitting routine. (b): Fitted fluctuation data, where the shaded regions indicate areas where the crossovers occur.

After the application of this fitting, see fig. 6.2b, we find two sharp crossovers between η^{-3} and $\eta^{-1/2}$ power laws. The shaded regions in fig. 6.2b represent the area in which we expect the boundaries corresponding to Γ/T_c and E_{Th}/T_c to lie. This behaviour can be seen in multiple different film thicknesses; we present the plots of this analysis for Klemencic et. al.'s 128nm, 160nm, 168nm, 204nm, and 564nm films in appendix L.

6.2 Theory Versus Experiment

To compare theory to experiment, we use the following parameters,

$$\begin{gathered} \delta = 5.6 \times 10^{-3}\text{K}, \qquad \Gamma = 2.62 \times 10^{-2}\text{K}, \qquad E_{Th} = 1\text{K}, \\ T_c = 3.8\text{K}, \qquad a = 10^{-7}\text{m}, \end{gathered} \tag{6.1}$$

where a is based upon the average grain size given in [28], and the mean level spacing corresponds to a carrier concentration of 10^{27}m^{-3}, which is taken from [77].[2] With these parameters, E_{Th} is too large for us to include any non-zero internal momenta associated to a virtual Cooper pair, such that we can still satisfy our assumption of the diffusive limit.

[2]For comparison to Klemencic et. al. [28], note that $E_{Th} = 1$K corresponds to $\mathcal{D} = 13.1$ cm s^{-1}.

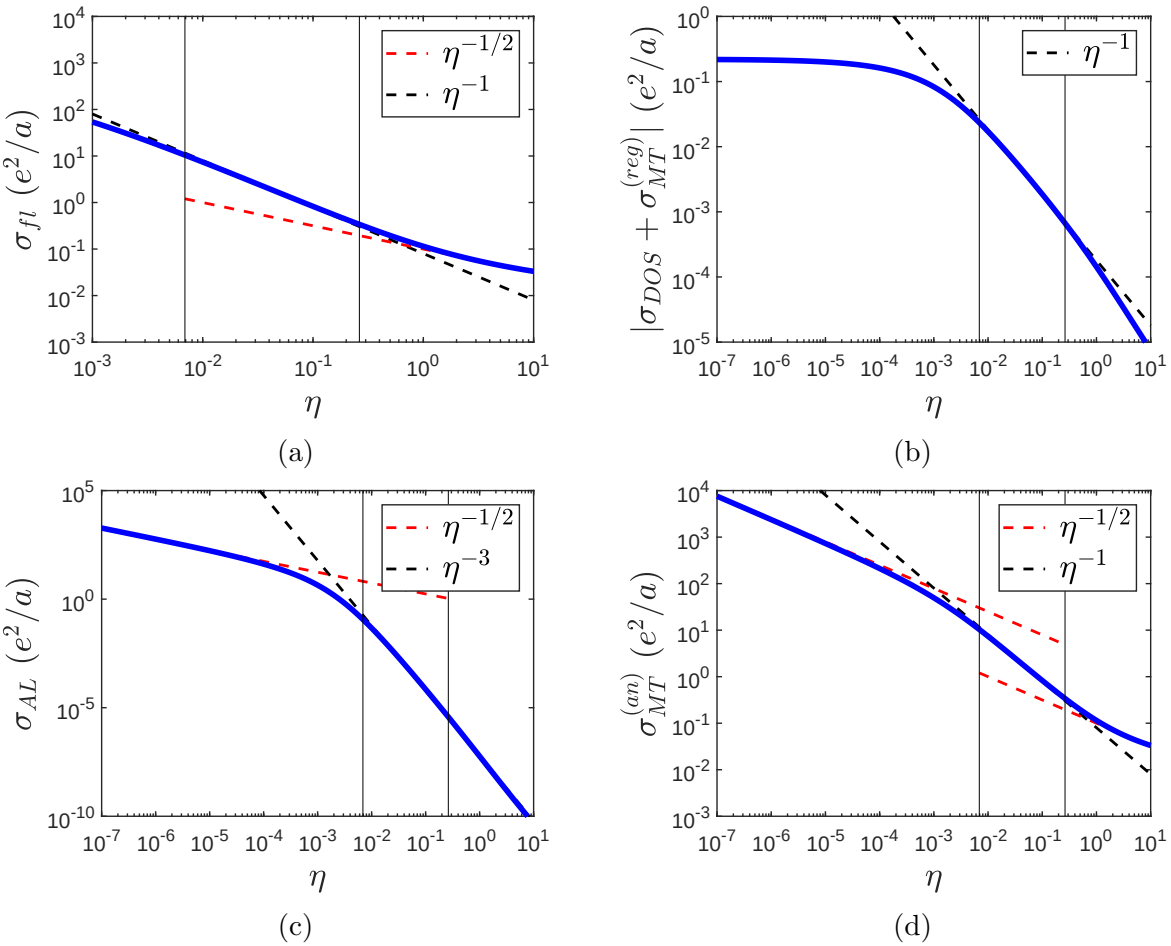

Figure 6.3: Theoretical predictions for the different contributions to the fluctuation conductivity, using the parameters listed in eq. 6.1, in the absence of phase breaking. The solid black vertical lines mark where $\eta = \Gamma/T_c$ and $\eta = E_{Th}/T_c$. (a): Total fluctuation conductivity. (b): DOS and regular MT contribution. (c): AL contribution. (d): Anomalous MT contribution. (These are the plots presented in Perkins et. al. [76].)

Therefore, we shall only consider the $\mathbf{q} = \mathbf{0}$ contributions of the fluctuation conductivity corrections presented in section 5.4. The theoretical fluctuation conductivity is presented in fig. 6.3, where we have initially assumed $\tau_\phi^{-1} = 0\text{K}$.

As expected, the AL contribution is completely dominated by the MT and DOS terms in the intermediate and far-from-T_c regions. However, we do in fact observe an $\eta^{-1/2}$ power law in the far-from-T_c region, despite the fact that we have not included the internal DOFs of the virtual Cooper pairs. This behaviour can be attributed to the anomalous MT term, see fig. 6.3d. The reason behind this apparent power law behaviour is not straightforward, and is unlikely to be as simple as being able to find an approximation

such that $\sigma_{MT}^{(an)} \sim \eta^{-1/2}$ in this region without the inclusion of internal DOFs. Given that this power law is seen in the region where $10^{-1} < \eta < 1$, we cannot take $\ln(T/T_c) \simeq \eta$ here, and so the fact we see power law type behaviour theoretically is most likely happenstance.

We should also note that the theory predicts a much more gradual change in power law behaviour, compared to the sharp crossovers seen in experiment. Additionally, the close-intermediate crossover in the theory appears at a much lower value of η than we might initially expect. The theory predicts that the close-to-T_c behaviour should not be visible within the experimental range of η; i.e. the theoretical close-to-T_c behaviour appears to start around at most $\eta \sim 10^{-4}$, whilst the experimental fluctuation data is only in the range $10^{-3} \leq \eta$. To shift the close-to-T_c $\eta^{-1/2}$ power law into the experimental range of η, we might wish to choose a larger value of Γ. It turns out that this does move the $\eta^{-1/2}$ behaviour to higher values of η, but the size of Γ required is much larger than expected, and still does not give a perfect power law within the experimental η range. We will return to this point shortly.

Let us now consider the effects of a constant phase breaking rate. This will allow us to check whether the anomalous MT contribution can be suppressed such that it cancels almost perfectly with the DOS and regular MT terms, thus allowing the AL term to be visible in the intermediate region. Fig. 6.4a shows total fluctuation conductivity for different values of τ_ϕ^{-1} using the parameters given in eq. 6.1. For large phase breaking, $\tau_\phi^{-1} \sim T_c$, we find that the η^{-3} power law does indeed become visible due to the near-perfect cancellation of the MT and DOS terms. However, we find that this introduces an uncharacteristic minimum in σ_{fl} and still does not give sharp crossovers.

For comparison, let us consider a different set of material parameters,

$$\begin{gathered} \delta = 5.6 \times 10^{-3}\text{K}, \qquad \Gamma = 0.1\text{K}, \qquad E_{Th} = 3\text{K}, \\ T_c = 3.8\text{K}, \qquad a = 10^{-7}\text{m}. \end{gathered} \tag{6.2}$$

Using these values, we obtain the fluctuation conductivity for different constant phase breaking rates shown in fig. 6.4b. We again find that the η^{-3} power law only becomes

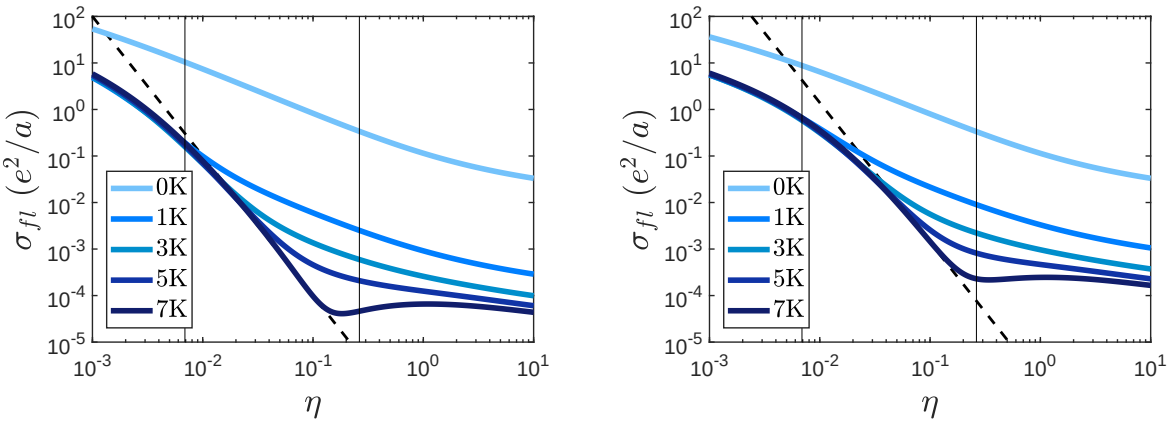

Figure 6.4: Total fluctuation conductivity corrections for different constant τ_ϕ^{-1}, using two different sets of material parameters. The solid black vertical lines mark where $\eta = \Gamma/T_c$ and $\eta = E_{Th}/T_c$ using the values for Γ and E_{Th} given in eq. 6.1. The dashed black line acts as a guide for η^{-3} behaviour. (a): Here we use the experimental parameters given in eq. 6.1. (b): Here we use the custom set of parameters given in eq. 6.2. (These are the plots presented in Perkins et. al. [76].)

visible when $\tau_\phi^{-1} \sim T_c$, and that the same minimum is still obtained. We also note that, whilst the close-intermediate crossover has move to a higher value of η, the fluctuation conductivity still has not rolled over to a clear $\eta^{-1/2}$ power law within the experimental η range when in the close-to-T_c region. Furthermore, the value of Γ is much larger than we might initially expect based upon the fitting in fig. 6.2b. We should also note that the range over which we see η^{-3} behaviour is smaller than before too.

Let us now include our model for the temperature dependence of τ_ϕ^{-1}. By assuming $\Gamma \ll \tau_\phi^{-1} \ll T$, we make use of eq. 5.203 for $\tau_{\phi,ee}^{-1}$ and eq. 5.206 for $\tau_{\phi,fl}^{-1}$, and we plot the resulting solution to the self-consistent equation in fig. 6.5. From this we can see that our assumption $T \gg \tau_\phi^{-1}$ holds true within reason, whilst the assumption $\tau_\phi^{-1} \gg \Gamma$ is not so clearly supported.[3] Within the intermediate region we note that τ_ϕ^{-1} follows an $\eta^{-0.55}$ power law. However, unlike the examples for τ_ϕ^{-1} behaviour we gave in section 5.5.2, we have only included the $\mathbf{q} = \mathbf{0}$ components and allowed the close-to-T_c and intermediate self-consistent solution to run across all η. As a result, we see that the minimum phase

[3]The notion of a quantity being much larger than 1, or rather sufficiently large is very situational. Sometimes we find the large parameter limit is reached relatively quickly. So the notion of large is smaller in some cases than others.

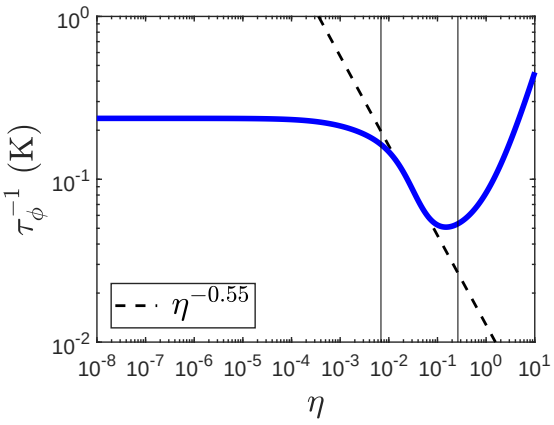

Figure 6.5: Total phase breaking rate based upon the parameters in eq. 6.1.

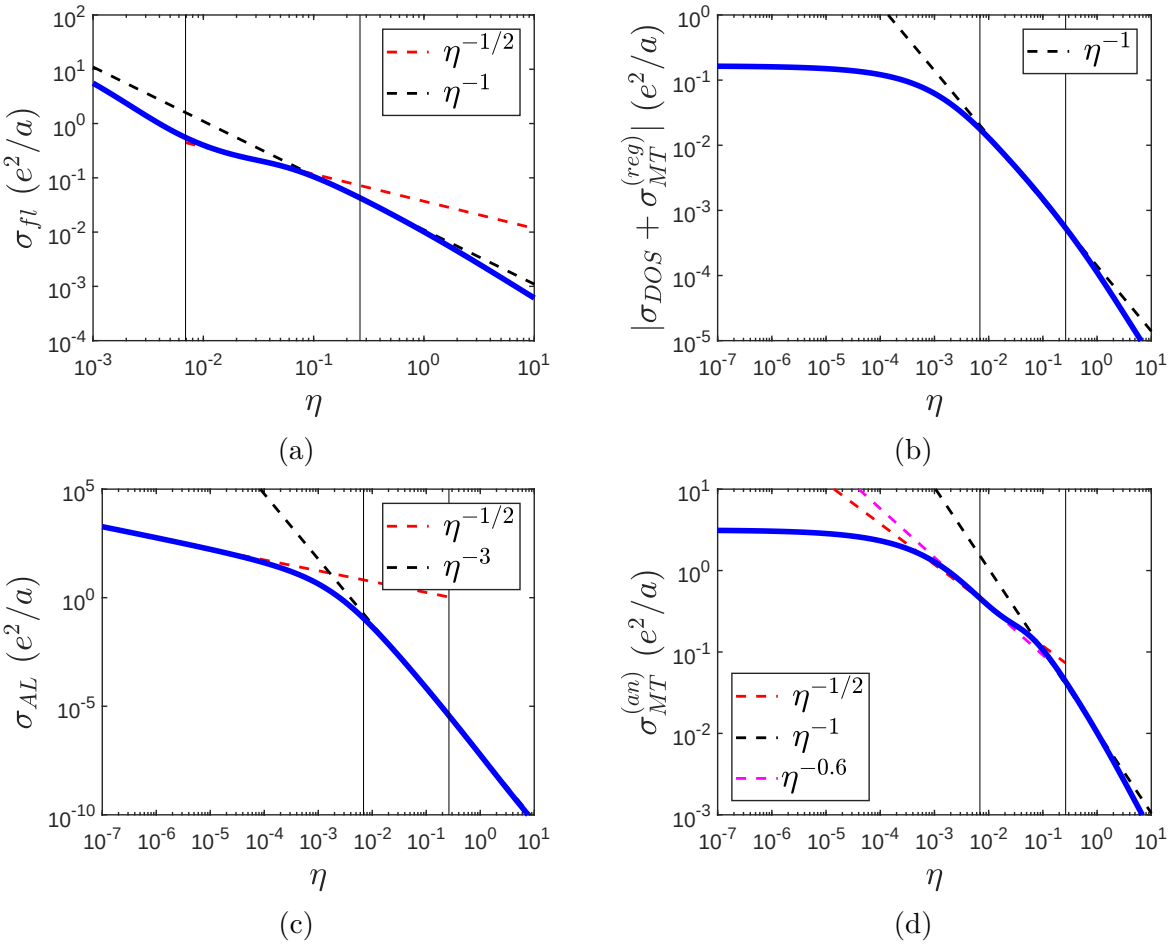

Figure 6.6: Theoretical predictions for the different contributions to the fluctuation conductivity including a temperature dependent phase breaking rate, using the parameters listed in eq. 6.1. The solid black vertical lines mark where $\eta = \Gamma/T_c$ and $\eta = E_{Th}/T_c$. (a): Total fluctuation conductivity. (b): DOS and regular MT contribution. (c): AL contribution. (d): Anomalous MT contribution.

breaking rate clearly occurs inside the intermediate region.

Our model of the phase breaking rate assumes that τ_ϕ^{-1} is small enough such that we may neglect its presence inside all digamma functions and digamma function derivatives. Hence, in the equations describing granular fluctuation conductivity in section 5.4, we take $\epsilon(\mathbf{0}, T) \simeq \ln(T/T_c)$ and $\alpha_n(\mathbf{0}, T) \simeq \psi^{(n)}(1/2)$. With these approximations, we obtain the plots shown in fig. 6.6, where we see that phase breaking has the effect of suppressing the anomalous MT contribution in the close-to-T_c region, whilst leaving the AL and DOS terms unaffected. Additionally, the behaviour of the anomalous MT term appears to be altered such that it no longer has an η^{-1} power law in the intermediate region. Rather, the anomalous MT contribution now appears to have a slight wobble in its behaviour. Around the close-intermediate boundary it has an approximately $\eta^{-0.6}$ power law, in the middle of the intermediate region an $\eta^{-1/2}$ power law can be seen, and finally an η^{-1} relation around the intermediate-far boundary.

Looking at the far-from-T_c region, we see that the anomalous MT term's $\eta^{-1/2}$ power law has also been suppressed. In the depths of the far-from-T_c region, the anomalous MT term begins to decrease with increasing temperature at a faster rate than η^{-1}, and resembles the DOS and regular MT behaviour in the same region. Combining the AL, MT, and DOS terms whilst including the temperature dependence of τ_ϕ^{-1}, see fig. 6.6a, we find a conductivity that does not possess an η^{-3} power law in the intermediate region, and bears no resemblance of Klemencic et. al.'s data. Let us now discuss what we can deduce from comparing theory to experiment.

6.3 Discussion

In the above we have seen that, without the inclusion of phase breaking mechanisms, we cannot reproduce a dominant η^{-3} power law over the range $10^{-2} \lesssim \eta \lesssim 10^{-1}$. In a naïve approach we initially assumed a constant phase breaking rate, and found that only for $\tau_\phi^{-1} \sim T_c$, were we able to obtain an η^{-3} power law over approximately one order

of magnitude in η. Phase breaking rates of a size comparable to T_c have been observed before in other systems [78, 79], and so we should not be too concerned regarding the size of τ_ϕ^{-1} in this case. However, this model introduced an uncharacteristic minimum into σ_{fl}, which is not seen experimentally. The minimum appearing in σ_{fl} may seem unphysical; however the experimental data for G_{fl} is extremely small, and so is very sensitive to the fitting of EEIs plus Drude. Hence, a small change in the high temperature fitting may allow for a minimum to exist in the fluctuation conductivity. Overall, this assumption of a constant τ_ϕ^{-1} allowed for a semi-quantitative agreement between theory and experiment.

Despite the lack of η^{-3} behaviour in the intermediate region when $\tau_\phi^{-1} = 0$K, we did obtain an $\eta^{-1/2}$ power law in the far-from-T_c region without the inclusion of intragranular momenta. This behaviour was a consequence of the anomalous MT term. Whilst this power law behaviour is serendipitous, we may be able to probe whether it is the result of the anomalous MT contribution by applying a magnetic field to increase the phase breaking rate. If the observed far-from-T_c behaviour is due to the anomalous MT term, we would expect it to be replaced by DOS type behaviour at higher field strengths.

After considering a constant phase breaking rate, we applied our model for the temperature dependence of τ_ϕ^{-1} and found that $\tau_\phi^{-1} \sim 10^{-1}$K, under the assumption that $\Gamma \ll \tau_\phi^{-1} \ll T$. We saw that the resulting phase breaking rate only varied significantly in the intermediate region, where it obeyed an $\eta^{-0.55}$ power law and reached a minimum value of $\tau_\phi^{-1} \sim 0.05$K. Upon substituting this into the AL, MT, and DOS terms, we saw that the total fluctuation conductivity was drastically different to the case with no phase breaking, and the case of a constant phase breaking rate. The changes we saw lead to an alteration of the anomalous MT contribution in all regions, such that it was heavily suppressed in the close-to-T_c and far-from-T_c regions. The intermediate behaviour became quite muddled, with different power laws appearing for short ranges of η. We therefore cannot assign a definite form of relation between $\sigma_{MT}^{(an)}$ and η in this region.

In all cases we were unable to produce crossovers that were as sharp as those observed in experiment. This is a point that remains to be explored and replicated through some

means. Furthermore, our assumption $\tau_\phi^{-1} \gg \Gamma$ may not be valid, and so the reduced temperature dependence of τ_ϕ^{-1} plotted in fig. 6.5 may not be entirely accurate in the intermediate region. However, in the close-to-T_c region and deep in the far-from-T_c region, τ_ϕ^{-1} can be argued to be sufficiently large for our approximations to hold. In any case, we can expect the phase breaking rate to be in the range $0.01\text{K} \lesssim \tau_\phi^{-1} \lesssim 0.1\text{K}$, and so not suppress the intermediate MT sufficiently to allow the AL term to dominate. Given that the crossovers in both σ_{fl} and τ_ϕ^{-1} are not sharp changes, it is unlikely that the model we are currently considering will produce a phase breaking rate sufficient to modify the anomalous MT term, such that it replicates an η^{-3} power law in the intermediate region.

Finally, let us address the assumptions behind the fitting procedure. By fitting a function of the form $1/(aT^{1/2} + b)$ to the high temperature resistance data, we have assumed the standard homogeneous 3D form for the EEI contribution to the electrical conductivity. To obtain such behaviour in granular systems requires $\Gamma \gg T$, see section 5.3. However, to see crossovers in the fluctuation conductivity requires us to assume $\Gamma \ll T_c$, and so the two models we are trying to apply to the data appear to be from contradicting limits. This leaves us with a very interesting set of questions regarding the physics observed in BNCD systems that are yet to be answered.

If the high temperature fit is correct, what exactly is the physics we are seeing in the fluctuation conductivity? Crossovers in σ_{fl} are not seen in 3D homogeneous systems,[4] so clearly this must be a result of granularity. However, the only model we have seen describing two crossovers is the one originally presented by Lerner et. al. [27], which we have extended in this thesis. If other mechanisms are present, we will need to first understand what is responsible for their presence. It is not currently clear what other physics may play a role in this system.

If the fluctuation theory is correct, what is the origin of the $T^{1/2}$ high temperature behaviour? Perhaps phonons play a more significant role in granular systems, or BNCD

[4]Crossovers can be seen in homogeneous thin films, as far from the transition the virtual cooper pair coherence length is much smaller than the film thickness, and so the material appears 3D. Approaching T_c, the cooper pair coherence length becomes greater than the film thickness, and so the system now appears 2D in nature. Hence we see a 3D-2D crossover when approaching the transition from above.

in particular. To check this would require further work beyond that presented in this thesis.

On the topic of phonons, perhaps our assumption of the BCS interaction only being local to a grain is not always applicable. To deal with two-body interactions that have both internal and external DOFs is an area for further study. We should note that spin glass behaviour has also been observed by Klemencic et. al. [28] in the same BNCD films, which suggests the ability for each grain to possess its own superconducting order parameter. For independent order parameters, a BCS interaction local to a grain would be an accurate description of the system. However, if the order parameter phases are able to interact this would suggest some form of Cooper pair interaction between grains. Hence, an accurate description of BNCD may require a theory of superconducting fluctuations that allows for an intergranular BCS interaction.

CHAPTER 7

CONCLUSION

In this thesis we started by deriving the building blocks for diagrammatic quantum field theory in chapter 2. In chapter 3, we showed how these ideas could be used to calculate the electrical conductivity of a disordered homogeneous metal to obtain the Drude conductivity and the weak localisation correction to this result. Furthermore, we showed how to reproduce the temperature dependence of the conductivity corrections due to the Coulomb interaction between electrons (EEIs), and due to virtual Cooper pairs appearing near the superconducting transition whilst in the normal state; these results are well known in the literature, see [39] and [56] respectively. Finally, this chapter showed how to calculate the temperature dependence of the phase breaking rate, τ_ϕ^{-1}, generated by EEIs and virtual Cooper pairs. Understanding τ_ϕ^{-1} is vital in avoiding the divergences that appear in 1D and 2D systems when considering the effects of weak localisation and superconducting fluctuations.

Following on from this in chapter 4, we developed a set of diagrammatic rules analogous to those obtained in chapter 2, which allowed us to construct a field theoretic description of a granular system. These ideas were based upon the prior works of Beloborodov et. al. [26], Biagini et. al. [67], Lerner et. al. [27], and Barone and Paternò [71]. Unlike prior works, however, we incorporated the DOFs internal to a grain and external to a grain (i.e. the lattice DOFs) simultaneously. We further introduced a statistical distribution to

describe the random distribution of tunnelling energies associated to each grain boundary. This allowed us to perform a disorder average over tunnelling events, and so obtain a granular disorder-averaged electron Green's function which had knowledge of internal impurity scattering and of tunnelling between grains. This amounted to replacing τ_0^{-1}, the elastic scattering rate of electrons off of impurities, by $\tau^{-1} = \tau_0^{-1} + z\Gamma$ in the homogeneous disorder-averaged electron Green's function. Here Γ is the electron tunnelling rate between two grains, and z is the coordination number of grains. The inclusion of both sets of DOFs also led to two-particle propagators and interactions having two momentum arguments: internal momenta associated to motion inside a grain, and external/lattice momenta associated to hopping between grains.

After this, chapter 5 showed how these rules for a granular system could be applied to a disordered granular metal to obtain the temperature dependence of the electrical conductivity in such materials. Here we provided an explicit derivation of the granular Drude conductivity, followed by the calculations of the WL, EEI, and superconducting fluctuation corrections to the electrical conductivity. We finished this chapter by calculating the phase breaking rate present in granular systems, where we found that a large number of parameters were involved, and hence allowed for several limits to exist in such materials. We considered two limits: one which gave results analogous to the homogeneous case, and a second to demonstrate what novel phase breaking rates might be present in disordered granular metals.

In these calculations we introduced a new limit in analogy to the homogeneous case, which we named the *granular diffusive limit*. This limit allowed for a simple mapping between the homogeneous results and granular results, where by letting $\mathcal{D} \to \mathcal{D}_T$ in the homogeneous corrections we obtained the granular results in the limit $\Gamma \gg T$.

In the limit $\Gamma \ll T$, we obtained new results unique to disordered granular metals in the case of EEIs, superconducting fluctuations, and phase breaking rates. For EEIs we saw that, in all dimensionalities, the conductivity correction would have a T^{-1} power law. For superconducting fluctuations we found three regions of behaviour to exist near

T_c, which agreed with the ideas of Lerner et. al. [27]. We found that in the *close-to-T_c region*, $\eta \ll \Gamma/T_c$ ($\eta = (T - T_c)/T_c$), the fluctuation conductivity, σ_{fl}, reflected the dimensionality of the system. Moving away from the transition into the *intermediate region*, $\Gamma/T_c \ll \eta \ll E_{Th}/T_c$, we found that the power law dependence of σ_{fl} upon η changed drastically, such that the AL contribution became quasi-0D in exhibiting an η^{-3} power law, whilst the anomalous MT and DOS terms generated η^{-1} power laws. Finally, by moving further away from the transition into the *far-from-T_c region*, $E_{Th}/T_c \ll \eta \ll 1$, the behaviour of the anomalous MT and DOS terms returned to power laws that resembled the dimensionality of the system: the anomalous MT term behaved as $\eta^{(d-4)/2}$, whilst the DOS term became approximately constant. In contrast, the AL term produced an $\eta^{(d-6)/2}$ correction.

In general, the anomalous MT and DOS terms have d-dimensional behaviour in the close-to-T_c and far-from-T_c regions due to being second order in tunnelling. However, the AL term is fourth order in tunnelling, and so each block of its diagram generates a factor of $Q_\alpha a$, where a is the typical grain size, but no analogous factor for the internal momentum $\mathbf{q}$. Hence, the internal and external momentum integrals give rise to different power laws.

Regarding the order of each term, we saw that, in the absence of phase breaking, the AL term was always dominated by the anomalous MT term in the intermediate and far-from-T_c regions. The DOS was also dominated by the anomalous MT term in these regions when phase breaking was negligible, and so we expect in granular systems with $\Gamma \ll E_{Th} \ll T_c$,

$$\sigma_{fl} \sim \frac{e^2}{a} \times \begin{cases} \sqrt{\dfrac{T_c}{\Gamma}}\eta^{-1/2}, & \eta \ll \dfrac{\Gamma}{T_c} \\ \eta^{-1}, & \dfrac{\Gamma}{T_c} \ll \eta \ll \dfrac{E_{Th}}{T_c} \\ \sqrt{\dfrac{\Gamma^2 T_c}{E_{Th}^3}}\eta^{-1/2}, & \dfrac{E_{Th}}{T_c} \ll \eta \ll 1, \end{cases} \tag{7.1}$$

when $\tau_\phi^{-1} = 0$.

Furthermore, each region of behaviour can also be related to the coherence length of a virtual Cooper pair compared to the size of a grain. We showed that the virtual Cooper pair propagator contained two coherence lengths: one associated to the internal DOFs, $\xi_{v,g}$, and another associated to the external DOFs, $\xi_{v,T}$. The close-to-T_c region corresponds to when $\xi_{v,g}, \xi_{v,T} \gg a$, the intermediate region occurs when $\xi_{v,g} \gg a \gg \xi_{v,T}$, and the far-from-$T_c$ region can be seen when $a \gg \xi_{v,g}, \xi_{v,T}$.

Finally, in chapter 6 we compared our model of a disordered granular metal to the experiments of Klemencic et. al. [77], who measured the temperature variation of resistance in boron-doped nanocrystalline diamond (BNCD) films. In their work they observed three crossovers in the fluctuation conductivity, and so used the ideas of Lerner et. al. [27] to determine the values of Γ and E_{Th} in various BNCD films. Specifically, they saw $\eta^{-1/2}$ behaviour in the close-to-T_c and far-from-T_c regions, whilst the intermediate region possessed an η^{-3} power law. Hence, the fluctuation conductivity has 3D-q0D-3D behaviour.

To understand the results of Klemencic et. al. [28], we started the chapter by reproducing their data analysis to obtain the fluctuation conductivity, which required a high temperature conductivity fitting of the form $\sigma_0 + bT^{1/2}$. This would imply that the system is not only 3D, but also in the limit $\Gamma \gg T$. However, in looking at the data and using an approximate temperature for where the resistance vanishes, the remaining fluctuation conductivity clearly exhibited three regions of behaviour, with the intermediate region displaying an η^{-3} power law. According to our model, this appears to disagree with the high temperature fitting, as this would require $\Gamma \ll E_{Th} \ll T_c$. Not only do we have a discrepancy, but the intermediate power law is also indicative of the AL term. Under the assumption that our model for σ_{fl} is applicable to BNCD, this would require a significant phase breaking rate to suppress the anomalous MT term, such that it would cancel almost perfectly with the DOS term. Without a phase breaking rate, the fluctuation conductivity gave the same behaviour as that listed in eq. 7.1 and gave rise to gradual crossovers, rather than the sharp changes at the region boundaries that are seen in experiment.

The inclusion of a constant phase breaking rate would require $\tau_\phi^{-1} \sim T_c$ to produce an η^{-3} power law, but then gave rise to a minimum not seen in the fluctuation data. However the magnitude of the data at this point is rather small, and so can be affected notably by the high temperature fitting. Therefore, a slight change in the high temperature fitting might allow for a minimum to arise near the intermediate-far crossover.

Finally, by including our model for a temperature dependent phase breaking rate, we found that τ_ϕ^{-1} was significantly smaller than the constant τ_ϕ^{-1} values we previously considered. Thus, the AL η^{-3} power law was not observable with the inclusion of our model for a temperature dependent phase breaking rate. We also saw that the behaviour of τ_ϕ^{-1} modified the anomalous MT contribution, not only by suppressing it slightly, but also changing its apparent power law behaviour. However, this change in the anomalous MT term's behaviour also did not produce an η^{-3} power law in the intermediate region.

We are therefore left with several questions regarding both the theoretical model and the physics observed experimentally. The first major point to clarify is can we obtain a $T^{1/2}$ dependence far away from T_c when $\Gamma \ll T_c$? If this behaviour is purely the result of EEIs, then we will have to search for extra diagrams in the theory that may be of equal importance to those already considered. Perhaps the behaviour seen experimentally might correspond to the granular analogue of the intermediate region of behaviour between the diffusive and ballistic limits. If the $T^{1/2}$ dependence is not due to EEIs, we are left needing to determine what the appropriate mechanism is from both a theoretical and experimental perspective. One possible avenue is to consider the role of phonons in granular metals beyond the standard BCS treatment.

In contrast, we could ask: if $\Gamma \gg T$, can we still obtain a fluctuation conductivity with three regions of behaviour? If so, what do the region boundaries correspond to? These questions are far less straightforward to answer, as our current understanding leads us to believe the crossovers can only occur due to the singular nature of the pair propagator near the transition. Our task would be to see if we are able to introduce other scales into the pair propagator that allowed for $\Gamma \gg T$, such that η could be smaller or greater

than the new scales whilst still satisfying $\eta \ll 1$. One possible avenue to explore is the modification of our BCS term to allow it to couple electrons in different grains.

Given that an η^{-3} power law is seen in σ_{fl} experimentally, it would be reasonable to attribute this to the AL term we calculated in chapter 5. Our focus should therefore be on trying to explain how the AL term might dominate over the anomalous MT contribution. At present, it is not possible to say which route will ensure this to be true, whilst still producing three regions of behaviour in σ_{fl} close to the transition.

APPENDIX A

SECOND QUANTISATION & THE PICTURES OF QUANTUM MECHANICS

In this appendix we provide an outline of the ideas underlying second quantisation, and how we may write quantum many-body problems in a second-quantised form. We shall also cover the different pictures of quantum mechanics we may consider when understanding the time evolution of observables from the operators and states relevant to the problem.

A.1 Second Quantisation

Let us first summarise the construction of second quantisation, where we closely follow the style of [34].[1] Starting from a single-particle picture, we define the set of normalised single-particle states, $\{|\lambda\rangle\}$, in terms of a set of eigenvalues we collectively refer to as λ, which also form a set, $\{\lambda\}$.[2] We may then construct a many-body state vector with N

[1] Second quantisation is sometimes referred to as the occupation number representation.

[2] Example eigenvalues include the energy, spin, and position of the particle. In the case of the hydrogen atom the eigenvalues we have are the energy level, n, angular momentum, l, and the z-component of angular momentum m, and so $\lambda = \{n, l, m\}$.

particles, for a specific realisation of the particles' distribution amongst $\{|\lambda\rangle\}$, by taking a direct product of the N single-particle states,

$$|\lambda_1, \lambda_2, ..., \lambda_N\rangle' = |\lambda_1\rangle_1 \otimes |\lambda_2\rangle_2 \otimes ... \otimes |\lambda_N\rangle_N \,, \tag{A.1}$$

where λ_i is eigenvalue of the i^{th} particle, the subscript on each single-particle state's ket emphasises the particle to which the state belongs, and the prime on the many-body state vector denotes the fact this is not the general N-particle state for a given $\{\lambda_i\}$, but rather one possible state we can make with N particles. We also assume a natural ordering to the set $\{\lambda_i\}$, such that we have a positive coefficient for the the state with the set of λ_i ordered such that i is ascending. This is a simple convention of convenience, as we are only concerned with the change of phase caused by changing the order of the λ_i between different many-body states.

Another possible many-body state that has the same distribution of particles can be created by simply swapping $|\lambda_1\rangle_1$ and $|\lambda_2\rangle_2$ in the direct product,

$$|\lambda_1, \lambda_2, ..., \lambda_N\rangle' = -\eta\, |\lambda_2\rangle_2 \otimes |\lambda_1\rangle_1 \otimes ... \otimes |\lambda_N\rangle_N \,, \tag{A.2}$$

recalling $\eta = +1$ for fermions, and $\eta = -1$ for bosons. Clearly, a complete description of a general N-particle state with a specific $\{\lambda_i\}$ will have to be the superposition of all possible permutations of $\{\lambda_i\}$. Therefore, the most general normalised many-body state vector we can write in this case is,

$$|\lambda_1, \lambda_2, ..., \lambda_N\rangle = \frac{1}{\sqrt{N! \prod_\lambda (n_\lambda!)}} \sum_{\mathcal{P}} (-\eta)^{\frac{1-\text{sgn}(\mathcal{P})}{2}} |\lambda_{\mathcal{P}_1}\rangle_{\mathcal{P}_1} \otimes |\lambda_{\mathcal{P}_2}\rangle_{\mathcal{P}_2} \otimes ... \otimes |\lambda_{\mathcal{P}_N}\rangle_{\mathcal{P}_N} \,, \tag{A.3}$$

where $\mathcal{P}$ is the permutation of the $\{\lambda_i\}$, $\mathcal{P}_i$ is the i^{th} element of the permutation, $\text{sgn}(\mathcal{P}) = \pm 1$ for even/odd permutations,[3] and n_λ is the number of particles with the same set of

[3]For example, eq. A.1 has $\mathcal{P} = 1, 2, ..., N$ and $\text{sgn}(\mathcal{P}) = +1$, whilst eq. A.2 has $\mathcal{P} = 2, 1, ..., N$ and $\text{sgn}(\mathcal{P}) = -1$.

eigenvalues, λ.[4] The factor of $1/\sqrt{N!}$ comes from the $N!$ possible permutations of the N particles, whilst $1/\sqrt{\prod_\lambda (n_\lambda!)}$ is needed to prevent over-counting due to the indistinguishability of particles in the same state. Note that for bosons $n_\lambda \in \mathbb{Z}_0^+$ (all non-negative integers), whilst $n_\lambda \in \{0, 1\}$ for fermions.

In writing eq. A.3 it becomes clear this will be a rather cumbersome formulation of many-body quantum mechanics. In fact, we do not need to write down which state each particle occupies, but rather how many particles are in a specific state. Thus instead of having to write out the set $\{\lambda_i\}$ we can instead write the set of occupation numbers of each state λ, $\{n_\lambda\}$. Using this idea we can then rewrite the many-body state vector for N particles as,

$$|\lambda_1, \lambda_2, ..., \lambda_N\rangle = |n_1, n_2, ...\rangle = |\{n_\lambda\}\rangle\,, \qquad \text{subject to} \qquad \sum_\lambda n_\lambda = N, \tag{A.4}$$

where we now let $\lambda = 1, 2, 3, ...$ for convenience.

Now to construct a many-body state, we can imagine starting from the vacuum state and adding particles one-by-one until we have the state we wish to consider. In order to construct operators capable of this we need to generalise the N-particle Hilbert space, $\mathcal{H}_N$, to allow for changing particle numbers. When constructing the N-particle state vector in eq. A.3 we worked with a fixed distribution of particles. The complete basis spanning all of $\mathcal{H}_N$ is given by considering all possible distributions of the particles amongst the λ states. Therefore $\{|\{n_\lambda\}\rangle\}$ with $\sum_\lambda n_\lambda = N$ forms the complete basis for $\mathcal{H}_N$.

The space with varying particle number can then be constructed by performing the direct sum of Hilbert spaces for all possible number of particles,

$$\mathcal{F} = \mathcal{H}_0 \oplus \mathcal{H}_1 \oplus \mathcal{H}_2 \oplus ... = \bigoplus_{N=0}^{\infty} \mathcal{H}_N. \tag{A.5}$$

This is called a Fock space. The inclusion of $\mathcal{H}_0$ includes the state with no particles, the

[4]For example, if $\lambda_1 = \lambda_2 = \widetilde{\lambda}$ and all other λ_i for unique, then $n_\lambda = 0$ or $1\,\forall\,\lambda \neq \widetilde{\lambda}$ whilst $n_{\widetilde{\lambda}} = 2$. Note this is only concerned the single-particle states, and not the particle index.

vacuum state, which we denote by $|0\rangle$. The complete basis spanning the Fock space is then given by the set of all basis vectors for each Hilbert space in the direct sum,

$$\{|\{n_\lambda\}\rangle\} = \left\{ |0\rangle\,, \{|\lambda\rangle\}, \{|\{n_\lambda\}\rangle\}\Big|_{\sum_\lambda n_\lambda=2}, \{|\{n_\lambda\}\rangle\}\Big|_{\sum_\lambda n_\lambda=3}, ... \right\}. \tag{A.6}$$

We now define a set of operators responsible for creating and annihilating particles in the state λ. These allow us to move between the different N-particle Hilbert spaces, and to build up the many-body state we wish to consider.

Specifically, the operator $a^\dagger_\lambda$ creates a particle in state λ, whilst its partner a_λ annihilating a particle in the state λ. Fittingly, these operators are called creation and annihilation operators respectively. Formally, they act on a many-body state, in an extremely similar manner to the ladder operators of the harmonic oscillator, according to

$$\begin{aligned} a^\dagger_{\lambda'} |\{n_\lambda\}\rangle &= (-\eta)^{s_{\lambda'}} \sqrt{n_j + 1}\, |n_1, ..., n_{\lambda'} + 1, ...\rangle\,, \\ a_{\lambda'} |\{n_\lambda\}\rangle &= (-\eta)^{s_{\lambda'}} \sqrt{n_j}\, |n_1, ..., n_{\lambda'} - 1, ...\rangle\,, \end{aligned} \tag{A.7}$$

where $s_{\lambda'}$ is the number particles that occur in the states $\lambda < \lambda'$ according to our ordering convention,[5]

$$s_{\lambda'} = \sum_{\lambda<\lambda'} n_\lambda. \tag{A.8}$$

This allows us to write the many-body state vector, and so any basis vector for $\mathcal{F}$, in terms of creation operators acting upon the vacuum,

$$|\{n_\lambda\}\rangle = \prod_{\lambda'} \frac{1}{\sqrt{n_{\lambda'}!}} (a^\dagger_{\lambda'})^{n_{\lambda'}} |0\rangle\,. \tag{A.9}$$

Clearly acting a_λ on a state where $n_\lambda = 0$ annihilates the state, $a_\lambda |..., n_\lambda = 0, ...\rangle = 0$, and hence a_λ acting on the vacuum will always annihilate the state for any choice of λ. Similarly, acting $a^\dagger_\lambda$ on a state with $n_\lambda = 1$ for fermions also annihilates the state due to Pauli exclusion, $a^\dagger_\lambda |..., n_\lambda = 1, ...\rangle = 0$. This property is also hidden in eq. A.7. Whilst

[5] Our ordering convention changes slightly here compared to the case where we listed all λ_i explicitly. Our ordering now puts the λ in ascending order.

it may seem that we can consider $n_{\lambda'} \geq 1$ without the creation operator producing a factor of zero, the state itself can be shown to equal zero. Consider acting $a^\dagger_{\lambda'}$ on a state with $n_{\lambda'} = 1$, we would then have to pass commute $a^\dagger_{\lambda'}$ through $s_{\lambda'}$ operators before it arrived next to the $a^\dagger_{\lambda'}$ operator already present in generating the state. According to eq. A.7 this would produce a state with $n_{\lambda'} = 2$ with a prefactor of $(-1)^{s_{\lambda'}}\sqrt{2}$. However, we can exchange the two $a^\dagger_{\lambda'}$ operators which produces an additional factor of (-1), but produces an entirely equivalent state with $n_{\lambda'} = 2$. Hence, the new state is equivalent to its negative, and hence must be zero.

Using eq. A.7 we can easily obtain the (anti-)commutation relations for (fermionic) bosonic creation and annihilation operators,

$$[a_\lambda, a^\dagger_{\lambda'}]_\eta = \delta_{\lambda\lambda'}, \qquad [a_\lambda, a_{\lambda'}]_\eta = 0, \qquad [a^\dagger_\lambda, a^\dagger_{\lambda'}]_\eta = 0, \tag{A.10}$$

where $[A, B]_\eta$ is the generalised commutator given in eq. 2.2.

We now consider a change of basis from the set of single-particle states $\{|\lambda\rangle\}$ to a new set of single-particle states $\{|\mu\rangle\}$. To move our creation operators into the μ basis we consider the definition of $a^\dagger$ in both bases,

$$|\lambda\rangle = a^\dagger_\lambda |0\rangle , \qquad |\mu\rangle = a^\dagger_\mu |0\rangle . \tag{A.11}$$

By multiplying $|\mu\rangle$ by identity, $\mathcal{I} = \sum_\lambda |\lambda\rangle \langle\lambda|$, we see

$$\begin{aligned} |\mu\rangle = \sum_\lambda |\lambda\rangle \langle\lambda|\mu\rangle = \sum_\lambda a^\dagger_\lambda \langle\lambda|\mu\rangle |0\rangle = a^\dagger_\mu |0\rangle , \\ \Rightarrow a^\dagger_\mu = \sum_\lambda \langle\lambda|\mu\rangle a^\dagger_\lambda \\ \Rightarrow a_\mu = \sum_\lambda \langle\mu|\lambda\rangle a_\lambda \end{aligned} \tag{A.12}$$

Hence we have obtained the transformation that moves our creation and annihilation operators from one basis into another. The inverse transformation to move from $\{|\mu\rangle\}$

back to $\{|\lambda\rangle\}$ is also given by these relations.

For many systems the natural basis to work in is one with a continuous set of quantum numbers (e.g: position coordinates). This is most certainly the case in transport phenomena where we typically label particles by their position and time coordinates. In this case we move from a discrete notation of the quantum numbers to a continuous one, $a^\dagger_\lambda \to a^\dagger(x)$. The transformations in eq. A.12 are left unchanged when moving from the $\{|\lambda\rangle\}$ basis to the $\{|x\rangle\}$ basis. The inverse transformation, however, replaces the sums with integrals due to the continuous nature of the basis being transformed from. That is to say,

$$\begin{aligned} a^\dagger_\lambda &= \int dx\, \langle x|\lambda\rangle\, a^\dagger(x), \qquad a_\lambda = \int dx\, \langle \lambda|x\rangle\, a(x), \\ a^\dagger(x) &= \sum_\lambda \langle \lambda|x\rangle\, a^\dagger_\lambda, \qquad a(x) = \sum_\lambda \langle x|\lambda\rangle\, a_\lambda. \end{aligned} \tag{A.13}$$

Let us therefore define a special set of operators in the basis of d-dimensional real space and spin, σ,

$$\psi^\dagger_\sigma(\mathbf{r}) = \sum_\lambda \langle \lambda|\mathbf{r}\rangle\, a^\dagger_{\lambda\,\sigma}, \qquad \psi_\sigma(\mathbf{r}) = \sum_\lambda \langle \mathbf{r}|\lambda\rangle\, a_{\lambda\,\sigma}. \tag{A.14}$$

We refer to these operators as field operators, where $\psi^\dagger_\sigma(\mathbf{r})$ creates a particle with spin σ at position $\mathbf{r}$, whilst $\psi_\sigma(\mathbf{r})$ annihilates a particle with spin σ at position $\mathbf{r}$. Further connection can be made to more familiar ideas of first quantisation by noting that $\langle \mathbf{r}|\lambda\rangle = \phi_\lambda(\mathbf{r})$ is just the time independent wavefunction of a particle in the state λ. We therefore arrive at the commonly quoted definition of field operators

$$\psi^\dagger_\sigma(\mathbf{r}) = \sum_\lambda \phi^*_\lambda(\mathbf{r}) a^\dagger_{\lambda\,\sigma}, \qquad \psi_\sigma(\mathbf{r}) = \sum_\lambda \phi_\lambda(\mathbf{r}) a_{\lambda\,\sigma}. \tag{A.15}$$

These operators satisfy the generalised equal-time (anti-)commutation relations

$$\begin{aligned} [\psi_\sigma(\mathbf{r}), \psi^\dagger_{\sigma'}(\mathbf{r}')]_\eta &= \delta^{(d)}(\mathbf{r}-\mathbf{r}')\delta_{\sigma\sigma'}, \\ [\psi_\sigma(\mathbf{r}), \psi_{\sigma'}(\mathbf{r}')]_\eta = 0, \qquad & [\psi^\dagger_\sigma(\mathbf{r}), \psi^\dagger_{\sigma'}(\mathbf{r}')]_\eta = 0. \end{aligned} \tag{A.16}$$

We will introduce time dependence to these operators when we consider the different pictures of quantum mechanics. Currently, these operators are written in the Schrödinger picture (i.e: they are time independent).

Having outlined the construction of a more intuitive representation of quantum mechanics for many-body systems, we now show how one translates general operators describing particle interactions from first quantisation to second quantisation.

A.1.1 Single-Particle Operators

Single particle operators act upon one particle at a time, and do not model the effects of interactions between particles. Examples of these operators include the kinetic energy, $\widehat{T}$, and potential $\widehat{U}$,

$$\widehat{T} = \sum_{i=1}^{N} \frac{1}{2m}\hat{p}_i^2, \qquad \widehat{U} = \sum_{i=1}^{N} U(\hat{x}_i), \tag{A.17}$$

where $\hat{p}_i$ is the momentum operator acting on the i^{th} particle, and $\hat{x}_i$ is the position operator of the i^{th} particle. This section focuses on representing operators of this type on a second-quantised form.

We start by defining the occupation number operator,

$$\hat{n}_\lambda = a^\dagger_\lambda a_\lambda, \tag{A.18}$$

which simply counts the number of particles occupying the state λ, $\hat{n}_{\lambda'} |\{n_\lambda\}\rangle = n_{\lambda'} |\{n_\lambda\}\rangle$. Let us now consider a generic single-particle operator, $\mathcal{O}_1$, formed of the individual operators $\hat{o}_i$ acting on the i^{th} particle, $\mathcal{O}_1 = \sum_i \hat{o}_i$. The individual operators are diagonal in the λ basis with eigenvalues o_λ, $\hat{o}_i |\lambda\rangle_i = o_\lambda |\lambda\rangle_i$.

Using this definition of $\mathcal{O}_1$ we see

$$\langle\{n'_\lambda\}|\,\mathcal{O}_1\,|\{n_\lambda\}\rangle = \left(\sum_\lambda o_\lambda n_\lambda\right)\langle\{n'_\lambda\}|\{n_\lambda\}\rangle = \langle\{n'_\lambda\}|\left(\sum_\lambda o_\lambda \hat{n}_\lambda\right)|\{n_\lambda\}\rangle\,. \tag{A.19}$$

Hence we may write the second-quantised form of $\mathcal{O}_1$ in a diagonal basis as,

$$\mathcal{O}_1 = \sum_\lambda \langle\lambda|\,\hat{o}\,|\lambda\rangle\, a^\dagger_\lambda a_\lambda, \tag{A.20}$$

where $\hat{o}$ is the one particle operator acting on a generic particle. Finally, we move to a general set of bases by inserting the identity between $\hat{o}$ and the two state vectors, making use of eq. A.12, and noting that due to being in a diagonal basis we may write,

$$\mathcal{O}_1 = \sum_{\lambda,\lambda'} \langle\lambda|\,\hat{o}\,|\lambda'\rangle\, a^\dagger_\lambda a_{\lambda'}. \tag{A.21}$$

Using these ideas we arrive at

$$\mathcal{O}_1 = \sum_{\mu,\nu} \langle\mu|\,\hat{o}\,|\nu\rangle\, a^\dagger_\mu a_\nu. \tag{A.22}$$

Thus we have arrived at the general expression for a single-particle operator written in second-quantised form. For continuous variables eq. A.22 becomes

$$\mathcal{O}_1 = \int d^d r \int d^d r'\, \langle\mathbf{r}|\,\hat{o}\,|\mathbf{r}'\rangle\, a^\dagger(\mathbf{r}) a(\mathbf{r}'). \tag{A.23}$$

The Hamiltonian for a system of non-interacting particles in the presence of a single-particle potential may now be written as

$$H = \sum_{\mu,\nu} \left[T_{\mu\nu} + U_{\mu\nu}\right] a^\dagger_\mu a_\nu. \tag{A.24}$$

To give this Hamiltonian a more intuitive form in terms of variables we are familiar with, let us try and write eq. A.24 in real space. Clearly the operator $\widehat{U}$ is diagonal in the real

space basis, and so we need only treat the kinetic energy piece differently. We note that the kinetic energy is diagonal in momentum space, and so we start from this basis

$$\begin{aligned}
\widehat{T} &= \int \frac{d^d p}{(2\pi)^d} \frac{p^2}{2m} a^\dagger(\mathbf{p}) a(\mathbf{p}) \\
&= \int \frac{d^d p}{(2\pi)^d} \int d^d p' \frac{\mathbf{p}\cdot\mathbf{p}'}{2m} a^\dagger(\mathbf{p}) a(\mathbf{p}')\, \delta^{(d)}(\mathbf{p}-\mathbf{p}') \\
&= \int \frac{d^d p}{(2\pi)^d} \int d^d p' \frac{\mathbf{p}\cdot\mathbf{p}'}{2m} a^\dagger(\mathbf{p}) a(\mathbf{p}') \int d^d r e^{i\mathbf{r}\cdot(\mathbf{p}'-\mathbf{p})} \\
&= \int d^d r \frac{1}{2m} \nabla \left[\int \frac{d^d p}{(2\pi)^{d/2}} e^{-i\mathbf{p}\cdot\mathbf{r}} a^\dagger(\mathbf{p}) \right] \cdot \nabla \left[\int \frac{d^d p'}{(2\pi)^{d/2}} e^{i\mathbf{p}'\cdot\mathbf{r}} a(\mathbf{p}') \right] \\
&= \int d^d r \frac{1}{2m} \nabla\psi^\dagger(\mathbf{r}) \cdot \nabla\psi(\mathbf{r}) \\
&= -\int d^d r\, \psi^\dagger(\mathbf{r}) \frac{\nabla^2}{2m} \psi(\mathbf{r}).
\end{aligned} \tag{A.25}$$

In the last line we integrated by parts in the knowledge that the surface term vanishes. Therefore we may write our single-particle interaction Hamiltonian as

$$H = \int d^d r\, \psi^\dagger(\mathbf{r}) \left[\frac{-\nabla^2}{2m} + U(\mathbf{r}) \right] \psi(\mathbf{r}). \tag{A.26}$$

Looking at the above we can see that the second-quantised form of the Hamiltonian is easily related to the single-particle operators, which are simply sandwiched between two field operators and integrated over all space.

A.1.2 Two-particle operators

Let us consider a generic two-particle operator, $\mathcal{O}_2$, which is formed of individual two-body interactions represented by the operator $\hat{V}$. For the problems we consider, we further assume $\hat{V}$ is symmetric between states, $\hat{V}_{mn} = \hat{V}_{nm}$, where m and n label the particles in states m and n respectively. Thus we may write

$$\mathcal{O}_2 = \sum_{m<n} \hat{V}_{mn} = \frac{1}{2} \sum_{m\neq n} \hat{V}_{mn}, \tag{A.27}$$

We may rewrite $\mathcal{O}_2$ in terms of the number of particles occupying the single-particle state $|\lambda\rangle$, which we assume to be the diagonal basis [80],

$$\begin{gathered}\mathcal{O}_2 = \frac{1}{2}\sum_{\lambda\neq\lambda'}\hat{n}_\lambda\hat{n}_{\lambda'}V_{\lambda\lambda'} + \frac{1}{2}\sum_{\lambda}\hat{n}_\lambda(\hat{n}_\lambda - 1)V_{\lambda\lambda} = \frac{1}{2}\sum_{\lambda,\lambda'}\hat{n}_\lambda(\hat{n}_{\lambda'} - \delta_{\lambda\lambda'})V_{\lambda\lambda'}, \\ V_{\lambda\lambda'} = V_{\lambda\lambda'\lambda'\lambda} = \langle\lambda,\lambda'|\,\hat{V}\,|\lambda,\lambda'\rangle\end{gathered} \tag{A.28}$$

where the second term of the first line describes a particle interacting with the remaining particles in the same state, which clearly vanishes in the case of fermions where $n_\lambda = 0, 1$.

Further progress is made by using the commutation relation,

$$[a_\lambda, \hat{n}_{\lambda'}] = \delta_{\lambda\lambda'}a_{\lambda'}, \tag{A.29}$$

to show

$$\begin{aligned}\hat{n}_\lambda(\hat{n}_{\lambda'} - \delta_{\lambda\lambda'}) &= a_\lambda^\dagger\left(a_\lambda^\dagger\hat{n}_{\lambda'} - [a_\lambda, \hat{n}_{\lambda'}]\right) \\ &= a_\lambda^\dagger a_{\lambda'}^\dagger a_{\lambda'}a_\lambda.\end{aligned} \tag{A.30}$$

Consequently, the second-quantised form of a two-particle operator in a diagonal single-particle basis is

$$\mathcal{O}_2 = \frac{1}{2}\sum_{\lambda,\lambda'}a_\lambda^\dagger a_{\lambda'}^\dagger V_{\lambda\lambda'}a_{\lambda'}a_\lambda. \tag{A.31}$$

As before, let us now move to a general non-diagonal basis. To do this we require the identity operator for a two-particle Hilbert space[6],

$$\mathcal{I}_2 = \sum_{\alpha,\beta}|\alpha,\beta\rangle\langle\alpha,\beta|\,. \tag{A.32}$$

Inserting this between $\hat{V}$ and the two state vectors in conjunction with eq. A.12, we

[6]In general a many-body state is written as the direct product of single-particle states, $|\alpha,\beta\rangle = |\alpha\rangle_1 \otimes |\beta\rangle_2$. Here $|\alpha\rangle$ is the single-particle state of particle 1, whilst $|\beta\rangle$ is the single-particle state of particle 2. See [34, 81] for in depth discussions on this topic.

obtain the well known second-quantised form for a two-particle operator

$$\begin{aligned} \mathcal{O}_2 &= \frac{1}{2}\sum_{\alpha,\beta,\gamma,\delta} a_\alpha^\dagger a_\beta^\dagger V_{\alpha\beta\gamma\delta} a_\gamma a_\delta, \\ V_{\alpha\beta\gamma\delta} &= \langle \alpha,\beta|\, \hat{V}\, |\gamma,\delta\rangle\,. \end{aligned} \tag{A.33}$$

In the case of a continuous basis, eq. A.33 becomes

$$\mathcal{O}_2 = \frac{1}{2}\int d^d r_1 \int d^d r_2 \int d^d r_3 \int d^d r_4 a^\dagger(\mathbf{r}_1) a^\dagger(\mathbf{r}_2) V(\mathbf{r}_1,\mathbf{r}_2,\mathbf{r}_3,\mathbf{r}_4) a(\mathbf{r}_3) a(\mathbf{r}_4). \tag{A.34}$$

As an example consider the Coulomb interaction, $V(\mathbf{r},\mathbf{r}') = V(\mathbf{r}-\mathbf{r}')$, which is in the form of a two-particle operator written in a diagonal single-particle position and spin basis. The resulting second-quantised operator may therefore be written in terms of field operators as

$$H_{\text{int}} = \frac{1}{2}\sum_{\sigma,\sigma'} \int d^d r \int d^d r' \psi_\sigma^\dagger(\mathbf{r}) \psi_{\sigma'}^\dagger V(\mathbf{r}-\mathbf{r}') \psi_{\sigma'}(\mathbf{r}') \psi_\sigma(\mathbf{r}). \tag{A.35}$$

A.1.3 The Pictures of Quantum Mechanics

Within quantum mechanics there exist different ways in which to view the time evolution of a system. The first, and most intuitive, picture of quantum mechanics most physicists encounter is the Schrödinger picture, in which all time evolution of a system is carried by the wave functions (states) of the particles involved. In this case the operators remain constant whilst the states evolve according to the unitary time evolution operator, $\mathcal{U}$,

$$|\psi(t)\rangle_S = \mathcal{U}(t)\,|\psi(0)\rangle_S = e^{-iHt}\,|\psi(0)\rangle_S\,, \tag{A.36}$$

where we have assumed a time independent Hamiltonian.

In contrast to this, we may choose all time evolution to be contained in the operators, thus leaving us with the time-independent states $|\psi\rangle_H = |\psi(0)\rangle_S = e^{iHt}\,|\psi(t)\rangle_S$. This

leads us to the Heisenberg picture. Here the operators evolve in time via

$$\mathcal{O}_H(t) = \mathcal{U}^\dagger(t)\,\mathcal{O}_S\,\mathcal{U}(t) = e^{iHt}\,\mathcal{O}_S\,e^{-iHt}. \tag{A.37}$$

These two pictures are physically equivalent as they give rise to the same expectation values of any observable. This can be seen by considering an expectation value in the Schrödinger picture

$${}_S\langle\psi(t)|\mathcal{O}_S\,|\psi(t)\rangle_S = \langle\psi(0)|\,\mathcal{U}^\dagger(t)\,\mathcal{O}_S\mathcal{U}(t)\,|\psi(0)\rangle = {}_H\langle\psi|\mathcal{O}_H(t)\,|\psi\rangle_H\,. \tag{A.38}$$

A consequence of this picture is a resulting equation of motion for the operators. It is easy to show

$$\frac{d\mathcal{O}_H}{dt} = i\,[H, \mathcal{O}_H]\,, \tag{A.39}$$

which is known as the Heisenberg equation of motion (EOM).

Finally, a third viewpoint can be taken which allows for perturbative treatment of interactions in a system. Fittingly, this is referred to as the interaction picture. Here both operators and states evolve in time, though through different relations. Consider a Hamiltonian described by an exactly soluble (typically non-interatcting) piece, H_0, whose corrseponding single-particle Green's function can be found through the methods of section 2.3, and a two-particle interacting piece we wish to focus on, H_{int},

$$H = H_0 + H_{\text{int}}. \tag{A.40}$$

We define the operators and states in the interaction picture as

$$\widetilde{\mathcal{O}}(t) = e^{iH_0t}\,\mathcal{O}_S\,e^{-iH_0t} = \mathcal{U}_0^\dagger(t)\,\mathcal{O}_S\,\mathcal{U}_0(t), \tag{A.41a}$$

$$|\widetilde{\psi}(t)\rangle = e^{iH_0t}\,|\psi(t)\rangle_S = \mathcal{U}_0^\dagger(t)\,\mathcal{U}(t)\,|\psi\rangle_H\,, \tag{A.41b}$$

which looks extremely similar to the Heisenberg picture, but with H_0 in place of H.

Naïvely, this can be thought of as removing the non-interacting piece of the time evolution from the states and putting it on the operators.[7] From Heisenberg's EOM and eq. A.41, we can show that operators and states in the interaction picture evolve according to

$$\frac{d\widetilde{\mathcal{O}}}{dt} = i\left[H_0, \widetilde{\mathcal{O}}\right], \qquad\qquad i\frac{d}{dt}\left|\widetilde{\psi}(t)\right\rangle = \widetilde{H}_{\text{int}}(t)\left|\widetilde{\psi}(t)\right\rangle. \tag{A.42}$$

Clearly both time evolution relations look similar to their respective forms in the Heisenberg picture and Schrödinger picture respectively.

Following the formalism of [30], we integrate the second part of eq. A.42 to write down a solution for the state $|\widetilde{\psi}(t)\rangle$,[8]

$$\left|\widetilde{\psi}(t)\right\rangle = \left|\widetilde{\psi}(t_0)\right\rangle - i\int_{t_0}^{t} dt' \widetilde{H}_{\text{int}}(t')\left|\widetilde{\psi}(t')\right\rangle. \tag{A.43}$$

This can be solved iteratively by repeatedly substituting eq. A.43 into itself to produce an infinite series solution

$$\begin{aligned} \left|\widetilde{\psi}(t)\right\rangle &= \sum_{n=0}^{\infty}\left|\widetilde{\psi}^{(n)}(t)\right\rangle, \quad \left|\widetilde{\psi}^{(0)}(t)\right\rangle = \left|\widetilde{\psi}(t_0)\right\rangle, \\ \left|\widetilde{\psi}^{(n)}(t)\right\rangle &= (-i)^n \int_{t_0}^{t} dt_1 \ldots \int_{t_0}^{t_{n-1}} dt_n\, \widetilde{H}_{\text{int}}(t_1)\ldots\widetilde{H}_{\text{int}}(t_n)\left|\widetilde{\psi}(t_0)\right\rangle, \end{aligned} \tag{A.44}$$

where $t \geq t_1 \geq t_2 \geq \ldots \geq t_n$. Clearly the state $|\widetilde{\psi}(t_0)\rangle$ is a time independent common factor and may be factorised out of the series given in eq. A.44. This allows us to define a new type of time evolution operator as the left over series of integrals,

$$\begin{aligned} \left|\widetilde{\psi}(t)\right\rangle &= S(t,t_0)\left|\widetilde{\psi}_0(t_0)\right\rangle, \\ S(t,t_0) &= \sum_{n=0}^{\infty}(-i)^n \int_{t_0}^{t} dt_1 \ldots \int_{t_0}^{t_{n-1}} dt_n\, \widetilde{H}_{\text{int}}(t_1)\ldots\widetilde{H}_{\text{int}}(t_n). \end{aligned} \tag{A.45}$$

Next we may simplify this expression by understanding the combinatorics of the n^{th}

[7] Clearly this isn't completely true as H_0 and H_{int} do not necessarily commute.

[8] Since $\widetilde{H}_{\text{int}}(t)$ taken at different times don't necessarily commute with each other, we cannot employ the simple solution $|\widetilde{\psi}(t)\rangle = \text{const.}\exp\left(\int_{-\infty}^{t} dt' \widetilde{H}_{\text{int}}(t')\right)$.

term in the above sum. Let us first consider $n = 2$,

$$S^{(2)}(t,t_0) = (-i)^2 \int_{t_0}^{t} dt_1 \int_{t_0}^{t_1} dt_2 \widetilde{H}_{\rm int}(t_1)\widetilde{H}_{\rm int}(t_2). \tag{A.46}$$

Clearly the dummy variables, t_1 and t_2, can be exchanged with each other to give an equivalent contribution to $S^{(2)}(t,t_0)$ meaning

$$\begin{aligned} S^{(2)}(t,t_0) &= \frac{(-i)^2}{2} \int_{t_0}^{t} dt_1 \int_{t_0}^{t_1} dt_2 \widetilde{H}_{\rm int}(t_1)\widetilde{H}_{\rm int}(t_2) \\ &\qquad + \frac{(-i)^2}{2} \int_{t_0}^{t} dt_2 \int_{t_0}^{t_2} dt_1 \widetilde{H}_{\rm int}(t_2)\widetilde{H}_{\rm int}(t_1) \\ &= \frac{(-i)^2}{2} \int_{t_0}^{t} dt_1 \int_{t_0}^{t} dt_2 \Big[\widetilde{H}_{\rm int}(t_1)\widetilde{H}_{\rm int}(t_2)\Theta(t_1 - t_2) \\ &\qquad + \widetilde{H}_{\rm int}(t_2)\widetilde{H}_{\rm int}(t_1)\Theta(t_2 - t_1) \Big] \\ &= \frac{(-i)^2}{2!} \int_{t_0}^{t} dt_1 \int_{t_0}^{t} dt_2 T_t \left\{ \widetilde{H}_{\rm int}(t_1)\widetilde{H}_{\rm int}(t_2) \right\}, \end{aligned} \tag{A.47}$$

where $\Theta(x)$ is the Heaviside function and T_t is the real time ordering operator. For a set of operators, $A(t)$, $B(t)$, ..., taken at different times, T_t orders the operators such that the later occurring operators appear to the left of earlier occurring operators,

$$T_t \left\{ A(t_1)B(t_2)C(t_3)... \right\} = \begin{cases} A(t_1)B(t_2)C(t_3)... & t_1 > t_2 > t_3 > ... \\ (-\eta)B(t_2)A(t_1)C(t_3)... & t_2 > t_1 > t_3 > ... \\ (-\eta)A(t_1)C(t_3)B(t_2)... & t_1 > t_3 > t_2 > ... \\ (-\eta)^2 B(t_2)C(t_3)A(t_1)... & t_2 > t_3 > t_1 > ... \\ (-\eta)^2 C(t_3)A(t_1)B(t_2)... & t_3 > t_1 > t_2 > ... \\ (-\eta)^3 C(t_3)B(t_2)A(t_1)... & t_3 > t_2 > t_1 > ..., \\ ... \end{cases} \tag{A.48}$$

where the factor of $(-\eta)^n$ is due to the swapping of fermionic ($\eta = 1$) and bosonic ($\eta = -1$), with n being the number of neighbouring swaps needed to make achieve time

ordering.

In general, for the n^{th} order contribution to $S(t,t_0)$ we see that the number of unique exchanges of the dummy variables is $n!$, which yields

$$S^{(n)}(t,t_0) = \frac{(-i)^n}{n!}\int_{t_0}^{t} dt_1 ... \int_{t_0}^{t} dt_n T_t \left\{ \widetilde{H}_{\text{int}}(t_1) ... \widetilde{H}_{\text{int}}(t_n) \right\}, \tag{A.49}$$

and hence we may write

$$S(t,t_0) = T_t \left\{ \exp\left(-i \int_{t_0}^{t} dt' \widetilde{H}_{\text{int}}(t') \right) \right\}. \tag{A.50}$$

Here we pulled the time ordering outside of the integrals, as T_t will only act upon the $\widetilde{H}_{\text{int}}(t)$ operators. We refer to this operator as the double time S-matrix.

At this point it is worth noting a few useful properties of the S-matrix. Clearly $S(t_1,t_2) = S(t_1,t_3)S(t_3,t_2)$, where $t_1 > t_3 > t_2$, since

$$|\widetilde{\psi}(t_1)\rangle = S(t_1,t_3)\,|\widetilde{\psi}(t_3)\rangle = S(t_1,t_3)S(t_3,t_2)\,|\widetilde{\psi}(t_2)\rangle = S(t_1,t_2)\,|\widetilde{\psi}(t_2)\rangle\,. \tag{A.51}$$

On top of this S is a unitary matrix, $S^{\dagger}(t,t_0) = S^{-1}(t,t_0)$, in order to maintain normalised state vectors, $\langle\widetilde{\psi}(t)|\widetilde{\psi}(t)\rangle = 1$.

Now that we understand time evolution in the interaction picture, and how to link this picture back to the Schrödinger picture, we next aim to find the relation between the Heisenberg and interaction pictures. We may define

$$|\widetilde{\psi}(t)\rangle = Q(t)\,|\psi\rangle_H\,, \tag{A.52}$$

where $Q(t)$ is a unitary operator, which together with eq. A.45 implies

$$Q(t) = S(t,t_0)Q(t_0). \tag{A.53}$$

Table A.1: Summary of the relations between different quantum mechanical pictures.

	Schrödinger	Heisenberg	Interaction
Schrödinger	$\|\psi(t)\rangle_S = \|\psi(t)\rangle$	$\|\psi(t)\rangle_S = \mathcal{U}(t)\|\psi\rangle_H$	$\|\psi(t)\rangle_S = \mathcal{U}_0(t)\|\widetilde{\psi}(t)\rangle$
Heisenberg	$\|\psi\rangle_H = \mathcal{U}^\dagger(t)\|\psi(t)\rangle$	$\|\psi\rangle_H = \|\psi\rangle_H$	$\|\psi\rangle_H = Q^\dagger(t)\|\widetilde{\psi}(t)\rangle$
Interaction	$\|\widetilde{\psi}(t)\rangle = \mathcal{U}_0^\dagger(t)\|\psi(t)\rangle$	$\|\widetilde{\psi}(t)\rangle = Q(t)\|\psi\rangle_H$	$\|\widetilde{\psi}(t)\rangle = \|\widetilde{\psi}(t)\rangle$

Using eq. A.41 we then see

$$\begin{aligned} \mathcal{U}_0^\dagger(t)\mathcal{U}(t) &= S(t,t_0)Q(t_0), \\ \Rightarrow \quad Q(t_0) &= \mathcal{U}_0^\dagger(t_0)\mathcal{U}(t_0), \quad \text{given} \quad S(t_0,t_0) = 1. \end{aligned} \tag{A.54}$$

Let us now use the idea of an adiabatically turned on interaction, that is to say at $t = -\infty$ the interaction vanishes, and as t increases the interaction is turned on infinitely slowly to its normal value at finite times. Thus we take $t_0 \to -\infty$ and note that $H = H_0$ at this time. Therefore $Q(t_0) = 1$ and we may relate the states of the Heisenberg and interaction pictures via

$$|\widetilde{\psi}(t)\rangle = S(t)\,|\psi\rangle_H\,, \tag{A.55}$$

where $S(t) = S(t,-\infty)$ is commonly referred to as the S-matrix. Given we can now link the states of the interaction and Heisenberg pictures, we can easily deduce the relation between their respective operators,

$$\begin{aligned} \langle\widetilde{\psi}(t)|\,\widetilde{\mathcal{O}}(t)\,|\widetilde{\psi}(t)\rangle &= \langle\psi|_H\,\mathcal{O}_H\,|\psi\rangle_H \\ \Rightarrow \quad \widetilde{\mathcal{O}}(t) &= S^{-1}(t)\mathcal{O}_H(t)S(t). \end{aligned} \tag{A.56}$$

In this subsection we have discussed the different pictures of quantum mechanics, and given details on how to derive the interaction picture. We summarise the relations between these formalisms in table A.1, before moving on to the last topic of this appendix.

Thus far we have not introduced the notion of temperature, and so have been dealing

purely with zero temperature. Let us now move to considering finite temperature by moving to the grand canonical ensemble. In this case time evolution is dictated by the GCE Hamiltonian $\mathscr{K} = H - \mu N$, where μ is the chemical potential and N is the particle number operator, that is to say time evolution in the Schrödinger and Heisenberg pictures is defined by

$$\begin{gathered} |\psi(\tau)\rangle_S = \mathscr{U}(\tau)\,|\psi(0)\rangle_S = \mathscr{U}(\tau)\,|\psi\rangle_H\,, \qquad \mathcal{O}_H(\tau) = \mathscr{U}^\dagger(\tau)\,\mathcal{O}_S\,\mathscr{U}(\tau), \\ \text{where} \qquad \mathscr{U}(\tau) = e^{-\mathscr{K}\tau}, \end{gathered} \tag{A.57}$$

and $\tau = it$ is imaginary time. To understand the interaction picture in this language we closely follow the procedure of Matsubara's original paper [9].

Let us consider the $\mathcal{S}$-matrix defined by

$$e^{-\beta\mathscr{K}} = e^{-\beta\mathscr{K}_0}\mathcal{S}(\beta) \qquad \Rightarrow \qquad -\frac{\partial\mathcal{S}}{\partial\beta} = \widetilde{H}_{\text{int}}(\beta)S(\beta), \tag{A.58}$$

subject to $\mathcal{S}(0) = 1$, where $\mathscr{K} = \mathscr{K}_0 + H_{\text{int}}$, $\beta = 1/T$, and

$$\widetilde{H}_{\text{int}}(\beta) = e^{\beta\mathscr{K}_0}H_{\text{int}}e^{-\beta\mathscr{K}_0} = \mathscr{U}_0^\dagger(\beta)H_{\text{int}}\mathscr{U}_0(\beta). \tag{A.59}$$

We see that $\mathcal{S}$ plays a similar role to the S-matrix from before. In fact, this is how we define the interaction picture for finite temperature, and consequently we write operators in the interaction picture according to

$$\widetilde{\mathcal{O}}(\tau) = \mathscr{U}_0^\dagger(\tau)\,\mathcal{O}_S\,\mathscr{U}_0(\tau), \tag{A.60}$$

where τ is imaginary time defined on the interval of 0 to β. We solve the differential equation for $\mathcal{S}(\beta)$ in the same manner as the zero temperature case for $|\widetilde{\psi}\rangle$. This yields

$$\mathcal{S}(\beta) = T_\tau\left\{\exp\left(-\int_0^\beta d\tau'\widetilde{H}_{\text{int}}(\tau')\right)\right\}. \tag{A.61}$$

In a similar fasion we define the matrix

$$\mathcal{S}(\tau_2,\tau_1) = T_\tau\left\{\exp\left(-\int_{\tau_1}^{\tau_2} d\tau' \widetilde{H}_{\text{int}}(\tau')\right)\right\}, \tag{A.62}$$

which has the properties

$$\begin{aligned} \mathcal{S}(\tau_2,\tau_1) &= \mathcal{S}(\tau_2,\tau_3)\mathcal{S}(\tau_3,\tau_1), \qquad \tau_2 > \tau_3 > \tau_1, \\ \mathcal{S}(\tau_2,\tau_1) &= \mathcal{S}(\tau_2)\mathcal{S}^{-1}(\tau_1). \end{aligned} \tag{A.63}$$

Now we consider the single-particle Green's function defined in eq. 2.27, and write the time evolution of the operators explicitly,

$$\begin{aligned} \mathscr{G}_{\alpha\alpha'}(\mathbf{r},\tau;\mathbf{r}',\tau') &= -\frac{1}{\mathcal{Z}}\text{Tr}\left[T_\tau\left\{e^{-\beta\mathscr{H}}e^{\mathscr{H}\tau}\psi_\alpha(\mathbf{r})e^{-\mathscr{H}\tau}e^{\mathscr{H}\tau'}\psi^\dagger_{\alpha'}(\mathbf{r}')e^{-\mathscr{H}\tau'}\right\}\right] \\ &= -\frac{1}{\mathcal{Z}}\text{Tr}\Big[T_\tau\Big\{e^{-\beta\mathscr{H}_0}\mathcal{S}(\beta)\mathcal{S}^{-1}(\tau)e^{\mathscr{H}_0\tau}\psi_\alpha(\mathbf{r})e^{-\mathscr{H}_0\tau}\mathcal{S}(\tau) \\ &\qquad\qquad \times \mathcal{S}^{-1}(\tau')e^{\mathscr{H}_0\tau'}\psi^\dagger_{\alpha'}(\mathbf{r}')e^{-\mathscr{H}_0\tau'}\mathcal{S}(\tau')\Big\}\Big] \\ &= -\frac{1}{\mathcal{Z}}\text{Tr}\left[e^{-\beta\mathscr{H}_0}T_\tau\left\{\mathcal{S}(\beta,\tau)\widetilde{\psi}_\alpha(\mathbf{r},\tau)\mathcal{S}(\tau,\tau')\widetilde{\psi}^\dagger_{\alpha'}(\mathbf{r}',\tau')\mathcal{S}(\tau',0)\right\}\right] \\ &= -\frac{1}{\mathcal{Z}}\text{Tr}\left[e^{-\beta\mathscr{H}_0}T_\tau\left\{\widetilde{\psi}_\alpha(\mathbf{r},\tau)\widetilde{\psi}^\dagger_{\alpha'}(\mathbf{r}',\tau')\mathcal{S}(\beta)\right\}\right]. \end{aligned} \tag{A.64}$$

Here we noted that any operator evaluated at imaginary time β will always appear to the left of all operators, hence why we were able to factor out the $e^{-\beta\mathscr{H}_0}$ term from the time ordering operation in the third line. In the fourth line we moved all the $\mathcal{S}$ matrices through the field operators to combine them into one $\mathcal{S}$ matrix, without incurring any sign changes due to the bosonic nature of the two-particle interactions represented by H_{int} appearing in $\mathcal{S}$. The time ordering operation means that we needn't worry about commutation relations too. Lastly we defined the operators $\widetilde{\psi}$ and $\widetilde{\psi}^\dagger$ as the finite temperature interaction picture field operators according to eq. A.60.

To write the single-particle Green's function more elegantly, we define $\langle ... \rangle_0$ as the average over the non-interacting Hamiltonian. Next we rewrite the partition function in

terms of this average,

$$\mathcal{Z} = \mathrm{Tr}\left[e^{-\beta\mathscr{H}}\right] = \mathrm{Tr}\left[e^{-\beta\mathscr{H}_0}\mathcal{S}(\beta)\right] = \langle\mathcal{S}(\beta)\rangle_0\,. \tag{A.65}$$

Therefore, using the non-interacting average definition and eq. A.65, we obtain

$$\mathscr{G}_{\alpha\alpha'}(\mathbf{r},\tau;\mathbf{r}',\tau') = -\frac{\left\langle T_\tau\left\{\widetilde{\psi}_\alpha(\mathbf{r},\tau)\widetilde{\psi}^\dagger(\mathbf{r}',\tau')\mathcal{S}(\beta)\right\}\right\rangle_0}{\langle\mathcal{S}(\beta)\rangle_0}. \tag{A.66}$$

APPENDIX B

WICK'S THEOREM

This appendix is intended as a reference for how to apply Wick's theorem, rather than how it is derived. The statement of Wick's theorem, based upon Bruus and Flensberg [31], is as follows,

> *Any many-particle Green's function that is taken as a correlation of field operators with respect to a non-interacting Hamiltonian – one that is quadratic in field operators – can be decomposed into a sum of single-particle Green's function products.*

A general N-particle Green's function is composed of $2N$ operators, half of which are creation operators, whilst the other half are annihilation operators. The N-particle temperature Green's function is therefore

$$\begin{aligned} &G(x_1, x_2, ..., x_N; x'_1, x'_2, ..., x'_N) \\ &\qquad = (-1)^N \left\langle T_\tau \left\{ \psi(x_1)\psi(x_2)...\psi(x_N)\psi^\dagger(x'_N)...\psi^\dagger(x'_2)\psi^\dagger(x'_1) \right\} \right\rangle . \end{aligned} \tag{B.1}$$

In applying Wick's theorem to this Green's function, we must know the statistics obeyed by the field operators. This will dictate the way we sum all possible single-particle Green's function products generated by the N-particle Green's function. If we start from the order of operators given in eq. B.1, we create one realisation of a single-particle Green's function product by pairing neighbouring operators, such that the pairs

do not share operators, so that each pair forms a correlator,

$$\begin{aligned} G_1(x_1, x_2, ..., x_N; x_1', x_2', ..., x_N') =& (-1)^N \langle T_\tau \{\psi(x_1)\psi(x_2)\}\rangle \langle T_\tau \{\psi(x_3)\psi(x_4)\}\rangle ... \\ & \times \left\langle T_\tau \left\{\psi^\dagger(x_4)\psi^\dagger(x_3)\right\}\right\rangle \left\langle T_\tau \left\{\psi^\dagger(x_2)\psi^\dagger(x_1)\right\}\right\rangle , \end{aligned} \tag{B.2}$$

where the subscript 1 on the N-particle Green's function denotes this is the first possible pairing of operators.

In this case the product we find is not actually of single-particle Green's functions, but rather we have correlators containing a pair of creation operators or a pair of annihilation operators.[1] Hence, this contribution will vanish.[2]

To generate other possible products from these operators, we will have to re-order them by commuting them passed one another. For example, another product we could generate would be from simply swapping the positions of $\psi(x_2)$ and $\psi(x_3)$. However, since we have performed a single commutation, we must introduce the appropriate multiplicative factor according to their statistics. Thus, we find this second product to be

$$\begin{aligned} G_1(x_1, x_2, ..., x_N; x_1', x_2', ..., x_N') = & (-1)^N(-\eta) \langle T_\tau \{\psi(x_1)\psi(x_3)\}\rangle \\ & \times \langle T_\tau \{\psi(x_2)\psi(x_4)\}\rangle ... \left\langle T_\tau \left\{\psi^\dagger(x_4)\psi^\dagger(x_3)\right\}\right\rangle \left\langle T_\tau \left\{\psi^\dagger(x_2)\psi^\dagger(x_1)\right\}\right\rangle , \end{aligned} \tag{B.3}$$

where we recall

$$\eta = \begin{cases} +1, & \text{fermions} \\ -1, & \text{bosons.} \end{cases} \tag{B.4}$$

Again, this realisation vanishes, but it acts as a simple demonstration as to how we generate different products and how we account for their multiplicative permutation factors.

So, to get contributions that are actually products of single-particle Green's functions we will have to perform several permutations. In generating new products, we will never

[1] If N is even, then all the correlators would be a pair of just creation operators or just annihilation operators. If N is odd, then we will find just one correlator of a creation and annihilation operator.

[2] Technically, in systems like superconductors the correlator $-\langle T_\tau \{\psi(x_1)\psi(x_2)\}\rangle$ does not vanish, since cooper pairs and cooper hole pairs exist in these systems. These are refered to as anomalous Green's functions. See [29, 30, 31] for a more in depth discussion of this.

consider a product that differs from another through swapping the order of operators within a pair. More generally, the pairs we will consider will always be ordered such that the leftmost operator of a pair, prior to pairing, will appear to the left within the pair. Let us show this mathematically.

Using the Green's function in eq. B.1, an allowed pairing, which generates a single-particle Green's function, is

$$\left\langle T_\tau \left\{ \psi(x_1)\psi^\dagger(x_1) \right\} \right\rangle . \tag{B.5}$$

However, we are not allowed the pairing

$$\left\langle T_\tau \left\{ \psi^\dagger(x_1)\psi(x_1) \right\} \right\rangle , \tag{B.6}$$

as $\psi(x_1)$ is the leftmost operator of the pair in the original ordering of the operators in eq. B.1, and so should appear to the left within the pairing, as in eq. B.5.

To demonstrate the application of Wick's theorem, let us look at the two-particle and three-particle Green's functions explicitly. These are defined as

$$G(x_1, x_2; x_1', x_2') = \left\langle T_\tau \left\{ \psi(x_1)\psi(x_2)\psi^\dagger(x_2')\psi^\dagger(x_1') \right\} \right\rangle , \tag{B.7a}$$

$$G(x_1, x_2, x_3; x_1', x_2', x_3') = -\left\langle T_\tau \left\{ \psi(x_1)\psi(x_2)\psi(x_3)\psi^\dagger(x_3')\psi^\dagger(x_2')\psi^\dagger(x_1') \right\} \right\rangle , \tag{B.7b}$$

respectively. Using Wick's theorem on these Green's functions gives

$$\begin{aligned} G(x_1, x_2; x_1', x_2') &= \left\langle T_\tau \left\{ \psi(x_1)\psi^\dagger(x_1') \right\} \right\rangle \left\langle T_\tau \left\{ \psi(x_2)\psi^\dagger(x_2') \right\} \right\rangle \\ &\quad - \eta \left\langle T_\tau \left\{ \psi(x_1)\psi^\dagger(x_2') \right\} \right\rangle \left\langle T_\tau \left\{ \psi(x_2)\psi^\dagger(x_1') \right\} \right\rangle \qquad \text{(B.8a)} \\ &= G(x_1, x_1')G(x_2, x_2') - \eta G(x_1, x_2')G(x_2, x_1'), \end{aligned}$$

$$
\begin{aligned}
&G(x_1, x_2, x_3; x_1', x_2', x_3') \\
&\quad = \left\langle T_\tau \left\{ \psi(x_1)\psi^\dagger(x_1') \right\} \right\rangle \left\langle T_\tau \left\{ \psi(x_2)\psi^\dagger(x_2') \right\} \right\rangle \left\langle T_\tau \left\{ \psi(x_3)\psi^\dagger(x_3') \right\} \right\rangle \\
&\qquad - \eta \left\langle T_\tau \left\{ \psi(x_1)\psi^\dagger(x_2') \right\} \right\rangle \left\langle T_\tau \left\{ \psi(x_2)\psi^\dagger(x_1') \right\} \right\rangle \left\langle T_\tau \left\{ \psi(x_3)\psi^\dagger(x_3') \right\} \right\rangle \\
&\qquad - \eta \left\langle T_\tau \left\{ \psi(x_1)\psi^\dagger(x_3') \right\} \right\rangle \left\langle T_\tau \left\{ \psi(x_2)\psi^\dagger(x_2') \right\} \right\rangle \left\langle T_\tau \left\{ \psi(x_3)\psi^\dagger(x_1') \right\} \right\rangle \\
&\qquad - \eta \left\langle T_\tau \left\{ \psi(x_1)\psi^\dagger(x_1') \right\} \right\rangle \left\langle T_\tau \left\{ \psi(x_2)\psi^\dagger(x_3') \right\} \right\rangle \left\langle T_\tau \left\{ \psi(x_3)\psi^\dagger(x_2') \right\} \right\rangle \\
&\qquad + \left\langle T_\tau \left\{ \psi(x_1)\psi^\dagger(x_2') \right\} \right\rangle \left\langle T_\tau \left\{ \psi(x_2)\psi^\dagger(x_3') \right\} \right\rangle \left\langle T_\tau \left\{ \psi(x_3)\psi^\dagger(x_1') \right\} \right\rangle \\
&\qquad + \left\langle T_\tau \left\{ \psi(x_1)\psi^\dagger(x_3') \right\} \right\rangle \left\langle T_\tau \left\{ \psi(x_2)\psi^\dagger(x_1') \right\} \right\rangle \left\langle T_\tau \left\{ \psi(x_3)\psi^\dagger(x_2') \right\} \right\rangle
\end{aligned}
\tag{B.8b}
$$

$$
\begin{aligned}
&= -G(x_1, x_1')G(x_2, x_2')G(x_3, x_3') + \eta G(x_1, x_2')G(x_2, x_1')G(x_3, x_3') \\
&\quad + \eta G(x_1, x_3')G(x_2, x_2')G(x_3, x_1') + \eta G(x_1, x_1')G(x_2, x_3')G(x_3, x_2') \\
&\quad + G(x_1, x_2')G(x_2, x_3')G(x_3, x_1') + G(x_1, x_3')G(x_2, x_1')G(x_3, x_2').
\end{aligned}
$$

We have so far demonstrated how to calculate many-particle Green's functions using Wick's theorem in a very hands on approach. We can, however, write down a compact equation that naturally generates all allowed decompositions of a many-particle Gren's function into a sum over single-particle Green's function products. The most compact form of Wick's theorem we can write, given by Bruus and Flensberg [31], is thus

$$
G_1(x_1, x_2, ..., x_N; x_1', x_2', ..., x_N') = \begin{cases} \det \mathcal{M}, & \text{fermions} \\ \text{perm } \mathcal{M}, & \text{bosons,} \end{cases}
\tag{B.9a}
$$

$$
\mathcal{M} = \begin{pmatrix} G(x_1, x_1') & ... & G(x_1, x_N') \\ \vdots & \ddots & \vdots \\ G(x_N, x_1') & ... & G(x_N, x_N') \end{pmatrix}, \qquad \mathcal{M}_{ji} = G(x_j, x_i').
\tag{B.9b}
$$

Here perm $\mathcal{M}$ is the permanent of the matrix $\mathcal{M}$. This function is similar to the determinant, except that no minus signs appear in the permanent. I.e. all the minus signs in the determinant become plus signs in the permanent.

APPENDIX C

THE DENSITY MATRIX

In the following discussion of the density matrix we follow the ideas explored in [31] and [81]. The density matrix is an extremely useful object to consider, and is related to the probability of finding a system in a certain state. Consider a many body system that has access to the ensemble of states $\{|\psi\rangle\}$, where each $|\psi\rangle$ represents a different overall configuration of the many body system (i.e: particle number, occupation number, total energy, etc can all vary). We define the density matrix as being the statistical collection of these states,

$$\rho(t) = \sum_{\psi} p_{\psi} \left|\psi(t)\right\rangle \left\langle\psi(t)\right|, \tag{C.1}$$

where we have allowed for time evolution and p_{ψ} is the statistical weighting of the state $|\psi\rangle$.

To better understand the time evolution of $\rho(t)$, we take it's partial time derivative ($\hbar = 1$),

$$\begin{aligned} i\frac{\partial \rho}{\partial t} &= \sum_{\psi} p_{\psi} \left[\left(i\frac{\partial}{\partial t} \left|\psi(t)\right\rangle \right) \left\langle\psi(t)\right| + \left|\psi(t)\right\rangle \left(i\frac{\partial}{\partial t} \left\langle\psi(t)\right| \right) \right] \\ &= \sum_{\psi} p_{\psi} \Big[H \left|\psi(t)\right\rangle \left\langle\psi(t)\right| - \left|\psi(t)\right\rangle \left\langle\psi(t)\right| H \Big] \\ &= [H, \rho(t)]. \end{aligned} \tag{C.2}$$

In obtaining the second line we used the Schrödinger equation,

$$i\frac{\partial}{\partial t}\left|\psi(t)\right\rangle = H\left|\psi(t)\right\rangle, \qquad -i\frac{\partial}{\partial t}\left\langle\psi(t)\right| = \left\langle\psi(t)\right| H, \tag{C.3}$$

where H is the Hamiltonian of the system. Therefore the time evolution of the density matrix is governed by

$$i\frac{\partial\rho}{\partial t} = [H,\rho]. \tag{C.4}$$

Thinking about this in terms of statistical mechanics, when the system occupies a specific state, say $|\phi\rangle \in \{|\psi\rangle\}$, the remaining states form a reservoir with which the system can interact through energy and particle exchange. Assuming the system is in thermal equilibrium, p_ψ is just the statistical weight for the GCE,

$$p_\psi = \frac{1}{\mathcal{Z}}e^{-\beta(E_\psi-\mu N_\psi)}, \tag{C.5}$$

where E_ψ is the energy of state $|\psi\rangle$, N_ψ is the number of particles in state $|\psi\rangle$, μ is the chemical potential, and $\mathcal{Z} = \sum_\psi e^{-\beta(E_\psi-\mu N_\psi)}$ is the partition function. In writing this, we have subtly assumed that $\{|\psi\rangle\}$ are eigenstates of the Hamiltonian and the number operator. So in the basis of eigenstates the density matrix is

$$\rho = \frac{1}{\mathcal{Z}}\sum_\psi e^{-\beta(E_\psi-\mu N_\psi)}\left|\psi\right\rangle\left\langle\psi\right|, \tag{C.6}$$

where $\{|\psi\rangle\}$ are now stationary states.

As a final step we can write our density matrix without defining a basis by noting that H and the number operator, N, are diagonal in $|\psi\rangle$ we can write

$$\rho = \frac{1}{\mathcal{Z}}e^{-\beta(H-\mu N)}. \tag{C.7}$$

Therefore we may choose a basis to write our operators, H and N, in and hence the basis ρ is written in. It is worth noting the only basis that we interpret physically is the

eigenbasis. We may now define the partition function generally as

$$\mathcal{Z} = \mathrm{Tr}\left[e^{-\beta(H-\mu N)}\right], \tag{C.8}$$

which ensures that $\mathrm{Tr}\left[\rho\right] = 1$.

Lastly, we stress that the expressions given in eq. C.7 and eq. C.8 are only true for a system in equilibrium. If an external field is applied or another form of perturbation is introduced, then we cannot treat ρ as being written simply in terms of an exponentiated Hamiltonian. This point is of importance when deriving Kubo's formula for linear response.

APPENDIX D

DISORDER AVERAGING, SELF-ENERGY, AND THE BORN APPROXIMATION

In chapter 3 we considered the effects of impurities and how they adjust the electron Green's function. There we simply stated the consequence of impurity averaging, and approximated the electron self-energy via the first non-zero impurity scattering term after averaging, which is commonly known as the *first order Born approximation*. In this appendix we will show how the results quoted in chapter 3 are obtained, and how we may include higher order corrections. We start by providing the details of how to perform disorder averaging, before turning our attention to relaxing our approximations step by step to consider higher order corrections, following closely the ideas set out in [31].

D.1 Disorder Averaging - The Gruesome Details

Let us start by calculating the averages given in eq. 3.4 explicitly. We begin by assuming our system has periodic boundary conditions and a total volume $\mathcal{V}$, which allows us to

Figure D.1: Diagrammatic representation of the first order correction to the electron Green's function after disorder averaging. The dashed line and cross represent the interaction due to eq. D.2, and the solid lines denote G_0.

rewrite the impurity potential as a Fourier series,

$$U(x_n) = \frac{1}{\mathcal{V}} \sum_i \sum_{\mathbf{k}} v_n(\mathbf{k}) e^{i\mathbf{k}\cdot(\mathbf{r}_n - \mathbf{R}_i)} \delta(\tau_n), \tag{D.1}$$

where we have introduced the subscript n to the single impurity potential to denote the cross $v_n(\mathbf{k})$ is associated to in the diagram of fig. 2.2. This will be important when averaging more than two impurity potentials. Applying $\langle ... \rangle_{\text{dis}}^{(0)}$ to rq. D.1 simply yields

$$\begin{aligned}
\langle U(x_1) \rangle_{\text{dis}}^{(0)} &= \frac{\delta(\tau_1)}{\mathcal{V}} \sum_i \sum_{\mathbf{k}_1} v_1(\mathbf{k}_1) e^{i\mathbf{k}\cdot\mathbf{r}_1} \left\langle e^{-i\mathbf{k}_1\cdot\mathbf{R}_i} \right\rangle_{\text{dis}}^{(0)} \\
&= \frac{\delta(\tau_1)}{\mathcal{V}} \sum_i \sum_{\mathbf{k}_1} v_1(\mathbf{k}_1) e^{i\mathbf{k}_1\cdot\mathbf{r}_1} \frac{1}{\mathcal{V}} \int d^d R_i \, e^{-i\mathbf{k}_1\cdot\mathbf{R}_i} \\
&= \frac{\delta(\tau_1)}{\mathcal{V}} \sum_i \sum_{\mathbf{k}_1} v_1(\mathbf{k}_1) e^{i\mathbf{k}_1\cdot\mathbf{r}_1} \delta_{\mathbf{k}_1,\mathbf{0}} \\
&= n_{\text{imp}} v(\mathbf{0}) \delta(\tau_1),
\end{aligned} \tag{D.2}$$

where $n_{\text{imp}} = N_{\text{imp}}/\mathcal{V}$. In the last line we used the fact that $v(\mathbf{k}) = v_n(\mathbf{k}) \equiv v_m(\mathbf{k}) \; \forall \; n$, m, as the subscript is purely a label of convenience. We represent this diagrammatically by moving the cross off the free electron Green's function lines and connecting it back to the Green's function lines via a dashed line, as illustrated in fig. D.1 This represents the electron scattering off the impurity through some interaction. This allows us to represent multiple scatterings from the same impurity with ease.[1]

[1]The process of multiple scatterings is only possible at second order and higher, where the number of impurity scatterings equals the order of the perturbative expansion.

Moving on to the second order term we see

$$\begin{aligned}
\langle U(x_1)U(x_2)\rangle^{(0)}_{\text{dis}} &= \frac{\delta(\tau_1)\delta(\tau_2)}{\mathcal{V}^2}\sum_{i,j}\sum_{\mathbf{k}_1,\mathbf{k}_2} v_1(\mathbf{k}_1)v_2(\mathbf{k}_2)e^{i\mathbf{k}_1\cdot\mathbf{r}_1+i\mathbf{k}_2\cdot\mathbf{r}_2}\left\langle e^{-i\mathbf{k}_1\cdot\mathbf{R}_i}e^{-i\mathbf{k}_2\cdot\mathbf{R}_j}\right\rangle^{(0)}_{\text{dis}} \\
&= \frac{\delta(\tau_1)\delta(\tau_2)}{\mathcal{V}^2}\sum_{\mathbf{k}_1,\mathbf{k}_2} v_1(\mathbf{k}_1)v_2(\mathbf{k}_2)e^{i\mathbf{k}_1\cdot\mathbf{r}_1+i\mathbf{k}_2\cdot\mathbf{r}_2} \\
&\qquad\times\left[\sum_{i\neq j}\frac{1}{\mathcal{V}^2}\int d^dR_i\int d^dR_j\, e^{-i\mathbf{k}_1\cdot\mathbf{R}_i-i\mathbf{k}_2\cdot\mathbf{R}_j}\right. \\
&\qquad\qquad\left.+\sum_i\frac{1}{\mathcal{V}}\int d^dR_i\, e^{-i\mathbf{R}_i\cdot(\mathbf{k}_1+\mathbf{k}_2)}\right] \qquad \text{(D.3)}\\
&= \frac{\delta(\tau_1)\delta(\tau_2)}{\mathcal{V}^2}\sum_{\mathbf{k}_1,\mathbf{k}_2} v_1(\mathbf{k}_1)v_2(\mathbf{k}_2)e^{i\mathbf{k}_1\cdot\mathbf{r}_1+i\mathbf{k}_2\cdot\mathbf{r}_2} \\
&\qquad\times\left[N_{\text{imp}}(N_{\text{imp}}-1)\delta_{\mathbf{k}_1,\mathbf{0}}\delta_{\mathbf{k}_2,\mathbf{0}}+N_{\text{imp}}\delta_{\mathbf{k}_1,-\mathbf{k}_2}\right] \\
&= \frac{\delta(\tau_1)\delta(\tau_2)}{\mathcal{V}^2}\left[N_{\text{imp}}(N_{\text{imp}}-1)v(\mathbf{0})^2\right. \\
&\qquad\left.+N_{\text{imp}}\sum_{\mathbf{k}} v_1(-\mathbf{k})v_2(\mathbf{k})e^{-i\mathbf{k}\cdot(\mathbf{r}_1-\mathbf{r}_2)}\right].
\end{aligned}$$

Applying our assumption that the impurity positions can be treated as independent (the sum over $i\neq j$ becomes the sum over i,j) we may approximate this expression as

$$\langle U(x_1)U(x_2)\rangle^{(0)}_{\text{dis}} = \left[n^2_{\text{imp}}v(\mathbf{0})^2+\frac{n_{\text{imp}}}{\mathcal{V}}\sum_{\mathbf{k}} v_1(-\mathbf{k})v_2(\mathbf{k})e^{-i\mathbf{k}\cdot(\mathbf{r}_1-\mathbf{r}_2)}\right]\delta(\tau_1)\delta(\tau_2). \qquad \text{(D.4)}$$

This approximation introduces an error of order $1/N_{\text{imp}}$ to the constant correction. Given we are dealing with disordered systems we may assume that $N_{\text{imp}}\gg 1$, and so this error becomes negligible.

The first term of eq. D.4 corresponds to two isolated impurities, analogous to what we saw in the first order correction.[2] In comparison, the second term looks like an effective two body interaction connecting two crosses, where a momentum $\mathbf{k}$ leaves the first cross and re-enters at the second cross.

[2]By this point in the literature most texts would argue that $v(\mathbf{0})=0$, as a non-zero value would only give an uninteresting constant shift to the ground state energy (see [29, 30]). However, we shall maintain a non-zero value for the time being and demonstrate how this statement can be realised. Though this is clearly going to become a painful decision when calculating higher order corrections.

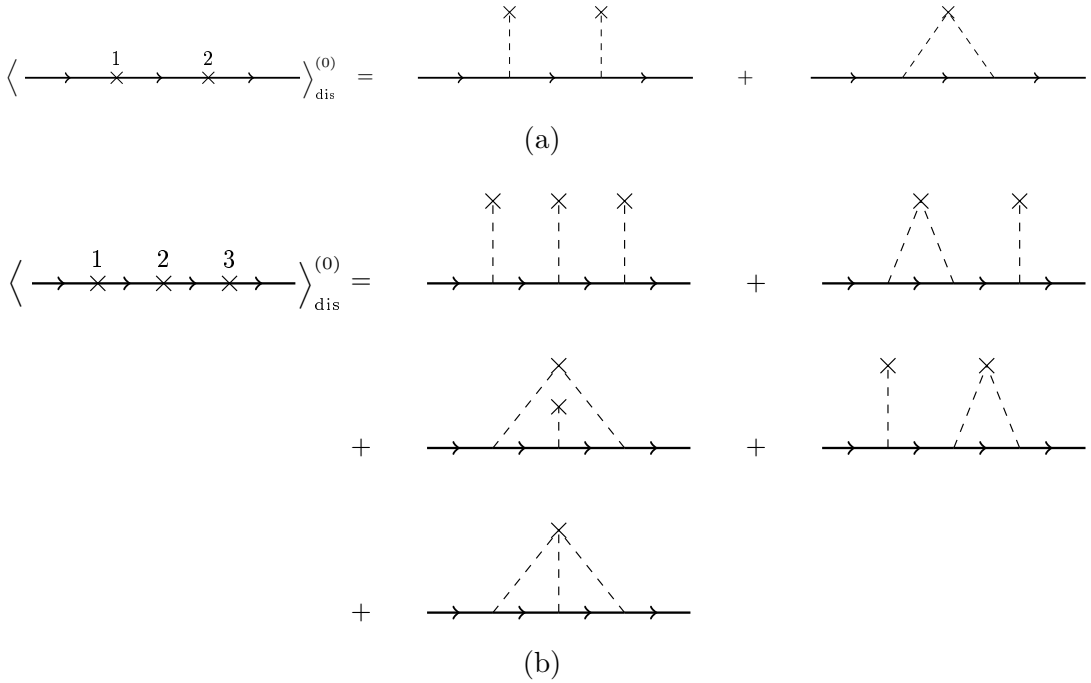

Figure D.2: Diagrammatic representation of the second (a) and third (b) order corrections to the electron Green's function after disorder averaging.

Turning to the diagrammatic representation of the second order contribution to the Green's function, we see that the first term of eq. D.4 leads to the first term in fig. D.2a. The second term in the diagrammatic series represents the correlated scattering events appearing in the second term of eq. D.4, where the cross represents the scattering events being due to the same impurity. In general we shall represent disorder averaging diagrammatically by using a single cross connected to Green's function via dashed lines to denote scattering from the same impurity.

In a similar vain we see that the third order term becomes

$$\begin{aligned}\langle U(x_1)U(x_2)U(x_3)\rangle^{(0)}_{\text{dis}} = \delta(\tau_1)\delta(\tau_2)\delta(\tau_3)\Big\{ & n^3_{\text{imp}} v(\mathbf{0})^3 \\ & + \frac{n^2_{\text{imp}}}{\mathcal{V}} v(\mathbf{0}) \sum_{\mathbf{k}} \Big[v_1(-\mathbf{k}) v_2(\mathbf{k}) e^{-i\mathbf{k}\cdot(\mathbf{r}_1-\mathbf{r}_2)} + v_1(-\mathbf{k}) v_3(\mathbf{k}) e^{-i\mathbf{k}\cdot(\mathbf{r}_1-\mathbf{r}_3)} \\ & \qquad + v_2(-\mathbf{k}) v_3(\mathbf{k}) e^{-i\mathbf{k}\cdot(\mathbf{r}_2-\mathbf{r}_3)} \Big] \\ & + \frac{n_{\text{imp}}}{\mathcal{V}^2} \sum_{\mathbf{k},\mathbf{q}} v_1(-\mathbf{k}-\mathbf{q}) v_2(\mathbf{k}) v_3(\mathbf{q}) e^{-i(\mathbf{k}+\mathbf{q})\cdot(\mathbf{r}_1-\mathbf{r}_2-\mathbf{r}_3)} \Big\},\end{aligned} \tag{D.5}$$

which leads to the diagrammatic correction in fig. D.2b. The first and second terms are clearly responsible for the first two terms of fig. D.2b, whilst the third term gives rise to a cross connected to the Green's functions by three dashed lines.

Lastly, at fourth order we find

$$\begin{aligned}
\langle U(x_1)U(x_2)U(x_3)U(x_4)\rangle^{(0)}_{\text{dis}} = \delta(\tau_1)\delta(\tau_2)\delta(\tau_3)\delta(\tau_4)\Big\{ & n_{\text{imp}}^4 v(\mathbf{0})^4 \\
& + \frac{n_{\text{imp}}^3 v(\mathbf{0})^2}{\mathcal{V}} \sum_{\mathbf{k}} \Big[v_1(-\mathbf{k})v_2(\mathbf{k})e^{-i\mathbf{k}\cdot(\mathbf{r}_1-\mathbf{r}_2)} + v_1(-\mathbf{k})v_3(\mathbf{k})e^{-i\mathbf{k}\cdot(\mathbf{r}_1-\mathbf{r}_3)} \\
& \qquad + v_1(-\mathbf{k})v_4(\mathbf{k})e^{-i\mathbf{k}\cdot(\mathbf{r}_1-\mathbf{r}_4)} + v_2(-\mathbf{k})v_3(\mathbf{k})e^{-i\mathbf{k}\cdot(\mathbf{r}_2-\mathbf{r}_3)} \\
& \qquad + v_2(-\mathbf{k})v_4(\mathbf{k})e^{-i\mathbf{k}\cdot(\mathbf{r}_2-\mathbf{r}_4)} + v_3(-\mathbf{k})v_4(\mathbf{k})e^{-i\mathbf{k}\cdot(\mathbf{r}_3-\mathbf{r}_4)} \Big] \\
& + \frac{n_{\text{imp}}^2}{\mathcal{V}} \sum_{\mathbf{k},\mathbf{q}} \Big[v_1(-\mathbf{k})v_2(\mathbf{k})v_3(-\mathbf{q})v_4(\mathbf{q})e^{-i\mathbf{k}\cdot(\mathbf{r}_1-\mathbf{r}_2)}e^{-i\mathbf{q}\cdot(\mathbf{r}_3-\mathbf{r}_4)} \\
& \qquad + v_1(-\mathbf{k})v_3(\mathbf{k})v_2(-\mathbf{q})v_4(\mathbf{q})e^{-i\mathbf{k}\cdot(\mathbf{r}_1-\mathbf{r}_3)}e^{-i\mathbf{q}\cdot(\mathbf{r}_2-\mathbf{r}_4)} \\
& \qquad + v_1(-\mathbf{k})v_4(\mathbf{k})v_2(-\mathbf{q})v_4(\mathbf{q})e^{-i\mathbf{k}\cdot(\mathbf{r}_1-\mathbf{r}_3)}e^{-i\mathbf{q}\cdot(\mathbf{r}_2-\mathbf{r}_3)} \Big] \\
& + \frac{n_{\text{imp}}^2 v(\mathbf{0})}{\mathcal{V}^2} \sum_{\mathbf{k},\mathbf{q}} \Big[v_1(-\mathbf{k}-\mathbf{q})v_2(\mathbf{k})v_3(\mathbf{q})e^{-i(\mathbf{k}+\mathbf{q})\cdot(\mathbf{r}_1-\mathbf{r}_2-\mathbf{r}_3)} \\
& \qquad + v_1(-\mathbf{k}-\mathbf{q})v_2(\mathbf{k})v_4(\mathbf{q})e^{-i(\mathbf{k}+\mathbf{q})\cdot(\mathbf{r}_1-\mathbf{r}_2-\mathbf{r}_4)} \\
& \qquad + v_1(-\mathbf{k}-\mathbf{q})v_3(\mathbf{k})v_4(\mathbf{q})e^{-i(\mathbf{k}+\mathbf{q})\cdot(\mathbf{r}_1-\mathbf{r}_3-\mathbf{r}_4)} \\
& \qquad + v_2(-\mathbf{k}-\mathbf{q})v_3(\mathbf{k})v_4(\mathbf{q})e^{-i(\mathbf{k}+\mathbf{q})\cdot(\mathbf{r}_2-\mathbf{r}_3-\mathbf{r}_4)} \Big] \\
& + \frac{n_{\text{imp}}}{\mathcal{V}^3} \sum_{\substack{\mathbf{k},\mathbf{q},\\ \mathbf{p}}} v_1(-\mathbf{k}-\mathbf{q}-\mathbf{p})v_2(\mathbf{k})v_3(\mathbf{q})v_4(\mathbf{p}) \Big\}.
\end{aligned} \tag{D.6}$$

This term gives rise to the correction represented in fig. D.3, where variations refers to the different possible correlated scattering events that have a similar structure to their prior term. The first term is trivially four unconnected scatterings. The second line deals with two correlated events and two uncorrelated events, and is generated by the second term in eq. D.6. The third and fourth lines all depict two sets of connected scattering events, and are the most significant contributions to the Green's function at this order. These lines are a consequence of the third term of eq. D.6. The fifth line denotes the fourth

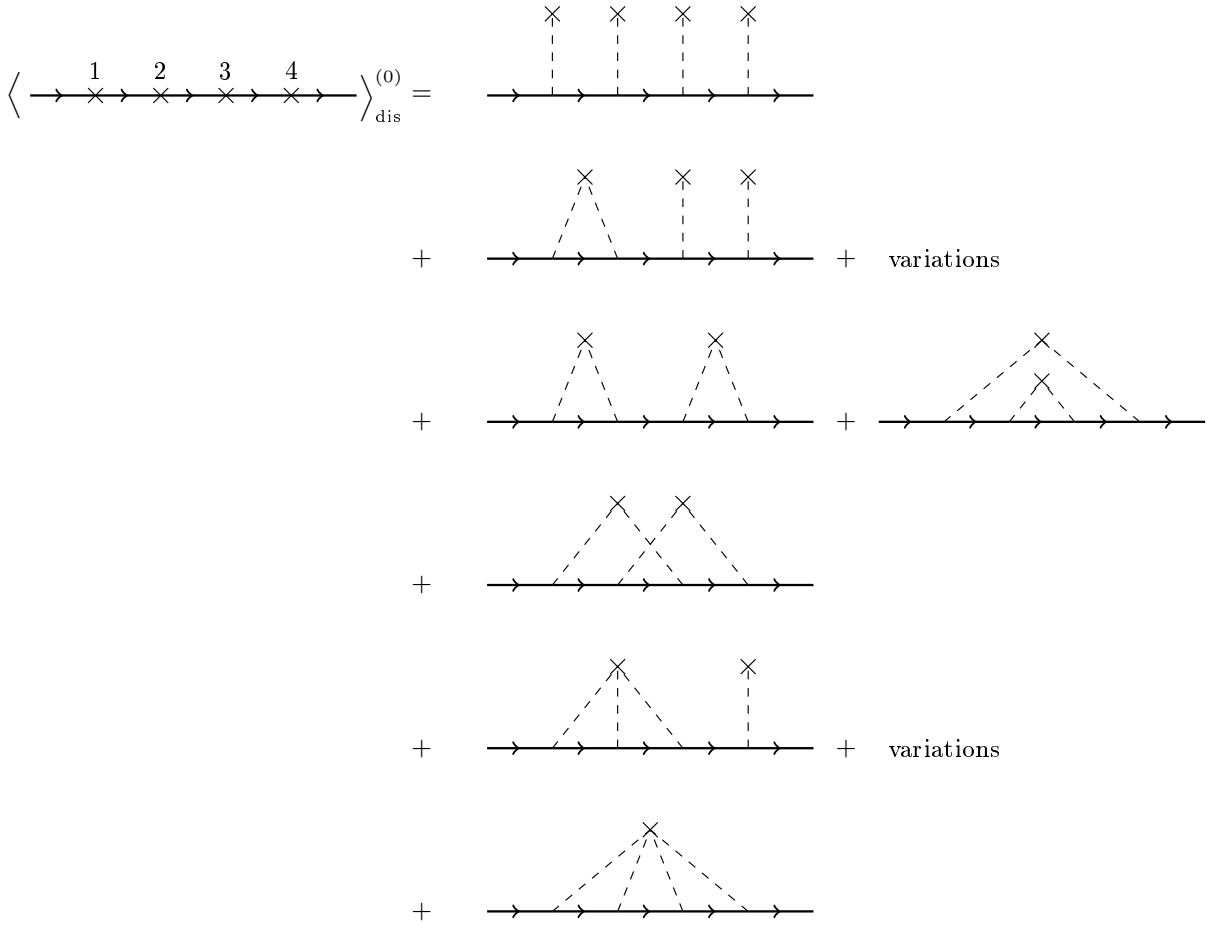

Figure D.3: Diagrammatic representation of the fourth order correction to the electron Green's function after disorder averaging.

term of eq. D.6, and the final line represents all four scattering events being correlated and hence describes the fifth term of eq. D.6.

Clearly, continuing this procedure analytically will quickly become unwieldy. We can see from these diagrams, however, that a clear pattern emerges where we consider all possible variations of connecting n impurities at the n^{th} order, such that these connections can leave an arbirtary number of scattering events unconnected. This pattern can be realised both diagrammatically and mathematically by using an object called the self-energy, Σ. The self-energy is defined as the collection of diagrams that are one particle irreducible. That is to say, it is formed of diagrams that may not be split into two separate pieces by cutting an internal propagator.[3]

[3]For example, consider fig. D.1: we may not cut any propagator here as there are no internal propagators to cut. Therefore it is one particle irreducible. The first term of fig. D.2a can be cut through it's

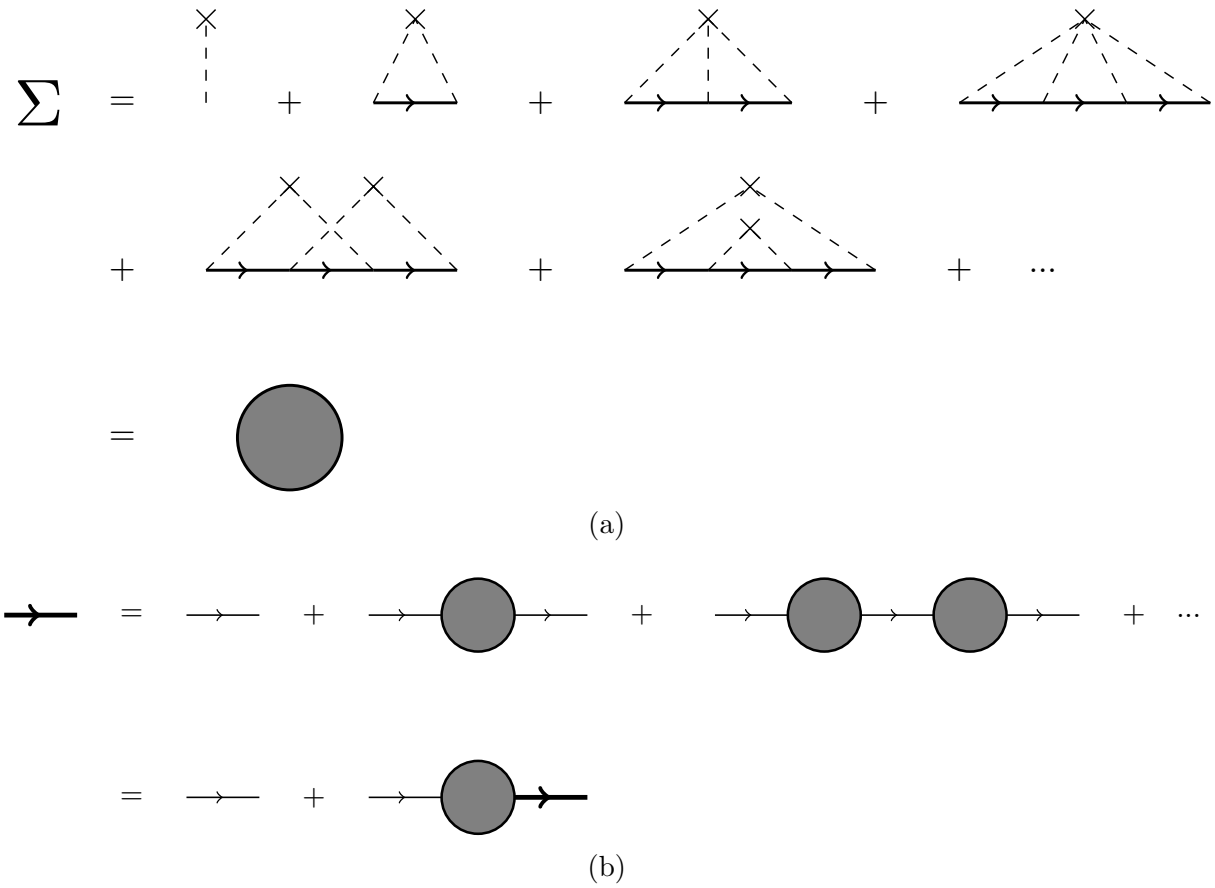

Figure D.4: (a): Diagrammatic series for the self-energy describing impurity averaging. Here solid lines represent G_0. (b): Diagrammatic representation of the Dyson equation, where the thin solid lines are G_0 propagators, and the thick solid lines are the full disorder-averaged electron Green's function, G.

In the case of disorder averaging, the self-energy may be written diagrammatically as shown in fig. D.4a. We may then insert this into the series describing the disorder-averaged electron Green's function in fig. D.4b. It is at this point we can begin to take different approximations to calculate the self-energy, and thus the resulting Green's function.

D.2 The First Order Born Approximation

The "first" order contribution to $\Sigma(\mathbf{k})$ is simply $n_{\text{imp}}v(\mathbf{0})$, which clearly just leads to a constant shift to the energy of the system. Therefore, we may neglect it by absorbing it

middle propagator, to form two separate pieces. Therefore, this term is not one particle irreducible. In contrast the second term in fig. D.2a is one particle irreducible.

into the ground state energy of the system, or equivalently set $v(\mathbf{0}) = 0$. Clearly, this means any diagrams we previously considered with an isolated impurity would vanish, leaving diagrams where all scattering events are correlated in some way.

So the real first (leading) order contribution to the self-energy is actually the second term in fig. D.4a,

$$\begin{aligned}\Sigma^{(1)}(\mathbf{k}, i\varepsilon) &= \frac{n_{\text{imp}}}{\mathcal{V}} \sum_{\mathbf{k}'} |v(\mathbf{k}-\mathbf{k}')|^2 \, G_0(\mathbf{k}', i\varepsilon) \\ &= -\frac{n_{\text{imp}}}{\mathcal{V}} \sum_{\mathbf{k}'} |v(\mathbf{k}-\mathbf{k}')|^2 \, \frac{i\varepsilon + \xi_{\mathbf{k}'}}{\varepsilon^2 + \xi_{\mathbf{k}'}^2},\end{aligned} \tag{D.7}$$

Here we used $v_n(\mathbf{k}) = v_m(\mathbf{k}) \equiv v(\mathbf{k})$, along with the knowledge that $V(\mathbf{r}-\mathbf{r}')$ is a real potential and hence gives $v(\mathbf{k})^* = v(-\mathbf{k})$. We also shifted our momentum variables, so that the free Green's function only had one momentum variable in its argument.

As before, we focus on energies close to the Fermi surface, $\xi_{\mathbf{k}'}/\varepsilon_F \ll 1$ (ε_F is the Fermi energy), as this region provides the most singular contribution. Approximating the sum via an integral, we find

$$\Sigma^{(1)}(\mathbf{k}, i\varepsilon) = -n_{\text{imp}} N(0) \int_{-\infty}^{+\infty} d\xi' |v(\mathbf{k}-\mathbf{k}')|^2 \frac{i\varepsilon + \xi'}{\varepsilon^2 + \xi'^2}. \tag{D.8}$$

Next, we assume that the function $v(\mathbf{k}-\mathbf{k}')$ does not vary significantly for small variations of $\mathbf{k}'$ about the Fermi surface, so we may take it to be constant $v(\mathbf{k}-\mathbf{k}') \simeq v(\mathbf{k}_F)$. Lastly, by identifying

$$n_{\text{imp}} |v(\mathbf{k}_F)|^2 = \frac{1}{2\pi N(0) \tau_0}, \tag{D.9}$$

we recover eq. 3.12, and thus proceed as in the main text.

To begin including higher order corrections, let us remove our last assumption. This means the reasoning used in moving from eq. 3.12 to eq. 3.13, in which we argued that the second term of the integrand appearing in the first equation was odd and hence vanished, is no longer necessarily true. Being completely honest and maintaining $v(\mathbf{k})$ as being a

non-constant function of $\mathbf{k}$, means we must deal with

$$\Sigma^{(1)}(\mathbf{k}, i\varepsilon) = -n_{\text{imp}} \int_{-\infty}^{+\infty} d\xi' N(\xi') |v(\mathbf{k}-\mathbf{k}')|^2 \frac{i\varepsilon + \xi'}{\xi'^2 + \varepsilon^2}. \tag{D.10}$$

This leads to a real and imaginary part of $\Sigma^{(1)}$. The real part clearly arises from the second term, and simply leads to a constant contribution in the denominator of the disorder-averaged electron Green's function. Hence, we may absorb it into the definition of the chemical potential, and so this terms has no physical significance. The parity argument can only be made when we focus on the behaviour in the region about the Fermi surface, where $|v(\mathbf{k}-\mathbf{k}')|$ can be treated as a slowly varying function, and extend it across the entire domain of $\xi' \in (-\infty, +\infty)$.[4]

Now, let us take another step back in writing $\Sigma^{(1)}$. By using the first line of eq. D.7 and performing analytic continuation to consider the retarded and advanced forms of $\Sigma^{(1)}$, $i\varepsilon \to \omega \pm i\delta$, we obtain

$$\begin{aligned} \Sigma^{(1),R/A}(\mathbf{k}, \omega) &= \frac{n_{\text{imp}}}{\mathcal{V}} \sum_{\mathbf{k}'} |v(\mathbf{k}-\mathbf{k}')|^2 \frac{1}{\omega - \xi_{\mathbf{k}'} \pm i\delta} \\ &= \frac{n_{\text{imp}}}{\mathcal{V}} \sum_{\mathbf{k}'} |v(\mathbf{k}-\mathbf{k}')|^2 \left[\frac{1}{\omega - \xi_{\mathbf{k}'}} \mp i\pi\delta(\omega - \xi_{\mathbf{k}'}) \right], \end{aligned} \tag{D.11}$$

where we used the sum form of the Plemelj formula to get the second line. The first term is real and so may be ignored. Let us now assume that the spectral function, $\mathcal{A}(\mathbf{k}, \omega)$, corresponding to the disorder-averaged electron Green's function is strongly peaked around $\xi_{\mathbf{k}}$, so that choices of ω far from $\xi_{\mathbf{k}}$ are negligible. This assumption is equivalent to saying that the number of states that may be accessed by the addition of a particle with momentum $\mathbf{k}$ and energy $\omega + \mu$ is small. This is ensured by focussing on energies close to the Fermi surface, meaning that $\xi_{\mathbf{k}}$ is small and hence few states are accessible. In any

[4] In treating $|v(\mathbf{k}-\mathbf{k}')|$ as effectively constant near Fermi surface, we've technically accounted for the effect of screening. That is to say that the electrons redistribute themselves to screen the impurity charges. More details are given in [31].

case, this assumption means we may set $\omega = \xi_{\mathbf{k}}$ in the self-energy,

$$\Sigma^{(1),R/A}(\mathbf{k}) = \mp i\pi \frac{n_{\text{imp}}}{\mathcal{V}} \sum_{\mathbf{k}'} |v(\mathbf{k}-\mathbf{k}')|^2 \delta(\xi_{\mathbf{k}} - \xi_{\mathbf{k}'}). \tag{D.12}$$

To further simplify the self-energy, we introduce the characteristic scattering time

$$\frac{1}{\tau_{0,\mathbf{k}}} = 2\pi \frac{n_{\text{imp}}}{\mathcal{V}} \sum_{\mathbf{k}'} |v(\mathbf{k}-\mathbf{k}')|^2 \delta(\xi_{\mathbf{k}} - \xi_{\mathbf{k}'}). \tag{D.13}$$

Thus, the more accurately written first Born self-energy is

$$\Sigma^{(1),R/A}(\mathbf{k}) = \mp \frac{i}{2\tau_{0,\mathbf{k}}}, \tag{D.14}$$

which corresponds to

$$\Sigma^{(1)}(\mathbf{k}, i\varepsilon) = -\frac{i}{2\tau_{0,\mathbf{k}}} \text{sgn}(\varepsilon), \tag{D.15}$$

in the Matsubara formalism.

To check for self-consistency we use this to determine the spectral function. Recalling from eq. 2.21 that the spectral function is related to the imaginary part of the retarded Green's function, it is straight forward to show that

$$\mathcal{A}(\mathbf{k}, \omega) = \frac{1}{2\pi\tau_{0,\mathbf{k}}} \frac{1}{(\omega - \xi_{\mathbf{k}})^2 + (2\tau_{0,\mathbf{k}})^{-2}}, \tag{D.16}$$

which is just a Lorentzian centred on $\omega = \xi_{\mathbf{k}}$ with width $2\tau_{0,\mathbf{k}}^{-1}$. Since the energies we focus on are close to ε_F, and for disordered metals $\varepsilon_F \ll \tau_{0,\mathbf{k}}^{-1}$, our argument that the spectral function is strongly peaked about $\xi_{\mathbf{k}}$ is self-consistent.

Finally, let us show how we can obtain the real time retarded and advanced Green's functions and the position space Green's function from the disordered electron Matsubara Green's function. For the sake of simplicity, we shall use approximate $\tau_{0,\mathbf{k}} \simeq \tau_0$. To obtain the retarded and advanced Green's functions we need only find one, as the other is simply the complex conjugate of the other. First we analytically continue $i\varepsilon \to \omega + i\delta$ in the

disordered electron Green's function, before making use of the inverse Fourier transform defined in eq. 2.10 to get

$$G^R(\mathbf{k},t) = \int_{-\infty}^{+\infty} d\omega \frac{e^{-i(\omega+i\delta)t}}{\omega - \xi_{\mathbf{k}} + \frac{i}{2\tau_0}}. \tag{D.17}$$

In writing eq. D.17 we have neglected the $+i\delta$ term appearing in the denominator as it is an infinitesimal, which is much smaller than $i/(2\tau_0)$. The analytic structure remains unchanged by this, as the sign of the impurity correction is the same as the retarded/advanced infinitesimal.

Now let us analytically continue ω into the complex plane and consider the pole structure of the integrand. For all choices of t there is a simple pole in the lower half plane at $\omega = \xi - i/(2\tau_0)$, however there exists an additional pole in the case where $t > 0$. Specifically, when $\mathrm{Im}[\omega] \to +\infty$ the integrand again diverges when $t > 0$. Therefore, for $t < 0$ we may choose to close our usual semi-circle contour in the upper half plane without generating any additional contributions due to the contour at infinity. Given there are no poles in the upper half plane, this contour encloses no poles, and hence the integral vanishes. In contrast to this, the $t > 0$ case has poles in both half planes and so does not necessarily vanish.

The easiest contour to consider is the semi-circle closed in the lower half plane, where the contour at infinity does not encounter any poles and gives no contribution. Thus the integral is given simply by the simple pole enclosed here at $\omega = \xi - i/(2\tau_0)$. This leads us to writing

$$G^R(\mathbf{k},t) = \begin{cases} -i\, e^{-i\xi_{\mathbf{k}}t}\, e^{-(1/(2\tau_0)-\delta)t}, & t > 0 \\ 0, & t < 0. \end{cases} \tag{D.18}$$

We may write this concisely by using the Heavisde function and appreciating that we may neglect δ,

$$G^R(\mathbf{k},t) = -i\, e^{-i\xi_{\mathbf{k}}t}\, e^{-t/(2\tau_0)}\, \Theta(t). \tag{D.19}$$

Hence, we have reproduced the result we quote in eq. 3.18.

Turning our attention to the three dimensional real space picture we choose to write our problem in terms of spherical coordinates due to the symmetry of the system,

$$G^R(\mathbf{r},\omega) = \int_0^{+\infty} \frac{dk}{(2\pi)^3} k^2 \int_0^{\pi} d\theta \sin(\theta) \int_0^{2\pi} d\phi \frac{e^{i\mathbf{k}\cdot\mathbf{r}}}{\omega - \xi_{\mathbf{k}} + \frac{1}{2\tau_0}}. \tag{D.20}$$

At this point we are free to choose the orientation of our axes, so for convenience we choose $\mathbf{r}$ to be aligned with the k_z axis so that $\mathbf{k}\cdot\mathbf{r} = kr\cos(\theta)$. This allows us to perform both the polar and azimuthal integrals by inspection,

$$G^R(\mathbf{r},\omega) = \int_0^{+\infty} \frac{dk}{2\pi^2} \frac{k}{r} \frac{\sin(kr)}{\omega - \xi_{\mathbf{k}} + \frac{i}{2\tau_0}}. \tag{D.21}$$

As with most transport problems we shall change variables to an integral over ξ, and approximate this about the Fermi surface in the usual fashion. This allows us to write,

$$G^R(\mathbf{r},\omega) = \frac{N(0)}{k_F r} \int_{-\infty}^{+\infty} d\xi \frac{\sin(kr)}{\omega - \xi + \frac{i}{2\tau_0}}. \tag{D.22}$$

To further approximate this integral, we use $(k - k_F) \simeq m\xi/k_F$ and rewrite $\sin(kr)$ in terms of exponentials[5]

$$\begin{aligned} G^R(\mathbf{r},\omega) = \frac{N(0)}{2ik_F r} \Bigg[&\int_{-\infty}^{+\infty} d\xi \frac{\exp\left(ik_F r + i\frac{mr}{k_F}\xi\right)}{\omega - \xi + \frac{i}{2\tau_0}} \\ &- \int_{-\infty}^{+\infty} d\xi \frac{\exp\left(-ik_F r - i\frac{mr}{k_F}\xi\right)}{\omega - \xi + \frac{i}{2\tau_0}} \Bigg]. \end{aligned} \tag{D.23}$$

Whilst this may seem ugly, we can quickly notice that the second term vanishes as all of its poles lie in the upper half plane. Hence, by complex analysis, we may consider a contour integral, whose contour is closed in the lower half plane thus enclosing no poles, to show this vanishes. In contrast, the first term has a simple pole in the upper half plane at $\xi = \omega + i/(2\tau_0)$, as well as a singularity in the lower half plane as $\mathrm{Im}[\xi] \to -\infty$. We

[5]To see this approximation of $(k - k_F)$ more clearly, consider expanding $\xi_{\mathbf{k}} = k^2/(2m) - k_F^2/(2m)$ about k_F with the assumption that $|k - k_F| \ll k_F$.

therefore choose to close our contour in the upper half plane for simplicity, thus enclosing the simple pole. This yields

$$G^R(\mathbf{r},\omega) = -\frac{\pi N(0)}{k_F r}\exp\left(ik_F r + i\frac{m\omega}{k_F}r\right)e^{-r/l}, \tag{D.24}$$

where $l = v_F\tau_0$ is the mean free path. In many situations involving metals we may consider $\omega \ll \varepsilon_F$ due to the sheer scale of the Fermi energy. In this case the retarded real space Green's function simplifies to

$$G^R(\mathbf{r},\omega) = -\frac{\pi N(0)}{k_F r}e^{ik_F r}e^{-r/l}. \tag{D.25}$$

Let us now move on to consider how to include the other diagrams appearing in the self-energy for the disordered electron gas.

D.3 The Full Born Approximation

In the *full Born approximation* (FBA), we not only account for diagrams describing the first order approximation, but also all diagrams that involve multiple scattering events connected to the same impurity. However, we ignore all nested diagrams[6] and those that involve crossings of the impurity scattering lines. We illustrate this self-energy, Σ^{FBA}, in fig. D.5. This expansion can be written in terms of a transition matrix, $t_{\mathbf{k},\mathbf{k}'}$, whose diagonal elements are equal to $\Sigma^{\mathrm{FBA}}(\mathbf{k})$. The equation corresponding to fig. D.5 is

$$\Sigma^{\mathrm{FBA}}(\mathbf{k},i\varepsilon) = n_{\mathrm{imp}}v(\mathbf{0}) + \frac{1}{\mathcal{V}}\sum_{\mathbf{k}'}v(\mathbf{k}-\mathbf{k}')G_0(\mathbf{k}',i\varepsilon)t_{\mathbf{k},\mathbf{k}'}, \tag{D.26a}$$

$$t_{\mathbf{k},\mathbf{k}'} = n_{\mathrm{imp}}v(\mathbf{k}-\mathbf{k}') + \frac{1}{\mathcal{V}}\sum_{\mathbf{q}}v(\mathbf{k}'-\mathbf{q})G_0(\mathbf{q},i\varepsilon)t_{\mathbf{k},\mathbf{q}}. \tag{D.26b}$$

[6]These are the diagrams that have a set of correlated scattering events contained completely within another set of correlated scattering events. The sixth term of fig. D.4a is the simplest example of this.

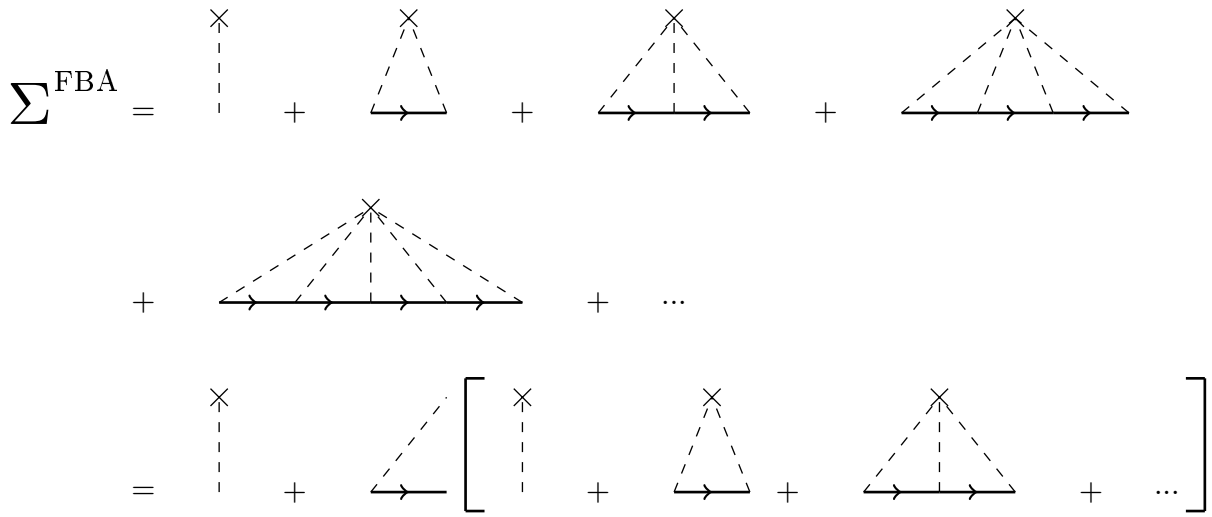

Figure D.5: Diagrammatic series for the self-energy in the FBA. The term written in the brackets after the second equality is the transition matrix, $t_{\mathbf{k},\mathbf{k}'}$.

Since we are only interested in electrons near the Fermi surface, we note that the real part of the diagonal elements of the transition matrix are close to constant. As such we may again ignore $\mathrm{Re}[t_{\mathbf{k},\mathbf{k}}]$ by absorbing it into the definition of the chemical potential. Thus all the physics of the problem is contained in $\mathrm{Im}[t_{\mathbf{k},\mathbf{k}}]$. To extract the imaginary part, we rewrite eq. D.26b as a matrix equation,

$$t = n_{\mathrm{imp}}\, u + \frac{1}{\mathcal{V}}\, u\, G_0\, t, \tag{D.27}$$

where the matrix u has the elements $u_{\mathbf{k},\mathbf{p}} = v(\mathbf{k}-\mathbf{p})$, and the matrix G_0 has the elements $G_{0,\mathbf{k},\mathbf{p}} = G_0(\mathbf{k}, i\varepsilon)\delta_{\mathbf{k},\mathbf{p}}$. Taking the Hermitian conjugate of t yields

$$t^\dagger = n_{\mathrm{imp}}\, u + \frac{1}{\mathcal{V}} t^\dagger G_0^\dagger u, \tag{D.28}$$

where we noted that u is Hermitian. Rearranging this equation, we see that

$$u = \frac{1}{n_{\mathrm{imp}}} t^\dagger - \frac{1}{\mathcal{V} n_{\mathrm{imp}}} t^\dagger G_0^\dagger u, \tag{D.29}$$

which can be substituted back into eq. D.27 to give

$$t = n_{\text{imp}} u - \frac{1}{\mathcal{V}^2 n_{\text{imp}}} t^\dagger G_0^\dagger u G_0 t + \frac{1}{\mathcal{V} n_{\text{imp}}} t^\dagger G_0 t. \tag{D.30}$$

Taking the diagonal components of this it is easy to see that the imaginary part of the transition matrix is determined solely by the final term above, due to being the only non-Hermitian contribution to $t_{\mathbf{k},\mathbf{k}'}$.[7] Therefore we have shown

$$\text{Im}[t_{\mathbf{k},\mathbf{k}}] = \frac{1}{\mathcal{V} n_{\text{imp}}} \text{Im}\left[\langle \mathbf{k}| \, t^\dagger G_0(i\varepsilon) t \, |\mathbf{k}\rangle\right] = \frac{1}{\mathcal{V} n_{\text{imp}}} \text{Im}\left[\sum_{\mathbf{k}'} t^\dagger_{\mathbf{k},\mathbf{k}'} G_0(\mathbf{k}', i\varepsilon) t^\dagger_{\mathbf{k}'\mathbf{k}}\right]. \tag{D.31}$$

Using the fact that $\text{Im}[\Sigma^{\text{FBA}}(\mathbf{k}, i\varepsilon)] = \text{Im}[t_{\mathbf{k},\mathbf{k}}]$ and ignoring real part of the self-energy, we find the correction to the disorder-averaged electron Green's function is

$$i \, \text{Im}[\Sigma^{\text{FBA}}(\mathbf{k}, i\varepsilon)] = \frac{i}{\mathcal{V} n_{\text{imp}}} \text{Im}\left[\sum_{\mathbf{k}'} |t_{\mathbf{k},\mathbf{k}'}|^2 G_0(\mathbf{k}', i\varepsilon)\right]. \tag{D.32}$$

Comparing this to the first order Born approximation, we see this calculation is now identical, but with $n_{\text{imp}}|v(\mathbf{k}-\mathbf{k}')|^2$ replaced by $|t_{\mathbf{k},\mathbf{k}'}|^2/n_{\text{imp}}$. This leads us to redefine the characteristic scattering time as

$$\frac{1}{\tau_{0,\mathbf{k}}} = \frac{2\pi}{\mathcal{V} n_{\text{imp}}} \sum_{\mathbf{k}'} |t_{\mathbf{k},\mathbf{k}'}|^2 \delta(\xi_{\mathbf{k}} - \xi_{\mathbf{k}'}). \tag{D.33}$$

This leads to an identical form for the self-energy, and hence disordered electron Green's function, where only the characteristic scattering rate changes.

D.4 The Self-Consistent Born Approximation

As the name suggests, the *self-consistent Born approximation* (SCBA) leads to an equation that must be solved self-consistently. In this case we use the same diagrammatic

[7] The fact we are looking at the diagonal is important here since the diagonal elements of Hermitian matrices are always real.

series as the FBA, see fig. D.5, but we now replace the free electron Green's function lines with the disorder-averaged electron Green's function. This accounts for all non-crossing diagrams that can occur in the scattering process. The corresponding equation is thus

$$\begin{aligned}\Sigma^{\mathrm{SCBA}}(\mathbf{k}, i\varepsilon) &= n_{\mathrm{imp}} v(\mathbf{0}) + \frac{1}{\mathcal{V}} \sum_{\mathbf{k}'} v(\mathbf{k}-\mathbf{k}')\, G(\mathbf{k}, i\varepsilon)\, t^{\mathrm{SCBA}}_{\mathbf{k},\mathbf{k}'} \\ &= n_{\mathrm{imp}} v(\mathbf{0}) + \frac{1}{\mathcal{V}} \sum_{\mathbf{k}'} v(\mathbf{k}-\mathbf{k}')\, t^{\mathrm{SCBA}}_{\mathbf{k},\mathbf{k}'} \frac{1}{i\varepsilon - \xi_{\mathbf{k}'} - \Sigma^{\mathrm{SCBA}}(\mathbf{k}', i\varepsilon)}.\end{aligned} \tag{D.34}$$

We repeat the same process as used for the FBA section, where we absorb the real part of the self-energy into the chemical potential and focus entirely on the imaginary part, to arrive at

$$\mathrm{Im}\left[\Sigma^{\mathrm{SCBA}}(\mathbf{k}, i\varepsilon)\right] = \mathrm{Im}\left[\frac{1}{\mathcal{V} n_{\mathrm{imp}}} \sum_{\mathbf{k}'} \frac{|t^{\mathrm{SCBA}}_{\mathbf{k},\mathbf{k}'}|^2}{i\varepsilon - \xi_{\mathbf{k}'} - i\,\mathrm{Im}\left[\Sigma^{\mathrm{SCBA}}(\mathbf{k}', i\varepsilon)\right]}\right]. \tag{D.35}$$

Rewriting this as

$$\mathrm{Im}\left[\Sigma^{\mathrm{SCBA}}(\mathbf{k}, i\varepsilon)\right] = -\frac{1}{\mathcal{V} n_{\mathrm{imp}}} \sum_{\mathbf{k}'} |t^{\mathrm{SCBA}}_{\mathbf{k},\mathbf{k}'}|^2 \frac{\varepsilon - \mathrm{Im}\left[\Sigma^{\mathrm{SCBA}}(\mathbf{k}', i\varepsilon)\right]}{\xi^2_{\mathbf{k}'} + \left(\varepsilon - \mathrm{Im}\left[\Sigma^{\mathrm{SCBA},\,R/A}(\mathbf{k}', \omega)\right]\right)^2}, \tag{D.36}$$

we note that the ansatz

$$\mathrm{Im}\left[\Sigma^{\mathrm{SCBA}}(\mathbf{k}, i\varepsilon)\right] = -\gamma_{\mathbf{k}} \mathrm{sgn}(\varepsilon), \tag{D.37}$$

where $\gamma_{\mathbf{k}} > 0$, satisfies the sign necessary for the self-energy. If we did not include the $\mathrm{sgn}(\varepsilon)$ factor, then choices of ε could exist that would lead to a contradiction in eq. D.36.

Next, we analytically continue eq. D.35, $i\varepsilon \to \omega \pm i\delta$, to yield

$$\mathrm{Im}\left[\Sigma^{\mathrm{SCBA},\,R/A}(\mathbf{k}, \omega)\right] = \frac{1}{\mathcal{V} n_{\mathrm{imp}}} \sum_{\mathbf{k}'} |t^{\mathrm{SCBA}}_{\mathbf{k},\mathbf{k}'}|^2 \frac{\mathrm{Im}\left[\Sigma^{\mathrm{SCBA},\,R/A}(\mathbf{k}', \omega)\right]}{(\omega - \xi_{\mathbf{k}'})^2 + \left(\mathrm{Im}\left[\Sigma^{\mathrm{SCBA},\,R/A}(\mathbf{k}', \omega)\right]\right)^2}. \tag{D.38}$$

The factor multiplying $|t^{\mathrm{SCBA}}_{\mathbf{k},\mathbf{k}'}|^2$ has a Lorentzian form of width $\mathrm{Im}\left[\Sigma^{\mathrm{SCBA}}(\mathbf{k}', i\varepsilon)\right]$ and centred on $\xi_{\mathbf{k}'}$. Under the assumption that the width is small, such that the Lorentzian, and hence $\mathcal{A}(\mathbf{k}, \omega)$, is strongly peaked around $\xi_{\mathbf{k}}$, we may approximate it by a delta

function as in the FBA,[8]

$$\mathrm{Im}\left[\Sigma^{\mathrm{SCBA},\,R/A}(\mathbf{k},\omega)\right] = \mp\frac{\pi}{\mathcal{V}n_{\mathrm{imp}}}\sum_{\mathbf{k}'}|t^{\mathrm{SCBA}}_{\mathbf{k},\mathbf{k}'}|^2\delta(\xi_{\mathbf{k}}-\xi_{\mathbf{k}'}). \tag{D.39}$$

Here we have included the $\mp$ to fix the sign generated by analytically continuing the ansatz in eq. D.37, as well as a factor of π to draw analogy to the first order Born approximation and FBA. This clearly has a similar form to the result we obtained using the FBA. Hence, by letting $\gamma_{\mathbf{k}} = (2\tau_{0\mathbf{k}})^{-1}$, we identify the characteristic scattering rate as

$$\frac{1}{\tau_{0,\mathbf{k}}} = \frac{2\pi}{\mathcal{V}n_{\mathrm{imp}}}\sum_{\mathbf{k}'}|t^{\mathrm{SCBA}}_{\mathbf{k},\mathbf{k}'}|^2\delta(\xi_{\mathbf{k}}-\xi_{\mathbf{k}'}). \tag{D.40}$$

Again, the general form of the self-energy is the same and hence the disorder-averaged electron Green's function takes the same form as in the FBA and first order approximation. This should come as no surprise as we can quickly show that all nested diagrams give no contribution in the weak scattering limit. In all nested diagrams, there will exist two or more Greens functions with the same momentum frequency arguments. Thus, when performing the momentum integrals as energy integrals linearised about the Fermi surface, all the poles of the integrand lie in the same half plane of the complex energy space. We may therefore choose to close our contour in the opposite half plane, which contains zero poles, and hence produce a vanishing result.

For example, consider the sixth term of fig. D.4a which depends on the following sums

$$\frac{1}{\mathcal{V}^2}\sum_{\mathbf{k},\mathbf{k}'}G_0(\mathbf{k},i\varepsilon)^2G_0(\mathbf{k}',i\varepsilon) = \frac{1}{\mathcal{V}}\sum_{\mathbf{k}'}G_0(\mathbf{k}',i\varepsilon)\int_{-\infty}^{+\infty}d\xi\frac{1}{(i\varepsilon-\xi)^2}. \tag{D.41}$$

The integral in the second line is clearly zero as the integrand's pole exists in only one half plane, and not on the real axis. This reasoning can be applied to higher order nested terms to justify their vanishing. Therefore, the fact that the SCBA gives a near identical answer in the limit of weak scattering is to be expected.

[8] If we did not assume weak scattering, then this would not be a simple delta function. In the case of strong scattering more thought has to be put into what this function could be.

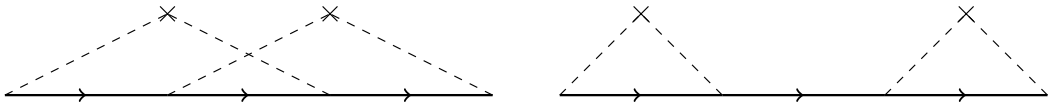

(a) (b)

Figure D.6: Left: Simplest crossing term correction to the disordered electron Green's function. Right: Second order term of the leading order approximation correction. The solid lines here represent free electron Green's functions.

D.5 Crossing Terms

So far we have included all types of diagrams besides those with crossing interactions. For a good conductor, that is one with $k_F l \gg 1$ ($\varepsilon_F \tau_0 \gg 1$) where l is the mean free path, these diagrams are negligible to those at the same order in scattering. Let us consider the simplest case shown in fig. D.6a, where the solid lines are free electron Green's functions.

Written mathematically, with an input momentum $\mathbf{p}$ and frequency $i\varepsilon$, this diagram yields

$$\frac{1}{(2\pi N(0)\tau_0)^2}\frac{1}{\mathcal{V}^2}\sum_{\mathbf{k},\mathbf{k}'} G_0(\mathbf{k}, i\varepsilon)G_0(\mathbf{k}', i\varepsilon)G_0(\mathbf{p}+\mathbf{k}'-\mathbf{k}, i\varepsilon). \tag{D.42}$$

We shall compare this to the second order contribution to the Green's function generated in the first order Born approximation, see fig. D.6b.[9] This term has the form,

$$\frac{1}{(2\pi N(0)\tau_0)^2}\left(\frac{1}{\mathcal{V}}\sum_{\mathbf{k}} G_0(\mathbf{k}, i\varepsilon)\right)^2. \tag{D.43}$$

Now, we start by appreciating that the free electron Green's functions are most singular close to the Fermi surface (i.e: sharply peaked about $\mathbf{k} = \mathbf{k}_F$), and so our sums give their most significant contributions when the Green's function momentum arguments are close to k_F. Given our earlier analysis of the spectral function, which we showed to be a Lorentzian of width $(2\tau_0)^{-1}$, for the disordered electron gas, we expect that the electrons that give rise to significant contributions lie within $(2\tau_0)^{-1}$ of the Fermi energy. Therefore

[9] We could choose to compare the crossing term to the nested diagram of the same order, and thus focus purely on the self-energy, which is entirely valid. The same argument applies, since both this diagram and the nested diagram have access to the full Fermi shell about the Fermi surface, and so have the same structure of summation. Though this assumes the nested diagram is non-vanishing.

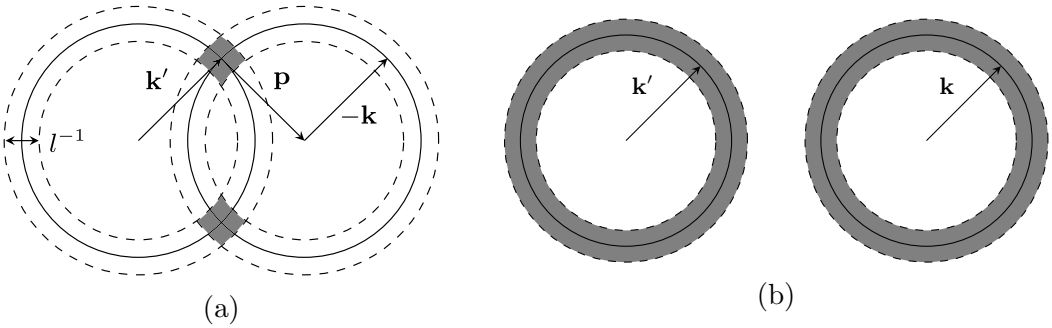

Figure D.7: Visualisation of the overlap of the Green's function momentum arguments. The shaded regions represent the parts where the product of Green's functions is significant. The solid circles are the Fermi surfaces at $\mathbf{k} = \mathbf{k}_F$, and the dashed lines are the shells of size l about the Fermi momentum. Left: significant momentum contributions for the crossed term. Right: significant momentum contributions for fig. D.43.

we wish to focus on the regions of momentum space that allow for the Green's function momentum arguments to be within $(2\tau_0^{-1})$ of the Fermi energy.

Whilst this gives us a region to work with in energy space, we wish to work in momentum space. Given there exists a small region about ε_F that leads to significant contributions, there must exist a corresponding small parameter, Δk, characterising the region about k_F in momentum space.[10] With this in mind we may say that

$$\varepsilon_F + \frac{1}{\tau_0} = \frac{(k_F + \Delta k)^2}{2m} \simeq \frac{k_F^2}{2m} + v_F \Delta k, \tag{D.44}$$

where $v_F = k_F/m$. This clearly gives $\Delta k = (v_F \tau_0)^{-1} = l^{-1}$, which is just the inverse of the mean free path, l. Therefore, only momenta within l^{-1} of k_F lead to significant contributions.

Let us now consider the crossed term in eq. D.42. We can see that if we were to sum freely over one of the two internal momenta, say $\mathbf{k}$, then the $\mathbf{k}'$ sum would be constrained in order to ensure that the magnitude of the argument $|\mathbf{k}' + \mathbf{p} - \mathbf{k}|$ was also close to k_F, whilst simultaneously keeping $\mathbf{k}'$ close to k_F. This is difficult to imagine without a diagram, so we refer to fig. D.7a to help visualise this line of argument.

Here we can see two annuli of radius k_F and thickness l^{-1}. The leftmost annulus is

[10] By saying we treat Δk as small, we mean in comparison to the Fermi momentum, k_F. Note that we also assume $\Delta\mathbf{k}$ is parallel to $\mathbf{k}_F$, hence we only need to consider their magnitudes.

centred on the origin, whilst the other is centred on $\mathbf{k}' + \mathbf{p}$. The left annulus represents the momentum space in which $G_0(\mathbf{k}', i\varepsilon)$ is notably singular, whilst the right annulus represents the region in which both $G_0(\mathbf{k}, i\varepsilon)$ and $G_0(\mathbf{k}' + \mathbf{p} - \mathbf{k}, i\varepsilon)$ are notably singular. Thus, we need only focus on the regions of overlap (the grey regions) between these Green's functions where they are all significant.

For comparison fig. D.7b shows the regions summed over for eq. D.43, which is clearly much larger than that of the crossed term. In this case there are no restrictions on the internal momenta, and so we may sum over all momentum space inside the annuli without concern. The volume of the phase space for a single sum $\sim k_F/l$, and so the phase space accessible to eq. D.43 is $\Omega_{\text{ind.}} \sim (k_F/l)^2$.

Turning to the crossed term, we can easily see that the volume of accessible phase space is comparable to $\Omega_{\text{cross}} \sim k_F/l^3$, where a factor of k_F/l comes from performing either the entire $\mathbf{k}$ or $\mathbf{k}'$ sum, and a factor of l^{-2} comes from the remaining sum. Therefore

$$\frac{\Omega_{\text{cross}}}{\Omega_{\text{ind.}}} \sim \frac{1}{k_F l}, \tag{D.45}$$

which shows that the significant phase space of the crossed term is smaller than the leading order term by a factor of $k_F l$ (assuming $k_F l > 1$). In the case of good conductors, where we must have $k_F l \gg 1$, we see that all cross terms are sub-dominant to the terms generator by the first order Born approximation. Therefore, we may neglect all terms involving crossings of impurity lines in the transport theory of metals.

As a final note, these ideas are applicable to different dimensionalities, but will give the same result that we have provided here. This concludes our appendix on the self-energy and the many different types of Born approximations one might want to apply to the problem of disorder averaging.

APPENDIX E

KUBO'S FORMULA AND LINEAR RESPONSE

Kubo originally derived his formula for linear response to determine the electrical conductivity tensor [10] as the linear response of the electrical current density to an applied electric field. In this appendix we present the most general form of Kubo's formula based on the books of Rickayzen [29] and Bruus & Flensberg [31].

Given the statistical nature of condensed matter field theory, we wish to understand and calculate the statistical averages of observables. We therefore concern ourselves with determining the quantity $\langle M \rangle$ when we wish to measure the observable M. This average, represented by the angled brackets, contains both a quantum average and a statistical average at finite temperature in the grand canonical ensemble.[1] Hence, the system's behaviour and measurable quantities are determined by its density matrix, ρ. This average is given in eq. 2.3, but we quote it here for ease of reference

$$\langle ... \rangle = \mathrm{Tr}\left[\rho \, ...\right], \qquad \rho = \frac{1}{\mathcal{Z}} e^{-\beta(H-\mu N)}, \qquad \mathcal{Z} = \mathrm{Tr}\left[e^{-\beta(H-\mu N)}\right], \tag{E.1}$$

[1] We can think of statistical averaging as "classical" averaging. The ideas used for this part of the averaging procedure are those used in statistical mechanics. The technical points and ideas behind quantum and statistical averages are of great importance in many-body systems, where mixed states are the dominant objects of concern, rather than simple many-body pure states. It is best to spend some time reading and thinking about what pure and mixed states are to truly appreciated the mathematics in condensed matter field theory.

where N is the number operator, μ is the chemical potential, and H is the Hamiltonian of our system. The trace can be written in terms of the eigenstates of H as

$$\mathrm{Tr}\left[...\right] = \sum_n \langle n| ... |n\rangle \,, \tag{E.2}$$

where the eigenstate $|n\rangle$ has the eigenvalue E_n. We shall use the same shorthand notation we defined in section 2.1 to take these eigenvalues relative to the chemical potential, $\widetilde{E}_n = E_n - \mu N_n$.

Let us now consider a system with an initial time independent and particle conserving Hamiltonian, H_0, which can be solved exactly (i.e. it can diagonalised/we can find its appropriate Green's function). We also assume the system is in equilibrium before the application of an external field. This last statement is equivalent to assuming the density matrix is time independent before any external field is applied. Suppose now that we apply a time dependent external field to the system described by the Hamiltonian $H'(t)$, which acts for times $t \geq t_0$ as a small perturbation. Our Hamiltonian for times greater than t_0 is the combination $H + H'(t)$. In general we may write our full Hamiltonian as

$$H = H_0 + H'(t)\Theta(t - t_0). \tag{E.3}$$

To find how the expectation value of an observable, M, evolves in time we need to understand how the density matrix evolves in time. Equivalently, we can ask how the eigenstates of H evolve with time. We explore the details behind the time evolution of the density matrix in appendix C, and so we start from the differential equation defining its time evolution

$$i\frac{\partial}{\partial t}\rho(t) = [H(t), \rho(t)]. \tag{E.4}$$

Next we apply a transformation to move our density matrix from the Schrödinger

picture, $\rho(t)$, to the interaction picture (see appendix A.1.3), $\widetilde{\rho}(t)$, which yields

$$\begin{aligned} i\frac{\partial\widetilde{\rho}}{\partial t} =& [\widetilde{H}'(t), \widetilde{\rho}], \\ \rho(t) = \mathcal{U}_0(t)\,\widetilde{\rho}(t)\,\mathcal{U}_0^\dagger(t) \qquad & \widetilde{H}'(t) = \mathcal{U}_0^\dagger(t)\,H'(t)\,\mathcal{U}_0(t) \end{aligned} \tag{E.5}$$

For $t \leq t_0$ the system is in equilibrium so $\rho(t \leq t_0) = \rho_0$, and the external field has not yet been applied meaning ρ and $\mathcal{U}_0(t)$ commute. Therefore, we have the initial condition

$$\widetilde{\rho}(t \leq t_0) = \rho_0. \tag{E.6}$$

Integrating the first line of eq. E.5 with respect to t generates a self-consistent integral equation,

$$\widetilde{\rho}(t) = \rho_0 - i\int_{t_0}^{t} dt'[\widetilde{H}'(t'), \widetilde{\rho}(t')]. \tag{E.7}$$

To obtain the linear response we only wish to retain terms that are either constant or linear in H', therefore can substitute eq. E.7 into itself and drop any $\mathcal{O}(H'^2)$ terms or higher. Doing so gives the density matrix, in the Schrödinger picture, to first order in H' to be

$$\rho(t) = \rho_0 - i\,\mathcal{U}_0(t)\int_{t_0}^{t} dt'[\widetilde{H}'(t'), \rho_0]\,\mathcal{U}_0^\dagger(t). \tag{E.8}$$

We may now consider the expectation value of an observable, M. Using eq. E.8 we see that

$$\begin{aligned} \langle M\rangle &= \mathrm{Tr}\,[\rho(t)M] \\ &= \mathrm{Tr}\,[\rho_0 M] - i\,\mathrm{Tr}\left[M\mathcal{U}_0(t)\int_{t_0}^{t} dt'[\widetilde{H}'(t'), \rho_0]\mathcal{U}_0^\dagger(t)\right] \\ &= \langle M\rangle_0 + i\int_{t_0}^{t} dt'\mathrm{Tr}\left[\rho_0[\widetilde{H}'(t'), \widetilde{M}(t)]\right], \\ &= \langle M\rangle_0 + \delta\langle M\rangle_0 \end{aligned} \tag{E.9}$$

where $\widetilde{M}(t) = \mathcal{U}_0^\dagger(t)M\mathcal{U}_0(t)$ is just the observable's operator in the interaction picture. This is the famous Kubo formula.

As a generic example, let us choose $H'(t) = A(t)B$, where $A(t)$ is the applied field and B is an operator belonging to the system.[2] The linear response of the observable can then be written as

$$\begin{aligned}\delta \langle M \rangle_0 &= i \int_{t_0}^{t} dt' A(t') \mathrm{Tr} \left[\rho_0 [\widetilde{B}(t'), \widetilde{M}(t)] \right] \\ &= \int_{t_0}^{+\infty} dt' A(t') G^R(t, t'),\end{aligned} \tag{E.10}$$

where

$$G^R(t, t') = -i \left\langle [\widetilde{M}(t), \widetilde{B}(t')] \right\rangle_0 \Theta(t - t') \tag{E.11}$$

is a retarded Green's function.

E.1 Electrical Current

Here let us consider the case of electrical current specifically. We gave the result in section 3.2 when we derived the Drude conductivity for a homogeneous system, so we shall give the details skipped in obtaining eq. 3.26.

By applying an electric field, $\mathbf{E}$, to a system, the electrical current density, $\mathbf{J}$, response is determined by the conductivity tensor, $\sigma_{\alpha\beta}$,

$$J_\alpha(\mathbf{r}, t) = \sum_\beta \int_{-\infty}^{+\infty} dt' \int d^d r' \sigma_{\alpha\beta}(\mathbf{r} - \mathbf{r}', t - t') \mathbf{E}(\mathbf{r}', t'). \tag{E.12}$$

By working in the Coulomb gauge we may write the electric field purely in terms of the vector potential, $\mathbf{A}$,

$$\mathbf{E} = -\frac{\partial \mathbf{A}}{\partial t}. \tag{E.13}$$

To find the temporal Fourier transform of the current density, we write σ and $\mathbf{A}$ in terms

[2] Using the example given by Rickayzen [29], the field could be a magnetic field whilst the operator could be the magnetic moment density operator.

of their inverse Fourier transforms,

$$\begin{aligned}
J_\alpha(\mathbf{r},t) &= -\sum_\beta \int_{-\infty}^{+\infty} dt' \int d^d r' \int_{-\infty}^{+\infty} \frac{d\omega}{2\pi} \sigma_{\alpha\beta}(\mathbf{r}-\mathbf{r}',\omega) e^{-i\omega(t-t')} \\
&\qquad\qquad \times \frac{\partial}{\partial t'} \int_{-\infty}^{+\infty} \frac{d\omega'}{2\pi} A_\beta(\mathbf{r}',\omega') e^{-i\omega' t'} \\
&= \sum_\beta \int d^d r' \int_{-\infty}^{+\infty} \frac{d\omega}{2\pi} \int_{-\infty}^{+\infty} d\omega' \sigma_{\alpha\beta}(\mathbf{r}-\mathbf{r}',\omega) e^{-i\omega t} i\omega' A_\beta(\mathbf{r}',\omega') \\
&\qquad\qquad \times \int_{-\infty}^{+\infty} \frac{dt'}{2\pi} e^{i(\omega-\omega')t'} \qquad \text{(E.14)} \\
&= \sum_\beta \int d^d r' \int_{-\infty}^{+\infty} \frac{d\omega}{2\pi} \int_{-\infty}^{+\infty} d\omega' \sigma_{\alpha\beta}(\mathbf{r}-\mathbf{r}',\omega) e^{-i\omega t} i\omega' A_\beta(\mathbf{r}',\omega') \delta(\omega-\omega') \\
&= \sum_\beta \int d^d r' \int_{-\infty}^{+\infty} \frac{d\omega}{2\pi} i\omega \sigma_{\alpha\beta}(\mathbf{r}-\mathbf{r}',\omega) A_\beta(\mathbf{r}',\omega) e^{-i\omega t} \\
&= \int_{-\infty}^{+\infty} \frac{d\omega'}{2\pi} J_\alpha(\mathbf{r},\omega) e^{-i\omega t}.
\end{aligned}$$

Therefore we arrive at

$$J_\alpha(\mathbf{r},\omega) = i\omega \sum_\beta \int d^d r' \sigma_{\alpha\beta}(\mathbf{r}-\mathbf{r}',\omega) A_\beta(\mathbf{r}',\omega). \qquad \text{(E.15)}$$

From this it is clear that the conductivity tensor is given by the linear response of the current density to the vector potential. Next, we need to determine the perturbation to the Hamiltonian created by the external field's vector potential. We will only consider the linear behaviour of the Hamiltonian, as we are concerning ourselves with weak changes meaning higher orders in $\mathbf{A}$ are negligible.

In the presence of a vector potential the GC Hamiltonian for a disordered system written in terms of field operators is (see eq. 3.23)

$$\mathscr{H} = \sum_\sigma \int d^d r\, \psi_\sigma^\dagger(\mathbf{r}) \left[\frac{(-i\nabla - e\mathbf{A}(\mathbf{r},t))^2}{2m} + U(\mathbf{r}) - \mu \right] \psi_\sigma(\mathbf{r}). \qquad \text{(E.16)}$$

If we expand this to isolate terms containing $\mathbf{A}$ this becomes

$$\begin{aligned}\mathscr{H} &= \sum_\sigma \int d^d r\, \psi_\sigma^\dagger(\mathbf{r}) \left[-\frac{\nabla^2}{2m} - \mu + U(\mathbf{r})\right] \psi_\sigma(\mathbf{r}) \\ &\qquad + i\sum_\sigma \int d^d r\, \psi_\sigma^\dagger(\mathbf{r}) \left[\frac{ie}{2m}\nabla\cdot\mathbf{A} + \frac{ie}{2m}\mathbf{A}\cdot\nabla + \frac{e^2}{2m}A^2\right] \psi_\sigma(\mathbf{r}) \\ &= \mathscr{H}_0 + \sum_\sigma \int d^d r \left[\frac{ie}{2m}\left[\psi_\sigma^\dagger(\mathbf{r})\left\{\nabla\psi_\sigma(\mathbf{r})\right\} - \left\{\nabla\psi_\sigma^\dagger(\mathbf{r})\right\}\psi_\sigma(\mathbf{r})\right]\right. \\ &\qquad \left. + \frac{e^2}{2m}\mathbf{A}\psi_\sigma^\dagger(\mathbf{r})\psi_\sigma(\mathbf{r})\right]\cdot\mathbf{A}\end{aligned} \tag{E.17}$$

where in the second line we integrated by parts to shift the gradient operator from acting on $\mathbf{A}\psi$ to act on $\psi^\dagger$.

Now, in retaining only terms that are at most linear in $\mathbf{A}$, we may write $\mathscr{H} = \mathscr{H}_0 + H'(t)$ with

$$H'(t) = -\int d^d r\, \mathbf{j}_0(\mathbf{r})\cdot\mathbf{A}(\mathbf{r},t), \tag{E.18}$$

Here, $\mathbf{j}_0$ is the electrical current density operator in the absence of a vector potential,

$$\mathbf{j}_0(\mathbf{r}) = -\frac{ie}{2m}\sum_\sigma \left[\left\{\nabla\psi_\sigma^\dagger(\mathbf{r})\right\}\psi_\sigma(\mathbf{r}) - \psi_\sigma^\dagger(\mathbf{r})\,\nabla\psi_\sigma(\mathbf{r})\right]. \tag{E.19}$$

The full current operator in the presence of a vector potential is found by minimally coupling $\mathbf{j}_0$,

$$\mathbf{j}(\mathbf{r},t) = \mathbf{j}_0(\mathbf{r}) - \frac{e^2}{m}\mathbf{A}(\mathbf{r},t)\sum_\sigma \psi_\sigma^\dagger(\mathbf{r})\psi_\sigma(\mathbf{r}), \tag{E.20}$$

Given the current density operator and linearised Hamiltonian, we may now apply Kubo's formula from eq. E.9 (more specifically eq. E.10) to determine the response of the total current density of the system, $\mathbf{j}$, to an electric field applied for times $t \geq t_0$. In

applying Kubo's formula, we find

$$\begin{aligned}\langle j_\alpha(\mathbf{r},t)\rangle &= \langle \mathbf{j}_0(\mathbf{r})\rangle - \frac{e^2}{m}A_\alpha(\mathbf{r},t)\sum_\sigma \left\langle \psi^\dagger_\sigma(\mathbf{r})\psi_\sigma(\mathbf{r})\right\rangle \\ &\simeq \langle \mathbf{j}_0(\mathbf{r})\rangle_0 - i\sum_\beta \int d^dr' \int_{t_0}^{t} dt' A_\beta(\mathbf{r}',t')\mathrm{Tr}\left[\rho_0[\,\widetilde{j}_{0\beta}(\mathbf{r}',t'),\widetilde{j}_{0\alpha}(\mathbf{r},t)\,]\right] \\ &\quad - \frac{e^2}{m}A_\alpha(\mathbf{r},t)\sum_\sigma \left\langle \psi^\dagger_\sigma(\mathbf{r})\psi_\sigma(\mathbf{r})\right\rangle_0 \\ &= \langle j_{0\alpha}(\mathbf{r})\rangle_0 - i\sum_\beta \int d^dr' \int_{t_0}^{+\infty} dt' A_\beta(\mathbf{r}',t')\mathcal{G}^R_{\alpha\beta}(\mathbf{r},t;\mathbf{r}',t') \\ &\quad - \frac{n'(\mathbf{r})e^2}{m}A_\alpha(\mathbf{r},t),\end{aligned} \tag{E.21}$$

where $n'(\mathbf{r}) = \sum_\sigma \left\langle \psi^\dagger_\sigma(\mathbf{r})\psi_\sigma(\mathbf{r})\right\rangle_0$ is the electron number density for a specific impurity distribution, and

$$\mathcal{G}^R_{\alpha\beta}(\mathbf{r},t;\mathbf{r}',t') = -i\left\langle \left[\widetilde{j}_{0\alpha}(\mathbf{r},t),\widetilde{j}_{0\beta}(\mathbf{r}',t')\right]\right\rangle_0 \Theta(t-t'), \tag{E.22}$$

is the retarded microscopic current-current correlator. Lastly, to isolate the driven response of the system we extend the lower limit of the t' integral to $-\infty$. This ensures that the transient response due to switching the electric field on at t_0 decays by the time of measurement, t.

So far we have considered a specific distribution of impurities, and thus a microscopic current density. If we wish to model the macroscopic current density we observe, we need to average over all possible impurity distributions. That is to say $\mathbf{J}(\mathbf{r},t) = \langle\langle \mathbf{j}(\mathbf{r},t)\rangle\rangle^{(0)}_{\mathrm{dis}} = \langle \mathbf{j}(\mathbf{r},t)\rangle_{\mathrm{dis}}$. We shall also assume after disorder averaging that the electron number density is constant and uniform, $n = \langle n'(\mathbf{r})\rangle^{(0)}_{\mathrm{dis}}$.

After averaging over impurity distributions, we arrive at the linear response of the electrical current density to the application of an external electric field described by the

vector potential $\mathbf{A}$,

$$J_\alpha(\mathbf{r},t) = \langle j_{0,\alpha}(\mathbf{r},t)\rangle_{\rm dis} - \frac{ne^2}{m}A_\alpha(\mathbf{r},t) - \sum_\beta \int_{-\infty}^{+\infty} dt' \int d^d r'\, \mathcal{G}^R_{\alpha\beta}(\mathbf{r},t;\mathbf{r}',t')A_\beta(\mathbf{r}',t'), \tag{E.23}$$

where

$$\mathcal{G}^R_{\alpha\beta}(\mathbf{r},t;\mathbf{r}',t') = -i\Big\langle \Big[\widetilde{j}_{0,\alpha}(\mathbf{r},t), \widetilde{j}_{0,\beta}(\mathbf{r}',t') \Big] \Big\rangle_{0,\rm dis} \Theta(t-t'), \tag{E.24}$$

is the retarded current-current correlator.

APPENDIX F

OBSERVING WEAK LOCALISATION

In section 3.3.2 we found the temperature dependence of WL corrections to the electrical DC conductivity, so it is only natural to ask "how might we observe such a phenomenon experimentally?", to which there is a simple answer: we apply a magnetic field. This works because the cooperon lacks time reversal symmetry, unlike the diffuson; the cooperon is a particle-particle (hole-hole) propagator which is mapped onto a hole-hole (particle-particle) propagator by time reversal. In comparison, the diffuson is a particle-hole propagator, so under time reversal it remains a particle-hole propagator.

Alternatively, we could imagine threading a self-intersecting loop with the magnetic field. This means the phase picked up by an electron traversing the loop in one direction will be different to the phase obtained by travelling in the opposite direction around the loop. Naturally, we would expect this to produce oscillatory behaviour in the magneto-resistance of a material, as certain field strengths would allow for the two phases to differ by an integer multiple of 2π.

To show how oscillatory behaviour appears in the magneto-resistance, let us start by considering the experiments of Sharvin et. al. [49] and Al'tshuler et. al. [50]. These experiments used a thin metallic cylinder threaded with a magnetic field, which we illus-

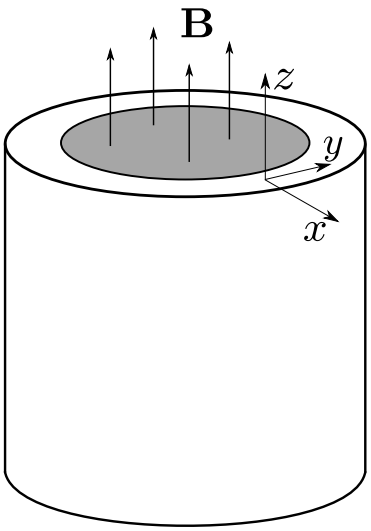

Figure F.1: Set up of a thin metal cylinder threaded by a magnetic field. The alignment of our coordinate axes is also shown.

trate in fig. F.1. The extent of the cylinder along the z axis dictates whether the observed phenomenon will be one or two dimensional in nature. These correspond to a short and long cylinder respectively.

The magnetic field dependence of the WL corrections in $d = 1$ and $d = 2$ was developed theoretically in 1981 by Al'tshuler et. al. [82]. In this work they showed that the WL correction oscillated as a function of the magnetic flux threading the cylinder, Φ_B, with a period of the magnetic flux quantum $\Phi_0 = hc/(2e)$ (not using natural units).[1]

To obtain these results from the diagrammatics, we need to introduce the knowledge of a magnetic field into the cooperon. Let us consider the Green's functions that build the cooperon, $G(\mathbf{q} + \mathbf{k}, i\varepsilon + i\omega)$ and $G(-\mathbf{k}, i\varepsilon)$. We define our magnetic field in terms of a vector potential, $\mathbf{A}$, which varies slowly in space (i.e. weak spatial dependence). This allows us to neglect the commutators between the momentum operator and vector potential. As a result the free electron piece of the Hamiltonian transforms according to

[1]The magnetic flux quantum written here is in Gaussian cgs units, which is a more convenient choice when dealing with electromagnetic phenomena. If we were to write this in SI units it would simply be $\Phi_0 = h/(2e)$.

$(c = 1)$,

$$\mathscr{H}_0 = \sum_\sigma \sum_{\mathbf{k}} \left[\frac{k^2}{2m} - \mu \right] c^\dagger_{\mathbf{k}\sigma} c_{\mathbf{k},\sigma} \to \sum_\sigma \sum_{\mathbf{k}} \left[\frac{1}{2m} (\mathbf{k} + e\mathbf{A})^2 - \mu \right] c^\dagger_{\mathbf{k}\sigma} c_{\mathbf{k},\sigma}. \tag{F.1}$$

Hence, the inclusion of a vector potential simply replaces k^2 with $(\mathbf{k} + e\mathbf{A})^2$. We may therefore deduce the disorder-averaged electron Green's function in the presence of $\mathbf{A}$ to be,

$$G(\mathbf{k}, i\varepsilon; \mathbf{A}) = G(\mathbf{k} + e\mathbf{A}, i\varepsilon) = \frac{1}{i\varepsilon + \xi_{\mathbf{k}+e\mathbf{A}} + \frac{i}{2\tau_0}\mathrm{sgn}(\varepsilon)}. \tag{F.2}$$

Now, the cooperon is determined by $G(\mathbf{q}+\mathbf{k}, i\varepsilon+i\omega)G(-\mathbf{k}, i\varepsilon)$, which becomes $G(\mathbf{q}+e\mathbf{A}+\mathbf{k}, i\varepsilon+i\omega)G(e\mathbf{A}-\mathbf{k}, i\varepsilon)$ upon $\mathbf{A}$'s inclusion, summed over the "fast" momentum, $\mathbf{k}$.[2] We may freely transform this momentum by $\mathbf{k} \to \mathbf{k} + e\mathbf{A}$ without affecting the sum. Doing so gives the cooperon self-energy to be

$$\sum_{\mathbf{k}} G(\mathbf{q} + 2e\mathbf{A} + \mathbf{k}, i\varepsilon + \omega) G(-\mathbf{k}, i\varepsilon), \tag{F.3}$$

which is the same as shifting $\mathbf{q} \to \mathbf{q} + 2e\mathbf{A}$ in the original problem. Thus, the cooperon in the presence of a vector potential (with weak spatial dependence) is simply,

$$\widetilde{C}(\mathbf{q}, i\varepsilon + i\omega, i\varepsilon; \mathbf{A}) = \frac{1}{2\pi N(0)\tau_0^2} \frac{1}{\mathcal{D}(\mathbf{q} + 2e\mathbf{A})^2 + |\omega| + \tau_\phi^{-1}}. \tag{F.4}$$

This approach is exactly the same as that used in [34].

It is clear to see that the cooperon has become less singular for $q, \omega \to 0$, and therefore reduces the size of the WL correction. If we now use this cooperon, we find the general formula for the WL correction in the presence of a magnetic field to be,

$$\sigma_{WL}(i\Omega) = -\frac{2e^2\mathcal{D}}{\pi} \sum_{\mathbf{q}} \frac{1}{\mathcal{D}(\mathbf{q} + 2e\mathbf{A})^2 + \Omega + \tau_\phi^{-1}}. \tag{F.5}$$

[2]The momentum $\mathbf{k}$ we can typically associate to being the electron's initial momentum before being affected by the "transfer" momentum $\mathbf{q}$. Since we generally take $\mathbf{k}$ to be near the Fermi surface, it is characteristically large and hence a fast momentum.

Here the system's dimensionality and geometry become extremely important. We shall now consider the system to be a thin cylinder that is either quasi-1D or quasi-2D to compare to the observations in [49, 50]. Hence, we closely follow the methodology of [82].

We model this as a system that is extended in both the y and z axes ($d = 2$) or just the y axis ($d = 1$), and impose periodic boundary conditions along the y axis. This means we align the axes as shown in fig. F.1, where the x axis is radial, the y axis runs along the circumference of the thin cylinder, and the z axis runs parallel to the applied magnetic field.

We may rewrite eq. F.5 as a hybrid between an integral and sum. The x and z components of the momentum are integrated over, as they can be viewed as extended without periodic boundary conditions, and so are effectively continuous. However, the y component of momentum is quantised according to $2\pi n/L_y$, where $L_y = 2\pi R$ is the circumference of the cylinder, and R is the cylinder's radius.[3] This quantisation arises from the requirement that the electron wave function must satisfy $\phi(x, y, z) = \phi(x, y + L_y, z)$ due to periodic boundary conditions.

The hybrid form of eq. 3.84 in the DC limit is then

$$\begin{aligned}\sigma_{WL} &= \frac{2e^2\mathcal{D}}{\pi}\frac{1}{L_y}\int\frac{dq_x dq_z}{(2\pi)^2}\sum_{n=-\infty}^{+\infty}\frac{1}{\mathcal{D}(q_x^2+q_z^2)+\mathcal{D}(\frac{2\pi n}{L_y}-2eA)^2+\tau_\phi^{-1}} \\ &= \frac{2e^2}{\pi}\frac{1}{L_y}\int\frac{dq_x dq_z}{(2\pi)^2}\sum_{n=-\infty}^{+\infty}\frac{1}{q_x^2+q_z^2+(\frac{2\pi}{L_y})^2(n-\frac{\Phi_B}{\Phi_0})^2+l_\phi^{-1}},\end{aligned} \tag{F.6}$$

where the factor of L_y^{-1} comes from us accounting for the factor of $\mathcal{V}^{-1}$ explicitly, and we have chosen a gauge that makes the y component of $\mathbf{A}$ its only non-zero component. By writing $\mathcal{V} = L_x L_y L_z$, the x and z system lengths are cancelled by replacing their sums with integrals, leaving just L_y. To relate Φ_B to A, we used

$$\Phi_B = \int_S \mathbf{B}\cdot d\mathbf{S} = \oint_C \mathbf{A}\cdot d\mathbf{r} = L_y A, \tag{F.7}$$

[3] L_y is just the system's size in the y direction within a unit cell.

where in the last equality we used the fact that $\mathbf{A}$ is purely along the y axis, and therefore parallel to the contour traversed, C.

Given the cylinder is thin, we may neglect the q_x component and treat the system as being two dimensional. If we further restrict the cylinder to be short in the z axis, then we have a quasi-one dimensional system meaning we may ignore the q_z component as well. Let us only consider the $d = 1$ case as a way to illustrate the oscillatory behaviour.[4] Here we use the identity (see appendix M.3)

$$\begin{aligned}\sum_{n=-\infty}^{+\infty} \frac{1}{\alpha^2(n-\beta)^2+\gamma^2} &= \frac{\pi}{2\alpha\gamma}\left[\coth\left(\frac{\pi\gamma}{\alpha}+i\pi\beta\right)+\coth\left(\frac{\pi\gamma}{\alpha}-i\pi\beta\right)\right] \\ &= \frac{\pi}{\alpha\gamma}\frac{\sinh\left(\frac{2\pi\gamma}{\alpha}\right)}{\cosh\left(\frac{2\pi\gamma}{\alpha}\right)-\cos\left(2\pi\beta\right)},\end{aligned} \tag{F.8}$$

to yield

$$\sigma_{WL} = \frac{e^2}{\pi} l_\phi \frac{\sinh\left(\frac{L_y}{l_\phi}\right)}{\cosh\left(\frac{L_y}{l_\phi}\right)-\cos\left(2\pi\frac{\Phi_B}{\Phi_0}\right)}, \qquad (d=1). \tag{F.9}$$

Clearly the the WL correction oscillates as a function of the magnetic flux threading the cylinder with a period of the flux quantum Φ_0.

The appearance of the flux quantum implies that the charge carrier responsible for this process has a charge of $2e$, due to the $2e$ in the denominator of Φ_0. This is a direct reflection of the underlying physical process responsible for weak localisation. Specifically, it is a result of the coherent back scattering of an electron (hole), which is equivalent to particle-particle (hole-hole) diffusion and so the diffusive process is described by a particle of charge $2e$.

[4] For those interested in the 2D case, the calculation is performed by Al'tshuler et. al. in [50].

APPENDIX G

ELECTRON-ELECTRON INTERACTION – CALCULATION DETAILS

In this appendix we give the details behind the calculation of the screened Coulomb interaction using RPA in section G.1. In section G.2, we provide the details for the EEI correction to the electrical conductivity regarding the cancellation of the first three diagrams, A-C. Finally, in section G.3, we show how to deal with the integrals and sums appearing in the EEI correction to the electrical conductivity in different dimensions.

G.1 Screened Coulomb and RPA

Here we evaluate the first term of the screened Coulomb interaction's polarisation bubble, $\Pi_0(\mathbf{q}, i\omega)$, in eq. 3.89, following ideas similar to Rickayzen's analysis of the Drude conductivity [29].[1] We start by approximating the momentum sum as an integral linearised

[1] Other approaches to computing this term exist, see [34] for example. However, I would also like to thank Jacob Spink in finding this approach to computing the empty bubble.

around the Fermi surface and writing the Green's functions in spectral form,

$$\Pi_0(\mathbf{q}, i\varepsilon) = -2N(0) \int d\hat{\Omega}_d \int_{-\infty}^{+\infty} d\xi \times \int_{-\infty}^{+\infty} dx \int_{-\infty}^{+\infty} dy\, T \sum_{\varepsilon} \frac{\mathcal{A}(\mathbf{k}+\mathbf{q}, x)\mathcal{A}(\mathbf{k}, y)}{[i(\varepsilon+\omega) - x][i\varepsilon - y]}. \tag{G.1}$$

We must perform the frequency sum first due to issues of convergence in the summand preventing us from freely swapping the order of summation. With the details given in appendix M.4, we find

$$\Pi_0(\mathbf{q}, i\varepsilon) = -2N(0) \int d\hat{\Omega}_d \int_{-\infty}^{+\infty} d\xi_{\mathbf{k}} \times \int_{-\infty}^{+\infty} dx \int_{-\infty}^{+\infty} dy \frac{\mathcal{A}(\mathbf{k}+\mathbf{q}, x)\mathcal{A}(\mathbf{k}, y)[f(y) - f(x)]}{y - x + i\omega}. \tag{G.2}$$

Using eq. 2.21, we see that

$$\mathcal{A}(\mathbf{k}, x) = \frac{1}{2\pi\tau_0} \frac{1}{(x - \xi_{\mathbf{k}})^2 + \frac{1}{4\tau_0^2}}. \tag{G.3}$$

We then perform the the x integral for the term containing $f(y)$ and the y integral for the term containing $f(x)$ to yield[2]

$$\Pi_0(\mathbf{q}, i\omega) = -2N(0) \int d\hat{\Omega}_d \int_{-\infty}^{+\infty} d\xi_{\mathbf{k}} \times \int_{-\infty}^{+\infty} dx f(x) \left[\frac{\mathcal{A}(\mathbf{k}, x)}{x - \xi_{\mathbf{k}+\mathbf{q}} + i\omega + \frac{i}{2\tau_0}} - \frac{\mathcal{A}(\mathbf{k}+\mathbf{q}, x)}{\xi_{\mathbf{k}} - x + i\omega + \frac{i}{2\tau_0}} \right]. \tag{G.4}$$

Since only the electrons near the Fermi surface contribute significantly and $\mathbf{k}$ is the momentum of the electron Green's function, we see that only small momentum transfers, $\mathbf{q}$, are of notable importance. Given this condition, $q \ll k \sim k_F$, we may approximate

$$\xi_{\mathbf{k}+\mathbf{q}} \simeq \xi_{\mathbf{k}} + \frac{\mathbf{k} \cdot \mathbf{q}}{m} \simeq \xi_{\mathbf{k}} + \mathbf{v}_F \cdot \mathbf{q}. \tag{G.5}$$

[2]We use complex analysis with semi-circular contours closed in the upper half plane (y integral) and the lower half plane (x integral) to evaluate these integrals.

Substituting this into eq. G.4 produces an integral of the form

$$I = \int_{-\infty}^{+\infty} d\xi \int_{-\infty}^{+\infty} dx f(x) F(x-\xi), \tag{G.6}$$

inside the angular integral. We now use the same trick as Rickayzen by integrating this expression by parts, whilst assuming $F(x-\xi) \sim \xi^{-n}$ with $n > 1$ for $|\xi| \to \infty$,[3] to obtain

$$\begin{aligned} I &= -\int_{-\infty}^{+\infty} d\xi \xi \frac{d}{d\xi} \int_{-\infty}^{+\infty} dx f(x) F(x-\xi) \\ &= -\int_{-\infty}^{+\infty} d\xi \xi \int_{-\infty}^{+\infty} dx f(x) \frac{d}{d\xi} F(x-\xi) \\ &= \int_{-\infty}^{+\infty} d\xi \xi \int_{-\infty}^{+\infty} dx f(x) \frac{d}{dx} F(x-\xi) \\ &= -\int_{-\infty}^{+\infty} d\xi \xi \int_{-\infty}^{+\infty} dx \frac{df}{dx} F(x-\xi). \end{aligned} \tag{G.7}$$

In the final line we performed integration by parts on the x integral. We may now freely interchange the orders of integration as df/dx is sufficiently convergent as $|x| \to \infty$. Hence,

$$\begin{aligned} \Pi_0(\mathbf{q}, i\omega) =& 2N(0) \int d\hat{\Omega}_d \int_{-\infty}^{+\infty} dx \frac{df}{dx} \\ & \times \int_{-\infty}^{+\infty} d\xi \xi \left[\frac{\mathcal{A}(\mathbf{k}, x)}{x - \xi - \mathbf{v}_F \cdot \mathbf{q} + i\omega + \frac{i}{2\tau_0}} - \frac{\mathcal{A}(\mathbf{k}+\mathbf{q}, x)}{\xi - x + i\omega + \frac{i}{2\tau_0}} \right]. \end{aligned} \tag{G.8}$$

Performing the ξ integral via complex analysis gives

$$\Pi_0(\mathbf{q}, i\omega) = 2N(0) \int d\hat{\Omega}_d \int_{-\infty}^{+\infty} dx \frac{df}{dx} \frac{\mathbf{v}_F \cdot \mathbf{q} - \frac{i}{\tau_0}}{i\omega + \frac{i}{\tau_0} - \mathbf{v}_F \cdot \mathbf{q}}. \tag{G.9}$$

The x integral is trivial and yields

$$\Pi_0(\mathbf{q}, i\omega) = -2N(0) \int d\hat{\Omega}_d \frac{\mathbf{v}_F \cdot \mathbf{q} - \frac{i}{\tau_0}}{i\omega + \frac{i}{\tau_0} - \mathbf{v}_F \cdot \mathbf{q}} = -2N(0) \int d\hat{\Omega}_d \frac{\tau_0 \mathbf{v}_F \cdot \mathbf{q} - i}{i(1+\omega\tau_0) - \tau_0 \mathbf{v}_F \cdot \mathbf{q}}. \tag{G.10}$$

[3] This is to ensure that all surface terms vanish.

We may neglect the $\omega\tau_0$ piece in the imaginary part of the denominator as we are in the diffusive limit. Therefore we see that $\Pi_0(\mathbf{q}, i\omega) = 2N(0)$ for any choice of dimensionality.

G.2 Cancellation of Diagrams A, B, and C

We begin by calculating the diagrams A and B in fig. 3.18a and fig. 3.18b respectively,[4] in the presence of an electric field with Matsubara frequency $\Omega > 0$. The electromagnetic response functions these diagrams are

$$\begin{aligned} K^{(A)}_{\alpha\beta}(i\Omega) = -\frac{4e^2}{m^2}T^2 \sum_{\varepsilon,\omega}\sum_{\mathbf{k},\mathbf{q}} \Big[& k_\alpha k_\beta V(\mathbf{q}, i\omega) G(\mathbf{k}, i\varepsilon + i\Omega)^2 G(\mathbf{k}, i\varepsilon) \\ & \times G(\mathbf{k}+\mathbf{q}, i\varepsilon + i\Omega + i\omega) D(\mathbf{q}, i\varepsilon + i\Omega + i\omega, i\varepsilon + i\Omega)^2 \Big], \end{aligned} \tag{G.11a}$$

$$\begin{aligned} K^{(B)}_{\alpha\beta}(i\Omega) = -\frac{4e^2}{m^2}\frac{T^2}{2\pi N(0)\tau_0} \sum_{\varepsilon,\omega}\sum_{\mathbf{k},\mathbf{k}',\mathbf{q}} \Big[& k_\alpha k_\beta V(\mathbf{q}, i\omega) G(\mathbf{k}, i\varepsilon + i\Omega)^2 G(\mathbf{k}, i\varepsilon) \\ & \times G(\mathbf{k}', i\varepsilon + i\Omega)^2 G(\mathbf{k}'+\mathbf{q}, i\varepsilon + i\Omega + i\omega) \\ & \times D(\mathbf{q}, i\varepsilon + i\Omega + i\omega, i\varepsilon + i\Omega)^2 \Big]. \end{aligned} \tag{G.11b}$$

The factors of 4 out front in these expressions come from a factor of 2 for electron spin, and an additional factor of 2 for the variant diagrams with the interaction, and single correlated impurity scattering event, on the lower half of the diagram. The minus sign is due to the interaction carrying a minus sign.[5]

The presence of the diffusons at either end of the interaction only allow for certain sign choices of the frequencies to give non-zero contributions to the diagram's correction. The Green's functions involved with the diffuson must be of opposite sign, and so we are left with three possible sign choices, as illustrated in fig. G.1. In the case of fig. 3.18a we may break the electromagnetic response function into three parts: $\varepsilon, (\varepsilon + \Omega) < 0$ and $\varepsilon + \Omega + \omega > 0$ (fig. G.1a), which gives $K^{(A1)}_{\alpha\beta}$; $\varepsilon, (\varepsilon + \Omega) > 0$ and $\varepsilon + \Omega + \omega < 0$ (fig. G.1b), which gives $K^{(A2)}_{\alpha\beta}$; $\varepsilon + \Omega > 0$ and $\varepsilon, (\varepsilon + \Omega + \omega) < 0$ (fig. G.1c), which gives $K^{(A3)}_{\alpha\beta}$. These

[4] These are sometimes referred to as DOS type diagrams.

[5] Recall an interaction introduces $-V(\mathbf{q}, i\omega)$.

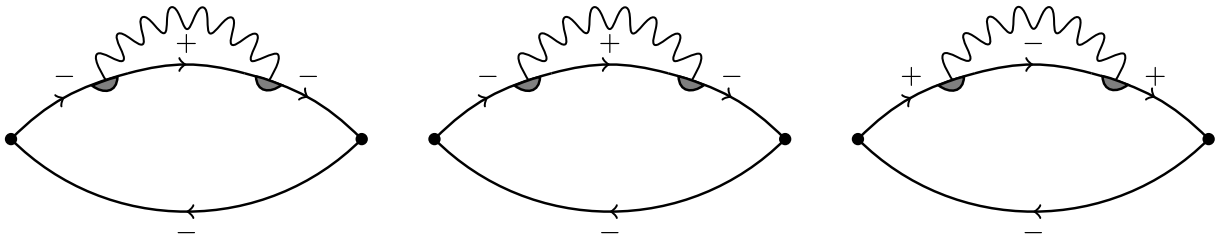

Figure G.1: Sign choices for the DOS diagram in fig. 3.18a. (a), (b), and (c) correspond to the $A1$, $A2$, and $A3$ contributions respectively. (c) is also the only possible sign configuration for fig. 3.18b, as the single impurity line does not change the electron's energy.

response functions are given by,

$$K_{\alpha\beta}^{(A1)}(i\Omega) = -\frac{4e^2}{m^2}T^2 \times \sum_{\omega>0} \sum_{-(\Omega+\omega)<\varepsilon<-\Omega} \sum_{\mathbf{k},\mathbf{q}} \Big[k_{F\alpha}k_{F\beta}V(\mathbf{q},i\omega)G^-(\mathbf{k})^3G^+(\mathbf{k})D(\mathbf{q},i\omega)^2\Big], \tag{G.12a}$$

$$K_{\alpha\beta}^{(A2)}(i\Omega) = -\frac{4e^2}{m^2}T^2 \times \sum_{\omega<-\Omega} \sum_{0<\varepsilon<-(\Omega+\omega)} \sum_{\mathbf{k},\mathbf{q}} \Big[k_{F\alpha}k_{F\beta}V(\mathbf{q},i\omega)G^+(\mathbf{k})^3G^-(\mathbf{k})D(\mathbf{q},i\omega)^2\Big], \tag{G.12b}$$

$$K_{\alpha\beta}^{(A3)}(i\Omega) = -\frac{4e^2}{m^2}T^2 \left[\sum_{-\Omega\le\omega<0} \sum_{-\Omega<\varepsilon<-(\Omega+\omega)} + \sum_{\omega<-\Omega} \sum_{-\Omega<\varepsilon<0}\right] \times \sum_{\mathbf{k},\mathbf{q}} \Big[k_{F\alpha}k_{F\beta}V(\mathbf{q},i\omega)G^+(\mathbf{k})^2G^-(\mathbf{k})^2D(\mathbf{q},i\omega)^2\Big]. \tag{G.12c}$$

Here we have already accounted for the fact that only the electrons close to Fermi surface contribute significantly the sums and hence transport, $|\mathbf{k}| \simeq k_F$. In doing this, we have also assumed that $\mathbf{q}$ is small compared to k_F.[6]

The electron momenta, $\mathbf{k}$, are summed over using the diffusive momentum sum identity in eq. 3.75. We then let $\omega \to -\omega$ in eqs. G.12b and G.12c, making note that $V(\mathbf{q}, i\omega)$

[6]This is natural as larger values of $\mathbf{q}$ would give rise to less singular contributions, as $G(\mathbf{k}+\mathbf{q}, i\varepsilon + i\Omega + i\omega)$ will significantly smaller for larger $\mathbf{q}$.

and $D(\mathbf{q}, i\omega)$ are unaffected by this,[7] to yield

$$K_{\alpha\beta}^{(A1)}(i\Omega) = \frac{8\pi N(0)e^2k_F^2\tau_0}{m^2d}\delta_{\alpha\beta}\,T^2\sum_{\omega>0}\sum_{-(\Omega+\omega)<\varepsilon<-\Omega}\sum_{\mathbf{q}}\frac{V(\mathbf{q},i\omega)}{(\omega+\mathcal{D}q^2)^2}, \tag{G.13a}$$

$$K_{\alpha\beta}^{(A2)}(i\Omega) = \frac{8\pi N(0)e^2k_F^2\tau_0}{m^2d}\delta_{\alpha\beta}\,T^2\sum_{\omega>\Omega}\sum_{0<\varepsilon<\omega-\Omega}\sum_{\mathbf{q}}\frac{V(\mathbf{q},i\omega)}{(\omega+\mathcal{D}q^2)^2}, \tag{G.13b}$$

$$\begin{aligned}K_{\alpha\beta}^{(A3)}(i\Omega) = &-\frac{16\pi N(0)e^2k_F^2\tau_0}{m^2d}\delta_{\alpha\beta}\,T^2\\ &\times\left[\sum_{0<\omega\leq\Omega}\sum_{-\Omega<\varepsilon<\omega-\Omega}+\sum_{\omega>\Omega}\sum_{-\Omega<\varepsilon<0}\right]\sum_{\mathbf{q}}\frac{V(\mathbf{q},i\omega)}{(\omega+\mathcal{D}q^2)^2}.\end{aligned} \tag{G.13c}$$

These expressions have ε independent summands, meaning the ε sums can be evaluated with ease. We are thus left with

$$K_{\alpha\beta}^{(A1)}(i\Omega) = 4N(0)e^2\mathcal{D}\,\delta_{\alpha\beta}\,T\sum_{\omega>0}\sum_{\mathbf{q}}\omega\frac{V(\mathbf{q},i\omega)}{(\omega+\mathcal{D}q^2)^2}, \tag{G.14a}$$

$$K_{\alpha\beta}^{(A2)}(i\Omega) = 4N(0)e^2\mathcal{D}\,\delta_{\alpha\beta}\,T\sum_{\omega>\Omega}\sum_{\mathbf{q}}(\omega-\Omega)\frac{V(\mathbf{q},i\omega)}{(\omega+\mathcal{D}q^2)^2}, \tag{G.14b}$$

$$K_{\alpha\beta}^{(A3)}(i\Omega) = -8N(0)e^2\mathcal{D}\,\delta_{\alpha\beta}\,T\left[\sum_{0<\omega\leq\Omega}\omega+\sum_{\omega>\Omega}\Omega\right]\sum_{\mathbf{q}}\frac{V(\mathbf{q},i\omega)}{(\omega+\mathcal{D}q^2)^2}. \tag{G.14c}$$

Now, considering fig. 3.18b it might appear that the same sign choices can be made as in fig. 3.18a. However, the presence of the single impurity line causes the first and second sign choices to vanish, as the Green's functions with momentum $\mathbf{k}$ will all have poles in the same half plane, meaning the $\mathbf{k}$ sum, when analytically continued, can have its contour closed in the empty half plane. Therefore, we need only evaluate the third

[7] Look back at their expressions in eq. 3.94 and eq. 3.74 and see that they depend upon $|\omega|$.

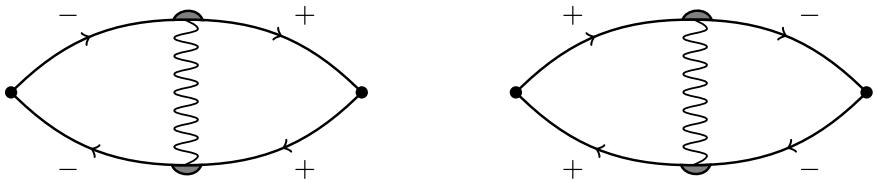

Figure G.2: Sign choices for the diagram in fig. 3.18c. Panels a and b correspond to the $C1$ and $C2$ contributions respectively.

sign choice. The resulting contribution is then[8]

$$K^{(B)}_{\alpha\beta}(i\Omega) = 4N(0)e^2\mathcal{D}\,\delta_{\alpha\beta}\,T\left[\sum_{0<\omega\leq\Omega}\omega + \sum_{\omega>\Omega}\Omega\right]\sum_{\mathbf{q}}\frac{V(\mathbf{q},i\omega)}{(\omega+\mathcal{D}q^2)^2}, \tag{G.15}$$

which is clearly $-K^{(A3)}_{\alpha\beta}(i\Omega)/2$.

Moving on to diagram C in fig. 3.18c, we may write the response function

$$\begin{aligned} K^{(C)}_{\alpha\beta}(i\Omega) = -\frac{2e^2}{m^2}T^2\sum_{\omega,\varepsilon}\sum_{\mathbf{k},\mathbf{q}}\Big[&k_\alpha(\mathbf{k}+\mathbf{q})_\beta V(\mathbf{q},i\omega)G(\mathbf{k},i\varepsilon+i\Omega)G(\mathbf{k},i\varepsilon)\\ &\times G(\mathbf{k}+\mathbf{q},i\varepsilon+i\Omega+i\omega)G(\mathbf{k}+\mathbf{q},i\varepsilon+i\omega)\\ &\times D(\mathbf{q},i\varepsilon+i\omega,i\varepsilon)D(\mathbf{q},i\varepsilon+i\Omega,i\varepsilon+i\Omega+i\omega)\Big]. \end{aligned} \tag{G.16}$$

First we note that the momentum $\mathbf{k}$ is the electron momentum, and so is close to the Fermi momentum. In comparison, $\mathbf{q}$ is a small momentum exchange in the diffusive limit, such that we may approximate $(\mathbf{k}+\mathbf{q})_\beta \simeq k_\beta$. Next, the diffusons enforce the two possible sign choices shown in fig. G.2; $\varepsilon, (\varepsilon+\Omega) < 0$ and $(\varepsilon+\Omega+\omega), (\varepsilon+\omega) > 0$ (fig. G.2a), which corresponds to $K^{(C1)}_{\alpha\beta}(i\Omega)$; $\varepsilon, (\varepsilon+\Omega) > 0$ and $(\varepsilon+\Omega+\omega), (\varepsilon+\omega) < 0$ (fig. G.2b), which corresponds to $K^{(C2)}_{\alpha\beta}(i\Omega)$. Performing the $\mathbf{k}$ sum in the diffusive limit followed by the ε sum, we find that both sign choices give the same result, $K^{(C1)}_{\alpha\beta}(i\Omega) = K^{(C2)}_{\alpha\beta}(i\Omega)$. Thus,

$$K^{(C)}_{\alpha\beta}(i\Omega) = -8N(0)e^2\mathcal{D}\,\delta_{\alpha\beta}\,T\sum_{\omega>\Omega}\sum_{\mathbf{q}}(\omega-\Omega)\frac{V(\mathbf{q},i\omega)}{(\omega+\mathcal{D}q^2)^2}, \tag{G.17}$$

[8]We skip the details here, as we have given a large amount of detail on how to perform these types of calculations when dealing with fig. 3.18a. Extra details will only be included where necessary from here onwards. For example, in the case of tricks or new technical points.

which is just $-2K^{(A2)}_{\alpha\beta}(i\Omega)$.

Combining the contributions of the first three diagrams we see that,

$$\begin{aligned} K^{(A)}_{\alpha\beta}(i\Omega) + K^{(B)}_{\alpha\beta}(i\Omega) + K^{(C)}_{\alpha\beta}(i\Omega) & \\ &= K^{(A1)}_{\alpha\beta}(i\Omega) + K^{(A2)}_{\alpha\beta}(i\Omega) + K^{(A3)}_{\alpha\beta}(i\Omega) + K^{(B)}_{\alpha\beta}(i\Omega) + K^{(C)}_{\alpha\beta}(i\Omega) \\ &= K^{(A1)}_{\alpha\beta}(i\Omega) + \frac{1}{2}K^{(A3)}_{\alpha\beta}(i\Omega) - K^{(A2)}_{\alpha\beta}(i\Omega) \\ &= 0. \end{aligned} \tag{G.18}$$

The last line is most easily seen by noting that the $\omega > \Omega$ sum of $K^{(A3)}_{\alpha\beta}(i\Omega)$ and the term with Ω in the numerator of $K^{(A2)}_{\alpha\beta}(i\Omega)$ cancel in the above combination. The remaining pieces of $K^{(A2)}_{\alpha\beta}(i\Omega)$ and $K^{(A3)}_{\alpha\beta}(i\Omega)$ in the above then sum to give $-K^{(A1)}_{\alpha\beta}(i\Omega)$, and hence a trivial result for the sum of the first three diagrams.

G.3 EEI Corrections in Different Dimensions

In this section we provide the details for calculating eq. 3.103 for different dimensionalities,

$$K_{\alpha\beta}(i\Omega) = -\frac{16N(0)e^2\mathcal{D}^2}{d}\,\delta_{\alpha\beta}\,T\left[\sum_{0<\omega\leq\Omega}\omega + \sum_{\omega>\Omega}\Omega\right]\sum_{\mathbf{q}}\frac{q^2V(\mathbf{q},i\omega)}{(\mathcal{D}q^2+\omega)^2(\mathcal{D}q^2+\omega+\Omega)}. \tag{G.19}$$

For $d = 2$ we can perform the momentum sum followed by the frequency sum without issue, though the momentum sum will require an appropriate upper cut-off. However, the $d = 1$ and $d = 3$ cases do not require the same cut-off to obtain convergent results.[9]

Starting with $d = 2$ and we approximating the sum by an integral, we are left to evaluate

$$\int_0^\infty \frac{dq}{2\pi}\frac{q}{(\mathcal{D}q^2+\omega)^2} = \frac{1}{4\pi\mathcal{D}}\int_0^{1/\tau_0}\frac{dx}{(x+\omega)^2}, \tag{G.20}$$

where we used eq. 3.97 for $V(\mathbf{q}, i\omega)$ due to being in the diffusive limit, and $x = \mathcal{D}q^2$. We also introduced a cut-off in the upper limit for consistency with the diffusive limit,

[9]Technically all dimensions should have a cut-off based on the diffusive limit, $\mathcal{D}q_c^2 = \tau_0^{-1}$, but we can obtain the same approximate results by replacing this with infinity for $d = 1$ and $d = 3$ due to the convergent nature of their integrals.

$\mathcal{D}q^2 \ll \tau_0^{-1}$.[10] Performing the integral yields,

$$\frac{1}{4\pi\mathcal{D}}\int_0^{1/\tau_0}\frac{dx}{(x+\omega)^2} = \frac{1}{4\pi\mathcal{D}}\left(\frac{1}{\omega}-\frac{\tau_0}{1+\omega\tau_0}\right) \simeq \frac{1}{4\pi\mathcal{D}\omega}, \tag{G.21}$$

where we have approximated using the diffusive limit, $\omega\tau_0 \ll 1$. This thus leaves,

$$K_{\alpha\beta}(i\Omega) = -\frac{e^2}{\pi}\delta_{\alpha\beta}T\left[\sum_{0<\omega\leq\Omega}1+\sum_{\omega>\Omega}\frac{\Omega}{\omega}\right]. \tag{G.22}$$

The first of these sums is trivial and gives $\Omega/(2\pi T)$, whilst the second sum diverges logarithmically at its upper limit. As with the momentum integral, we can introduce a physical cut-off to the upper limit based upon the diffusive limit. Since $\omega = 2\pi nT$ and $\omega\tau_0 \ll 1$, we define $n_{\max} = (2\pi T\tau_0)^{-1}$. Similarly, since $\omega > \Omega$ we also define $n_{\min} = \Omega/(2\pi T)+1$. Hence, we may write the second sum as

$$\frac{1}{2\pi T}\sum_{n=n_{\min}}^{n_{\max}}\frac{\Omega}{n} = \frac{1}{2\pi T}\sum_{n=0}^{n_{\max}-n_{\min}}\frac{\Omega}{n+\frac{\Omega}{2\pi T}+1}. \tag{G.23}$$

We evaluate this sum as a difference of digamma functions, $\psi(x)$,[11]

$$\frac{1}{2\pi T}\sum_{n=0}^{\frac{1}{2\pi T\tau_0}-\frac{\Omega}{2\pi T}-1}\frac{\Omega}{n+\frac{\Omega}{2\pi T}+1} = \frac{\Omega}{2\pi T}\left[\psi\left(\frac{1}{2\pi T\tau_0}\right)-\psi\left(\frac{\Omega}{2\pi T}+1\right)\right]. \tag{G.24}$$

In the limit $x \gg 1$, $\psi(x) \simeq \ln(x)$, which can be applied to the first digamma function in eq. G.24 due to the diffusive limit, $T\tau_0 \ll 1$, to give

$$\frac{1}{2\pi T}\sum_{n=0}^{\frac{1}{2\pi T\tau_0}-\frac{\Omega}{2\pi T}-1}\frac{\Omega}{n+\frac{\Omega}{2\pi T}+1} = \left[\ln\left(\frac{1}{2\pi T\tau_0}\right)-\psi\left(\frac{\Omega}{2\pi T}+1\right)\right]. \tag{G.25}$$

[10] We simply set the upper limit to be equal to the largest scale set by the limit. In this case the largest "allowed" value of $\mathcal{D}q^2$ is τ_0^{-1}.

[11] Details of this function are given in appendix N.

We therefore find

$$\begin{aligned} K_{\alpha\beta}(i\Omega) &= -\frac{e^2\Omega}{2\pi^2}\delta_{\alpha\beta}\left[1+\ln\left(\frac{1}{2\pi T\tau_0}\right)-\psi\left(\frac{\Omega}{2\pi T}+1\right)\right] \\ &\simeq -\frac{e^2\Omega}{2\pi^2}\delta_{\alpha\beta}\left[\ln\left(\frac{1}{2\pi T\tau_0}\right)-\psi\left(\frac{\Omega}{2\pi T}+1\right)\right]. \end{aligned} \tag{G.26}$$

Finally, by using $K_{\alpha\beta}(i\Omega) = \Omega\sigma_{\alpha\beta}(i\Omega) = \Omega\delta_{\alpha\beta}\sigma(i\Omega)$,[12] we arrive at the corrections to the electrical conductivity for a disordered thin metallic film,

$$\sigma^{(2\mathrm{D})}_{\mathrm{EEI}}(i\Omega) = -\frac{e^2}{2\pi^2}\left[\ln\left(\frac{1}{2\pi T\tau_0}\right)-\psi\left(\frac{\Omega}{2\pi T}+1\right)\right]. \tag{G.27}$$

Hence, the DC conductivity is simply

$$\sigma^{(2\mathrm{D})}_{\mathrm{EEI}} = -\frac{e^2}{2\pi^2}\ln\left(\frac{1}{2\pi T\tau_0}\right), \tag{G.28}$$

as $\psi(1) = -\gamma$, where γ the Euler-Mascheroni constant, is at most of order unity.

To find the $d = 1$ and $d = 3$ results, let us return to eq. G.19 and again perform the momentum integral. However, we are only interested in the leading order behaviour in Ω, so we may expand to $\mathcal{O}(\Omega)$.[13] This yields

$$\sigma_{\mathrm{EEI}} = -\frac{e^2}{2\pi^2}\frac{\alpha_d}{d}\mathcal{D}^{1-\frac{d}{2}}T\left[\lim_{\Omega\to 0}\frac{1}{\Omega}\sum_{0<\omega\leq\Omega}\omega^{\frac{d}{2}-1}+\sum_{\omega>0}\omega^{\frac{d}{2}-2}\right], \tag{G.29}$$

where

$$\alpha_d = \begin{cases} 4\pi^2, & d=1 \\ 2\pi, & d=3. \end{cases} \tag{G.30}$$

[12] This simplification is not true in general, but in all the cases we explore in this thesis we will only encounter diagonal conductivity tensors.

[13] This trick can be shown to produce the correct answer if we consider the sum using the standard analytic continuation tricks.

Manipulating the frequency sums produces Hurwitz zeta functions,[14]

$$\begin{aligned}\sum_{\omega>0}\omega^{\frac{d}{2}-2} &= \frac{1}{(2\pi T)^{2-\frac{d}{2}}}\sum_{n=1}^{\infty} n^{\frac{d}{2}-2} \\ &= \frac{1}{(2\pi T)^{\frac{d}{2}-2}}\sum_{n=0}^{\infty}\frac{1}{(n+1)^{2-\frac{d}{2}}} = \frac{1}{(2\pi T)^{2-\frac{d}{2}}}\zeta\left(2-\frac{d}{2},1\right),\end{aligned} \tag{G.31a}$$

$$\begin{aligned}\frac{1}{\Omega}\sum_{0<\omega\leq\Omega}\omega^{\frac{d}{2}-1} &= \frac{1}{(2\pi T)^{1-\frac{d}{2}}}\frac{1}{\Omega}\sum_{n=1}^{\frac{\Omega}{2\pi T}} n^{\frac{d}{2}-1} \\ &= \frac{1}{(2\pi T)^{1-\frac{d}{2}}}\frac{1}{\Omega}\left[\sum_{n=1}^{\infty} n^{\frac{d}{2}-1} - \sum_{n=\frac{\Omega}{2\pi T}+1}^{\infty} n^{\frac{d}{2}-1}\right] \\ &= \frac{1}{(2\pi T)^{1-\frac{d}{2}}}\frac{1}{\Omega}\left[\zeta\left(1-\frac{d}{2},1\right) - \zeta\left(1-\frac{d}{2},1+\frac{\Omega}{2\pi T}\right)\right] \\ &\overset{\Omega\to 0}{=} -\frac{1}{(2\pi T)^{2-\frac{d}{2}}}\frac{d}{dx}\left[\zeta\left(1-\frac{d}{2},x\right)\right]\Big|_{x=1} \\ &= \frac{1}{(2\pi T)^{2-\frac{d}{2}}}\left(1-\frac{d}{2}\right)\zeta\left(2-\frac{d}{2},1\right).\end{aligned} \tag{G.31b}$$

Substituting these into eq. G.29 leads to

$$\sigma_{\text{EEI}}^{(d=1,3)} = -\frac{e^2}{2\pi^2}\left(\frac{T}{\mathcal{D}}\right)^{\frac{d}{2}-1}\frac{\alpha_d}{(2\pi)^{2-\frac{d}{2}}}\frac{4-d}{2d}\zeta\left(2-\frac{d}{2},1\right), \tag{G.32}$$

which is exactly what was given in eq. 3.104.

[14] See appendix N for its properties.

APPENDIX H

THE PAIR PROPAGATOR: AN HONEST DERIVATION

In this appendix we shall follow Larkin and Varlamov [56] to show how the pair propagator term with no impurity scattering between BCS interactions is included. To do this we must calculate the vertex part denoted by the hatched region in fig. 3.22. We shall associate $\Gamma_c(\mathbf{q}, i\varepsilon_1, i\varepsilon_2)$ to this object with a closed end, see fig. H.1. This vertex part is given by the self-consistent equation[1]

$$\begin{aligned}\Gamma_c(\mathbf{q}, i\varepsilon + i\omega, -i\varepsilon) &= 1 + \sum_{\mathbf{k}} \frac{G(\mathbf{k}+\mathbf{q}, i\varepsilon + i\omega)G(-\mathbf{k}, -i\varepsilon)}{2\pi N(0)\tau_0}\Gamma_c(\mathbf{q}, i\varepsilon + i\omega, -i\varepsilon) \\ &= 1 + \Sigma_c\,\Gamma_c(\mathbf{q}, i\varepsilon + i\omega, -i\varepsilon).\end{aligned} \tag{H.1}$$

This can be easily rearranged to give Γ_c in terms of Σ_c, and so leaves us to evaluate the $\mathbf{k}$ sum. Before we assume that we are in the diffusive limit, let us show how we can obtain the expression given in eq. 5.26 of [56].

[1] This type of equation is also known as a Bethe-Salpeter equation, see [34].

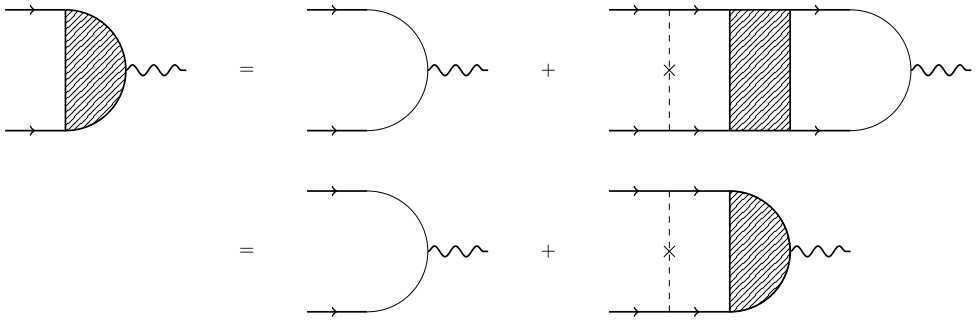

Figure H.1: Modified cooperon vertex part to include no scatterings between the Green's functions.

As usual, we linearise the momentum integral about the Fermi surface to produce,

$$\begin{aligned}
&\sum_{\mathbf{k}} G(\mathbf{k}+\mathbf{q}, i\varepsilon + i\omega)G(-\mathbf{k}, -i\varepsilon) \\
&\qquad \simeq -N(0)\int d\hat{\Omega}_d \int_{-\infty}^{+\infty} d\xi \Bigg[\frac{1}{i\varepsilon + \xi + \frac{i}{2\tau_0}\mathrm{sgn}(\varepsilon)} \\
&\qquad\qquad \times \frac{1}{i\varepsilon + i\omega - \xi - \mathbf{v}_F\cdot\mathbf{q} + \frac{i}{2\tau_0}\mathrm{sgn}(\varepsilon+\omega)} \Bigg] \\
&\qquad = \pi i N(0)\int d\hat{\Omega}_d \frac{\Theta(\varepsilon(\varepsilon+\omega))[\mathrm{sgn}(\varepsilon+\omega)+\mathrm{sgn}(\varepsilon)]}{2i\varepsilon + i\omega - \mathbf{v}_F\cdot\mathbf{q} + \frac{i}{2\tau_0}[\mathrm{sgn}(\varepsilon+\omega)+\mathrm{sgn}(\varepsilon)]} \\
&\qquad = 2\pi i N(0)\int d\hat{\Omega}_d \frac{\Theta(\varepsilon(\varepsilon+\omega))\mathrm{sgn}(2\varepsilon+\omega)}{2i\varepsilon + i\omega - \mathbf{v}_F\cdot\mathbf{q} + \frac{i}{\tau_0}\mathrm{sgn}(2\varepsilon+\omega)} \\
&\qquad = 2\pi i N(0)\int d\hat{\Omega}_d \frac{\Theta(\varepsilon(\varepsilon+\omega))}{i|2\varepsilon+\omega| - \mathbf{v}_F\cdot\mathbf{q} + \frac{i}{\tau_0}} \\
&\qquad = 2\pi N(0)\int d\hat{\Omega}_d \frac{\Theta(\varepsilon(\varepsilon+\omega))}{|2\varepsilon+\omega| + \frac{1}{\tau_0} + i\mathbf{v}_F\cdot\mathbf{q}}.
\end{aligned} \tag{H.2}$$

At this point, Larkin and Varlamov [56] expand in powers of $\mathbf{v}_F\cdot\mathbf{q}$ by considering only small momenta, and retain terms up to order $(\mathbf{v}_F\cdot\mathbf{q})^2$. This is entirely analogous to what we did for the diffuson in section 3.3.1, however we have not assumed the diffusive limit

here as we have not stated anything about the relative size of T (and hence the Matsubara frequencies ε and ω) compared to τ_0^{-1}. This expansion gives,

$$\begin{aligned}\sum_{\mathbf{k}} G(\mathbf{k}+\mathbf{q}, i\varepsilon + i\omega)G(-\mathbf{k}, -i\varepsilon) \\ &\simeq \frac{2\pi N(0)}{|2\varepsilon+\omega| + \frac{1}{\tau_0}} \int d\hat{\Omega}_d \left(1 - \frac{(\mathbf{v}_F \cdot \mathbf{q})^2}{(|2\varepsilon+\omega| + \frac{1}{\tau_0})^2}\right) \Theta(\varepsilon(\varepsilon+\omega)) \\ &= \frac{2\pi N(0)}{|2\varepsilon+\omega| + \frac{1}{\tau_0}} \left(1 - \frac{1}{(|2\varepsilon+\omega| + \frac{1}{\tau_0})^2} \frac{v_F^2 q^2}{d}\right) \Theta(\varepsilon(\varepsilon+\omega)),\end{aligned} \tag{H.3}$$

and hence

$$\Sigma_c = \frac{1}{\tau_0} \frac{1}{|2\varepsilon+\omega| + \frac{1}{\tau_0}} \left(1 - \frac{1}{(|2\varepsilon+\omega| + \frac{1}{\tau_0})^2} \frac{v_F^2 q^2}{d}\right) \Theta(\varepsilon(\varepsilon+\omega)). \tag{H.4}$$

For comparison to [56], we have assumed that our Fermi surface is spherical in computing the angular integral for the $(\mathbf{v}_F \cdot \mathbf{q})^2$ piece. If the Fermi surface was not trivial (i.e. anisotropic) the angular integral would give a different result, and may not even be possible to calculate in general. In this case, the $(\mathbf{v}_F \cdot \mathbf{q})^2$ term can be thought of as being averaged over the Fermi surface, which is exactly how Larkin and Varlamov [56] treat this problem. In their notation, instead of performing the angular integral for the $(\mathbf{v}_F \cdot \mathbf{q})^2$ term, they simply write it as $\langle (\mathbf{v}_F \cdot \mathbf{q})^2 \rangle_{\text{F.S.}}$ to denote the average over the Fermi surface.

Substituting eq. H.4 into eq. H.1 and rearranging for Γ_c, we see,

$$\Gamma_c(\mathbf{q}, i\varepsilon + i\omega, -i\varepsilon) = \frac{|2\varepsilon+\omega| + \frac{1}{\tau_0}}{|2\varepsilon+\omega| + \frac{1}{\tau_0} + (\frac{1}{|2\varepsilon+\omega|\tau_0+1}\mathcal{D}q^2 - \frac{1}{\tau_0})\Theta(\varepsilon(\varepsilon+\omega))}, \tag{H.5}$$

which is an entirely identical result to Larkin and Varlamov's eq. 5.26 [56] for a spherically symmetric Fermi surface. If we now apply the diffusive limit, where $T\tau_0 \ll 1$ and so $|2\varepsilon+\omega|\tau_0 \ll 1$, eq. H.5 simply collapses to the result we're used to dealing with, where we did not include the term with no scatterings between the Green's functions,

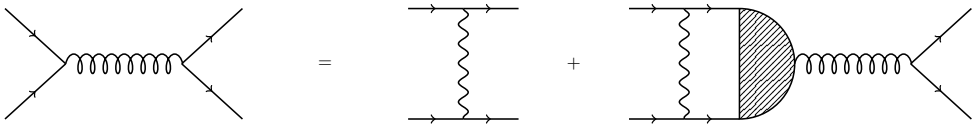

Figure H.2: Alternate, but equivalent, way of writing the diagrammatic series for the pair propagator given in fig. 3.22.

$$\begin{aligned}\widetilde{\Gamma}_c(\mathbf{q}, i\varepsilon + i\omega, -i\varepsilon) &\simeq \Theta(-\varepsilon(\varepsilon+\omega)) + \frac{1}{\tau_0}\frac{\Theta(\varepsilon(\varepsilon+\omega))}{|2\varepsilon+\omega| + \mathcal{D}q^2} \\ &\simeq \frac{1}{\tau_0}\frac{\Theta(\varepsilon(\varepsilon+\omega))}{|2\varepsilon+\omega| + \mathcal{D}q^2} \\ &= C(\mathbf{q}, i\varepsilon + i\omega, -i\varepsilon).\end{aligned} \tag{H.6}$$

Now, we can write the pair propagator as a Dyson equation based on the series show in fig. H.2. This diagram is entirely equivalent to what we dealt with previously in section 3.5.1. The pair propagator's self-energy (fluctuation ploarisation operator), which was originally split up into $\Pi_{fl,0}(\mathbf{q}, i\omega)$ and $\Pi_{fl,1}(\mathbf{q}, i\omega)$, can now be written as one compact object,

$$\Pi_{fl}(\mathbf{q}, i\omega) = T\sum_{\varepsilon}\sum_{\mathbf{k}} G(\mathbf{k}+\mathbf{q}, i\varepsilon + i\omega)G(-\mathbf{k}, -i\varepsilon)\widetilde{\Gamma}_c(\mathbf{q}, i\varepsilon + i\omega, -i\varepsilon). \tag{H.7}$$

In applying the diffusive limit, $\widetilde{\Gamma}_c(\mathbf{q}, i\varepsilon+i\omega, -i\varepsilon) \simeq C(\mathbf{q}, i\varepsilon+i\omega, -i\varepsilon)$, and so $\Pi_{fl}(\mathbf{q}, i\omega) \simeq \Pi_{fl,1}(\mathbf{q}, i\omega)$. We therefore see that the contribution of $\Pi_{fl,0}(\mathbf{q}, i\omega)$ is negligible in the diffusive limit.

APPENDIX I

FLUCTUATION CONDUCTIVITY – CALCULATION DETAILS

In this appendix we provide the details behind some of the points made in the section 3.5.3, as well as section 5.4.2. Namely, we will show how sum of the diagrams in fig. 3.23 vanishes in the limit of zero external frequency, as well as why we choose to focus on diagrams A, B, C, and F. In doing this, we provide the outline of how to set up the response functions we quote in the main text. In a similar manner, we also show how the analogous diagrams for granular systems, see fig. 5.13, sum to zero in the absence of a non-zero external frequency.

Showing that the sum of all diagrams vanish when the external frequency is zero is vital to assuring that we have accounted for all diagrams. Since this only justifies that we have accounted for all diagrams and does not provide any insight into the physics we observe, these details would have simply clogged the main body of this thesis. In a similar vain, we need only worry about the parts of calculation unique to superconducting fluctuations in the main text. Therefore, the necessary, but repetitive, procedure of setting up the response functions, determining their non-zero sign choices, and the contributions arising from each choice would have also made chapter 3 bloated and an arduous read. We therefore expand upon these details here.

I.1 Vanishing Zero Frequency Response – Homogeneous Metals

The total leading order correction to the conductivity due to superconducting fluctuations is given by the diagrams in fig. 3.23. Let us begin by writing each diagram's electromagnetic response function,

$$K^{(A)}_{\alpha\beta}(i\Omega) = -\frac{4e^2}{m^2}T^2\sum_{\varepsilon,\omega}\sum_{\mathbf{k},\mathbf{q}}\Big[k_\alpha k_\beta G(\mathbf{k},i\varepsilon+i\Omega)^2 G(\mathbf{q}-\mathbf{k},i\omega-i\varepsilon-i\Omega) \times G(\mathbf{k},i\varepsilon)C(\mathbf{q},i\varepsilon+i\Omega,i\omega-i\varepsilon-i\Omega)^2 L(\mathbf{q},i\omega)\Big], \tag{I.1a}$$

$$K^{(B)}_{\alpha\beta}(i\Omega) = -\frac{4e^2}{m^2}\frac{T^2}{2\pi N(0)\tau_0}\sum_{\varepsilon,\omega}\sum_{\mathbf{k},\mathbf{k}',\mathbf{q}}\Big[k_\alpha k_\beta G(\mathbf{k},i\varepsilon+i\Omega)^2 G(\mathbf{k},i\varepsilon) \times G(\mathbf{k}',i\varepsilon+i\Omega)^2 G(\mathbf{q}-\mathbf{k}',i\omega-i\varepsilon-i\Omega) \times C(\mathbf{q},i\varepsilon+i\Omega,i\omega-i\varepsilon-i\Omega)^2 L(\mathbf{q},i\omega)\Big], \tag{I.1b}$$

$$K^{(C)}_{\alpha\beta}(i\Omega) = -\frac{2e^2}{m^2}T^2\sum_{\varepsilon,\omega}\sum_{\mathbf{k},\mathbf{q}}\Big[k_\alpha(\mathbf{q}-\mathbf{k})_\beta G(\mathbf{k},i\varepsilon+i\Omega)G(\mathbf{q}-\mathbf{k},i\omega-i\varepsilon-i\Omega) \times G(\mathbf{k},i\varepsilon)G(\mathbf{q}-\mathbf{k},i\omega-i\varepsilon)C(\mathbf{q},i\varepsilon+i\Omega,i\omega-i\varepsilon-i\Omega) \times C(\mathbf{q},i\varepsilon,i\omega-i\varepsilon)L(\mathbf{q},i\omega)\Big], \tag{I.1c}$$

$$K^{(D)}_{\alpha\beta}(i\Omega) = -\frac{4e^2}{m^2}T^2\sum_{\varepsilon,\omega}\sum_{\mathbf{k},\mathbf{k}',\mathbf{q}}\Big[k_\alpha k'_\beta G(\mathbf{k},i\varepsilon+i\Omega)G(\mathbf{q}-\mathbf{k},i\omega-i\varepsilon-i\Omega) \times G(\mathbf{k},i\varepsilon)G(\mathbf{k}',i\varepsilon)G(\mathbf{k}',i\varepsilon+i\Omega)G(\mathbf{q}-\mathbf{k}',i\omega-i\varepsilon-i\Omega) \times C(\mathbf{q},i\varepsilon+i\Omega,i\omega-i\varepsilon-i\Omega)^2\widetilde{C}(\mathbf{q},i\omega-i\varepsilon-i\Omega,i\varepsilon)L(\mathbf{q},i\omega)\Big], \tag{I.1d}$$

$$K^{(E)}_{\alpha\beta}(i\Omega) = -\frac{4e^2}{m^2}T^2\sum_{\varepsilon,\omega}\sum_{\mathbf{k},\mathbf{k}',\mathbf{q}}\Big[k_\alpha k'_\beta G(\mathbf{k},i\varepsilon+i\Omega)G(\mathbf{q}-\mathbf{k},i\omega-i\varepsilon-i\Omega) \times G(\mathbf{k},i\varepsilon)G(\mathbf{k}',i\omega-i\varepsilon-i\Omega)G(\mathbf{q}-\mathbf{k}',i\varepsilon)G(\mathbf{k}',i\omega-i\varepsilon) \times C(\mathbf{q},i\varepsilon+i\Omega,i\omega-i\varepsilon-i\Omega)C(\mathbf{q},i\varepsilon,i\omega-i\varepsilon) \times \widetilde{C}(\mathbf{q},i\omega-i\varepsilon-i\Omega,i\varepsilon)L(\mathbf{q},i\omega)\Big], \tag{I.1e}$$

$$
\begin{aligned}
K^{(F)}_{\alpha\beta}(i\Omega) = -\frac{4e^2}{m^2}T^3 \sum_{\varepsilon,\varepsilon',\omega} \sum_{\mathbf{k},\mathbf{k}',\mathbf{q}} \Big[& G(\mathbf{k}, i\varepsilon + i\Omega) G(\mathbf{q}-\mathbf{k}, i\omega - i\varepsilon) G(\mathbf{k}, i\varepsilon) \\
& \times C(\mathbf{q}, i\varepsilon + i\Omega, i\omega - i\varepsilon) C(\mathbf{q}, i\varepsilon, i\omega - i\varepsilon) G(\mathbf{k}', i\varepsilon' + i\Omega) \\
& \times G(\mathbf{q}-\mathbf{k}', i\omega - i\varepsilon') G(\mathbf{k}', i\varepsilon') C(\mathbf{q}, i\varepsilon' + i\Omega, i\omega - i\varepsilon') \\
& \times C(\mathbf{q}, i\varepsilon', i\omega - i\varepsilon') L(\mathbf{q}, i\omega) L(\mathbf{q}, i\omega + i\Omega) \Big].
\end{aligned}
\tag{I.1f}
$$

The minus signs appearing in diagrams A-E are due to $L(\mathbf{q}, i\omega)$ being an effective interaction, and hence carrying an extra minus sign according to the standard diagrammatic rules. The additional factors of 2 in the DOS type diagrams is a result of their two variations: the ones shown in fig. 3.23, and the same with the pair propagator on the lower branch. Similarly, diagram E carries an extra factor of 2 due to its variants: the pair propagator and cooperon can be crossed in the order shown in fig. 3.23e, as well as in the opposite order. Finally, the minus sign in diagram F is due to the second closed fermion loop.

First, we shall focus on diagrams A-E as these are relatively straightforward. Diagram F has a few nuances that will require a little more attention. A lot of the ideas used in the EEI calculation can be used here, but let us give a brief outline of the process.

Each diagram has an allowed set of sign choices yielding non-zero values due to the cooperons present. These are illustrated in fig. I.1. Any current vertices containing both fast and slow momenta we approximate as $(\mathbf{q}-\mathbf{k})_\beta \simeq -k_\beta$, and similarly we approximate the arguments of the electron Green's functions in the same way where appropriate. However, if the fast momentum sum is odd in $\mathbf{k}$ due to the current vertex, we expand the Green's functions dependent on $\mathbf{q}$ to first order, so that we produce factors that look like $k_\beta(\mathbf{k}\cdot\mathbf{q})$, which do not vanish upon summation over $\mathbf{k}$. This expansion is the same trick we used for diagrams D and E of the EEI corrections. By doing this we find the leading order contributions to the electrical conductivity. We lastly assume $\Omega > 0$ without loss of generality.

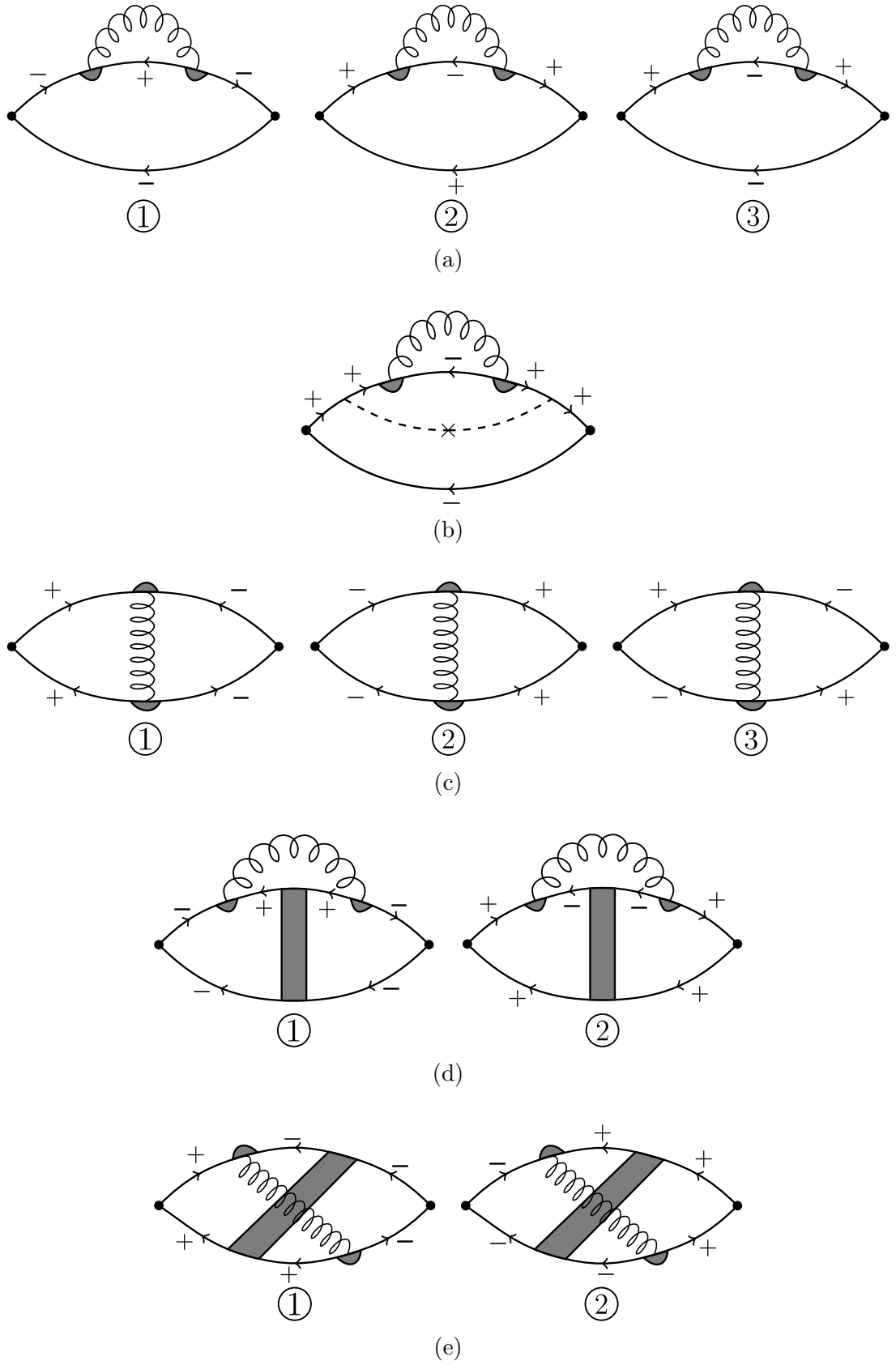

Figure I.1: Sign choices for diagrams A-E describing superconducting fluctuation corrections to the electrical conductivity in disordered homogeneous metals.

The maths behind each diagram and sign choice is long and arduous, so we simply quote the results of performing the fast momentum sums (those over $\mathbf{k}$ and $\mathbf{k}'$). By following the ideas listed above, and using the EEI calculation as a reference point, one can reproduce the following,

$$\begin{aligned} K_{\alpha\beta}^{(A1)}(i\Omega) &= 16\pi N(0)e^2\mathcal{D}\delta_{\alpha\beta}T^2\sum_{\omega>0}\sum_{\varepsilon>0}\sum_{\mathbf{q}}\frac{L(\mathbf{q},i\omega)}{(\mathcal{D}q^2+2\varepsilon+\omega)^2} \\ &\quad + 8\pi N(0)e^2\mathcal{D}\delta_{\alpha\beta}T^2\sum_{\varepsilon>0}\sum_{\mathbf{q}}\frac{L(\mathbf{q},0)}{(\mathcal{D}q^2+2\varepsilon)^2}, \end{aligned} \tag{I.2a}$$

$$\begin{aligned} K_{\alpha\beta}^{(A2)}(i\Omega) &= 8\pi N(0)e^2\mathcal{D}\delta_{\alpha\beta}T^2 \\ &\quad \times\sum_{\varepsilon>0}\sum_{\mathbf{q}}\left[\sum_{\omega>\Omega}\frac{L(\mathbf{q},i\omega)}{(\mathcal{D}q^2+2\varepsilon+\omega)^2}+\sum_{\omega<\Omega}\frac{L(\mathbf{q},i\omega)}{(\mathcal{D}q^2+2\varepsilon+2\Omega-\omega)^2}\right] \\ &\quad + 8\pi N(0)e^2\mathcal{D}\delta_{\alpha\beta}T^2\sum_{\varepsilon>0}\sum_{\mathbf{q}}\frac{L(\mathbf{q},i\Omega)}{(\mathcal{D}q^2+2\varepsilon+\Omega)^2} \end{aligned} \tag{I.2b}$$

$$\begin{aligned} K_{\alpha\beta}^{(A3)}(i\Omega) &= -2K_{\alpha\beta}^{(B)}(i\Omega) \\ &= -16\pi N(0)e^2\mathcal{D}\delta_{\alpha\beta}T^2 \\ &\quad \times\sum_{\mathbf{q}}\left[\sum_{\omega\leq 0}\sum_{0<\varepsilon<\Omega}+\sum_{0<\omega<\Omega}\sum_{0<\varepsilon<\Omega-\omega}\right]\frac{L(\mathbf{q},i\omega)}{(\mathcal{D}q^2+2\varepsilon+|\omega|)^2}, \end{aligned} \tag{I.2c}$$

$$\begin{aligned} K_{\alpha\beta}^{(C1)}(i\Omega) &= K_{\alpha\beta}^{(C2)}(i\Omega) \\ &= 16\pi N(0)e^2\mathcal{D}\delta_{\alpha\beta}T^2 \\ &\quad \times\sum_{\omega>0}\sum_{\varepsilon>0}\sum_{\mathbf{q}}\frac{L(\mathbf{q},i\omega)}{(\mathcal{D}q^2+2\varepsilon+\omega)}\frac{1}{(\mathcal{D}q^2+2\varepsilon+2\Omega+\omega)} \\ &\quad + 8\pi N(0)e^2\mathcal{D}\delta_{\alpha\beta}T^2\sum_{\varepsilon>0}\sum_{\mathbf{q}}\frac{L(\mathbf{q},0)}{(\mathcal{D}q^2+2\varepsilon)}\frac{1}{(\mathcal{D}q^2+2\varepsilon+2\Omega)}, \end{aligned} \tag{I.2d}$$

$$\begin{aligned} K_{\alpha\beta}^{(C3)}(i\Omega) &= 16\pi N(0)e^2\mathcal{D}\delta_{\alpha\beta}T^2 \\ &\quad \times\sum_{0<\omega<\Omega}\sum_{0<\varepsilon<\Omega-\omega}\sum_{\mathbf{q}}\frac{L(\mathbf{q},i\omega)}{(\mathcal{D}q^2+2\varepsilon+\omega)}\frac{1}{(\mathcal{D}q^2+2\Omega-2\varepsilon-\omega)} \\ &\quad + 8\pi N(0)e^2\mathcal{D}\delta_{\alpha\beta}T^2\sum_{0<\varepsilon<\Omega}\sum_{\mathbf{q}}\frac{L(\mathbf{q},0)}{(\mathcal{D}q^2+2\varepsilon)}\frac{1}{(\mathcal{D}q^2+2\Omega-2\varepsilon)}, \end{aligned} \tag{I.2e}$$

$$
\begin{aligned}
K^{(D1)}_{\alpha\beta}(i\Omega) &= -64\pi N(0)e^2\mathcal{D}^2T^2 \\
&\quad\times\sum_{\omega>0}\sum_{\varepsilon>0}\sum_{\mathbf{q}}\frac{L(\mathbf{q},i\omega)}{(\mathcal{D}q^2+2\varepsilon+\omega)^2}\frac{q_\alpha q_\beta}{(\mathcal{D}q^2+2\varepsilon+\Omega+\omega)} \\
&\quad-32\pi N(0)e^2\mathcal{D}^2T^2\sum_{\varepsilon>0}\sum_{\mathbf{q}}\frac{L(\mathbf{q},0)}{(\mathcal{D}q^2+2\varepsilon)^2}\frac{q_\alpha q_\beta}{(\mathcal{D}q^2+2\varepsilon+\Omega)},
\end{aligned}
\tag{I.2f}
$$

$$
\begin{aligned}
K^{(D2)}_{\alpha\beta}(i\Omega) &= -32\pi N(0)e^2\mathcal{D}^2T^2 \\
&\quad\times\sum_{\varepsilon>0}\sum_{\mathbf{q}}q_\alpha q_\beta\Bigg[\sum_{\omega<\Omega}\frac{L(\mathbf{q},i\omega)}{(\mathcal{D}q^2+2\varepsilon+2\Omega-\omega)^2}\frac{1}{(\mathcal{D}q^2+2\varepsilon+\Omega-\omega)} \\
&\qquad\qquad+\sum_{\omega>\Omega}\frac{L(\mathbf{q},i\omega)}{(\mathcal{D}q^2+2\varepsilon+\omega)^2}\frac{1}{(\mathcal{D}q^2+2\varepsilon+\omega-\Omega)}\Bigg] \\
&\quad-32\pi N(0)e^2\mathcal{D}^2T^2\sum_{\varepsilon>0}\sum_{\mathbf{q}}\frac{L(\mathbf{q},i\Omega)}{(\mathcal{D}q^2+2\varepsilon+\Omega)^2}\frac{q_\alpha q_\beta}{(\mathcal{D}q^2+2\varepsilon)},
\end{aligned}
\tag{I.2g}
$$

$$
\begin{aligned}
K^{(E1)}_{\alpha\beta}(i\Omega) &= K^{(E2)}_{\alpha\beta}(i\Omega) \\
&= -64\pi N(0)e^2\mathcal{D}^2T^2 \\
&\quad\times\sum_{\omega>0}\sum_{\varepsilon>0}\sum_{\mathbf{q}}q_\alpha q_\beta\Bigg[\frac{L(\mathbf{q},i\omega)}{(\mathcal{D}q^2+2\varepsilon+\omega)} \\
&\qquad\qquad\times\frac{1}{(\mathcal{D}q^2+2\varepsilon+2\Omega+\omega)}\frac{1}{(\mathcal{D}q^2+2\varepsilon+\Omega+\omega)}\Bigg] \\
&\quad-32\pi N(0)e^2\mathcal{D}^2T^2 \\
&\quad\times\sum_{\varepsilon>0}\sum_{\mathbf{q}}q_\alpha q_\beta\frac{L(\mathbf{q},0)}{(\mathcal{D}q^2+2\varepsilon)}\frac{1}{(\mathcal{D}q^2+2\varepsilon+2\Omega)}\frac{1}{(\mathcal{D}q^2+2\varepsilon+\Omega)}.
\end{aligned}
\tag{I.2h}
$$

For simplicity we have ignored the phase breaking rate, τ_ϕ^{-1}, in the cooperons. However, their inclusion would not change the result of what we show here. The mathematics would simply become more cumbersome and filled with more parameters to keep track of. The simplest way to re-include τ_ϕ^{-1} would be to let $\mathcal{D}q^2 \to \mathcal{D}q^2+\tau_\phi^{-1}$ in the denominators. Later on this would simply amount to doing the same replacement inside digamma functions.

Turning our attention towards diagram F, we may deal with each block of electron Green's functions (the triangles) appearing either side of the diagram independently from

Figure I.2: Sign choices of the blocks appearing in the AL diagram. Panel a corresponds to $B_\alpha^{(a)}(\mathbf{q}, i\omega, i\Omega)$, whilst panel b corresponds to $B_\alpha^{(b)}(\mathbf{q}, i\omega, i\Omega)$.

the other. These blocks are entirely equivalent, and so we only need to calculate a single block. The sign choices of a single Green's function block are shown in fig. I.2.

However, before we rush in to calculating the contributions of these sign choices, we first need to understand the analytic structure of the ω sum due to the presence of two pair propagators with different frequencies. If we were to analytically continue the ω sum in the response function for diagram F, we would find two branch cuts in the complex ω plane. These different branch cuts are the result of the pair propagators switching from retarded to advanced Green's functions at different points in the complex plane. Therefore we should consider three different regions of the ω sum,

$$\begin{array}{lll} \omega{+}\Omega > 0 & \omega{+}\Omega \leq 0 & \omega{+}\Omega > 0 \\ \omega \geq 0 \quad , & \omega < 0 \quad , & \omega < 0 \quad , \\ \text{Region I} & \text{Region II} & \text{Region III} \end{array} \tag{I.3}$$

where region I is the retarded-retarded part, region II is the advanced-advanced part, and region III is the retarded-advanced part. Finally, for notational ease, let us first rewrite the response function in terms of the block functions,

$$\begin{aligned} B_\alpha(\mathbf{q}, i\omega, i\Omega) = T \sum_\varepsilon \sum_{\mathbf{k}} \Big[& \frac{k_\alpha}{m} G(\mathbf{k}, i\varepsilon + i\Omega) G(\mathbf{k}, i\varepsilon) G(\mathbf{q}-\mathbf{k}, i\omega - i\varepsilon) \\ & \times C(\mathbf{q}, i\varepsilon + i\Omega, i\omega - i\varepsilon) C(\mathbf{q}, i\varepsilon, i\omega - i\varepsilon) \Big], \end{aligned} \tag{I.4}$$

so that

$$K_{\alpha\beta}^{(F)}(i\Omega) = -4e^2T\sum_{\omega}\sum_{\mathbf{q}} B_\alpha(\mathbf{q}, i\omega, i\Omega)B_\beta(\mathbf{q}, i\omega, i\Omega)L(\mathbf{q}, i\omega + i\Omega)L(\mathbf{q}, i\omega). \tag{I.5}$$

Clearly each block vanishes unless we expand $G(\mathbf{q}-\mathbf{k}, i\omega - i\varepsilon)$ in terms of $\mathbf{q}$. Expanding to leading order in $\mathbf{q}$ yields[1]

$$\begin{aligned} B_\alpha(\mathbf{q}, i\omega, i\Omega) = -T\sum_{\varepsilon}\sum_{\mathbf{k}}\Bigg[&\frac{k_\alpha(\mathbf{k}\cdot\mathbf{q})}{m^2}G(\mathbf{k}, i\varepsilon + i\Omega)G(\mathbf{k}, i\varepsilon)G(\mathbf{k}, i\omega - i\varepsilon)^2 \\ &\times C(\mathbf{q}, i\varepsilon + i\Omega, i\omega - i\varepsilon)C(\mathbf{q}, i\varepsilon, i\omega - i\varepsilon)\Bigg]. \end{aligned} \tag{I.6}$$

Considering each sign choice then gives (approximated about the Fermi surface)

$$\begin{aligned} B_\alpha^{(a)}(\mathbf{q}, i\omega, i\Omega) &= 4\pi N(0)\mathcal{D}q_\alpha T{\sum_{\varepsilon}}' \frac{1}{\mathcal{D}q^2 + |2\varepsilon + \Omega - \omega|}\frac{1}{\mathcal{D}q^2 + |2\varepsilon - \omega|}, \\ B_\alpha^{(b)}(\mathbf{q}, i\omega, i\Omega) &= 4\pi N(0)\mathcal{D}q_\alpha T{\sum_{\varepsilon}}'' \frac{1}{\mathcal{D}q^2 + |2\varepsilon + \Omega - \omega|}\frac{1}{\mathcal{D}q^2 + |2\varepsilon - \omega|}, \end{aligned} \tag{I.7}$$

where the primes on the sums denote a restricted sum over ε based upon the sign choices of the block and the region we are considering.

Let us now calculate a block inside each region of ω. We present the ε summation range within each ω region for a given block sign configuration in table I.1, and list how we then manipulate the Matsubara sums within the brackets of each case.[2] Using the above we find,

$$\begin{aligned} B_\alpha^{(\mathrm{I},a)}(\mathbf{q}, i\omega, i\Omega) &= B_\alpha^{(\mathrm{II},a)}(\mathbf{q}, i\omega, i\Omega) \\ &= 4\pi N(0)\mathcal{D}q_\alpha T\sum_{\varepsilon>0}\frac{1}{\mathcal{D}q^2 + 2\varepsilon + \Omega + \omega}\frac{1}{\mathcal{D}q^2 + 2\varepsilon + 2\Omega + \omega}, \end{aligned} \tag{I.8a}$$

[1] The extra minus sign appearing in the block here comes from the fact that $G(\mathbf{q}-\mathbf{k}, i\omega - i\varepsilon)$ has a minus sign difference between $\mathbf{k}$ and $\mathbf{q}$. Thus $+(\mathbf{v}\cdot\mathbf{q})$ appears in the denominators of the Green's function rather than $-(\mathbf{v}\cdot\mathbf{q})$.

[2] In the case of region II, we use the transformation $\omega \to -\omega - \Omega$ to regain an ω sum that is for $\omega > 0$. We may use this transformation since $L(\mathbf{q}, i\omega)$ is unaffected by $\omega \to -\omega$, hence the combination $L(\mathbf{q}, i\omega)L(\mathbf{q}, i\omega + i\Omega)$ is unaffected by $\omega \to -\omega - \Omega$.

Table I.1: Ranges of ε that give a non-zero contribution to $K^{(F)}_{\alpha\beta}$. The brackets within each resultant cell gives the transformation we use to manipulate the Matsubara sums to obtain the results given in eq. I.8. For multiple transformations in the same cell, the order they are written is the order in which they are applied.

	Block sign choice	
	a $(\varepsilon+\Omega<0,\ \varepsilon<0,\ \omega-\varepsilon>0)$	b $(\varepsilon+\Omega>0,\ \varepsilon>0,\ \omega-\varepsilon<0)$
Region I $(\omega\geq 0)$	$\varepsilon<-\Omega$ $(\varepsilon\to-\varepsilon-\Omega)$	$\varepsilon>\omega$ $(\varepsilon\to\varepsilon+\omega)$
Region II $(\omega\leq-\Omega)$	$\varepsilon<\omega$ $(\varepsilon\to-\varepsilon+\omega,$ $\omega\to-\omega-\Omega,\Rightarrow\omega\geq 0)$	$\varepsilon>0$ $(\omega\to-\omega-\Omega,\Rightarrow\omega\geq 0)$
Region III $(-\Omega<\omega<0)$	$\varepsilon<-\Omega$ $(\varepsilon\to-\varepsilon-\Omega)$	$\varepsilon>0$

$$\begin{aligned} B^{(\mathrm{I},b)}_{\alpha}(\mathbf{q},i\omega,i\Omega) &= B^{(\mathrm{II},b)}_{\alpha}(\mathbf{q},i\omega,i\Omega) \\ &= 4\pi N(0)\mathcal{D}q_\alpha\, T\sum_{\varepsilon>0}\frac{1}{\mathcal{D}q^2+2\varepsilon+\Omega+\omega}\frac{1}{\mathcal{D}q^2+2\varepsilon+\omega}, \end{aligned} \tag{I.8b}$$

$$B^{(\mathrm{III},a)}_{\alpha}(\mathbf{q},i\omega,i\Omega) = 4\pi N(0)\mathcal{D}q_\alpha\, T\sum_{\varepsilon>0}\frac{1}{\mathcal{D}q^2+2\varepsilon+\Omega+\omega}\frac{1}{\mathcal{D}q^2+2\varepsilon+2\Omega+\omega}, \tag{I.8c}$$

$$B^{(\mathrm{III},b)}_{\alpha}(\mathbf{q},i\omega,i\Omega) = 4\pi N(0)\mathcal{D}q_\alpha\, T\sum_{\varepsilon>0}\frac{1}{\mathcal{D}q^2+2\varepsilon+\Omega-\omega}\frac{1}{\mathcal{D}q^2+2\varepsilon-\omega}. \tag{I.8d}$$

To use these block expressions, we note that the AL response function is simply the sum of the response functions within each ω region, $\mathcal{R}$,

$$K^{(F)}_{\alpha\beta}(i\Omega) = K^{(F,\mathrm{I})}_{\alpha\beta}(i\Omega) + K^{(F,\mathrm{II})}_{\alpha\beta}(i\Omega) + K^{(F,\mathrm{III})}_{\alpha\beta}(i\Omega), \tag{I.9a}$$

$$\begin{aligned} K^{(F,\mathcal{R})}_{\alpha\beta}(i\Omega) = -4e^2T\sum_{\omega\in\mathcal{R}}\sum_{\mathbf{q}}\Big\{&\Big[B^{(\mathcal{R},a)}_{\alpha}(\mathbf{q},i\omega,i\Omega)+B^{(\mathcal{R},b)}_{\alpha}(\mathbf{q},i\omega,i\Omega)\Big] \\ &\times\Big[B^{(\mathcal{R},a)}_{\beta}(\mathbf{q},i\omega,i\Omega)+B^{(\mathcal{R},b)}_{\beta}(\mathbf{q},i\omega,i\Omega)\Big]L(\mathbf{q},i\omega+i\Omega)L(\mathbf{q},i\omega)\Big\}. \end{aligned} \tag{I.9b}$$

We choose to deal with the regional contributions of the AL response function instead of the complete AL response function, as they allow for an easy demonstration of a vanishing zero frequency response. The regional contributions are thus,

$$\begin{aligned} K_{\alpha\beta}^{(F,\mathrm{I})}(i\Omega) &= K_{\alpha\beta}^{(F,\mathrm{II})}(i\Omega) \\ &= -64e^2\pi^2 N(0)^2\mathcal{D}^2 T\sum_{\omega\geq 0}\Bigg\{\sum_{\mathbf{q}} q_\alpha q_\beta L(\mathbf{q},i\omega)L(\mathbf{q},i\omega+i\Omega) \\ &\times\left(T\sum_{\varepsilon>0}\left[\frac{1}{\mathcal{D}q^2+2\varepsilon+\omega}+\frac{1}{\mathcal{D}q^2+2\varepsilon+2\Omega+\omega}\right]\frac{1}{\mathcal{D}q^2+2\varepsilon+\Omega+\omega}\right)^2\Bigg\} \end{aligned} \tag{I.10a}$$

$$\begin{aligned} K_{\alpha\beta}^{(F,\mathrm{III})}(i\Omega) &= -64e^2\pi^2 N(0)^2\mathcal{D}^2 T\sum_{-\Omega<\omega<0}\Bigg\{\sum_{\mathbf{q}} q_\alpha q_\beta L(\mathbf{q},i\omega)L(\mathbf{q},i\omega+i\Omega) \\ &\times\Bigg(T\sum_{\varepsilon>0}\Bigg[\frac{1}{\mathcal{D}q^2+2\varepsilon+\Omega-\omega}\frac{1}{\mathcal{D}q^2+2\varepsilon-\omega} \\ &\qquad+\frac{1}{\mathcal{D}q^2+2\varepsilon+2\Omega+\omega}\frac{1}{\mathcal{D}q^2+2\varepsilon+\Omega+\omega}\Bigg]\Bigg)^2\Bigg\}. \end{aligned} \tag{I.10b}$$

Let us now set $\Omega = 0$ and consider the sum of all the response functions we have listed in eq. I.2 and eq. I.10. Clearly $K_{\alpha\beta}^{(A3)}(i\Omega)$, $K_{\alpha\beta}^{(B)}(i\Omega)$, $K_{\alpha\beta}^{(C3)}(i\Omega)$, and $K_{\alpha\beta}^{(F,\mathrm{III})}(i\Omega)$ all vanish. This leaves us with summing the following,

$$\begin{aligned} K_{\alpha\beta}^{(A1)}(0) &= K_{\alpha\beta}^{(A2)}(0) = K_{\alpha\beta}^{(C1)}(0) = K_{\alpha\beta}^{(C2)}(0) \\ &= 16e^2\pi N(0)\mathcal{D}\delta_{\alpha\beta}T^2\sum_{\omega>0}\sum_{\mathbf{q}}\sum_{\varepsilon>0}\frac{L(\mathbf{q},i\omega)}{(\mathcal{D}q^2+2\varepsilon+\omega)^2} \\ &\quad+8e^2\pi N(0)\mathcal{D}\delta_{\alpha\beta}T^2\sum_{\mathbf{q}}\sum_{\varepsilon>0}\frac{L(\mathbf{q},0)}{(\mathcal{D}q^2+2\varepsilon)^2}, \end{aligned} \tag{I.11a}$$

$$\begin{aligned} K_{\alpha\beta}^{(D1)}(0) &= K_{\alpha\beta}^{(D2)}(0) = K_{\alpha\beta}^{(E1)}(0) = K_{\alpha\beta}^{(E2)}(0) \\ &= -64e^2\pi N(0)\mathcal{D}^2T^2\sum_{\omega>0}\sum_{\mathbf{q}}\sum_{\varepsilon>0}\frac{q_\alpha q_\beta L(\mathbf{q},i\omega)}{(\mathcal{D}q^2+2\varepsilon+\omega)^3} \\ &\quad-32\pi N(0)e^2\mathcal{D}^2T^2\sum_{\varepsilon>0}\sum_{\mathbf{q}} q_\alpha q_\beta\frac{L(\mathbf{q},0)}{(\mathcal{D}q^2+2\varepsilon)^3}, \end{aligned} \tag{I.11b}$$

$$\begin{aligned} K_{\alpha\beta}^{(F,\mathrm{I})}(0) &= K_{\alpha\beta}^{(F,\mathrm{II})}(0) \\ &= -256e^2\pi^2 N(0)^2\mathcal{D}^2 T \\ &\times \sum_{\omega>0}\sum_{\mathbf{q}} q_\alpha q_\beta L(\mathbf{q},i\omega)^2 \left(T\sum_{\varepsilon>0} \frac{1}{(\mathcal{D}q^2+2\varepsilon+\omega)^2}\right)^2 \\ &- 128e^2\pi^2 N(0)^2\mathcal{D}^2 T \sum_{\mathbf{q}} q_\alpha q_\beta L(\mathbf{q},0)^2 \left(T\sum_{\varepsilon>0} \frac{1}{(\mathcal{D}q^2+2\varepsilon)^2}\right)^2 . \end{aligned} \tag{I.11c}$$

In the above we have separated out the $\omega = 0$ pieces explicitly, as these have different prefactors compared to the $\omega \neq 0$ pieces. There is one subtlety we used in writing eq. I.11c. The ω sum written in eq. I.10a would imply the $\omega = 0$ and $\omega \neq 0$ pieces would have the same prefactor. However, if we consider how each region is written, we can see that we would double count the $\omega = 0$ term if we used this expression with $\Omega = 0$. This is easily seen by recalling that region I considers $\omega \geq 0$ whilst region II considers $\omega \leq -\Omega$. So in taking $\Omega = 0$, we would have region II being over $\omega \leq 0$, and hence we double count $\omega = 0$. Therefore, when we set $\Omega = 0$, the $\omega = 0$ component of the sum simply carries an additional factor $1/2$ compared to the $\omega \neq 0$ components.

Next we tidy up these expressions by replacing the ε sums with digamma function derivatives (see appendix N for the definition of the digamma function and its derivatives in terms of sums). Specifically, we note that

$$T\sum_{\varepsilon>0} \frac{1}{(\mathcal{D}q^2+2\varepsilon+\omega)^2} = \frac{1}{16\pi^2 T}\psi'\left(\frac{1}{2}+\frac{\mathcal{D}q^2+\omega}{4\pi T}\right), \tag{I.12a}$$

$$T\sum_{\varepsilon>0} \frac{1}{(\mathcal{D}q^2+2\varepsilon+\omega)^3} = -\frac{1}{128\pi^3 T^2}\psi''\left(\frac{1}{2}+\frac{\mathcal{D}q^2+\omega}{4\pi T}\right). \tag{I.12b}$$

So the total zero frequency response function is given by

$$\begin{aligned}
K_{\alpha\beta}(0) &= K^{(A1)}_{\alpha\beta}(0) + K^{(A2)}_{\alpha\beta}(0) + K^{(C1)}_{\alpha\beta}(0) + K^{(C2)}_{\alpha\beta}(0) \\
&\quad + K^{(D1)}_{\alpha\beta}(0) + K^{(D2)}_{\alpha\beta}(0) + K^{(E1)}_{\alpha\beta}(0) + K^{(E2)}_{\alpha\beta}(0) \\
&\quad + K^{(F,\mathrm{I})}_{\alpha\beta}(0) + K^{(F,\mathrm{II})}_{\alpha\beta}(0), \\
&= \frac{4e^2N(0)\mathcal{D}}{\pi}\delta_{\alpha\beta}\sum_{\omega>0}\sum_{\mathbf{q}} L(\mathbf{q},i\omega)\psi'\left(\frac{1}{2}+\frac{\mathcal{D}q^2+\omega}{4\pi T}\right) \\
&\quad + \frac{2e^2N(0)\mathcal{D}}{\pi^2T}\sum_{\omega>0}\sum_{\mathbf{q}} q_\alpha q_\beta L(\mathbf{q},i\omega)\psi''\left(\frac{1}{2}+\frac{\mathcal{D}q^2+\omega}{4\pi T}\right) \\
&\quad - \frac{2e^2N(0)^2\mathcal{D}^2}{\pi^2T^2}\sum_{\omega>0}\sum_{\mathbf{q}} q_\alpha q_\beta L(\mathbf{q},i\omega)^2\psi'\left(\frac{1}{2}+\frac{\mathcal{D}q^2+\omega}{4\pi T}\right)^2 \\
&\quad + (\omega = 0 \text{ terms})
\end{aligned} \tag{I.13}$$

Here we have avoided writing the $\omega = 0$ piece explicitly as this simply carries an additional factor of $1/2$ and no ω sum. Hence, any tricks we use for the $\omega \neq 0$ part can be equally applied to the $\omega = 0$ part, provided it does not involve manipulating the ω sum. We now make use of the pair propagator's explicit form in eq. 3.116 in the absence of phase breaking,

$$L(\mathbf{q},i\omega) = \frac{1}{N(0)}\left[\ln\left(\frac{T}{T_c}\right) + \psi\left(\frac{1}{2}+\frac{|\omega|+\mathcal{D}q^2}{4\pi T}\right) - \psi\left(\frac{1}{2}\right)\right]^{-1}. \tag{I.14}$$

To progress, let us consider taking derivatives of the function

$$\ln\left[\ln\left(\frac{T}{T_c}\right) + \psi\left(\frac{1}{2}+\frac{|\omega|+\mathcal{D}q^2}{4\pi T}\right) - \psi\left(\frac{1}{2}\right)\right]. \tag{I.15}$$

The derivatives of this function are,

$$\begin{aligned}
&\frac{\partial}{\partial q_\beta}\ln\left[\ln\left(\frac{T}{T_c}\right) + \psi\left(\frac{1}{2}+\frac{|\omega|+\mathcal{D}q^2}{4\pi T}\right) - \psi\left(\frac{1}{2}\right)\right] \\
&\qquad = N(0)L(\mathbf{q},i\omega)\psi'\left(\frac{1}{2}+\frac{|\omega|+\mathcal{D}q^2}{4\pi T}\right)\frac{\mathcal{D}q_\beta}{2\pi T}
\end{aligned} \tag{I.16a}$$

$$\begin{aligned}
&\frac{\partial^2}{\partial q_\alpha \partial q_\beta} \ln\left[\ln\left(\frac{T}{T_c}\right) + \psi\left(\frac{1}{2} + \frac{|\omega| + \mathcal{D}q^2}{4\pi T}\right) - \psi\left(\frac{1}{2}\right)\right] \\
&\qquad = N(0) L(\mathbf{q}, i\omega) \psi'\left(\frac{1}{2} + \frac{|\omega| + \mathcal{D}q^2}{4\pi T}\right) \frac{\delta_{\alpha\beta}}{2\pi T} \\
&\qquad\quad + N(0) L(\mathbf{q}, i\omega) \psi''\left(\frac{1}{2} + \frac{|\omega| + \mathcal{D}q^2}{4\pi T}\right) \frac{\mathcal{D}^2 q_\alpha q_\beta}{4\pi^2 T^2} \\
&\qquad\quad - N(0)^2 L(\mathbf{q}, i\omega)^2 \psi'\left(\frac{1}{2} + \frac{|\omega| + \mathcal{D}q^2}{4\pi T}\right)^2 \frac{\mathcal{D}^2 q_\alpha q_\beta}{4\pi^2 T^2}.
\end{aligned} \tag{I.16b}$$

Clearly the first, second, and third lines of eq. I.16b are related to the first, second, and third lines of the second equality in eq. I.13, respectively. The expression in eq. I.13 can thus be rewritten as

$$\begin{aligned}
K_{\alpha\beta}(0) &= 8e^2 T \sum_{\omega>0} \sum_{\mathbf{q}} \frac{\partial^2}{\partial q_\alpha \partial q_\beta} \ln\left[\ln\left(\frac{T}{T_c}\right) + \psi\left(\frac{1}{2} + \frac{|\omega| + \mathcal{D}q^2}{4\pi T}\right) - \psi\left(\frac{1}{2}\right)\right] \\
&\quad + (\omega = 0 \text{ terms}) \\
&= 8e^2 T \sum_{\omega>0} \sum_{\mathbf{q}} \mathbf{e}_\alpha \cdot \nabla \frac{\partial}{\partial q_\beta} \ln\left[\ln\left(\frac{T}{T_c}\right) + \psi\left(\frac{1}{2} + \frac{|\omega| + \mathcal{D}q^2}{4\pi T}\right) - \psi\left(\frac{1}{2}\right)\right] \\
&\quad + (\omega = 0 \text{ terms}),
\end{aligned} \tag{I.17}$$

where $\mathbf{e}_\alpha$ is a unit vector in the α direction. Next, we replace the $\mathbf{q}$ sum by a volume integral and use the divergence theorem to rewrite this as a surface integral over the surface S, whose normal vector is $\hat{\mathbf{n}}$, to obtain

$$\begin{aligned}
K_{\alpha\beta}(0) &= 8e^2 T \sum_{\omega>0} \\
&\quad \times \oint_S d^{d-1}q\, \mathbf{e}_\alpha \cdot \hat{\mathbf{n}} \frac{\partial}{\partial q_\beta} \ln\left[\ln\left(\frac{T}{T_c}\right) + \psi\left(\frac{1}{2} + \frac{|\omega| + \mathcal{D}q^2}{4\pi T}\right) - \psi\left(\frac{1}{2}\right)\right] \\
&\quad + (\omega = 0 \text{ terms}) \\
&= \frac{4e^2 N(0)\mathcal{D}}{\pi} \sum_{\omega>0} \oint_S d^{d-1}q\, \mathbf{e}_\alpha \cdot \hat{\mathbf{n}}\, L(\mathbf{q}, i\omega) \psi'\left(\frac{1}{2} + \frac{|\omega| + \mathcal{D}q^2}{4\pi T}\right) q_\beta \\
&\quad + (\omega = 0 \text{ terms}).
\end{aligned} \tag{I.18}$$

By taking the surface to infinity, we find that the integrand vanishes, and hence the

surface integral must also vanish.[3] Thus, $K_{\alpha\beta}(0) = 0$ as desired, therefore confirming that we have accounted for all diagrams when calculating the correction to the electrical conductivity due to superconducting fluctuations.

Technically speaking, the upper limit of the surface should be $q_{\max} = 1/\sqrt{\mathcal{D}\tau_0} = 1/l$ due to the diffusive limit. However, this is much larger than T, and hence the argument of the digamma function appears to be large. So by taking this to infinity is yet another approximation, but at least within reason.

I.2 Non-Singular Contributions

In the main body of the thesis we argued that the most singular behaviour arose from diagrams A, B, C, and F of fig. 3.23, and that diagrams D and E were unimportant. Let us now show that these are indeed less singular than the other diagrams.

In the previous section we found the electromagnetic response functions for diagrams D and E, and so let us consider their $\omega = 0$ components as they only possess a single pair propagator. The expressions we therefore concern ourselves with are

$$\begin{aligned}\bar{K}^{(D)}_{\alpha\beta}(i\Omega) = &-32\pi N(0)e^2\mathcal{D}^2T^2 \\ &\times \sum_{\mathbf{q}}\sum_{\varepsilon>0} \frac{q_\alpha q_\beta L(\mathbf{q},0)}{\mathcal{D}q^2+2\varepsilon+\Omega}\left[\frac{1}{(\mathcal{D}q^2+2\varepsilon)^2}+\frac{1}{(\mathcal{D}q^2+2\varepsilon+2\Omega)^2}\right],\end{aligned} \tag{I.19a}$$

$$\begin{aligned}\bar{K}^{(E)}_{\alpha\beta}(i\Omega) = &-64\pi N(0)e^2\mathcal{D}^2T^2 \\ &\times \sum_{\varepsilon>0}\sum_{\mathbf{q}} q_\alpha q_\beta \frac{L(\mathbf{q},0)}{(\mathcal{D}q^2+2\varepsilon)}\frac{1}{(\mathcal{D}q^2+2\varepsilon+2\Omega)}\frac{1}{(\mathcal{D}q^2+2\varepsilon+\Omega)}.\end{aligned} \tag{I.19b}$$

For ease of comparison to σ_{DOS} and $\sigma^{(reg)}_{MT}$, we wish to perform the fermionic Matsubara sums to obtain digamma functions and derivatives of the digamma function. Hence, we split the fractions in eq. I.19 using partial fractions, which leaves us to evaluate the

[3]The integrand falls of as $1/q$ as we take q to infinity. This is due to the digamma function derivative falling off sufficiently fast, $\psi'(x) \sim 1/x$ when $x \gg 1$.

following ε sums for diagrams D and E respectively,

$$\sum_{\varepsilon>0}\Bigg[\frac{1}{\Omega^2}\left(\frac{2}{\mathcal{D}q^2+2\varepsilon+\Omega}-\frac{1}{\mathcal{D}q^2+2\varepsilon}-\frac{1}{\mathcal{D}q^2+2\varepsilon+2\Omega}\right) + \frac{1}{\Omega}\left(\frac{1}{(\mathcal{D}q^2+2\varepsilon)^2}-\frac{1}{(\mathcal{D}q^2+2\varepsilon+2\Omega)^2}\right)\Bigg], \tag{I.20a}$$

$$-\frac{1}{2}\sum_{\varepsilon>0}\frac{1}{\Omega^2}\left[\frac{2}{\mathcal{D}q^2+2\varepsilon+\Omega}-\frac{1}{\mathcal{D}q^2+2\varepsilon}-\frac{1}{\mathcal{D}q^2+2\varepsilon+2\Omega}\right]. \tag{I.20b}$$

Writing these sums in terms of digamma functions, and derivatives thereof, and substituting them into their respective response functions, we see

$$\begin{aligned}\bar{K}^{(D)}_{\alpha\beta}(i\Omega) &= -32\pi N(0)e^2\mathcal{D}^2T^2\sum_{\mathbf{q}}q_\alpha q_\beta L(\mathbf{q},0)\\ &\times\Bigg\{\frac{1}{4\pi T}\frac{1}{\Omega^2}\left[\psi\left(\frac{1}{2}+\frac{\mathcal{D}q^2}{4\pi T}\right)+\psi\left(\frac{1}{2}+\frac{\mathcal{D}q^2+2\Omega}{4\pi T}\right)-2\psi\left(\frac{1}{2}+\frac{\mathcal{D}q^2+\Omega}{4\pi T}\right)\right]\\ &+\frac{1}{(4\pi T)^2}\frac{1}{\Omega}\left[\psi'\left(\frac{1}{2}+\frac{\mathcal{D}q^2}{4\pi T}\right)-\psi'\left(\frac{1}{2}+\frac{\mathcal{D}q^2+2\Omega}{4\pi T}\right)\right]\Bigg\},\end{aligned} \tag{I.21a}$$

$$\begin{aligned}\bar{K}^{(E)}_{\alpha\beta}(i\Omega) &= \frac{8N(0)e^2\mathcal{D}^2T}{\Omega^2}\sum_{\mathbf{q}}q_\alpha q_\beta L(\mathbf{q},0)\\ &\times\left[\psi\left(\frac{1}{2}+\frac{\mathcal{D}q^2}{4\pi T}\right)+\psi\left(\frac{1}{2}+\frac{\mathcal{D}q^2+2\Omega}{4\pi T}\right)-2\psi\left(\frac{1}{2}+\frac{\mathcal{D}q^2+\Omega}{4\pi T}\right)\right].\end{aligned} \tag{I.21b}$$

We can then perform our usual trick of analytically continuing $\Omega\to i\Omega$ to consider the retarded response function, expand in power of Ω, and then convert back to the Matsubara formalism, since there is no odd pole structure in the digamma functions. This is equivalent to simply treating the Mastubara Ω as continuous for the purpose of differentiation to obtain an expansion in terms of Ω. So, without worrying about the analytic continuation, we expand the above expressions to third order in Ω to consider the $\mathcal{O}(\Omega)$ piece as this gives the DC conductivity, $\sigma^{(D,E)}$. We find that the $\mathcal{O}(\Omega^{-2})$ and $\mathcal{O}(\Omega^{-1})$ pieces have vanishing coefficients, as expected, since there were no divergence

issues before we used partial fractions. We then ignore the $\mathcal{O}(\Omega^0)$ piece as we have shown that this cancels when all diagrams are considered. We therefore find

$$\sigma^{(D)} = -\frac{N(0)e^2\mathcal{D}^2}{8d\pi^3T^2}\psi^{(3)}\left(\frac{1}{2}\right)\sum_{\mathbf{q}} q^2 L(\mathbf{q},0), \tag{I.22a}$$

$$\sigma^{(E)} = \frac{N(0)e^2\mathcal{D}^2}{8d\pi^3T^2}\psi^{(3)}\left(\frac{1}{2}\right)\sum_{\mathbf{q}} q^2 L(\mathbf{q},0), \tag{I.22b}$$

where we have neglected the $\mathcal{D}q^2$ in the digamma function as we are only interested in small momenta. We have also accounted for the factor of $1/d$ that appears in the diagonal part of the conductivity tensor due to the $q_\alpha q_\beta$ factor in the summand.

Clearly, these contributions are equal and opposite, meaning they cancel exactly in the DC limit. If their prefactors were different, or if we considered higher order terms where they do not cancel exactly, we can see that their contributions will be less singular than the DOS and MT diagrams. In both cases, the extra factor of q^2 generates an additional factor of η in the result. This is easy to see through power counting q after converting the momentum sum to an integral. So neither diagram is singular in η. Thus we can simply neglect their contribution when calculating the DC conductivity corrections due to superconducting fluctuations.

I.3 AL Integration Details

Let us consider the $d = 2$ case separately to the $d = 1$ and $d = 3$ cases. In the 2D case eq. 3.144 becomes

$$\sigma_{AL} = \frac{e^2}{\pi}\epsilon^{-1}\int_0^{+\infty} dx \int_0^{+\infty} d\phi \frac{x^3}{\left[(1+x^2)^2+\phi^2\right]^2}. \tag{I.23}$$

By letting $y = x^2$, this simplifies to

$$\sigma_{AL} = \frac{e^2}{2\pi}\epsilon^{-1}\int_0^{+\infty} dy \int_0^{+\infty} d\phi \frac{y}{\left[(1+y)^2+\phi^2\right]^2}. \tag{I.24}$$

Let us focus on the integrals for now,

$$\begin{aligned}\int_0^{+\infty} dy \int_0^{+\infty} d\phi \frac{y}{\left[(1+y)^2+\phi^2\right]^2} \\ &= \int_0^{+\infty} d\phi \int_0^{+\infty} dy \left[\frac{1+y}{\left[(1+y)^2+\phi^2\right]^2} - \frac{1}{\left[(1+y)^2+\phi^2\right]^2}\right] \\ &= \frac{1}{2}\int_0^{+\infty} d\phi \frac{1}{1+\phi^2} - \int_0^{+\infty} d\phi \int_0^{+\infty} dy \frac{1}{\left[(1+y)^2+\phi^2\right]^2}.\end{aligned} \tag{I.25}$$

The remaining y integral can be computed by noting that the use of partial fractions gives

$$\frac{1}{\left[(1+y)^2+\phi^2\right]^2} = \frac{1}{2\phi^2}\frac{1}{(1+y)^2+\phi^2} - \frac{1}{4\phi^2}\left(\frac{1}{(1+y+i\phi)^2} + \frac{1}{(1+y-i\phi)^2}\right). \tag{I.26}$$

Substituting this into eq. I.25 leaves us to perform the remaining y integral,

$$\begin{aligned}\int_0^{+\infty} dy \frac{1}{\left[(1+y)^2+\phi^2\right]^2} \\ &= \left[\frac{1}{2\phi^3}\arctan\left(\frac{y+1}{\phi}\right) + \frac{1}{4\phi^2}\left(\frac{1}{(1+y+i\phi)} + \frac{1}{(1+y-i\phi)}\right)\right]_0^{+\infty} \\ &= \frac{1}{2\phi^3}\left[\frac{\pi}{2} - \arctan\left(\frac{1}{\phi}\right)\right] - \frac{1}{2\phi^2}\frac{1}{1+\phi^2} \\ &= \frac{1}{2\phi^3}\arctan\phi - \frac{1}{2\phi^2}\frac{1}{1+\phi^2},\end{aligned} \tag{I.27}$$

where we used the reflection formula,

$$\arctan\phi = \frac{\pi}{2} - \arctan\left(\frac{1}{\phi}\right), \qquad \phi > 0, \tag{I.28}$$

to obtain the last line. Now, putting eq. I.27 into eq. I.25 gives

$$\int_0^{+\infty} dy \int_0^{+\infty} d\phi \frac{y}{\left[(1+y)^2+\phi^2\right]^2} = \frac{1}{2}\int_0^{+\infty} d\phi \left[\frac{1}{\phi^2} - \frac{1}{\phi^3}\arctan\phi\right]. \tag{I.29}$$

The leftover ϕ integral might seem to have divergence issues at $\phi = 0$, however the divergences of the two terms are equal and opposite as $\phi \to 0$, meaning the integrand is

well behaved at the lower limit. The ϕ integral can be resolved as follows: we start by integrating the first term simply and use integration by parts on the second term,

$$\frac{1}{2}\int_0^{+\infty} d\phi \left[\frac{1}{\phi^2} - \frac{1}{\phi^3}\arctan\phi\right] = \frac{1}{2}\left[-\frac{1}{\phi} + \frac{1}{2\phi^2}\arctan\phi\right]_0^{+\infty} - \frac{1}{4}\int_0^{+\infty}\frac{d\phi}{\phi^2}\frac{1}{1+\phi^2}. \quad \text{(I.30)}$$

Then we use partial fractions on the new ϕ integral,

$$\int_0^{+\infty}\frac{d\phi}{\phi^2}\frac{1}{1+\phi^2} = \int_0^{+\infty} d\phi\left(\frac{1}{\phi^2} - \frac{1}{1+\phi^2}\right) = -\left[\frac{1}{\phi} + \arctan\phi\right]_0^{+\infty}. \quad \text{(I.31)}$$

Hence,

$$\int_0^{+\infty} dy \int_0^{+\infty} d\phi \frac{y}{\left[(1+y)^2+\phi^2\right]^2} = \frac{1}{4}\left[\frac{1}{\phi^2}\arctan\phi - \frac{1}{\phi} + \arctan\phi\right]_0^{+\infty} = \frac{\pi}{8}, \quad \text{(I.32)}$$

since the first two terms cancel when $\phi \to 0$. As we are working close to T_c, $\epsilon \simeq \eta$, and so the 2D AL conductivity is simply,

$$\sigma_{AL}^{(2\mathrm{D})} = \frac{e^2}{16}\frac{1}{\eta}. \quad \text{(I.33)}$$

In reality, a thin film is still three dimensional, albeit with a thin thickness of δ in the short dimension. Therefore, in experiment the observable conductivity would be,

$$\sigma_{AL}^{(\mathrm{film})} = \frac{e^2}{16\delta}\frac{1}{\eta}. \quad \text{(I.34)}$$

Let us now consider a more general method that will allow us to consider the other dimensionalities at the same time as $d = 2$.

Starting again from eq. 3.144, we now perform the ϕ integral first. This is most easily

calculated by considering an integral of the form,

$$\begin{aligned}\int_0^{+\infty} d\phi \frac{1}{(\phi^2+a^2)^2} &= -\frac{d}{d(a^2)}\int_0^{+\infty} d\phi \frac{1}{\phi^2+a^2} \\ &= -\frac{1}{2a}\frac{d}{da}\left[\frac{1}{a}\arctan\left(\frac{\phi}{a}\right)\right]_0^{+\infty} = -\frac{1}{2a}\frac{d}{da}\frac{\pi}{2a} = \frac{\pi}{4a^3}.\end{aligned} \tag{I.35}$$

Clearly, this is the same as the ϕ integral in eq. 3.144 with $a = 1 + x^2$. Hence, we are left to evaluate

$$\frac{\pi}{4}\int_0^{+\infty} \frac{x^{d+1}}{(1+x^2)^3}, \tag{I.36}$$

which converges for $d < 4$. This integral is straightforward to calculate using integration by parts, and so we find

$$\int_0^{+\infty} dx \int_0^{+\infty} d\phi \frac{x^{d+1}}{\left[(1+x^2)^2+\phi^2\right]^2} = \frac{\pi}{64} \times \begin{cases} 3\pi, & d = 3 \\ 4, & d = 2 \\ \pi, & d = 1. \end{cases} \tag{I.37}$$

Substituting this back into eq. 3.144 gives the result we quote in eq. 3.148.

As a final note, the conductivity we would expect to see in a real experiment for the 1D case would correspond to a thin wire of radius a. Thus in reality, the conductivity for a quasi-1D system would be

$$\sigma_{AL}^{(wire)} = \frac{e^2}{a^2}\frac{\pi^{3/2}\sqrt{2}}{256}\sqrt{\frac{\mathcal{D}}{T}}\frac{1}{\eta^{1/2}}, \tag{I.38}$$

which is just the $d = 1$ case of eq. 3.148 divided by the wire's cross-sectional area.

The reason for division by πa^2 in the 1D case, and δ in the 2D case can be justified by considering the the replacement of the $\mathbf{q}$ sum by an integral. In our calculations we usually ignore the factor of volume that appears with each momentum sum, however, let

us include it explicitly here. Written accurately the momentum sum appears as

$$\frac{1}{\mathcal{V}}\sum_{\mathbf{q}} \tag{I.39}$$

where $\mathcal{V}$ is the system volume. For $d = 3$, replacing the momentum sum via an integral is simple and neatly cancels the factor of $\mathcal{V}^{-1}$,

$$\frac{1}{\mathcal{V}}\sum_{\mathbf{q}} \to \int \frac{d^3q}{(2\pi)^3}. \tag{I.40}$$

However, for $d = 2$ the volume can be written as $\mathcal{V} = \delta L_x L_y$, where L_x and L_y are the system's lengths in the extended dimensions. Therefore, when we replace the sum via a 2D momentum integral we see only the extended length factors are cancelled

$$\frac{1}{\mathcal{V}}\sum_{\mathbf{q}} \to \frac{1}{\delta}\int \frac{d^2q}{(2\pi)^2}. \tag{I.41}$$

This idea can be applied in exactly the same way for $d = 1$, where $\mathcal{V} = \pi a^2 L_x$,

$$\frac{1}{\mathcal{V}}\sum_{\mathbf{q}} \to \frac{1}{\pi a^2}\int \frac{dq}{2\pi}. \tag{I.42}$$

I.4 Anomalous MT Integration Details

The integral in eq. 3.154 cannot be done in a nice simple manner that encompasses all choices of dimensionality at once, so we have to compute each case separately. Thankfully these integrals are relatively straightforward. Let us start with the integral for $d = 3$,

$$\begin{aligned}\int_0^{+\infty} dx\, x^2\left(\frac{1}{x^2+\frac{\pi}{8T\tau_\phi\eta}}-\frac{1}{1+x^2}\right) &= \int_0^{+\infty} dx\left(\frac{1}{1+x^2}-\frac{\pi}{8T\tau_\phi\eta}\frac{1}{x^2+\frac{\pi}{8T\tau_\phi\eta}}\right)\\ &= \left[\arctan x-\sqrt{\frac{\pi}{8T\tau_\phi\eta}}\arctan\left(\sqrt{\frac{8T\tau_\phi\eta}{\pi}}x\right)\right]_0^{+\infty}\\ &= \frac{\pi}{2}\left(1-\sqrt{\frac{\pi}{8T\tau_\phi\eta}}\right)\simeq\frac{\pi}{2},\end{aligned} \tag{I.43}$$

where in the last line we recalled that we are working with small phase breaking rates, $\tau_\phi^{-1} \ll T$. For $d = 2$ the integral becomes,

$$\int_0^{+\infty} dx\, x\left(\frac{1}{x^2+\frac{\pi}{8T\tau_\phi\eta}}-\frac{1}{1+x^2}\right)=\left[\frac{1}{2}\ln\left(\frac{x^2+\frac{\pi}{8T\tau_\phi\eta}}{x^2+1}\right)\right]_0^{+\infty}=\frac{1}{2}\ln\left(\frac{8T\tau_\phi\eta}{\pi}\right), \quad \text{(I.44)}$$

whilst for $d = 1$,

$$\begin{aligned}&\int_0^{+\infty} dx\left(\frac{1}{x^2+\frac{\pi}{8T\tau_\phi\eta}}-\frac{1}{1+x^2}\right)\\ &\qquad=\left[\sqrt{\frac{8T\tau_\phi\eta}{\pi}}\arctan\left(\sqrt{\frac{8T\tau_\phi\eta}{\pi}}x\right)-\arctan x\right]_0^{+\infty}=\frac{\pi}{2}\sqrt{\frac{8T\tau_\phi\eta}{\pi}}.\end{aligned} \quad \text{(I.45)}$$

Clearly, τ_ϕ is vital to preventing the 1D and 2D results from diverging.

Finally, to produce the prefactor given in eq. 3.155, we note

$$\frac{\pi\Omega_d}{2(2\pi)^d}\times\begin{cases}\frac{\pi}{2}, & d=3\\ \frac{1}{2}, & d=2\\ \frac{\pi}{2}, & d=1\end{cases}=\begin{cases}\frac{1}{8}, & d=2,3\\ \frac{\pi}{4}, & d=1.\end{cases} \quad \text{(I.46)}$$

I.5 Regular MT & DOS Integration Details

Here we focus on the case when τ_ϕ^{-1} is small, as we may neglect its role in the regular MT and DOS contributions. In this case, the two regular MT parts become equivalent and so $\sigma_{MT}^{(reg)} = \sigma_{DOS}$. If we did not have this luxury, then $\sigma_{MT}^{(reg2)} = \sigma_{DOS}/2$ and $\sigma_{MT}^{(reg1)}$ would be stand-alone contributions. This is the case we study in granular systems, and is discussed in section 5.4.

Let us compute the integral in eq. 3.159 for the different dimensionalities. Starting with $d = 3$ we see that

$$\int_0^{+\infty} dx\frac{x^2}{1+x^2}=\int_0^{+\infty} dx\left(1-\frac{1}{1+x^2}\right), \quad \text{(I.47)}$$

which has a divergence due to the first term. However, in obtaining these integrals we made assumptions about the size of the virtual Cooper pair momentum, $\mathbf{q}$, as so we have a natural upper cut-off for q and hence x. There two possible cut-offs we could pick: in taking the diffusive limit we may take $\mathcal{D}q_c^2 = 1/\tau_0$; but in neglecting $\mathcal{D}q^2$ inside the digamma function and its derivatives we could also define $\mathcal{D}q_c^2 = 4\pi T$. Due to the latter being more restrictive, we use this to define the cut-off. In this case, the upper limit of the x integral's diverging piece is given by

$$x_c = \frac{\pi}{\sqrt{2\epsilon}}, \tag{I.48}$$

and so

$$\int_0^{+\infty} dx \frac{x^2}{1+x^2} \simeq \frac{\pi}{\sqrt{2\epsilon}} - \frac{\pi}{2}. \tag{I.49}$$

Considering that we are looking at temperatures close to T_c, $\epsilon \simeq \eta \ll 1$, the above integral can be approximated by its first term. Given that the regular MT and DOS type contributions have a factor of $\eta^{d/2-1}$ outside the integral, we see that the 3D reduced temperature dependence of these terms is constant.

For the choice $d = 2$ the integral is trivial to evaluate,

$$\int_0^{+\infty} dx \frac{x}{1+x^2} = \left[\frac{1}{2}\ln(1+x^2)\right]_0^{+\infty}, \tag{I.50}$$

which suffers an ultra-violet divergence similar to the 3D case. Using the same cut-off as before, we see that

$$\int_0^{+\infty} dx \frac{x}{1+x^2} \simeq \frac{1}{2}\ln\left(1+\frac{\pi^2}{2\epsilon}\right) \simeq \frac{1}{2}\ln\left(\frac{\pi^2}{2\eta}\right) \tag{I.51}$$

The integral for $d = 1$ is a standard integral, so we do not provide the details of its calculation here.

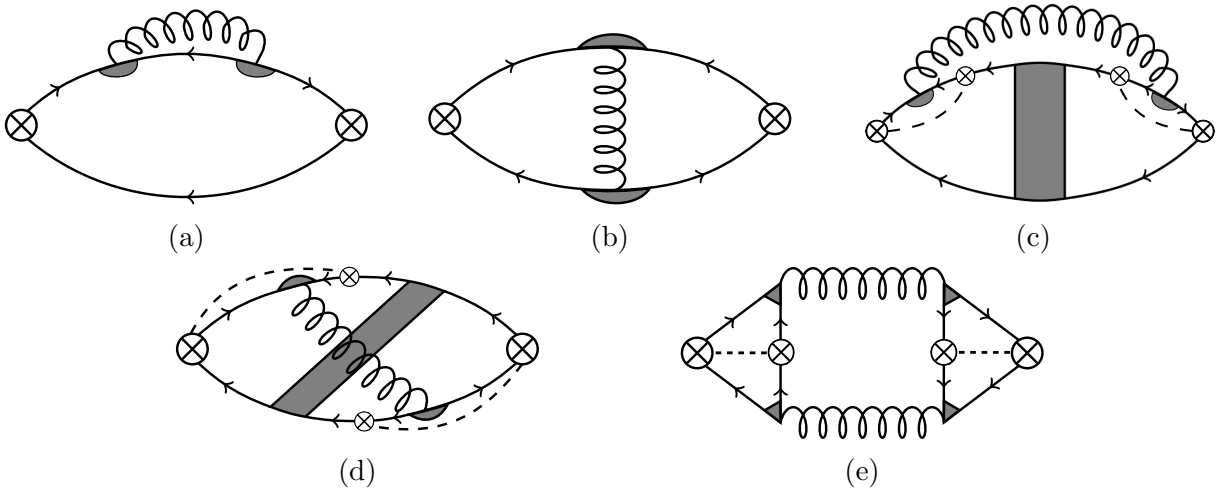

Figure I.3: Leading order corrections to the electrical conductivity due to superconducting fluctuations in granular metals.

I.6 Vanishing Zero Frequency Response – Granular Metals

For reference, the diagrams describing the fluctuation conductivity in disordered granular metals are shown in fig. I.3. The diagrams shown here have the same sign choices as their homogeneous analogues, so we use the same labelling convention employed in section I.1 to denote each sign choice.[4] Given the similarity in the method and results of the granular and homogeneous response functions, we shall simply quote the contributions generated by each sign choice. The response functions for each sign contribution are as follows,

$$\begin{aligned} K_{\alpha\beta}^{(A1)}(i\Omega) = \frac{16\pi N(0)e^2\mathcal{D}_T}{\mathcal{N}a^d}\delta_{\alpha\beta}T^2\sum_{\omega>0}\sum_{\varepsilon>0}\sum_{\mathbf{Q}}\sum_{\mathbf{q}}\frac{L(\mathbf{Q},\mathbf{q},i\omega)}{(\Gamma\lambda_{\mathbf{Q}}+\mathcal{D}q^2+2\varepsilon+\omega)^2} \\ + \frac{8\pi N(0)e^2\mathcal{D}_T}{\mathcal{N}a^d}\delta_{\alpha\beta}T^2\sum_{\varepsilon>0}\sum_{\mathbf{Q}}\sum_{\mathbf{q}}\frac{L(\mathbf{Q},\mathbf{q},0)}{(\Gamma\lambda_{\mathbf{Q}}+\mathcal{D}q^2+2\varepsilon)^2}, \end{aligned} \tag{I.52a}$$

[4]The only diagram that has no analogue here is diagram B of the homogeneous calculation, though its analogous contribution is effectively absorbed into the calculation of the granular analogue of the homogeneous A3 contribution.

$$
\begin{aligned}
K_{\alpha\beta}^{(A2)}(i\Omega) = & \frac{8\pi N(0)e^2\mathcal{D}_T}{\mathcal{N}a^d}\delta_{\alpha\beta}T^2 \\
& \times \sum_{\varepsilon>0}\sum_{\mathbf{Q}}\sum_{\mathbf{q}}\left[\sum_{\omega>\Omega}\frac{L(\mathbf{Q},\mathbf{q},i\omega)}{(\Gamma\lambda_{\mathbf{Q}}+\mathcal{D}q^2+2\varepsilon+\omega)^2}\right. \\
& \qquad \left. + \sum_{\omega<\Omega}\frac{L(\mathbf{Q},\mathbf{q},i\omega)}{(\Gamma\lambda_{\mathbf{Q}}+\mathcal{D}q^2+2\varepsilon+2\Omega-\omega)^2}\right] \\
& + \frac{8\pi N(0)e^2\mathcal{D}_T}{\mathcal{N}a^d}\delta_{\alpha\beta}T^2\sum_{\varepsilon>0}\sum_{\mathbf{Q}}\sum_{\mathbf{q}}\frac{L(\mathbf{Q},\mathbf{q},i\Omega)}{(\Gamma\lambda_{\mathbf{Q}}+\mathcal{D}q^2+2\varepsilon+\Omega)^2}
\end{aligned}
\tag{I.52b}
$$

$$
\begin{aligned}
K_{\alpha\beta}^{(A3)}(i\Omega) = & -\frac{8\pi N(0)e^2\mathcal{D}_T}{\mathcal{N}a^d}\delta_{\alpha\beta}T^2 \\
& \times \sum_{\mathbf{Q}}\sum_{\mathbf{q}}\left[\sum_{\omega\le 0}\sum_{0<\varepsilon<\Omega} + \sum_{0<\omega<\Omega}\sum_{0<\varepsilon<\Omega-\omega}\right]\frac{L(\mathbf{Q},\mathbf{q},i\omega)}{(\Gamma\lambda_{\mathbf{Q}}+\mathcal{D}q^2+2\varepsilon+|\omega|)^2},
\end{aligned}
\tag{I.52c}
$$

$$
\begin{aligned}
K_{\alpha\beta}^{(B1)}(i\Omega) = & K_{\alpha\beta}^{(B2)}(i\Omega) \\
= & \frac{16\pi N(0)e^2\mathcal{D}_T}{\mathcal{N}a^d}\delta_{\alpha\beta}T^2 \\
& \times \sum_{\omega>0}\sum_{\varepsilon>0}\sum_{\mathbf{Q}}\sum_{\mathbf{q}}\frac{L(\mathbf{Q},\mathbf{q},i\omega)}{(\Gamma\lambda_{\mathbf{Q}}+\mathcal{D}q^2+2\varepsilon+\omega)}\frac{\cos(Q_\alpha a)}{(\Gamma\lambda_{\mathbf{Q}}+\mathcal{D}q^2+2\varepsilon+2\Omega+\omega)} \\
& + \frac{8\pi N(0)e^2\mathcal{D}_T}{\mathcal{N}a^d}\delta_{\alpha\beta}T^2 \\
& \times \sum_{\varepsilon>0}\sum_{\mathbf{Q}}\sum_{\mathbf{q}}\frac{L(\mathbf{Q},\mathbf{q},0)}{(\Gamma\lambda_{\mathbf{Q}}+\mathcal{D}q^2+2\varepsilon)}\frac{\cos(Q_\alpha a)}{(\Gamma\lambda_{\mathbf{Q}}+\mathcal{D}q^2+2\varepsilon+2\Omega)},
\end{aligned}
\tag{I.52d}
$$

$$
\begin{aligned}
K_{\alpha\beta}^{(B3)}(i\Omega) = & \frac{16\pi N(0)e^2\mathcal{D}_T}{\mathcal{N}a^d}\delta_{\alpha\beta}T^2\sum_{0<\omega<\Omega}\sum_{0<\varepsilon<\Omega-\omega} \\
& \times \sum_{\mathbf{Q}}\sum_{\mathbf{q}}\frac{L(\mathbf{Q},\mathbf{q},i\omega)}{(\Gamma\lambda_{\mathbf{Q}}+\mathcal{D}q^2+2\varepsilon+\omega)}\frac{\cos(Q_\alpha a)}{(\Gamma\lambda_{\mathbf{Q}}+\mathcal{D}q^2+2\Omega-2\varepsilon-\omega)} \\
& + \frac{8\pi N(0)e^2\mathcal{D}_T}{\mathcal{N}a^d}\delta_{\alpha\beta}T^2\sum_{0<\varepsilon<\Omega} \\
& \times \sum_{\mathbf{Q}}\sum_{\mathbf{q}}\frac{L(\mathbf{Q},\mathbf{q},0)}{(\Gamma\lambda_{\mathbf{Q}}+\mathcal{D}q^2+2\varepsilon)}\frac{\cos(Q_\alpha a)}{(\Gamma\lambda_{\mathbf{Q}}+\mathcal{D}q^2+2\Omega-2\varepsilon)},
\end{aligned}
\tag{I.52e}
$$

$$
\begin{aligned}
K_{\alpha\beta}^{(C1)}(i\Omega) = &-\frac{64\pi N(0)e^2\mathcal{D}_T^2}{\mathcal{N}a^{d+2}}T^2\sum_{\omega>0}\sum_{\varepsilon>0}\\
&\times\sum_{\mathbf{Q}}\sum_{\mathbf{q}}\frac{L(\mathbf{Q},\mathbf{q},i\omega)}{(\Gamma\lambda_{\mathbf{Q}}+\mathcal{D}q^2+2\varepsilon+\omega)^2}\frac{\sin(Q_\alpha a)\sin(Q_\beta a)}{(\Gamma\lambda_{\mathbf{Q}}+\mathcal{D}q^2+2\varepsilon+\Omega+\omega)}\\
&-\frac{32\pi N(0)e^2\mathcal{D}_T^2}{\mathcal{N}a^{d+2}}T^2\sum_{\varepsilon>0}\\
&\times\sum_{\mathbf{Q}}\sum_{\mathbf{q}}\frac{L(\mathbf{Q},\mathbf{q},0)}{(\Gamma\lambda_{\mathbf{Q}}+\mathcal{D}q^2+2\varepsilon)^2}\frac{\sin(Q_\alpha a)\sin(Q_\beta a)}{(\Gamma\lambda_{\mathbf{Q}}+\mathcal{D}q^2+2\varepsilon+\Omega)},
\end{aligned}
\tag{I.52f}
$$

$$
\begin{aligned}
K_{\alpha\beta}^{(C2)}(i\Omega) = &-\frac{32\pi N(0)e^2\mathcal{D}_T^2}{\mathcal{N}a^{d+2}}T^2\sum_{\varepsilon>0}\sum_{\mathbf{Q}}\sum_{\mathbf{q}}\sin(Q_\alpha a)\sin(Q_\beta a)\\
&\times\Bigg[\sum_{\omega<\Omega}\frac{L(\mathbf{Q},\mathbf{q},i\omega)}{(\Gamma\lambda_{\mathbf{Q}}+\mathcal{D}q^2+2\varepsilon+2\Omega-\omega)^2}\frac{1}{(\Gamma\lambda_{\mathbf{Q}}+\mathcal{D}q^2+2\varepsilon+\Omega-\omega)}\\
&\qquad+\sum_{\omega>\Omega}\frac{L(\mathbf{Q},\mathbf{q},i\omega)}{(\Gamma\lambda_{\mathbf{Q}}+\mathcal{D}q^2+2\varepsilon+\omega)^2}\frac{1}{(\Gamma\lambda_{\mathbf{Q}}+\mathcal{D}q^2+2\varepsilon+\omega-\Omega)}\Bigg]\\
&-\frac{32\pi N(0)e^2\mathcal{D}_T^2}{\mathcal{N}a^{d+2}}T^2\\
&\times\sum_{\varepsilon>0}\sum_{\mathbf{Q}}\sum_{\mathbf{q}}\frac{L(\mathbf{Q},\mathbf{q},i\Omega)}{(\Gamma\lambda_{\mathbf{Q}}+\mathcal{D}q^2+2\varepsilon+\Omega)^2}\frac{\sin(Q_\alpha a)\sin(Q_\beta a)}{(\Gamma\lambda_{\mathbf{Q}}+\mathcal{D}q^2+2\varepsilon)},
\end{aligned}
\tag{I.52g}
$$

$$
\begin{aligned}
K_{\alpha\beta}^{(D1)}(i\Omega) &= K_{\alpha\beta}^{(D2)}(i\Omega)\\
&=-\frac{64\pi N(0)e^2\mathcal{D}_T^2}{\mathcal{N}a^{d+2}}T^2\sum_{\omega>0}\sum_{\varepsilon>0}\sum_{\mathbf{Q}}\\
&\times\sum_{\mathbf{q}}\Bigg[\frac{L(\mathbf{Q},\mathbf{q},i\omega)}{(\Gamma\lambda_{\mathbf{Q}}+\mathcal{D}q^2+2\varepsilon+\omega)}\frac{\sin(Q_\alpha a)\sin(Q_\beta a)}{(\Gamma\lambda_{\mathbf{Q}}+\mathcal{D}q^2+2\varepsilon+2\Omega+\omega)}\\
&\qquad\times\frac{1}{(\Gamma\lambda_{\mathbf{Q}}+\mathcal{D}q^2+2\varepsilon+\Omega+\omega)}\Bigg]\\
&-\frac{32\pi N(0)e^2\mathcal{D}_T^2}{\mathcal{N}a^{d+2}}T^2\sum_{\varepsilon>0}\sum_{\mathbf{Q}}\\
&\times\sum_{\mathbf{q}}\Bigg[\frac{L(\mathbf{Q},\mathbf{q},0)}{(\Gamma\lambda_{\mathbf{Q}}+\mathcal{D}q^2+2\varepsilon)}\frac{\sin(Q_\alpha a)\sin(Q_\beta a)}{(\Gamma\lambda_{\mathbf{Q}}+\mathcal{D}q^2+2\varepsilon+2\Omega)}\\
&\qquad\times\frac{1}{(\Gamma\lambda_{\mathbf{Q}}+\mathcal{D}q^2+2\varepsilon+\Omega)}\Bigg].
\end{aligned}
\tag{I.52h}
$$

$$
\begin{aligned}
K_{\alpha\beta}^{(E,\mathrm{I})}(i\Omega) &= K_{\alpha\beta}^{(E,\mathrm{II})}(i\Omega) \\
&= -\frac{64e^2\pi^2N(0)^2\mathcal{D}_T^2}{\mathcal{N}a^{d+2}}T\sum_{\omega\geq 0}\Bigg\{\sum_{\mathbf{Q}}\sum_{\mathbf{q}}\sin(Q_\alpha a)\sin(Q_\beta a)L(\mathbf{Q},\mathbf{q},i\omega) \\
&\quad\times L(\mathbf{Q},\mathbf{q},i\omega+i\Omega)\Bigg(T\sum_{\varepsilon>0}\Bigg\{\Bigg[\frac{1}{\Gamma\lambda_{\mathbf{Q}}+\mathcal{D}q^2+2\varepsilon+\omega} \\
&\quad+\frac{1}{\Gamma\lambda_{\mathbf{Q}}+\mathcal{D}q^2+2\varepsilon+2\Omega+\omega}\Bigg]\frac{1}{\Gamma\lambda_{\mathbf{Q}}+\mathcal{D}q^2+2\varepsilon+\Omega+\omega}\Bigg\}\Bigg)^2\Bigg\}
\end{aligned}
\tag{I.52i}
$$

$$
\begin{aligned}
K_{\alpha\beta}^{(E,\mathrm{III})}(i\Omega) &= -\frac{64e^2\pi^2N(0)^2\mathcal{D}_T^2}{\mathcal{N}a^{d+2}}T\sum_{-\Omega<\omega<0}\Bigg\{\sum_{\mathbf{Q}}\sum_{\mathbf{q}}\sin(Q_\alpha a)\sin(Q_\beta a) \\
&\quad\times L(\mathbf{Q},\mathbf{q},i\omega)L(\mathbf{Q},\mathbf{q},i\omega+i\Omega)\Bigg(T\sum_{\varepsilon>0}\Bigg[\frac{1}{\Gamma\lambda_{\mathbf{Q}}+\mathcal{D}q^2+2\varepsilon+\Omega-\omega} \\
&\quad\times\frac{1}{\Gamma\lambda_{\mathbf{Q}}+\mathcal{D}q^2+2\varepsilon-\omega}+\frac{1}{\Gamma\lambda_{\mathbf{Q}}+\mathcal{D}q^2+2\varepsilon+2\Omega+\omega} \\
&\quad\times\frac{1}{\Gamma\lambda_{\mathbf{Q}}+\mathcal{D}q^2+2\varepsilon+\Omega+\omega}\Bigg]\Bigg)^2\Bigg\}.
\end{aligned}
\tag{I.52j}
$$

In the granular diffusive limit, $Q \ll a^{-1}$, we may approximate $\cos(Q_\alpha a) \simeq 1$, $\sin(Q_\alpha a) \simeq Q_\alpha a$, and $\Gamma\lambda_{\mathbf{Q}} \simeq \mathcal{D}_T Q^2$. Doing so, the above response functions collapse to forms equivalent to the homogeneous case, such that they obey the typical mapping $\mathcal{D} \to \mathcal{D}_T$ in the prefactor, and $\mathcal{D}q^2 \to \mathcal{D}q^2 + \mathcal{D}_T Q^2$ in the diffusive propagators. We may then handle the sum of these functions for $\Omega = 0$ in exactly the same manner as before, where we instead focus on the $\mathbf{Q}$ sum rather than the $\mathbf{q}$ sum. We thus find

$$
\begin{aligned}
K_{\alpha\beta}(0) &= K_{\alpha\beta}^{(A1)}(0)+K_{\alpha\beta}^{(A2)}(0)+K_{\alpha\beta}^{(B1)}(0)+K_{\alpha\beta}^{(B2)}(0) \\
&\quad+K_{\alpha\beta}^{(C1)}(0)+K_{\alpha\beta}^{(C2)}(0)+K_{\alpha\beta}^{(D1)}(0)+K_{\alpha\beta}^{(D2)}(0) \\
&\quad+K_{\alpha\beta}^{(E,\mathrm{I})}(0)+K_{\alpha\beta}^{(E,\mathrm{II})}(0) \\
&= \frac{8e^2}{\mathcal{N}a^{d+2}}T\sum_{\omega>0}\sum_{\mathbf{Q}}\sum_{\mathbf{q}}\frac{\partial^2}{\partial Q_\alpha\partial Q_\beta}\ln\left[\ln\left(\frac{T}{T_c}\right)+\psi\left(\frac{1}{2}+\frac{\omega+\mathcal{D}q^2+\Gamma\lambda_{\mathbf{Q}}}{4\pi T}\right)-\psi\left(\frac{1}{2}\right)\right] \\
&\quad+(\omega=0\text{ terms}).
\end{aligned}
\tag{I.53}
$$

By replacing the $\mathbf{Q}$ sum by an integral, we again manipulate it into a surface integral and take the surface to infinity where the integrand vanishes.

On a technical point, taking the surface to infinity might seem unreasonable as we have assumed the granular diffusive limit, which imposes a finite upper limit. However, even in the homogeneous case, where we assume the regular diffusive limit, we have a finite upper limit, $q \ll l^{-1}$. We therefore have to appreciate that the vanishing of $K_{\alpha\beta}(0)$ is an approximate result.

If we wanted to show that all diagrams cancelled exactly in the zero frequency limit, we would need to repeal our assumption of the granular diffusive limit and consider diagrams that would otherwise appear as higher order corrections. This would correspond to including diagrams that produce extra factors of $\mathcal{D}q^2\tau_0$ in the homogeneous case, of which there is an infinite set.[5] In the case of granular systems, we would need to include diagrams containing extra factors of $Q_\alpha a$. In homogeneous metals, this set of circumstances is known as the *intermediate limit*; disorder is still present in the system and cannot be neglected, but it is not as abundant as in the diffusive limit.[6] Hence, to get exact cancellation in the granular case, we would need to consider the granular analogue of the intermediate limit.

So, let the set of diagrams generated in the granular intermediate limit produce the electromagnetic response function $K^{(X)}_{\alpha\beta}(i\Omega)$. Now, let us suppose that $K^{(X)}_{\alpha\beta}(i\Omega)$ produces the following contributions to $K_{\alpha\beta}(i\Omega)$,

$$\begin{aligned} K^{(X1)}_{\alpha\beta}(i\Omega) = &-\frac{16\pi N(0)e^2\mathcal{D}_T}{\mathcal{N}a^d}\delta_{\alpha\beta}T^2\sum_{\omega>0}\sum_{\varepsilon>0}\sum_{\mathbf{Q}}\sum_{\mathbf{q}}\frac{L(\mathbf{Q},\mathbf{q},i\omega)(1-\cos(Q_\alpha a))}{(\Gamma\lambda_{\mathbf{Q}}+\mathcal{D}q^2+2\varepsilon+\omega)^2} \\ &-\frac{8\pi N(0)e^2\mathcal{D}_T}{\mathcal{N}a^d}\delta_{\alpha\beta}T^2\sum_{\varepsilon>0}\sum_{\mathbf{Q}}\sum_{\mathbf{q}}\frac{L(\mathbf{Q},\mathbf{q},0)(1-\cos(Q_\alpha a))}{(\Gamma\lambda_{\mathbf{Q}}+\mathcal{D}q^2+2\varepsilon)^2}, \end{aligned} \tag{I.54a}$$

[5] We could have diagrams that produce $\mathcal{D}q^2\tau_0$, $(\mathcal{D}q^2\tau_0)^2$, etc, which would all become relevant outside of the diffusive limit.

[6] The intermediate limit is the middle ground between diffusive and ballistic behaviour. In the former, disorder is extremely abundant and scattering happens more frequently. In contrast, ballistic behaviour is related to clean systems, where electrons move far more freely inside the material, and hence scatter off the material's edges more often than they do off internal impurities.

$$
\begin{aligned}
K_{\alpha\beta}^{(X2)}(i\Omega) = &-\frac{8\pi N(0)e^2\mathcal{D}_T}{\mathcal{N}a^d}\delta_{\alpha\beta}T^2 \\
&\times\sum_{\varepsilon>0}\sum_{\mathbf{Q}}\sum_{\mathbf{q}}\left[\sum_{\omega>\Omega}\frac{L(\mathbf{Q},\mathbf{q},i\omega)(1-\cos(Q_\alpha a))}{(\Gamma\lambda_{\mathbf{Q}}+\mathcal{D}q^2+2\varepsilon+\omega)^2}\right. \\
&\qquad\left.+\sum_{\omega<\Omega}\frac{L(\mathbf{Q},\mathbf{q},i\omega)(1-\cos(Q_\alpha a))}{(\Gamma\lambda_{\mathbf{Q}}+\mathcal{D}q^2+2\varepsilon+2\Omega-\omega)^2}\right] \\
&-\frac{8\pi N(0)e^2\mathcal{D}_T}{\mathcal{N}a^d}\delta_{\alpha\beta}T^2\sum_{\varepsilon>0}\sum_{\mathbf{Q}}\sum_{\mathbf{q}}\frac{L(\mathbf{Q},\mathbf{q},i\Omega)(1-\cos(Q_\alpha a))}{(\Gamma\lambda_{\mathbf{Q}}+\mathcal{D}q^2+2\varepsilon+\Omega)^2}
\end{aligned}
\tag{I.54b}
$$

$$
\begin{aligned}
K_{\alpha\beta}^{(X3)}(i\Omega) = &\frac{8\pi N(0)e^2\mathcal{D}_T}{\mathcal{N}a^d}\delta_{\alpha\beta}T^2 \\
&\times\sum_{\mathbf{Q}}\sum_{\mathbf{q}}\left[\sum_{\omega\le 0}\sum_{0<\varepsilon<\Omega}+\sum_{0<\omega<\Omega}\sum_{0<\varepsilon<\Omega-\omega}\right]\frac{L(\mathbf{Q},\mathbf{q},i\omega)(1-\cos(Q_\alpha a))}{(\Gamma\lambda_{\mathbf{Q}}+\mathcal{D}q^2+2\varepsilon+|\omega|)^2}.
\end{aligned}
\tag{I.54c}
$$

In the granular diffusive limit, $K_{\alpha\beta}^{(X)}(i\Omega)$ clearly carries an extra factor of $(Q_\alpha a)^2$ compared to $K_{\alpha\beta}^{(A)}(i\Omega)$, and hence is a higher order correction. The sum of $K_{\alpha\beta}^{(X)}(i\Omega)$ and $K_{\alpha\beta}^{(A)}(i\Omega)$ produces

$$
\begin{aligned}
\hat{K}_{\alpha\beta}^{(A1)}(i\Omega) = &\frac{16\pi N(0)e^2\mathcal{D}_T}{\mathcal{N}a^d}\delta_{\alpha\beta}T^2\sum_{\omega>0}\sum_{\varepsilon>0}\sum_{\mathbf{Q}}\sum_{\mathbf{q}}\frac{L(\mathbf{Q},\mathbf{q},i\omega)\cos(Q_\alpha a)}{(\Gamma\lambda_{\mathbf{Q}}+\mathcal{D}q^2+2\varepsilon+\omega)^2} \\
&+\frac{8\pi N(0)e^2\mathcal{D}_T}{\mathcal{N}a^d}\delta_{\alpha\beta}T^2\sum_{\varepsilon>0}\sum_{\mathbf{Q}}\sum_{\mathbf{q}}\frac{L(\mathbf{Q},\mathbf{q},0)\cos(Q_\alpha a)}{(\Gamma\lambda_{\mathbf{Q}}+\mathcal{D}q^2+2\varepsilon)^2},
\end{aligned}
\tag{I.55a}
$$

$$
\begin{aligned}
\hat{K}_{\alpha\beta}^{(A2)}(i\Omega) = &\frac{8\pi N(0)e^2\mathcal{D}_T}{\mathcal{N}a^d}\delta_{\alpha\beta}T^2 \\
&\times\sum_{\varepsilon>0}\sum_{\mathbf{Q}}\sum_{\mathbf{q}}\left[\sum_{\omega>\Omega}\frac{L(\mathbf{Q},\mathbf{q},i\omega)\cos(Q_\alpha a)}{(\Gamma\lambda_{\mathbf{Q}}+\mathcal{D}q^2+2\varepsilon+\omega)^2}\right. \\
&\qquad\left.+\sum_{\omega<\Omega}\frac{L(\mathbf{Q},\mathbf{q},i\omega)\cos(Q_\alpha a)}{(\Gamma\lambda_{\mathbf{Q}}+\mathcal{D}q^2+2\varepsilon+2\Omega-\omega)^2}\right] \\
&+\frac{8\pi N(0)e^2\mathcal{D}_T}{\mathcal{N}a^d}\delta_{\alpha\beta}T^2\sum_{\varepsilon>0}\sum_{\mathbf{Q}}\sum_{\mathbf{q}}\frac{L(\mathbf{Q},\mathbf{q},i\Omega)\cos(Q_\alpha a)}{(\Gamma\lambda_{\mathbf{Q}}+\mathcal{D}q^2+2\varepsilon+\Omega)^2}
\end{aligned}
\tag{I.55b}
$$

$$\hat{K}^{(A3)}_{\alpha\beta}(i\Omega) = -\frac{8\pi N(0)e^2\mathcal{D}_T}{\mathcal{N}a^d}\delta_{\alpha\beta}T^2 \times \sum_{\mathbf{Q}}\sum_{\mathbf{q}}\left[\sum_{\omega\leq 0}\sum_{0<\varepsilon<\Omega} + \sum_{0<\omega<\Omega}\sum_{0<\varepsilon<\Omega-\omega}\right]\frac{L(\mathbf{Q},\mathbf{q},i\omega)\cos(Q_\alpha a)}{(\Gamma\lambda_{\mathbf{Q}}+\mathcal{D}q^2+2\varepsilon+|\omega|)^2}, \tag{I.55c}$$

where $\hat{K}^{(A)}_{\alpha\beta}(i\Omega) = K^{(A)}_{\alpha\beta}(i\Omega)+K^{(X)}_{\alpha\beta}(i\Omega)$. Clearly $\hat{K}^{(A)}_{\alpha\beta}(i\Omega)$ resembles $K^{(A)}_{\alpha\beta}(i\Omega)$, but has an extra factor of $\cos(Q_\alpha a)$ in the summand. Note that $\hat{K}^{(A)}_{\alpha\beta}(i\Omega) \simeq K^{(A)}_{\alpha\beta}(i\Omega)$ in the granular diffusive limit, as expected.

With the extra contributions of $K^{(X)}_{\alpha\beta}(i\Omega)$, the zero frequency response function is now given by

$$\begin{aligned}
K_{\alpha\beta}(0) &= \hat{K}^{(A1)}_{\alpha\beta}(0) + \hat{K}^{(A2)}_{\alpha\beta}(0) + K^{(B1)}_{\alpha\beta}(0) + K^{(B2)}_{\alpha\beta}(0) \\
&\quad + K^{(C1)}_{\alpha\beta}(0) + K^{(C2)}_{\alpha\beta}(0) + K^{(D1)}_{\alpha\beta}(0) + K^{(D2)}_{\alpha\beta}(0) \\
&\quad + K^{(E,\mathrm{I})}_{\alpha\beta}(0) + K^{(E,\mathrm{II})}_{\alpha\beta}(0) \\
&= \frac{8e^2}{\mathcal{N}a^{d+2}}T \\
&\quad \times \sum_{\omega>0}\sum_{\mathbf{Q}}\sum_{\mathbf{q}}\frac{\partial^2}{\partial Q_\alpha \partial Q_\beta}\ln\left[\ln\left(\frac{T}{T_c}\right)+\psi\left(\frac{1}{2}+\frac{\omega+\mathcal{D}q^2+\Gamma\lambda_{\mathbf{Q}}}{4\pi T}\right)-\psi\left(\frac{1}{2}\right)\right] \\
&\quad + (\omega = 0 \text{ terms}).
\end{aligned} \tag{I.56}$$

The second equality of eq. I.56 is found using the same approach we implemented in obtaining eq. I.16b. By rewriting $K_{\alpha\beta}(0)$ in terms of a surface integral in Q-space,

$$\begin{aligned}
K_{\alpha\beta}(0) &= \frac{8e^2T}{a^2}\sum_{\omega>0}\sum_{\mathbf{q}} \\
&\quad \times \oint_S d^{d-1}Q\,\mathbf{e}_\alpha\cdot\hat{\mathbf{n}}\,\frac{\partial}{\partial Q_\beta}\ln\left[\ln\left(\frac{T}{T_c}\right)+\psi\left(\frac{1}{2}+\frac{|\omega|+\mathcal{D}q^2+\Gamma\lambda_{\mathbf{Q}}}{4\pi T}\right)-\psi\left(\frac{1}{2}\right)\right] \\
&\quad + (\omega = 0 \text{ terms}) \\
&= -\frac{4e^2N(0)\Gamma}{\pi a^2}\sum_{\omega>0}\sum_{\mathbf{q}} \\
&\quad \times \oint_S d^{d-1}Q\,\mathbf{e}_\alpha\cdot\hat{\mathbf{n}}\,L(\mathbf{Q},\mathbf{q},i\omega)\psi'\left(\frac{1}{2}+\frac{|\omega|+\mathcal{D}q^2+\Gamma\lambda_{\mathbf{Q}}}{4\pi T}\right)\sin(Q_\beta a) \\
&\quad + (\omega = 0 \text{ terms}),
\end{aligned} \tag{I.57}$$

and taking the surface to the boundary of the first Brillouin zone,[7] which is a cube in our case, we see that $K_{\alpha\beta}(0)$ vanishes. This is because the surfaces on opposite sides of the Brillouin zone produce the near identical contributions to the integral, where they only differ in sign due to the factor of $\mathbf{e}_\alpha \cdot \hat{\mathbf{n}}$.

We therefore expect that a diagram, or set of diagrams, would produce the response function $K^{(X)}_{\alpha\beta}(i\Omega)$. These diagrams are not included in those shown in fig. I.3, and must be related to higher order corrections in the granular diffusive limit. Therefore, the diagrams shown in fig. I.3 constitute the full set of diagrams describing the first order contributions to the fluctuation conductivity in the granular diffusive limit.

The diagrams generating $K^{(X)}_{\alpha\beta}(i\Omega)$ only become relevant in the *granular intermediate limit*, where $Q_\alpha a \sim 1$ is allowed. This is analogous to the intermediate limit of the homogeneous case ($q \sim l^{-1}$). To determine the set of diagrams that become relevant in the granular intermediate limit, we should first understand the set of diagrams describing the fluctuation conductivity in the intermediate limit for homogeneous systems.

I.6.1 EEI Side Note

A similar argument can be made for the vanishing of the electromagnetic response function for granular EEIs. In section 5.3.2, we saw that diagrams A and B did not cancel exactly, unlike their homogeneous analogues. However, we did see that their sum was a higher order correction due to the factor of $1-\cos(Q_\alpha a) \sim (Q_\alpha a)^2$ in the granular diffusive limit. Terms analogous to this would only appear in the homogeneous calculation if we chose to work in the intermediate limit, as opposed to the diffusive limit.

Here, we again suggest that there may be a set of diagrams that we have not accounted for that are relevant in the granular intermediate limit, such that their inclusion would amount to adding an extra factor of $\cos(Q_\alpha a)$ into the summand of $K^{(A)}_{\alpha\beta}(i\Omega)$. This would lead to the exact cancellation of diagrams A and B with the extra set of diagrams. This is entirely analogous to what we proposed above for granular superconducting fluctuations.

[7] This is analogous to the surface to infinity in the homogeneous case

APPENDIX J

PHASE BREAKING RATES IN HOMOGENEOUS SYSTEMS – CALCULATION DETAILS

In this appendix we provide the details of how to calculate the phase breaking rates, τ_ϕ^{-1}, due to electron-electron interactions via Coulomb and superconducting fluctuations in disordered homogeneous metals. In section J.1 we look at the EEI contribution, after which we provide the details for the superconducting fluctuation contribution in section J.2.

J.1 Coulomb Contribution

In this section we concern ourselves with the calculation of the diagrams in fig. J.1, where the wavy lines represent the screened Coulomb interaction. To the diagrams A, B, and C we may associate

$$\Sigma^{(A)}_{\phi,ee} = -T\sum_{\mathbf{k},\mathbf{q}}\sum_{\omega}\Big[V(\mathbf{q},i\omega)D(\mathbf{q},i\varepsilon+i\Omega,i\varepsilon+i\Omega+i\omega)^2G(\mathbf{k},i\varepsilon+i\Omega)^2 \times G(\mathbf{k}+\mathbf{q},i\omega+i\varepsilon+i\Omega)G(\mathbf{k},i\varepsilon)\Big], \tag{J.1a}$$

$$\Sigma^{(B)}_{\phi,ee} = -T\sum_{\mathbf{k},\mathbf{k}',\mathbf{q}}\sum_{\omega}\Bigg[\frac{V(\mathbf{q},i\omega)}{2\pi N(0)\tau_0}D(\mathbf{q},i\varepsilon+i\Omega,i\varepsilon+i\Omega+i\omega)^2G(\mathbf{k},i\varepsilon+i\Omega)^2 \times G(\mathbf{k},i\varepsilon)G(\mathbf{k}',i\varepsilon+i\Omega)^2G(\mathbf{k}'+\mathbf{q},i\omega+i\varepsilon+i\Omega)\Bigg], \tag{J.1b}$$

$$\Sigma^{(C)}_{\phi,ee} = -T\sum_{\mathbf{q}}\sum_{\omega}\Bigg[\frac{V(\mathbf{q},i\omega)}{2\pi N(0)\tau_0}D(\mathbf{q},i\varepsilon+i\Omega,i\varepsilon+i\Omega+i\omega)^2 \times\left(\sum_{\mathbf{k}}G(\mathbf{k},i\varepsilon+i\Omega)G(\mathbf{k}+\mathbf{q},i\omega+i\varepsilon+i\Omega)G(\mathbf{k},i\varepsilon)\right)^2\Bigg], \tag{J.1c}$$

respectively. We shall assume $\varepsilon+\Omega>0$ and $\varepsilon<0$ without loss of generality, as explained in the main body of the thesis. The diffusons present in these diagrams enforce $\omega+\varepsilon+\Omega<0$. Hence, we may rewrite these expressions as

$$\Sigma^{(A)}_{\phi,ee} = -T\sum_{\mathbf{k},\mathbf{q}}\sum_{\omega<-(\varepsilon+\Omega)}V(\mathbf{q},i\omega)D(\mathbf{q},i\omega)^2G^+(\mathbf{k})^2G^-(\mathbf{k}+\mathbf{q},i\omega+i\varepsilon+i\Omega)G^-(\mathbf{k}), \tag{J.2a}$$

$$\Sigma^{(B)}_{\phi,ee} = -T\sum_{\mathbf{k},\mathbf{k}',\mathbf{q}}\sum_{\omega<-(\varepsilon+\Omega)}\Bigg[\frac{V(\mathbf{q},i\omega)}{2\pi N(0)\tau_0}D(\mathbf{q},i\omega)^2G^+(\mathbf{k})^2 \times G^-(\mathbf{k})G^+(\mathbf{k}')^2G^-(\mathbf{k}'+\mathbf{q},i\omega+i\varepsilon+i\Omega)\Bigg], \tag{J.2b}$$

$$\Sigma^{(C)}_{\phi,ee} = -T\sum_{\mathbf{q}}\sum_{\omega<-(\varepsilon+\Omega)}\Bigg[\frac{V(\mathbf{q},i\omega)}{2\pi N(0)\tau_0}D(\mathbf{q},i\omega)^2 \times\left(\sum_{\mathbf{k}}G^+(\mathbf{k})G^-(\mathbf{k}+\mathbf{q},i\omega+i\varepsilon+i\Omega)G^-(\mathbf{k})\right)^2\Bigg]. \tag{J.2c}$$

We next expand the electron Green's functions in powers of $\mathbf{q}$ and ω, retaining leading order terms that are not zeroth order,[1] and linearise the fast momentum sums ($\mathbf{k}$ and $\mathbf{k}'$) around the Fermi surface. This yields,

[1] Terms containing a single power of $\mathbf{q}$ vanish due to carrying a factor of $\mathbf{k}$, and hence is odd in $\mathbf{k}$.

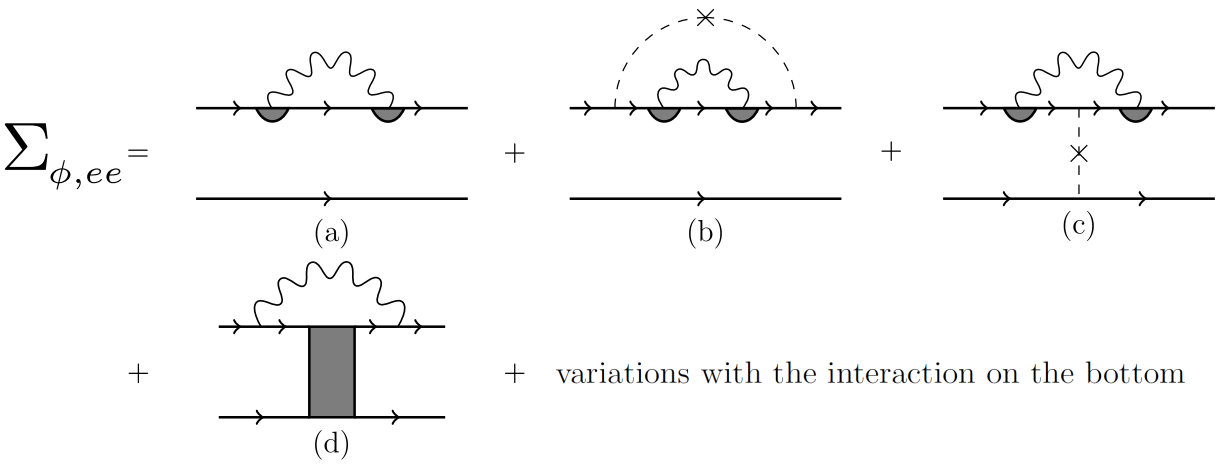

Figure J.1: Diagrams describing the phase coherence corrections to the cooperon in homogeneous systems due to Coulomb interactions.

$$\Sigma^{(A)}_{\phi,ee} = -T\sum_{\mathbf{k},\mathbf{q}}\sum_{\omega<-(\varepsilon+\Omega)}\Big\{V(\mathbf{q},i\omega)D(\mathbf{q},i\omega)^2G^+(\mathbf{k})^2G^-(\mathbf{k}) \times\Big[G^-(\mathbf{k})-i\omega G^-(\mathbf{k})^2+(\mathbf{v}_F\cdot\mathbf{q})^2G^-(\mathbf{k})^3\Big]\Big\}, \tag{J.3a}$$

$$\Sigma^{(B)}_{\phi,ee} = -T\sum_{\mathbf{k},\mathbf{k}',\mathbf{q}}\sum_{\omega<-(\varepsilon+\Omega)}\left\{\frac{V(\mathbf{q},i\omega)}{2\pi N(0)\tau_0}D(\mathbf{q},i\omega)^2G^+(\mathbf{k})^2G^-(\mathbf{k})G^+(\mathbf{k}')^2 \times\Big[G^-(\mathbf{k}')-i\omega G^-(\mathbf{k}')^2+(\mathbf{v}'_F\cdot\mathbf{q})^2G^-(\mathbf{k}')^3\Big]\right\}, \tag{J.3b}$$

$$\Sigma^{(C)}_{\phi,ee} = -T\sum_{\mathbf{q}}\sum_{\omega<-(\varepsilon+\Omega)}\left\{\frac{V(\mathbf{q},i\omega)}{2\pi N(0)\tau_0}D(\mathbf{q},i\omega)^2 \times\left(\sum_{\mathbf{k}}G^+(\mathbf{k})G^-(\mathbf{k})\Big[G^-(\mathbf{k})-i\omega G^-(\mathbf{k})^2+(\mathbf{v}_F\cdot\mathbf{q})^2G^-(\mathbf{k})^3\Big]\right)^2\right\}, \tag{J.3c}$$

where the prime on the $\mathbf{v}'_F$ reminds us that it comes from $\mathbf{k}'$, and so is independent of the $\mathbf{k}$ sum but not the $\mathbf{k}'$ sum.

We next evaluate the fast momentum sums using the diffusive momentum sum identity in eq. 3.75. This produces,

$$\Sigma^{(A)}_{\phi,ee} = -2\pi N(0)\tau_0^3T\sum_{\mathbf{k},\mathbf{q}}\sum_{\omega<-(\varepsilon+\Omega)}V(\mathbf{q},i\omega)D(\mathbf{q},i\omega)^2(2+3\omega\tau_0-4\mathcal{D}q^2\tau_0), \tag{J.4a}$$

$$\Sigma^{(B)}_{\phi,ee} = -2\pi N(0)\tau_0^3 T \sum_{\mathbf{k},\mathbf{k}',\mathbf{q}} \sum_{\omega<-(\varepsilon+\Omega)} V(\mathbf{q},i\omega)D(\mathbf{q},i\omega)^2(-1-2\omega\tau_0+3\mathcal{D}q^2\tau_0), \tag{J.4b}$$

$$\Sigma^{(C)}_{\phi,ee} = -2\pi N(0)\tau_0^3 T \sum_{\mathbf{q}} \sum_{\omega<-(\varepsilon+\Omega)} V(\mathbf{q},i\omega)D(\mathbf{q},i\omega)^2(-1-2\omega\tau_0+2\mathcal{D}q^2\tau_0), \tag{J.4c}$$

where we retained terms up to order ω and $\mathcal{D}q^2$ in eq. J.4c. By adding these contributions together, we find

$$\begin{aligned}\Sigma^{(ABC)}_{\phi,ee} &= -2\pi N(0)\tau_0^4 T \sum_{\mathbf{q}} \sum_{\omega<-(\varepsilon+\Omega)} V(\mathbf{q},i\omega)D(\mathbf{q},i\omega)^2(\mathcal{D}q^2-\omega) \\ &= -2\pi N(0)\tau_0^2 T \sum_{\mathbf{q}} \sum_{\omega<-(\varepsilon+\Omega)} V(\mathbf{q},i\omega)\frac{\mathcal{D}q^2-\omega}{(\mathcal{D}q^2+|\omega|)^2}.\end{aligned} \tag{J.5}$$

Recalling eq. 3.73, noting that $|\omega| = -\omega$ in the above Matsubara frequency sum, and letting $\omega \to -\omega$, we can rewrite eq. J.5 as

$$\Sigma^{(ABC)}_{\phi,ee} = -T(2\pi N(0)\tau_0^2)^2 \sum_{\mathbf{q}} \sum_{\omega>\varepsilon+\Omega} \widetilde{D}(\mathbf{q},i\varepsilon+i\Omega+i\omega,i\varepsilon+i\Omega)V(\mathbf{q},i\omega), \tag{J.6}$$

which is exactly the result we quote for the sum of diagrams A, B, and C in eq. 3.169.

The counterpart to the sum of diagrams A, B, and C where the interaction is on the bottom electron Green's function can be calculated using the exact same ideas as above. The only change is that the ω sum is taken over the range $\omega > -\varepsilon$. We shall not show this explicitly, as this would simply repeat what we have just done.

Diagram D is given by,

$$\begin{aligned}\Sigma^{(D)}_{\phi,ee} &= -T\sum_{\mathbf{q}}\sum_{\omega} \widetilde{C}(\mathbf{q},i\varepsilon+i\Omega+i\omega,i\varepsilon)V(\mathbf{q},i\omega) \\ &\qquad \times \left(\sum_{\mathbf{k}} G(\mathbf{k},i\varepsilon+i\Omega)G(\mathbf{k}+\mathbf{q},i\varepsilon+\Omega+i\omega)G(\mathbf{k},i\varepsilon)\right)^2 \\ &\simeq -T\sum_{\mathbf{q}}\sum_{\omega<-(\varepsilon+\Omega)} \widetilde{C}(\mathbf{q},i\Omega+i\omega)V(\mathbf{q},i\omega)\left(\sum_{\mathbf{k}} G^+(\mathbf{k})G^-(\mathbf{k})^2\right)^2,\end{aligned} \tag{J.7}$$

where in the second equality we appreciated that $|\mathbf{k}| \simeq k_F$, so only small $\mathbf{q}$ are significant ($|\mathbf{q}| \ll k_F$), hence we may neglect its presence inside the electron Green's functions. Evaluating the $\mathbf{k}$ sum using eq. 3.75, we find the expression quoted in eq. 3.171

$$\Sigma^{(D)}_{\phi,ee} = T(2\pi N(0)\tau_0^2)^2 \sum_{\mathbf{q}} \sum_{\omega > -(\varepsilon+\Omega)} \widetilde{C}(\mathbf{q}, i\Omega + i\omega) V(\mathbf{q}, i\omega). \tag{J.8}$$

In complete analogy to the counterpart to diagrams A, B, and C, the counterpart to diagram D which has the interaction appearing on the bottom electron Green's function will have exactly same form as above, but with the Matsubara sum taken for $\omega > \varepsilon$. Again, we shall not give the details for the calculation of this piece as it simply repeats the process we presented above.

To progress further, we next need to perform analytic continuation for the ω sums. These details are given in chapter 3, so we shall not repeat them here. What we shall do next, however, is give the details for evaluating the integral and sum in eq. 3.184 for two and three dimensions. For reference, eq. 3.184 is

$$\frac{1}{\tau_{\phi,ee}} \simeq -4N(0)\tau_0^2 \sum_{\mathbf{q}} \int_{-T}^{+T} dz \frac{\widetilde{C}^R(\mathbf{q}, z)}{\sinh(\beta z)} \mathrm{Im}\left[V^R(\mathbf{q}, z)\right]. \tag{J.9}$$

In both cases, we will need to approximate the screened Coulomb interaction,

$$V^R(\mathbf{q}, z) = \frac{V_{0,d}(\mathbf{q})}{1 + \frac{\kappa_d^{d-1}\mathcal{D}q^{3-d}}{\mathcal{D}q^2 - iz}}, \qquad d = 2, 3, \tag{J.10}$$

where $V_{0,d}(\mathbf{q})$ is the unscreened Coulomb interaction in d dimensions, see eq. 3.87, and κ_d is the Thomas-Fermi wave vector in d dimensions. In general, $\kappa_d \gg |\mathbf{q}|$, and hence

$$\begin{aligned} V^R(\mathbf{q}, z) &= V_{0,d}(\mathbf{q}) \frac{\mathcal{D}q^2 - iz}{\mathcal{D}q^2 - iz + \kappa_d^{d-1}\mathcal{D}q^{3-d}} \\ &\simeq V_{0,d}(\mathbf{q}) \frac{\mathcal{D}q^2 - iz}{\kappa_d^{d-1}\mathcal{D}q^{3-d} - iz}. \end{aligned} \tag{J.11}$$

Therefore,

$$\begin{aligned} \mathrm{Im}[V^R(\mathbf{q},z)] &= zV_{0,d}(\mathbf{q})\frac{\mathcal{D}q^2-\kappa_d^{d-1}\mathcal{D}q^{3-d}}{(\kappa_d^{d-1}\mathcal{D}q^{3-d})^2+z^2} \\ &\simeq -zV_{0,d}(\mathbf{q})\frac{\kappa_d^{d-1}\mathcal{D}q^{3-d}}{(\kappa_d^{d-1}\mathcal{D}q^{3-d})^2+z^2}. \end{aligned} \tag{J.12}$$

Finally, we note that

$$\widetilde{C}^R(\mathbf{q},z) = \frac{1}{2\pi N(0)\tau_0^2}\frac{1}{\mathcal{D}q^2-iz+\tau_\phi^{-1}}. \tag{J.13}$$

J.1.1 Two Dimensions

Let us now consider $d=2$ and substitute eq. J.12 and eq. J.13 into eq. J.9,

$$\frac{1}{\tau_{\phi,ee}} = 4e^2\mathcal{D}\kappa_2\sum_{\mathbf{q}}\int_{-\infty}^{+\infty}\frac{dz}{\sinh(\beta z)}\frac{1}{\mathcal{D}q^2-iz+\tau_\phi^{-1}}\frac{z}{\mathcal{D}^2\kappa_2^2q^2+z^2}. \tag{J.14}$$

We now replace the $\mathbf{q}$ sum by an integral,

$$\frac{1}{\tau_{\phi,ee}} = \frac{2e^2\mathcal{D}\kappa_2}{\pi}\int_{-\infty}^{+\infty}dz\frac{z}{\sinh(\beta z)}\int_0^\infty dq\,q\,\frac{1}{\mathcal{D}q^2-iz+\tau_\phi^{-1}}\frac{1}{\mathcal{D}^2\kappa_2^2q^2+z^2}. \tag{J.15}$$

We shall focus on performing the q integral first,

$$I(z) = \int_0^\infty dq\,q\,\frac{1}{q^2+a}\frac{1}{q^2+b^2}, \tag{J.16a}$$

where

$$a = \frac{\tau_\phi^{-1}-iz}{\mathcal{D}}, \qquad b = \frac{z}{\mathcal{D}\kappa_2}, \tag{J.16b}$$

and

$$\frac{1}{\tau_{\phi,ee}} = \frac{2e^2}{\pi\mathcal{D}^2\kappa_2}\int_{-\infty}^{+\infty}dz\frac{z}{\sinh(\beta z)}I(z). \tag{J.17}$$

We evaluate eq. J.16a as follows,

$$I(z) = \int_0^\infty dq\, q \left[\frac{1}{q^2+a} - \frac{1}{q^2+b^2}\right]\frac{1}{b^2-a} = \frac{1}{b^2-a}\left[\ln\left(\frac{q^2+a}{q^2+b^2}\right)\right]_0^\infty = \frac{1}{b^2-a}\ln\left(\frac{b^2}{a}\right). \quad \text{(J.18)}$$

Next, by appreciating that we will only be interested in small values of z (which have the most singular contributions to the z integral), we may write

$$b^2 - a = \frac{z^2}{\mathcal{D}^2\kappa_2^2} + \frac{iz}{\mathcal{D}} - \frac{\tau_\phi^{-1}}{\mathcal{D}} \simeq \frac{iz - \tau_\phi^{-1}}{\mathcal{D}}. \quad \text{(J.19)}$$

Therefore, upon substituting eq. J.19 into eq. J.18, and the result of this into eq. J.17, we find that

$$\begin{aligned}\frac{1}{\tau_{\phi,ee}} &= \frac{e^2}{\pi\mathcal{D}\kappa_2}\int_{-\infty}^{+\infty}\frac{dz}{\sinh(\beta z)}\frac{z}{\tau_\phi^{-1}-iz}\ln\left(\frac{\mathcal{D}\kappa_2^2(\tau_\phi^{-1}-iz)}{z^2}\right) \\ &= \frac{2e^2}{\pi\mathcal{D}\kappa_2}\int_0^{+\infty} dz\frac{z}{\sinh(\beta z)}\mathrm{Re}\left[\frac{1}{\tau_\phi^{-1}-iz}\ln\left(\frac{\mathcal{D}\kappa_2^2(\tau_\phi^{-1}-iz)}{z^2}\right)\right],\end{aligned} \quad \text{(J.20)}$$

where, in writing the second line, we appreciated that the integrand of the first line had the property $g(-z) = g(z)^*$.[2] We again make use of the fact that only values of $z \ll T$ contribute significantly to the integral, so $\sinh(\beta z) \simeq \beta z$. Consequently, eq. J.20 can be approximated as

$$\frac{1}{\tau_{\phi,ee}} = \frac{2e^2T}{\pi\mathcal{D}\kappa_2}\int_0^T dz\mathrm{Re}\left[\frac{1}{\tau_\phi^{-1}-iz}\ln\left(\frac{\mathcal{D}\kappa_2^2(\tau_\phi^{-1}-iz)}{z^2}\right)\right]. \quad \text{(J.21)}$$

By letting $z \to z\tau_\phi^{-1}$, this expression becomes

$$\begin{aligned}\frac{1}{\tau_{\phi,ee}} &= \frac{2e^2T}{\pi\mathcal{D}\kappa_2}\mathrm{Re}\left[\int_0^{\tau_\phi T} dz\frac{1+iz}{1+z^2}\ln\left(\frac{\mathcal{D}\kappa_2^2\tau_\phi(1-iz)}{z^2}\right)\right] \\ &= \frac{2e^2T}{\pi\mathcal{D}\kappa_2}\mathrm{Re}\left[\int_0^{\tau_\phi T} dz\frac{1+iz}{1+z^2}\left(\ln\left(\mathcal{D}\kappa_2^2\tau_\phi\right) + \ln(1-iz) - 2\ln z\right)\right] \\ &= \frac{2e^2T}{\pi\mathcal{D}\kappa_2}(I_1 - 2I_2 + \mathrm{Re}\,[I_3]),\end{aligned} \quad \text{(J.22)}$$

[2]Here $g(z)$ is some generic function.

where

$$I_1 = \int_0^{\tau_\phi T} dz\, \frac{\ln\left(\mathcal{D}\kappa_2^2\tau_\phi\right)}{1+z^2}, \quad I_2 = \int_0^{\tau_\phi T} dz\, \frac{\ln z}{1+z^2}, \quad I_3 = \int_0^{\tau_\phi T} dz\, \frac{\ln(1-iz)}{1-iz}. \tag{J.23}$$

Simplifying eq. J.22 comes down to our ability to evaluate I_1, I_2, and I_3. Since we expect $\tau_\phi^{-1} \ll T$, we may set the $T\tau_\phi \to \infty$ in the upper limits of I_1 and I_2, as their integrands converge sufficiently fast for $z \to \infty$. This is not the case for I_3, however.

The first integral, I_1, is trivial to evaluate, and yields

$$I_1 = \frac{\pi}{2} \ln\left(\mathcal{D}\kappa_2^2\tau_\phi\right). \tag{J.24}$$

We tackle I_2 as follows,

$$\begin{aligned} I_2 &= \int_0^\infty dz \frac{\ln z}{1+z^2} \\ &= \int_0^1 dz \frac{\ln z}{1+z^2} + \int_1^\infty dz \frac{\ln z}{1+z^2} \\ &= \int_0^1 dz \frac{\ln z}{1+z^2} - \int_1^0 \frac{dz}{z^2} \frac{\ln(z^{-1})}{1+z^{-2}}, \end{aligned} \tag{J.25}$$

where we let $z \to z^{-1}$ in the second integral to obtain the final line. Clearly this integral vanishes, $I_2 = 0$.

Finally, we compute I_3,

$$\begin{aligned} I_3 &= \int_0^{\tau_\phi T} dz \frac{1}{1-iz} \ln(1-iz) \\ &= \left[\frac{i}{2}\Big(\ln\left(1-iz\right)\Big)^2\right]_0^{T\tau_\phi} \\ &= \frac{i}{2}\Big[\ln\left(1-iT\tau_\phi\right)\Big]^2. \end{aligned} \tag{J.26}$$

To take the real part of this, we note that

$$\ln(x+iy) = \frac{1}{2}\ln(x^2+y^2) + i\arctan\left(\frac{y}{x}\right), \tag{J.27}$$

which gives

$$\mathrm{Re}\,[I_3] = \frac{1}{2}\ln(1+T^2\tau_\phi^2)\arctan(T\tau_\phi). \tag{J.28}$$

Recalling our expectation that $1 \ll T\tau_\phi$, eq. J.28 becomes

$$\mathrm{Re}\,[I_3] = \frac{\pi}{2}\ln(1+T\tau_\phi). \tag{J.29}$$

Substituting our results for I_1, I_2, and I_3 into eq. J.22, we find

$$\frac{1}{\tau_{\phi,ee}} = \frac{e^2T}{\mathcal{D}\kappa_2}\ln(\mathcal{D}\kappa_2^2T\tau_\phi^2). \tag{J.30}$$

Recalling that $\kappa_2 = 4\pi N(0)e^2 = 2me^2$, we recover the self-consistent result quoted in eq. 3.185.

J.1.2 Three Dimensions

Again we substitute eq. J.12 and eq. J.13 into eq. J.9, replace the $\mathbf{q}$ sum by a 3D integral, and apply the fact that only $z \ll T$ contributions are important, to produce

$$\begin{aligned}\frac{1}{\tau_{\phi,ee}} &= \frac{4\mathcal{D}\kappa_3^2e^2}{\pi^2}T\int_{-T}^{+T}\frac{dz}{\mathcal{D}^2\kappa_3^4+z^2}\int_0^\infty dq\frac{1}{\mathcal{D}q^2-iz+\tau_\phi^{-1}}\\ &= \frac{2\sqrt{\mathcal{D}}\kappa_3^2e^2}{\pi}T\int_{-T}^{+T}\frac{dz}{\mathcal{D}^2\kappa_3^4+z^2}\frac{1}{\sqrt{\tau_\phi^{-1}-iz}}\\ &= \frac{4\sqrt{\mathcal{D}}\kappa_3^2e^2}{\pi}T\int_0^{T}\frac{dz}{\mathcal{D}^2\kappa_3^4+z^2}\mathrm{Re}\left[\frac{1}{\sqrt{\tau_\phi^{-1}-iz}}\right].\end{aligned} \tag{J.31}$$

In obtaining the final line, we used the same trick that we used for the 2D case in eq. J.20. Next, we appreciate that $\mathcal{D}\kappa_3^2 \gg T$, and so $\mathcal{D}\kappa_3^2 \gg z$, so we may approximate eq. J.31 as

$$\frac{1}{\tau_{\phi,ee}} = \frac{4e^2}{\pi\mathcal{D}^{3/2}\kappa_3^2}T\int_0^T dz\mathrm{Re}\left[\frac{1}{\sqrt{\tau_\phi^{-1}-iz}}\right] \tag{J.32}$$

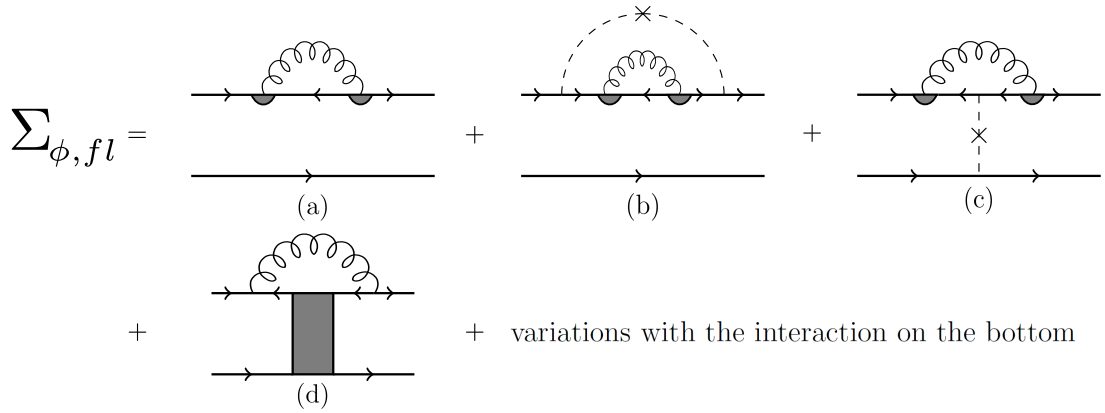

Figure J.2: Diagrams describing the phase coherence corrections to the cooperon in homogeneous systems due to superconducting fluctuations.

Letting $z \to \tau_\phi^{-1} z$,

$$\begin{aligned}\frac{1}{\tau_{\phi,ee}} &= \frac{4e^2\tau_\phi^{-1/2}}{\pi\mathcal{D}^{3/2}\kappa_3^2} T \,\mathrm{Re}\left[\int_0^{T\tau_\phi} dz \frac{1}{\sqrt{1-iz}}\right] \\ &= \frac{4e^2\tau_\phi^{-1/2}}{\pi\mathcal{D}^{3/2}\kappa_3^2} T \,\mathrm{Re}\left[2i(\sqrt{1-iT\tau_\phi}-1)\right] \\ &= -\frac{8e^2\tau_\phi^{-1/2}}{\pi\mathcal{D}^{3/2}\kappa_3^2} T \,\mathrm{Im}\left[\sqrt{1-iT\tau_\phi}\right].\end{aligned} \tag{J.33}$$

In taking the imaginary part of this complex square root, we must take the negative sign choice since $\tau_{\phi,ee}^{-1}$ must be positive,

$$\mathrm{Im}\left[\sqrt{1-iT\tau_\phi}\right] = -\sqrt{\frac{-1+\sqrt{1+T^2\tau_\phi^2}}{2}} \simeq \sqrt{T\tau_\phi}. \tag{J.34}$$

Substituting eq. J.34 into eq. J.33 gives

$$\frac{1}{\tau_{\phi,ee}} = -\frac{8e^2}{\pi\mathcal{D}^{3/2}\kappa_3^2} T^{3/2}. \tag{J.35}$$

Recalling that

$$\kappa_3^2 = 8\pi N(0)e^2, \qquad N(0) = \frac{1}{\pi^2}\sqrt{\frac{m_e^3}{2}\varepsilon_F}, \tag{J.36}$$

we arrive at the answer we gave in eq. 3.188.

J.2 Superconducting Fluctuations Contribution

The diagrams describing the superconducting fluctuation contribution to the phase breaking rate are shown in fig. J.2. The expressions corresponding to diagrams A, B, and C respectively are,

$$\Sigma^{(A)}_{\phi,fl} = -T\sum_{\mathbf{k},\mathbf{q}}\sum_{\omega}\Big[L(\mathbf{q},i\omega)C(\mathbf{q},i\varepsilon+i\Omega,i\omega-i\varepsilon-i\Omega)^2G(\mathbf{k},i\varepsilon+i\Omega)^2 \times G(\mathbf{q}-\mathbf{k},i\omega-i\varepsilon-i\Omega)G(\mathbf{k},i\varepsilon)\Big], \tag{J.37a}$$

$$\Sigma^{(B)}_{\phi,efl} = -T\sum_{\mathbf{k},\mathbf{k}',\mathbf{q}}\sum_{\omega}\left[\frac{L(\mathbf{q},i\omega)}{2\pi N(0)\tau_0}C(\mathbf{q},i\varepsilon+i\Omega,i\omega-i\varepsilon-i\Omega)^2G(\mathbf{k},i\varepsilon+i\Omega)^2 \times G(\mathbf{k},i\varepsilon)G(\mathbf{k}',i\varepsilon+i\Omega)^2G(\mathbf{q}-\mathbf{k}',i\omega-i\varepsilon-i\Omega)\right], \tag{J.37b}$$

$$\Sigma^{(C)}_{\phi,fl} = -T\sum_{\mathbf{q}}\sum_{\omega}\left[\frac{L(\mathbf{q},i\omega)}{2\pi N(0)\tau_0}C(\mathbf{q},i\varepsilon+i\Omega,i\omega-i\varepsilon-i\Omega)^2 \times\left(\sum_{\mathbf{k}}G(\mathbf{k},i\varepsilon+i\Omega)G(\mathbf{q}-\mathbf{k},i\omega-i\varepsilon-i\Omega)G(\mathbf{k},i\varepsilon)\right)^2\right], \tag{J.37c}$$

Again, we consider the case where $\varepsilon+\Omega>0$ and $\varepsilon<0$ without loss of generality, and so the cooperons in these diagrams enforce that $\omega>\varepsilon+\Omega$. As before, we expand these Green's function in powers of ω and $\mathbf{q}$, keeping only terms up to first order in ω and second order in $\mathbf{q}$. This yields

$$\Sigma^{(A)}_{\phi,fl} = -T\sum_{\mathbf{k},\mathbf{q}}\sum_{\omega>\varepsilon+\Omega}\Big\{L(\mathbf{q},i\omega)C(\mathbf{q},i\omega-2i\varepsilon-2i\Omega)^2G^+(\mathbf{k})^2G^-(\mathbf{k}) \times\Big[G^-(\mathbf{k})-i\omega G^-(\mathbf{k})^2+(\mathbf{v}_F\cdot\mathbf{q})^2G^-(\mathbf{k})^3\Big]\Big\}, \tag{J.38a}$$

$$\Sigma^{(B)}_{\phi,fl} = -T\sum_{\mathbf{k},\mathbf{k}',\mathbf{q}}\sum_{\omega>\varepsilon+\Omega}\left\{\frac{L(\mathbf{q},i\omega)}{2\pi N(0)\tau_0}C(\mathbf{q},i\omega-2i\varepsilon-2i\Omega)^2G^+(\mathbf{k})^2G^-(\mathbf{k})G^+(\mathbf{k}')^2 \times\Big[G^-(\mathbf{k}')-i\omega G^-(\mathbf{k}')^2+(\mathbf{v}'_F\cdot\mathbf{q})^2G^-(\mathbf{k}')^3\Big]\right\}, \tag{J.38b}$$

$$\Sigma^{(C)}_{\phi,fl} = -T\sum_{\mathbf{q}}\sum_{\omega>\varepsilon+\Omega}\left\{\frac{L(\mathbf{q},i\omega)}{2\pi N(0)\tau_0}C(\mathbf{q},i\omega-2i\varepsilon-2i\Omega)^2 \times\left(\sum_{\mathbf{k}}G^+(\mathbf{k})G^-(\mathbf{k})\Big[G^-(\mathbf{k})-i\omega G^-(\mathbf{k})^2+(\mathbf{v}_F\cdot\mathbf{q})^2G^-(\mathbf{k})^3\Big]\right)^2\right\}. \tag{J.38c}$$

By evaluating the fast momentum sums using eq. 3.75, we find

$$\Sigma^{(A)}_{\phi,fl} = -2\pi N(0)\tau_0^3 T \sum_{\mathbf{k},\mathbf{q}} \sum_{\omega>\varepsilon+\Omega} \Big[L(\mathbf{q}, i\omega) C(\mathbf{q}, i\omega - 2i\varepsilon - 2i\Omega)^2 \times (2 + 3\omega\tau_0 - 4\mathcal{D}q^2\tau_0) \Big], \tag{J.39a}$$

$$\Sigma^{(B)}_{\phi,fl} = -2\pi N(0)\tau_0^3 T \sum_{\mathbf{k},\mathbf{k}',\mathbf{q}} \sum_{\omega>\varepsilon+\Omega} \Big[L(\mathbf{q}, i\omega - 2i\varepsilon - 2i\Omega) C(\mathbf{q}, i\omega)^2 \times (-1 - 2\omega\tau_0 + 3\mathcal{D}q^2\tau_0) \Big], \tag{J.39b}$$

$$\Sigma^{(C)}_{\phi,fl} = -2\pi N(0)\tau_0^3 T \sum_{\mathbf{q}} \sum_{\omega>\varepsilon+\Omega} \Big[L(\mathbf{q}, i\omega) C(\mathbf{q}, i\omega - 2i\varepsilon - 2i\Omega)^2 \times (-1 - 2\omega\tau_0 + 2\mathcal{D}q^2\tau_0) \Big], \tag{J.39c}$$

and hence

$$\begin{aligned} \Sigma^{(ABC)}_{\phi,fl} &= -2\pi N(0)\tau_0^4 T \sum_{\mathbf{q}} \sum_{\omega>\varepsilon+\Omega} L(\mathbf{q}, i\omega) C(\mathbf{q}, i\omega - 2i\varepsilon - 2i\Omega)^2 (\mathcal{D}q^2 - \omega) \\ &= -(2\pi N(0)\tau_0^2)^3 T \sum_{\mathbf{q}} \sum_{\omega>\varepsilon+\Omega} L(\mathbf{q}, i\omega) \widetilde{C}(\mathbf{q}, i\omega - 2i\varepsilon - 2i\Omega)^2 (\mathcal{D}q^2 - \omega). \end{aligned} \tag{J.40}$$

If we consider the variations of diagrams A, B, and C with the pair propagator on the bottom electron Green's function, we find the same expression as above, but with the sum taken over $\omega < -\varepsilon$, and $C(\mathbf{q}, i\omega + 2i\varepsilon)$ in place of $C(\mathbf{q}, i\omega - 2i\varepsilon - 2i\Omega)$. Therefore, eq. J.40, and its variant, give the first and second lines of eq. 3.190 respectively.

Diagram D can be written as,

$$\begin{aligned} \Sigma^{(D)}_{\phi,fl} &= -T \sum_{\mathbf{q}} \sum_{\omega} \widetilde{D}(\mathbf{q}, i\varepsilon + i\Omega + i\omega, i\varepsilon) L(\mathbf{q}, i\omega) \\ &\qquad \times \left(\sum_{\mathbf{k}} G(\mathbf{k}, i\varepsilon + i\Omega) G(\mathbf{q} - \mathbf{k}, i\omega - i\varepsilon - \Omega) G(\mathbf{k}, i\varepsilon) \right)^2 \\ &\simeq -T \sum_{\mathbf{q}} \sum_{\omega>\varepsilon+\Omega} \widetilde{D}(\mathbf{q}, i\omega - 2i\varepsilon - i\Omega) L(\mathbf{q}, i\omega) \left(\sum_{\mathbf{k}} G^+(\mathbf{k}) G^-(\mathbf{k})^2 \right)^2 . \end{aligned} \tag{J.41}$$

Evaluating the fast momentum sum yields,

$$\Sigma^{(D)}_{\phi,fl} = T(2\pi N(0)\tau_0^2)^2 \sum_{\mathbf{q}} \sum_{\omega>\varepsilon+\Omega} \widetilde{D}(\mathbf{q}, i\omega - 2i\varepsilon - i\Omega) L(\mathbf{q}, i\omega). \tag{J.42}$$

The variant of diagram D with the pair propagator on the bottom Green's function, is found using the same approach. This variant is given by eq. J.42 with the Matsubara sum taken over $\omega > -\varepsilon$, and $\widetilde{D}(\mathbf{q}, i\omega - 2i\varepsilon - i\Omega)$ replaced by $\widetilde{D}(\mathbf{q}, i\omega + 2i\varepsilon + i\Omega)$. Hence, eq. J.42, and its variant, give the third and fourth lines of eq. 3.190 respectively.

The details regarding the analytic continuation of the ω sum are discussed in section 3.6.2, and so we do not provide these details here. Instead, we turn our attention to evaluating the result of analytic continuation in eq. 3.192. Substituting eq. 3.194 for the retarded pair propagator in to eq. 3.192, we see

$$\frac{1}{\tau_{\phi,fl}} = 64N(0)\tau_0^4 T^2 \sum_{\mathbf{q}} \int_{-T}^{+T} dz \, \frac{1}{(\mathcal{D}q^2 + \tau_{GL}^{-1})^2 + z^2} \, (\mathcal{D}q^2 + iz) \, \widetilde{C}^A(\mathbf{q}, z)^2. \tag{J.43}$$

Noting that $\widetilde{C}^A(\mathbf{q}, z) = \widetilde{C}^R(\mathbf{q}, z)^*$, we write

$$\begin{aligned} \frac{1}{\tau_{\phi,fl}} &= \frac{16}{\pi^2 N(0)} T^2 \sum_{\mathbf{q}} \int_{-T}^{+T} dz \, \frac{1}{(\mathcal{D}q^2 + \tau_{GL}^{-1})^2 + z^2} \, \frac{\mathcal{D}q^2 + iz}{(\mathcal{D}q^2 + \tau_\phi^{-1} + iz)^2} \\ &\simeq \frac{32}{\pi^2 N(0)} T^2 \sum_{\mathbf{q}} \int_{0}^{T} dz \, \frac{1}{(\mathcal{D}q^2 + \tau_{GL}^{-1})^2 + z^2} \, \mathrm{Re}\left[\frac{\mathcal{D}q^2 + iz}{(\mathcal{D}q^2 + \tau_\phi^{-1} + iz)^2} \right]. \end{aligned} \tag{J.44}$$

Letting $z \to \tau_\phi^{-1} z$,

$$\begin{aligned} \frac{1}{\tau_{\phi,fl}} &= \frac{32(T\tau_\phi)^2}{\pi^2 N(0)} \sum_{\mathbf{q}} \int_0^\infty dz \, \frac{1}{(\tau_\phi \mathcal{D}q^2 + \tau_\phi \tau_{GL}^{-1})^2 + z^2} \, \mathrm{Re}\left[\frac{\tau_\phi \mathcal{D}q^2 + iz}{(\tau_\phi \mathcal{D}q^2 + 1 + iz)^2} \right] \\ &= \frac{32(T\tau_\phi)^2}{\pi^2 N(0)} \\ &\quad \times \sum_{\mathbf{q}} \int_0^\infty dz \, \frac{1}{(\tau_\phi \mathcal{D}q^2 + \tau_\phi \tau_{GL}^{-1})^2 + z^2} \, \frac{\tau_\phi \mathcal{D}q^2 (\tau_\phi \mathcal{D}q^2 + 1)^2 + z^2(\tau_\phi \mathcal{D}q^2 + 2)}{[(\tau_\phi \mathcal{D}q^2 + 1)^2 + z^2]^2} \end{aligned} \tag{J.45}$$

where we let the upper limit $T\tau_\phi \to \infty$, as we expect $T\tau_\phi \gg 1$.

To evaluate eq. J.45, we define the following integrals,

$$\widetilde{I}(a,b) = \int_0^\infty dz \frac{1}{(a^2+z^2)(b^2+z^2)}, \tag{J.46a}$$

$$I(a,b) = -\frac{\partial \widetilde{I}}{\partial(a^2)} = -\frac{1}{2a}\frac{\partial \widetilde{I}}{\partial a} = \int_0^\infty dz \frac{1}{(a^2+z^2)^2(b^2+z^2)}, \tag{J.46b}$$

$$\widetilde{J}(a,b) = \int_0^\infty dz \frac{z^2}{(a^2+z^2)(b^2+z^2)}, \tag{J.46c}$$

$$J(a,b) = -\frac{\partial \widetilde{J}}{\partial(a^2)} = -\frac{1}{2a}\frac{\partial \widetilde{J}}{\partial a} = \int_0^\infty dz \frac{z^2}{(a^2+z^2)^2(b^2+z^2)}, \tag{J.46d}$$

which allow us to write

$$\begin{aligned}\frac{1}{\tau_{\phi,fl}} = \frac{32(T\tau_\phi)^2}{\pi^2 N(0)} \sum_{\mathbf{q}} \Big[& \tau_\phi \mathcal{D} q^2 (\tau_\phi \mathcal{D} q^2 + 1)^2 \; I(\tau_\phi \mathcal{D} q^2 + 1, \tau_\phi \mathcal{D} q^2 + \tau_\phi \tau_{GL}^{-1}) \\ & + (\tau_\phi \mathcal{D} q^2 + 2) \; J(\tau_\phi \mathcal{D} q^2 + 1, \tau_\phi \mathcal{D} q^2 + \tau_\phi \tau_{GL}^{-1}) \Big].\end{aligned} \tag{J.47}$$

The only integrals we are now required to evaluate directly, are those in eq. J.46a and eq. J.46c. Below we show how these are calculated,

$$\begin{aligned}\widetilde{I}(a,b) &= \frac{1}{b^2-a^2}\int_0^\infty dz \left[\frac{1}{a^2+z^2} - \frac{1}{b^2+z^2}\right] \\ &= \frac{1}{b^2-a^2}\left[\frac{1}{a}\arctan\left(\frac{z}{a}\right) - \frac{1}{b}\arctan\left(\frac{z}{b}\right)\right]_0^\infty \\ &= \frac{\pi}{2}\frac{1}{b^2-a^2}\left(\frac{1}{a}-\frac{1}{b}\right) = \frac{\pi}{2}\frac{1}{ab(a+b)},\end{aligned} \tag{J.48}$$

and

$$\begin{aligned}\widetilde{J}(a,b) &= \frac{1}{b^2-a^2}\int_0^\infty dz \left[\frac{z^2}{a^2+z^2} - \frac{z^2}{b^2+z^2}\right] \\ &= \frac{1}{b^2-a^2}\int_0^\infty dz \left[\frac{b^2}{b^2+z^2} - \frac{a^2}{a^2+z^2}\right] \\ &= \frac{1}{b^2-a^2}\left[b\arctan\left(\frac{z}{b}\right) - a\arctan\left(\frac{z}{a}\right)\right]_0^\infty \\ &= \frac{\pi}{2}\frac{b-a}{b^2-a^2} = \frac{\pi}{2}\frac{1}{a+b}.\end{aligned} \tag{J.49}$$

Hence, substituting eq. J.48 and eq. J.49 into eq. J.46b and eq. J.46d, we find

$$I(a,b) = \frac{\pi}{4}\frac{b+2a}{a^3 b(a+b)^2}, \tag{J.50a}$$

$$J(a,b) = \frac{\pi}{4}\frac{1}{a(a+b)^2}. \tag{J.50b}$$

To simplify the expression,

$$\begin{aligned}\tau_\phi \mathcal{D}q^2(\tau_\phi \mathcal{D}q^2+1)^2\, I(\tau_\phi \mathcal{D}q^2+1, \tau_\phi \mathcal{D}q^2+\tau_\phi\tau_{GL}^{-1}) \\ + (\tau_\phi \mathcal{D}q^2+2)\, J(\tau_\phi \mathcal{D}q^2+1, \tau_\phi \mathcal{D}q^2+\tau_\phi\tau_{GL}^{-1})\end{aligned} \tag{J.51}$$

appearing in eq. J.47, we let $x = \tau_\phi\tau_{GL}^{-1}$ and $y = \tau_\phi \mathcal{D}q^2$. Using these variables, we substitute eq. J.50a and eq. J.50b into eq. J.51 to get

$$\begin{aligned}&\frac{\pi}{4}\left[\frac{y(y+1)^2(3y+2+x)}{(y+1)^3(y+x)(2y+1+x)^2} + \frac{y+2}{(y+1)(2y+1+x)^2}\right] \\ &\qquad = \frac{\pi}{4}\frac{1}{(2y+1+x)^2}\left[\frac{2y}{y+x} + \frac{y}{y+1} + \frac{1}{y+1} + 1\right] \\ &\qquad = \frac{\pi}{2}\frac{1}{(2y+1+x)^2}\left[\frac{y}{y+x} + 1\right].\end{aligned} \tag{J.52}$$

Finally, by substituting eq. J.52, with the definitions for x and y, into eq. J.47, we arrive at

$$\frac{1}{\tau_{\phi,fl}} = \frac{16T^2}{\pi N(0)}\sum_{\mathbf{q}}\left[1 + \frac{\mathcal{D}q^2}{\mathcal{D}q^2+\tau_{GL}^{-1}}\right]\frac{1}{(\tau_\phi^{-1}+\tau_{GL}^{-1}+2\mathcal{D}q^2)^2}, \tag{J.53}$$

which is exactly what we gave in the main body of the thesis, see eq. 3.195.

J.2.1 Two Dimensional Systems

In 2D systems, eq. J.53 becomes

$$\frac{1}{\tau_{\phi,fl}} = \frac{8T^2}{\pi^2 N(0)}\int_0^\infty dq\, q\left[1 + \frac{\mathcal{D}q^2}{\mathcal{D}q^2+\tau_{GL}^{-1}}\right]\frac{1}{(\tau_\phi^{-1}+\tau_{GL}^{-1}+2\mathcal{D}q^2)^2}. \tag{J.54}$$

By making the substitution $x = \mathcal{D}q^2$, this simplifies to

$$\frac{1}{\tau_{\phi,fl}} = \frac{4T^2}{\pi^2 N(0)\mathcal{D}} \int_0^\infty dx \left[1 + \frac{x}{x + \tau_{GL}^{-1}}\right] \frac{1}{(\tau_\phi^{-1} + \tau_{GL}^{-1} + 2x)^2}. \tag{J.55}$$

The first term of the integral is solved trivially,

$$\int_0^\infty dx \frac{1}{(\tau_\phi^{-1} + \tau_{GL}^{-1} + 2x)^2} = \frac{1}{2} \frac{1}{\tau_\phi^{-1} + \tau_{GL}^{-1}}, \tag{J.56}$$

whilst the second term can be handled by considering an integral of the form

$$I(a,b) = \int_0^\infty dx \frac{x}{(x+a)(2x+b)^2}. \tag{J.57}$$

Using partial fractions on the integrand of $I(a,b)$, we find

$$\begin{aligned} I(a,b) &= \int_0^\infty dx \left[\frac{a}{(2a-b)^2}\left(\frac{2}{2x+b} - \frac{1}{x+a}\right) - \frac{b}{2a-b}\frac{1}{(2x+b)^2}\right] \\ &= \frac{a}{(2a-b)^2} \ln\left(\frac{2a}{b}\right) - \frac{1}{2}\frac{1}{2a-b} \end{aligned} \tag{J.58}$$

Therefore, using the results in eq. J.56 and eq. J.58, with $a = \tau_{GL}^{-1}$ and $b = \tau_{GL}^{-1} + \tau_\phi^{-1}$, in eq. J.55, we obtain

$$\frac{1}{\tau_{\phi,fl}} = \frac{4T^2\tau_\phi}{\pi^2 N(0)\mathcal{D}} \left[\frac{\tau_\phi \tau_{GL}}{(\tau_\phi - \tau_{GL})^2} \ln\left(\frac{2\tau_\phi}{\tau_\phi + \tau_{GL}}\right) + \frac{\tau_{GL}^2}{\tau_{GL}^2 - \tau_\phi^2}\right]. \tag{J.59}$$

By recalling that $N(0) = m_e/(2\pi)$ and $\mathcal{D} = v_F\tau_0/2$, we arrive at the result given in eq. 3.196.

J.2.2 Three Dimensional Systems

In 3D systems, eq. J.53 becomes

$$\frac{1}{\tau_{\phi,fl}} = \frac{8T^2}{\pi^3 N(0)} \int_0^\infty dq\, q^2 \left[1 + \frac{\mathcal{D}q^2}{\mathcal{D}q^2 + \tau_{GL}^{-1}}\right] \frac{1}{(\tau_\phi^{-1} + \tau_{GL}^{-1} + 2\mathcal{D}q^2)^2}. \tag{J.60}$$

which we simplify by making the substitution $x = \sqrt{\mathcal{D}}q$,

$$\frac{1}{\tau_{\phi,fl}} = \frac{8T^2}{\pi^3 N(0)\mathcal{D}^{3/2}} \int_0^\infty dx\, x^2 \left[2 - \frac{\tau_{GL}^{-1}}{x^2 + \tau_{GL}^{-1}}\right] \frac{1}{(\tau_\phi^{-1} + \tau_{GL}^{-1} + 2x^2)^2}. \tag{J.61}$$

We first focus on the first term of eq. J.61,

$$\int_0^\infty dx \frac{2x^2}{(\tau_\phi^{-1} + \tau_{GL}^{-1} + 2x^2)^2} = \int_0^\infty dx \left[\frac{1}{\tau_\phi^{-1} + \tau_{GL}^{-1} + 2x^2} - \frac{\tau_\phi^{-1} + \tau_{GL}^{-1}}{(\tau_\phi^{-1} + \tau_{GL}^{-1} + 2x^2)^2}\right]. \tag{J.62}$$

To evaluate this integral, we note that the second term of its integrand is related to its first term by simple differentiation,

$$\int_0^\infty dx \frac{\tau_\phi^{-1} + \tau_{GL}^{-1}}{(\tau_\phi^{-1} + \tau_{GL}^{-1} + 2x^2)^2} = -(\tau_\phi^{-1} + \tau_{GL}^{-1}) \frac{d}{db} \left[\int_0^\infty dx \frac{1}{b + 2x^2}\right] \Bigg|_{b=\tau_\phi^{-1}+\tau_{GL}^{-1}}. \tag{J.63}$$

The integral inside the derivative, which is just the first term of eq. J.62's integrand, is trivial to compute, and so

$$\int_0^\infty dx \frac{1}{\tau_\phi^{-1} + \tau_{GL}^{-1} + 2x^2} = \frac{\pi}{2\sqrt{2}} \frac{1}{\sqrt{\tau_\phi^{-1} + \tau_{GL}^{-1}}}, \tag{J.64a}$$

$$\int_0^\infty dx \frac{\tau_\phi^{-1} + \tau_{GL}^{-1}}{(\tau_\phi^{-1} + \tau_{GL}^{-1} + 2x^2)^2} = \frac{\pi}{4\sqrt{2}} \frac{1}{\sqrt{\tau_\phi^{-1} + \tau_{GL}^{-1}}}. \tag{J.64b}$$

Thus, eq. J.62 becomes

$$\int_0^\infty dx \frac{2x^2}{(\tau_\phi^{-1} + \tau_{GL}^{-1} + 2x^2)^2} = \frac{\pi}{8} \sqrt{\frac{2}{\tau_\phi^{-1} + \tau_{GL}^{-1}}}. \tag{J.65}$$

Turning our attention towards the second term of eq. J.61, we note that

$$\int_0^\infty dx \frac{x^2}{(x^2 + \tau_{GL}^{-1})(\tau_\phi^{-1} + \tau_{GL}^{-1} + 2x^2)^2} = -\frac{\partial}{\partial b} J(a,b) \Big|_{\substack{a=\tau_{GL}^{-1} \\ b=\tau_\phi^{-1}+\tau_{GL}^{-1}}}, \tag{J.66}$$

where

$$J(a,b) = \int_0^\infty dx \frac{x^2}{(x^2+a)(2x^2+b)}. \tag{J.67}$$

Hence, our ability to evaluate the second term of eq. J.61 depends on our ability to perform the integral $J(a,b)$. We start by writing

$$\begin{aligned} J(a,b) &= \frac{1}{2}\int_0^\infty dx \left[\frac{1}{x^2+a} - \frac{b}{(x^2+a)(2x^2-b)}\right] \\ &= \frac{1}{2}\int_0^\infty dx \left[\frac{1}{x^2+a} - \frac{b}{b-2a}\left(\frac{1}{x^2+a} - \frac{2}{2x^2+b}\right)\right]. \end{aligned} \tag{J.68}$$

This integral is now straightforward to compute and yields,

$$J(a,b) = \frac{\pi}{4}\frac{2\sqrt{a}-\sqrt{2b}}{2a-b}. \tag{J.69}$$

Therefore, we find that

$$\int_0^\infty dx \frac{x^2}{(x^2+\tau_{GL}^{-1})(\tau_\phi^{-1}+\tau_{GL}^{-1}+2x^2)^2} = \frac{\pi}{8}\sqrt{\frac{2}{\tau_{GL}^{-1}+\tau_\phi^{-1}}}\left(\frac{\sqrt{2\tau_{GL}^{-1}}-\sqrt{\tau_{GL}^{-1}+\tau_\phi^{-1}}}{\tau_{GL}^{-1}-\tau_\phi^{-1}}\right)^2. \tag{J.70}$$

Finally, by substituting eq. J.65 and eq. J.70 into eq. J.61, we obtain

$$\frac{1}{\tau_{\phi,fl}} = \frac{T^2}{\pi^2 N(0)\mathcal{D}^{3/2}}\sqrt{\frac{2}{\tau_{GL}^{-1}+\tau_\phi^{-1}}}\left[1-\tau_{GL}^{-1}\left(\frac{\sqrt{2\tau_{GL}^{-1}}-\sqrt{\tau_{GL}^{-1}+\tau_\phi^{-1}}}{\tau_{GL}^{-1}-\tau_\phi^{-1}}\right)^2\right]. \tag{J.71}$$

Recalling that,

$$N(0) = \frac{1}{\pi^2}\sqrt{\frac{m_e^3}{2}\varepsilon_F}, \qquad \mathcal{D} = \frac{v_F^2\tau_0}{3}, \tag{J.72}$$

in 3D, we see that eq. J.70 is the same result we gave in eq. 3.199.

APPENDIX K

LATTICES AND PERIODIC BOUNDARY CONDITIONS

This appendix acts as background to the ideas we use when modelling granular materials, which we assume to form lattices with periodic boundary conditions. The ideas we present here are based upon Simon's book [4].

Consider a d-dimensional lattice with $\mathcal{N}$ sites, whose locations form the set $\{\mathbf{R}_i\}$, which is spanned by the set of primitive lattice vectors $\{\mathbf{a}_\alpha\}$. In this case, any site location can be written as

$$\mathbf{R}_i = \sum_{\alpha=1}^{d} n_{i,\alpha}\mathbf{a}_\alpha, \qquad n_{i,1}, n_{i,2}, ... \in \mathbb{Z}. \tag{K.1}$$

The corresponding reciprocal lattice's site locations form the set $\{\mathbf{G}_i\}$. The reciprocal lattice is spanned by the set of primitive reciprocal lattice vectors $\{\mathbf{b}_i\}$, and so any site on the reciprocal lattice can be expressed as

$$\mathbf{G}_i = \sum_{\alpha=1}^{d} m_{i,\alpha}\mathbf{b}_\alpha, \qquad m_{i,1}, m_{i,2}, ... \in \mathbb{Z}. \tag{K.2}$$

The spanning vectors, $\{\mathbf{a}_i\}$ and $\{\mathbf{b}_i\}$, are related by

$$\mathbf{a}_i \cdot \mathbf{b}_j = 2\pi\delta_{ij}. \tag{K.3}$$

With these definitions in mind, we may now tackle how to write a Fourier series expansion for a function subject to periodic boundary conditions.

We define our lattice to be periodic such that there are $\mathcal{N}_\alpha$ sites in the direction of $\mathbf{a}_\alpha$, before looping back round. As a result, any function existing inside the lattice that depends upon position must exhibit the same periodicity,

$$F(\mathbf{r} + \mathcal{N}_\alpha \mathbf{a}_\alpha) = F(\mathbf{r}), \qquad \alpha = 1, 2, ..., d. \tag{K.4}$$

We also note that the total number of sites is simply the product of the periodic lengths,

$$\mathcal{N} = \prod_{\alpha=1}^{d} \mathcal{N}_\alpha. \tag{K.5}$$

Now, let us expand the function $F(\mathbf{r})$ as a Fourier series with an arbitrary normalisation constant, A,

$$F(\mathbf{r}) = A \sum_{\mathbf{Q}\in\mathcal{V}_{\mathrm{B1}}} \widetilde{F}(\mathbf{Q}) e^{i\mathbf{Q}\cdot\mathbf{r}}, \qquad \widetilde{F}(\mathbf{Q}) = \int_{\mathcal{V}} d^d r F(\mathbf{r}) e^{-i\mathbf{Q}\cdot\mathbf{r}}, \tag{K.6}$$

where $\mathcal{V}$ is the volume of the lattice and $\mathcal{V}_{\mathrm{B1}}$ is the volume of the first Brillouin zone. In writing the momentum sum to only be over the modes within the first Brillouin zone, we have appreciated that all unique modes occur in this region of reciprocal space: modes outside this can be mapped back to the the first Brillouin zone by shifts using the reciprocal lattice vectors in eq. K.2.

For eq. K.6 to obey the periodic boundary conditions in eq. K.4, we must have

$$e^{i\mathcal{N}_\alpha \mathbf{Q}\cdot\mathbf{a}_\alpha} = 1. \tag{K.7}$$

By writing the lattice momentum, $\mathbf{Q}$, in terms of the primitive reciprocal lattice vectors,

$$\mathbf{Q} = \sum_{\alpha=1}^{d} c_\alpha \mathbf{b}_\alpha, \tag{K.8}$$

we see that the components are quantised according to

$$c_\alpha = \frac{l_\alpha}{\mathcal{N}_\alpha}, \qquad l_\alpha \in \mathbb{Z}, \qquad -\frac{\mathcal{N}_\alpha}{2} \leq l_\alpha < \frac{\mathcal{N}_\alpha}{2}. \tag{K.9}$$

The inequality above ensures that we do not double count momenta leading to the same physical mode: all unique components of $\mathbf{Q}$ lie within the first Brillouin zone. That is to say, the lattice is periodic on the length $|\mathbf{a}_\alpha|$ in the α direction.[1]

The volume associated to each mode is given by the appropriate formula for the volume of a d-dimensional parallelepiped, whose edges are described by the fundamental vectors composing $\mathbf{Q}$,

$$\mathcal{V}_Q = \mathcal{V}_d\left(\left\{\frac{\mathbf{b}_\alpha}{\mathcal{N}_\alpha}\right\}\right) = \mathcal{V}_d(\{\mathbf{b}_\alpha\}) \prod_{\alpha=1}^{d} \frac{1}{\mathcal{N}_\alpha}. \tag{K.10}$$

For $d = 1, 2$, and 3 this function is,

$$\mathcal{V}_d(\{\mathbf{b}_\alpha\}) = \begin{cases} \mathbf{b}_1 \cdot (\mathbf{b}_2 \times \mathbf{b}_3), & d = 3 \\ |\mathbf{b}_1 \times \mathbf{b}_2|, & d = 2 \\ |\mathbf{b}_1|, & d = 1. \end{cases} \tag{K.11}$$

However, the function $\mathcal{V}_d(\{\mathbf{b}_\alpha\})$ is just the volume of the first Brillouin zone, which, in conjunction with eq. K.5, yields

$$\mathcal{V}_Q = \frac{\mathcal{V}_{\mathrm{B1}}}{\mathcal{N}}. \tag{K.12}$$

Therefore, there are $\mathcal{N}$ momentum modes in the first Brillouin zone.

[1] It is worth noting that there are two levels of periodicity at play here. The first period we mentioned was the system's periodicity, where we loop the lattice back round onto itself in each direction. The second period we have just mentioned is that of the lattice, which is inherently smaller than the system's periodicity. The period of the lattice defines the first Brillouin zone in reciprocal space, and leads to a reciprocal lattice with period $2\pi/|\mathbf{a}_\alpha|$ in the direction of $\mathbf{b}_\alpha$. In contrast, the system's periodicity defines the modes within the first Brillouin zone, which are given by eq. K.8 and eq. K.9

To make use of this fact, we write eq. K.6 as

$$\begin{aligned} F(\mathbf{r}) &= A\int_{\mathcal{V}} d^d r' F(\mathbf{r}') \sum_{\mathbf{Q}\in\mathcal{V}_{\mathrm{B1}}} e^{i\mathbf{Q}\cdot(\mathbf{r}-\mathbf{r}')} \\ &= A\int_{\mathcal{V}} d^d r' F(\mathbf{r}')\, \mathcal{N}\, \delta^{(d)}(\mathbf{r}-\mathbf{r}'). \end{aligned} \tag{K.13}$$

Hence, we define $A = 1/\mathcal{N}$. If we instead chose to treat $\mathbf{Q}$ as continuous,[2] we would write eq. K.6 using an integral over $\mathbf{Q}$ instead of a sum,

$$F(\mathbf{r}) = A\int_{\mathcal{V}_{\mathrm{B1}}} d^d Q \widetilde{F}(\mathbf{Q}) e^{i\mathbf{Q}\cdot\mathbf{r}}, \qquad \widetilde{F}(\mathbf{Q}) = \int_{\mathcal{V}} d^d r F(\mathbf{r}) e^{-i\mathbf{Q}\cdot\mathbf{r}}. \tag{K.14}$$

Substituting $\widetilde{F}(\mathbf{Q})$ into $F(\mathbf{r})$ produces,

$$\begin{aligned} F(\mathbf{r}) &= A\int_{\mathcal{V}} d^d r' F(\mathbf{r}') \int_{\mathcal{V}_{\mathrm{B1}}} d^d Q e^{i\mathbf{Q}\cdot(\mathbf{r}-\mathbf{r}')} \\ &= A\int_{\mathcal{V}} d^d r' F(\mathbf{r}')\, \mathcal{V}_{\mathrm{B1}}\, \delta^{(d)}(\mathbf{r}-\mathbf{r}'), \end{aligned} \tag{K.15}$$

therefore meaning we must choose $A = 1/\mathcal{V}_{\mathrm{B1}}$ in this case.

So in general, we may write any function that is position dependent in the lattice in terms of a sum over $\mathbf{Q}$ when we have discrete quantised modes, or an integral over $\mathbf{Q}$ when the reciprocal space is continuous. This leads to the expressions,

$$F(\mathbf{r}) = \frac{1}{\mathcal{N}} \sum_{\mathbf{Q}\in\mathcal{V}_{\mathrm{B1}}} \widetilde{F}(\mathbf{Q}) e^{i\mathbf{Q}\cdot\mathbf{r}}, \qquad F(\mathbf{r}) = \frac{1}{\mathcal{V}_{\mathrm{B1}}} \int_{\mathcal{V}_{\mathrm{B1}}} d^d Q \widetilde{F}(\mathbf{Q}) e^{i\mathbf{Q}\cdot\mathbf{r}}. \tag{K.16}$$

For the granular systems we consider in the main body of this thesis, we assume the lattice is simple cubic with side length a. Therefore, the volume of the first Brillouin zone is trivially,

$$\mathcal{V}_{\mathrm{B1}} = \left(\frac{2\pi}{a}\right)^d. \tag{K.17}$$

[2] This is the same as letting $\mathcal{N}_\alpha \to \infty\, \forall\, \alpha$. Consequently, $\mathcal{V}$ becomes the volume over all space.

APPENDIX L

ANALYSIS OF RESISTANCE VERSUS TEMPERATURE DATA FOR VARIOUS BNCD FILMS

This appendix reproduces the data analysis of Klemencic et. al.'s experimental work in [28]. We use the same methods as those detailed in chapter 6, and consider films of thickness 564nm, 204nm, 168nm, 160nm, and 128nm, in addition to the 329nm film presented earlier. Table L.1 presents the values of T_c and a found for each film, as well as the range of possible values for Γ and E_{Th}.

Table L.1: Summary of the T_c and a values found to various BNCD films, and the range of values Γ and E_{Th} might take.

Thickness (nm)	T_c (K)	a (nm)	Γ ($\times 10^{-2}$K)	E_{Th} (K)
564	3.83	102	$2.6 < \Gamma < 7.2$	$0.9 < E_{Th} < 1.2$
339	3.81	102	$2.7 < \Gamma < 6.8$	$0.825 < E_{Th} < 1$
204	3.72	79.0	$3.4 < \Gamma < 6.3$	$0.8 < E_{Th} < 1$
168	3.61	71.9	$3.6 < \Gamma < 6.5$	$1 < E_{Th} < 1.2$
160	3.34	64.3	$3 < \Gamma < 6.7$	$0.9 < E_{Th} < 1.1$
128	2.83	56.9	$4 < \Gamma < 9.9$	$1.2 < E_{Th} < 1.5$

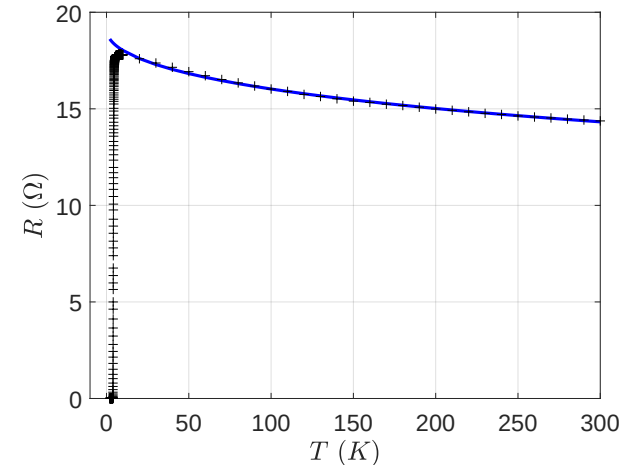

(a)

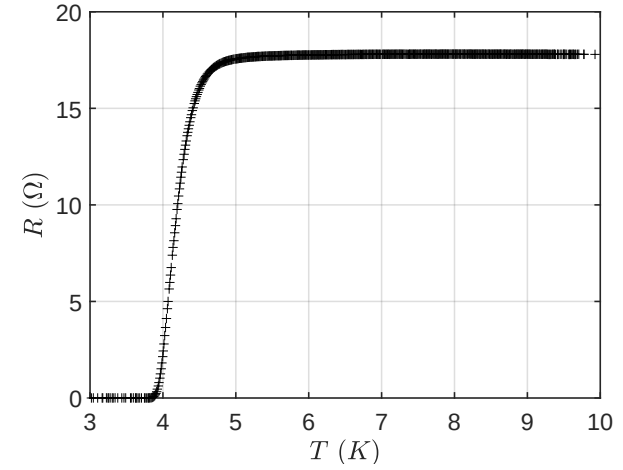

(b)

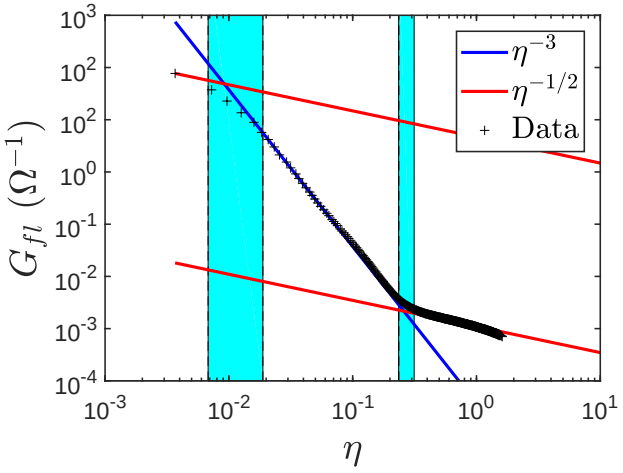

(c)

Figure L.1: The plots above show the fittings to Klemencic et. al.'s data [28] for a 564nm BNCD film. (a): EEI fitting to high temperature data. (b): focus on the superconducting transition. (c): Fitted fluctuation data, where the shaded regions indicate areas where the crossovers may exist.

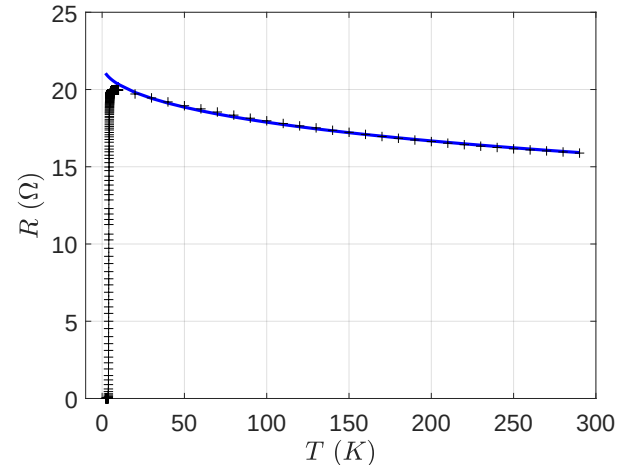

(a)

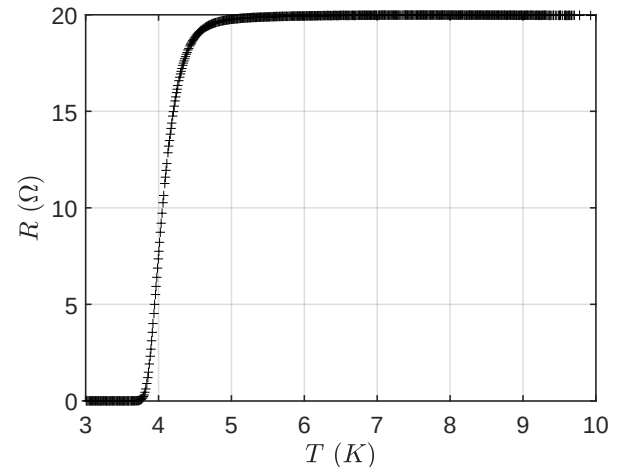

(b)

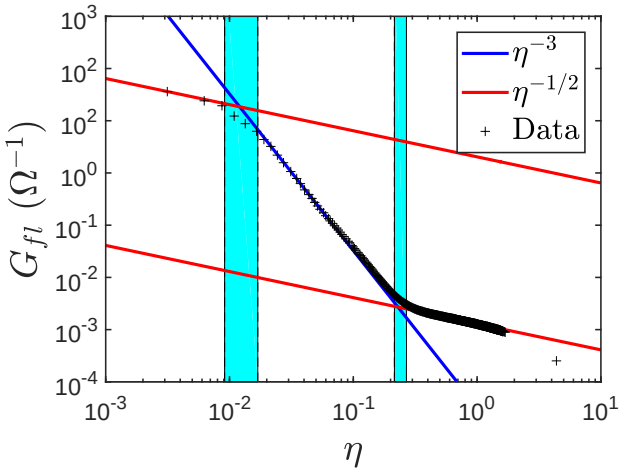

(c)

Figure L.2: The plots above show the fittings to Klemencic et. al.'s data [28] for a 204nm BNCD film. (a): EEI fitting to high temperature data. (b): focus on the superconducting transition. (c): Fitted fluctuation data, where the shaded regions indicate areas where the crossovers may exist.

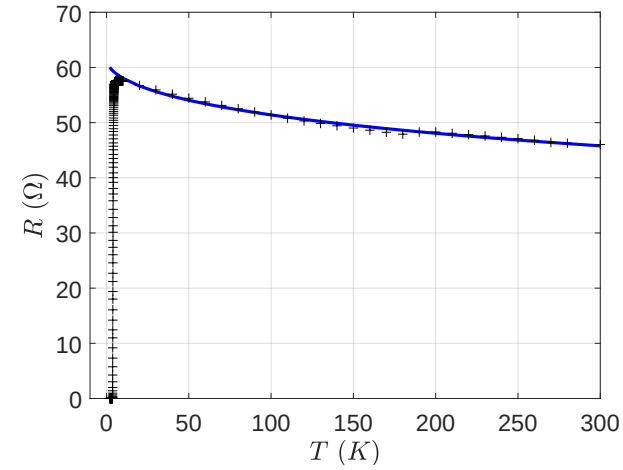

(a)

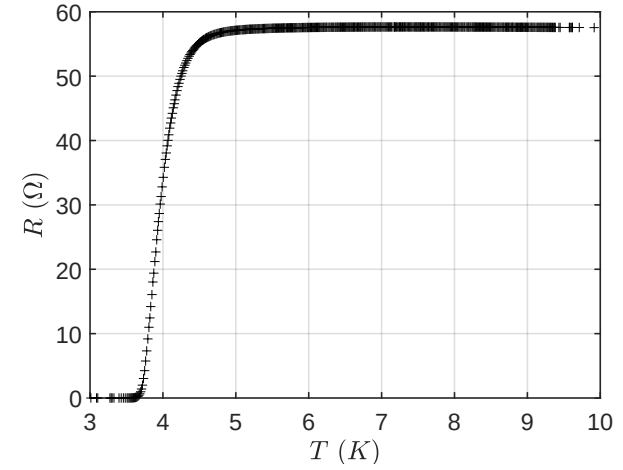

(b)

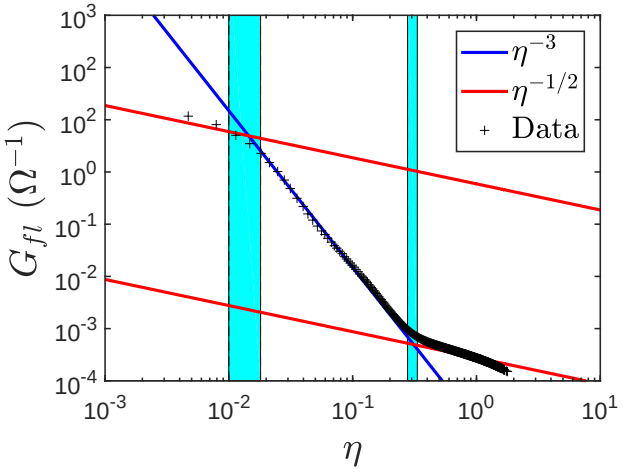

(c)

Figure L.3: The plots above show the fittings to Klemencic et. al.'s data [28] for a 168nm BNCD film. (a): EEI fitting to high temperature data. (b): focus on the superconducting transition. (c): Fitted fluctuation data, where the shaded regions indicate areas where the crossovers may exist.

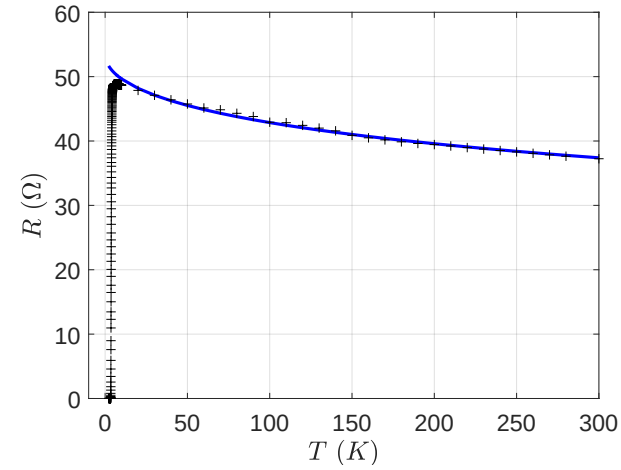

(a)

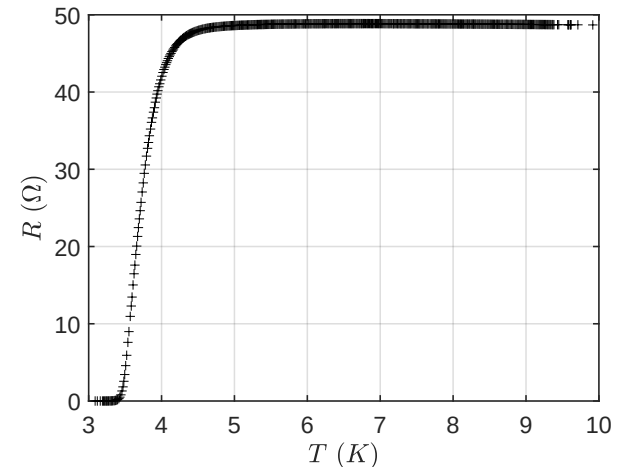

(b)

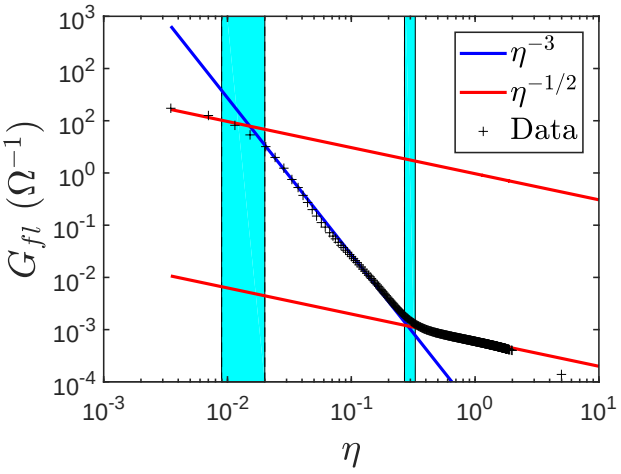

(c)

Figure L.4: The plots above show the fittings to Klemencic et. al.'s data [28] for a 160nm BNCD film. (a): EEI fitting to high temperature data. (b): focus on the superconducting transition. (c): Fitted fluctuation data, where the shaded regions indicate areas where the crossovers may exist.

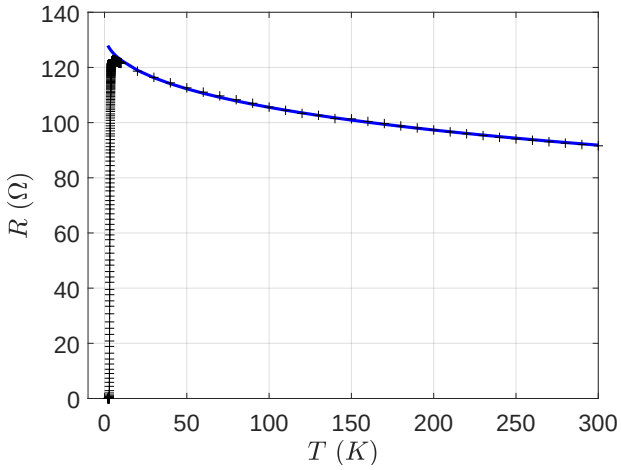

(a)

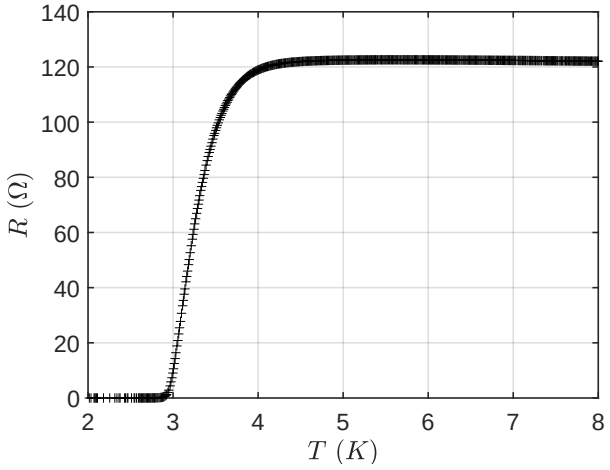

(b)

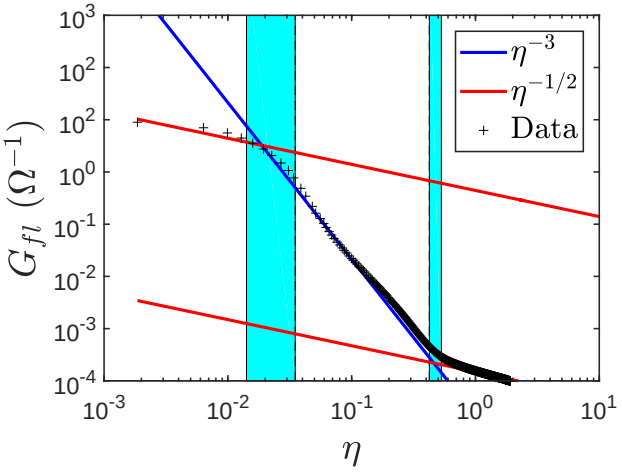

(c)

Figure L.5: The plots above show the fittings to Klemencic et. al.'s data [28] for a 128nm BNCD film. (a): EEI fitting to high temperature data. (b): focus on the superconducting transition. (c): Fitted fluctuation data, where the shaded regions indicate areas where the crossovers may exist.

APPENDIX M

SUMMIN' ABOUT SUM IDENTITIES

M.1 Matsubara Sums

In general a Matsubara sum is dealt with by performing analytic continuation so that we may consider an integral in the complex plane taken over some contour C, which can be shown to be related to our original sum of interest. This Matsubara trick is heavily used when dealing with sums over Matsubara frequencies, but can be applied very generally. Given the focus of this thesis, we will phrase this method in terms of Matsubara frequenices, however we will use a generalisation of the ideas presented in this section to derive the "difference of coths" identity quoted in eq. F.8 in section M.3.

Let us start by considering some function, $F(i\nu)$, that depends on the Matsubara frequency ν, which can be bosonic or fermionic, and is summed over this frequency,

$$S = \sum_{\nu} F(i\nu) \tag{M.1}$$

We now make a key assumption that underpins the Matsubara trick: we assume that the function $F(z)$, where $z \in \mathbb{C}$, has a finite number of poles whose locations form the set $\{z_0\}$, but none of which occur at $z = i\nu$. In this case we may analytically continue our

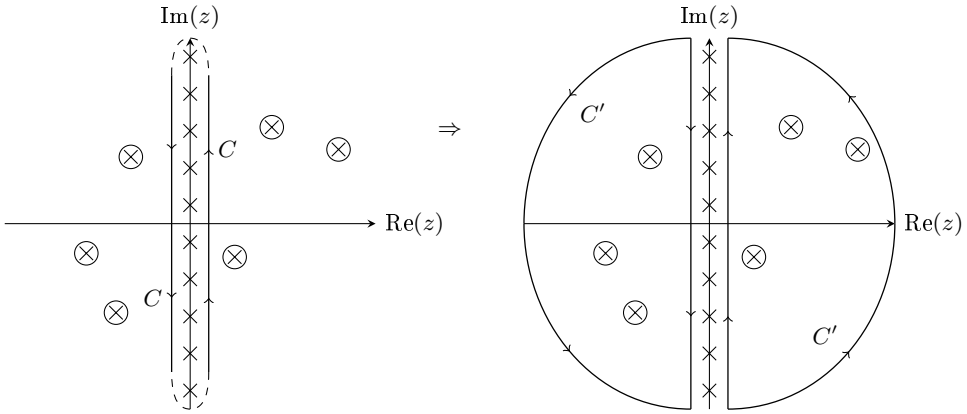

Figure M.1: Reinterpretation of the contour integral over C as a contour integral over C'. The crosses represent poles, with bare crosses arising from the counting function, $p(z)$, and the circled crosses being generated by $F(z)$. The dashed line on C represents the contour being taken to infinity on the imaginary axis.

Matsubara sum into the complex plane by introducing some counting function, $p(z)$, and letting $i\nu \to z$. This counting function has poles at $z = i\nu$, so when we consider our contour of integration in the complex plane we can enclose only the poles of $p(z)$ meaning the residue theorem sums over all the Matsubara frequencies. Written mathematically this reads

$$\oint_C dz\, p(z)F(z) = 2\pi i \sum_\nu F(i\nu)\mathrm{Res}\left(p(z), i\nu\right), \tag{M.2}$$

where the contour C is illustrated on the left set of axes in fig. M.1. If the counting function has the same residue at each pole, $R_0 = \mathrm{Res}\left(p(z), i\nu_1\right) = \mathrm{Res}\left(p(z), i\nu_2\right) = ...$, then we recover our original sum of interest

$$\oint_C dz\, p(z)F(z) = 2\pi i R_0 S. \tag{M.3}$$

Next, let us reinterpret the contour integral in eq. M.3. Instead of considering the poles inside the contour, we may instead consider the poles outside of the contour which introduces an additional minus sign due to the reversal of contour direction in the perspective of the poles "enclosed". We may picture this as taking the integral over the contour C' as shown in fig. M.1.

The poles exterior to C, but enclosed by C', are the poles associated to $F(z)$. Provided

that $F(z)$ decays sufficiently quickly,

$$\lim_{|z|\to\infty} |zp(z)F(z)| = 0, \tag{M.4}$$

we may write the integral as a sum over these poles

$$\oint_C dz\, p(z)F(z) = \oint_{C'} dz\, p(z)F(z) = -2\pi i \sum_{z_0} p(z_0)\mathrm{Res}\left(F(z), z_0\right). \tag{M.5}$$

Thus, by combining eq. M.3 and eq. M.5 we may evaluate a Matsubara type sum using

$$\sum_{\nu} F(i\nu) = -\frac{1}{R_0}\sum_{z_0} p(z_0)\mathrm{Res}\left(F(z), z_0\right) \tag{M.6}$$

Now the type of Matsubara frequency becomes important as bosonic and fermionic frequencies have different counting functions. For each type there are two common choices for $p(z)$ which we present in table M.1, where $f(z)$ is the Fermi-Dirac distribution and $n(z)$ is the Bose-Einstein distribution,

$$f(z) = \frac{1}{e^{\beta z}+1}, \qquad n(z) = \frac{1}{e^{\beta z}-1}. \tag{M.7}$$

Using the statistical distributions is quite intuitive and gives the correct Matsubara frequencies, however the second set of choices may appear less obvious. We can relate $\coth(\beta z/2)$ and $\tanh(\beta z/2)$ back to the distributions with ease using

$$\tanh\left(\frac{\beta z}{2}\right) = 1 - 2f(z), \qquad \coth\left(\frac{\beta z}{2}\right) = 1 + 2n(z). \tag{M.8}$$

Given that a simple constant has no poles (here that constant is just 1), we can ignore it inside the contour integral as it will simply give zero. Therefore, the poles of $f(z)$ and $\tanh(\beta z/2)$ are identical, but due to the factor of 2 relating these functions the residue of $\tanh(\beta z/2)$ is twice that of $f(z)$ at their poles. The same is clearly true for $n(z)$ and $\coth(\beta z/2)$, where they have identical pole structures and the residue of $\coth(\beta z/2)$ is

Table M.1: Choices of Matsubara counting functions and their residues for fermionic and bosonic frequencies, $\varepsilon = (2n+1)\pi T$ and $\omega = 2\pi n T$ respectively.

	Choice 1		Choice 2	
	$p(z)$	$\mathrm{Res}\,(p(z), i\nu)$	$p(z)$	$\mathrm{Res}\,(p(z), i\nu)$
Fermions ($\nu = \varepsilon$)	$f(z)$	$-T$	$\tanh\left(\frac{\beta z}{2}\right)$	$-2T$
Bosons ($\nu = \omega$)	$n(z)$	T	$\coth\left(\frac{\beta z}{2}\right)$	$2T$

twice that of $n(z)$ at the poles due the factor of 2 relating them.

If we now use these counting functions we see

$$\begin{aligned}
p(z) = f(z) \quad &\Rightarrow \quad T\sum_{\varepsilon} F(i\varepsilon) = \sum_{z_0} f(z_0)\mathrm{Res}\,(F(z), z_0)\,, \\
p(z) = \tanh\left(\frac{\beta z}{2}\right) \quad &\Rightarrow \quad T\sum_{\varepsilon} F(i\varepsilon) = \frac{1}{2}\sum_{z_0} \tanh\left(\frac{\beta z_0}{2}\right)\mathrm{Res}\,(F(z), z_0)\,, \\
p(z) = n(z) \quad &\Rightarrow \quad T\sum_{\varepsilon} F(i\varepsilon) = -\sum_{z_0} n(z_0)\mathrm{Res}\,(F(z), z_0)\,, \\
p(z) = \coth\left(\frac{\beta z}{2}\right) \quad &\Rightarrow \quad T\sum_{\varepsilon} F(i\varepsilon) = -\frac{1}{2}\sum_{z_0} \coth\left(\frac{\beta z_0}{2}\right)\mathrm{Res}\,(F(z), z_0)\,.
\end{aligned} \tag{M.9}$$

M.2 Momentum Sums in the Diffusive Limit

Here we study two sums. The first is the most commonly used result through this thesis, and the second is a special case. Both sums relate to a sum over momentum of a number of disorder averaged Green's functions in the diffusive limit, which we recall as being defined as,

$$q \ll \frac{1}{l}, \qquad T \ll \frac{1}{\tau_0}, \tag{M.10}$$

where q is the momentum difference between Green's functions, l is the elastic mean free path, and τ_0^{-1} is the elastic scattering rate.

Let us now consider the sum of two Green's functions with the same momentum[1] but

[1]This is the point we arrive at after neglecting the small momentum difference between the Green's functions.

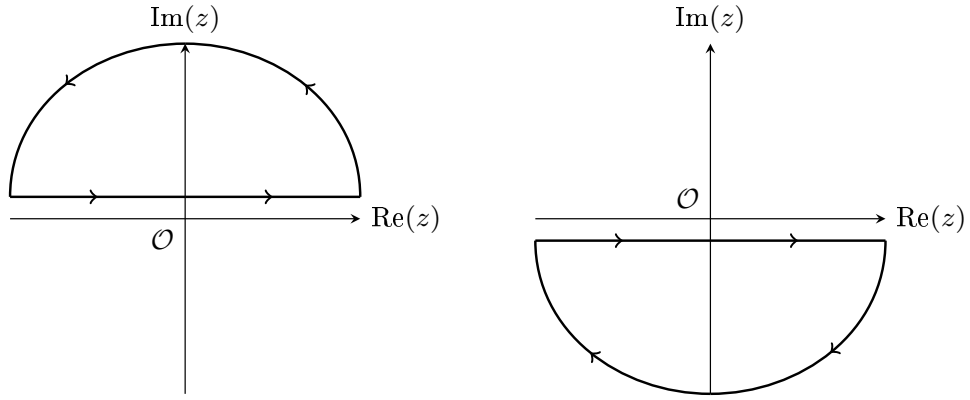

Figure M.2: Contour choices for the integral in eq. M.13.

differing frequencies, ε and $\varepsilon + \omega$. The sum we construct will contain an arbitrary integer power of each Green's function. Written mathematically the sum reads,[2]

$$S = \sum_{\mathbf{k}} G(\mathbf{k}, i\varepsilon)^m G(\mathbf{k}, i\varepsilon + i\omega)^n, \qquad m, n \in \mathbb{Z}^+. \tag{M.11}$$

We approximate this sum via an integral to yield

$$\begin{aligned} S &= \int \frac{d^d k}{(2\pi)^d} \frac{1}{[i\varepsilon - \xi_{\mathbf{k}} + \frac{i}{2\tau_0}\mathrm{sgn}(\varepsilon)]^m} \frac{1}{[i\varepsilon + i\omega - \xi_{\mathbf{k}} + \frac{i}{2\tau_0}\mathrm{sgn}(\varepsilon + \omega)]^n} \\ &= N(0) \int_{-\infty}^{+\infty} d\xi \frac{1}{[i\varepsilon - \xi + \frac{i}{2\tau_0}\mathrm{sgn}(\varepsilon)]^m} \frac{1}{[i\varepsilon + i\omega - \xi + \frac{i}{2\tau_0}\mathrm{sgn}(\varepsilon + \omega)]^n}, \end{aligned} \tag{M.12}$$

where $N(0)$ is the single spin DOS per unit volume.

Given that m, $n \geq 1$, the integrand falls off sufficiently rapidly for us to write it as an integral over a semi-circular contour whose radius is taken to infinity.[3] This means the sum becomes,

$$S = (-1)^{n+m} N(0) \oint_C dz \frac{1}{[z - i\varepsilon - \frac{i}{2\tau_0}\mathrm{sgn}(\varepsilon)]^m} \frac{1}{[z - i(\varepsilon + \omega) - \frac{i}{2\tau_0}\mathrm{sgn}(\varepsilon + \omega)]^n}, \tag{M.13}$$

where C is the semi-circular contour we integrate over. The two choices for this type of contour are shown in fig. M.2. This integral's value is thus dictated by its poles at

[2]Recall we are using the standard convention of dropping the volume factor of $\mathcal{V}^{-1}$ in front of the momentum sum.

[3]I.e: the integral over the semi-circle arc at infinity vanishes.

$z = i\varepsilon + i\,\mathrm{sgn}(\varepsilon)/(2\tau_0)$ and $z = i(\varepsilon+\omega) + i\,\mathrm{sgn}(\varepsilon+\omega)/(2\tau_0)$. These poles are of order m and n respectively.

If both frequencies, ε and $\varepsilon+\omega$, have the same sign, then both poles in the integrand will lie in the same half plane. We may then choose our contour to close in the opposite half plane (that with no poles), meaning this case trivially gives $S = 0$. However, if the frequencies are of opposite sign, then we are unable to choose a contour that does not enclose any poles. Both choices shown in fig. M.2 we will enclose one of the poles.

For simplicity we assume $\varepsilon+\omega > 0$ and $\varepsilon < 0$, and close our contour in the upper half plane. Cauchy's residue theorem allows us to write

$$\begin{aligned} S &= \frac{2\pi i(-1)^{n+m}N(0)}{(m-1)!}\frac{d^{m-1}}{dz^{m-1}}\left[\frac{1}{(z-i\varepsilon+\frac{i}{2\tau_0})^n}\right]\Bigg|_{z=i(\varepsilon+\omega)+i/(2\tau_0)} \\ &= \frac{2\pi i(-1)^{n-1}N(0)}{(m-1)!}\frac{n(n+1)(n+2)...(n+m-4)(n+m-3)(n+m-2)}{(\frac{i}{\tau_0}+i\omega)^{n+m-1}} \\ &= 2\pi N(0)\frac{(m+n-2)!}{(m-1)!(n-1)!}\frac{1}{(1+\omega\tau_0)}\frac{(-1)^{n-1}}{i^{(n+m-1)}}\tau_0^{n+m-1}i \\ &= 2\pi N(0)\frac{(m+n-2)!}{(m-1)!(n-1)!}\frac{1}{(1+\omega\tau_0)}(-i\tau_0)^m(i\tau_0)^{n-1}i \end{aligned} \tag{M.14}$$

Recalling that we are working in the diffusive limit, $T \ll \tau_0^{-1}$, and that $\omega = 2\pi LT$ ($L \in \mathbb{Z}$) is a bosonic Matsubara frequency, we may take $\omega\tau_0 \ll 1$. Using this limit we see that the result for frequencies of opposite sign does not depend upon the actual value of frequencies at all. We thus arrive at our final answer for a diffusive sum of Matsubara Green's functions,

$$\sum_{\mathbf{k}} G^+(\mathbf{k})^m G^-(\mathbf{k})^n = 2\pi N(0)\frac{(m+n-2)!}{(m-1)!(n-1)!}(-i\tau_0)^m(i\tau_0)^{n-1}i, \tag{M.15}$$

for m, $n \in \mathbb{Z}^+$, where we have used $G^\pm$ to denote a Green's function with a positive or negative frequency respectively.

M.2.1 A Single Green's Function

Let us now consider the momentum sum of a single disorder averaged electron Green's function of any frequency,

$$S_0 = \sum_{\mathbf{k}} G(\mathbf{k}, i\varepsilon). \tag{M.16}$$

This sum is of notable importance when calculating the self energy of the disorder average electron Green's function's Dyson equation.

We can approach this in two ways: analytically continue the sum to the complex plane and use Cauchy's residue theorem (*Method 1*); or standard algebraic tricks inside a real integral (*Method 2*). In both approaches we will start from the integral approximation of eq. M.16,

$$S_0 = N(0) \int_{-\infty}^{+\infty} d\xi \frac{1}{i\varepsilon - \xi + \frac{i}{2\tau_0}\mathrm{sgn}(\varepsilon)} \tag{M.17}$$

Method 1

We start by considering the contour integral

$$\begin{aligned} J_R &= \oint_{C_R} dz \frac{1}{z - i\varepsilon - \frac{i}{2\tau_0}\mathrm{sgn}(\varepsilon)} \\ &= \int_{-R}^{+R} dx \frac{1}{x - i\varepsilon - \frac{i}{2\tau_0}} + \int_{\Gamma_R} dz \frac{1}{z - i\varepsilon - \frac{i}{2\tau_0}\mathrm{sgn}(\varepsilon)}, \end{aligned} \tag{M.18}$$

where C_R is the contour defined by a semi-circle of radius R, and Γ_R is the contour running along the arc of the semi-circle. We may choose C_R to be one of two variants as before, see fig. M.2. The integrand has a simple pole at $z = i\varepsilon + i\mathrm{sgn}(\varepsilon)/(2\tau_0)$, and falls of as z^{-1} as $|z| \to \infty$ meaning the integral along Γ_R does not necessarily vanish.

In the limit $R \to \infty$ the first term produces S_0 upon multiplication by $-N(0)$. We may calculate J_R using Cauchy's residue theorem, so our choice of contour is important. Since the integrand has just one pole, we may choose to close our contour in the empty half plane (i.e: that which doesn't contain the pole) to produce $J_R = 0$. Therefore eq.

M.18 in the limit $R \to \infty$ yields

$$\begin{aligned} S_0^{\pm} &= \lim_{R\to\infty} N(0) \int_{\Gamma_R} dz \frac{1}{z - i\varepsilon \mp \frac{i}{2\tau_0}} \\ &= \lim_{R\to\infty} N(0) i \int_0^{\mp\pi} d\theta \frac{Re^{i\theta}}{Re^{i\theta} - i\varepsilon \mp \frac{i}{2\tau_0}} \\ &= N(0) i \int_0^{\mp\pi} d\theta \\ &= \mp\pi N(0) i, \end{aligned} \tag{M.19}$$

where the $\pm$ on $S_0^{\pm}$ refers to the sign of ε. In the second line of eq. M.19 we let $z = Re^{i\theta}$ on the contour Γ_R, where the upper limit of θ was dictated by whether we closed the C_R in the lower ($\varepsilon > 0$) or upper ($\varepsilon < 0$) half plane.

So the final result for the momentum sum of a single disorder averaged electron Green's function in the diffusive limit is,

$$\sum_{\mathbf{k}} G(\mathbf{k}, i\varepsilon) = -i\pi N(0) \mathrm{sgn}(\varepsilon) \tag{M.20}$$

Method 2

We may rewrite the integral in eq. M.17 as

$$S_0 = -N(0) \int_{-\infty}^{+\infty} d\xi \frac{\xi + i\varepsilon + \frac{i}{2\tau_0}\mathrm{sgn}(\varepsilon)}{\xi^2 + \left(\varepsilon + \frac{1}{2\tau_0}\mathrm{sgn}(\varepsilon)\right)^2}. \tag{M.21}$$

The real part vanishes due to being odd in ξ, whilst the imaginary part is easily evaluated to give,

$$S_0 = -N(0) i \left[\arctan\left(\frac{\xi}{\varepsilon + \frac{1}{\tau_0}\mathrm{sgn}(\varepsilon)} \right) \right]_{-\infty}^{+\infty}. \tag{M.22}$$

Clearly the integral produces a factor of $+\pi$ when $\varepsilon > 0$, and a factor of $-\pi$ when $\varepsilon < 0$. This therefore reproduces the result given in eq. M.20.

M.3 A Difference of coths

We use this identity in evaluating the inclusion of a vector potential **A** into the weak localisation corrections of a 1D cylinder (appendix F). Let us start by considering the sum

$$\begin{aligned} S &= \sum_{n=-\infty}^{+\infty} \frac{1}{\alpha^2(n-\beta)^2+\gamma^2} \\ &= \frac{1}{\alpha^2}\sum_{n=-\infty}^{+\infty} \frac{1}{(n-\beta)^2+\widetilde{\gamma}^2}, \end{aligned} \tag{M.23}$$

where $\gamma = \alpha\widetilde{\gamma}$. We now use the standard Matsubara trick using $\coth(az)$ as our pole counting function, where a is to be determined such that we can recover the correct summand. This counting function has poles at $z = i\pi n/a$, where $n \in \mathbb{Z}$, each with a residue of a^{-1}. Letting

$$F(n) = \frac{1}{(n-\beta)^2+\widetilde{\gamma}}, \tag{M.24}$$

we may write

$$I = \oint_C dz \coth(az)F(z) = \frac{2\pi i}{a}\sum_{n=-\infty}^{+\infty} F\left(\frac{i\pi n}{a}\right). \tag{M.25}$$

Therefore by letting $a = i\pi$ we recover the original sum in eq. M.25, such that $I = 2\alpha^2 S$.

Now, by considering the poles outside the contour C, which arise at $z_\pm = b \pm ia$ due to $F(z)$, we may also write

$$I = -2\pi i\left[\coth(z_+)\mathrm{Res}\left(F(z), z_+\right) + \coth(z_-)\mathrm{Res}\left(F(z), z_-\right)\right]. \tag{M.26}$$

This is then easily shown to be

$$I = \frac{\pi}{\widetilde{\gamma}}[\coth(\pi\widetilde{\gamma} + i\pi\beta) + \coth(\pi\widetilde{\gamma} - i\pi\beta)], \tag{M.27}$$

and hence

$$S = \frac{\pi}{2\alpha\gamma}\left[\coth\left(\frac{\pi\gamma}{\alpha} + i\pi\beta\right) + \coth\left(\frac{\pi\gamma}{\alpha} - i\pi\beta\right)\right]. \tag{M.28}$$

Thus we have obtained the result given in the first line of eq. F.8.

To get the second line, we write the coth functions in their exponential form and construct a common denominator. In doing this we see that

$$\begin{aligned}\coth(x+iy)+\coth(x-iy) &= 2\frac{e^{2x}-e^{-2x}}{e^{2x}+e^{-2x}-(e^{2iy}+e^{-2iy})} \\ &= 2\frac{\sinh(2x)}{\cosh(2x)-\cos(2y)}.\end{aligned} \tag{M.29}$$

Using this in conjunction with eq. M.28 we arrive at the final identity quoted in eq. F.8

$$S = \frac{\pi}{\alpha\gamma}\frac{\sinh\left(\frac{2\pi\gamma}{\alpha}\right)}{\cosh\left(\frac{2\pi\gamma}{\alpha}\right)-\cos\left(2\pi\beta\right)}. \tag{M.30}$$

M.4 A Sum of a Product of Green's Functions in Spectral Function Form

In computing the empty bubble of the polarisation operator for the screened Coulomb interaction in appendix G, we encountered the following sum,

$$S = T\sum_{\varepsilon}\frac{\mathcal{A}(\mathbf{k}+\mathbf{q},x)\mathcal{A}(\mathbf{k},y)}{[i(\varepsilon+\omega)-x][i\varepsilon-y]}. \tag{M.31}$$

Here $\mathcal{A}(\mathbf{k},x)$ is the spectral function of the disorder-averaged Green's function for a homogeneous metal,

$$G(\mathbf{k},i\varepsilon) = \frac{1}{i\varepsilon-\xi_{\mathbf{k}}+\frac{i}{2\tau_0}\mathrm{sgn}(\varepsilon)}, \tag{M.32}$$

ε is a fermionic Matsubara frequency, and ω is a bosonic Matsubara frequency. To evaluate this sum we will employ the same method used by Rickayzen in [29], where the sum in eq. M.31 appeared in the calculation of the Drude conductivity.

Using the standard Matsubara trick, we may rewrite the sum in eq. M.31 as

$$\begin{aligned} S &= \mathcal{A}(\mathbf{k}+\mathbf{q},x)\mathcal{A}(\mathbf{k},y)\frac{i}{2\pi}\oint_C dz \frac{f(z)}{(z+i\omega-x)(z-y)} \\ &= -\frac{i}{2\pi}\mathcal{A}(\mathbf{k}+\mathbf{q},x)\mathcal{A}(\mathbf{k},y)\oint_{C'} dz \frac{f(z)}{(z+i\omega-x)(z-y)}, \end{aligned} \tag{M.33}$$

where C and C' are the contours shown in fig. M.1. The contour integral taken over C' is then evaluated using the calculus of residues to yield

$$S = \mathcal{A}(\mathbf{k}+\mathbf{q},x)\mathcal{A}(\mathbf{k},y)\left[\frac{f(x-i\omega)}{x-y-i\omega}+\frac{f(y)}{y-x+i\omega}\right]. \tag{M.34}$$

Given that ω is a bosonic Matsubara frequency, we see that $f(x-i\omega)=f(x)$ and hence

$$S = \mathcal{A}(\mathbf{k}+\mathbf{q},x)\mathcal{A}(\mathbf{k},y)\frac{f(y)-f(x)}{y-x+i\omega}. \tag{M.35}$$

This is exactly the result that connects eq. G.1 and eq. G.2.

APPENDIX N

SPECIAL FUNCTIONS

This appendix serves as a quick reference for properties of the special functions used in this thesis. All identities and properties shown here are given in [83], or can be obtained from the identities listed there.

N.1 The Digamma Function

The digamma function, $\psi(x)$, is defined as the logarithmic derivative of the Gamma function, $\Gamma(x)$, [83],

$$\psi(x) = \frac{d}{dx} \ln \left[\Gamma(x)\right]. \tag{N.1}$$

The digamma function also has the following series representation,

$$\psi(x) = -\gamma - \sum_{n=0}^{\infty} \left[\frac{1}{x+n} - \frac{1}{n+1}\right], \tag{N.2}$$

where γ is the Euler-Mascheroni constant. Other series representations exist, but this is the one we will make most use of here. From eq. N.2, we may write,

$$\psi(x+m) - \psi(x) = \sum_{n=0}^{m-1} \frac{1}{x+n}. \tag{N.3}$$

Furthermore, eq. N.2 allows us to write the m^{th} derivative of the digamma function as

$$\psi^{(m)}(x) = (-1)^{m+1} m! \sum_{n=0}^{\infty} \frac{1}{(x+n)^{m+1}}. \tag{N.4}$$

Finally, let us note some useful values for the digamma function and its derivatives,

$$\begin{aligned} \psi(1) &= -\gamma, \\ \psi\left(\frac{1}{2}\right) &= -\gamma - 2\ln 2, \\ \psi'(1) &= \frac{\pi^2}{2}, \\ \psi'\left(\frac{1}{2}\right) &= \frac{\pi^2}{2}, \\ \psi''\left(\frac{1}{2}\right) &= -14\zeta(3). \end{aligned} \tag{N.5}$$

N.2 The Hurwitz Zeta Function

The Hurwtiz zeta function, $\zeta(x, a)$, is a generalisation of the Riemann zeta function, $\zeta(x)$. The Hurwitz zeta function can be represented by the series [83]

$$\zeta(z, a) = \sum_{n=0}^{\infty} \frac{1}{(n+a)^z}, \qquad \text{Re}[z] > 1,\ a \notin \mathbb{Z}_0^-, \tag{N.6}$$

where $\mathbb{Z}_0^-$ is the set of negative integers and zero. We note that eq. N.6 helps to illustrate $\zeta(z, 1) = \zeta(z)$. By differentiating eq. N.6 with respect to a we find [84]

$$\frac{d}{da}\zeta(z, a) = -z\zeta(z+1, a). \tag{N.7}$$

Another useful identity, which can be used to prove $\psi''(1/2) = -14\zeta(3)$, is

$$\zeta\left(z, \frac{1}{2}\right) = (2^z - 1)\zeta(z), \qquad \text{Re}[z] > 1. \tag{N.8}$$

BIBLIOGRAPHY

[1] P. Drude. Zur Elektronentheorie der Metalle. (German) [On the Electron Theory of Metals]. *Annalen der Physik*, 306(3):566 – 613, 1900.

[2] J. J. Thomson. XL. Cathode Rays. *The London, Edinburgh, and Dublin Philosophical Magazine and Journal of Science*, 44(269):293 – 316, 1897.

[3] P. Debye. Zur Theorie der spezifischen Wärmen. *Annalen der Physik*, 344(14):789 – 839, 1912.

[4] S. H. Simon. *The Oxford Solid State Basics*. Oxford University Press, Oxford, 1976.

[5] W. Heisenberg. Über quantentheoretische Umdeutung kinematischer und mechanischer Beziehungen. *Zeitschrift für Physik*, 33(1):879 – 893, 1925.

[6] E. Schrödinger. Quantisierung als Eigenwertproblem. *Annalen der Physik*, 384(4):361 – 376, 1926.

[7] A. Somerfeld. Zur Elektronentheorie der Metalle. (German) [On the Electron Theory of Metals]. *Naturwissenschaften*, 15(41):825 – 832, 1927.

[8] N. W. Ashcroft and N. D. Mermin. *Solid State Physics*. Brook/Cole Cengage Learning, United States of America, 1976.

[9] T. Matsubara. A New Approach to Quantum-Statistical Mechanics. *Progress of Theoretical Physics*, 14(4):351 – 378, 1955.

[10] R. Kubo. A General Expression for the Conductivity Tensor. *Canadian Journal of Physics*, 34(12A):1274 – 1277, 1956.

[11] R. Edwards. A New Method for the Evaluation of Electric Conducitivity in Metals. *Philisophical Magazine*, 3(8):1020 – 1031, 1958.

[12] J. S. Langer. Theory of Impurity Resistance in Metals. *Physical Review*, 120(3):714 – 725, 1960.

[13] J. S. Langer. Theory of Impurity Resistance in Metals II. *Physical Review*, 124(4):1003 – 1010, 1961.

[14] J. S. Langer. Evaluation of Kubo's Formula for the Impurity Resistance of an Interacting Electron Gas. *Physical Review*, 127(1):5 – 16, 1962.

[15] J. Bardeen, L. N. Cooper, and J. R. Schrieffer. Theory of Superconductivity. *Physical Review*, 108(5):1175 – 1204, 1957.

[16] Y. Nambu. Quasi-Particles and Gauge Invariance in the Theory of Superconductivity. *Physical Review*, 117(3):648 – 663, 1960.

[17] L. P. Gor'kov. On the Energy Spectrum of Superconductors. *Soviet Physics JETP*, 7(3):505 – 508, 1958.

[18] L. G. Aslamazov and A. I. Larkin. Effect of Fluctuations on the Properties of a Supercondutor Above the Critical Temperature. *Soviet Physics - Solid State*, 10(4):23 – 28, 1968.

[19] K. Maki. Critical Fluctuation of the Order Parameter in a Supercondutor. I. *Progress of Theoretical Physics*, 40(2):193 – 200, 1968.

[20] R. S. Thompson. Microwave, Flux Flow, and Fluctuation Resistance of Dirty Type-II Superconductors. *Physical Review B*, 1(1):327 – 333, 1970.

[21] B. L. Al'tshuler and A. G. Aronov. Contribution to the theory of disordered metals in strongly doped semiconductors. *Soviet Physics JETP*, 50(5):968 – 976, 1979.

[22] E. Abrahams, P. W. Anderson, D. C. Licciardello, and T. V. Ramakrishnan. Scaling Theory of Localization: Absence of Quantum Diffusion in Two Dimensions. *Physical Review Letters*, 42(10):673 – 676, 1979.

[23] L. P. Gor'kov, A. I. Larkin, and D. E. Kheml'nitskii. Particle conductivity in a two-dimensional random potential. *Soviet Physics JETP Letters*, 30(4):228 – 232, 1979.

[24] C. J. Adkins. Hopping Conductivity in Granular Metals Revisited. In P. P. Edwards and C. N. R. Rao, editors, *Metal-Insulator Transitions Revisited*. Taylor and Francis, London, 1995.

[25] B. Abeles, P. Sheng, M.D. Coutts, and Y. Arie. Structural and electrical properties of granular metal films. *Advances in Physics*, 24(3):407 – 461, 1975.

[26] I. S. Beloborodov, A. V. Lopatin, V. M. Vinokur, and K. B. Efetov. Granular electronic systems. *Reviews of Modern Physics*, 79(2):469 – 518, 2007.

[27] I. V. Lerner, A. A. Varlamov, and V. M. Vinokur. Fluctuation Spectroscopy of Granularity in Superconducting Structures. *Physical Review Letters*, 100(11):117003, 2008.

[28] G. M. Klemencic, J. M. Fellows, J. M. Werrell, S. Mandal, S. R. Giblin, R. A. Smith, and O. A. Williams. Fluctuation spectroscopy as a probe of granular superconducting diamond films. *Physical Review Materials*, 1(4):044801, 2017.

[29] G. Rickayzen. *Green's Functions and Condensed Matter*. Dover Publications, New York, corrected edition, 2013.

[30] A. A. Abrikosov, L. P. Gorkov, and I. E. Dzyaloshinski. *Methods Of Quantum Field Theory In Statistical Physics*. Dover Publications, New York, 1975.

[31] H. Bruus and K Flensberg. *Many-Body Quantum Theory in Condensed Matter Physics: An Introduction*. Oxford University Press, New York, 2004.

[32] D. A. Greenwood. The Boltzmann Equation in the Theory of Electrical Conduction in Metals. *Proceedings of the Physical Society*, 71(4):585 – 596, 1958.

[33] A. A. Abrikosov and L. P. Gorkov. On the Theory of Superconducting Alloys; I. The Electrodynamics of Allyos at Absolute Zero. *Philisophical Magazine*, 8(6):1090 – 1098, 1959.

[34] A. Altland and B. Simons. *Condensed Matter Field Theory*. Cambridge University Press, Cambridge, 2nd edition, 2010.

[35] I. V. Lerner. Nonlinear Sigma Model for Normal and Superconducting Systems: A Pedestrians Approach [Internet]. `https://arxiv.org/abs/cond-mat/0307471`, 2002. [Last accessed: 12/03/2021].

[36] K. Efetov. *Supersymmetry in Disorder and Chaos*. Cambridge University Press, Cambridge, 1996.

[37] D. T. S. Perkins and R. A. Smith. Drude Conductivity of a Granular Metal. *Annals of Physics*, 418:168170, 2020.

[38] S. Datta. *Electronic Transport in Mesoscopic Systems*. Cambridge University Press, Cambridge, 1995.

[39] B. L. Altshuler and A. G. Aronov. Electron-Electron Interaction In Disordered Conductors. In A. L. Efros and M. Pollak, editors, *Electron-Electron Interactions in Disordered Systems*. North-Holland Physics Publishing, Amsterdam, 1985.

[40] P. W. Anderson. Absence of Diffusion in Certain Random Lattices. *Physical Review*, 109(5):1492 – 1505, 1958.

[41] P. A. Lee and T. V. Ramakrishnan. Disordered Electronic Systems. *Reviews of Modern Physics*, 57(2):287 – 337, 1985.

[42] G. Bergmann. Weak Locaization in Thin Films. *Physical Reports*, 107(1):1– 58, 1984.

[43] H. Fukuyama. Interaction Effects in the Weakly Localized Regime of Two- and Three-Dimensional Disordered Systems. In A. L. Efros and M. Pollak, editors, *Electron-Electron Interactions in Disordered Systems*. North-Holland Physics Publishing, Amsterdam, 1985.

[44] B. R. Patton. Fluctuation Theory of the Superconducting Transition in Restricted Dimensionality. *Physical Review Letters*, 27(19):1273 – 1276, 1971.

[45] J. S. Langer and T. Neal. Breakdown of the Concentration Expansion for the Impurity Resistivity of Metals. *Phys. Rev. Lett.*, 16(22):984 – 986, 1966.

[46] E. Abrahams and T. V. Ramakrishnan. Scaling Theory of Locaization and Non-Ohmic Effects in Two Dimensions. *Journal of Non-Crystalline Solids*, 35:15 – 20, 1980.

[47] S. Kawaji and Y. Kawaguchi. A New Type of Anomalous Magnetoresistance in Two Dimensional Transport in InAs. *Journal of the Physical Society of Japan*, 24(4):963–963, 1968.

[48] Y. Kawaguchi and S. Kawaji. Negative Magnetoresistance in Silicon (100) MOS Inversion Layers. *Journal of the Physical Society of Japan*, 48(2):699–700, 1980.

[49] D. Yu. and Yu. V. Sharvin. Magnetic-flux quantization in a cylindrical film of a normal metal. *Soviet Physics JETP Letters*, 34(5):272 – 275, 1981.

[50] B. L. Al'tshuler, A. G. Aronov, B. Z. Spivak, D. Yu. Sharvin, and Yu. V. Sharvin. Observation of the Aaronov-Bohm effect in hollow metal cylinders. *Soviet Physics JETP Letters*, 35(11):588 – 591, 1982.

[51] G. D. Mahan. *Many-Particle Physics*. Kluwer Academic/Plenun Publishers, New York, third edition, 2000.

[52] M. Tinkham. *Introduction to Superconductivity*. Dover Publications, New York, 2nd edition, 2004.

[53] J. E. Crow, R. S. Thompson, M. A. Klenin, and A. K. Bhatnagar. Divergent Fluctuations in Superconducting Films. *Physical Review Letters*, 24(8):371 – 475, 1970.

[54] J. Keller and V. Korenman. Regularization of the Maki Conductivity by Fluctuations. *Physical Review Letters*, 27(19):1270 – 1273, 1971.

[55] J. Keller and V. Korenman. Fluctuation-Induced Conductivity of Superconductors above the Transition Temperature: Regularization of the Maki Diagram. *Physical Review B*, 5(11):4367 – 4375, 1972.

[56] A. Larkin and A. Varlamov. *Theory of Fluctuations in Superconductors*. Oxford University Press, New York, 2005.

[57] E. Abrahams, P. W. Anderson, P. A. Lee, and T. V. Ramakrishnan. Quasiparticle lifetime in disordered two-dimensional metals. *Physical Review B*, 24(12):6783 – 6789, 1981.

[58] H. Fukuyama and E. Abrahams. Inelastic scattering time in two-dimensional disordered metals. *Physical Review B*, 27(10):5976 – 5980, 1983.

[59] W. Brenig, M.C. Chang, E. Abrahams, and P. Wölfle. Inelastic scattering time above the superconductivity transition in two dimensions: Dependence on disorder and magnetic field. *Physical Review B*, 31(11):7001 – 7005, 1985.

[60] J. M. Gordon, C. J. Lobb, and M. Tinkham. Divergent phase-breaking rate in aluminum films from magnetoconductance measurements. *Physical Review B*, 29(9):5232 – 5235, 1984.

[61] I. S. Beloborodov and K. B. Efetov. Negative Magnetoresistance of Granular Metals in a Strong Magnetic Field. *Physical Review Letters*, 82(16):3332 – 3335, 1999.

[62] I. S. Beloborodov, K. B. Efetov, and A. I. Larkin. Magnetoresistance of granular superconducting metals in a strong magnetic field. *Physical Review B*, 61(13):9145 – 9161, 2000.

[63] I. S. Beloborodov, K. B. Efetov, A. Altland, and F. W. J. Hekking. Quantum interference and Coulomb interaction in arrays of tunnel junctions. *Physical Review B*, 63(11):115109, 2001.

[64] I. S. Beloborodov, K. B. Efetov, A. V. Lopatin, and V. M. Vinokur. Transport Properties of Granular Metals at Low Temperatures. *Physical Review Letters*, 91(24):246801, 2003.

[65] I. S. Beloborodov, A. V. Lopatin, and V. M. Vinokur. Universal description of granular metals at low temperatures: Granular Fermi liquid. *Physical Review B*, 70(20):205120, 2004.

[66] I. S. Beloborodov, A. V. Lopatin, and V. M. Vinokur. Coulomb effects and hopping transport in granular metals. *Physical Review B*, 72(12):125121, 2005.

[67] C. Biagini, T. Caneva, V. Tognetti, and A. A. Varlamov. Weak localization effects in granular metals. *Physical Review B*, 72(4):041102, 2005.

[68] C. Biagini, R. Ferone, R. Fazio, F. W. J. Hekking, and V. Tognetti. Superconducting fluctuation corrections to the thermal conductivity in granular metals. *Physical Review B*, 72(13):134510, 2005.

[69] B. S. Skrzynski, I. S. Beloborodov, and K. B. Efetov. Superconducting fluctuations in granular metals with a large coupling between the grains. *Physical Review B*, 65(9):094516, 2002.

[70] K. B. Efetov and A. Tschersich. Coulomb effects in granular materials at not very low temperatures. *Physical Review B*, 67(17):174205, 2003.

[71] A. Barone and G. Paternò. *Physics and Applications of the Josephson Effect*. Wiley-Interscience, New York, 1982.

[72] R. Peierls. Zur Theorie des Diamagnetismus von Leitungselektronen. (German) [On the Theory of Diamagnetism of Conduction Electrons]. *Zeitschrift für Physik*, 80(11):763 – 791, 1933.

[73] V. Turkowski and J. K. Freericks. Nonlinear response of Bloch electrons in infinite dimensions. *Physical Review B*, 71(8):085104, 2005.

[74] R. P. Feynman, R. B. Leighton, and Sands M. *The Feynman Lectures on Physics. Volume III: Quantum Mechanics*. Basic Books, New York, the new millennium edition edition, 2011.

[75] A. A. Varlamov and V. V. Dorin. Fluctuation resistance of Josephson junctions. *Soviet Physics JETP*, 57(5):1089 – 1096, 1970.

[76] D. T. S. Perkins, G. M. Klemencic, J. M. Fellows, and R. A. Smith. Fluctuation spectroscopy in granular superconductors with application to boron-doped nanocrystalline diamond. *Physical Review B*, 104(9):094513, 2021.

[77] G. M. Klemencic, J. M. Fellows, J. M. Werrell, S. Mandal, S. R. Giblin, R. A. Smith, and O. A. Williams. Observation of a superconducting glass state in granular superconducting diamond. *Scientific Reports*, 9(1):4578, 2019.

[78] M. Giannouri, E. Rocofyllou, C. Papastaikoudis, and W. Schilling. Weak-localization, Aslamazov-Larkin, and Maki-Thompson superconducting fluctuation effects in disordered $Zr_{1-x}Rh_x$ films above T_c. *Physical Review B*, 56(10):6148 – 6156, 1997.

[79] K. Meiners-Hagen and W. Gey. Maki-Thompson correction to magnetoresistance in three-dimensional disordered alloys. *Physical Review B*, 63(5):052507, 2001.

[80] P. E. Parris. Many Particle Systems [Internet]. `https://web.mst.edu/~parris/QuantumOne/Class_Notes/ManyParticleSystems.pdf`, 2002. [Last accessed: 12/03/2021].

[81] R. Shankar. *Principles of Quantum Mechanics*. Springer, New York, 2nd edition, 2014.

[82] B. L. Al'tshuler, A. G. Aronov, and B. Z. Spivak. The Aaronov-Bohm effect in disordered conductors. *Soviet Physics JETP Letters*, 33(2):94 – 97, 1981.

[83] I. S. Gradshteyn and I. M. Ryzhik. *Table of Integrals, Series, and Products*. Academic Press, London, corrected and enlarged edition, 1980.

[84] J. Sondow and E. W. Weisstein. Hurwitz Zeta Function [Internet]. `https://mathworld.wolfram.com/HurwitzZetaFunction.html`, Publication year unknown. [Last accessed: 08/06/2021].